Department of Chemical
and Biochemical Engineering
Technical University of Denmark

Graduate Schools Yearbook 2009

Editors:
Kim Dam-Johansen
Victor Darde
Krist V. Gernaey

Address: Department of Chemical and Biochemical Engineering
Søltofts Plads, Building 229
Technical University of Denmark
DK-2800 Kgs. Lyngby
Denmark

Telephone: +45 4525 2800
Fax: +45 4588 2258
Email: kt@kt.dtu.dk
Internet: http://www.kt.dtu.dk

Print: J&R Frydberg A/S
København
May 2010

Cover: Suzanne Fog

Cover Photo: Klaus Holsting

ISBN-13: 978-87-92481-14-6

Contents

Contributions

Preface

The number of PhD students at DTU Chemical Engineering has grown significantly over the last couple of years. This increase is caused by expanding activities in our traditional core disciplines of Chemical Engineering as well as a substantial number of new research projects in our groups in the field of Biochemical Engineering focusing on enzymes and process technology.

Thanks to very talented graduate students from all over the world, active and ambitious supervisors combined with support from administration, technicians and our workshop we have attracted more public grants than ever before. We have also established cooperation with an expanding number of research based companies not only from Denmark – but from all regions of the world. In addition to that, we have seen a further extension of our collaborations with sister departments at universities all over the world.

In the Graduate Schools yearbook 2009 our PhD students present their individual projects. Some of the students have just initiated their research whereas others are close to concluding their work. We hope that the readers will find the Yearbook interesting and we invite you to contact us in case you would like to receive more details of specific projects.

Yours Sincerely

Kim Dam-Johansen
Professor, Head of Department

Krist V. Gernaey
Associate Professor, Editor

Jane Agger
Phone: +45 4525 2943
Fax: +45 4593 2906
E-mail: jag@kt.dtu.dk
WWW: http://bioeng.kt.dtu.dk
Supervisors: Anne Meyer

Anders Viksø-Nielsen, Novozymes A/S

PhD Study
Started: March 2007
To be completed: December 2010

Deacetylation Rather than Deferuloylation Increase the Depolymerization of Corn Fiber Arabinoxylan

Abstract
Corn fiber is a prospective source of biofuels, chemicals and food ingredients and may be upgraded by enzymatic modifications. In the present work enzymatic hydrolysis of arabinoxylan from pretreated corn fiber (190 ºC, 10 min) was evaluated by measuring the release of xylose and arabinose using a designed mixture of mono-component enzymes consisting of α-L-arabinofuranosidases, endo-xylanase and β-xylosidase. The pretreatment divided the corn fiber material equally into a soluble and an insoluble fraction. The latter was less substituted with arabinose than the original material and enzymatic hydrolysis released up to 15% of the xylose. Addition of acetyl xylan esterase activity to the mono-component mixture almost doubled the xylose release. Expressed as mole equivalents, the acetyl xylan esterase boosted the release of one mole of xylose pr. mole of acetate released, whereas a feruloyl esterase promoted the release of approx. 0.4 mole of xylose pr. mole of released ferulic acid. On the soluble material, the release of one mole equivalent of acetate released up to 0.5 mole xylose, whereas ferulic acid release was equivalent to the release of one mole equivalent of xylose. The results implied that on the insoluble material the acetyl xylan esterase activity was a more important component for the enzymatic degradation than feruloyl esterase activity, whereas on soluble arabinoxylan the feruloyl esterase activity seemed to be more important for the arabinoxylan depolymerization.

Introduction
Enzymatic hydrolysis of corn fiber is of great interest because of corn fibers potential of becoming a source of renewable biofuels or food ingredients. However, enzymatic hydrolysis of corn fiber has proven difficult due to complex polysaccharide structures and interactions [1]. Corn fiber consists of the pericarp tissue and the tip of the corn kernel and originates from a gramineaceous plant whose primary cell wall is mainly composed of heteroxylans (approx. 50% by dry weight) notably arabinoxylan [2]. Fig. 1 depicts a possible sketch of the arabinoxylan structure. The arabinoxylan backbone is composed of a β-1,4-linked D-xylose backbone. Linkage analysis has suggested that up to 85% of the xylose moieties are substituted with various components [3]. The main substitutions are α-L-arabinose linked to the O-2 or O-3 position on monosubstituted xylose (40%) or to both O-2 and O-3 on one xylose monomer (20%). Arabinose substitutions have also been suggested as short side chains linking arabinose moieties by C2 or C3. As much as 40% the total arabinose substitutions have been reported as non-terminal [3]. Xylan is furthermore directly substituted with D-galactose and D-glucuronic acid which may each account for approx. 3-5% of the biomass dry weight [2,4]. It has also been suggested that xylan is further substituted with xylose by a C1 to C3 linkage and that arabinose can be further decorated with xylose or even L-galactose [4,5]. Besides glycosidic linkages arabinoxylan is also substituted by esterifications. Acetate is found to constitute 3-5% of the dry matter and is esterified directly to the xylose backbone in position O-2 or O-3 while the hydroxycinnamic acids (3-6%) are esterified to arabinose in position O-5 [5,6]. The hydroxycinnamates are mainly ferulic acid and dehydrodimers of ferulic acid [5,7-9]. Suggestions have been made that ferulic acid can be positioned on arabinose in short chain substitutions rather than terminally on the arabinose moiety [5]. It is known that in particular diferulates cross-link arabinoxylan molecules thereby creating covalent intermolecular relations [9-11]. Finally corn fiber also contains cellulose (~20%), lignin (~10%) and structural proteins (~5%). In particular the lignin and structural proteins have been suggested to also participate in intermolecular interactions with arabinoxylan through diferulate cross-linking giving rise to a highly complex network of heterogeneous molecules [5,12,13].

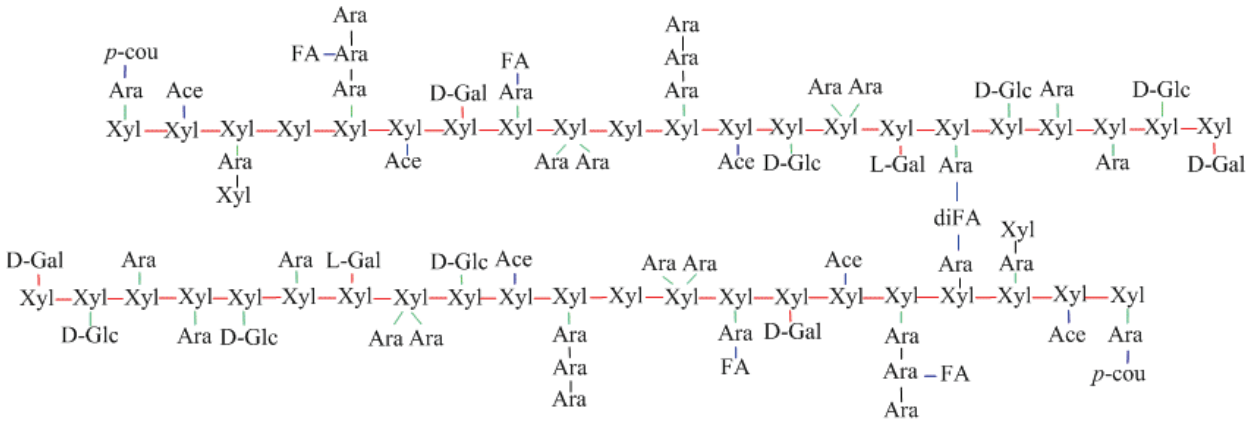

Figure 1: Schematic drawing of arabinoxylan structure in corn fiber. Xyl: D-xylose, Ara: L-arabinose, D/L-Gal: D/L-galactose, D-Glc: D-glucuronic acid, FA: ferulic acid, diFA: dehydrodimer of ferulic acid, *p*-cou: *p*-coumaric acid, Ace: acetate.

In order to achieve reasonable enzymatic hydrolysis pretreatment has been applied with success [14,15] and seems inevitable at present. The recalcitrance to degradation has been ascribed to be a consequence of the highly branched structure of the arabinoxylan and indeed feruloylation has been held responsible [16,17]. In contrast, acetylation has been given very little attention even though early studies with other substrates such as wheat and aspen xylans have shown that enzymatic digestibility of both cellulose and xylan remarkably increased with increasing chemical deacetylation [18].

Specific Objective

We hypothesized that deacetylation could be important for the overall enzymatic digestibility of xylan. The purpose of the present work was to assess and compare the overall depolymerization of corn fiber arabinoxylan using relevant monocomponent enzyme activities and hereby to obtain indications as to the significance of deacetylation for enzymatic depolymerization of corn fiber arabinoxylan.

Materials and methods

Substrate

Raw corn fiber was provided by Archer Daniel Midlands Company, Decatur Illinois, USA. The material was milled, enzymatically destarched, freeze dried and milled again before use. Initial wet milling was performed at 2% dry matter (DM) and destarching was carried out using a thermostable α-amylase (Termamyl® SC) incubated at pH 6, 95 ºC for half an hour, followed by incubation with amyloglucosidase (Spirizyme® Plus FG) at pH 5, 60 ºC for 1 hour. The material was washed in water and decanted to remove liberated glucose. Freeze drying was done over 5 days and the biomass was milled again to reduce the particle size to less than 1 mm.

Enzymes

All enzymes were provided by Novozymes A/S, Bagsværd, Denmark. Cellic™ CTec is a commercially available cellulase preparation based on the *Trichoderma reesei* complex while the others were mono-component preparations (Table 1).

Table 1: Enzymes used for hydrolysis of pretreated corn fiber. [a]Mixed cellulase preparation. Hemicellulases were the same as the minimal cocktail from [19]. FAE [20,21]

Enzyme	Microorganism	Family/Type
Endoxylanase	*Humicola insolens*	GH10
β-xylosidase	*Trichoderma reesei*	GH3
α-L-arabinofuranosidase	*Meripilus giganteus*	GH51
α-L-arabinofuranosidase	*Humicola insolens*	GH43
Acetyl xylan esterase (AXE)	*Flavolaschia sp.*	CE1
Ferulic acid esterase (FAE)	*Aspergillus niger*	A
Cellic™ CTec[a]	*Trichoderma reesei*	-

Pretreatment

60 g of destarched corn fiber was suspended in 1 L of water and pretreated at 190 ºC with a 10 min holding time. Heating and cooling periods together added up to 6 min. The pretreatment was conducted in a loop autoclave at Risø DTU. No chemicals or gasses were added to the suspension neither before during or after the treatment. Afterwards the material was separated into a solid and a supernatant fraction by filtration and were characterized and enzymatically hydrolyzed individually.

Enzymatic hydrolysis

All enzymatic hydrolysis experiments were performed at a 2% DM concentration in 0.1 M succinate buffer, pH 5 and incubated at 50 ºC for 24 hours with mixing at 1400 rpm. Samples were withdrawn after 0, 2, 4, 6 and 24 hours. After incubation the samples were inactivated

immediately at 100 ºC for 10 min. Enzymes were loaded according to their enzyme protein (EP) concentration with 0.25 g EP/kg DM for each of the hemicellulases, 0.5 g EP/kg DM for the esterases and 4 g EP/kg DM for the cellulase preparation. All hydrolyses were performed in triplicate.

Results and discussion

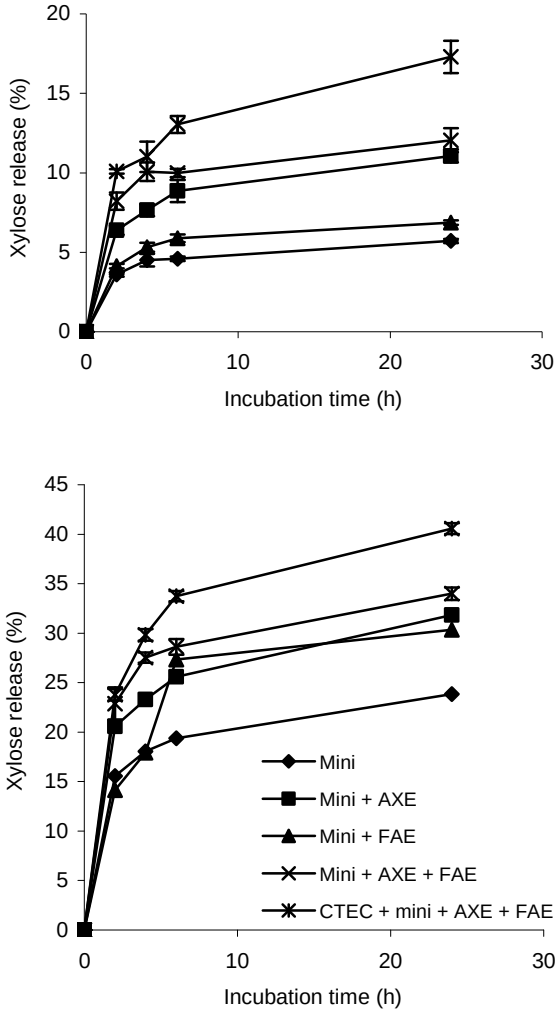

Figure 2: Xylose release after enzymatic hydrolysis. Upper graph: solid fraction, lower graph: supernatant fraction. Mini (hemicellulases), AXE (acetyl xylan esterase), FAE (feruloyl esterase), CTEC (Cellic™ CTec)

Fig. 2 shows that enzymatic release of xylose was affected by the presence of other enzymes than hemicellulases (mini). In particular depolymerization of xylose in the solid fraction was promoted by the presence of acetyl xylan esterase and cellulases. When comparing the 24 hours data points it was evident that ferulic acid esterase was not responsible for any additional release of xylose compared to the hemicellulases alone, whereas the acetyl xylan esterase caused release of approximately twice the amount of xylose compared to the hemicellulases alone. In the experiment combining the two types of esterases the xylose release was not higher than when compared to the acetyl xylan esterase incubated alone with the hemicellulases. Furthermore, the cellulase preparation induced additional release of xylose and this was most likely a consequence of simultaneous cellulose degradation revealing more substrate for the endo-xylanase.

The effect of acetyl xylan esterase versus ferulic acid esterase was not pronounced to the same degree for the solubilized fraction indicating that the accessibility for the hemicellulases was not restricted in the same manner as on the insoluble fraction. In addition, the yield of xylose in the solubilized material was higher (up to 36% of the fraction, 10% of the original amount of xylose) than in the insoluble material (approx. 15%, 4% of the original amount of xylose) meaning that the enzymatic accessibility had indeed improved by the solubilization. The cellulase preparation seemed not to have any noteworthy effect on the solubilized material owing to a low content of cellulose. Appropriate controls of esterases incubated alone did not show any release of xylose (data not shown).

When the acetate and ferulic acid release were compared to the respective xylose release (Table 2) it was clear that deacetylation promoted the depolymerization of xylan to a greater extent than deferuloylation in the insoluble material. Here the reaction ratio was 1:1 leading to the release of one mole equivalent of xylose for every released mole equivalent of acetate. The corresponding release of ferulic acid was 0.39 moles of xylose released for every mole of ferulic acid. This fact implied that catalysis by the endo-xylanase was entirely dependent of the degree of substitution directly on the xylan backbone rather than on the removal of extended branching. Furthermore, these data support that reactions catalyzed by these types of enzymes (glycosyl hydrolases) could be promoted even on insoluble substrates if the appropriate activities were present and accompanying each other.

Table 2: Xylose release related to acetate or ferulic acid release

	AXE (mol xylose/mol acetate)	**FAE** (mol xylose/mol ferulic acid)
Solid	1.06	0.39
Supernatant	0.51	1.01

The opposite effect was observed for the solubilized oligosaccharides (Table 2). Here the release of xylose compared to ferulic acid release was 1:1, whereas deacetylation only caused 0.5 mole equivalents of xylose per mole equivalent acetate. In this case it would have been expected that the arabinose release would have increased equally but this was not the case. Arabinose release was not affected by the presence of either of the esterases (data not shown). This result has several implications one of them being that the enzymes may be highly dependent on the overall substrate

structure rather than just the presence of the bonds to be hydrolyzed. The lack of arabinose release also clearly envisions the diversity of the enzymatic attack performed by the same enzymes. The solubilized oligosaccharides represented a completely different substrate both with respect to substitution pattern, degree of substitution and most probably also the degree of polymerization (DP) as compared to the insoluble material. The increased release of xylose occurring with deferuloylation without the simultaneous release of arabinose could indicate that the feruloyl substitutions hindered the endo-xylanase and/or β-xylosidase action differently than by steric hindrance alone. The endo-xylanase used here was from the GH10 family of xylanases known to attack close to arabinose substitutions [22]. However, hydrophobic interactions, such as feruloylation could possibly influence how close to arabinose substitutions the GH10 xylanase would attack the substrate and deferuloylation would therefore remove this obstacle for depolymerization. Combined with the presumed low DP of the substrate this could perhaps make it possible for the endo-xylanase to associate with the substrate closer to arabinose substitutions compared to the distance necessary on the insoluble substrate. The lack of arabinose release further questions the significance of the present α-L-arabinofuranosidases. However, if arabinose substitutions were to some degree made up of short chains rather than entirely of single moiety substitutions [3,4], ferulic acid maybe positioned along these short chains instead of terminally. The release of ferulic acid from this position would then in turn not render the arabinose substitutions available for the α-L-arabinofuranosidases and therefore simultaneous release of arabinose would not occur. It could also be speculated that ferulic acid was not solely esterified to arabinose but also to xylose in the same manner as acetate. The release of ferulic acid would then open the xylan backbone for endo-xylanase attack. Yet no previous suggestions towards this argument have been reported in literature and it therefore seems less plausible.

These results also signified that the degree of substitution on the poly-/oligomeric substrates was not necessarily a hindrance for the release of ferulic acid as postulated previously [16,17]. In these experiments it has been evident that the highly substituted material was more accessible to both esterases. However the accessibility was most likely related to the solubility of the substrate rather than the degree of substitution. Even though the extent of substitution had declined in the insoluble arabinoxylan as a result of pretreatment it might have only resulted in a limited boost in enzymatic accessibility, because longer stretches of unsubstituted xylan could precipitate as a result of hydrogen bonding.

Conclusion

The results of this study showed that deacetylation was important for the overall depolymerisation of insoluble corn fiber arabinoxylan, whereas deferuloylation was important for depolymerisation of soluble arabinoxylan. Future work will focus on obtaining even higher degradation of corn fiber by combining more different relevant enzyme activities.

Acknowledgement

This study is co-financed by FOOD Graduate School and Novozymes A/S.

References

[1] C. B. Faulds, P. A. Kroon, L. Sauliner, J. F. Thibault, G. Williamson, Carbohyr. Polym. 27 (1997) 187-190.

[2] L. Sauliner, J. Thibault, J.Sci.Food Agric., 402 (1999), 396-402

[3] E. Chanliaud, L. Sauliner, J. Thibault, J. Cereal Sci. 21 (1995), 195-203

[4] L. Sauliner, C. Marot, E. Chanliaud, J. F. Thibault, Carbohydr. Polym. 26 (1995), 279-287

[5] L. Sauliner, J. Vigouroux, J. Thibault, Carbohydr. Res. 272 (1995), 241-253

[6] P. Biely, Xylanolytic enzymes In Handbook of food enzymes. Marcel Dekker, Inc. New York (2003) 879-915

[7] M. Smith, R. Hatley, Carbohydr. Res. 118 (1983), 65-30

[8] M. Bunzel, J. Ralph, J. M. Marita, R. D. Hatfield, H. Steinhart, J. Sci. Food. Agric. 81 (2001), 653-660

[9] E. Allerdings, J. Ralph, P. F. Schatz, D. Gniechwitz, H. Steinhart, Phytochemistry 66 (2005), 113-124

[10] R. Hatfield, J. Ralph, J. Grabber, J. Sci. Food Agric. 79 (1999) 403-407

[11] J. Ralph, M. Bunzel, J. M. Marita, R. D. Hatfield, F. Lu, H. Kim, P. F. Schatz, J. H. Grabber, H. Steinhart, Phytochem. Rev. 3 (2004) 79-96

[12] C. Lapierre, B. Pollet, M. C. Ralet, L. Saulnier, Phytochemistry 57 (2001) 765-772

[13] M. Piber, P. Koehler, J. Agric. Food Chem. 53 (2005) 5276-5284

[14] L. Sauliner, C. Marot, M. elgorriaga, E. Bonnin, J. F. Thibault, Carbohydr. Polym. 45 (2001) 269-275

[15] B. Saha, R. Bothast, Appl. Biochem. Biotechnol. 76 (1999), 65-77

[16] B. Bartolomé, C. Faulds, G. Williamson, J. Cereal Sci. 25 (1195), 285-288

[17] C. Faulds, B. Bartolomé, G. Williamson, Ind. Crop. Prod. 6 (1997) 367-374

[18] K. Grohmann, D. J. Mitchell, M. E. Himmel, B. E. Dale, H. A. Schroeder, Appl. Biochem. Biotechnol. 20 (1989) 45-61

[19] H. R. Sørensen, S. Pedersen, C. T. Jørgensen, A. S. Meyer, Biotechnol. Prog. 23 (2007) 100-107

[20] C. B. Faulds, G. Williamson, Microbiology (Reading, U.K.) 140 (1994) 779-787

[21] C. B. Faulds, G. Williamson, Appl. Microbiol. Biotechnol. 43 (1995) 1082-1087

[22] P. Biely, M. Vrsanská, M. Tenkanen, D. Kluepfel, J. Biotechnol. 57 (1997) 151-166

Mads Orla Albæk

Phone: +45 6126 4748
Fax: +45 4588 2258
E-mail: maa@kt.dtu.dk
WWW: http://www.kt.dtu.dk
Supervisors: Krist V. Gernaey
Morten S. Hansen, Novozymes A/S
Stuart M. Stocks, Novozymes A/S

Industrial PhD Study
Started: April 2009
To be completed: March 2012

Investigation of the Efficiency of Alternative Enzyme Production Technologies

Abstract
The aim of this industrial Ph.D project is to investigate the efficiency of alternative technologies for enzyme production and evaluate these objectively in a comparison with the existing production platform. The stirred tank reactor is the standard technology for most biotech processes; however this may not always be the most economical production technology. In this project the reference process is a submerged fed batch fermentation of the filamentous fungus *Trichoderma reesei.* A model of the reference process is used to compare literature data from promising alternative technologies, which have typically been tested in laboratory scale. The overall goal of the project is to verify alternative technologies with the model predictions at an industrial relevant scale.

Introduction
Industrial enzymes are currently mainly produced in stirred tank reactors using what might be termed traditional technology. This technology platform is well known since it has been the most popular technology for about 50 years. There have been many attempts to improve the current technology by changing dosing strategy, optimizing impeller design, implementing more advanced control strategies etc. A number of alternative technologies which might replace the current one exist and have been reported in the open literature.

The underlying hypothesis for this research project is that alternative technologies exist that profitably could be used in industrial enzyme production so that the energy- and or resource consumption would be lowered. In order to objectively evaluate alternative technologies it is necessary to use similar scale. Research in bioreactors is often based on geometric similarity, which is why the Novozymes Fermentation Pilot Plant provides an obvious setting for this work.

Specific objectives
The purpose of this paper is to describe the general approach that will be employed in this project. The main activities of this project are: I) Determination of the key parameters for the reference process. II) Modeling of the reference process. III) Identification of alternative production technologies. IV) Characterization of a least 1 alternative technology. V) Conclusion on performance of at least 1 alternative technology.

Results and discussion
In an effort to determine the key parameters for the reference process, data from 40 production batches of *T. reesei* have been collected and analyzed. These batches have been run in two different tank sizes, $80m^3$ and $160m^3$ respectively, with geometrical similarity. In the $80m^3$ fermentors a slightly higher power draw is used for the agitation of the vessel due to the difference in volume. In Table 1 the key parameters of each fermentor size are compared.

Table 1: Key parameters for the reference process, an aerobic submerged fed batch fermentation of *T. reesei* (work in progress). Data is scaled for commercial reasons.

	Unit	$80m^3$	$160m^3$
Endo glucanase activity (scaled)	-	1.00	0.93
Energy yield (agitation + aeration)	g protein/ kWh	0.89	1.00
Substrate yield	g protein/ g substrate	1.00	0.99
Productivity	g protein/ h/m^3	1.00	0.91

This data supports the general reported trend stating that higher productivity as seen in the $80m^3$ is often correlated with a lower efficiency [1]. Here this lower efficiency is reflected in a lower energy yield and thus higher energy consumption. The protein yield per unit of substrate uptaken up is identical in the two different scales which is expected as the same strain and process parameters are used.

Some examples of alternative technologies for production of enzymes are shown in Figure 1.

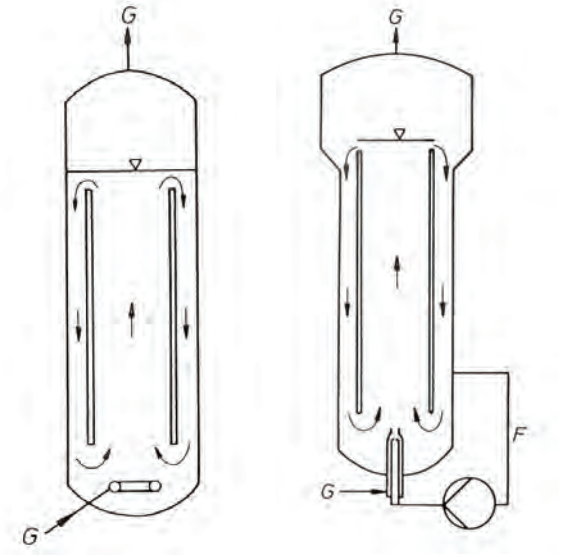

Figure 1: Examples of alternative technologies for production of enzymes. Left: An airlift tower reactor with a draft tube. Right: A tower jet reactor with a draft tube. G: Gas. F: Liquid flow.

Neither the airlift reactor nor the tower jet reactor consume energy for mechanical stirring of the fermentation broth. In turn these technologies have higher energy consumption for sparging of compressed gas and liquid circulation.

The limiting rate in fermentations of filamentous fungi is often mass transfer of oxygen from the gas to the liquid phase. Therefore, in comparison of alternative reactor designs and technologies that oxygen transfer rate (OTR) and especially the efficiency of the oxygen transfer (E_{O2}) is of great importance. In this project it has been decided to look at the collective energy consumption for the fermentation including the following factors: Energy use by mechanical mixing, energy use by liquid circulation, energy use by compressed gas, and energy use by cooling of the fermentor.

The first three of these can usually be calculated from data provided in academic publications. The energy consumption used for cooling will however depend on the process and the metabolic heat development associated with growth. To make the data comparable the heat development is therefore determined from the reference process and assumed equal for each technology. Based on this approach the units of oxygen transfer rate and efficiency of oxygen transfer are:

OTR: kg $O_2/m^3/h$

E_{O2}: kg O_2/kWh

The energy consumption included in this definition is all contributions mentioned earlier except for energy consumed for cooling. However in the definition of the total energy consumption per produced gram of protein all energy consumption is included.

Energy yield: g protein/kWh

This final result will determine whether a given technology is competitive with the stirred tank reactor. Here the same yields are assumed and the expenses for medium, sterilization and manpower have not been included.

A modeling approach has previously been developed which is able to predict the progress of a fed-batch fermentation of a filamentous fungus [2,3]. It is the intention to use a similar approach to describe the reference process of this study. This is the current state of the project. The result of this comparison will show which technologies should be pursued further. It is the aim of this project to verify the results of these "theoretical" comparisons with experimental data.

Conclusions

A number of alternative technologies will be compared in an approach as objective as possible to the current technological platform. The energy efficiency of alternative technologies will determine if they are economically competitive. It is the aim of this project to verify the results of the theoretical comparisons based on both model predictions and experimental data.

References/List of Publications

1. K. Schügerl, Bioreaction Engineering: Characteristic Features of Bioreactors, John Wiley and Son Ltd, Chichester, U.K., 1991, p. 324.
2. M.O. Albaek, K.V. Gernaey, S.M. Stocks, Modelling of an industrial enzyme fermentation by mass transfer estimation. Presented at 8th World Congress of Chemical Engineering, August 2009, Montreal, Canada
3. M.O. Albaek, S.M. Stocks and A.W. Nienow, Comparison of Traditional Rushton Disc Turbines with Up-pumping Hydrofoil B2 Impellers in 550 L Pilot Scale Aerobic Submerged Fermentations. Presented at AIChE Annual Meeting, November 2009, Nashville, Tennessee

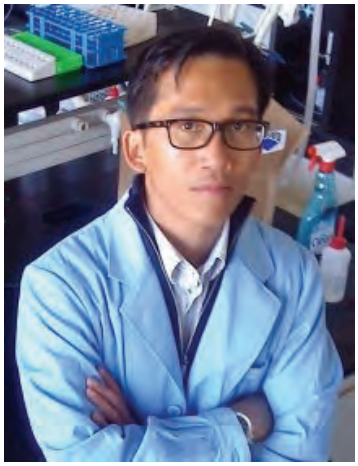

Marcel Tutor Ale
Phone: +45 4525 2861

E-mail: mta@kt.dtu.dk
Website: http://www.kt.dtu.dk
Supervisors: Prof. Anne S. Meyer
Prof. Jørn Dalgaard Mikkelsen

PhD Study
Started: March 2008
To be completed: June 2011

Assessment of Algae Productivity Responses and Biomass Potentials

Abstract
Seaweed can efficiently assimilate nutrients such as N or C and effectively capture light energy for biomass accumulation. Successful exploitation of seaweed requires our understanding of seaweed growth kinetics. The different nutrient flux has affected seaweed growth and nutrient uptake mechanism. This may have profound influence on the yield and properties of the seaweed products. The aim of this study is to assess growth responses to different nutrient source; and to evaluate the influences of this nutrients supply on the potential product of seaweed biomass.

Introduction
Algae are simple unicellular organisms, either found as single or in groups as colonies, or they can be present as macroscopic multicellular organisms sometimes collaborating together as simple tissues (i.e. seaweed). Seaweed or algae are like land plants, they can efficiently capture solar energy by photosynthetic processes and assimilate nutrients e.g. C and N for growth. Exponential growth can be achieved only in short period thus they can accumulate biomass faster than terrestrial plants. Seaweeds are classified according to their physiology, morphology and taxonomic characteristics into three groups: Chlorophyta (green), Rhodophyta (red) and Phaeophyta (brown). Each species have their own distinct characteristics and differ generally on chemical composition, structure and properties. The diversity of the seaweeds and their products are an unused potential for new products and applications. Most common seaweed products are agar, alginate and carrageenans.

The utilization of seaweed for food; feed stuff and alternative medicine have existed for many centuries ago. Recently, algae have gained more attention from commercial as well as scientific interests. Micro and macro algae sales account approximately for 22% of the 39.4 million metric tons of aquaculture products sold worldwide [1]. The production of alternative fuels from non-starch biomass has directed attention to utilization of the micro and macroalgae or seaweed as sources of biomass for biofuels production. The utilization of seaweed has increased popularity in cosmetics and has also been proposed for functional foods and functional food ingredients; as well as pharmaceutical applications.

Seaweed farming and collection is an integral part for commercial exploitation and mass production. Most of commercially exploited seaweed species such as *K. alvarezii* and *E. denticulatum* for hydrocolloid production are farmed offshore while other important species such as *Laminaria* and *Macrocystis* are often harvested or collected naturally. For this reason monitoring of productivity responses and growth kinetics is a challenge. However, there are few who have successfully cultivated seaweed in culture tanks. This paves the way for scientific investigation on seaweed growth responses to different nutrient under controlled condition [2]. Major prerequisite for successful exploitation of cultivated seaweed for commercial application is that the growth rate and yields are optimized. This in turn requires both an understanding of the influence of different nutrients response and a precise methodology to measure the growth.

Working Objectives
During the course of this study, the objectives are: to develop a simple technique to quantitatively monitor algae growth; to assess growth responses to different nutrient source; and to evaluate the influences of this nutrients supply on the potential product of seaweed biomass.

Experimental work

A photo-scanning evaluation of Ulva lactuca growth response to different nitrogen sources

Ulva lactuca a.k.a. "sea lettuce" is an important macroalga in marine ecology. *Ulva* species are particularly rich in dietary fiber, mainly soluble fiber [3] and have been proposed as being a good source of Vitamin A, B2, B12 and C and is rich in γ-tocopherol and *U. lactuca* extracts exhibit antioxidant, anti-microbial, and anti-viral activities [4].

It has been shown previously, that *U. lactuca* is suitable for propagation under controlled conditions [5]. Precise monitoring of the growth for obtaining maximal yields is a crucial prerequisite for achieving these goals. Current methods for growth monitoring of macroalgae rely on gravimetric assessment of samples of the fronds. This approach requires removal of surface moisture from the fronds and is therefore inherently prone to inaccuracy. The objective of this work was to assess the applicability of photo-scanning technology for monitoring of the growth kinetics of *U. lactuca*.

Results

A simple and non-destructive growth monitoring technique based on assessment of area expansion of prepared *U. lactuca* discs was developed [6]. Growth was evaluated quantitatively by use of photo-scanning for taking digital images and image processing software for measuring disc area. The images revealed differential increases of the surface area of *U. lactuca* discs with time in response to different N-nutrient enrichments (Figure 1).

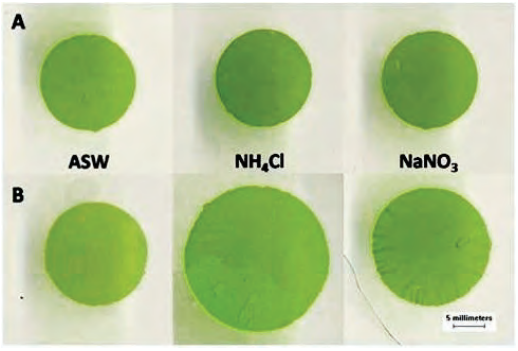

Figure 1: The growth difference of the surface area in the images (A) Day-1 and, (B) Day-10 culture in artificial sea water (ASW) enriched with different N-nutrients. Images were generated after photo-scanning using Canon Scan 5600F scanner at 300 dpi resolution.

The NH_4Cl and $NaNO_3$ rich media accelerated *U. lactuca* growth to a maximum specific growth rate of 16.4 ± 0.18% d^{-1} and 9.4 ± 0.72% d^{-1}. The highest biomass production rate obtained was 22.6 ± 0.24 mg-DW· m^{-2}·d^{-1} (Figure 2).

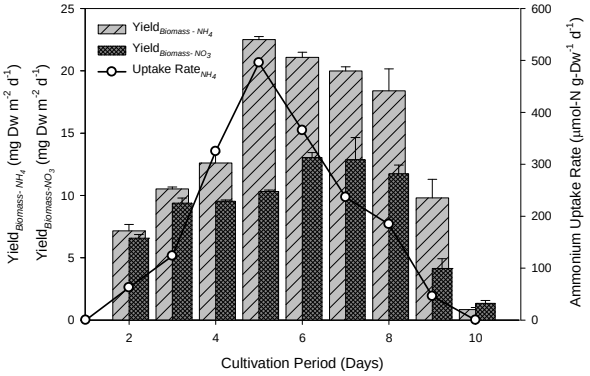

Figure 2: The ammonium uptake rate of *U. lactuca* as function of time and the influence of ammonium-N and nitrate-N source on the biomass yield. The maximum specific uptake rate was 495.59 ± 0.22 µmol-N·g-DW^{-1} d^{-1} and maximum biomass yield were 22.50 ± 0.24 mg m^{-2} d^{-1} by ammonium and 13.03 ± 0.40 mg m^{-2} d^{-1} by nitrate enrichment.

Conclusion

We have introduced a novel method to monitor the growth development including nutrient uptake of *U. lactuca* [6]. The method was able to assess distinct and subtle differences in growth response to two different nitrogen sources. The images provided information that enabled us to determine the biomass productivity, and provided a better understanding of the importance of N-nutrients on the growth kinetics of this important benthic macrophyte.

References

1. R.A. Andersen, Algal Culturing Techniques, Elsevier Academic Press, London, UK, 2005, p. IX.
2. Jimenez del Rio et. al., Ulva rigida (Ulvales, Chlorophyta) tank culture as biofilters for dissolved inorganic nitrogen from fishpond effluents, Hydrobiologia 326/327, p 61-66, 1996
3. M. Lahaye, Marine algae as sources of fibres: Determination of soluble and insoluble dietary fibre contents in some sea vegetables. J Sci Food Agric., 54, p587-594, 1991
4. H.H. Abd El-Baky et. al., Evaluation of marine alga *Ulva lactuca* L. as a source of natural preservative ingredient. EJEAFChe, 7(11), p3353-3367, 2008.
5. H.F. Christensen, K. Sand-Jensen, Growth rate and carbon affinity of *Ulva lactuca* under controlled levels of carbon, pH and oxygen. Mar. Biol., 104, p497-501,1990
6. M.T. Ale et. al. A photo-scanning methodology for evaluation of Ulva lactuca growth response to different nitrogen sources. [submitted manuscript]

Naweed Al-Haque
Phone: +45 4525 2926
Fax: +45 4593 2906
E-mail: nah@kt.dtu.dk
WWW: http://www.kt.dtu.dk
Supervisors: John M. Woodley
Rafiqul Gani
Pär Tufvesson

PhD Study
Started: November 2009
To be completed: October 2012

Modelling of Controlled Supply of Substrate Using Solid Sorbents in Biocatalysis

Abstract
Biocatalysts (as both isolated enzyme and whole-cell systems) are increasingly being used to assist in synthetic routes to complex molecules of industrial interest. The attractive features of higher selectivity and benign reactive operations make it an alternative worth investigating. There are some limitations (product inhibition, toxicity) to biocatalysis which can be overcome with methods such as slow release of substrates combined with *in-situ* product removal (ISPR) using solid sorbents. The investigation of this approach will be performed with a mechanistic model to predict the reactor performance for a slow release and ISPR system. A prototype reactor will be built to test and verify the research findings.

Introduction
For many processes in the chemical and pharmaceutical industries, the easiest means for chemical production is by using the conventional chemical synthetic route. However, with the development of biocatalysts, greener technologies have become more accessible to industry. Biocatalysis has become increasingly common in all industrial sectors such as chemicals, fuels, food and pharmaceuticals [1 – 3]. The obvious advantage of this technology is selectivity which is necessary to obtain a high yield of a specific product. In this specific project, a novel substrate release technique will be investigated by controlling the diffusion rate of the substrate in the reaction medium, or in other word the slow release of the substrate using a solid resin.

In bioprocesses, especially in bioconversions, the substrate and the product may inhibit or damage the biological catalyst or interfere with other components in the reaction medium above a crtical concentration [4]. In this project we will examine the use of a solid sorbent support to slowly release the substrate and adsorb the product simultaneously, to overcome this limitation. This novel technology will behave such that the resin will act as a 'reservoir' for the substrate and the product. The substrate via mass transfer will slowly diffuse into the solution. The slow release will maintain the aqueous concentration beneath the inhibitory level. The biocatalyst will react with the substrate(s) producing the required product(s) which can subsequently be recovered by means of *in-situ* product removal (ISPR). At the end of the reaction, the product is eluted to give a high concentration solution. Such an approach will be investigated in this project. This therefore represents a novel way of intensifying bioprocesses, via the combination of controlled substrate supply, reaction and product removal in an integrated unit operation. Figure 1 displays a schematic of the methodology.

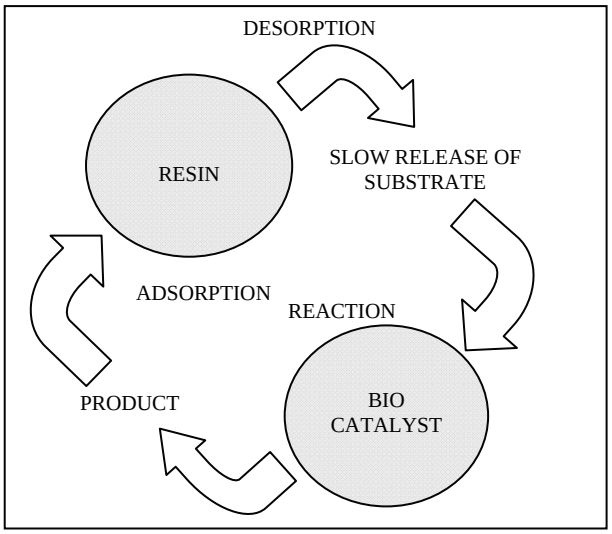

Figure 1: Principle of a resin based ISPR using the slow release mechanism

The outcome of the proposed research will provide a strong foundation for future research in the application of biocatalysis and fermentation. As biocatalytic technology and fermentation finds new application in lower value chemicals and fuels, the pressure on a cost effective process intensifies. Consequently, the new concepts in this proposal will have a direct impact on the future implementation of biocatalysis and fermentation.

Specific Objectives

- understand the influence of process configuration and mode of operation for this reaction scheme via the development of a suitable mathematical model
- test experimentally the approach on a variety of biocatalytic reactions using soluble and immobilized enzymes
- devise a mechanistic model for the use of a sorbent based substrate supply and product removal as a basis for resin selection

Systematic Methodology for Design/Analysis

To approach this project, a methodology has to be constructed to develop this novel scheme in an optimized manner. The main stages in the proposed methodology are briefly described below.

1. Data collection of the process to establish a base case design
2. Modeling and simulation of the base case design to generate data for analysis
3. Perform experiments to quantify kinetic and equilibrium data to fit into the model
4. Optimal reactor design can be generated based on the mechanistic model
5. A database and a model can then be devised for the systematic selection of a sorbent

Case Studies

Two case studies will be use to validate the approach. The first uses a microbial catalyst for the Baeyer-Villiger (BV) oxidation. The main limitation to the process is substrate and product inhibition [5]. Figure 2 below shows the reaction scheme.

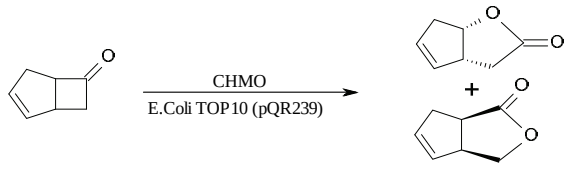

Figure 2: Microbial Baeyer-Villiger oxidation scheme of rac-bicyclohept-2-en-6-one

The second uses transaminases (TA) as a biocatalyst for the production of chiral amines. However, in this reaction, both substrate and product inhibit the enzyme activity [6]. It would be favorable to apply this novel technique to overcome the limitation. Figure 3 below illustrate a scheme for transamination of acetophenone with alanine as the amino group donor to yield methylbenzyl amine.

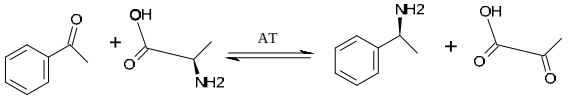

Figure 3: Transamination catalysed by ω-transaminase

Conclusions

With the current research, a mechanistic model can be developed which would incorporate the novel technique of controlled release of substrate. With the creation of this robust model, the optimal recovery method can be selected. Upon which a resin selection guide can be created to assist in predicting the appropriate sorbent for the desired system.

Acknowledgement

The author kindly expresses his gratitude to the Technical University of Denmark for the financial support.

References

1. DJ Pollard, JM Woodley. Biocatalysis for pharmaceutical intermediates: the future is now. Trend Biotechnol 25 (2007) 66 – 73.
2. VJ Shorrock, M Chartain, JM Woodley. An alternative bioreactor concept for application of an isolated oxidoreductase for asymmetric keton reduction. Tetrahedron 60 (2004) 781 – 788.
3. T Rojanarta, D Isarangul, S Wiyakrutta, V Meevootisom, JM Woodley. Controlled release biocatalysis for the synthesis of D-phenylglycine. Biocat Biotrans 22 (2004) 195 – 201.
4. RP Chauhan; JM Woodley. Increasing the productivity of bioconversion processes. Chemtech June (1997) 26-30.
5. JD Stewart. Dehydrogenases and transaminases in asymmetric synthesis. Current Opinion in Chemical Biology 5 (2001) 120-129.
6. IG Fotheringham, N Grinter, DP Pantaleone, RF Senkpeil, PP Taylor. Engineering of a novel biochemical pathway for the biosynthesis of L-2-aminobutyric acid in E.Coli K12. Bioorganic & Medicinal Chemistry 7 (1999) 2209-2213.

Muhammad Shafique Bashir

Phone: +45 4525 2853
Fax: +45 4588 2258
E-mail: msb@kt.dtu.dk
WWW: http://chec.kt.dtu.dk
Supervisors: Kim Dam-Johansen
Peter Arendt Jensen
Flemming Frandsen
Stig Wedel
Johan Wadenbäck, Vattenfall AB

PhD Study
Started: September 2008
To be completed: August 2011

Characterization and Quantification of Deposits Buildup and Removal in Straw Suspension Fired Boilers

Abstract
The deposit formation and removal in biomass-fired boilers has been the objectives for several studies; however some biomass deposit related processes are still not well described. Most studies have been based on measurements in grate boilers, while only limited data is available from biomass suspension-firing, where improved knowledge on the transient deposit formation process, the influence of fuel characteristics and mechanisms of ash deposits removal are needed. The aim of this project is to investigate ash deposition and shedding in suspension-fired straw boilers and to provide recommendations for the optimal operation strategy of boilers with respect to minimization of deposit related problems.

Introduction
One of the main sources for sustainable energy now and in the near future is biomass. In Denmark, straw and wood chips are the most abundant biomass sources used for power production. A fairly large surplus of wheat straw exists in certain parts of Denmark, and it can be a better substitute for coal [1]. Use of straw may cause severe operational problems i.e. when 100% straw fuel is applied in large suspension-fired boilers, the heat transfer surfaces may be covered by severe ash deposits impeding the plant operation. The reason is that when straw is burned, potassium vapors, salts and silicates with relatively low melting temperatures are formed. These potassium components play a significant role in the deposit formation because they act as glue bonding the individual fly ash particles together [1]. In order to make the operation of 100% straw-fired suspension boilers more efficient, improved technologies for deposit removal are needed.

Research on slagging, fouling and shedding has been carried out by researchers but most studies are related to coal-fired boilers. Shedding is a process of removal of deposits by thermal shock, soot blowing, erosion or gravity. Zbogar et al [4] performed experiments in the superheater area of a straw fired grate boiler and the results indicate that surface melting for the inserted probe is the main mechanism of deposit removal for flue gas temperatures greater than 1000^{o}C. The experimental findings indicate that at 1100^{o}C or above, the surface layer is completely melted, at 1000^{o}C it is partially melted and at flue gas temperatures below than 900^{o}C, the deposits contain mainly porous solid phase. The intention of this project is provide accurate data related to shedding of biomass ash deposits naturally or by soot blowing where limited accurate knowledge is available.

Project Description and Specific Objectives
The objective of this project is to provide recommendations for the optimal operation strategy of suspension fired straw boilers with respect to minimization of deposit related problems. The specific objectives of the project are:

- Understanding removal behaviour of deposits in the boiler chamber and superheater region (convective pass) of biomass fired boilers.
- Investigating the influence of load, operation conditions and fuel changes (straw, wood or coal firing) on boiler deposits.
- A model based description of the influence of fuel changes on deposits. The model needs to account for deposit formation and removal with changed temperature, ash composition and flow conditions. The model is intended to describe the deposit related processes as a function of the local parameters as gas velocity, ash particle size distribution, ash

particle composition and gas and surface temperature.
- Provide measuring data that can support activities on fuel characterization and CFD modeling.

Based on the obtained knowledge, innovative ideas for deposit removal will be provided and tested. The practical probe measurements will form the basis for the transient mathematical model for ash deposition and shedding.

Methodology

- Full scale measurements in suspension-fired boilers to investigate characterization and shedding of ash deposits for different fuels, using air and water cooled horizontal and vertical deposition/shedding probe.
- Development of sub-models for ash deposition and shedding in the boiler furnace region.
- Comparison of simulation results against observations from real furnaces.

Full Scale Experiments

Using an advanced horizontal deposition/shedding probe, a series of full scale measurements were performed. The deposit probe is cooled by water and air, with a total length of 3 m and an outer diameter of 40.5 mm. The probe is a double annular probe, made of stainless steel. The probe hung on a hinge which is connected to a flange. The flange was mounted on the boiler wall. A balance at the rear was used to oppose fluctuations in the boiler and to keep the probe horizontally. A load cell was used to detect variations of the force caused by the mass of the ash deposit on the probe inside the boiler. Total 12 thermocouples were placed inside the outer probe metal tube with four thermo-elements at three different positions. In each position, the thermocouple provided temperature at north, south, east and west of the probe. The intention of the study was to identify the ash deposition/shedding rate for changed fuel composition and boiler operation in the superheater region and in the tube bank region just after the convective pass. The measurements were conducted at Amager Power Plant unit II (suspension-fired boiler) utilizing different shares of Russian wood and Danish straw. Amager Power Plant Unit 2 (AMVII) located in the Copenhagen area, was previously a coal dust-fired suspension drum type boiler. It was retrofitted in 2003, to entirely use biomass fuel with different shares of wood and straw. AMVII is a 91MWe front wall-fired boiler with 12 burners at three levels. The results were compared with the previous full scale measurements are Avedøre power plant (AVV2).

Table 1 shows the composition of the fuels applied during full scale measurements. The most important difference between wood and straw is that straw has significant amounts of potassium, chlorine and ash. The high ash content implies a considerably higher content of alkali. The slight difference between the fuel analysis of straw applied for experiments at AVV2 and straw pellets applied at AMVII is possibly due to the straw season (rain and time of harvesting) and pelleting.

Table 1: Ultimate, proximate and ash analysis of fuel applied

Analysis	Straw [a]	Straw [b]	Wood [c]
Proximate Analysis			
Moisture (wt% a.r.[d])	10.20	7.40	9.45
Ash (wt% d.b.[e])	4.70	5.90	3.30
Volatiles(wt% d.b.)	76.60	75.50	79.50
MJ/kg : a.r.	–	16.00	16.65
Dry Basis (MJ/kg)	–	17.50	18.65
Ultimate Analysis (wt% d.b.)			
C	47.23	45.00	49.10
H	6.34	5.90	6.20
N	0.406	0.630	0.130
S	0.093	0.100	0.0185
Ash Analysis (wt% d.b.)			
Si	23.40	23.00	25.61
Al	0.18	0.47	1.92
Ca	7.23	7.30	6.67
Fe	0.16	0.78	1.27
K	19.57	14.00	2.83
Cl	7.62	6.75	0.45
Mg	1.38	1.60	1.05
Na	0.51	1.60	0.73
P	1.28	1.20	0.33

[a]Straw Bundles; Avedøre
[b]Straw Pellets; Amager
[c]Wood Pellets; Amager
[d]as received
[e]dry basis

Comparison of all conducted experimental campaigns regarding probe temperature, probe exposure time, flue gas temperature, mass uptake and heat uptake, is shown in Table 2. Average value of initial 2 hours and final values are presented. It is clear that flue gas temperature remains more or less constant in the start and final stage of all tests. For test 1 at AMVII, the initial mass uptake is least compared to all tests and is 105.7 g/m^2. The maximum initial mass uptake is 707.7 g/m^2 for test 4 at AMVII when pure straw is used. The initial deposition rate is remarkably dependent on the straw share. It is clear that mass uptake and primarily initial mass uptake increases significantly when straw share is increased. Possibly condensed material can increase the contact area between particles with several orders of magnitude, and when in contact with heat transfer surface, increase the bonding strength of the deposit leading to difficult removal of the deposit. The mean mass uptake ranges between 1040-1700 g/m^2 in the superheater region while the mass uptake is very small in the tube bank region. For test 5, the fuel used is pure wood and the probe weight measurements were not sufficiently accurate to provide deposit uptake data since most of the time very little material accumulated on the probe. Deposit fluxes were therefore calculated are not accurate.

The difference between the initial and the final heat uptake is higher for test 2 at AMVII, where the initial

heat uptake is 33.22 KW/m^2 and final is 21.32 KW/m^2. The possible reason for that is the formation of blackish upper layer in the windward direction during this test. Least reduction in heat uptake is for test 3, where initial value is 30.10 KW/m^2 and final is 23.15 KW/m^2. For test 5, heat uptake difference between the initial and final hours is lesser because of very thin deposit layer formed during this test. For AVV2, tests, heat uptake reduction is higher as compared to the tests at AMVII because of higher deposition. The heat uptake reduction is very small in the tube bank region of AMVII, where very few deposits are formed. The heat uptake after large deposit build up is reasonably constant at fixed probe temperatures even the deposit mass increase continuously indicating that the heat transfer from the flue gas to the probe is dominated by the rear side of the probe when a thick front deposit is formed.

Table 2: Comparison of all experimental campaigns regarding flue gas temp, mass uptake and heat uptake.

Boiler	AMV II	AMV II	AMV II	AMV II	AMV II
Test No.	**1(SH)**	**2(SH)**	**3(SH)**	**4(SH)**	**5(TB)**
Start	23.02.09	27.02.09	09.03.09	20.03.09	30.03.09
End	27.02.09	04.03.09	12.03.09	23.03.09	31.03.09
Total hours	90.00	124.15	72.70	76.55	23.80
Probe Metal Temp. (°C)	500	500	500	500	500
Fuel Share (%)[a]					
Straw	35	80	65	100	0
Wood	65	20	35	0	100
Flue Gas Temp. (°C)					
Initial (2 h)	850.8	864.9	839.5	860.4	602.9
Mean	848.3	849.3	819.7	837.57	581.2
Final (2 h)	851.9	833.8	842.3	844.3	588.6
Mass Uptake (g/(m^2)					
Initial (2 h)	105.7	198.2	150.38	747.7	3.4
Final (2 h)	1041.0	1520.1	1475.5	1670.0	-0.6
Heat Uptake (kW/m^2)					
Initial (2 h)	31.94	33.22	30.10	36.47	12.46
Final (2 h)	23.27	21.32	23.15	28.34	10.20

[a] Mass basis

The deposits obtained after test 1 at AMVII, are brownish in the windward direction with thickness of approximately 5 mm and 2 mm thick in the leanward direction, of brownish yellow layer. The total mass of the deposits collected from the sampling area was 77.59 g. For test 2, the deposits are randomly distributed, with three layers in the windward direction up to certain length (20 cm), starting from tip of probe and the rest part of the probe is more or less evenly distributed. The upper most layer in the front side is blackish and very porous, the middle layer is light brownish yellow. There are two layers in the leanward direction up to the mid of the probe starting from the tip of the probe. The total mass of the deposits collected is 336.85 g and the major contribution for weight comes from the middle layer in the windward direction. For test 3, the deposits are not strongly adhered to the probe and deposits are evenly distributed in the front side of the probe. The deposits are evenly distributed with thickness of 20 mm in the front side and 3 mm in the rear side. The collected mass for this test is 320.06 g mainly from the front side. For pure straw firing at AMVII (test 4), the deposits are more sintered and formed three layers in the front side and two distinct layers in the rear side of the probe. The collected mass during this test is 585.15 g. For test 5, the deposits are powder like and evenly distributed along the entire circumference of the probe and can be easily removed through sootblowing. The deposits in the front side are blackish for the upper layer and light gray for the layer attached to the probe.

Elemental analysis of the fuel ash, fly ash and deposit samples was made using Inductively Coupled Plasma-Optical Emission Spectroscopy (ICP-OES) in order to identify concentrations of the major elements Al, Ca, Fe, K, Mg, Na, P, Si, S and Cl. The elemental composition of straw, wood, fly ash and deposit samples collected during experiments at AMVII and AVV2 is shown in Table 3. The elemental representation of fuel is actually fuel ash analyzed at 550^{o}C. The composition of wood ash was not analyzed, but based on the data provided by Vattenfall (Ash analysis from Vattenfall Europe PowerConsult GmbH). The fly ash samples were collected from almost all silos of electrostatic precipitators and finally an overall representative sample was selected for ICP-OES analysis. The fly ash samples were taken from the bag house filter during AVV2 experiments. Scanning Electron Microscopy (SEM) combined with Energy Dispersive X-ray (EDX) was used to investigate morphology of fly ash and deposit samples collected after experiments to get better understanding of ash transformation in biomass-fired boilers.

Table 3: Elemental representation of fuel ash, fly ash and deposit layers

Sample	Al	Ca	Fe	K	Mg	Na	P	Si	S	Cl	K/(2S+Cl)
Straw (AMVII)	0.47	7.30	0.78	14.00	1.60	1.60	1.20	23.00	1.50	6.75	2.81
Wood (AMVII)	1.24	5.57	0.74	1.21	0.91	0.33	1.12	36.08	6.25	2.25	0.07
Straw (AVV2)	0.18	7.23	0.16	19.57	1.38	0.51	1.28	23.40	–	7.62	–
Flyash [a]	0.54	6.50	1.00	17.00	1.30	0.57	0.98	20.00	2.30	8.00	1.18
Flyash [b]	0.04	1.05	0.053	38.9	0.18	0.78	2.62	3.46	5.22	23.5	1.04
Test 1 [c]	0.64	15.00	2.00	18.00	2.70	0.43	1.20	9.00	4.50	5.30	1.07
Test 2 [d]	0.40	9.10	0.31	27.00	1.60	0.59	1.20	10.00	4.50	16.00	0.94
Test 2 [e]	0.44	9.20	0.32	16.00	1.70	0.58	1.40	20.00	3.00	3.10	1.49
Test 4 [f]	0.35	9.90	0.32	25.00	1.90	0.60	1.10	11.00	5.90	11.00	0.94
Test 1 [g]	0.25	5.69	0.17	32.9	0.788	0.35	1.28	8.39	4.72	19.05	1.01
Test 2 [h]	0.18	4.41	0.11	35.3	0.71	0.22	1.36	8.6	4.88	19.1	1.07

[a] 80% Straw, AMVII, Electrostatic Precipitator
[b] 100% Straw, AVV2, Bag Filter
[c] 35% Straw, AMVII, Upper Windward Layer
[d] 80% Straw, AMVII, Middle Windward Layer
[e] 80% Straw, AMVII, Upper Windward Layer
[f] 100% Straw, AMVII, Upper Windward Layer
[g] 100% Straw, AVV2, Upper Windward Layer
[h] 100% Straw, AVV2, Upper Windward Layer

The remarkable difference between grate-firing and suspension-firing is the significant release of Si, Mg and Ca during suspension-firing as shown in Table 2.

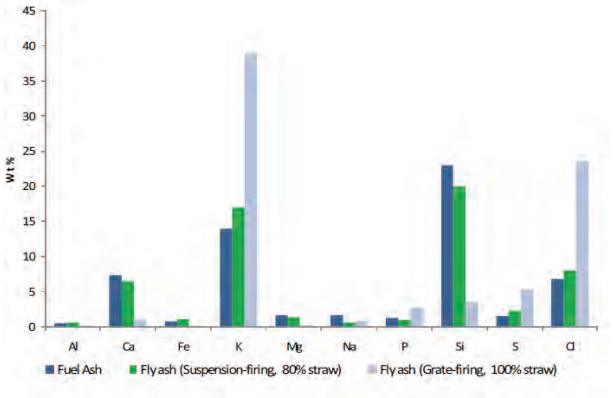

Figure 1: Enrichment of fly ash elements during grate and suspension-firing of biomass.

Figure 1 indicates that volatile elements (K, Cl and S) has enrichment ratio higher during grate-firing, while enrichment ratio for non-volatile elements (Si, Mg and Ca) is higher during suspension-firing. The higher Fe

contents investigated for test one at AMVII are possibly due to corrosion of the probe (first test on probe in the season). Less KCl is formed during test 1, because of lesser amount of potassium and chlorine present in the fuel. For suspension-firing, the average temperature is higher as compared to the grate-fired, therefore, more HCl(g) is gone to the flue gas. More calcium is released when wood share is higher and calcium content in the front layer of deposits in the windward direction is 15% for test with 65% wood on mass basis. Deposits enriched with K_2SO_4 and $CaSO_4$ are formed for co-firing of wood with straw. The formation of blackish layer in the front side during test 2, indicates that the blackish particles have composition comparable with fly with exception of Cl which is possibly released in the gas phase for increased deposit surface temperature. For test 2, the middle layer is dominated by K and Cl and the composition of this layer is more or less similar to the upper layer in the windward side during test for pure straw as shown in Figure 2. There is indication that for pure straw, uppermost layer in the front direction is sintered and fly ash particles are not adhered, while for test 2, the middle layer is not so sintered and has provided sites for the deposition of fly ash particles.

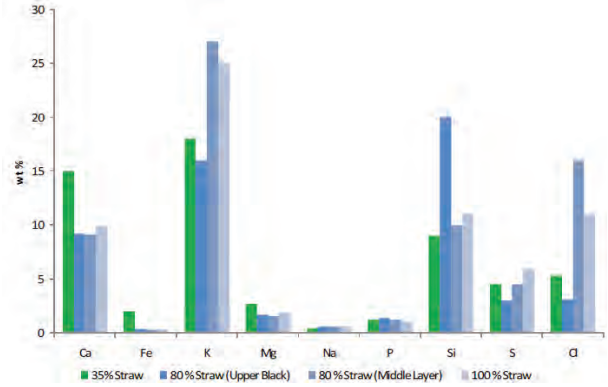

Figure 2: Enrichment of elements in the deposits during suspension-firing of biomass for different shares of straw.

Conclusions and Future Work

A series of full-scale and long duration experiments have been conducted in biomass suspension-fired boiler (AMVII) to investigate ash deposition and shedding for different shares of straw and wood. Ash deposit formation and removal experiments have been conducted using air and water cooled deposition/shedding probe at probe metal temperature of 500^{o}C. The experiments were conducted near the convective pass regions of Danish biomass-fired boiler, utilizing Danish straw and Russian wood. It was identified that mass uptake and primarily initial mass uptake increases significantly when straw share is increased. The mean mass uptake ranges between 1040-1700 g/m^2 in the superheater region while the mass uptake is very small in the tube bank region. It was identified that for test with 35% straw, the deposition rate is not significant and deposits can be easily removed through 2-3 sootblowing events after 2-3 hours. However, for increased straw share (80% straw), increased sootblowing frequency is needed and better to use 2-3 intervals of sootblowing in an hour rather than larger number of single sootblowing events. It was also observed that shedding through debonding took place during test with 80% straw, when fuel switching was made. Ash deposit shedding was investigated using CCD camera for test with 80% straw share. The shedding event was confirmed through camera images and mass uptake signals. For 100% wood firing in the tube bank region at AMVII, the probe weight measurements were not sufficiently accurate to provide deposit flux data since most of the time very little material accumulated on the probe. The heat uptake reduction for all tests at AMVII is reasonably constant except for the tests where shedding took place. The heat uptake reduction is very small in the tube bank region of AMVII, where very few deposits are formed. The elemental composition of front deposits and fly ash samples indicate that during suspension-firing, lesser amount of volatile elements (K, Cl and S) are found compared to grate-firing. However, significant amounts of Ca and Si are released during suspension-firing of biomass.

Transient model accounting for ash deposit formation and removal with changed temperature, ash composition and flow conditions is in the development phase. Further improvement is the horizontal probe system has been made using sootbowling probe along with shedding probe. A vertical deposition and shedding probe is also in the development phase which will provide online information about deposit weight and heat uptake with video monitoring and local flue gas measurement. These probes will be used for full scale measurements at Amager Power Plant unit I (suspension-fired boiler).

Acknowledgment

The project is funded by PSO system and is carried out at CHEC Research Center in cooperation with Vattenfall AB. People from Vattanfall are acknowledged for significant cooperation during the experiments.

References

1. H. P. Nielsen, Deposition and High Temperature Corrosion in Biomass Fired Boilers. PhD Thesis, (1998), Technical University of Denmark.
2. A. Zbogar, F. J. Frandsen, P. A. Jensen and P. Glarborg, Literature Study: Shedding of Ash Deposits. PSO Project 4106 (2006), CHEC Research Center, Technical University of Denmark.
3. F. J. Frandsen, Fuel. 84 (2005) 1277-1294.
4. A. Zabogar, F. J. Frandsen, P. A. Jensen P. Glaborg, and P. Hansen, Energy Fuel. 20(2) (2006) 512-519.
5. H. Zhou, P. A. Jensen and F. J. Frandsen, Fuel. (86) (2007) 1519-1533.

Matthias Josef Beier

Phone: +45 4525 2936
Fax: +45 4588 2258
E-mail: mjb@kt.dtu.dk

Supervisors: Prof. Jan-Dierk Grunwaldt
Prof. Georgios Kontogeorgis

PhD Study
Started: February 2008
To be completed: February 2011

Selective Oxidation Reactions Using Green Oxidants Catalyzed by Silver-based Heterogeneous Catalysts

Abstract
Selective oxidations are key reactions in the chemical industry. While numerous catalysts are available for these type of reactions often expensive oxidizing agents are employed additionally causing the formation of (toxic) waste. This Ph.D. project aims at the investigation of new catalysts and catalytic processes suitable for the selective oxidation of alcohols, alkyl aromatic compounds and olefins both in organic solvents and supercritical carbon dioxide. Ceria modified silver-impregnated silica has been found to be a suitable catalyst for the selective oxidation of alcohols using inexpensive molecular oxygen as the oxidizing agent.

Introduction
Due to the high versatility, oxidation reactions have always played a major role in the production of commodity and fine chemicals. While for a long time toxic stoichiometric oxidants such as Cr(VI) or Mn(VII) were employed, increased awareness for environmental issues demands the use of benign oxidizing agents such as hydrogen peroxide, *tert.*-butyl hydroperoxide or in the most ideal case molecular oxygen.

This Ph.D. thesis aims at exploring and understanding new heterogeneous catalysts for "green" oxidation reactions, i.e. using benign oxidants and where possible pressurized "supercritical" CO_2 as a replacement for organic solvents making catalytic processes involving oxidations both safer and environmentally more acceptable. The high availability of CO_2 additionally offers the opportunity of rendering the process less cost-intensive. Oxidations studied involve the selective oxidation of alcohols to aldehydes and ketones, alkyl aromatic compounds to side chain oxidized products and olefins to epoxides.

The selective oxidation of alcohols to aldehydes and ketones in the liquid phase is used in the production of fine chemical such as drugs, perfumes and artificial flavors. During the last 10 – 15 years, heterogeneous noble metal catalysts based mainly on platinum, gold, palladium or ruthenium [1] were developed which are capable of using molecular oxygen as oxidizing agent. Less expensive silver being highly active in gas phase oxidations has rarely been used in liquid phase oxidations often showing inferior performance to the established noble metal catalysts. In this project a silver catalyst was found which was effectively promoted by ceria nanoparticles showing comparable or even better performance than gold and palladium catalysts. Since the structure of a metal catalyst often is crucial for its activity, X-ray absorption spectroscopy (XAS), X-ray diffraction (XRD) and Transmission electron microscopy (TEM) were utilized to gain a more fundamental insight into the catalyst structure.

Flame-spray pyrolysis (FSP) as a new synthesis method for nanoparticles and catalysts offers the opportunity of synthesizing more effective supported catalysts with high metal dispersions. It was shown that FSP-prepared catalysts perform superior compared to impregnated catalysts in the side chain oxidation of *p*-xylene, ethyl benzene and cumene to the corresponding hydroperoxide, alcohol, aldehyde and carboxylic acid.

Results and Discussion
In a special screening approach testing catalyst mixtures instead of single catalysts a strong collaborative effect between ceria nanoparticles and silver-on-silica ($10\%Ag/SiO_2$) was found [2]. The mixture was significantly more active than the single components in the aerobic oxidation of benzyl alcohol to benzaldehyde (Table 1). Comparing the new silver catalyst with typically used Pd- and Au-based catalysts resulted in two interesting findings: (1) ceria in general promotes noble metal catalysts used in alcohol oxidation and (2) ceria-promoted silver is more active than the

investigated ceria-promoted gold catalysts and more selective than the Pd catalyst which became significantly more active.

Table 1: Comparison of the optimized Ag catalyst with Pd and Au catalysts. Conditions: 20 mL xylene, 0.10 g biphenyl, 2.00 mmol benzyl alcohol, 50 mg catalyst, 2 h reflux in O_2 atmosphere.

	10% Ag-SiO_2	**1% Au-ZnO**	**1% Au-Al_2O_3**	**0.5% Pd-Al_2O_3**
Conv. / %	6	45	72	81
Sel. / %	> 99	90	90	67
Catalyst with CeO_2 (25 mg)				
Conv. / %	98	75	77	94[a]
Sel. / %	95	93	93	58[a]

[a] Reaction time: 30 min.

TEM analysis revealed the presence of large silver particles >10 nm while most particles were in the range of 2-3 nm (Figure 2a and b). XAS analysis showed that freshly calcined catalyst was metallic. After the reaction ceria was well-dispersed on the silica support (Figure 2c and d) which indicates that a direct interaction of silver and ceria is crucial for the collaborative effect. This is also supported by catalytic investigations with separated ceria and 10%Ag/SiO_2 containers which exhibited a low catalytic activity and ICP-MS investigations for leaching showing almost no Ag and Ce present in solution. Using a Pd catalyst, "supercritical" CO_2 as a solvent increased the oxidation rate efficient [3]. Future studies will elucidate whether a similar effect can also be observed for the new silver catalyst and give a deeper insight into the phase behavior of the benzyl alcohol/O_2/CO_2 system accompanied by theoretical studies [4].

A similar system based on silver is capable of catalyzing the selective side-chain oxidation of alkyl aromatic compounds such as toluene, *p*-xylene, ethyl benzene and cumene with molecular oxygen [5]. Products were the corresponding alcohols, carbonyl compounds and carboxylic acids. Catalysts were prepared both by impregnation as well as flame spray pyrolysis the latter giving the highest turn-over numbers upon addition of a modifier of up to 2000 at elevated temperature under ambient pressure. Addition of a radical scavenger stopped the reaction suggesting a radical autoxidation mechanism. The role of silver is likely to initiate the radical reaction. Interestingly, for cumene oxidation the impregnated catalyst was more active than the flame-synthesized catalyst indicating a change in the reaction mechanism from *p*-xylene to cumene.

Conclusion

Silver was successfully used as a heterogeneous catalyst in oxidation reactions using molecular oxygen as oxidant. A collaborative effect between silver and ceria nanoparticles was found to improve the catalytic performance in the oxidation of alcohols. Ceria was also found to have a beneficial effect on gold and palladium catalysts. The promoting effect of ceria is likely to be connected to a close interaction between ceria and the noble metal particles. Silver was found to catalyze the side-chain oxidation of alkyl aromatic compounds. Flame-synthesized catalysts performed superior to standard impregnation catalysts.

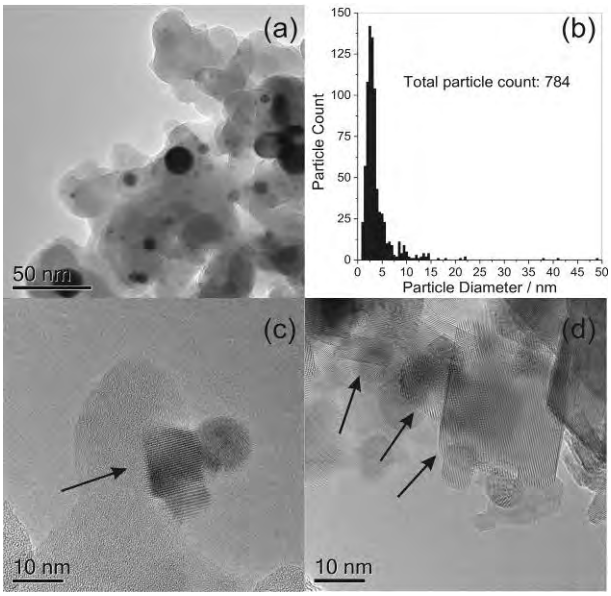

Figure 1: TEM images of calcined 10% Ag/SiO_2 (a) and particle corresponding size distribution of 10% Ag-SiO_2 (b). Catalyst mixture of 10% Ag/SiO_2 and CeO_2 after 15 min (c) and 300 min (d) reaction time. Arrows indicate CeO_2 nanoparticles. Dark circles are silver particles on the silica support.

Acknowledgements

Financial support of the study by DTU and the Danish Research Council (FTP-project) as well the support of the PhD grant by DTU, the Graduate School MP_2T and Haldor Topsøe A/S are gratefully acknowledged. We thank HASYLAB at DESY, Hamburg, for beamtime and financial support (Contract RII13-CT-2004-506008). The A.P. Møller and Chastine Mc-Kinney Møller Foundation is gratefully acknowledged for their contribution towards establishment of Center for Electron Nanoscopy.

References

1. T. Mallat, A. Baiker, Chem. Rev. 104 (2004) 3037-3058.
2. M.J. Beier, T.W. Hansen, J.-D. Grunwaldt, J. Catal. 266 (2009) 320.
3. M. Caravati, J.-D. Grunwaldt, A. Baiker, Phys. Chem. Chem. Phys. 7, (2005), 278.
4. G. M. Kontogeorgis, M. L. Michelsen, G. Folas, S. Derawi, N. v. Solms, E.H.Stenby, Ind. Eng. Chem. Res. 45 (2006) 4855-4868 and 4869-4878.
5. M. J. Beier, B. Schimmöller, T. W. Hansen, J. E. T. Andersen, S. E. Pratsinis, J.-D. Grunwaldt, *in preparation.*

Rasmus Risum Boesen

Phone: +45 4525 2982
Fax: +45 4588 2258
E-mail: rrb@kt.dtu.dk
WWW: http:// www.ivc-sep.kt.dtu.dk
Supervisors: Nicolas von Solms
Michael L. Michelsen
Kim G. Knudsen, Haldor Topsøe A/S

PhD Study
Started: March 2007
To be completed: March 2010

Development of a Component-Based Reactor Model for a Distillate Hydrotreater

Abstract
Due to environmental concerns many countries have moved towards an ultra low sulfur specification for diesel oil, and therefore the hydrotreating process, in which sulfur is removed from the oil, has received increased attention within recent years. In order to improve the process, and develop more active catalysts, a better understanding of the interplay between the kinetics and the physical phenomena in the process is desirable. The purpose of this project is to develop a model for a hydrotreating reactor that includes kinetic models for the most important reactions, which can describe the most important inhibiting effects. The model should also account for physical phenomena such as phase equilibria and mass transfer limitations in the reactor. Knowledge about the details of the kinetics are obtained from model compound experiments using representative compounds.

Introduction
Due to environmental concerns, many countries have tightened the legislations regarding the sulfur content of diesel to an ultra low sulfur diesel (ULSD) specification of 10-15 ppm S [1]. The sulfur compounds present in diesel oils are mainly thiophenic compounds, and the sulfur is removed through a catalytic reaction with hydrogen, typically on sulfided $CoMo/Al_2O_3$ or $NiMo/Al_2O_3$ catalysts.

The main types of compounds present in diesel oil besides sulfur compounds are aromatics, naphthenes, paraffins and nitrogen compounds. During the hydrotreating process, several types of reactions are taking place. The most important reactions are hydrodesulfurization (HDS), hydrodenitrogenation (HDN) and hydrodearomatization (HDA).

In HDS, sulfur is removed from the organic sulfur compounds under the formation of hydrogen sulfide. The sulfur compounds present in diesel covers are large range of reactivities, and in order to meet ULSD specifications it is necessary to remove sulfur from sterically hindered dibenzothiophenes, which are known to be the among the most refractive compounds. Figure 1 show some typical sulfur compounds and the order of their reactivity. Thiophenes and benzothiophenes are among the most reactive compounds, while dibenzothiophenes with substituents in the 4 and/or 6 positions are more slow reacting species [2].

Dibenzothiophenes can react through two parallel reaction routes, a direct desulfurization route and a pre-hydrogenation route, as illustrated in figure 2 [3]. The sterically hindered sulfur compounds mainly react through the pre-hydrogenation route, while non-hindered mainly reacts through the direct desulfurization route.

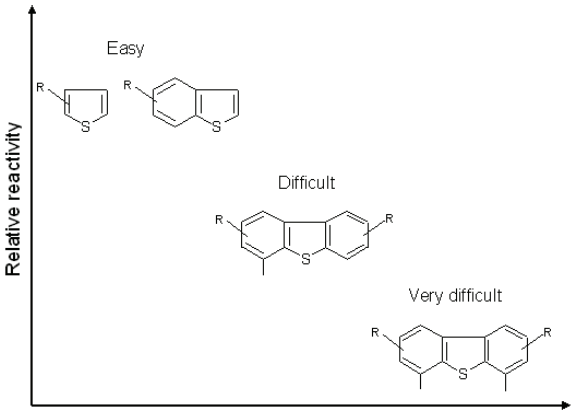

Figure 1: Typical sulfur compounds in diesel oil fractions and their order of reactivity

In HDA, aromatic rings are reacting with hydrogen to form naphthenes. In fused ring systems the reaction involving the first ring is significantly faster than of

monoaromatic rings. Furthermore the HDA reactions are often limited by a thermodynamic equilibrium. The HDA reactions are important, since the aromatics content has a significant influence on physical product properties of the diesel such as density and cetane number [4]. In HDN reactions nitrogen is removed and ammonia is formed, this reaction is important, as nitrogen compounds can act as inhibitors for the other reactions.

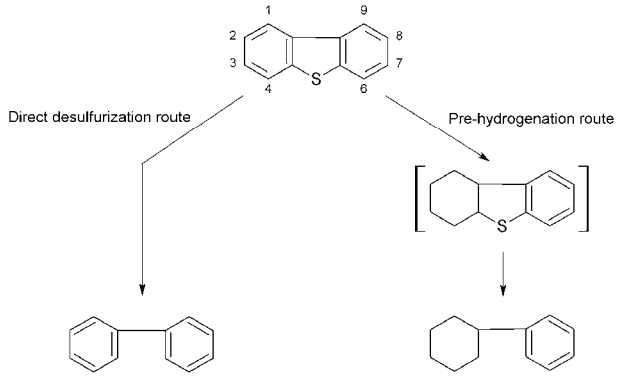

Figure 2: Reaction pathways for HDS of dibenzothiophene [3].

A hydrotreating reactor is a fixed bed catalytic reactor where gas and liquid flow co-currently from the top. It can be described as a trickle-bed reactor in which the liquid trickles from pellet to pellet and the gas forms a continuous phase. Thus equilibrium between gas and liquid phase and internal / external mass transport limitations can influence the performance of the reactor.

The purpose of this project has been to increase understanding of the hydrotreating process through experimental and modeling work.

Specific Objectives

The purpose of this project is to develop a component-based reactor model for a diesel hydrotreater, which describes the kinetics for a number of the most important reactions, including hydrodsulfurization (HDS) of sulfur-compounds with different reactivity, saturation of aromatics and hydrodenitrogenation (HDN) of nitrogen compounds. Certain compounds such as basic nitrogen compounds will act as inhibitor for other reactions, and this will be taken into account.

A hydrotreater is best modeled as a trickle-bed reactor in. In the reactor model, the thermodynamic equilibrium between the diesel oil components and the gaseous compounds (hydrogen, hydrogen sulfide and ammonia) are accounted for. An assumption is that the reactions only take place in the liquid phase inside the pores of the catalyst, and the model should be able to describe the diffusion limitations inside the catalyst pellets and any external mass transfer limitations.

Among the different parts of this project, has been setting up a mathematical model for a trickle-bed hydrotreater, an experimental study of the effect of particle size on the fast reaction of naphthalene has been investigated experimentally and an experimental study of the effect of different (basic and non-basic) nitrogen compounds on the HDS of 4,6-dimethyl-dibenzothiophene has also been done. The most recent work has been an experimenal study of hydrotreating of a model diesel mixture.

Experimental Work

Experiments are performed using a lab-scale reactor at Haldor Topsøe A/S. The reactor is illustrated in figure 2. As can be seen in the figure, hydrogen gas and liquid feed enters at the top of the reactor, and mixed before reaching the catalyst bed. The product stream is analyzed online in a gas chromatograph. Liquid product samples can be collected for further analysis.

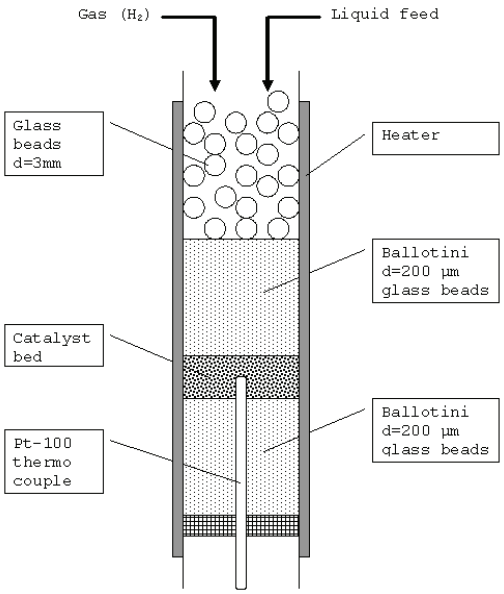

Figure 3: Lab-scale reactor used for kinetic experiments with model compounds.

Effect of nitrogen compounds on HDS

The effect of basic and non-basic nitrogen compounds on the HDS 4,6-dimethyldibenzothiophene has been investigated at a temperature of 350 °C and pressure of 50 barg on a commercial $NiMo/Al_2O_3$ catalyst. This was done by preparing feeds with different nitrogen content as shown in table 1.

Table 1: S and N concentrations in the liquid feeds. 4,6-dmdbt: 4,6-dimethyldibenzothiophene 1,4-dmcbz: 1,4-dimethylcarbazole 3-mein: 3-methylindole

Feed	4,6-dmdbt (ppm S)	Acridine (ppm N)	1,4-dmcbz (ppm N)	3-mein (ppm N)
I	1000	0	0	0
II	1000	300	0	0
III	1000	0	300	0
IV	1000	0	0	300
V	1000	150	150	0

The structures of the nitrogen compounds and 4,6-dimethyldibenzothiophene are shown in figure 4.

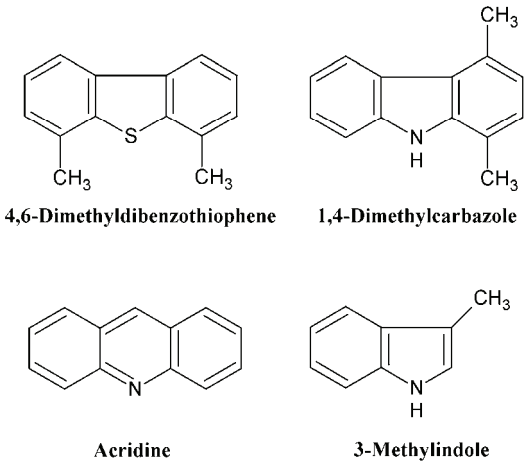

Figure 4: Structures of selected model compounds.

Model diesel mixture

Diesel oil is a complicated mixture of many compounds with normal boiling points between 230 and 360 °C. In an attempt to simplify the study of the hydrotreating of a diesel a simplified model diesel has been used for a series experiments. Compounds representating the different groups have been chosen, and the overall composition of the 14-component diesel is shown in table 2.

Table 2: Compounds in a model diesel mixture used for hydrotreating experiments.

Aromatics	**20 %**
pentyl-benzene	
tetralin	
naphthalene	
phenanthrene	
Naphthenes	**30 %**
butyl-cyclohexane	
decalin	
Paraffins	**43.7 %**
nonane	
hexadecane	
Sulfur Compounds	**6 %**
benzothiophene	
dibenzothiophene	
4,6-dimethyldibenzothiophene	
Nitrogen Compounds	**0.3 %**
acridine (basic)	
3-methylindole (non-basic)	
1,4-dimethylcarbazole (non-basic)	

The mixture in table 2 has been hydrotreated at temperatures between 300 and 380 °C, pressures between 30 and 80 barg and hydrogen to oil ratios of 125-500 Nml H_2/ ml oil. The catalyst used was a commercial $NiMo/Al_2O_3$ catalyst. Experiments have been done at weight hourly space velocity (WHSV) values of 4 and 8 hr^{-1}.

Results

Effect of nitrogen compounds on HDS

Figure 5 shows the conversion of 4,6-dimethyl-dibenzothiophene as a function of the inverse space velocity for solutions I-V. It is clear that the presence of nitrogen compounds have an influence on the conversion.

For solution III and IV the conversions are very similar, which indicates that the two non-basic compounds 1,4-dimethylcarbazole and 3-methylindole have a similar inhibition strength. Of the three nitrogen compounds acridine is the strongest inhibitor resulting in solution II having the lowest conversion.

Solution V contains equal amounts of acridine and 1,4-dimethylcarbazole, and this mixture show a similar inhibiting strength as when only acridine was present.

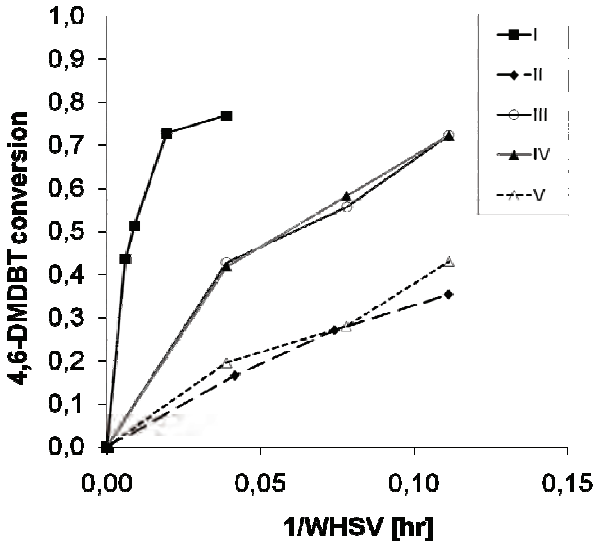

Figure 5: 4,6-dimethyldibenzothiophene conversion in solution I-V

There is good agreement between what has been observed in this experiment and what is presented in literature [5,6].

The experiments show that the inhibitors have a stronger effect on the pre-hydrogenation route than the direct desulfurization route.

Model diesel mixture

Using the model feed, it is possible to study the different reactions simultaneously.

Figure 6 show the conversion of different sulfur compounds, at 2 different temperatures. As can be seen benzothiophene is completely converted at both temperatures. The conversion of dibenzothiophene increases from 0.5 to close to 1, while the conversion of the most refractive sulfur compound, 4,6-dimethyldibenzothiphene, increases from 0.2 to almost 0.4. This illustrates the significant difference in

reactivity among sulfur compounds in diesel. Even though the feed concentration of benzothiophene and dibenzothiophene is larger than of 4,6-dimethyldibenzothiophene the conversion of the sterically hindered dibenzothiophene is much lower.

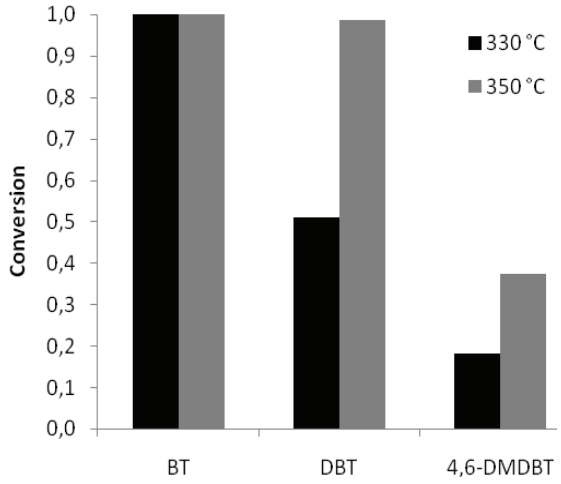

Figure 6: Conversion of sulfur compounds at P= 50 barg, H_2/oil = 125 Nml/ml and WHSV = 4 hr^{-1}. BT: Benzothiophene DBT: Dibenzothiophene 4,6-DMDBT: 4,6-dimethyldibenzothiophene.

Figure 7 show the conversion of naphthalene as a function of temperature. It shows how initially the conversion increases with the temperature, but at a certain point it decrease again. This most likely happens because the reaction becomes limited by thermodynamic equilibrium at high temperature. Increasing the temperature will increase the reaction rate, but move the equilibrium towards the aromatic species.

Conclusions

It has been shown how nitrogen compounds present in diesel oil can significantly inhibit the hydrodesulfurization reaction. Especially basic nitrogen compounds have a strong effect, and since the inhibiting effect is strongest on the pre-hydrogenation route, this is particularly important for sterically hindered dibenzothiophenes.

A set of experiments have been done, in which a model diesel mixture has been hydrotreated. This has provided information about the relative reactivities of the different compounds in a mixture where they are subject to the same amount of inhibitors and matrix effects. It has been shown how hydrogenation of fused rings can be limited by equilibrium at high temperatures.

This project has involved studies of different aspects of the hydrotreating process: The fast hydrogenation of fused aromatic rings that might lead to significant diffusion limitations, the effect of inhibitors on a very refractive sulfur compound and the reactions taking place simultaneously during hydrotreating of a model diesel oil.

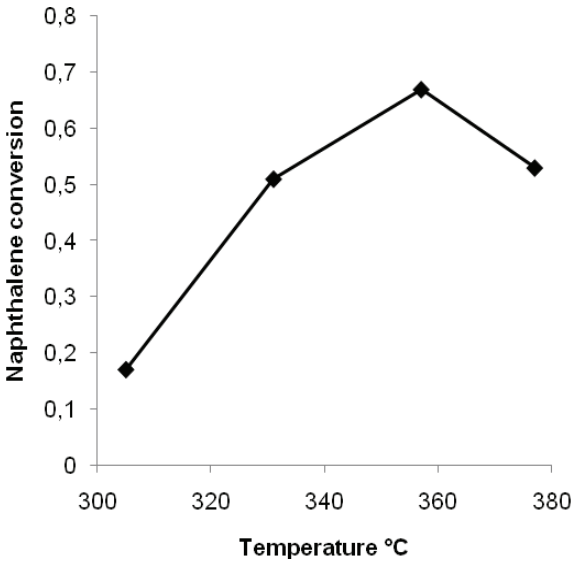

Figure 7: Naphthalene conversion at P= 30 barg, H_2/oil = 500 Nml/ml and WHSV = 8 hr^{-1}.

Future work

The results and knowledge obtained through the experiments can be used in combination with a mathematical model, including important physical effects, to simulate a trickle-bed hydrotreating unit.

Acknowledgements

This project is funded by Haldor Topsøe A/S, the MP_2T Graduate School in Chemical Engineering and the Technical University of Denmark.

References

1. T. Song, Z. Zhang,J. Chen, Z. Ring, H. Yang, Y. Zheng, Energy Fuels, 20, (2006), 2344-2349.
2. C. Song, Catalysis Today, 86, (2003), 211-263.
3. K. G. Knudsen, B. H. Cooper, H. Topsøe, Applied Catalysis A: General, 189 (1999), 205-215.
4. B. H. Cooper, B.B.L. Donnis, Applied Catalysis A: General, 137 (1996) 203-223.
5. B. H. Cooper, K. G. Knudsen, in: C.S. Hsu, P. R. Robinson (Eds.), Practical Advances in Petroleum Processing, Springer, New York, 2006, p. 297
6. V. Rabarihoela-Rakotovao, F. Diehl, S. Brunet, Catalysis Letters, 129, (2009), 50-60

Jacob Brix

Phone: +45 4525 2922
Fax: +45 4588 2258
E-mail: jac@kt.dtu.dk
WWW: http://chec.kt.dtu.dk
Supervisors: Anker Degn Jensen
Peter Arendt Jensen

PhD Study
Started: October 2007
To be completed: September 2010

Oxy-Fuel Combustion of Coal and the Evolution of NO_x

Abstract
Increasing awareness of the alleged global temperature increase, caused by an increasing level of anthropogenic CO_2 in the atmosphere has increased the interest for a CO_2-friendly use of coal for heat and power generation. A promising method to achieve this goal is oxy-fuel combustion, a process where coal is burned in a mixture of oxygen and recycled flue gas (RFG). This gives a process exit gas consisting mostly of H_2O and CO_2 along with impurities such as NO_x and SO_x. After condensation of H_2O and flue gas cleaning for impurities a near pure CO_2 stream is obtained, which is ready for underground sequestration. The purpose of this project is to investigate the impact of a changed gaseous environment on fuel conversion and NO_x emissions.

Introduction
In the recent years there has been an increased focus on the environmental role of CO_2 and this focus has initiated stricter environmental legislations both globally and within the EU [1]. To overcome these legislations and to solve the problems related to CO_2 emission, the energy industry relaying on coal will need to find technological alternatives to the present combustion processes that will utilize coal in a more environmentally friendly way. This technological development is necessary since the dependence on coal as an energy source can be expected to be present for many years to come [1], [2].

One solution that seems to be promising in the nearby to midterm future is oxy-fuel combustion [2]. Oxy-Fuel combustion is a combustion technique, which has been shown considerable research attention in recent years [3], [4], [5], [6], [7], [8], [9]. There are several reasons for this continuously increasing interest, among which the following should be emphasized:

- Existing plants can be retrofitted to function under oxy-fuel conditions relatively easy using O_2 concentrations of ~ 30 vol. % in the inlet gas [2].
- Oxy-Fuel combustion produces an exit stream with a very high CO_2 content (~90-95 %) [2], [8], [10], which is ready for sequestration. The CO_2 purity of the exit gas on industrial scale mainly depends on the efficiency of the Air Separation Unit (ASU) and the degree of leakage into the furnace.
- Combustion in an oxy-fuel environment has the potential to reduce NO_x emissions, when compared to traditional air-blown plants [2], [3], [4].

As a further benefit all of the oxy-fuel combustion unit operations, except the boiler, are in some sense relaying on existing and known equipment [11]. A scheme of the oxy-fuel combustion process can be seen in figure 1.

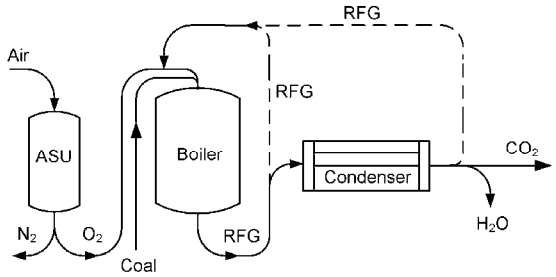

Figure 1: The overall idea behind the oxy-fuel combustion process is shown. Units such as flue gas cleaning units and compressors are omitted. The need for desulphurization will depend on the feedstock and if recycle is wet or dry.

Specific Objectives

This project is devoted to the kinetic investigation of char burnout and the evolution of NO_x under oxy-fuel combustion.

Combustion of char in oxygen enriched CO_2 atmospheres, such as those prevailing in oxy-fuel combustion, is not fully understood, and the influence of gasification at higher temperatures has been observed [12] though the conditions under which it occurs are not well documented. The possible differences in combustion behavior between conventional air-blown furnaces and oxy-fuel furnaces make a detailed study of the fuel combustion kinetics necessary. Such an investigation will need to focus on both effects arising from increased levels of CO_2 but also on kinetic effects of elevated oxygen concentrations [13]. Along with experiments accurate models predicting and interpreting test results are necessary before large scale plant construction can be initiated.

The NO_x evolution changes between air-blown combustion and oxy-fuel combustion [1]. This is mostly due to the recirculation of the flue gas into the flame and the reduction of NO over char. These effects are functions of O_2 concentration, temperature and fuel feed rate [14]. It is also possible that increased levels of CO facilitate an increased reduction of especially NO over the char surface [3]. These dependences on NO_x evolution are important to understand in detail in order to benefit fully from the possibilities oxy-fuel combustion gives for reducing the NO_x emission [15].

Experimental

Experiments relating to fuel conversion are carried out using an entrained flow reactor (EFR) located at the department. A schematic representation of the reactor is shown in figure 2.

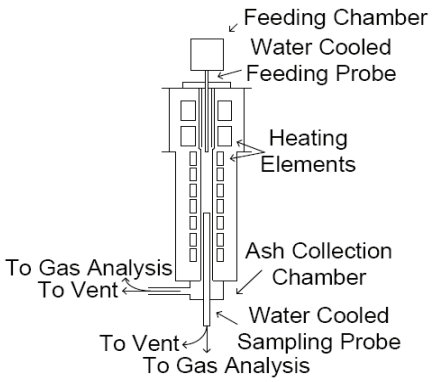

Figure 2: The electrically heated isothermal EFR used to investigate char conversion rate in N_2 /O_2 and CO_2/O_2 atmospheres.

Using the EFR experiments have been carried out in both CO_2/O_2 and N_2/O_2 mixtures in order to compare trends in char conversion profiles. Experiments have been carried out using bituminous coal particles sieved to be in the size interval 90 -106 µm. To obtain a broad set of experimental data the reactor temperature has been varied from 1073 K to 1673 K along with changes in O_2 concentration from 5 to 28 vol. %. To obtain conversion profiles for the different experimental conditions char is sampled through an adjustable water cooled probe. For selected particle samples Scanning Electron Microscopy (SEM) and N_2-BET is used to characterize particle morphology. In order to evaluate the fuel consumption due to char conversion devolatilization experiments have been carried out at each of the experimental temperatures using an oxygen concentration of 5 – 6 vol. % to avoid problems with tar.

Experiments carried out to investigate NO_x formation are conducted using a laboratory scale fixed bed reactor also located at the department. The reactor is equipped with a 16 bit Charged-Coupled Device (CCD) camera that measures the surface temperature of the burning particles from their emitted radiation in the near infra red spectrum. A schematic representation of the reactor is shown in figure 3.

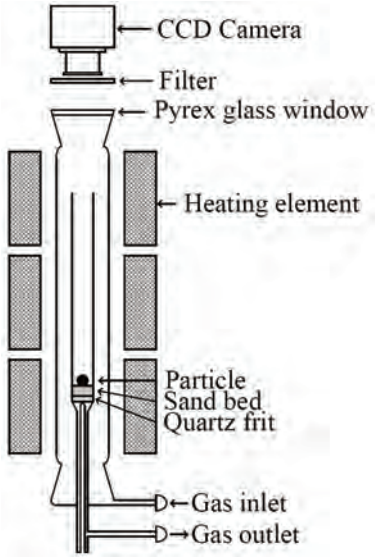

Figure 3: The laboratory scale fixed bed reactor used to measure NO emissions in N_2/O_2 and CO_2/O_2 atmospheres.

The experiments on NO_x emission are ongoing. The data obtained at present covers three types of experiments. To investigate the influence of particle size the oxygen concentration was held constant at app. 30 vol. % in N_2 or CO_2 while the particle size varied between 1.3-12.5 mm. The effect of the number of particles have been found by burning 5, 10, 15 or 20 particles in the size range 1.7 – 2.36 mm in app. 30 vol. % oxygen using either N_2 or CO_2 as carrier gas. The effect of oxygen concentration was found in the interval 5 – 80 vol. % by burning particles between 2.6 - 3.9 mm, also with either N_2 or CO_2 as carrier gas. All of the

experiments have been carried out using a pre-pyrolysed bituminous coal char obtained at 1173 K in N_2.

Results

Most of the devolatilization experiments have been carried out in CO_2. At 1573 K and 1673 K the experiments have been repeated using N_2 as carrier gas. Figure 4 shows the volatile weight losses found from mass balances at each of the experimental temperatures.

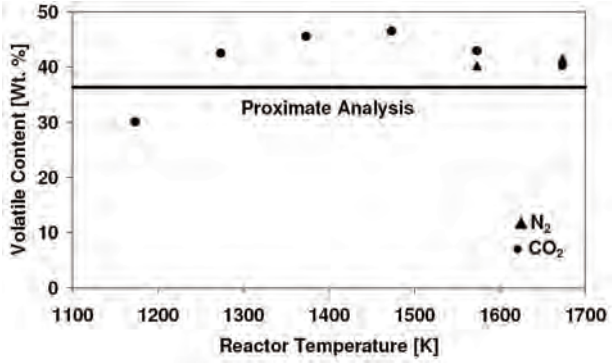

Figure 4: Volatile content as a function of reactor temperature.

It can be seen from figure 4 that no differences in volatile yields are found when N_2 is replaced with CO_2. That the volatile yields decreases slightly at the two highest temperatures is due to low sampling residence times. That no differences exist between chars obtained in N_2 and CO_2 based atmospheres is supported by figure 5 that shows SEM images of chars obtained at 1673 K. N_2-BET measurements on the chars in figure 5 show specific surface areas of 270 and 280 $m^2\ g^{-1}$ when devolatilization is carried out in N_2 and CO_2, respectively.

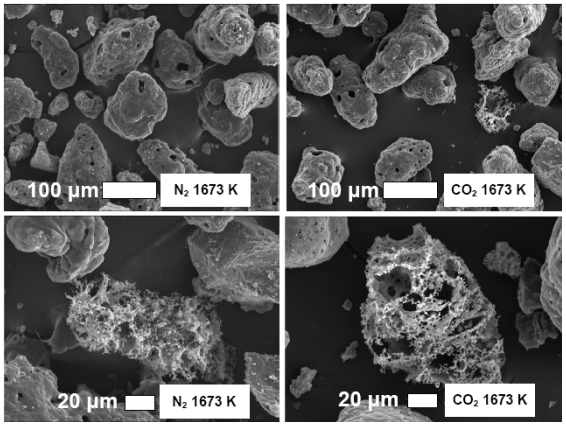

Figure 5: SEM images of chars obtained at 1673 K in N_2 and CO_2.

Results obtained for char conversion are in line with the conclusion on devolatilization. In figure 6 char conversion, X, does not seem to depend differently on bulk oxygen concentration when N_2 is replaced with CO_2 at neither low nor high degrees of char conversion.

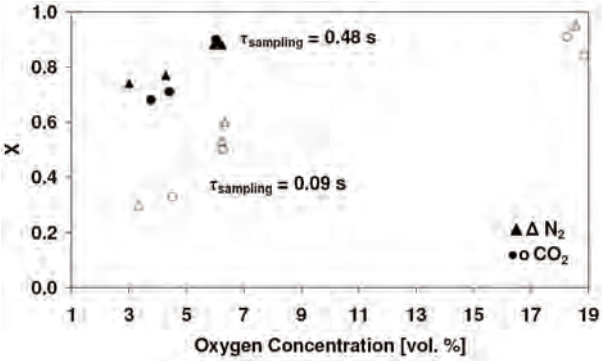

Figure 6: Char conversions vs. oxygen concentrations at 1373 K for two different sampling residence times. $\lambda \sim 2.4 - 10.2$.

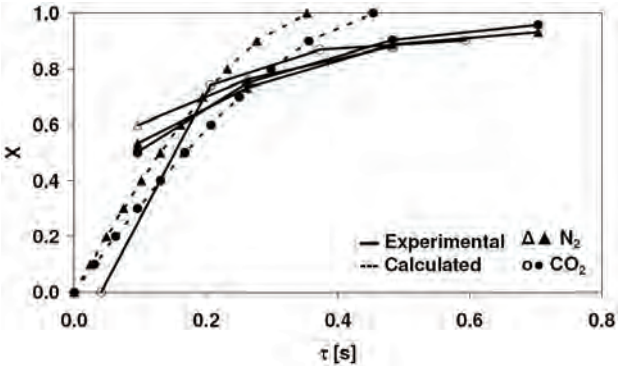

Figure 7: Char conversion profiles obtained at 1373 K. The calculated profiles are found for a shrinking sphere burning in zone III. (▲ 6.2 vol. % O_2)(Δ 6.3 vol. % O_2)(● 6.1 vol. % O_2)(o 5.9 vol. % O_2). Oxygen concentrations are the averages of the local concentrations measured in each experiment. $\lambda \sim 4.1$.

The char conversion profiles in figure 7 confirm the conclusion of figure 6, namely that similar conversion profiles can be expected in N_2/O_2 and CO_2/O_2 when combustion is taking place in zone I and II. Results obtained at the temperatures 1573 K and 1673 K showed that the lower diffusion coefficient (~ 22 %) of O_2 in CO_2 compared to N_2 causes the char conversion rate to be lower in CO_2 during zone III combustion.

Temperatures measured by the CCD camera during experiments in the laboratory scale fixed bed reactor are shown in figure 8. Here it is seen that there is not much difference in measured particle temperatures whether the combustion is taking place in N_2/O_2 or CO_2/O_2. For the same experiments a significant difference is however found in NO emission as shown in figure 9. Figure 9 confirms literature observations [14], [15] of lower NO emission in CO_2/O_2 compared to N_2/O_2. The reason for this is at present not fully understood and will be a subject for modeling in the further work. Figure 10 confirms the observations in figure 9 namely that the NO emission in lower when CO_2 is used as carrier gas.

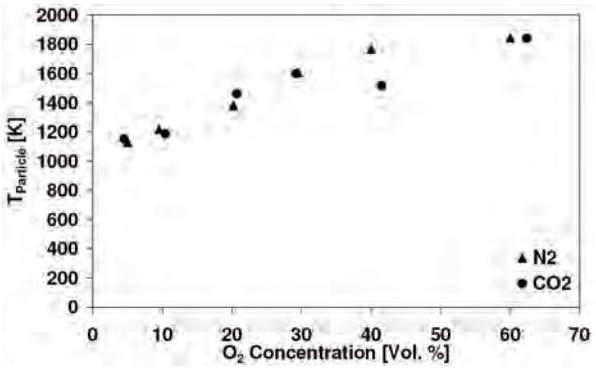

Figure 8: Particle temperatures vs. oxygen concentration measured during single particle combustion. $d_{particle}$ ~ 2.6 – 3.9 mm. $T_{reactor}$ ~ 1073 K.

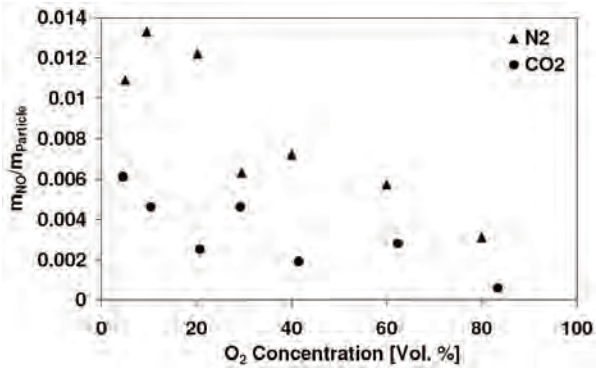

Figure 9: Mass emission of NO pr. particle mass vs. oxygen concentration measured during single particle combustion. $d_{particle}$ ~ 2.6 – 3.9 mm. $T_{reactor}$ ~ 1073 K.

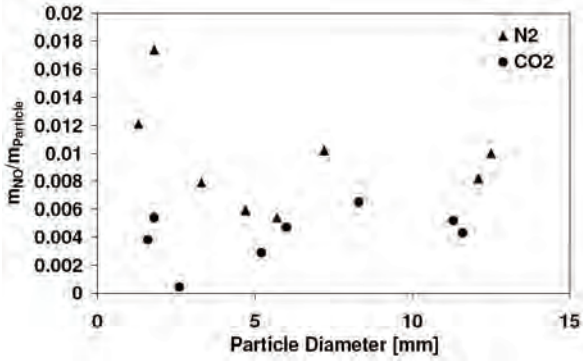

Figure 10: Mass emission of NO pr. particle mass vs. particle diameter measured during single particle combustion. $d_{particle}$ ~ 1.3 – 12.5 mm. $T_{reactor}$ ~ 1073 K. Oxygen concentration ~ 30 vol. %.

Conclusions and Discussion

On the basis of the results obtained in the EFR no apparent differences can be found in char combustion kinetic between N_2/O_2 and CO_2/O_2 environments as shown in figures 6 and 7. The results obtained for devolatilization both with respect to volatile weight loss, shown in figure 4, and char morphology, shown in figures 5, does not reveal noticeable differences between the two different gaseous environments either. Effects of transport properties have however been observed at high temperatures (1573 K and 1673 K) where the lower diffusion coefficient of O_2 in CO_2 compared to N_2 lowers the char conversion rate in CO2 when combustion is taking place under external mass transfer control (zone III). Experiments carried out using the laboratory scale fixed bed reactor with a CCD camera mounted on the top have proven a reliable method to conduct in-situ temperature measurements of burning particles. Measurements of NO emissions have so far confirmed literature results, showing a decrease in emissions when combustion is taking place in CO_2/O_2 as shown in figures 9 and 10.

Acknowledgements

This project is part of the EU project Friendly Coal and it is also sponsored by the Danish Agency for Science, Technology and Innovation. The support and funding from these partners are greatly valued.

References

1. R. Tan, G. Corragio, S. Santos, Oxy-Coal Combustion with Flue Gas Recycle for the Power Generation Industri, Report No. G 23/y/1, International Flame Research Foundation, 2005.
2. B. J. P. Buhre, L. K. Elliott, C. D. Sheng, R. P. Gupta, T. F. Wall, Prog. Energy Combust. Sci. (31) (2005) 283-307.
3. K. Okazaki, T. Ando, Energy (22) (1997) 207-215.
4. H. Liu, R. Zailani, B. M. Gibbs, Fuel (84) (2005) 2109-2115
5. Y. Q. Hu, N. Kobayashi, M. Hasatani, Fuel (80) (2001) 1851-1855
6. Y. Hu, S. Naito, N. Kobayashi, M. Hasatani, Fuel (79) (2000) 1925-1932
7. K. Andersson, F. Normann, F. Johnsson, B. Leckner, Ind. Eng. Chem. Res. (47) (2008) 1835-1845
8. H. Liu, R. Zailani, B. M. Gibbs, Fuel (84) (2005)
9. P. A. Bejarano, Y. A. Levendis, Combust. Flame (153) (2008) 270-287
10. C. S. Wang, G. F. Berry, K. C. Chang, A. M. Wolsky, Combust. Flame (72) (1988) 301-310
11. L. Strömberg, Combustion in a CO_2/O_2 Mixture for a CO_2 Emission Free Process, Second Nordic Minisymposium on Carbon Dioxide Capture and Storage, 2001, 58-63.
12. T. F. Wall, Proc. Combust. Inst. (31) (2007) 31-47.
13. J. J. Murphy, C. R. Shaddix, Combust. Flame (144) (2006) 710-729.
14. Y. Q. Hu, N. Kobayashi, M. Hasatani, Energy Convers. Manage. (44) (2003) 2331-2340.
15. Y. Tan, E. Croiset, M. A. Douglas, K. V. Thambimuthu, Fuel (85) (2006) 507-512.

Albert E. Cervera Padrell

Phone: +45 4525 2861
Fax: +45 4593 2906
E-mail: acp@kt.dtu.dk
WWW: www.kt.dtu.dk
Supervisors: Krist V. Gernaey
Rafiqul Gani
Søren Kiil
Tommy Skovby, Lundbeck A/S

PhD Study
Started: August 2008
To be completed: July 2011

Moving from Batch towards Continuous Organic-Chemical Pharmaceutical Production

Abstract
Organic-chemical pharmaceuticals have traditionally been produced in batch reactors, and it is custom to tailor the synthetic routes to work well in these reactors instead of using reactor set ups designed to handle the relevant chemistry. The aim of this PhD project is to develop continuous operation units optimized for a certain type of reaction or separation process, ideally preserving flexibility. Such approach should yield a methodology and a set of toolboxes applicable to similar design problems.

Introduction
A major problem of many batch reactions for pharmaceutical production is that the process is typically based on a long sequence of reactions, which thus results in time-consuming production processes that often need expensive storage of reaction intermediates as well. As such, batch production also implies that the full benefits of the Process Analytical Technology (PAT) initiative of the FDA cannot be realized in the pharmaceutical production process.

In contrast, a continuous production environment may potentially lead to improved safety against e.g. runaway reactions, higher productivity and reduced costs, and reduction or elimination of stocks. Furthermore, continuous production inherently implies an improved capability to react on process disturbances (e.g. changes in the quality of the raw materials used) via appropriate control loops, thus resulting in a more robust production process and a more consistent product quality.

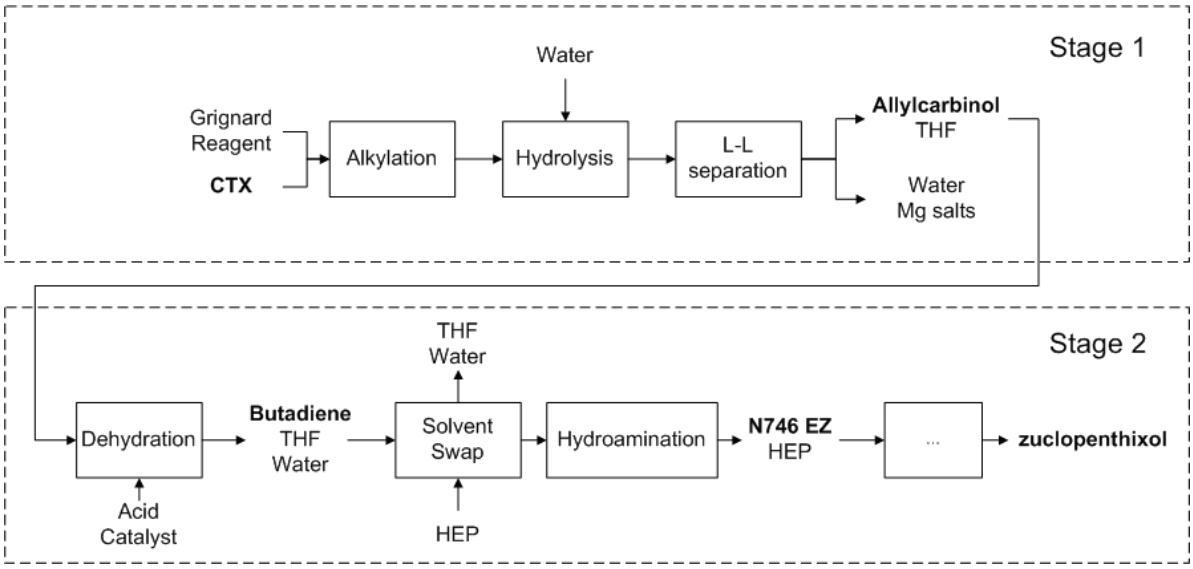

Figure 1. Simplified process flowsheet for the production of zuclopenthixol.

Specific Objectives

The case study of this project is the production of an active pharmaceutical ingredient (API) developed by Lundbeck: zuclopenthixol. The first objective is to eliminate intermediate production steps in order to obtain a less time-consuming and less complex production process. The original batch-wise process is divided into two stages. The first stage consists of the alkylation of chlorothioxanthone (CTX) with a Grignard reagent in THF, and the isolation of the first intermediate in the synthetic route: allylcarbinol. This product is separated by a crystallization step, dried and stored. In the second stage, allylcarbinol is dissolved in toluene, dehydrated and hydroaminated to obtain the API after several separation and purification steps.

A simplified process flowsheet has been proposed (Figure 1). The intermediate crystallization step and subsequent storage of allylcarbinol has been removed, thereby connecting the two stages in the process. Besides, the use of toluene for the dehydration of allylcarbinol is avoided by performing this reaction directly in THF.

Once the process flowsheet has been modified to a continuous production system, each unit operation needs to be analyzed in detail individually, but also in combination with the rest of operations. Therefore, the main objectives are:

- Propose continuous unit operations for reaction, L-L separation, distillation, etc.
- Operate the individual operations so that the full potential of the physical and chemical properties is exploited. Continuous operation may enable operation at very low temperatures, superheating under microwave radiation, etc.
- Study the effect of impurities which are carried on in the process and their effect on process performance.
- Seek for opportunities for process intensification. For example, obtain synergy combining reaction and separation.
- Apply a solvent selection methodology so that not only reaction conditions are improved but also down-stream processing.

The experience gained throughout the redesign process will serve as a basis for developing a methodology to convert pharmaceutical production processes from batch to continuous. The individual unit operations will be included in a library of pharmaceutical continuous manufacturing operations, which should be easily adaptable to other production processes. Therefore, an effort will be done to obtain standardized units which can be connected as modules in a short development time [1].

One of the additional demands of the pharmaceutical industry is the fast development of a new product and launching it to the market in the shortest time [1]. This implies that a large amount of knowledge must be gained from the API production process in a short time, and this knowledge should not be lost when scaling-up the process. Therefore, one of the objectives of this project is developing fast experimentation methods, involve modeling in the design of new processes, and when applicable follow a scale-out approach to facilitate moving the production from lab scale to industrial scale.

Last but not least, quality should be built in the process and not analyzed in the product obtained [2]. A set of process analytical technologies (PAT) need to be implemented in order to monitor the process in real time, ensuring that the process status remains within the design space through appropriate control loops [2].

Results and discussion

The process flowsheet shown in Figure 1 was selected as the simplest process option. This decision was based on a study of thermodynamic properties using databases and a simulation package (ICAS), and performing laboratory experiments to check the feasibility of the dehydration of allylcarbinol in THF as solvent.

The dehydration reaction was tested at different temperatures and acid catalyst concentrations using a simple design of experiments. From these results a simple kinetic model was obtained. Sensitivity analysis of the process parameters was performed and the confidence intervals for model predictions were obtained. The model has been used to design a continuous reactor. Plug-flow, CSTR and several CSTR in series were compared, concluding that two CSTR in series will be optimal to approach plug-flow conditions under reduced flow rate.

The study of all the other unit operations has also been initiated. The alkylation reaction to obtain allylcarbinol (Grignard reaction) poses interesting challenges. It is a highly exothermic reaction, with very fast kinetics with a reaction mechanism that is not well understood. Furthermore, the substrate of this reaction (CTX) has a very low solubility in many solvents. A design for a continuous reactor has been proposed and is currently being tested.

L-L separation and solvent exchange operations will soon be studied. A first suggestion to carry out L-L separation in continuous mode is to employ a centrifugal separator. Solvent exchange will be performed by either distillation or short path evaporation.

References

1. Behr, V.A. Brehme, C.L.J. Ewers, H. Grön, T. Kimmel, S. Küppers, I. Symietz, Eng. Life Sci. 4 (1) (2004) 15-24.
2. Q8(R2) ICH Quality Guideline (2009)

List of publications

1. N. Petersen, P. Ödman, A.E. Cervera Padrell, S. Stocks, A. Eliasson Lantz, K.V. Gernaey. Biotechnol Progr. (2009 in press). (doi: 10.1021/bp.288)
2. A.E. Cervera, N. Petersen, A. Eliasson Lantz, A. Larsen and K.V. Gernaey. Biotechnol. Progr. (2009 in press). (doi: 10.1021/bp.280)

Jakob Munkholt Christensen
Phone: +45 4525 2927
Fax: +45 4588 2258
E-mail: jmc@kt.dtu.dk
WWW: http://www.kt.dtu.dk
Supervisors: Anker Jensen
Peter Arendt Jensen

PhD Study
Started: September 2007
To be completed: January 2011

Catalytic Conversion of Syngas to Mixed Long Chain Alcohols

Abstract
A way to produce liquid biofuels for the transportation sector is a gasification of biomass to form syngas followed by a catalytic conversion of the syngas into fuel chemicals. A mixture of methanol and higher alcohols has a high octane number, a reasonable miscibility with gasoline, and can be synthesized directly from syngas over various catalysts. Here investigations of the alcohol synthesis over potassium promoted cobalt-molybdenum sulfide are presented. These investigations have revealed that the presence of H_2S in the syngas stabilizes a high fraction of higher alcohols in the product, but leads to incorporation of sulfur species into the alcohol product. The results also indicate the existence of a novel reaction mechanism, where higher alcohols are formed by coupling of lower alcohols.

Introduction
In the recent years there has been a growing interest in reducing the CO_2 emissions from the transportation sector. One way to achieve this target could be through an increased use of biofuels in the transportation sector. An interesting route to biofuels is a gasification of biomass to form syngas (a mixture of H_2 and CO) followed by a catalytic conversion of the syngas into fuel chemicals.

One possible group of fuel chemicals is alcohols. High octane numbers make alcohols well suited as additives to, or substitutes for, oil-derived gasoline. However the smaller alcohols (particularly methanol) have the problem that they can cause an undesirable phase separation in alcohol/gasoline mixtures, if the temperature is too low, or the water content of the mixture is too large. These miscibility problems can largely be avoided by including higher alcohols in the alcohol/gasoline mixture, since the higher species act as co-solvents and stabilize the blend [1]. This is illustrated in figure 1, which shows the water content that various alcohol/gasoline mixtures can tolerate before phase separation occurs.

Figure 1 shows that methanol containing mixtures have a low water tolerance, but that the water tolerance can be improved by adding a higher alcohol like iso-butanol to the mixture. Figure 1 also shows that the water tolerance of an ethanol/gasoline mixture can be improved by adding a higher alcohol like 1-butanol to the mixture. The results in figure 1 could suggest that it in some ways is easier to integrate a mixture of methanol, ethanol and higher alcohols into the existing fuel infrastructure, than it is to integrate e.g. pure methanol. Such a mixture of alcohols can be formed directly from syngas over various catalysts.

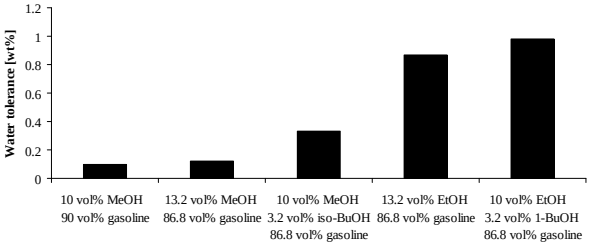

Figure 1: The water content that various alcohol/gasoline mixtures can tolerate before phase separation occurs (at 10 °C). The data are from Keller [1].

Possible catalysts for the synthesis of higher alcohols are Alkali/Cu, Co/Cu and Alkali/MoS_2 [2]. The present work has so far focused on alkali promoted cobalt-molybdenum sulfide. For syngas conversion it has previously been determined that addition of alkali salts to MoS_2 shifts the selectivity from hydrocarbons to alcohols, and that addition of Co to the Alkali/MoS_2 catalysts shifts the product distribution towards the desirable higher alcohols [3]. With the sulfide catalyst

the main product of syngas conversion is primary, linear alcohols, while the predominant by-product is short-chained hydrocarbons. The typical conditions for the alcohol synthesis over the sulfide catalyst are T = 250-350 °C, P = 50-150 bar, GHSV = 0-5000 h^{-1}.

That addition of the mixed alcohol product (formed over an Alkali/MoS_2 catalyst) to gasoline boosts the octane number is illustrated in figure 2, which shows the research octane number of a blend of gasoline and mixed alcohols as a function of the alcohol content in the mixture.

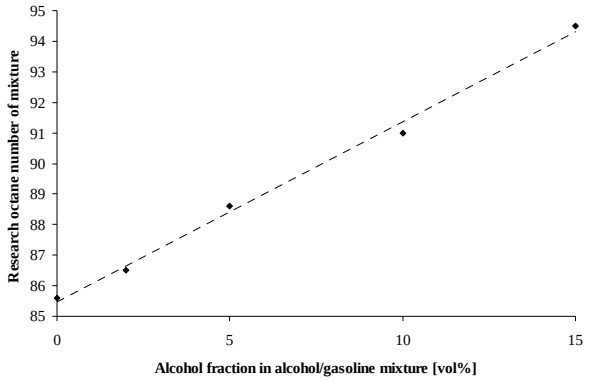

Figure 2: The research octane number of an alcohol/gasoline blend as a function of the alcohol content. The added alcoholic component is the mixed alcohol product formed over an Alkali/MoS_2 catalyst. The data are from Quarderer [4].

The objectives in our investigations of the alcohol synthesis are to gain an understanding of the catalyst and the reaction mechanism, and to develop improved catalysts and processes for the alcohol synthesis.

Experimental work

The experimental work has mainly been performed using a high pressure, flow reactor setup and a K_2CO_3/Co/MoS_2/C catalyst (13.60 wt% Mo, 2.71 wt% Co, 9.0 wt% K, BET area: 526 m^2). The catalyst has been provided by Haldor Topsøe A/S. Prior to use the catalyst is converted to the sulfide form by sulfidation in a flow of 2 mol% H_2S in H_2. A detailed description of the experimental setup and the experimental procedure is available elsewhere [5].

In short a bed of catalyst is placed in a quartz tube contained inside a stainless steel pressure shell. As the inside of the quartz tube is pressurized, nitrogen is dosed to the pressure shell to ensure an equal pressure on both sides of the quartz tube wall. Gases are supplied from pressurized cylinders. Product characterization downstream of the reactor is typically conducted using a GC-FID/TCD detection system. The experimental setup also allows for condensation and collection of the liquid alcohol product. Recently the experimental setup has been supplemented with a feeding system that allows normally liquid components to be fed to the high pressure reactor. A simplified diagram illustrating the experimental setup is shown in figure 3 below.

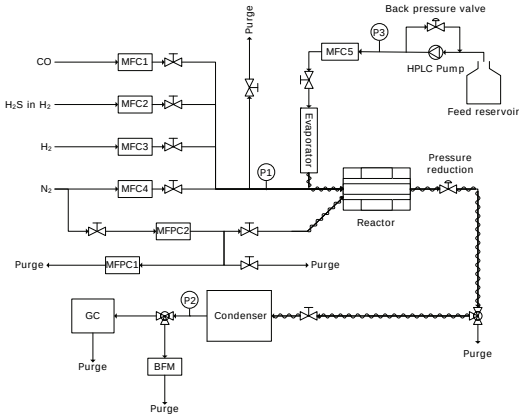

Figure 3: The experimental setup. BFM: Bubble flow meter; GC: Gas Chromatograph; MF(P)C: Mass flow (pressure) controller; P: Manometer; Heat tracing is indicated by sinusoidal curves.

The evaluation of the catalytic activity is supplemented by spectroscopic investigations of the catalyst structure by means of X-ray absorption spectroscopy and transmission electron microscopy.

Results

One of the main arguments that has been forwarded for the use of a sulfide catalyst has been that the sulfide is quite tolerant towards sulfur impurities that may be present in the syngas (typically as H_2S). Part of our investigations has focused on testing this claimed sulfur tolerance, and testing how sulfur in the form of H_2S affects the catalytic properties. Generally sulfur in the form of H_2S leads to an increased production of higher alcohols, but reduces the alcohol selectivity by enhancing the hydrocarbon formation [5].

It seems that a certain H_2S level is required to stabilize a large production of higher alcohols. This is illustrated in figure 4, which shows the ratio between higher alcohols and methanol in the alcohol product as a function of time on stream with various H_2S levels in the syngas feed.

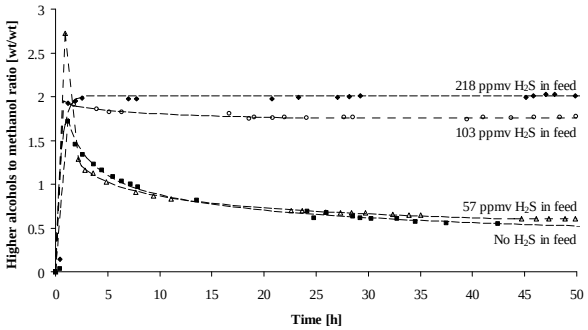

Figure 4: The weight ratio between higher alcohols and methanol as a function of time on stream with different H_2S levels in the syngas. Experimental conditions: T = 326 °C; P = 100 bar; GHSV = 5300 h^{-1}. Feed: 50 vol% H_2; 50 vol% CO. This figure is from Christensen et al. [5].

Figure 4 shows that with more than 103 ppmv H_2S in the syngas this ratio rapidly stabilizes at a value of around 2. However with less than 57 ppmv H_2S in the syngas this ratio decreases over time. The decreasing ratio reflects a decreasing fraction of higher alcohols in the product.

The results in figure 4 illustrate that the presence of H_2S may result in a high fraction of the desired higher alcohols in the product. While hydrogen sulfide has the positive effect of enhancing the fraction of the desirable higher alcohols, the presence of H_2S in the syngas also leads to an undesirable incorporation of sulfur species (mainly thiols) into the alcohol product [5]. Figure 5 shows that the weight fraction of sulfur in the condensed alcohol product rises linearly with the H_2S level in the syngas feed.

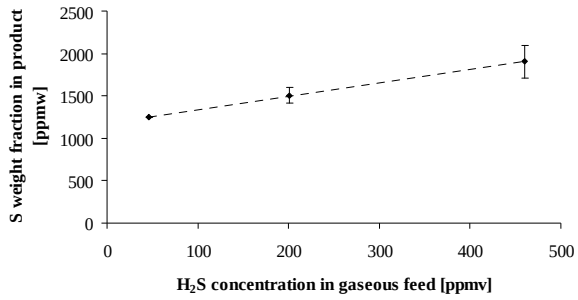

Figure 5: The weight fraction of sulfur in the condensed alcohol product as a function of the H_2S concentration in the syngas feed. The experimental conditions are T = 345 ºC, P = 100 bar, GHSV = 5100±200 h^{-1}, Feed: 50±1 vol% H_2, 50±1 vol% CO. The condensation of the liquid product is conducted at atmospheric pressure and dry ice temperature (-78.5 °C) [5].

The introduction of sulfur species into the alcohol product with H_2S in the syngas means that it could be prudent to operate the catalyst with a sulfur free syngas. In a sulfur free syngas we have observed that sulfur initially is incorporated into the alcohol product, but in this case the amount of incorporated sulfur decreases over time [5]. If the use of a sulfure free syngas is desired, it is important to establish the cause of the changes in the product distribution, which occur, when the catalyst is operated with a sulfur free syngas. Investigations are ongoing to determine, why the fraction of higher alcohols in the product decreases over time when the syngas contains little or no H_2S. Here the initial results might suggest that a contributing factor to the decreasing fraction of higher alcohols is a gradual incorporation of the cobalt component into an inactive phase. As it has been described in the introduction, cobalt is added to the catalyst to enhance the chain growth, and it is therefore quite reasonable that an incorporation of cobalt into an inactive phase would cause a reduction in the fraction of higher alcohols in the product.

One way to boost the production of the desirable higher alcohols might be to co-feed lower alcohols along with the syngas sent to the reactor. We have investigated how the addition of ethanol to the syngas affects the alcohols synthesis over K_2CO_3/Co/MoS_2/C. Due to the negative effects of H_2S in the syngas these investigations have been conducted with a sulfur free syngas. Because the catalyst in a sulfur free syngas has been observed to require a long initiation period (see figure 4) the present addition of ethanol to the syngas is commenced after the catalyst has been given 30 hours to stabilize in a sulfur free syngas (at the conditions listed in the caption of figure 6). Figure 6 shows the production rates of various alcohols as functions of the ethanol fraction in the feed.

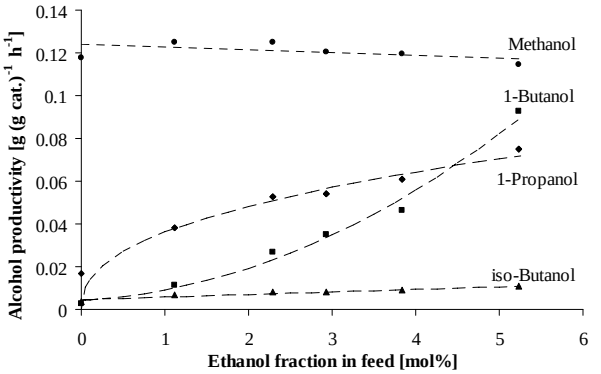

Figure 6: The production rates of various alcohols as functions of the ethanol fraction in the syngas feed. Experimental conditions: T = 325.3 °C; P = 100 bar; GHSV = 5500 h^{-1}. Feed excl. EtOH : 49.1 vol% H_2; 50.9 vol% CO; +30 hr on stream. This figure is from Christensen et al. [6].

The most interesting thing to observe in figure 5 is that the production of 1-butanol benefits the most from addition of ethanol to the syngas. This indicates that one route to chain growth for this catalyst is the coupling of alcohols – here exemplified by the coupling of ethanol or ethanol-derived species into 1-butanol. Such coupling reactions have not previously been reported for this type of catalyst.

Another way to alter the distribution of the alcohol product could be to change the composition of the syngas feed. Figure 7 shows the production rates of methanol and higher alcohols as functions of the H_2/CO ratio in the syngas feed. Also this investigation is conducted with a sulfur free feed, and in this case the catalyst has been given a 40 h initiation period at H_2/CO = 0.96 mol/mol, before the H_2/CO ratio is varied. Figure 7 shows that the methanol production increases with an increasing hydrogen content in the syngas. The stagnation in the methanol production that is observed at $H_2/CO \geq 3$ mol/mol does in fact occur because the methanol formation begins to reach its equilibrium. Contrary to the case for methanol it can be seen that the production of higher alcohols is optimal with an equimolar mixture of H_2 and CO. If it is assumed that all water formed in the reaction is converted to H_2 and CO_2 via the water-gas shift reaction an equimolar mixture of H_2 and CO does in fact constitute the stoichiometric feed for ethanol synthesis from syngas:

$$3CO + 3H_2 \rightarrow CH_3CH_2OH + CO_2$$

From figure 7 it can thus be seen that the distribution of the alcohol product depends upon the H_2/CO ratio in the feed . Ethanol and higher alcohols dominate the product for H_2/CO < 0.6 mol/mol, while methanol dominates the product above this limit.

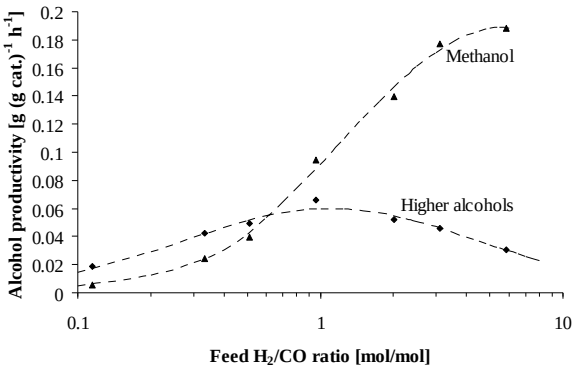

Figure 7: The production rates of methanol and higher alcohols as a function of the H_2/CO ratio in the syngas feed. Experimental conditions: T = 326 °C; P = 100 bar; GHSV = 2600 h^{-1}; No H_2S in the feed; +40 hr on stream.

Future work

So far the work has focused on alkali promoted molybdenum sulfide. Earlier investigations [3, 4] have revealed that the sulfide under the right conditions can provide both a good alcohol selectivity and a satisfactory distribution of the alcohol product. The observation that sulfur species may be incorporated into the alcohol product is however a significant drawback for the sulfide based catalyst. The investigations are therefore moving on to the exploration of other types of molybdenum based alcohol synthesis catalysts – especially catalysts based upon molybdenum carbide. Woo et al. [7] have previously observed that alcohol synthesis over K_2CO_3/Mo_2C can provide a reasonable alcohol selectivity and an alcohol product with a promising fraction of higher alcohols.

The development of new catalysts will encompass an optimization of the catalyst composition and of the catalyst preparation. Furthermore the development will include a search for novel additives that can improve the properties of the molybdenum based alcohol synthesis catalysts.

Conclusions

In conclusion the synthesis of methanol and mixed higher alcohols from syngas is a potential way to produce liquid biofuels via biomass gasification. Molybdenum based systems are interesting catalysts for the alcohol synthesis.

Investigations of a carbon supported $K_2CO_3/Co/MoS_2$ catalyst has revealed that the presence of H_2S above 103 ppmv of hydrogen sulfide in the syngas feed stabilizes a large fraction of higher alcohols in the product. In a sulfur free syngas the fraction of higher alcohols in the product decreases over time, although the fraction of higher alcohols may begin to stabilize after 30-40 h on stream. Unfortunately the presence of H_2S in the syngas feed leads to the incorporation of sulfur species, mainly thiols, into the condensed alcohol product.

The present investigations have also revealed the existence of a reaction mechanism in which higher alcohols may form by coupling of lower alcohols. Such couplings have never been reported for this type of catalyst.

Finally the present investigations have revealed that the distribution of the alcohol product depends upon the H_2/CO ratio in the syngas feed. While the production of methanol benefits from increasing hydrogen content in the syngas, the production of higher alcohols is optimal with an equimolar mixture of CO and H_2.

References

1. J.L. Keller, Hydrocarbon Process. 58 (1979) 127-138.
2. J.J. Spivey, A. Egbebi, Chem. Soc. Rev. 36 (2007) 1514-1528.
3. C.B. Murchison, M.M. Conway, R.R. Stevens, G.J. Quarderer, in: M.J. Phillips, M. Ternan (Eds.) Proceedings of the 9th International Congress of Catalysis, Calgary, Vol. 2, Chemical Institute of Canada, Ottawa, 1988, pp. 626-633.
4. G.J. Quarderer, Mixed alcohols from synthesis gas, AIChE Spring National Meeting, New Orleans, USA, 1986, Paper 25a.
5. J. M. Christensen, P. M. Mortensen, R. Trane, P. A. Jensen, A. D. Jensen, App. Catal. A 366 (2009) 29-43.
6. J. M. Christensen, P. A. Jensen, N. C. Schiødt, A. D. Jensen, ChemCatChem, submitted.
7. H.C. Woo, K.Y. Park, Y.G. Kim, I.S. Nam, J.S. Chung and J.S. Lee, App. Catal. 75 (1991) 267-280.

Acknowledgments

This work is part of the CHEC (Combustion and Harmful Emission Control) Research Center. This project is financed by Haldor Topsøe A/S, the Technical University of Denmark and the Danish Research Council for Technology and Production.

Elisa Conte

Phone: +45 4525 2959
Fax: +45 4593 2906
E-mail: elc@kt.dtu.dk
WWW: http://www.capec.dtu.dk
Supervisors: Rafiqul Gani
Jens Abildskov

PhD Study
Started: July 2007
To be completed: July 2010

Innovation in Integrated Chemical Product-Process Design - Development through a Model-Based Systems Approach

Abstract
The objective of this paper is to illustrate the new advances in the virtual product-process design laboratory (virtual PPD-lab) which has been previously presented [1, 2]. Through the virtual PPD-lab, it is possible to generate and/or analyze alternatives for products and processes matching a set of predefined targets by performing virtual experiments in order to verify product feasibility, identify problems and validate the product. The significance of the virtual laboratory is that the experimental effort during the development of new products and processes can be reduced, sparing therefore, valuable time and resources. This paper highlights the new advances in the capabilities of the virtual PPD-lab and illustrates them through an industrial case study involving the analysis of a hair spray.

Introduction
Chemical product-process design involves the identification of product candidates (molecules and/or mixtures) that exhibit specific desirable or targeted behavior and the design of a process that can manufacture them with the same qualities. The common practice for the design and development is experiment-based trial and error approach, where past and expert knowledge play an important role. The virtual PPD-lab is an innovative and alternative approach to product-process design. It contains methods, tools, work-flows/templates for different types of design problems corresponding to different activities within the design work-flow. As a number of the needed methods, tools and models are already available in ICAS [3], they are accessed from the virtual PPD-lab through an established interface. The current version of the virtual PPD-lab consists of templates for the design of microcapsules for the controlled release of active ingredients; for the design of pesticide formulations; and the newly added template for the design of personal care formulation [1, 2].

Computer-Aided design and analysis of formulations
Many chemicals based products used by millions of people everyday are formulations where Active Ingredients (AIs), solvents and additives are blended together in order to obtain a product with specific properties and a particular form (spray, cream,…) which meet the targets defined by the consumers, market and/or regulatory. The AIs are responsible for the main function of a product, for example, the activity of an insect repellent is to be effective against mosquitoes. The solvent mixture is the carrier for the AIs and it is therefore present in high concentrations. Also, it needs to be carefully selected (designed) in order to completely dissolve the AIs and to give the formulated product the desired (target) behavior. Additives such as wetting agents, perfumes, preservatives, etc., are added to enhance the end-use properties of the product, while other additives such as emulsifiers in a cream product are responsible for conferring the right form to the product.

The formulations considered in this work are lotions, that is, formulation with a liquid form and a work-flow for their design has been developed [2] and consists of four main tasks (see Fig. 1). At first, a market analysis is performed to understand the consumer needs, which are then translated into target properties on which constraints are set. All these actions contribute to the definition of the design problem (task 1). At task 2 database alternatives are screened in order to identify the most suitable AI/AIs. If the AI/AIs chemical properties are not available in the database they have to be calculated. In the solvent mixture design task, candidate one phase liquid mixtures matching the predefined property targets are identified. Additives are then selected in task 4. This methodology has been applied for the design of a paint [1], a liquid-spray insect repellent and a liquid-spray sunscreen [2].

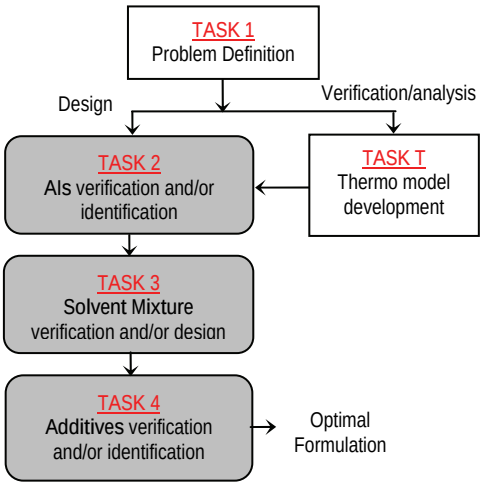

Figure 1: The modified flowchart of the virtual laboratory allows the verification and analysis of existing products.

While the above methodology (work-flow) is sufficient for the design of new products, modifications are needed for analysis, verification and possible improvements of existing formulated products. The aim of this paper is therefore to extend the current methodology to allow these new features and to highlight the application of this extended version through an industrial case study involving a hair-spray product.

Computer-Aided analysis of formulations

Unlike the design of formulations where the identities of the chemicals present are not known, in the verification and analysis of formulations, the identities of most of the chemicals are known, avoiding thereby the step of screening numerous alternatives. The aim in analysis of liquid formulated products is to verify the (liquid) phase stability of the actual formula and to calculate its chemical and physical properties to check the product performance. In some cases, the exact formula may not be available and a small number of candidates may need to be generated from an available short list of AIs, solvents or additives. The main issue is how to predict the phase stability and liquid mixture properties for very complex mixtures consisting of AIs (pigments, polymers), solvents (organic chemicals and water), additives (aroma chemicals, surfactants, preservatives, etc.). Models to predict properties of such mixtures do not exist while experimental verification is a reliable but time consuming and expensive option. The objective, therefore, is to manage this complexity by breaking down the problem into a number of sub-problems where available data and/or models can be used. At first the binary solvent mixtures, for which models and data are available, are studied. Then, binary mixtures of AIs and solvents are considered. Here, if models or data are not available, they can easily be adopted through a few data-points (measured or generated through other models). Next, only those binary mixtures that satisfy the requirements are combined to form ternary mixtures and the models ver3ified for binary mixtures are now tested for ternary mixtures. That is, the binary parameters are being extrapolated to the ternary composition space. Few experimental data .are needed to verify the model performance. Finally, systems with more than two solvents are considered, if necessary, with the same models. It is worth to note that verification and analysis of the specified product is made indirectly without using the actual multicomponent complex mixture. Based on the above, the previously developed work-flow [2] for the design of formulated products has been modified to introduce the option verification/analysis (see Fig. 1). The problem definition task (task 1) is common to both the options of design and verification. If the verification/analysis option is chosen, an appropriate set of thermodynamic models is developed, if necessary, in task T (T stands for 'Thermo'). The chemical systems under consideration are complex because of the nature of formulation, therefore the problem is decomposed into sub-problems. The actions to be performed in task T are the following:

Sub-task T.1: The solvent mixture is analyzed. At first, a search of the open literature is performed to look for availability of experimental (solubility) data/information. Then, available property model (such as UNIFAC, NRTL, UNIQUAC) usually able to handle the prediction of liquid equilibria for the systems under consideration are used to generate the phase diagrams.

Sub-task T.2: Analysis of binary systems AI-solvent. A search of the open literature is also performed to look for solubility information for the involved AIs. Here, an appropriate property model, capable of prediction of solubility and miscibility needs to be used. At first, the ability of available models (group/segment contribution based) to handle the systems under consideration is tested, that is, the necessary interaction parameters should be available. If not, new parameters need to be regressed or the existing parameters may be fine-tuned on experimental data. If experimental data are not available, pseudo-experimental data could be generated. Once the interaction parameters are available, binary phase equilibrium diagrams can be generated.

Sub-task T.3: Analysis of ternary systems AI-solvents. Literature search is performed, as in the previous steps. If new binary or ternary interaction parameters are needed, the same procedure used in T.2 is employed.

Sub-task T.4: Analysis of systems with more than two solvents. The procedure is the same as above.

If more than one AI needs to be considered, the procedure outlined above is repeated for each AI. As a last sub-task, the multicomponent system including the AIs and solvents should be considered. Additives are not included in task T since their concentration is usually very low and it can be assumed they will not influence the phase behavior of the system. If a choice between several AIs needs to be performed, further modeling may be required in task 2 in order to choose the most promising AI. If a solvent mixture needs to be

designed, further modeling may be needed in task 3, in order to compare the properties of different candidates and select the most promising. In task 4, the influence of the additives on the properties of designed formula can be evaluated.

Case study

A hair spray is usually constituted by a polymer blend, a solvent mixture, a propellant and some additives such as neutralizing agents, plasticizers and aromas [4]. The polymer blend constitutes the active ingredient (AI) with the function of holding the curls. The solvent mixture is usually a water-based mixture of organic chemicals and it constitutes the delivery system together with the propellant. The neutralizing agents are usually alkaline and are needed to rend the product water soluble (rinsable with water).

In this case study, the AI and the neutralizing agent are known, while the solvent mixture has not been defined yet, but a short list of candidate solvents is available. Because of confidentiality reasons, details such as chemical identity can not be given. However, sufficient explanations are provided for the reader to understand the main concepts. The AI is the co-polymer $M1_xM2_yM3_z$ where $M1$, $M2$ and $M3$ are three polymer repeat-units and x, y, z are the weight fractions of each repeat unit (note that $x >> y > z$). Molecular weight and polydispersity index are also known. The list of solvents includes 5 candidates: *A*, *B*, *C*, *D* and *E*. The objective of the case study is to investigate the stability of the formulation in terms of single liquid phase solvent mixtures that satisfy the performance criteria set by the market and that can at the same time dissolve the AI. The temperature of interest is room temperature (298 K). According to task 1 of the methodology (see Fig. 1), consumer preferences have to be identified. Market survey has indicated that consumers want a hair spray to give good curl retention and holding power, without giving a harsh and brittle feeling to the hair [5]. Shine and luster are also required attributes [6]. It must be possible to easily rinse the product with water [5] and with short drying time. In addition, the spray does not have to retain electric charge, which is responsible of the 'electric look' [6]. Flammability and toxicity concerns must also be taken into considerations [6] and environmental friendly products are preferred therefore VOCs emissions must be below the regulated limit [4,6].

The curl retention/holding power, shine and luster are provided by the AI. The tacky or gummy feeling also depends on the AI. The solvent mixture is responsible for the product drying time, flammability and toxicity. The overall mixture should contain less than 80% (by weight) of alcohol in order to limit the VOCs emissions. In addition, the static charge of the solvent mixture should be kept low. Numerical values for the constraints are also set: drying time is set between 480 and 960 seconds, toxicity parameter LC_{50} has to be higher than 0.1 mol/l, dielectric constant ε is fixed close to the one of the water (between 50 and 70) to avoid the dielectric behavior, the flash point has to be at least higher than the room temperature.

For the problem defined above (task 1), the appropriate property models need now to be developed.

Development of the thermodynamic model

The decomposition of the problem into sub-problems as outlined in section 2.1 is illustrated in Figure 2 (additional sub-tasks are needed because the AI is a copolymer). Sub-tasks T.2, T.3 and T.4 have to be performed for each polymer *P*1, *P*2 and *P*3. At the end of sub-task T.4, the polymer repeat units can be combined and the whole picture of the complex formulation can be obtained.

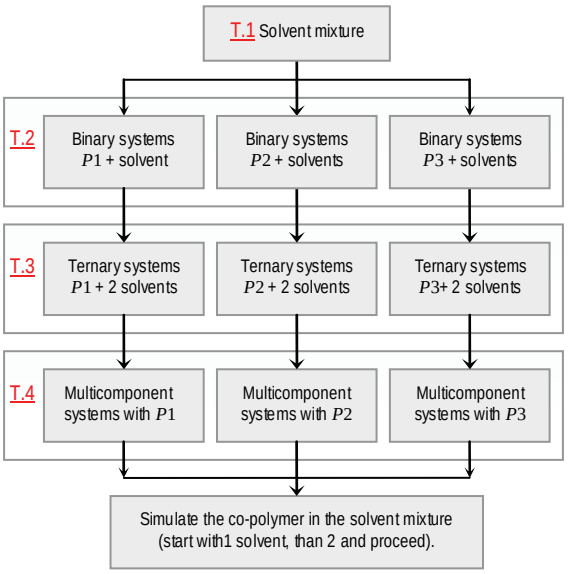

Figure 2: The thermodynamic task T of the verification/analysis option.

At this moment, binary and ternary solvent mixtures have been analyzed, and the first polymer *P*1 constituted by the repeat unit *M*1 has been considered. UNIFAC GC-method has been employed and it has been found that total miscibility cannot be guaranteed for the following solvent binary mixtures: (*A*, *D*), (*A*, *E*), (*C*, *D*) and (*D*, *E*). Since solvent *D* is causing immiscibility in many of the binary solvent mixtures, it is eliminated from further consideration. Ternary phase diagrams have also been investigated for the remaining solvents. In sub-task T.2, binary systems composed of a polymer *P*1 and one solvent have been analyzed. Experimental data for the following systems have been found: (*P*1, *A*), (*P*1, *B*) and (*P*1, *C*). The FV-UNIQUAC model [7, 8], which is suitable for polymer-solvent solubility calculations, has been selected from the model library to perform the phase stability checks. Even though the model is available in the model library, the needed interaction parameters are not available. The existing experimental data has been used to regress the parameters for the systems (*P*1, *A*), (*P*1, *B*) and (*P*1, *C*) while for the remaining two systems (*P*1, *D*) and (*P*1, *E*), pseudo-data have been generated based on the assumption that the energetic interactions between segments are not significantly dependent on molar mass,

and therefore, pseudo-experimental data generated with low molecular weight compounds can be used for the regression of the polymer-solvent parameters [7]. The UNIFAC GC-method has been employed for the pseudo-data generation. Systems (*P*1, *A*) and (*P*1, *B*) are found to show a two phase region with an Upper Critical Solution Temperature behaviour. In sub-task T.3, ternary mixtures are considered. No information on the ternary systems have been found. Models used in sub-task T.3 do not require ternary interaction parameters, but additional binary interaction parameters have to be regressed (interaction solvent-solvent).

Design of the solvent mixture

In task 1 the performance criteria were fixed and constraints on the target properties were defined. According to task 3 a solvent mixture matching the targets has to be identified from the combinations of solvents *A*, *B*, *C*, *D* and *E*. The mixture property models employed for this screening are linear mixing rules for the toxicity parameter and the dielectric constant, while rigorous models based on group contributions are selected to check the evaporation rate [8] and the flash point of the mixtures [9]. A constraint on the composition of the mixtures is also applied to account for the VOCs emissions. Table 1 shows the results: the mixtures matching the constraints, their composition in terms of weight fraction w_1, and the values of the properties LC_{50} (mol/l), ε (-), T_{90} (s), T_{flash} (°C).

Table 1: Feasible solvent mixtures.

Sol.1	Sol.2	w_1	LC_{50}	ε	T_{90}	T_{flash}
A	B	0.645	0.706	70.0	945.95	30.35
A	C	0.597	0.637	70.0	849.85	28.95

The last step is to evaluate if the identified solvent mixtures form a single liquid phase with the polymer *P*1. Figure 3 shows the ternary phase diagrams for the systems (*P*1, *A*, *B*) and (*P*1, *A*, *C*). The composition of interest is also reported (the polymer weight fraction is fixed at 5%). The ternary diagrams show that the first formula falls in the single phase region, while the second formula is in the two phase region. Therefore the only feasible formula, in the case the AI is constituted by the only polymer P1, is the formula (*P*1, *A*, *B*) with the corresponding composition (0.05, 0.613, 0.337).

Conclusions

The computer-aided methodology for the design of formulated products has been extended to include the verification and analysis of specified formulations. A procedure for the development of models needed for the new options has been suggested. Through an industrial case study, the application of the new developments has been highlighted. The case study has also shown how to face the problem of non-availability of experimental data for model parameter regression, and how the complexity of a problem can be managed with computer-aided tools.

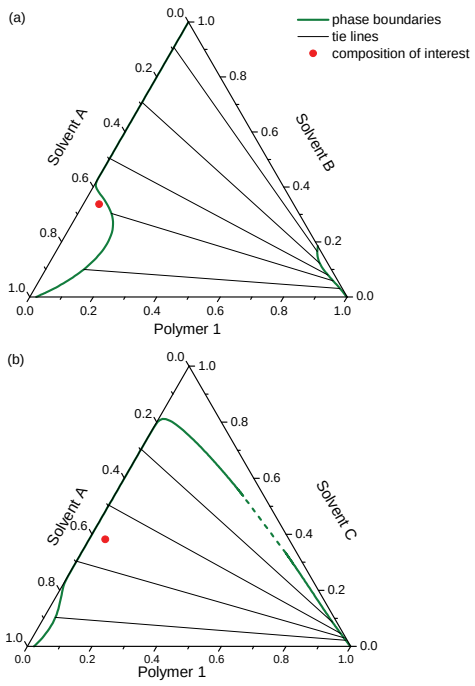

Figure 3: (a) Weight based ternary phase diagram for the system (*P*1, *A*, *B*) and (b) for the system (*P*1, *A*, *C*).

References

1. E. Conte, R. Morales-Rodriguez, R. Gani, Proceedings of 19th European Symposium on Computer Aided Process Engineering, 2009, 249-254.
2. E. Conte, R. Morales-Rodriguez, R. Gani, Proceedings of 10th International Symposium on Process System Engineering, 2009, 825-830.
3. ICAS Documentation, 2003, Internal report, CAPEC, KT-DTU, Lyngby, Denmark.
4. Shah, S. M., Fernandez, C. A.,1992, US Patent 5294437.
5. Varco, J., Williams, C. E., 1985, US Patent 4567040.
6. S. Shernv, 1989, US Patent 5053218.
7. G. Bogdanic, J. Vidal, *Fluid Phase Equlib.*, 2000, 173, 241-252.
8. Klein, J. A., Wu, D. T., Gani, R., *Comp. and Chem. Eng.*, 1992,16(5), 229-236.
9. H.-J. Liaw, Y.-H. Lee, C.-L. Tang, H.-H. Hsu, J.-H. Liu, *J. of Loss Prev. in the Proc. Ind.*, 2002, 15, 429-438.

Publication list

1. E. Conte, A. Martinho, H. A. Matos, R.Gani, *Ind. Eng. Chem. Res.*, 2008, 47(20), 7940-7954.
2. H. Modarresi, E. Conte, J. Abildskov, R. Gani., P. Crafts, *Ind. Eng. Chem. Res.*, 2008, 47(15), 5234-5242.

Victor Darde
Phone: +45 9955 4667
Fax: +45 4588 2258
E-mail: vid@kt.dtu.dk
WWW: www.cere.dtu.dk
Supervisors: Kaj Thomsen
Erling H. Stenby
Willy JM van Well, DONG Energy

Industrial PhD Study
Started: February 2008
To be completed: January 2011

CO_2 Capture using Aqueous Ammonia

Abstract
CO_2 capture process using aqueous ammonia shows good perspectives for decreasing the energy requirement thanks to the low enthalpy of absorption of CO_2 by NH_3. However, a scientific understanding of the process is required. The properties of the NH_3-CO_2-H_2O system were described using an upgraded version of the Extended UNIQUAC electrolyte model developed by Thomsen and Rasmussen in a temperature range from 0 to 150°C. [1] The results show that solid phases consisting of ammonium bicarbonate are formed in the absorber at low temperature. The enthalpy calculations show that a heat requirement for the desorber lower than 2 GJ/ton CO_2 can be reached. The thermodynamic model will then be implemented on the commercial simulator ASPEN in order to optimize the configuration of the process. In addition, the rate of absorption of carbon dioxide by ammonia solvent is being experimentally measured using a wetted wall column apparatus. The overall mass transfer coefficient measured when MEA and aqueous ammonia solutions are used will be compared.

Introduction

The amount of carbon dioxide emissions from power production is very significant in industrialized countries. Carbon dioxide capture implies separating the CO_2 from the flue gases from a power plant or other industry instead of releasing the CO_2 in the atmosphere. Post-combustion techniques separate the carbon dioxide from the flue gas after a traditional combustion process. Amine solutions have been commonly used for the commercial production of CO_2. However, this technology requires a large amount of energy, especially in the desorption part of the process. Therefore, new alternatives for post-combustion capture are searched for. Processes using aqueous ammonia as solvent are some of the promising alternatives. They can be found in two variants. The first variant absorbs the CO_2 at low temperature (2-10°C) and is called chilled ammonia process. It is a patented process. [2] This process allows precipitation of several ammonium carbonate compounds in the absorber. The second process absorbs CO_2 at ambient temperature (25-40°C) and does not allow precipitation.

Specific objective

The purpose of this study is to get a scientific understanding of the CO_2 capture process using aqueous ammonia. It is based on the extended UNIQUAC thermodynamic model developed for the CO_2-NH_3-H_2O system by Thomsen and Rasmussen [1]. An updated version of the model has been developed with an enlarged range of temperature by using additional experimental data. The process will then be simulated in order to optimize its configuration and its integration in the power plant process. The rate of absorption will also be investigated by designing and using a wetted wall column apparatus and comparing the rate of absorption of CO_2 by ammonia and amine solvents.

Results and discussion

The study of this process requires the use of a thermodynamic model that can take into account the speciation, the vapor liquid equilibrium (VLE), the solid liquid equilibrium (SLE) and the enthalpy change entailed by the mix of ammonia, carbon dioxide and water.

Model description

The model allows for calculating the activity coefficient for the liquid phase using the extended UNIQUAC model, and the gas phase fugacity using the Soave-Redlich-Kwong (SRK) equation for the volatile compounds. The original version of the model has shown to be capable of describing accurately the vapor-liquid-solid equilibria and thermal properties for the CO_2-NH_3-H_2O system for a wide range of concentration (up to 80 molal NH3), for a temperature in the range of

0-110°C and for a pressure up to 100 bars [1]. In this new version of the model, additional experimental data were used in order to extend the valid temperature range up to 150°C. More than 3800 experimental data from various publications were used to fit the parameters. In addition, some new features have been added in order to improve the accuracy of the model. The analysis of the CO_2-NH_3-H_2O system implies the study of several equilibrium processes. The following reactions are considered in the model:

Speciation equilibria

$$NH_3(aq)+H_2O \longleftrightarrow NH_4^+ + OH^-$$
$$CO_2(aq)+H_2O(l) \longleftrightarrow HCO_3^- + H^+$$
$$HCO_3^- \longleftrightarrow CO_3^{2-} + H^+$$
$$H_2O(l) \longleftrightarrow OH^- + H^+$$
$$NH_3(aq)+HCO_3^- \longleftrightarrow NH_2COO^- + H_2O(l)$$

Vapor-liquid equilibria

$$CO_2(g) \longleftrightarrow CO_2(aq)$$
$$NH_3(g) \longleftrightarrow NH_3(aq)$$
$$H_2O(g) \longleftrightarrow H_2O(l)$$

Liquid-solid equilibria

$$NH_4^+ + HCO_3^- \longleftrightarrow NH_4HCO_3(s)$$
$$NH_4^+ + NH_2COO^- \longleftrightarrow NH_2COONH_4(s)$$
$$2NH_4^+ + CO_3^{2-} + H_2O \longleftrightarrow (NH_4)_2CO_3.H_2O(s)$$
$$4NH_4^+ + CO_3^{2-} + 2HCO_3^- \longleftrightarrow (NH_4)_2CO_3.2NH_4HCO_3(s)$$
$$H_2O(l) \longleftrightarrow H_2O(s)$$

To extend the valid temperature range of the model, additional VLE data have been included for the parameter estimation. Figure 1 plots the pressure calculated with the extended UNIQUAC model for NH_3-CO_2-H_2O mixtures at 120°C and various molality of ammonia as a function of the molality of carbon dioxide. The corresponding results from two different publications have also been included [3, 4].

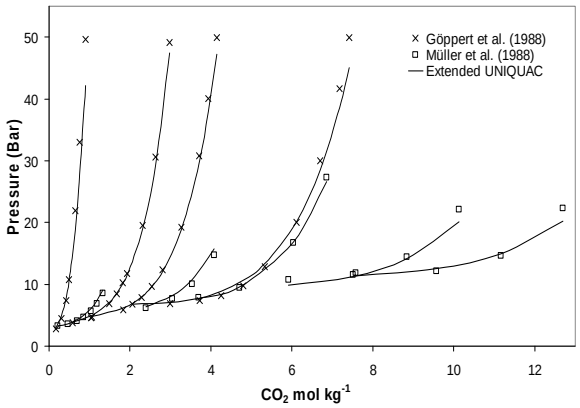

Figure 1: Total pressure in NH_3-CO_2-H_2O mixtures at 120°C

The model is able to predict the formation of solid phases. Figure 2 plots the solubility isotherm for the carbon dioxide-ammonia-water system at 40°C together with the experimental data from Jänecke [5]. It can be observed that the agreement between the model and the experimental data is satisfactory.

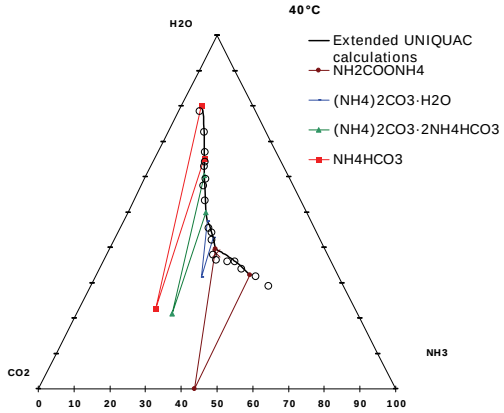

Figure 2: 40°C solubility isotherm in the ammonia-carbon dioxide-water system. The lines connect each part of the isotherm to the point that corresponds to the composition of the solid phase. The unit is mass %.

Compared to the previous version of the model, new types of experimental data were used for parameter estimation.

First, IR spectrometry data from Lichtfers [6] were used. These are speciation data for the NH_3-CO_2-H_2O system that were measured at a temperature from 40 to 120°C at various concentrations of ammonia and carbon dioxide. The ratio between the amount of ammonium carbamate ion and the total amount of ammonia was used in the object function during the determination of the parameters. Figure 3 plots speciation calculations at 80°C for the NH_3-CO_2-H_2O system for a molality of ammonia of 4.1mol/kg as a function of the molality of carbon dioxide. The experimental data from Lichtfers have also been plotted.

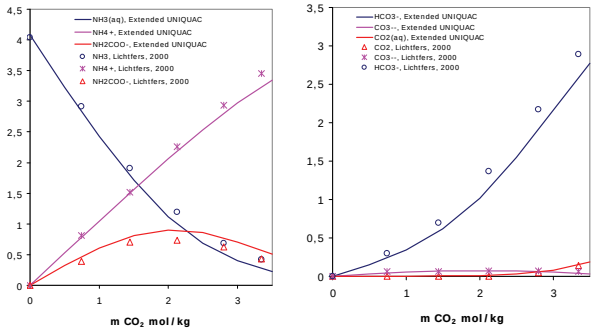

Figure 3: Speciation calculations at 80°C for a molality of ammonia of 4.1mol/kg

Enthalpy data from partial evaporation of CO_2-NH_3-H_2O mixtures published by Rumpf et al. in 1998 [7] were also used during the parameter estimation. The object function that was used consists of minimizing the difference of the calculated and the experimental enthalpy, based on a flash calculation simulating the experiment.

Hence, this model is capable of describing accurately the vapor-liquid-solid equilibria and thermal properties for this system for a wide range of concentrations (up to 80 molal), for a temperature in the range of 0-150°C and for a pressure up to 100 bars.

Results from the model

Based on the model and on the information from the patent of the process [2], the equilibrium composition of the different streams of the process has been studied. The results shown here describe the compositions of the streams in the absorber and in the desorber. A typical initial mass fraction of ammonia in the solvent is 10wt%. This value has been used in this study. Figure 4 shows the nature and amount of solid phase as a function of the CO_2 loading at 8°C, and Figure 5 shows the bubble point pressures as a function of the CO_2 loading at 120°C.

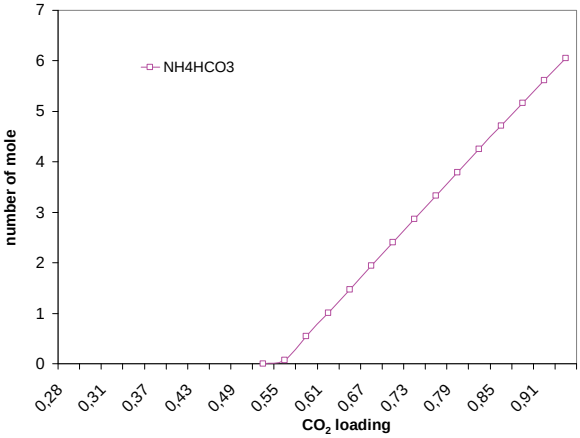

Figure 4: Nature and amount of solid phase of a 10wt% ammonia solvent with a temperature of 8°C as a function of the CO_2 loading

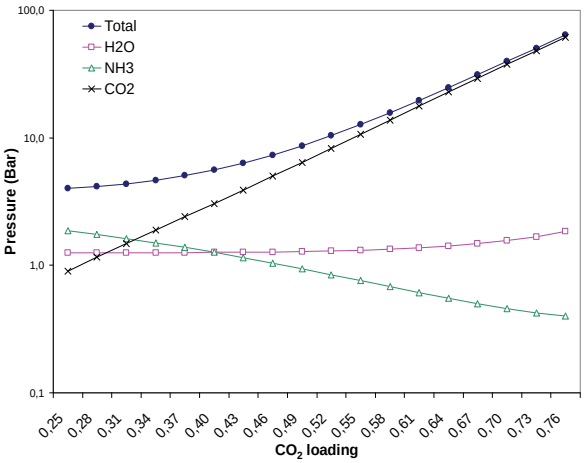

Figure 5: Bubble point pressures of a 10wt% ammonia solvent with a temperature of 120°C as a function of the CO_2 loading

Figure 4 shows that at 8°C, a solid phase consisting of ammonium bicarbonate appears for loadings higher than 0.52. Figure 5 shows that at high temperature, it is possible to get a pressurized and nearly pure CO_2 stream.

The heat requirement is a key parameter of a capture process. The cost of the capture is strongly linked to the heat that has to be supplied to ensure the desorption. The use of ammonia is supposed to lower the energy requirement. A reference configuration has been set up according to the information from the patent. Then, different parameters were modified individually in order to assess their influence. For the reference configuration, the energy requirement in the desorber was found to be below 1800 kJ/kg CO_2 captured. The CASTOR project that consists of a pilot capture plant using aqueous alkanolamines resulted in an energy consumption in the stripper of about 3700 kJ/kg CO_2 captured, with a capture efficiency of 90%. [8] Hence, this study shows that based on the equilibrium calculations, the use of ammonia as a solvent is a way to very significantly decrease the energy consumption in the desorber. In addition, the configuration studied here can be optimized to reduce the energy requirement. Moreover, the CO_2 stream that is obtained at the end of the process is pressurized when ammonia is used, which would result in additional energy savings during compression of the carbon dioxide.

To thoroughly evaluate the process, it is necessary to be able to simulate it. The extended UNIQUAC thermodynamic model has been implemented on the commercial simulator ASPEN. To do so, a user model has been developed by Bjørn Maribo Mogensen. This allows for using the functionalities of ASPEN coupled with the calculations abilities of the thermodynamic model. Hence, this will allow for simulating the process, analyzing it and optimizing its configuration.

Later on, based on the results from the simulation, it will be possible to integrate the capture process with the power plant, and therefore optimize the global process.

Experimental measurement of the rate of absorption

The study of the kinetic rate of absorption of carbon dioxide by aqueous ammonia solvent is regarding the evaluation of the process. This study is crucial to size accurately absorber columns and to assess the capital cost of the capture process. To be able to perform this task, an experimental apparatus has been designed and built. It is called a wetted wall column. It allows for contacting counter currently an aqueous amine solution with a defined gaseous mixture of carbon dioxide and nitrogen on the surface of a stainless steel tube with a known contact area. The apparatus can be operated from atmospheric to a pressure up to 8 bars and at a temperature from 5 to 80°C. Figure 6 shows a schematic flow sheet of the apparatus.

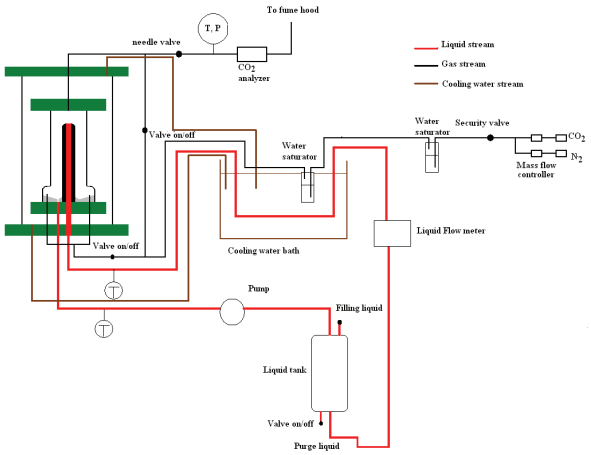

Figure 6: Schematic flow sheet of the apparatus

This study consists of comparing the overall mass transfer coefficient when MEA and ammonia solutions are used at various temperatures, loadings and amine concentrations. The absorption rate will be measured from 10 to 60°C using 0.1 to 5 mol.L^{-1} aqueous MEA with a loading from 0 to 0.5. It will be compared to the rate of absorption from 5 to 40°C for aqueous ammonia between 0.6 and 6 mol.L^{-1} with a loading varied from 0 to 0.8.

By measuring the flux of carbon dioxide at several partial pressure of carbon dioxide for given solvent and temperature, it is possible to obtain the overall mass transfer coefficient (K_G) as the slope of the linear curve between the flux and the partial pressure of carbon dioxide. Figure 7 plots the flux as a function of the partial pressure of CO_2 to show the linear trend that allows for determining the overall mass transfer coefficient. The solution used is a 1.2mol.L^{-1} MEA solution with a loading of 0.4.

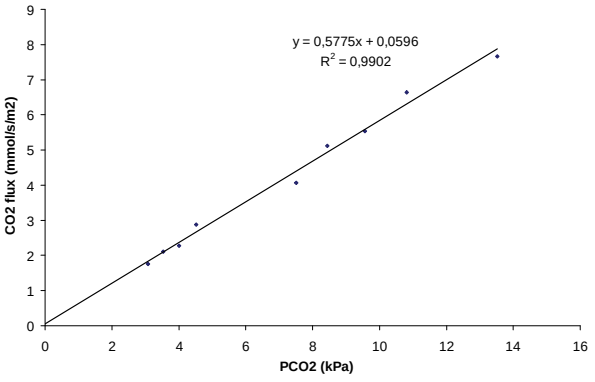

Figure 7: CO_2 flux as a function of the partial pressure of CO_2 for a 1.2mol.L^{-1} MEA solution with a loading of 0.4 at 40°C

Conclusions

This study showed the presence of precipitates in the absorber, and the formation of ammonium bicarbonate from the ammonium carbonate present in the CO_2-lean stream during the absorption process. It was also shown that the pure CO_2 stream that leaves the desorber column is pressurized. A reference configuration was used to assess the energy requirement both in the absorber and in the desorber. Based on equilibrium calculations, this study showed that the chilled ammonia process allows for a significant reduction of the energy consumption in the desorber compared to the energy consumption of the process using amines. This analysis will be completed by the results from the simulation of the process using ASPEN, and by the evaluation of the rate of absorption of CO_2 by ammonia solvents. In addition, the rate of absorption of carbon dioxide by aqueous ammonia will be investigated.

Acknowledgements

We want to thank the Danish Ministry of Science Technology and Innovation and DONG Energy for co-funding this industrial PhD project.

References

1. K. Thomsen, P. Rasmussen**,** Modeling of Vapor-liquid-solid equilibrium in gas-aqueous electrolyte system, Chem. Eng. Sci. 54 (1999)1787-1802
2. E. Gal, Ultra cleaning combustion gas including the removal of CO_2, World Intellectual Property, Patent WO 2006022885 (2006)
3. B. Rumpf, G. Maurer, Solubility of Ammonia Solutions of Sodium Sulfate and Ammonium Sulfate at temperatures from 333.15K to 433.15K and pressure up to 3MPa, ind. Eng. Chem. Res. 32(1993), 1780-1789
4. B. Rumpf, G. Maurer, An experimental and theoratical Investigation on the Solubility of Carbon Dioxide in Aqueous Solutions of Strong Electrolytes, Ber. Bunsenges. Phys. Chem. 97 (1993), 85-98
5. E. Jänecke, Über das System H2O, CO2 und NH3. Zeitschrift fuer Elektrochemie, 39 (1929) 332-334+716-728
6. Lichtfers U, Spektroskopische Untersuchungen zur ermittlung von Speziesverteilungen im System Ammoniak-Kohlendioxid-Wasser, (2001) Aachen, Shaker Verlag
7. B. Rumpf, F. Weyrich, G. Maurer, Enthalpy changes upon Partial Evaporation of Aqueous Solutions containing Ammonia and Carbon Dioxide, Ind. Eng. Chem. Res 37 (1998) 2983-2995
8. JN. Knudsen, JN. Jensen, O. Biede, Castor SP2: Experiments on Pilot Plant, CASTOR-ENCAP-CACHET-DYNAMIS common Technical Training Workshop (2008)

List of Publications

1. V. Darde, K. Thomsen, W. van Well, EH. Stenby, Chilled ammonia process for CO2 capture, Energy Procedia (2009), 1(1), 1035-1042

Martin Dela Ellegaard
Phone: +45 4525 2808
Fax: +45 4593 2906
E-mail: mec@kt.dtu.dk
WWW: http://www.capec.kt.dtu.dk
Supervisor: Jens Abildskov

PhD Study
Started: February 2008

Molecular Thermodynamic Modeling of Ionic Liquid Systems

Abstract
A simple method is employed for a molecular based description of systems of ionic liquids. These include pure liquids as well as gas solubilities in ionic liquds. The method stems from rigorous statistical mechanical theory, and results show excellent agreement with a variety of substances over a large range of state conditions for both pure liquid compression data and gas solubilities.

Specific Objectives
This paper aims to describe – in part – the contents of this Ph.D. project, which is divided in two main areas of research:

i. Quantitative thermodynamic modeling of systems of ionic liquids, incl. pure liquid compression and gas solubilities in pure ionic liquids.
ii. Modelling of mixed solvent solubilities.

This paper reports the latest progress on part i.

Introduction
Ionic liquids are salts composed of weakly coupled ions, where at least one has a delocalized charge and one component is an asymmetric organic. This prevents the formation of a stable crystal lattice. As a result ionic liquids have a range of favorable properties. They have negligible vapor pressures – a favorable property in chemical processing. This finds great usage – among others – in chemical reaction engineering, where ionic liquids may serve as medium, dissolving both organic and inorganic species. Additionally they may be used as fluids for separation processes, as well as electrolytes for electronic devices. To facilitate the usage of ionic liquids in process design it is crucial that their phase equilibria can be modeled to a high degree of accuracy. Much modeling of ionic liquid systems have been based on equations of state (EOS). Often simple, cubic equations have been deployed. However, these rely on vapour/liquid criticals, which for ionic liquids are hypothetical since they decompose before they reach a critical point.

The method given here proposes an easily generalizable approach for dealing with multicomponent phase equilbria. Although based on rigorous stastical mechanical theory, its application is easy and requires a minimum of parameters fitted to experimental phase equilibrium data.

Statistical Mechanical Solution Theory
Fluctuation solution theory of Kirkwood and Buff [1] relates integrals of molecular correlation functions to derivatives of thermodynamic quantities. One example is the activity coefficient derivative wrt. number density

$$\rho\frac{\partial \ln f_i / x_i}{\partial \rho_j}\bigg|_{T,\rho_{k\neq j}} = \rho\frac{\partial \ln \gamma_i}{\partial \rho_j}\bigg|_{T,\rho_{k\neq j}} = 1 - C_{ij}(T,\{\rho\}). \quad (1)$$

Here, C_{ij} is the spatial integral of the center-to-center direct correlation function between species i and j (DCFI). T is the absolute temperature and ρ is the molecular density. The derivative in Eq. 1 does not depend on the reference state chosen. The Gibbs/Duhem equation with Eq. 1 yields another relevant relation

$$\frac{\partial p / \mathrm{R}T}{\partial \rho_j}\bigg|_{T,\rho_{k\neq j}} = \frac{\overline{v}_j}{\kappa_T \mathrm{R}T} = \sum_i x_i\left[1 - C_{ij}(T,\{\rho\})\right], \quad (2)$$

where κ_T is the isothermal compressibility. If the system changes from a standard state $(T,p^r,\{x^r\}) = (T,\{\rho^r\})$ to $(T,p,\{x^f\}) = (T,\{\rho^f\})$, Eqs. 1 and 2 can be integrated to give activity coefficients and density provided temperature, pressure, and mole fractions.
Obviously, the formalism requires the DCFI can be modeled accurately. Previous investigations [2] have shown that this is feasible using a first order perturbation expansion in density

$$C_{ij}(T,\{\rho\}) = C_{ij}^{h.s.}(T,\{\rho\}) - 2\rho\left[B_{ij}(T) - B_{ij}^{h.s.}(T)\right]. \quad (3)$$

Here, $C^{h.s.}$ is calculable from a hard-sphere equation of state, B resembles the second virial coefficient for simple fluids, and $B^{h.s.}$ is the hard-sphere second virial coefficient. The two latter are calculated using a two-parameter corresponding states approach, with the functional forms and parameters adjusted to argon data. The pure component parameters are a characteristic volume and a characteristic temperature. Occasionally a binary parameter is required to properly scale the latter.

Results and Discussion

Molecular parameters for 28 ionic liquids and a variety of gases, incl. hydrogen, oxygen, and carbon dioxide have been obtained by reduction of isothermal compression data.

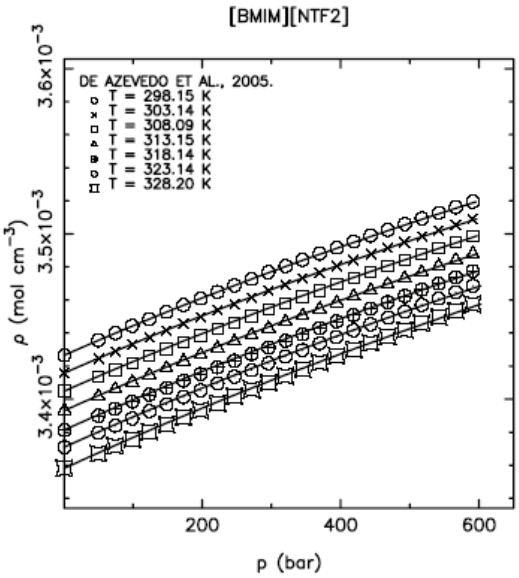

Figure 1. $p\rho T$ of [bmim][NTf_2].

Fig. 1 shows correlation of an ionic liquid [bmim][NTf_2] at pressures up to 600 bars. The agreement with experimental data is quantitative.

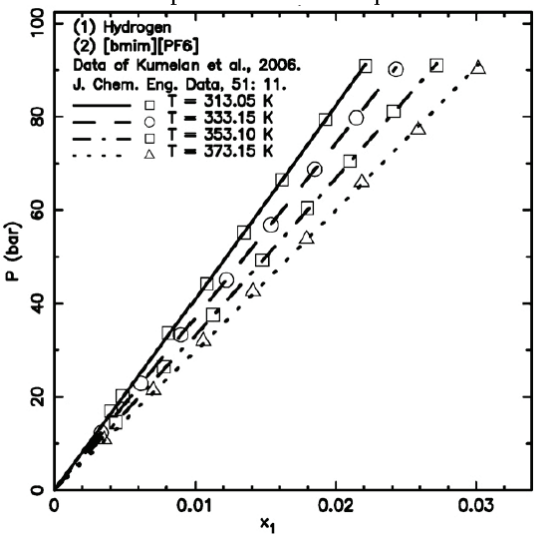

Figure 2. H_2 solubility in [bmim][PF_6], $k_{12} = 0$.

Fig. 2 plots the solubility of hydrogen in the ionic liquid [bmim][PF_6]. As before the agreement is quantitative over a large temperature range. The results are generally insensitive to the binary parameter, and for substances like hydrogen it can be neglected. However, the solubilities of more subcritical gases, such as carbon dioxide and hydrogen sulfide, the results are not quantitative.

Future Work

Current research is aimed at improving the model in Eq. 3 to better account for fluids closer to their critical point. In addition attempts to resolve the molecular parameters in group contributions are underway. This can potentially eliminate the need for experimental data for parameter estimation.

Conclusions

A simple method with a minimum of parmaeters has been applied to systems of ionic liquids. Results show that the agreement with experimental data generally is good.

Acknowledgements

The Technical University of Denmark is greatly acknowledged for financial support of this project. Prof. J.P. O'Connell of University of Virginia, USA, is also greatly acknowledged for many fruitful and helpful discussions.

References

1. J.G. Kirkwood, F.P. Buff. J. Chem. Phys. 19 (1951) 774-777.
2. P.M. Mathias, J.P. O'Connell. Chem. Eng. Sci. 36 (1981) 1123-1132.
3. J. Abildskov, M.D. Ellegaard, J.P. O'Connell. Fluid Phase Equil. 286 (2009) 85-96.

List of Publications

1. J. Abildskov, M.D. Ellegaard, J.P. O'Connell. Fluid Phase Equil. 286 (2009) 85–96.
2. M.D. Ellegaard, J. Abildskov, J.P. O'Connell. AIChE J. 55 (2009) 1256–1264.
3. M.D. Ellegaard, J. Abildskov, J.P. O'Connell in: Thermodynamics 2009, Imperial College, London, U.K., 2009.
4. M.D. Ellegaard, J. Abildskov, J.P. O'Connell in: J.-N. Jaubert (Ed.), Proceedings of the 23rd European Symposium of Applied Thermodynamics, Ecole Nationale Supériure des Indudsties Chimiques, France, 2008.
5. M.D. Ellegaard, J. Abildskov, J.P. O'Connell in: A. Arce, A. Soto (Eds.), 24th European Symposium of Applied Thermodynamics, University of Santiago de Compostela, Spain, 2009.
6. M.D. Ellegaard, J. Abildskov, J.P. O'Connell in: D.G. Friend, M.L. Huber, C.D. Muzny, G.R. Hardin (Eds.), Seventeenth Symposium on Thermophysical Properties, NIST / ASME / AIChE / IIR,, USA, 2009.
7. M. Ellegaard, J. Abildskov, J.P. O'Connell in: AIChE Anual Meeting 2008, AIChE, USA, 2008.

Leila Faramarzi
Phone: +45 4525 2892
Fax: +45 4588 2258
E-mail: lef@kt.dtu.dk
WWW: http://www.cere.kt.dtu.dk
Supervisors: Georgios M. Kontogeorgis
Kaj Thomsen
Erling H. Stenby

PhD Study
Started: February 2007
To be completed: March 2010

Modeling CO_2 Capture

Abstract
The purpose of the project has been to thermodynamically model the absorption of CO_2 in different aqueous alkanolamine solutions and also to model the absorber column using monoethanolamine as solvent. Both the thermodynamic model and the absorber model are validated against experimental data with good accuracy.

Introduction
Global increase in energy demand together with a continued dependence on fossil fuel resources have significantly contributed to the increase in the atmospheric levels of CO_2. International Energy Agency's (IEA's) World Outlook 2007 reports that the growth in energy demand will result in 57 percent energy related CO_2 emissions by 2030 (IEA 2007). The largest anthropogenic emission sources in the globe are the fossil fueled power plants causing approximately one-third of CO_2 emissions. Coal-fired plants emit significantly more CO_2 than natural gas plants. However coal is a very favorable energy source for power generation because it is relatively inexpensive compared to other fossil fuels.
Due to the apparent contribution of CO_2 to the global warming, more lately there has been an emphasis on mitigating CO_2 emission especially from the combustion processes associated with power generation. CO_2 separation from gaseous streams has been practiced for decades. Much of the work concerned the separation of CO_2 from methane for the purification of natural gas as many natural gas reservoirs contain significant amounts of acid gases such as CO_2.
Several different approaches have been proposed for removing CO_2 from flue gases on a large scale. The main approaches to the separation of CO_2 from other light gases are: cryogenic distillation, membrane purification, absorption with liquids, and adsorption using solids.
The absorption/stripping process for the post-combustion capture of CO_2 using alkanolamines is currently being extensively investigated as the process has decades of history in the chemical processes arena. Monoethanolamine (MEA) is the most studied alkanolamine.
In the current PhD project the purpose has been to develop a CO_2 capture process design model and validate it against the literature experimental data.

Thermodynamic Modeling
To properly simulate the reversible absorption process, a rate model is needed. However, it is essential to incorporate an accurate thermodynamic model with the rate model to calculate the driving forces for mass transfer correctly.
The purpose of the first phase of the work was to apply the in-house model, extended UNIQUAC to estimate various thermodynamic properties of the alkanolamine systems required for the design of CO_2 capture plants. In addition, the model proved capable to represent different types of thermodynamic properties of the aqueous CO_2-alkanolamin systems in a broad range of conditions using only one unique set of parameters [1].
Different types of data are used for modeling and they cover a wide range of conditions. Vapor-liquid equilibrium (VLE) data for the aqueous alkanolamine systems containing CO_2 in the pressure range of 3-13000 kPa and temperatures of 25-200ºC are used. The model is also regressed with the VLE and freezing point depression data of the binary aqueous alkanolamine systems (MEA-water and MDEA-water). The two just mentioned types of data cover the full concentration range of alkanolamines from extremely dilute to almost pure alkanolamine. The experimental freezing point depression data down to the temperature of -20ºC are used. Experimental excess enthalpy (H^E) data of the binary MEA-water and MDEA-water systems at 25, 40, 65 and 69ºC are used as well. In order to enhance the

calculation of the infinite dilution activity coefficients of MEA and MDEA, the pure alkanolamines vapor pressure data in a relevant temperature range (up to almost 230ºC) are included in the parameter estimation process.
The previously unavailable standard state properties of the alkanolamine ions of the interest of this project i.e. MEA protonate, MEA carbamate and MDEA protonate are determined.
The concentration of the species in both MEA and MDEA solutions containing CO_2 are predicted by the model and in the case of MEA compared to NMR spectroscopic data.
Compared to other modeling approaches in the literature, a quite extensive range of pressure, temperature and CO_2 concentration in the aqueous phase is addressed. Yet, the model's performance is quite satisfactory for the calculation of VLE of MEA, MDEA and MEA+MDEA systems.
Freezing point depression for the aqueous alkanolamine systems is also calculated very precisely by the model.
The model correlates the excess enthalpy of MEA-water and MDEA-water systems reasonably well considering the scatter of experimental data. The calculated concentration distributions for both MEA and MDEA systems show the expected behavior. Considering that the model is not tuned to any speciation data and the uncertainty of experimental measurements, the model calculations are reasonable. This fact also proves the accuracy of the activity coefficients and also the standard state properties determined in the present work.
Overall, it has been shown that extended UNIQUAC can accurately represent physical and chemical equilibria (H^E, VLE, SLE, speciation) over a wide range of conditions, thus being a valuable thermodynamic model for the design of the CO_2 absorption plants.

Modeling the Absorber

Packed column absorbers employing aqueous alkanolamine solutions have long been used for purification of natural gas and separation of acidic gases from industrial gaseous streams. Despite the fact that the process has been studied for many years and there have been many modeling approaches adopted by researchers, the available models need to be enhanced and there is room for developing new consistent ones.
Apart from the unsound design methods, the scarcity of the reliable design and pilot plant data has been a major obstacle in modeling the chemical absorption processes such as CO_2 capture in MEA solution.
In this project, the rate-based steady state model [3] for the design of the CO_2- 2-amino-2-methyl-propanol (AMP) absorbers is adopted and improved for the design of the CO_2- monoethanolamine (MEA) absorber. The influence of the application of different mass transfer correlations on the model's performance is investigated. Analytical expressions for the calculation of the enhancement factor for the second order as well as the pseudo-first order reaction regime are integrated in the model and their impact on the model's prediction is compared.
The model has been successfully applied to CO_2 absorber packed columns and validated against pilot plant data with good agreement. Three different rate equations were integrated in the model. The available rate models for the reaction of CO_2 with aqueous MEA are valid in a limited range of temperature and MEA concentration and they cannot be confidently extrapolated. Overall, the applied equations for the kinetic rate yielded similar results.
The accuracy of the model's predictions is dependent on the mass transfer correlations applied. However, mass transfer correlations are developed based on specific flow conditions and sometimes they are only suitable for specific types of packing. Consequently, these models may not be accurate at all hydrodynamic conditions.
The enhancement factor for the pseudo-first order reaction seemed to be not only sufficient, but the preferred approach for representing the experimental data for the loading ranges considered.
Overall, our simple model for the CO_2 absorber packed column is a valuable tool for simulating the capture process [2]. In cases where the quality of the essential fundamental data is dubious and the available correlations for the basic properties are not fully reliable, a simple model for CO_2 absorber design is a suitable approach.

Future Prospects

The extended UNIQUAC model proved a reliable tool for estimating the thermodynamic properties of alkanolamine solutions containing CO_2. The model will best serve the purpose of modeling the capture process if it is integrated in the absorber model. An Important future prospect is to integrate the thermodynamic model in the present absorber model.
The physical properties such as density, viscosity and heat capacity for the alkanolamine solutions containing CO_2 termed as loaded solutions are scarce and there is lots of room for performing experimental work on the field.
The pilot plant data for the CO_2 capture in aklanolamines are limited and not always consistent. This problem prevails even in the case of the most conventional alkanolamine, MEA. More pilot plant experiments need to be done.
It is also worthwhile to compare the performance of our absorber model to the other available models in literature and also to commercial packages.

References

[1] Faramarzi, L; Kontogeorgis, G.; Thomsen, K.; Stenby, E. H., Fluid Phase Equilib. 2009, 282, 121–132.
[2] Faramarzi, L; Kontogeorgis, G.; Michelsen, M. L.; Thomsen, K.; Stenby, E. H., Ind. Chem. Eng. Res. Submitted.
[3] Gabrielsen, J.; Michelsen, M. L.; Kontogeorgis, G. M.; Stenby, E. H. AICHE J. 2006, 52, 10, 1-9.

Rita Lencastre Fernandes
Phone: +45 4525 2994
Fax: +45 4593 2906
E-mail: rlf@kt.dtu.dk
WWW: -
Supervisors: Krist V. Gernaey
Anker D. Jensen
Ingmar Nopens, University of Ghent

PhD Study
Started: November 2009
To be completed: October 2012

Population Balance Models and Computational Fluid Dynamics: an Integrated Model Framework to Describe Heterogeneity in Fermentors

Abstract
Traditionally, a microbial population has been considered homogeneous in optimization studies of fermentation processes. However, research has shown that a typical microbial population in a fermentor is heterogeneous. The aim of this Ph.D. project is to establish a model framework where Population Balance Models (PBM) and Computational Fluid Dynamics (CFD) are integrated in order to describe heterogeneous microbial populations in stirred-tank reactors. Given the early stage of the project, this contribution presents an overall introduction to the project and a brief discussion on key issues that have been identified while developing a review of the available literature on PBM for microbial populations.

Introduction
Microbial cultures are, for simplification purposes, generally regarded as homogeneous mixtures of identical cells. This assumption does however not correspond to real systems. Individual cells exhibit heterogeneity, for example resulting from small variations in the cellular metabolism and cell-cycle dynamics. Therefore, mass and other single properties of the cells of a growing and proliferating cell population are distributed rather than uniform, and the distributions of such properties evolve with time. A typical biochemical experimental measurement represents, then, an average of the individual cell properties, and properties such as intracellular concentrations of metabolites should be described by distribution functions rather than scalar values.

Cell heterogeneity as result of metabolic or cell-cycle dynamics is greatly induced by changes in the extracellular environment that stimulate metabolic and stress responses. This phenomenon is particularly observed in large-scale reactors where substrate and oxygen gradients are formed due to mixing and aeration deficiencies [1]. Individual cell trajectories result in a succession of various extracellular stimuli that induce physiological responses leading to a heterogeneous cell population within the large-scale reactor.

In order to simulate the behavior of heterogeneous cell populations in large-scale reactors, it is necessary to integrate both models for the extracellular environment, including a description for the gradients of for example substrates and excreted metabolites, and for the cell population, including a description of growth and cell division.

On the one hand, a detailed description of the extracellular environment can be achieved by developing a computational fluid dynamics (CFD) model for the bioreactor. The trajectories of individual or groups of cells can also be simulated by using an Euler-Lagrange approach which allows one to describe population behavior as the outcome of the interaction between the intracellular state of the individual cells and the turbulent flow field in the reactor [2].

On the other hand, the most rigorous approach for describing the effects of cell heterogeneities on microbial culture dynamics is based on the population balance equation models (PBM) [3]. PBM consist of a mathematical description of how the number of individuals in a population and their properties changes with time and with the growth conditions.

Specific Objectives

The final aim of the project is to set up an integrated framework of CFD and PBM for dynamic simulation of distributed properties (e.g. size, composition, age, reaction rates,…) of microorganism populations in stirred tanks.

In a first phase of the project, attention is focused on establishing a PBM which is computationally solvable and provides a description of a microbial population which can be easily compared to experimental data.

In this early stage, a literature review on PBM for microbial populations is under development. The main conclusions and discussion topics identified so far are presented in the section below. In the short-term future the collected information and discussion will be compiled into a publishable review paper.

Results and Discussion

PBM models typically consist of population balance equations supplied with boundary conditions, initial conditions, and typically equations for the concentrations of growth-limiting nutrients in the medium, as well as other supporting equations describing cell division intensity and other kinetic functions. The complexity associated with describing the intracellular reaction network in detail leads to a computationally intractable, or difficultly tractable, model.

PBM presented in the literature can be generally divided into age or mass-structured models. As for the first, models cell subpopulations are grouped according to age – the time since the cells were "born". Nonetheless, age is virtually impossible to be experimentally determined and only in very limited conditions can be considered a good indicator of the cell state [5]. With regard to the mass-structured models, mass should be regarded as a general term for one or a vector of cellular variable(s) which can be correlated to the cellular metabolism, and therefore represent the state of each subpopulation. Historically, a key contribution to development of PBM for microbial populations was proposed in an article by Fredrickson, Ramskrishna and Tsuchiya in 1967, where the authors introduced a vectorial description of states into a population balance equation [4]. Ideally, the model would be more rigorous the more descriptive the state vector was. The problem that arises is that high-dimensional population balances are computationally intractable, and thus PBM state vectors typically include one or a maximum of two variables (i.e. 1-D or 2-D PBM).

Different methods for solving the integral partial differential equations defined within the PBM are discussed in the literature. These include finite differences methods [6], finite elements methods[7], spectral methods[8], and Monte Carlo procedures [9]. The choice of the adequate solving method will have to be discussed and investigated thoroughly in the course of the project. In fact, the solvability of the model is a critical issue that will have to be kept in mind in the frame of the project, especially as the developed PBM will be integrated with a CFD model, which will further aggravate the computational tractability issues.

Conclusions

Understanding the behavior of a microbial population in a large-scale bioreactor poses many challenges. Given the non-ideal mixing at this large-scale, gradients are formed within the reactor and individual cells experience a succession of different extracellular conditions along their cell trajectories. The variations in the extracellular environment stimulate physiological responses, resulting in a heterogeneous cell population which the common unstructured models do not account for.

It is therefore a challenge to establish a model framework which describes both the gradients found in the reactor by means of a CFD model, and the cell populations by means of a PBM model. In order to achieve a validated framework, it is necessary that the implemented models are computationally tractable and possible to validate using experimental data, Therefore, the PBM that will be developed will be based on one or two state variables which can be easily correlated to experimental data collected by flow cytometry and other single-cell level analysis methods.

References

1. S.-O. Enfors et al., J. of Biotech. 85 (2001) 175-185
2. A. Lapin, Schmid, J., Reuss, M., Chem. Eng. Sci. 61 (2006) 4783-4797
3. M. A. Henson, Curr. Opin. in Biotech. 14 (2003) 460-467
4. A. G. Fredrickson, D. Ramkrishna, H.M. Tsuchyia, Math. Biosci. 1 (3) (1967) 327-374
5. A. G. Fredrickson, N. V. Mantzaris, Chem. Eng. Sci. 57 (2002) 2265-2278
6. N. V. Mantzaris, P. Daoutidis, F. Srienc, Comp. and Chem. Eng. 25 (2001) 1411-1440
7. N. V. Mantzaris, P. Daoutidis, F. Srienc, Comp. and Chem. Eng. 25 (2001) 1463-1481
8. N. V. Mantzaris, P. Daoutidis, F. Srienc, Comp. and Chem. Eng. 25 (2001) 1441-1462
9. C. Hatzis, F. Srienc, A. G. Fredrickson, Biosystems 36 (1995) 19-35

José M. S. Fonseca
Phone: +45 4525 2858
Fax: +45 4588 2258
E-mail: jfo@kt.dtu.dk

Supervisor: Nicolas von Solms

PhD Study
Started: January 2007
To be completed: April 2010

Multiphase Equilibrium in Natural Gas / Hydrate Inhibitor Systems

Abstract
A considerable amount of money is currently spent in so-called “production chemicals”, used in order to increase or facilitate production from a reservoir and in pipelines. Examples of such chemicals are methanol and glycols, used as inhibitors to prevent the formation of gas hydrates. A better understanding of these systems will allow the reduction of the amounts used to the strictly necessary, with the inherent economical and environmental advantages. Therefore, we are working on the improvement of our experimental techniques with the design of new experimental set-ups for the measurement of phase equilibria through different methods, for the collection of more accurate and reliable data in a wide range of conditions.

Introduction
Gas hydrates are crystalline compounds formed by inclusion of low molecular weight compounds in lattice structures formed by water on hydrogen bonds. Small molecules from light gases stabilize the lattice structure with the formation of stable solids at temperatures above the freezing point of water. Additionally, hydrates form more readily from real natural gas mixtures than from the pure constituent components of natural gas, representing a frequent problem for the gas industry, especially at the high pressures and low temperatures typical in North Sea gas reserves.

Blocking of lines due to the formation of hydrates presents serious issues in what safety is concerned and it has disastrous economic consequences.

To face this problem, hydrate inhibitors such as ethylene glycol (MEG) or methanol are injected to the natural gas well stream, to prevent the formation of hydrates during transportation and further processing. In the case of offshore production, these inhibitors are transported through pipelines to the well. When a mixture of gas, water, MEG and condensate arrives onshore, all the components are distributed through all the phases, and it is essential to evaluate the amount of glycol lost in the gas phase, for environmental and for economical reasons. Also for environmental reasons it is necessary to determine the solubility of aromatics in the glycol rich phase, due to possible emissions during the regeneration process of the glycol.

Since the amount of inhibitor needed is not well known, and in order to avoid accidents, an excess of inhibitors is regularly used in these processes, with the inherent economical and environmental consequences.

A better knowledge of the phase equilibrium in these systems can allow the reduction of the amounts used to the strictly necessary.

This project we aim to improve our experimental techniques, with the designing of new experimental set-ups for the measurement of phase equilibria, which will allow the collection of more accurate and reliable data in a range of temperatures and pressures that can allow for example the replication of the polar conditions under which some pipelines are operated.

The methods for the analysis of the different phases include gas chromatography (GC), gas chromatography associated with mass spectroscopy (GC-MS), Karl Fisher and the use of adsorption columns (ATD).

Experimental
A new experimental set-up, was specially designed for the study of multi-phase equilibria in the systems hydrocarbon-water-hydrate inhibitor, at temperatures ranging from 203 K to 353 K and pressures up to 40 MPa. This apparatus, depicted in Figure 1, is based in the static analytical method [1], although the design of the cell allows for a recirculation method to be adopted very easily and with very small changes in the system.
The core of the apparatus is the high pressure cell shown in Figure 2, where a three dimensional computer generated image is presented, as well as a cut of the cell, showing its interior.

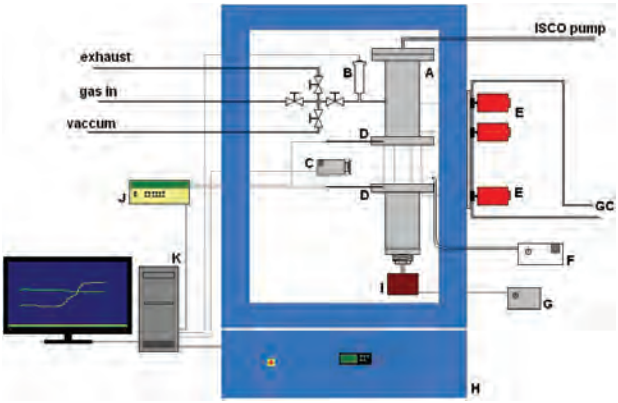

Figure 1: Schematic representation of the new experimental set-up for the measurement of multi-phase equilibria. – A: High pressure cell with 360º sapphire window. B: Temperature compensated high precision pressure sensor. C: video camera. D: Temperature sensors PT100. E: ROLSI™ samplers. F: Cold light source with optical fiber. G: Remote control for the stirring motor. H: Low temperature chamber. I: Stirring motor. J: Data logger. K: Computer.

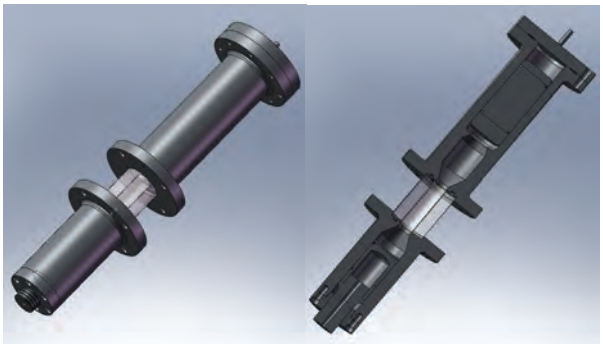

Figure 2: Three-dimensional computer generated images of the high pressure cell. – On the left: view of the cell. On the right: Cut of the cell showing its interior.

Equipped with a 360º sapphire window, this cell was entirely designed and built "in house" in Stainless Steel 316. Its air tightness is assured by high performance Mupu seals, consisting of a jacket of Kefloy energized by a metal spring, allowing to overcome the limitations of the more traditional sealing solutions, being suitable for pressures up to 60 MPa and temperatures as low as 200 K or even lower, depending on the polymers used.

The operating volume of the cell can be varied between 120 cm^3 and 207 cm^3, by means of two pistons.

A manual piston, in the lower part of the cell, comprises the magnetic stirrer in its interior and it can account for a displacement of 18 cm^3. It also allows the height of the interface between two phases to be conveniently located on the sapphire window.

An automatic piston is designed to compensate for any pressure drops that might result from the sampling processes and it can induce a variation in the volume of 69 cm^3. It is connected to a high pressure syringe pump ISCO 260D, using as pressure transmitting medium a commercial thermal fluid, based on polymetylsiloxanes, with a low viscosity at temperatures down to 188 K. This makes it ideal for this application, since an increase in the viscosity of the fluid could lead to delays in the piston actuation or even to its inoperability.

The cell is located inside a temperature chamber, specially customized by the manufacturer for this application, with an available volume of 240 dm^3 and an operating temperature range from 203 K to 453 K with a temperature constancy of ± 0.7 K over time, according to the manufacturer. The temperature stability of the cell inside is, however, better than this value, due to its thermal inertia.

The temperature of the cell is monitored through two platinum resistance thermometers PT100 class 1/10 DIN placed over and under the sapphire window, connected to a data acquisition system Agilent 34970A, connected to a computer via RS-232. The temperature is measured with a precision of 0.001 K, and according to the preliminary tests, its stability is better than 0.003 K.

The pressure inside the cell is monitored by a temperature compensated pressure transmitter for measurements up to 50 MPa with a resolution of 0.1 kPa and an accuracy of 0.1% FS (0.05 MPa). The stability of the measured values is better than 0.5 kPa. This transmitter is equipped with a digital output and it is connected directly to the computer via RS-485. The thermal compensation is performed internally by the transmitter through a mathematical model and using the information from its own internal temperature sensor.

The stirring on the cell is promoted magnetically, through a Neodymium Iron Boron magnet, placed inside the lower piston on the cavity observable in Figure 2. The magnet is connected to a low temperature motor with variable speed.

A digital video camera connected to the computer is used to observe in detail a phase interface, with the aid of a cold light source equipped with LED technology.

The use of an analytical method implies a higher complexity of the system, with the need of a sampling method and procedure, as well as the development of the analytical method itself. Nevertheless, this allows a better understanding of the systems in equilibrium, with the knowledge of the composition of all the different phases involved in the equilibrium.

In this stage of the work, the sampling system consists of three automatic electromagnetic capillary ROLSI™ samplers, directly coupled to an Agilent 6890 gas chromatograph equipped with a HP-PLOT Q capillary column.

Figure 3 shows a schematic representation of one of the samplers, which allows the withdrawing of extremely small sample volumes, reducing eventual pressure drops in the cell and making possible to take a large number of samples.

In a subsequent stage, the analysis of the samples will include other methods and techniques, such as GC-MS, Karl Fisher and the use of adsorption columns (ATD). The assessment of the composition of some of the phases will be possible by more than one method in order to test the respective accuracies.

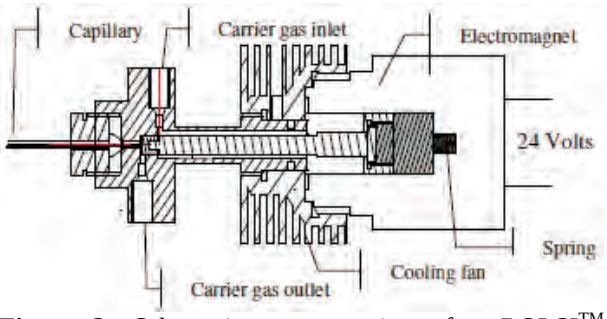

Figure 3: Schematic representation of a ROLSI™ electromagnetic sampler.

Meanwhile, a second experimental set-up was developed for the measurement of two-phase equilibria using a synthetic method [1], and making use of an old existing high pressure equilibrium cell, again aiming at a high precision and accuracy apparatus.

The existence of these two experimental set-ups allows the assessment of the consistency of the results yielded by both apparatus, permitting the establishment of a comparison between the two different methods, evincing the advantages and disadvantages of each one.

The new experimental set-up, presented in Figure 4, is suitable for measurements at temperatures ranging from 233 K to 353 K and at pressures up to 20 MPa.

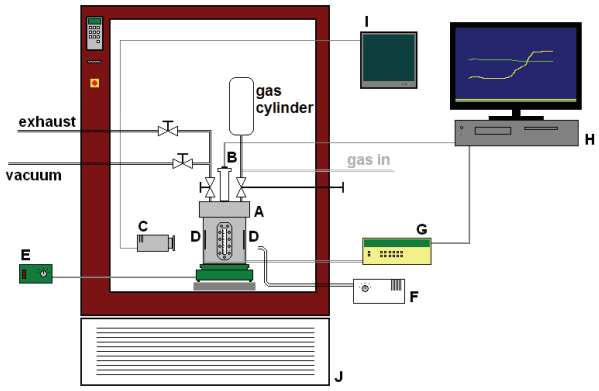

Figure 4: Representation of the new experimental set-up. – A: High pressure cell with two parallel sapphire windows. B: Temperature compensated high precision pressure sensor. C: camera. D: Temperature sensors PT100. E: Remote control for the magnetic stirrer. F: Cold light source with optical fiber. G: Data logger. H: Computer. I: TV monitor. J: Temperature chamber.

The core of the apparatus is the high pressure view cell, an upgraded version of the previously existing cell, with two parallel sapphire windows, for which the top was completely redesigned. The original cell was built in Stainless Steel 316 by TOP Industries, France, and had an internal volume around 560 cm^3. The main changes in the cell have to do with the reduction of the existing connections, from seven to three, improving its simplicity and reducing leak possibilities. A magnetic stirring system was also adopted, in opposition to the previously system where a rotating part was going through the top of the cell.

The cell is inside a temperature chamber, previously existing in our laboratory, with an available volume of 720 dm^3 and an operating temperature range from 233 K to 423 K, with a temperature stability of 0.5 K.

The temperature of the cell is monitored through two platinum resistance thermometers PT100 class 1/10 DIN placed in opposite sides of the cell inside its thick walls, in two holes specifically made for that purpose. These sensors are connected to a data acquisition system Agilent 34970A, connected to a computer via RS-232 for monitoring and recording of the experimental conditions. The temperature is measured with a precision of 0.001 K, and according to the preliminary tests, its long time stability is better than 0.05 K.

The pressure inside the cell is monitored by a temperature compensated pressure transmitter for measurements up to 20 MPa with a resolution of 0.1 kPa and an accuracy of 0.1% FS (0.02 MPa). The stability of the measured values is better than 0.2 kPa. This transmitter has a digital output and it is connected directly to the computer via RS-485. The thermal compensation is performed internally by the transmitter using a mathematical model together with the information from its own internal temperature sensor.

The stirring is promoted magnetically, through a commercial variable speed magnetic stirrer placed under the cell, adapted so that it can now be controlled from outside the temperature chamber.

One of the sapphire windows has a calibrated scale, allowing knowing the volume of each of the phases in equilibrium, through the observation of the phase interface by means of a video camera conveniently placed in front of the sapphire window, and with the aid of a cold light source using LED technology.

Most of the experiments are carried out with a gas cylinder with a volume from 150 cm^3 to 1000 cm^3, containing a precisely known amount of gas. The total volume of the system has a considerable influence in the reduction of the relative uncertainty when measuring the volumes of the phases involved in the equilibrium through the position of the interface.

Results

The quality of the pressure-temperature values measured with first apparatus, using the analytical method, was verified with the study of the vapor pressure of carbon dioxide, at temperatures ranging from 240 K up to its critical point at 304 K. The values are in close agreement with the literature, namely with the values recommended in the DIPPR database [2], as showed in Figure 5.

The agreement is better than 1% in the whole range, and although a deviation is noticeable for the values obtained at lower temperatures, this corresponds to a difference of only 10 kPa.

The study of the 3-phase coexisting line for the binary system methanol + ethane confirm the good quality of the PT values measured, as depicted in the plot in Figure 6. Figure 7 shows the GC results of one of the samples withdrawn from the methanol rich phase.

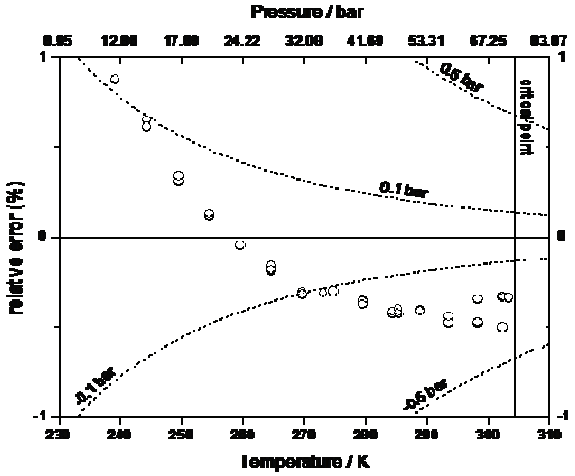

Figure 5: Comparison of the results obtained for the vapor pressure of carbon dioxide with the recommended values [2].

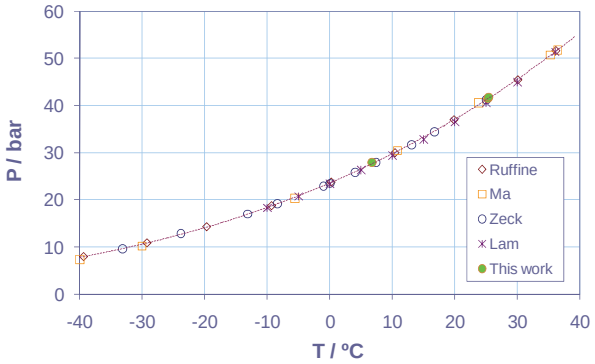

Figure 6: Comparison of the results obtained for the 3-phase coexisting line for the binary system methanol + ethane with data found in the literature [3-6].

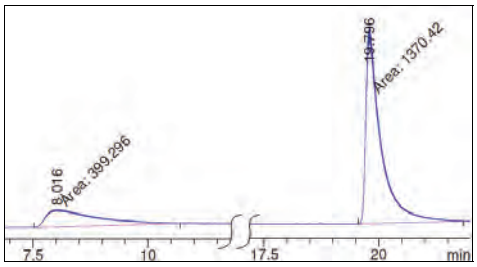

Figure 7: Chromatogram obtained from one of the samples withdrawn from the methanol rich phase during the study of the 3-phase coexisting line for the binary system methanol + ethane.

As for the second experimental set-up described, similar tests with carbon dioxide were performed in order to infer the quality of the PT measurements. The comparison with reference values [2] is presented in Figure 8. The agreement is again notable for the whole range of the measurements, from 260 K up to the critical point of carbon dioxide at 304 K.

The synthetic method was tested through the measurement of the solubility of methane in water at 298 K. The results, shown in Figure 9 are again in close agreement with the values found in the literature.

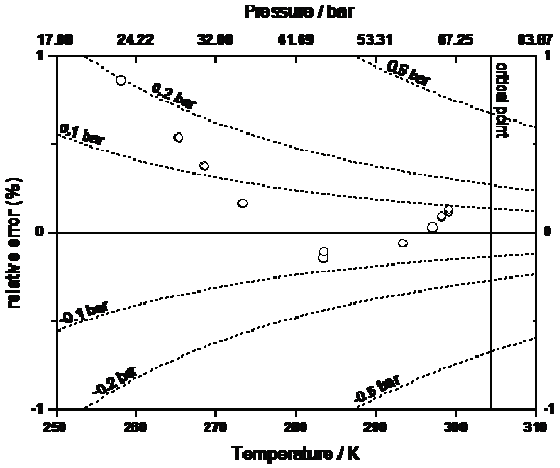

Figure 8: Comparison of the results obtained for the vapor pressure of carbon dioxide with the recommended values [2].

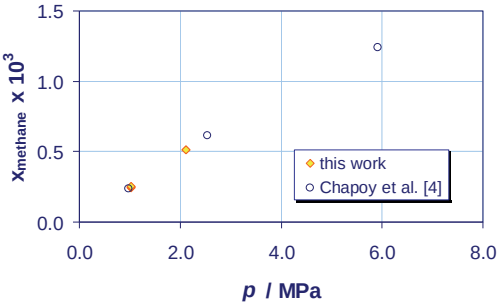

Figure 9: Comparison of the results obtained for the study of the solubility of methane in water at 298 K with data found in the literature [7].

References

1. R. Dohrn, S. Peper, J.M.S. Fonseca, Fluid Phase Equilib. 288 (2010) 1-54.
2. DIPPR DIADEM – The DIPPR Information and Data Evaluation Manager for the Design Institute for Physical Properties. 2006, Version 3.0.0.
3. L. Ruffine et al., Ind. Eng. Chem. Res. 44 (2005) 8387-8392.
4. Y. Ma, J. Kohn, J. Chem. Eng. Data, 9 (1964) 3-5.
5. S. Zeck, H. Knapp, Fluid Phase Equilib. 25 (1986) 303-322.
6. D. Lam, K. Luks, J. Chem. Eng. Data, 36 (1991) 307-311.
7. A. Chapoy, A.H. Mohammadi, D. Richon, B. Tohidi, Fluid Phase Equilib. 220 (2004) 113-121.

Acknowledgements

The author would like to thank the Danish Research Council for Technology and Production Sciences for the financial support through the project "Gas Hydrates – from Threat to Opportunity" and the Technical University of Denmark for the financial support through a Ph.D. scholarship.

Sarah Maria Frankær
Phone: +45 4525 6809
Fax: +45 4588 2161
E-mail: saf@kt.dtu.dk
WWW: http://www.dpc.kt.dtu.dk
Supervisors: Søren Kiil
Anne L. Skov
Kim Dam-Johansen

PhD Study
Started: May 2009
To be completed: April 2012

Stimuli-Adaptable Materials

Abstract
Materials that change properties after being exposed to external stimuli pose a new and very interesting field for development of new materials. This project focuses on making polymeric materials which change their material properties upon exposure to UV-light. The described materials consist of a permanent polymer network and a number of star molecules which are cross-linked under exposure to UV-light whereby they form a second network which penetrates the permanent network. The UV-light induced cross-linking of the star molecules is fully reversible.

Introduction
In 2005 Lendlein et al. published an article describing a system with light-induced shape memory. [1] The paper describes two systems: One where the reactive molecule is grafted onto the polymer network and one where the reactive molecule is introduced as a separate part of the system. Regardless of the system the reaction chemistry is the same.

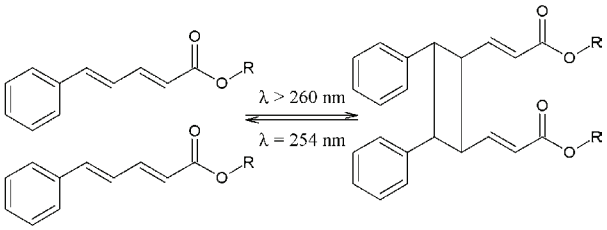

Figure 1: Schematic representation of the cross-linking of two cinnamylidene acetic acid residues to form a cyclobutane structure.

The chemistry is a cross-linking of the cinnamylidene acetic acid (CAA) residue with UV-light ($\lambda > 260$ nm), see Figure 1. The cross-linking is reversible by irradiation with another wavelength of light ($\lambda = 254$ nm). [2]

It is well known that cross-linking polymers to form polymer networks greatly influence the mechanical properties of the polymer material. However changing the degree of cross-linking can give very different materials from the same polymer – in fact, everything from materials which are highly viscous liquids to hard and strong rubbers is possible from the same initial polymer but depending on the ratio of crosslinker to polymer different properties are obtained.
The presented chemistry should allow creation of systems which contain a well characterized network as well as a network that can be switched on and off by external stimuli. As an example a soft liquid-like material could be present before irradiation with UV-light, and after irradiation the second network will have formed and the material will all of a sudden behave like a rubber.

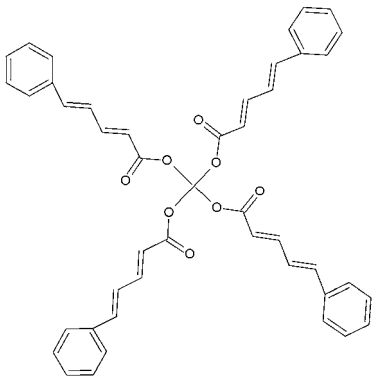

Figure 2: The poly(ethylene glycol) star with cinnamylidene acetic acid residues on each arm.

It is intended to introduce this switchable network by synthesizing 4-armed star molecules with the CAA-

residues at the end of the arms, see Figure 2. The star molecule itself consists of poly(ethylene glycol). [1]
By incorporating the star molecules into a polymer network a system like the one shown in Figure 3 will be made. It consists of a permanent network and the star molecules **(**Figure 3A**)** which form a network after irradiation with UV-light **(**Figure 3B**)**.

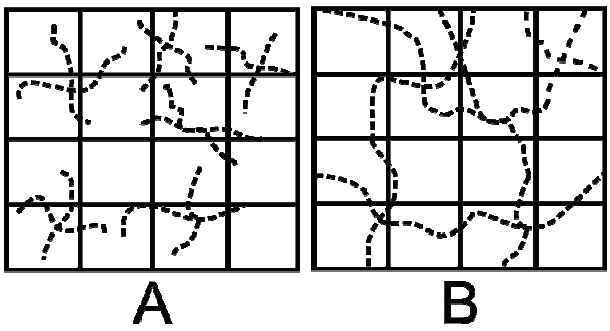

Figure 3: A: The permanent network with the star molecules inside. B: The permanent network and the network formed by the star molecules after irradiation.

Specific Objectives
The objective of the project is to develop materials which change properties upon external stimuli – in this case UV-radiation will be used. To do this many steps must be taken; first the chemistry must be understood and the systems reported in literature should be replicated. The reported systems also need further characterization since structural and physical data are scarce. It will be investigated if the technology can be applied to other polymers and polymer networks than the ones reported. If this proves to be successful many new materials could be made.

Results and discussion
The formation of the second network is time dependent and thus the change in mechanical properties is as well. While the second network is forming the concentration of the star molecules decreases which indicates that there is a link between the concentration of the star molecules and the mechanical properties of the sample. Tanaka *et al.* report that the reaction shown in Figure 1 follows a first-order kinetic equation. [2] This equation was combined with expressions for the concentration at a specific time to yield an equation which gives the concentration, *c*, of the star molecules at a given time:

$$c(t) = 1/(2.303\varepsilon l)*\log(\exp(c_1+c_2*t)+1$$

Where ε is the molar absorptivity for the CAA-residue and l is the thickness of the sample. c_1 and c_2 were found using data from Lendlein *et al.*
After irradiation of a sample for one hour Lendlein *et al.* obtained an increase in Young's modulus from 0.19 MPa to 0.24 MPa.
It is expected that optimizing the concentration of star molecules and the time of irradiation with UV-light will lead to materials which can be fine tuned to a large variety of applications.

Conclusion
The presented project gives rise to the possibility of creating many intriguing products. Imaging bulletproof materials that are soft and able to bend, or an adhesive that is soft and comfortable and still causes minimal trauma to the skin upon removal.
The results that have been found from literature indicate that materials with these properties could be made with the presented technology.

References

1. A. Lendlein, H. Jiang, O. Jünger, R. Langer, Nature, 434 (2005) 879-882.
2. H. Tanaka, K. Honda, J. Polym. Sci., Polym. Chem. Ed. 15 (1977) 2685-2689

Charlotte Juel Fristrup
Phone: +45 4525 6819
Fax: +45 4588 2161
E-mail: cjf@kt.dtu.dk
WWW: http://dpc.kt.dtu.dk
Supervisors: Søren Hvilsted
Katja Jankova
Rüya Eskimergen Nielsen, Novo Nordisk
Jens Thostrup Bukrinski, Novo Nordisk

PhD Study
Started: March 2007
To be completed: October 2010

Biofunctional Coatings by use of Surface-Initiated Atom Transfer Radical Polymerization

Abstract
The initial formation of initiating sites for Atom Transfer Radical Polymerization (ATRP) on various polymer surfaces and numerous inorganic and metallic surfaces is elaborated. The subsequent ATRP grafting of a multitude of monomers from such surfaces to generate thin covalently linked polymer coatings is discussed briefly in order to provide a readily accessible survey. The potential for achieving a range of well-defined biofunctionalities, such as inhibition of non-specific fouling, immobilization of biomolecules, separation of proteins, adsorbents for proteins or cells, antibacterial activity, and encapsulation of drugs in particular provided by these surface-grafted polymers is described.

Introduction
The most powerful changes in surfaces are achieved by grafting where an entire new surface layer is added to the substrate. Conventionally, polymerization is accomplished by the use of electrons, UV or plasma treatment of the surface followed by radical polymerization of various monomers, but there is generally only poor control of the new surface layer in terms of chemical functionality and morphology. Controlled radical polymerization techniques, especially Atom Transfer Radical Polymerization (ATRP) [1], provide the best control, where "control" means the ability to shape the polymer architecture and to design linear, block, graft, star or dendritic forms in a predictable manner including total control over the chain length (molecular weight). ATRP normally also offers the possibility to select the most convenient and appropriate initiator for the monomer in question. However, in *grafting* by ATRP *from* a polymer surface, there is one the restriction and complication that initiating sites need to be generated at the original surface. In principle, the concept of grafting from a polymer also allows an initiator gradient, enabling a variation in the grafting density. The grafted polymer layer can then be designed to vary from mushrooms or isolated chains to brushes or high grafting density, which has been shown to have large implications for some biofuntionalities [2,3]. On the other hand, we claim that the other possibility - *grafting onto* a polymer surface - requires both an anchoring group on the surface and a reactive group on the incoming polymer, in addition to an effective coupling mechanism. Steric hindrance or shielding from the first reacted polymers onto a surface often prevents subsequent polymer grafting and lead to a low surface coverage. Since these obstacles significantly lower the grafting densities of the polymer brushes, we do not consider this option here. The greatest challenge, however, is the analysis of the grafted polymers in terms of both the chain length and grafting density, since conventional polymer characterization techniques have been found to be insufficient.

Fabrication of the initiator for the Surface-Initiated ATRP (SI-ATRP)
The first stage in grafting from a surface is the immobilization of a suitable initiator for the particular monomer(s). Few synthetic materials contain inherent initiating groups for ATRP. Merrifield resins (with chloromethyl polystyrene) [4], and poly(4-vinylbenzyl chloride) (PVBC), either cross-linked [5,6] or not cross-linked [7] can be used as received for SI-ATRP. Interestingly, secondary fluorine atoms were available on the surface of poly(vinylidene fluoride) (PVDF) for the direct SI-ATRP of various monomers [8,9]. Unfortunately, the authors' attempts to repeat the method with a range of monomers were not satisfactory. All other

materials need immobilization of initiator on the surface prior to the SI-ATRP. Various methodologies have been developed which differ depending on the applied substrate - organic/polymeric or inorganic/metallic - and consequently we show them schematically in these two categories. Most of the implied pathways require functional groups on the surface for further reaction. The initiating groups on the surface are either formed in a synthetic cascade involving several chemical reactions, or a preformed bifunctional compound with suitable initiating groups for ATRP is attached to the substrate. Fig. 1 and Fig. 2 only contain methods producing biofunctional coatings. Additional information can be found in recent reviews dealing with SI-ATRP used either as a tool for the modification of polymer materials [10], silica nanoparticles [11] and carbon nanotubes [12] or as a tool for surface modification [13].

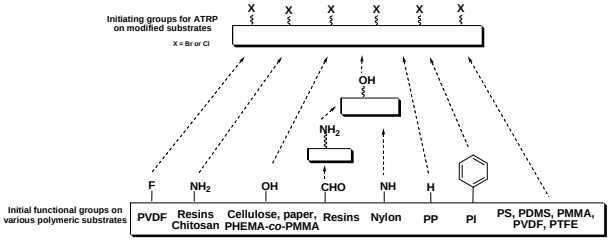

Figure 1: Preparation of initiating groups for ATRP on organic/polymeric substrates.

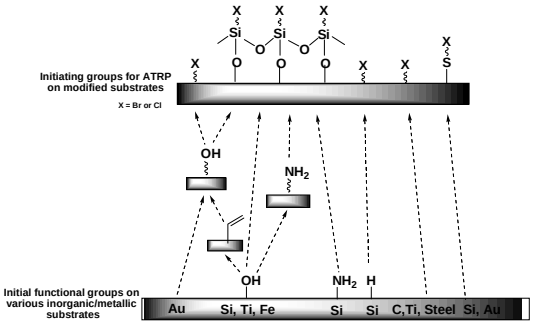

Figure 2: Formation of initiating groups on inorganic and metallic substrates (Au= Gold, gold coated QCM crystals; Si=Si/SiO_2, glass; Ti=Titanium; Fe=Fe_3O_4; C=(ultrananocrystalline) diamond; Steel=stainless steel).

For details about the chemical reactions in Fig. 1 and Fig. 2 we refer to our recent review article [14].

Biofunctional coatings

Various monomers have been used for SI-ATRP to prepare polymer coatings which can be applied within the field of biotechnology. The term biofunctionality is used to emphasize that the polymer coating is not only of interest in biological applications but also that it has been tested within these applications. We have chosen six classifications for biofunctionality in order to elucidate the applications of the monomers. The classifications include inhibition of non-specific fouling, immobilization of biomolecules, separation of proteins, adsorbents for proteins or cells, antibacterial activity, and encapsulation of drugs.

Inhibition of non-specific fouling, non-fouling, antifouling, and resistance against biofouling are terms to describe surfaces which reduce both protein adsorption and cell adhesion. Interactions between the proteins or cells and the surface determine the tendency to non-specific fouling. Hydrophobic and electrostatic interactions are considered to be the major driving forces for fouling; but the importance of these interactions depends on the protein structure and the surface properties. For instance, non-specific fouling depends on the surface wettability, specific chemical groups on the surface, surface charge, the balance between hydrophobic and hydrophilic groups, the mobility of the polymer brushes, and the structure of the adsorbed water [15]. Fig. 3 shows the monomers involved in preparation of non-fouling polymer brushes by SI-ATRP.

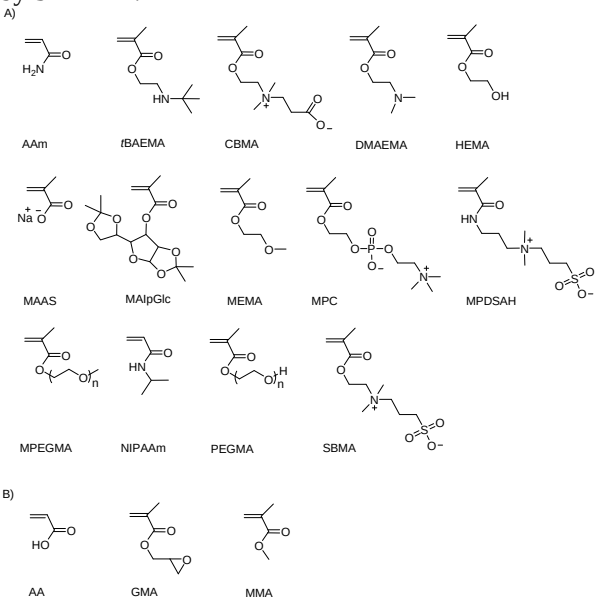

Figure 3: A) Polymer grafts on surfaces made from the monomers inhibit non-specific fouling; B) The monomers result in antifouling coatings when incorporated in copolymer structures.

Biomolecules including peptides, proteins, polysaccharides, antibiotics, biotin, and DNA have been immobilized on the substrates before or after SI-ATRP. The materials with grafted polymer brushes and anchored biomolecules can be applied as DNA-sensing devices, vascular graft materials, microarrays, bio- and molecular sensors, biomedical implants, and nanoparticles effective in preventing blood clotting in vitro [16]. Thus, the reason for anchoring biomolecules is either to reject or to adsorb e.g. proteins, peptides or cells. Fig. 4 illustrates the monomers which can be applied for immobilization of biomolecules.

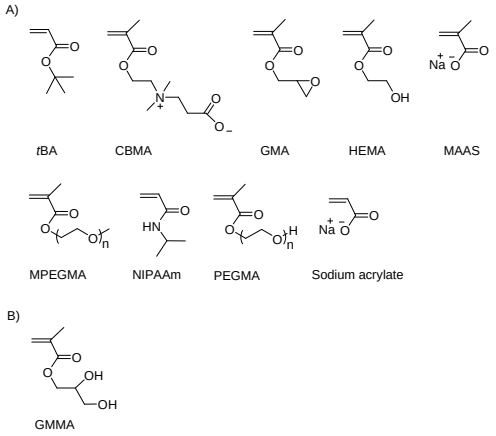

Figure 4: A) Monomers used for preparation of polymer coatings for immobilization of biomolecules; B) Copolymer grafts made from GMMA and GMA for immobilization of penicillin G acylase.

SI-ATRP is a suitable method to modify column material for various chromatographic techniques. The polymer coating must be uniform in order to avoid blocking of the pores; moreover, it should be covalently attached to the surface, as polymers formed in solution inside the pores will block the pores. SI-ATRP also offers the ability to control the thickness of the polymer coating as opposed to conventional radical polymerization [17]. If the purpose is to separate proteins by chromatography, e.g. Size Exclusion Chromatography, Capillary Electrophoresis or High Performance Liquid Chromatography, the column material could be modified with polymer brushes made from the monomers AAm, DMAAm, HEMA, NIPAAm, or SPM (Fig. 5).

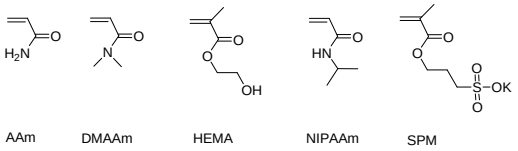

Figure 5: SI-ATRP of the monomers on column materials improves separation of proteins.

Adsorbents for proteins or cells, which is known as non-specific fouling, can be prepared for three purposes. The first is to apply the polymer brushes in adsorption studies or applications in which adsorption is needed. The second is to obtain polymer brushes which either adsorb or reject proteins or cells depending on the grafting density or the charge of the adsorbate. Thirdly, some polymer brushes are used for comparison, because they are known to adsorb proteins or cells. Fig. 6 shows the monomers which can be applied for SI-ATRP to prepare non-specific fouling surfaces.

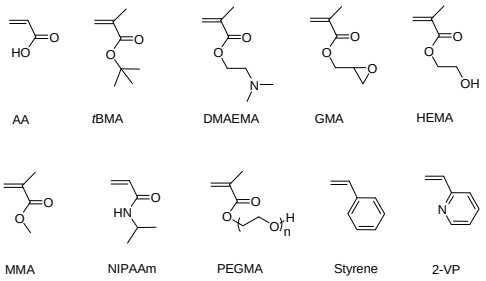

Figure 6: Non-specific fouling has been observed on surfaces with polymer grafts prepared from the monomers.

The term antibacterial is defined as being able to kill or reduce the harmful effect of bacteria (Cambridge Advanced Learner's Dictionary). Therefore, antibacterial polymer coatings should not only reject bacteria, they should also interfere with the growth and reproduction of bacteria. SI-ATRP of DMAEMA (Fig. 7) followed by quaternization of the tertiary amine groups is the most prevalent "grafting-from" method that leads to antibacterial polymer coatings.

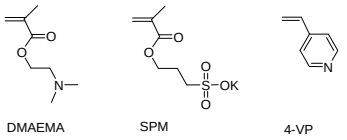

Figure 7: SI-ATRP of the monomers followed by quaternization or loading with silver results in antibacterial surfaces.

Stimuli-responsive polymers will be suitable for encapsulation of a drug as well as for load and release of the drug. The polymer brushes could be sensitive to external factors such as temperature, pH, or salt concentration [18]. Fig. 8 lists the monomers which have been reported to result in stimuli-responsive polymer grafts.

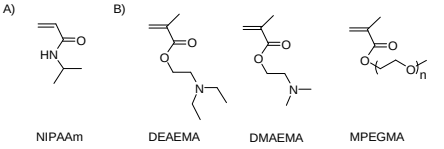

Figure 8: A) Polymer grafts prepared from NIPAAm can be used for encapsulation of drugs; B) Copolymer grafts from the monomers are suitable for encapsulation of drugs.

Conclusions

Possibilities of creating initiator sites for ATRP on various different polymer surfaces as well as on a variety of inorganic and metallic surfaces are described in detail, and a schematic presentation of a multitude of monomers grafted from such surfaces to provide thin covalently linked polymer coatings is provided. A relatively large number of polymeric substrates are used for applying biofunctional coatings. The well-defined biofunctionalities,

inhibition of non-specific fouling, immobilization of biomolecules, separation of proteins, adsorbents for proteins or cells, antibacterial activity, and encapsulation of drugs provided by these polymer coatings, are thoroughly discussed. Thus twelve years after its first appearance, SI-ATRP is shown to be a valuable technique to develop biofunctional coatings.

Acknowledgements
CJF acknowledges the Technical University of Denmark, Novo Nordisk, and the Danish Agency for Science Technology and Innovation for financial support.

Abbreviations
AA: Acrylic acid
AAm: Acrylamide
ATRP: Atom Transfer Radical Polymerization
*t*BA: *tert*-butyl acrylate
*t*BAEMA: 2-(*tert*-butylamino) ethyl methacrylate
*t*BMA: *tert*-Butyl methacrylate
Br-i-BuBr: 2-Bromoisobutyryl bromide
CBMA: 2-Carboxy-*N*,*N*-dimethyl-*N*-(2'-methacryloyloxyethyl)ethanaminium inner salt
DEAEMA: 2-(Diethylamino)ethyl methacrylate
DMAAm: *N*,*N*-Dimethylacrylamide
DMAEMA: 2-(*N*,*N*-dimethylamino)ethyl methacrylate
GMA: Glycidyl methacrylate
GMMA: Glycerol monomethacrylate
HEMA: 2-Hydroxyethyl methacrylate
MAAS: Methacrylic acid sodium salt
MAIpGlc: 3-*O*-Methacryloyl-1,2:5,6-di-*O*-isopropylidene-D-glucofuranose
MEMA: 2-Methoxyethyl methacrylate
MMA: Methyl methacrylate
MPC: 2-Methacryloyloxyethyl phosphorylcholine
MPDSAH: (3-(Methacryloylamino)propyl)-dimethyl(3-sulfopropyl) ammonium hydroxide
MPEG: Monomethoxy poly(ethylene glycol)
MPEGMA: Monomethoxy poly(ethylene glycol) methacrylate
NIPAAm: *N*-isopropylacrylamide
PDMS: Poly(dimethylsiloxane)
PEG: Poly(ethylene glycol)
PEGMA: Poly(ethylene glycol) methacrylate
PI: Polyimide
PP: Polypropylene
PS: Polystyrene
PVBC: Poly(4-vinylbenzyl chloride)
PVDF: Poly(vinylidene fluoride)
SBMA: Sulfobetaine methacrylate
SI-ATRP: Surface-Initiated Atom Transfer Radical Polymerization
SPM: 3-Sulfopropyl methacrylate potassium salt
2-VP: 2-Vinylpyridine
4-VP: 4-Vinylpyridine

References
1. (*a*) W. A. Braunecker, K. Matyjaszewski, Prog. Polym. Sci. 32 (2007) 93-146; (*b*) N. M. L. Hansen, K. Jankova, S. Hvilsted, European Polymer Journal 32 (2007) 255-293; (*c*) J. A. Opsteen, J. C. M. van Hest, in: K. Matyjaszewski, Y. Gnanou and L. Leibler (eds.), Macromolecular Engineering, Wiley-VCH, Weinheim, 2007, vol. IV, ch. 16.4, pp. 2662-2671; (*d*) N. V. Tsarevsky, K. Matyjaszewski, Chem Rev. 107 (2007) 2270-2299.
2. Y. Mei, T. Wu, C. Xu, K. J. Langenbach, J. T. Elliott, B. D. Vogt, K. L. Beers, E. J. Amis, N. R. Washburn, Langmuir 21 (2005) 12309-12314.
3. N. Singh, X. F. Cui, T. Boland, S. M. Husson, Biomaterials 28 (2007) 763-771.
4. C. P. Chen, B. T. Ko, S. L. Lin, M. Y. Hsu, C. Ting, Polymer 47 (2006) 6630-6635.
5. Z. P. Cheng, X. L. Zhu, Z. L. Shi, K. G. Neoh, E. T. Kang, Surf. Rev. Lett. 13 (2006) 313-318.
6. Z. P. Cheng, X. L. Zhu, Z. L. Shi, K. G. Neoh, E. T. Kang, Ind. Eng. Chem. Res. 44 (2005) 7098-7104.
7. A. Mizutani, A. Kikuchi, M. Yamato, H. Kanazawa, T. Okano, Biomaterials 29 (2008) 2073-2081.
8. Y. W. Chen, D. M. Liu, Q. L. Deng, X. H. He, X. F. Wang, J. Polym. Sci., Part A: Polym. Chem. 44 (2006) 3434-3443.
9. J. F. Hester, P. Banerjee, Y. Y. Won, A. Akthakul, M. H. Acar, A. M. Mayes, Macromolecules 35 (2002) 7652-7661.
10. P. Liu, E-Polymers (2007).
11. B. Rdahakrishnan, R. Ranjan, W. J. Brittain, Soft Matter, 2 (2006) 386-396.
12. C. M. Homenick, G. Lawson, A Adronov, Polymer Reviews 47 (2007) 265-290.
13. D. Bontempo, N. Tirelli, K. Feldman, G. Masci, V. Crescenzi, J. A. Hubbell, Adv. Mater. 14 (2002) 1239-1241.
14. C.J. Fristrup, K. Jankova, S. Hvilsted, Soft Matter 5 (2009) 4623-4634.
15. T. Tsukagoshi, Y. Kondo, N. Yoshino, Colloids Surf., B 54 (2007) 94-100
16. S. C. Wuang, K. G. Neoh, E. T. Kang, D. W. Pack, D. E. Leckband, Adv. Funct. Mater. 16 (2006) 1723-1730.
17. X. Y. Huang, L. J. Doneski, M. J. Wirth, ChemTech 28 (1998) 19-25.
18. Z. Y. Zhou, S. M. Zhu, D. Zhang, J. Mater. Chem. 17 (2007) 2428-2433.

Wenjing Fu

Phone: +45 4525 2804
Fax: +45 4593 2906
E-mail: wfu@kt.dtu.dk
WWW: www.kt.dtu.dk
Supervisors: John M Woodley
Rafiqul Gani
Anders Riisager (DTU Chemistry)

PhD Study
Started: March 2008
To be completed: February 2011

Process Design of Chemo-enzymatic Synthetic Cascades

Abstract
Limited fossil resources and the unstable oil price make it increasingly important to create new chemical processes based on renewable resources. For many of these new processes a combination of enzymatic as well as heterogeneous and homogeneous catalysis will be required to direct the reaction toward the desired products. Hence there is a need to create a suitable process model to manage a range of technologies and products in the optimal way starting from renewable resources, such as fructose or glucose. Specifically, this project focuses on the design of chemo-enzymatic synthetic cascades from glucose.

Introduction
Chemo-enzymatic synthesis is a method to achieve selective catalysis, with potential application to many classes of reaction where conventional approaches are very difficult. A combination of enzymatic as well as heterogeneous and homogeneous catalysis will direct the reaction toward the desired products. Some success in the application of chemo-enzymatic synthesis has already been shown in pharmaceutical processes to produce high-value products, as well as specialty chemicals. The challenge here will be how to apply this approach in the synthesis of lower-value bulk chemicals. For example, in a biorefinery, this approach can be used to develop entirely new routes from renewable resources to produce building blocks for the future chemical industry.

However, in many chemo-enzymatic processes, even a small reaction pathway, there are many alternative technologies and routes. Some can be integrated together, some give the required yield and selectivity, some are difficult to implement and others are untested at scale [1]. The consequence is that it is difficult to justify placing significant effort and resource on process design, especially in the early stages of process development, where the information is limited [2]. Thus, there is a need for a methodology capable of fast evaluation of different processes with limited information to reduce the number of potential process flowsheets and evaluate alternatives. For example, such a methodology could be used for setting targets for the best flowsheet candidates for further improvement, and finally identifying the optimal set of products and the best route for producing them [2, 3].

As an example, this PhD project examines the use of renewable resources as new, versatile feedstocks for the production of building blocks for the chemical industry. The study aims to examine the production of a new building block for the polymer industry, 2,5-furandicarboxylic acid (FDA), from glucose via the intermediate 5-hydroxymethyl furfural (HMF) and employs a combination of chemical and enzymatic catalysis. The new polymer building block (FDA) has applications and properties similar to terephthalic acid which is derived from fossil resources and is the main building block for polyester (e.g., PET) resins and fibers.

Glucose is chosen as the feedstock since it can be readily obtained from starch and the process from this point involves isomerization, dehydration and oxidation to synthesize FDA. Figure 1 shows the pathway. The reaction conditions for the three main reactions are listed in Table 1. One of the biggest challenges in this process is to match all three reaction conditions (reaction media, concentrations, temperatures, pH values) as well as reaction rates.

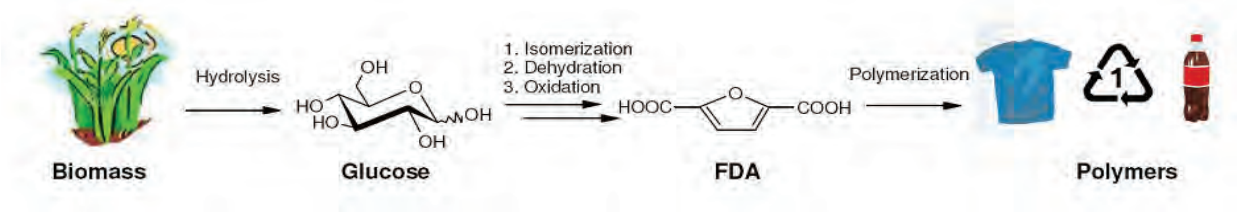

Figure 1: Main pathway for synthesis of FDA from glucose.

Table 1: Typical reaction conditions for the three main reactions involved in the synthesis of FDA from glucose.

Reaction	Temperature (°C)	pH	Catalyst
Isomerization	50 – 60	7 – 8	Glucose isomerase
dehydration	80- 200	acidic	Heterogeneous , Homogeneous
oxidation	room	basic	Inorganic

Objectives

The main objective is to develop a systematic modelling framework to address the necessary definition and design of an optimal process to produce FDA from glucose within specification and economic constraints as an example of the process design for chemo-enzymatic syntheses. The documented methodology and the tools involved in this study should form the basis for a framework for application to a range of similar chemo-enzymatic process designs.

Some specific objectives also include:

1) Identification of different possible flowsheets for routes from glucose to FDA, including both process options with integration and with intermediate separation.

2) Development of a systematic methodology using computer aided process modeling and cost analysis to compare the alternative technologies and routes from glucose to FDA within economic constraints.

3) Analysis of the potential process options to form the basis of process / cost models for detailed sensitivity analysis. Primarily this is with the purpose of setting targets for catalyst and process improvement.

4) Identification and documentation of the necessary type of property and thermodynamic data according to different types of modeling and analysis. This is required because collecting the correct and suitable property and thermodynamic data is essential for process modelling. However, for many chemicals involved in a biorefinery, such data are scarce or non-existent.

5) Examination and documentation of the feasibility of using different types of modelling software, which were developed for the conventional chemical processes, for the biorefinery design.

Methodology

The methodology of this study is shown in Figure 2.

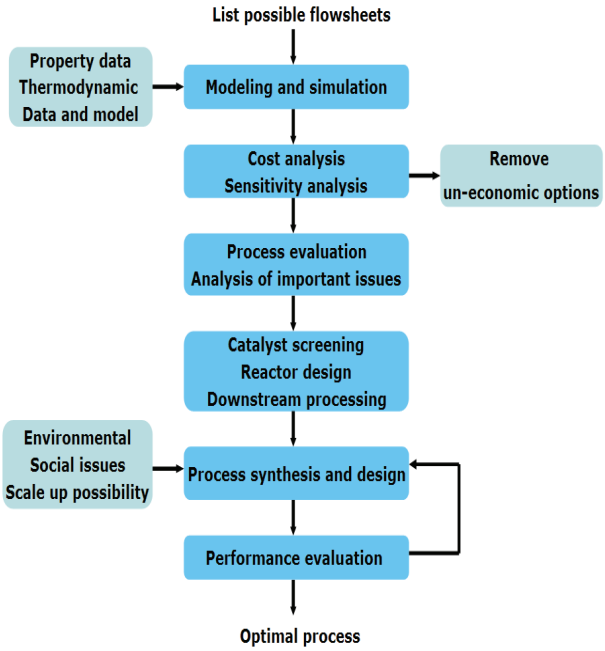

Figure 2: Plot of methodology of the study.

Acknowledgement

The author wants to thank the Technical University of Denmark, Novozymes A/S, and the Danish National Advanced Technology Foundation (DNATF) for financial support.

References

1. A. Boisen, T.B. Christiansen, W. Fu, Y.Y. Gorbanev, T.S. Hansen, J.S. Jensen, S.K. Klitgaard, S. Pedersen, A. Riisager, T. Ståhlberg and J.M. Woodley, Process integration for the conversion of glucose to 2,5-furandicarboxylic acid, Chemical engineering Research and Design,2008,87.1318
2. J. Shaeri, R. Wohlgemuth and J.M. Woodley, 2006, Semi-quantitative, Process Screening for the Biocatalytic Synthesis of D-Xylulose-5-phosphate, Organic process research & development, 10: 605-610.
3. N. Sammons, M. Eden, H. Cullinan, L. Perine and E. Connor, 2007, A flexible framework for optional biorefinery product allocation, Environmental Progress, 26:349 – 354.

Hassan Ahmadi Gavlighi
Phone: +45 4525 2947
Fax: +45 4593 2906
E-mail: HAG@kt.dtu.dk
WWW: http://www.bioeng.kt.dtu.dk/
Supervisors: Jørn Dalgaard Mikkelsen
Anne Meyer

PhD Study
Started: June 2009
To be completed: May 2012

Extraction and Production of Prebiotic and Hydrocolloids Oligosaccharides from Waste Streams from the Agricultural and Ingredient Industries

Abstract
A prebiotic oligosaccharide is a functional food component that confers a health benefit on the host which is associated with growth modulation of the gut microbiota. The interest in the use of nondigestible oligosaccharides (NDO) as functional food components targeted at gut health has increased during recent years. NDO are selectively fermented in the human colon and can be described as prebiotics. The waste streams from agricultural industry are a large source of oligosaccharides with potential prebiotic effects. The possibilities to manufacture new prebiotic oligosaccharides from large agricultural side-streams are therefore an attractive avenue and especially when it can be carried out using mono-component enzymes.

Introduction
It is now well established that the colonic microflora has a profound influence on health. Consequently, there is currently a great deal of interest in the use of prebiotic as functional food ingredients to manipulate the composition of colonic microflora in order to improve health. Prebiotics show both important technological characteristics and interesting nutritional properties. Several are found in vegetables and fruits and can be industrially processed from renewable materials. In food formulations, they can significantly improve organoleptic characteristics, upgrading both taste and mouthfeel. For prebiotics to serve as functional food ingredients, they must be chemically stable to food processing treatments, such as heat, low pH, and Maillard reaction conditions. That is, a prebiotic would no longer provide selective stimulation of beneficial microorganisms if the prebiotic was degraded to its component mono- and disaccharides or chemically altered so that it was unavailable for bacterial metabolism determined the effect of processing conditions on the prebiotic activity of commercial prebiotics using a prebiotic activity assay. The results showed that only heating at low pH caused a significant reduction in prebiotic activity, with one of the fructooligosaccharides (FOS) products being the least stable. The other conditions caused little change in activity. Stability of prebiotics to processing conditions has been considered. These results provide the basis for selecting prebiotics for use as functional food ingredients and for predicting the extent to which processing affects prebiotic activity. Most prebiotics and prebiotic candidates identified today are nondigestible oligosaccharides. They are obtained either by extraction from plants (e.g., chicory inulin), possibly followed by an enzymatic hydrolysis (e.g., oligofructose from inulin) or by synthesis (by trans-glycosylation reactions) from mono- or disaccharides such as sucrose (fructooligosaccharides) or lactose (trans-galactosylated oligosaccharides or galactooligosaccharides) .Among these prebiotics, inulin and oligosaccharides are the most studied prebiotics and have been recognized as dietary fibers in most countries.

Specific objectives
The main idea of the proposed project is to employ selective enzymatic catalysis to extract and design beneficial hydrocolloids and prebiotic oligosaccharides from agricultural industry.
Pectin is an abundant ubiquitous and multifunctional component of the cell wall of all land plants [1]. Pectic polysaccharides consist mostly of polymers rich in galacturonic acid (GalA), containing significant amounts of rhamnose (Rha), arabinose (Ara) and galactose (Gal) as well as other 13 different monosaccharides [2,3,4]. The three major pectic

polysaccharides currently defined are homogalacturonan (HG), rhamnogalacturonan I (RG-I) and rhamnogalacturonan II (RG-II) [5]. The industrial process for extraction of pectin is generally based on a chemical treatment at low pH. It generates large amounts of effluents (such as chemical waste) that need further treatment. It may also give rise to undesired degradation of pectin during extraction. There are a growing demand for sustainable processes with mild extraction and modification conditions to produce hydrocolloids and prebiotic oligosaccharides without the use and generation of hazardous substances. The present idea in this PhD study is to evaluate the use of new mono-component enzymes as an environmentally friendly method for pectin extraction and modification.

References

1. Willats, W. G. T.; Knox, P.; Mikkelsen, J. D., (2006). "Pectin: new insights into an old polymer are starting to gel". Trends in Food Science and Technology., 17, (3): 97-104.
2. Mohnen, D.,. (2008). "Pectin structure and biosynthesis". Current Opinion in Plant Biology., 11 (3): 266-277.
3. Vincken, J. P.; Schols, H. A.; Oomen, R.; McCann, M. C.; Ulvskov, P.; Voragen, A. G. J.; Visser, R. G. F., (2003). " If homogalacturonan were a side chain of rhamnogalacturonan I. Implications for cell wall architecture". Plant Physiology. 132, (4):1781-1789.
4. VINCKEN, J.; SCHOLS, H.; JFJ, R.; VORAGEN, A., (2003). “Pectin-The hairy thing”. Advances in Pectin and Pectinase Research, 47.
5. Waldron, K.; Parker, M.; Smith, A., (2003)." Plant cell walls and food quality ". Comprehensive reviews in food science and food safety, 2, (4): 128-146.

Fengxiao Guo
Phone: +45 4525 6821
Fax: +45 4588 2161
E-mail: feg@kt.dtu.dk
WWW: http://www.dpc.kt.dtu.dk/
Supervisors: Ole Hassager
Sokol Ndoni (Nanotech)
Katja Jankova

PhD Study
Started: November 2006
To be completed: February 2010

Ordered Nanoporous Scaffold for Conductive Polymers

Abstract
Nanoporous polymers of gyroid morphology are promising scaffolds to produce electronic materials with interconnected large surface area. We demonstrate the preparation of conductive nanoporous polymers by depositing polypyrrole onto nano cavity walls of nanoporous 1,2-polybutadiene films with gyroid morphology. The use of vapor phase polymerization of pyrrole with ferric *p*-toluenesulfonate as an oxidant can generate very thin films and avoid pore blocking. Infrared, Raman, and UV-Vis spectroscopies were used for confirmation of the incorporation of polypyrrole films. SAXS and TEM showed preservation of gyroid morphology after deposition of polypyrrole films. The conductivity of the resulting nanoporous polymers was verified by cyclic voltammetry.

Introduction
Polymeric materials with highly ordered nanopores have attracted considerable interest due to their unique nanometer-scaled structures. Self assembly of diblock copolymers spontaneously yields ordered nanostructures, including spheres, cylinders, gyroid and lamellae. Selective removal of one block can generate nanoporous polymers. Such nanoporous polymers can be used as a scaffold to grow nanostructured materials with controlled morphologies. Using nanoporous polymers as templates to synthesize conducting oxides and polymers may provide a means to shrink the dimensions of (opto)electronic devices.[1-3]

Polypyrrole (PPy) is one of the most common conducting polymers due to its simplicity of preparation, high conductivity and stability. A number of methods have been developed to produce PPy nanowires in both nanoporous organic and inorganic materials[4-6]. In addition to PPy nanowires, PPy ultrathin film incorporated onto nanopores of nanoporous polymers can also introduce conductivity to the previously insulating framework, and meanwhile the original porous structure is kept.

In this contribution we present the fabrication of conductive monolithic nanoporous polymers by coating PPy on nanopores of gyroid nanoporous 1,2-polybutadiene (PB). Gyroid nanoporous PB is prepared by cross-linking PB block from 1,2-polybutadiene-*b*-polydimethylsiloxane (PB-*b*-PDMS) diblock copolymer precursor and then etching away PDMS block. Gyroid morphology provides a continuous network. PPy thin film is deposited on the nanopores by vapor phase polymerization (VPP) with ferric *p*-toluenesulfonate (Fe(III)pTs) as an oxidant. Cyclic voltammogram of PPy modified nanoporous PB shows a promising electro activity. The prepared conductive nanoporous polymers may have interesting potential applications in sensing and catalysis due to their huge surface area.

Experimental Work
Colorless transparent gyroid nanoporous 1,2-polybutadiene (PB) monoliths (2 cm× 1 cm× 0.03 cm) with pore diameter of 14 ± 1 nm, surface area of 260 ± 30 m^2/g and porosity of 40 % used for this study were prepared from PB-*b*-PDMS by cross-linking the PB block with dicumyl peroxide followed by removal of the PDMS block with tetrabutylammonium fluoride according to ref 7. All other chemicals were received from Aldrich and used as received.

Fe(III)pTs solutions with concentration between 2.5% and 20% in ethanol were prepared. Nanoporous PB films were soaked in the Fe(III)pTs solutions for 30 min. When the films were taken out from oxidant solutions, the outside of the samples was washed with ethanol to remove excess Fe(III)pTs on the outside surface. The oxidant filled films were put into an oven at 80 – 100 °C to avoid crystallization of Fe(III)pTs before dry. After 5 min the solvent evaporated and the films became brownish. The films were then placed into a sealed chamber saturated with pyrrole vapors. After few minutes the color of the films changes from brown to black, indicating the formation of PPy. After 30 min

the films were taken out of the vapor chamber and placed into a petri dish to dry in air for 30 min before they were washed thoroughly in ethanol. VPP of pyrrole on glass slides was prepared in the same procedure as described for nanoporous PB.

Results and Discussion

The procedure of preparation of conductive nanoporous polymer films from original block copolymers is outlined in Figure 1.

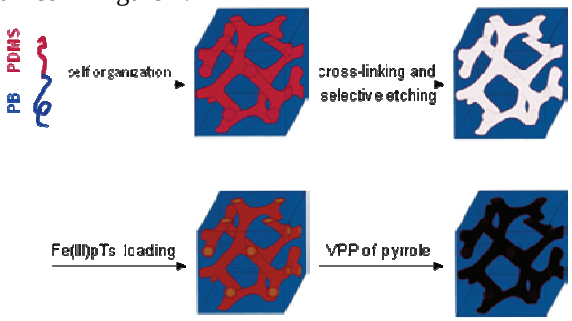

Figure 1. Schematic illustration of the preparation of conductive ordered nanoporous polymers.

Table 1. Mass uptake of nanoporous PB with PPy

Sample	Concentration of Fe(III)pTs solution	Mass uptake[a]
PB-PPy-I	2.5%	0%
PB-PPy-II	5%	0.6%
PB-PPy-III	10%	1.3%
PB-PPy-IV	20%	2.0%

[a] It is measured after films are washed in ethanol, and reference is the mass of nanoporous PB precursor.

The Fe(III)pTs was chosen as an oxidant here. Winther-Jensen et al. has reported that by using Fe(III)pTs oxidant VPP of pyrrole can leave very smooth and coherent coatings on a flat surface[8]. Gyroid morphology is known for its bicontinuous network, so it is easy accessible to gases and liquids, and probably less apt to have pore blockages[9]. The combination of VPP of pyrrole with Fe(III)pTs oxidant and gyroid morphology of nanoporous PB is to make continuous conductive PPy coatings throughout the nanopores. From Table 1, we can see that the mass of PPy in nanoporous PB increases with oxidant concentration.

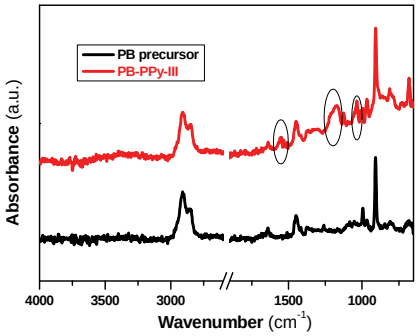

Figure 2. FT-IR spectra of PB precursor and PB-PPy-III.

To obtain evidence of PPy impregnation into nanoporous PB, FT-IR spectra of the film before and after modification were measured. As shown in Figure 2, compared to the spectrum of the PB precursor, additional characteristic peaks associated with PPy appear in the modified film, PB-PPy-III at 1550 cm^{-1} (ring stretching), 1180 and 1040 cm^{-1} (in-plane deformation of C-H bond). Furthermore, intensities of the two characteristic PPy peaks increase with increasing concentration of Fe(III)pTs. This is an indication that more PPy would be formed when more Fe(III)pTs is employed. UV-Vis spectroscopy was further used to confirm the presence of PPy in nanoporous PB. Figure 3 shows that the PB precursor does not absorb any light in the range from 350 to 900 nm. After modification, at 430 nm the typical $\pi - \pi^*$ absorption of conjugated PPy takes place. In addition, a broad band at 850 nm can be assigned to an extended conjugation in the backbone of the PPy.

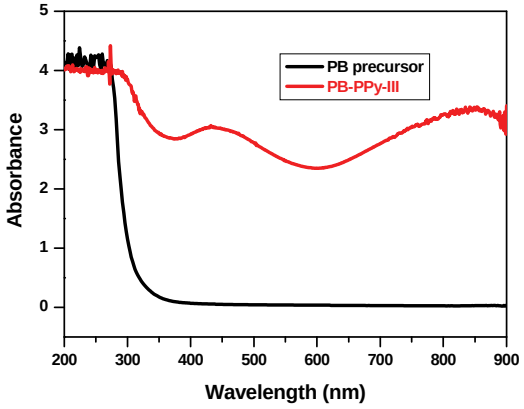

Figure 3. UV-Vis spectra of PB precursor and PB-PPy-III.

To investigate the thickness of PPy coating on the pore walls, PPy thin films were prepared on glass sides at same conditions as for nanoporous PB. Figure 4 shows the relationship between the coating thickness and absorbance of the coating at 430 nm. Based on this relation, the average coating thickness on pore walls of nanoporous PB can be calculated. Values for the four samples are close to the results obtained from mass uptake method, and are smaller than 1 Å, which means that the pore walls are not covered completely, and distribution of the coating is not homogeneous.

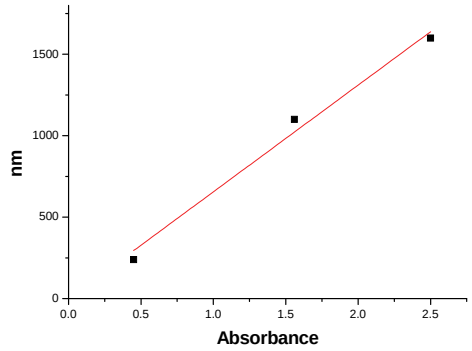

Figure 4. Relationship between PPy coating thickness and absorbance of the coating at 430 nm.

PPy inside network of the nanoporous PB was investigated by Raman spectroscopy with 632.8 nm diode laser excitation on a 300 lines/mm grating at room temperature on the cross section of PB-PPy-III. Raman spectrum in Figure 5 shows a typical Raman spectrum of PPy, similar to that of pure PPy polymerised under identical conditions. This not only confirms that the resulting composite material contains PPy, but also indicates that PPy coating has been incorporated into the whole thickness of the nanoporous PB.

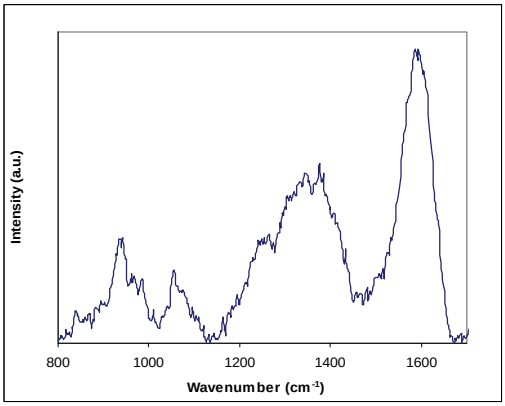

Figure 5. Raman Spectrum of PB-PPy-III with a 632.8 nm laser excitation and a 300 lines/mm grating.

Small angle x-ray scattering (SAXS) was used to investigate the morphology of nanoporous PB after modification. Figure 6 shows 1D scattering curves for the nanoporous PB precursor and PB-PPy-III. The ratio of the peak positions is characteristic for gyroid morphology. After VPP of pyrrole, the position of the scattering peaks PB-PPy-III does not change. This proves that the gyroid structure and lattice spacing of the sample were preserved during the modification sequence. Transmission electron microscopy (TEM) was employed to directly visualize the nanoporous structure. Figure 7 shows images of the PB precursor and one PB-PPy-III. Both images were observed nearly along the [111] direction. The center to center distances in the typical "wagon wheel" pattern (36±2 nm for PB precursor and 36±1 nm for PB-PPy-III) calculated by using the trigonometric relationships were in good agreement with those obtained from SAXS analysis (twice the spacing of the {211} planes, 37 nm for both samples). There is no observation of blocked pores or grainy structure of PPy particles in the pores through over the whole area of 1.5 μm×1.5 μm in TEM picture of PB-PPy-III. This confirms that the gyroid morphology and open pores were fully preserved after incorporation of PPy and that PPy were deposited onto the nanopore wallsurfaces.

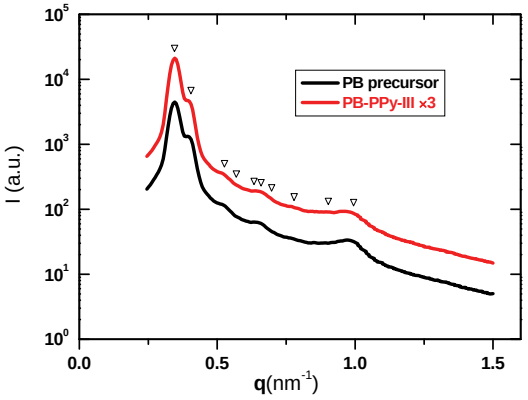

Figure 6. 1D SAXS profiles of PB precursor and PB-PPy-III. The [211], [220] and other characteristic peaks for gyroid structure are marked at $6^{1/2}q^*$, $8^{1/2}q^*$, $14^{1/2}q^*$, $16^{1/2}q^*$, $20^{1/2}q^*$, $22^{1/2}q^*$, $24^{1/2}q^*$, $30^{1/2}q^*$, $40^{1/2}q^*$ and $50^{1/2}q^*$ (q^* is the principle peak).

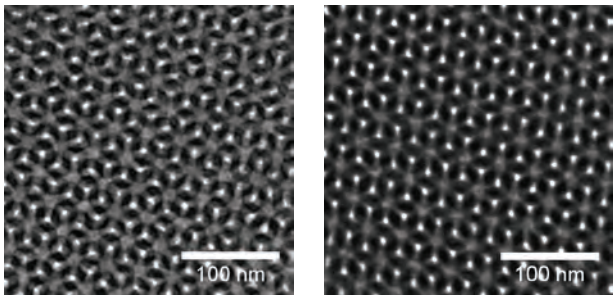

(a) (b)

Figure 7. TEM images of (a) PB precursor and (b) PB-PPy-III.

Figure 8 shows the cyclic voltammogram of PB-PPy-III electrode in 1.0 M $NaNO_3$ solution. It displays a typical stable redox couple (labelled A & B), which could be assigned to the PPy backbone. Even though the PPy does not cover the pore walls completely, partially continuous PPy coating exists in the network. That is why the sample shows the good electro activity. This suggests that the PPy/NPM has a potential as novel kind of nanoporous electromaterials.

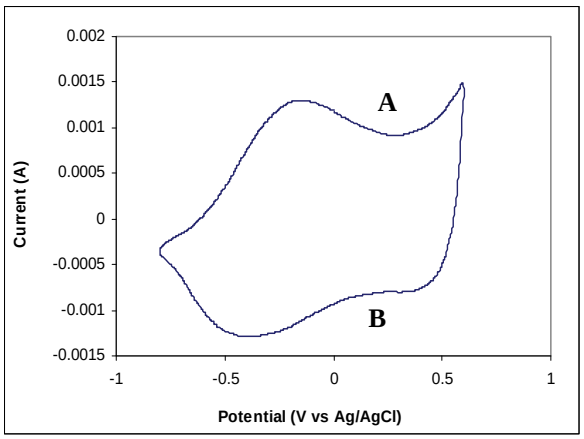

Figure 8. Cyclic voltammogram of PB-PPy-III. Range: -0.8 V to +0.6 V. Scan rate: 50 mV s^{-1}.

Conclusions

The conducting PPy thin coatings on nanopores of nanoporous PB were obtained by using vapor phase polymerization with ferric *p*-toluenesulfonate as oxidant. The highly ordered porous structure of PB precursor was preserved after modification as shown by SAXS and TEM. After incorporation of PPy coatings, previously insulating nanoporous polymers became conductive as verified by cyclic voltammogram. This method provides a general approach for producing conductive nanoporous polymers, which will have significant potential to be a novel nanometer-scaled electronic device.

References

1. E.J.W. Crossland, M. Kamperman, M. Nedelcu, C. Ducati, U. Wiesner, D.M. Smilgies, G.E.S. Toombes, M.A. Hillmyer, S. Ludwigs, U. Steiner, H.J. Snaith, Nano Letter 9 (2009) 2807-2812.
2. D.H. Kim, Z. Sun, T.P. Russell, W. Knoll, J.S. Gutmann, Adv. Funct. Mater. 15 (2005) 1160-1164.
3. B.J.S. Johnson, J.H. Wolf, A.S. Zalusky, M.A. Hillmyer, Chem. Mater. 16 (2004) 2909-2917.
4. T. Bein, P. Enzel, Angew. Chem. Int. Ed. 28 (1989) 1692 –1964.
5. M. Ikegame, K. Tajima, T. Aida, Angew. Chem. Int. Ed. 42 (2003) 2154-2157.
6. R. Guo, G. Li, W. Zhang, G. Shen, D. Shen, ChemPhysChem 6 (2005) 2025-2028.
7. F. Guo, J.W. Andreasen, M.E. Vigild, S. Ndoni, Macromolecules 40 (2007) 3669.
8. B. Winther-Jensen, J. Chen, K. West, G. Wallace, Macromolecules 37 (2004) 5930-5935.
9. S. Ndoni, M.E. Vigild, R.H. Berg, J. Am. Chem. Soc. 125 (2003) 13366.

List of Publications

1. F. Guo, K. Jankova, L. Schulte, M.E. Vigild, S. Ndoni, Langmuir (2009) DOI**:** 10.1021/la9025443.
2. S. Ndoni, L. Li, L. Schulte, P.P. Szewczykowski, T.W. Hansen, F. Guo, R.H. Berg, M.E. Vigild, Macromolecules 42 (2009) 3877.
3. F. Guo, K. Jankova, M.E. Vigild, S. Ndoni, Polymer Peprint 49 (2008) 540.
4. F. Guo, K. Jankova, L. Schulte, M.E. Vigild, S. Ndoni, Macromolecules 41 (2008) 1486.
5. F. Guo, J.W. Andreasen, M.E. Vigild, S. Ndoni, Macromolecules 40 (2007) 3669.

Mohd. Kamaruddin Abd. Hamid

Phone: +45 4525 2912
Fax: +45 4593 2906
E-mail: mka@kt.dtu.dk
WWW: http://capec.kt.dtu.dk
Supervisors: Prof. Rafiqul Gani
Asst. Prof. Gürkan Sin

PhD Study
Started: July 2007
To be completed: June 2010

Application of Decomposition Methodology to Solve Integrated Process Design and Control Problems for Reactor-Separator-Recycle Systems

Abstract
This paper addresses the integration of process design and control (*IPDC*) for reactor-separator-recycle (*RSR*) system and evaluates a decomposition-based methodology for solving a mixed integer dynamic optimization (*MIDO*) problem. The *MIDO* problem is decomposed into four hierarchical stages; (i) pre-analysis, (ii) design analysis, (iii) control analysis, and (iv) verification stage. In order to determine the optimal design-control decisions, the methodology makes use of graphical methods as an alternative to the use of optimization/search algorithms. The decomposition methodology was evaluated for the design of a *RSR* system involving consecutive reactions, $A \leftrightarrow B \rightarrow C$ and shown to provide effective solutions meeting design, control and cost criteria. The advantages of the methodology are that it is systematic, makes use of process knowledge and provides valuable insights to the solution of *IPDC* problem.

Introduction
A common feature of many chemical processes is the presence of recycle, where the unreacted reactant is recycled back to the reactor to increase the process economy when the conversion in the reactor is low. Integrating the reactor with separation unit through recycle stream however may exhibit the snowball effect where a small disturbance in the fresh rate will cause a very large disturbance to the recycle flow rate [1].

In this paper, we evaluated a decomposition-based methodology proposed by [2] for solving the integration of process design and control (*IPDC*) which is typically formulated as a mixed-integer dynamic optimization (*MIDO*) problem of a *reactor-separator-recycle* (*RSR*) involving consecutive reactions $A \leftrightarrow B \rightarrow C$. Accordingly the problem is decomposed and analyzed in four stages: (i) pre-analysis, (ii) design analysis, (iii) control analysis, and (iv) verification stage. This approach systematically reduces the search space of feasible solutions, thereby, making the solution of the final optimization problem easier to solve. In addition, the methodology makes use of graphical methods as an alternative to the use of optimization/search algorithms to help in determining the optimal design-control solution. The paper is structured as follows. The *IPDC* problem formulation based on decomposition methodology are introduced in the *Methods* section. Then, the implementation of the methodology in solving design-control problem of a *RSR* system is presented and discussed, which is followed by conclusions.

Methods
The *IPDC* problem is typically formulated as a *MIDO* problem in which a performance objective in terms of design, control and cost is optimized subject to process model, constitutive and process conditional constraints as shown in Figure 1.

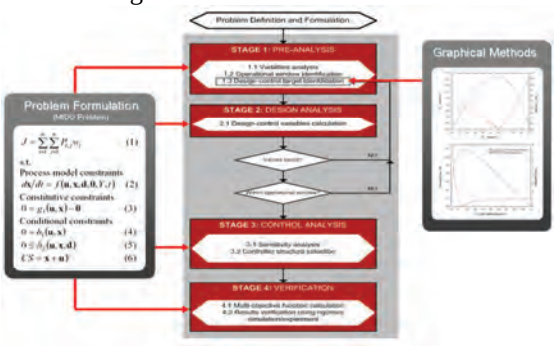

Figure 1: Decomposition-based solution strategy for *MIDO* problem [2].

The work flow and steps involved in the decomposition based solution strategy is also shown in Figure 1. Accordingly the problem is decomposed into four sequential stages: (1) pre-analysis; (2) design analysis;

(3) control analysis; and (4) verification stage. Detail descriptions of these four stages can be obtained in [3].

Results and Discussion

This section demonstrates the use of decomposition methodology in solving integrated design and control of a *RSR* system as illustrated in Fig. 2.

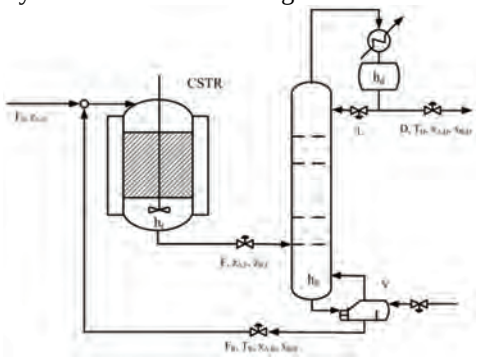

Figure 2: *RSR* flowsheet with a recycle of the distillation bottom flow rate.

We considered the following situation. In a continuous stirred tank reactor (*CSTR*), the product component *B* is to be produced from component *A*. Further reaction produces byproduct component *C* from *B*. The reaction scheme for this system is

$$A \underset{k_{-1}}{\overset{k_1}{\longleftrightarrow}} B \xrightarrow{k_2} C$$

The value of kinetic data are assumed to be k_1 = 5.1 s^{-1}, k_2 = 0.11 s^{-1}, and k_{-1} = 1.67 s^{-1}. We assume the effect of temperature on kinetic is negligible within the operating range. The pure component properties are tabulated in Table 1. The objective of the reactor is to produce component *B* ($z_{B,F}$), while the objective of the column is to keep 99% of component *A* in the bottom ($x_{A,R}$) (and 1% of component *A* in the top, $x_{A,D}$), i.e., $\mathbf{x}_1$ = [$z_{B,F}$ $x_{A,D}$ $x_{A,R}$]. The reactant-rich stream F_R is recycled back to the reactor. The objective is then to determine the design-control solution in which the multi-objective function is optimal. The feed conditions for this process are tabulated in Table 2.

Table 1: Pure component properties.

Property	*A*	*B*	*C*
M_w (g/mol)	100.24	100.24	100.24
T_c (K)	540.2	530.37	520.5
P_c (atm)	27.042	26.98	27.37
V_c (m^3/kmol)	0.43	0.42	0.42
T_m (K)	182.57	154.9	149.35
T_b (K)	371.58	363.20	352.34
$H_{combust}$ (kJ/kmol)	-4464730	-4459580	-4450820
Antoine equation			
A	7.10	7.20	7.08
B	1381.68	1429.67	1342.79
C	228.79	239.77	239.50

Stage 1: Pre-analysis.

Step 1.1: Analysis of variables

First, design and process variables are analyzed where the important variables which related to the objective function and operational constraints are identified. As shown in Fig. 2, five manipulated variables are available: reactor effluent (*F*), reflux flow (*L*), vapour boilup (*V*), product flow (*D*), and recycle (bottom) flow (F_R), hence $\mathbf{u}_0$ = [*F L V D* F_R]. As we need to control two liquid levels (condenser level h_d by manipulating *D* and column bottom level h_b by manipulating *Y*) to stabilize the column, we are left with three control degrees of freedom available for composition control, $\mathbf{x}_1$, which are here selected as $\mathbf{u}$ = [*F L V*].

Table 2: Feed conditions for a RSR system.

Variables	Value	Description
F_0	60 kmol/min	Feed flow rate
$z_{A,0}$	1.0 mole fraction A	Composition of *A*
T	433 K	Feed temperature
P	6 atm	Feed pressure

Step 1.2: Operational window identification

Next, the feasible operational window are identified in terms of dimensionless design variable (i.e. Damköhler number, $Da = k_1 C_{A,F} V/F$) where snowball effect can be avoided. Through manipulation of the mass balance equations, the dimensionless equations with respect to F_R and reactor effluent compositions ($z_{i,F}$) are obtained and plotted in Fig. 3. It can be observed that for the higher $z_{B,F}$ (see Fig. 3(a)) and also to eliminate the snowball effect (see Fig. 3(b)), the operational window for *Da* is identified within the range of $2 < Da < 50$ (Zone II).

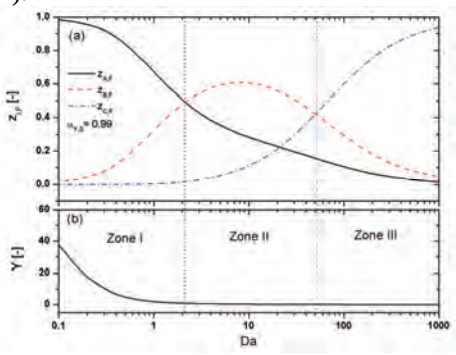

Figure 3: Operational windows for: (a) reactor outlet composition and (b) recycle flow rate F_R as a function of Da number.

Step 1.3: Optimal Design-Control Target Identification

Lastly, the target for the optimal design-control solution is identified using graphical methods; attainable region (*AR*) and driving force (*DF*) diagrams for reactor design and distillation design, respectively. The *AR* diagram is developed by plotting the response of the desired product, $z_{B,F}$ with respect to the response of reactant, $z_{A,F}$ as shown in Fig. 4(a). Then, the target for the optimal design-control solution for reactor is identified at the **maximum point of the *AR*** (point A). In Fig. 4(a) also, two other points which are not at the maximum are identified as candidate alternative designs for verification purposes (see stage 4). Fig. 5(a) shows plot of *DF* against composition. In this graphical method, the target for the optimal design-control solution for

distillation is identified at **the maximum point of the *DF*** (point D). The value of design variables that match targets at *AR* and *DF* diagrams are calculated for reactor and distillation, respectively, in the next stage.

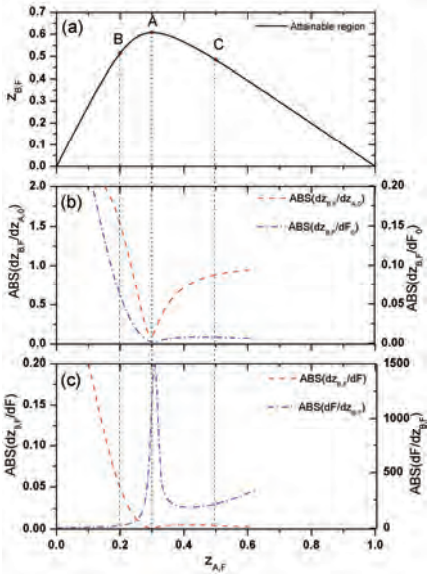

Figure 4: (a) *AR* diagram for the desired product composition, $z_{B,F}$ with respect to $z_{A,F}$, (b) Corresponding derivatives of $z_{B,F}$ with respect to disturbances ($z_{A,0}$ and F_0), (c) Corresponding derivatives of manipulated variable with respect to controlled variable.

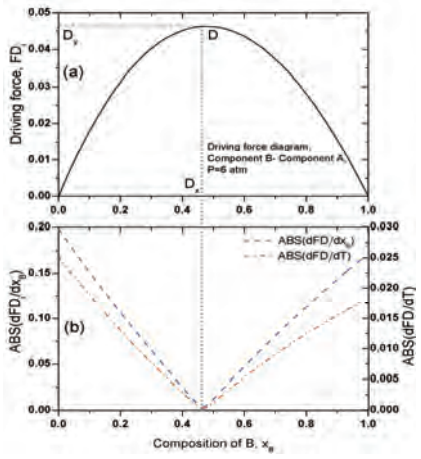

Figure 5: (a) *DF* diagram for the separation of components *B* and *A* by distillation, (b) Corresponding derivatives of the *DF* with respect to composition and temperature.

Stage 2: Design Analysis.

Step 2.1: Design Variables Calculation.

In this stage, the values of design variables are calculated for reactor and for distillation that match targets identified at the *AR* and *DF* diagrams in stage 1. The results are given in Table 3 and Table 4 for reactor and distillation, respectively. From Table 3, it can be seen that values of reactor volume and corresponding flow rates can be obtained for these three candidate reactor designs. In Table 4, values of distillation design variables corresponding to the maximum point of *DF* diagram (point D) for three different reactor designs can also be obtained.

Table 3: Values of controlled-manipulated variables at different reactor designs.

Reactor design	*Controlled*		*Manipulated*		
	$z_{A,F}$	$z_{B,F}$	F *(kmol/min)*	F_R *(kmol/min)*	V (m^3)
A	0.30	0.61	71.6	25.5	1.6
B	0.21	0.53	67.3	15.5	5.1
C	0.50	0.48	84.6	59.3	0.4

Table 4: Values of controlled-manipulated variables for distillation at point D for different reactor designs.

Reactor Design	*Controlled*					
	$x_{A,D}$	$x_{B,D}$	$x_{A,R}$	$x_{B,R}$	T_D *(K)*	T_R *(K)*
A	0.01	0.87	0.99	0.01	436.3	446.6
B	0.01	0.67	0.99	0.01	434.1	446.6
C	0.01	0.91	0.99	0.01	438.0	446.6
Reactor Design	*Manipulated*					
	N_S	N_F	L *(kmol/min)*	V *(kmol/min)*	Q_c *(kJ/min)x10*^{6}	Q_r *(kJ/min)x10*^{6}
A	65	34	730.8	337.5	-2.35	2.37
B	65	34	730.8	204.7	-2.33	2.34
C	65	34	730.8	784.3	-3.40	3.43

Stage 3: Control Analysis.

Step 3.1: Sensitivity Analysis.

In stage 3, the control structure design of the selected design candidates (reactor designs A, B, C) is analyzed for the purpose of validation. In this respect, two criteria are looked at: (a) process sensitivity with respect to disturbances, which should be low and (b) sensitivity of manipulated variable with respect to controlled variable, which should be high. The process sensitivity is analyzed by calculating the derivative of the controlled variables with respect to disturbances. Fig. 4(b) shows plots of derivative of $z_{B,F}$ with respect to $z_{A,0}$ and F_0 at different reactor designs. It can be seen that the derivative values are smaller for reactor design A compared to other designs (B and C). In Fig. 5(b) derivative plots of the *DF* with respect to composition of *B* and temperature are shown and at the maximum point of *DF* the derivative values are smaller. Smaller value of derivative to disturbances means process sensitivity is lower, hence the impact of disturbance on the process performance stability is less pronounced. As a result, from a control point of view, reactor design A and column design D are less sensitive to the effect of disturbances, which makes them easier to operate at the optimal set-points.

Step 3.2: Controller Structure Selection

Next, the controller structure is selected, i.e. pairing of manipulated-controlled variables and their set points. The controlled variable which is found less sensitive to the effect of disturbances is selected here. For a reactor it can be seen that $dz_{B,F}/dz_{A,0}=(dz_{B,F}/dh)(dh/dz_{A,0})\approx 0$ and $dz_{B,F}/dF_0=(dz_{B,F}/dh)(dh/dF_0)\approx 0$ at point A (see Fig. 4(b)). This means that the composition $z_{B,F}$ and reactor level controllers are optimal at the corresponding set-

points, i.e. the maximum point of *AR*. At this point, any big changes to the disturbances ($z_{A,0}$ and F_0) will result in smaller changes in the $z_{B,F}$ compared to other points. For controller structure, a cascade control is found suitable [4], in which controlling the product concentration ($z_{B,F}$) at the set point is the objective (master controller), while reactor level h_r is the secondary (slave) controlled variable which manipulates the effluent reactor flow rate, F (see Fig 6). As abovementioned, the optimal set point value of controlled variables ($z_{B,F}$) is selected at the highest *AR* point.

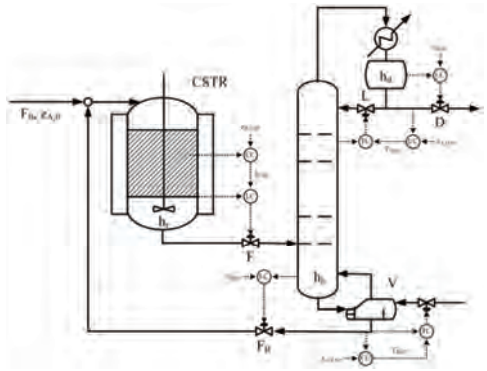

Figure 6: Proposed control structure for a *RSR* system.

The sensitivity of the manipulated variable (F) with respect to controlled variables ($z_{B,F}$) is then analyzed and shown in Fig. 4(c). It is clearly shown that, value of $dF/dz_{B,F}$ is bigger at reactor design A than reactor designs B and C. The big value of $dF/dz_{B,F}$ means the process gain is high, thus, the controlled variable is very sensitive to the changes in the manipulated variable thereby requiring smaller control action. Therefore, control action at a reactor design A is smaller meaning less costly than in designs B and C.

For the distillation column, it can bee seen that $dFD_i/dT=dFD_i/dx_B\approx 0$ at the maximum point of *DF* (see Fig. 5(b)). This means that the composition and temperature control is feasible [4]. At the highest *DF* point, both controllers are less sensitive to the composition and temperature variations (see Fig. 5(b)). Both composition and temperature control are feasible by manipulating reflux L and vapour boilup V for distillate and bottom controllers, respectively. Therefore, two composition-to-temperature cascade control structures were proposed for a distillation as shown in Fig. 6.

Stage 4: Verification.

Step 4.1: Multi-objective function calculation: verification of design.

The multi-objective function is calculated by summing up each objective function value using equal weights, meaning that the decision-maker doesn't have any preference of one objective over another. The multi-objective function is then reformulated as the maximization of $P_{1,j}$, $1/P_{2,1}$, $P_{2,2}$ and $1/P_{3,j}$. Since the range and unit of multi-objective values can be different, each objective value is normalized with respect to its maximum value. This is given in Table 5. $P_{1,1s}$ corresponds to the scaled value of $z_{B,F}$. $P_{2,1s}$ and $P_{2,2s}$ are the scaled value of $dz_{B,F}/dz_{A,0}$ and $dF/dz_{B,F}$, represent process sensitivity and process gain, respectively. Whereas, $P_{3,1s}$, $P_{3,2s}$, $P_{3,3s}$ and $P_{3,4s}$ are the scaled value of reactor volume, recycle flow rate, condenser and reboiler duties, respectively, which represent capital and operating costs. It can be seen that, value of J at reactor design A is higher followed by reactor designs C and B, respectively. Thus it is verified that the optimal solution to integrated design and control of a *RSR* system which satisfies the design, control and cost criteria is given at reactor design A, which is obtained using the graphical methods.

Table 5: Multi-objective function values at different reactor designs.

Point	$P_{1,1s}$	$P_{2,1s}$	$P_{2,2s}$	$P_{3,1s}$	$P_{3,2s}$	$P_{3,3s}$	$P_{3,4s}$	J
A	1.00	0.01	1.00	0.32	0.43	0.94	0.93	105
B	0.87	0.24	0.06	1.00	0.26	0.93	0.92	12
C	0.79	1.00	0.20	0.08	1.00	1.00	1.00	18

$P_{i,js}$ = scaled value

Conclusions

We presented the integration of process design and control (*IPDC*) for reactor-separator-recycle (*RSR*) system and evaluated a novel solution strategy based on decomposition for solving what is typically a mixed integer dynamic optimization (*MIDO*) problem. The *MIDO* problem is decomposed into four stages (i) pre-analysis, (ii) design analysis, (iii) control analysis, and (iv) verification, which became relatively easier to solve. The methodology also makes use of graphical methods as an alternative to the use of optimization/search algorithms for determining the optimal design-control decisions. The results showed that the methodology provided effective solutions to integrated design and control of a *RSR* system that meet design, control and cost criteria. The advantages of this new solution methodology are the following (a) it is systematic, (b) makes use of process knowledge and (c) provides valuable insights to the solution of *IPDC* problem.

References

1. W. L. Luyben, C. A. Floudas, Analyzing the interaction of design and control – 2. reactor-separator-recycle system.. *Comput. & Chem. Eng.*, 18 (10) (1994) 971-993.
2. M. K. A. Hamid, R. Gani, A model-based methodology for simultaneous process design and control for chemical processes. In: *Proceedings of the FOCAPO 2008*, Massachusetts, USA, 2008, p. 205-208.
3. M. K. A. Hamid, G. Sin, R. Gani, Determination of optimal design and control decisions for reactor-separator system with recycle. In: M. M. El-Hawagi & A. A. Linninger, *Design for energy and the environment*, CRC Press, 2009, p. 593-602.
4. D. E. Seborg, T. F. Edgar, D. A. Mellichamp, *Process dynamics and control, 2nd. Ed.* John Wiley & Sons, 2004.

Martina Heitzig

Phone: +45 4525 2986
Fax: +45 4588 2258
E-mail: mat@kt.dtu.dk
WWW: http://www.kt.dtu.dk
Supervisors: Rafiqul Gani
Peter Glarborg
Gürkan Sin

PhD Study
Started: December 2008
To be completed: November 2011

Computer-Aided Modelling for Efficient and Innovative Product-Process Engineering

Abstract
Model-based computer aided product-process engineering requires models of different types, forms and application mode. In this project a computer-aided modelling framework capable of handling the modelling needs for product-process design and analysis is being developed. The framework supports the systematic and efficient development of multi-scale models, their interconnections, numerical analysis, parameter regression and solution. Two case studies, one dealing with the thermal treatment of the off-gas stream of the adipic acid production and the second related to the batch uptake of lysozyme by sepharose are briefly presented to validate the methodology.

Introduction
Models are playing roles of increasing importance in design and analysis of chemicals/bio-chemicals based products and the processes that manufacture them because of the increasing use of computer-aided methods and tools. The advantage of using these model-based methods and tools is that they have the potential to reduce the number of experiments, which can be expensive and time consuming, while at the same time, lead to truly innovative solutions. As the required models may be complex and require multiple time and/or lengths scales, their development and application for product-process design is not trivial. Therefore, the modelling framework can contribute by reducing the time and resources needed for model development and application, thereby reducing the overall time and cost for product-process development.

Specific Objectives
The idea is to provide the wok-flow and the data-flow for solving model development problems from a large variety of chemical and biochemical engineering applications. Based on that a computer-aided modelling framework is developed which guides the user through the steps of the work-flow and at each step the required expertise, tools and database connections are provided.

Results and Discussion
So far, the modelling framework consists of two interconnected workflows (Figure 1). The first one is for the development of multi-scale models and the second one is for model identification. Certainly, both frameworks need to be interconnected but they can also be applied separate from each other if required.

The first step for multi-scale model development is to define the modelling objective. In the second step, corresponding to the modelling objective, available information on the system and the occurring phenomena is collected. With this information in place, the main assumptions which hold true for the different scenarios that need to be covered for the specific design problem are specified (step 3). In step 4 various modelling scenarios of interest are listed and models of the different scales are generated. In general, it is good practice to start with the simplest scenario and to gradually increase the model complexity by adding new scales. Steps 5-9 need to be repeated for each multi-scale scenario listed in step 4. First the model assumptions are formulated for each scale and based on that the model equations are derived or retrieved from library. The next step is to perform a numerical analysis of the models on each scale. That means that the types of the variables need to be specified, a degree of freedom analysis is performed, the incidence matrix is generated and based on that the equations are ordered to the optimal form for model solution. If there are parameters that need to be regressed, it is done in step 7. At this point the regression work-flow (Figure 1, right) will take over. In step 8, the models of different scales are combined according to the established work-flow.

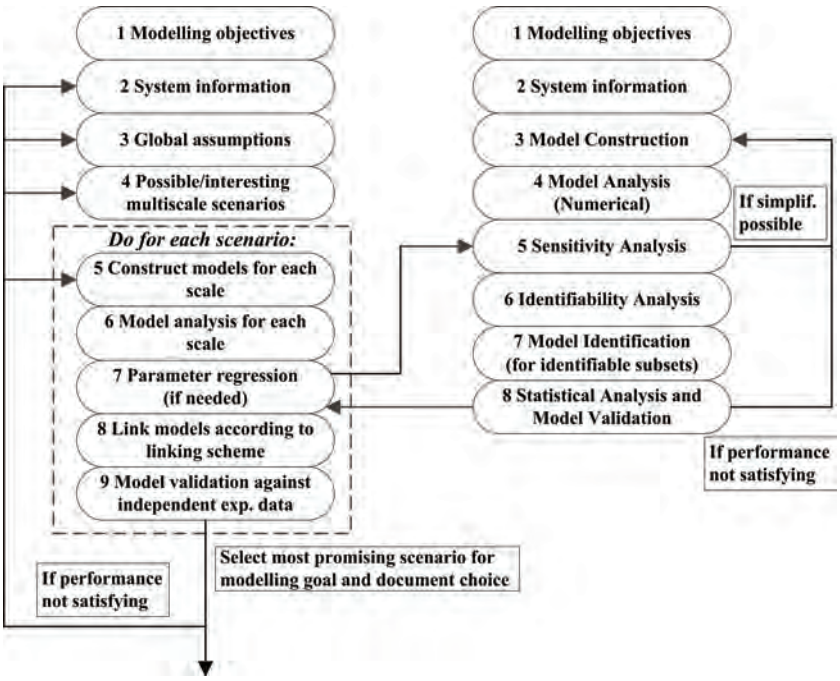

Figure 1: Work-flow for multi-scale modelling (left) and model identification (right)

All missing tools and features required to solve the different steps of the methodology are implemented into the modelling toolbox ICAS-MoT [1] which has a very friendly user-interface showing all the required steps for the model development. Figure 2 shows important features of ICAS-MoT.

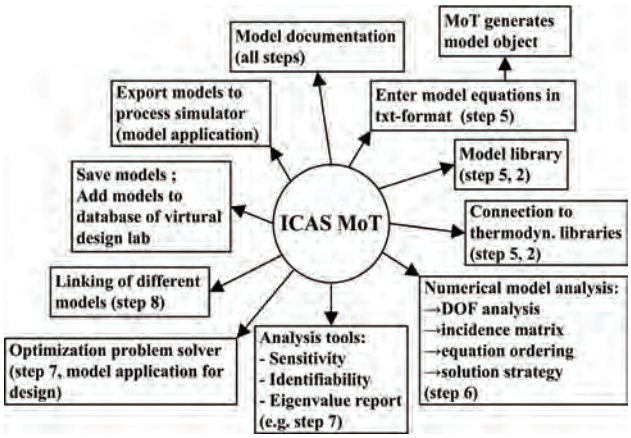

Figure 2: Overview over important ICAS-MoT features

Case Studies

Two different case studies in order to validate and further develop the methodology have been solved.

The first case study is related to combustion and deals with the thermal treatment of the off-gas stream of the adipic acid production in a flow reactor in order to reduce its N_2O- concentration [2]. The modelling objective is to provide a model for the reactor design.

The second case study deals with the batch uptake of lysozyme by sepharose beats and was taken from [3]. The goal is to provide a model that can be applied for product design and more precisely for monitoring the product behavior of the sepharose beats. This case study has been chosen because it requires the development and interconnection of models on multiple length scales like it is typically required for product design problems.

Conclusions

A generic methodology (work-flow and data-flow) to develop multi-scale models and for model identification have been developed. Based on that a conceptual computer-aided modelling framework has been constructed. All required tools and features of the framework have been implemented in the existing modelling toolbox ICAS-MoT. The methodology as well as the framework have been validated applying case studies from different areas in chemical engineering. Current and future work is the extension and refinement of the methodology by solving more case studies and the implementation of the corresponding features into ICAS-MoT so that interesting product-process design problems can be solved.

Acknowledgements

This PhD project is funded by a scholarship from the Technical University of Denmark.

References

[1] A. M. Sales-Cruz, Development of a Computer Aided Modelling System for Bio and Chemical Process and Product Design, PhD Thesis, Technical University of Denmark, 2006.
[2] P. Glarborg, J.E. Johnsson, K. Dam-Johansen, Combustion and Flame 99 (1994) 523-532.
[3] A.M. Lenhoff, Langmuir 24 (2008) 5991-5995.

Jesper Holck
Phone: +45 4525 2979
E-mail: jeh@kt.dtu.dk
WWW www.bioeng.kt.dtu.dk

Supervisors: Anne S. Meyer
Jørn Dalgaard Mikkelsen

PhD Study
Started: November 2007
To be completed: December 2010

Enzymatic Production of Prebiotics from Sugar Beet Pectin

Abstract
The potential importance of dietary fibres and oligosaccharides in modulating the microbial ecology of the human colon to exert beneficial health effects is currently receiving significant attention. By targeting dietary fibre structures and prebiotics by selective enzymatic hydrolysis of complex plant substrates, such as pectin, defined poly- and oligomers can be derived.

Introduction
Dietary fibres and prebiotics are non-digestible dietary carbohydrate structures that can be health promoting by supporting the growth of beneficial bacteria in the human colon, such as *Bifidobacterium sp*. and via other mechanisms [1]. This PhD project builds on that a significant potential exists for targeting dietary fibre and prebiotics structures by selective enzymatic hydrolysis of pectinaceous plant cell wall structures present in sugar beet pulp – the byproduct stream left over from industrial production of sugar.

Project outline
The focus of the project is on enzyme assisted modification of sugar beet pectin in order to manufacture target oligomer products which can have a potential beneficial effect. The production is made via an intelligent reaction optimisation and combination of monoactive experimental enzymes available in the Prebiotics Center. A particular focus area will be on characterising the action of these enzymes in modification of pectin rhamnogalacturonan I (RG I) (see Figure 1).

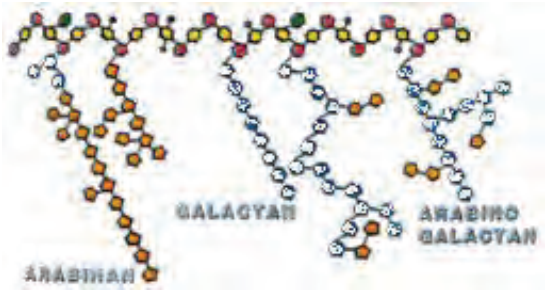

Figure 1. schematic structure of rhamnogalacturonan I

RG I is a heteropolysaccharide composed of a rhamnogalacturonan backbone with arabinan, galactan, and arabinogalactan side chains. The design of optimal enzyme reactions, including only the required activites for the particular target substrate and target product, will be done via an iteration of advanced structural substrate and product analyses in systematic enzymatic treatments using monoactive enzymes. The research will include reaction parameter optimisations of selected reactions. The experimental work will be conducted to allow obtainment of new realizations about enzyme cascade action patterns on RG I and other pectin structures, including quantitative kinetics on branched plant cell wall polysaccharides.

Specific objectives
In order to tailor the enzymatic treatment, the first challenge is to establish methods for thorough analysis of the substrate structure and the product oligomers. Therefore initial experiments on the monocomponent composition are required.
Secondly,

Results
A monocomponent composition analysis of modified high molecular weight pectin extracted from sugar beet pulp has been performed using standard acid hydrolysis followed by HPAEC-PAD analysis. The results on mole basis are compared to other published data for sugar beet pectin composition [2] on figure 2. These results showed a lower level of arabinose which might be due to loss of arabinan sidechains during the extraction. The decrease in arabinose content gives a relatively higher content of galacturonic acid. The ratio between

rhamnose and galacturonic acid indicate that a relatively large amount of the pectin consists of homogalacturonan.

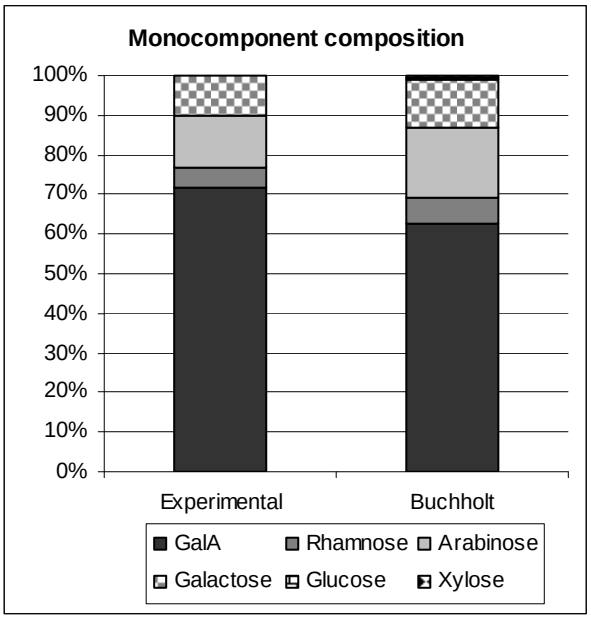

Figure 2. Comparison of composition on mole basis of modified sugar beet pectin from experimental data and [2].

These results is the first step in the progress of designing a properly targeted enzyme biocatalysis followed by construction of statistically designed combinations of monoactive experimental enzymes for contriving optimal "minimal" enzyme cocktails.

Acknowledgements

The project is anchored in the Center for Biological Production of Dietary Fibres and Prebiotics at DTU ("Prebiotics Center"), granted by DSF. The project has significant involvement from Danisco A/S which provides the sugar beet pectin and pulp.

References

1. Rastall, R.A., Gibson, G.R., Gill, H.S., Guarner, F., Klaenhammer, T.R., Pot, B., Reid, G., Rowland, I.R. and Sanders, M.E. (2005). Fems Microbiology Ecology 52, 145-152.
2. Buchholt, H.C., Christensen, T.M.I.E., Fallesen, B., Ralet, M.C. and Thibault, J.F. (2004). Carbohydrate Polymers 58, 149-161.

Martin Høj
Phone: +45 4525 2842
Fax: +45 4588 2258
E-mail: mh@kt.dtu.dk

Supervisors: Jan-Dierk Grunwaldt
Anker Degn Jensen

PhD Study
Started: September 2009
To be completed: September 2012

Nanoparticle Design using Flame Spray Pyrolysis for Catalysis

Abstract
Flame spray pyrolysis is a novel method for fast preparation of metal oxide nanoparticles. Precursors are dissolved in an organic solvent and sprayed into a supporting methane flame at high velocity forming small droplets. When the droplets are combusted metal oxides are formed as nanoparticles due to rapid temperature quenching. The project is to utilize this method for the preparation of heterogeneous catalysts. Interesting systems include selective oxidation, hydrotreating and higher alcohol synthesis catalysts. As part of the PhD project I am building up a catalyst test bench to study the selective oxidation of propane to propene.

Introduction
Production of nanoparticles by flame spray pyrolysis (FSP) was first demonstrated by Bickmore *et al.* in 1996 [1] and the full potential of the method for control of particle size and morphology was demonstrated by Mädler and Pratsinis *et al.* in 2001-2002[2-3].

The setup used by these researchers is similar to the setup at DTU Chemical Engineering, see Figure 1. The precursor solution is pumped by a syringe pump through a capillary tube into the middle of the nozzle where it is dispersed by a high velocity stream of oxygen. Surrounding the capillary tube a ring of premixed methane/oxygen flames ignites the flammable precursor solution.

The produced nanoparticles are collected on a glass fiber filter with the aid of a vacuum pump. The powder is collected from the filter and can be used in catalytic tests at microreactor scale or investigated by spectroscopy and electron microscopy [4-5]. It is also possible to collect the particles on a porous substrate, which is interesting for example in automotive catalysis.

Several examples of catalysts made by FSP can be found in the literature, like supported nobel metal catalysts [6] and mixed oxides [7]. The field of FSP made catalysts has been reviewed by Strobel *et al.* [8]. The materials are non-porous and can be prepared with very high surface area. High surface area is generally an advantage for high catalytic activity and mass-transfer is not limited by the size of the pores.

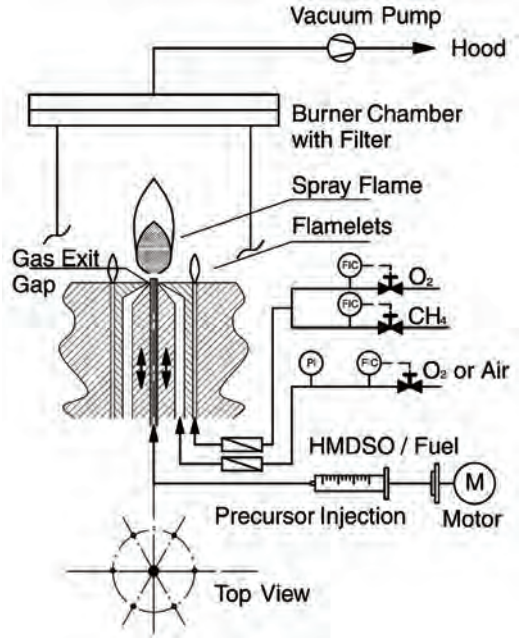

Figure 1: Schematic of the flame spray pyrolysis setup. The flamelets are small flames of methane and oxygen premixed at stoichiometric ratio. They ignite the flammable precursor solution and the twofold purpose of the dispersion gas is to spray the solution into small droplets and provide the oxidizer for the combustion. The solution contains metal precursors which are combusted to nanosized oxides. The nanoparticles are collected on the filter using a vacuum pump.

Specific objectives
The objectives of my project are to prepare catalytically

active nanomaterials using the FSP method. The catalysts will be tested for their catalytic activity and thephysical and chemical structure will be investigated using spectroscopy and electron microscopy. Especially X-ray absorption spectroscopy, which can only be performed at synchrotron facilities, is interesting for investigating the local chemical environment of metal atoms.

The prepared catalysts will be compared to similar catalysts prepared by conventional methods, both with respect to activity and physical and chemical structure.

Catalytic materials of interest include mixed metal oxides where the two metals have different valance, such as Al-Si, Al-Ti, Nb-Si, Nb-Ti and Mg-Al. These oxides have acidic sites and are used as catalysts for hydrocracking. Alumina supported Co-Mo oxides, which are catalysts for hydrodesulphurization and synthesis of higher alcohols from synthesis gas, are also of interest.

The final system to be investigated is selective oxidation of propane to propene using oxygen. This reaction is catalyzed by supported vanadium and molybdenum oxides, possibly mixed with Li, Mg, Cr, Co, Ni, Ga, Zr, Nb, Cs or W. Reaching high conversion, selectivity and productivity is a challenge [9].

Besides catalyst preparation, testing and characterization the project includes building a new automated test setup with three micro reactors and GC-MS analysis, where 50-500 mg of catalyst can be tested at ambient pressure at temperatures up to 750 °C.

Results

The flame spray pyrolysis setup has been taken into operation. The first test is to prepare silica from a solution of hexamethylsiloxane (HMDSO) in xylene or ethanol solution to test the effect of different experimental conditions. The powders produced are nanoparticles with BET specific surface areas 143 to 265 m^2/g.

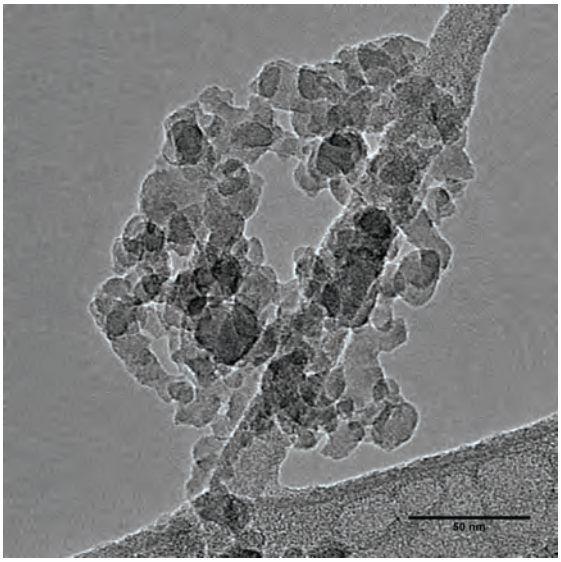

Figure 2: TEM image of FSP produced silica particles. The big fiber in the background is the TEM carbon grid.

This corresponds to approximately 10 to 19 nm particles, depending on flow rate of precursor solution and oxygen dispersion gas. The transmission electron microscopy (TEM) image in Figure 2 shows particles of this size, but they are irregularly shaped and polydisperse. This is expected for amorphous silica.

The catalytic test setup for selective oxidation of propane has been designed with three independent reactors in a series/bypass setup allowing automated sequential tests of three catalysts. The design includes a two channel GC-MS setup for gas analysis. Further detailed planning is needed before construction can begin in early 2010.

Discussion

Further work is needed to test the influence of the experimental conditions on the product powder, especially particle size.

Conclusions

Dispite the project is in its starting phase, the first nanoparticles have already successfully been prepared, but further investigations are needed before the FSP setup can be taken into normal operation.

Acknowledgements

Supervisors Jan-Dierk Grunwaldt and Anker Degn Jensen, Michael Brorson (Haldor Topsøe), Tobias Dokkedal Elmøe and help of Henrike Grossmann during her ERASMUS project.

References

1. C.R. Bickmore, K.F. Waldner, D.R. Treadwell, and R.M. Laine, J. Am. Ceram. Soc. 79 (1996) 1419-1423.
2. H.K. Kammler, L. Mädler, and S.E. Pratsinis, Chem. Eng. Technol. 24 (2001) 583-596.
3. L. Mädler, H.K. Kammler, R. Mueller, and S.E. Pratsinis, J. Aerosol Sci. 33 (2002) 369-389.
4. S. Hannemann, J.-D. Grunwaldt, P. Lienemann, D. Günther, F. Krumeich, S.E. Pratsinis, and A. Baiker, Appl. Catal., A 316 (2007) 226-239.
5. S. Hannemann, J.D. Grunwaldt, F. Krumeich, P. Kappen, and A. Baiker, Applied Surface Science 252 (2006) 7862-7873.
6. R. Strobel, J. Grunwaldt, A. Camenzind, S. Pratsinis, and A. Baiker, Catal. Lett. 104 (2005) 9-16.
7. W.Y. Teoh, R. Setiawan, L. Mädler, J.D. Grunwaldt, R. Amal, and S.E. Pratsinis, Chem. Mater. 20 (2008) 4069-4079.
8. R. Strobel, A. Baiker, and S.E. Pratsinis, Adv. Powder Technol. 17 (2006) 457-480.
9. F. Cavani, N. Ballarini, and A. Cericola, Catal. Today 127 (2007) 113-131.

Norazana binti Ibrahim
Phone: +45 4525 2922
Fax: +45 4588 2258
E-mail: nbi@kt.dtu.dk
WWW: http://www.chec.kt.dtu.dk
Supervisors: Prof. Kim Dam-Johansen
Assoc.Prof. Peter Arendt Jensen

PhD Study
Started: July 2007
To be completed: June 2010

Flash Pyrolysis of Biomass

Abstract
In this work, wheat straw, rice husk and pine wood were pyrolyzed in a pyrolysis centrifuge reactor (PCR) to produce liquid oil, solid char and non-condensable gasses. The main aim was to investigate the influence of biomass types, particularly the present of mineral matters, on the pyrolysis product yields. The reactor temperatures were varied between 475 °C to 575 °C. The ash content in wheat straw, rice husk and pine wood were 6.02, 13.6 and 0.5 % db, respectively. Wheat straw contains high potassium and magnesium, rice husk has a high silica content and pine wood characterized by high calcium content. The experimental results showed that the optimum yield temperature for straw was at 525 °C and at 550 °C for both rice husk and pine wood, with a maximum liquid organics yield of 50, 55 and 58 wt % (daf) respectively. The gas + water yield was higher for straw. The presence of alkali metals in biomass ash significantly affect the pyrolysis products yield and pyrolysis behavior by shifting the optimum degradation temperature and by catalyzing the conversion of tar to gasses.

Keywords: Flash pyrolysis, biomass, ash, bio-oil

Introduction
The flash pyrolysis process is a promising solid biomass thermal conversion route to produce a nearly ash-free liquid fuel with a high volumetric energy density. During pyrolysis, biomass is thermally decomposed without an oxidizing agent to produce a solid charcoal, liquid oil and gases. The char contain most of the inorganic components and it can be used as an energy carrier or as a soil fertilizer [1,2]. The pyrolysis gas can be used to generate electricity or to provide heat for the pyrolysis process. The pyrolysis gas consists mainly of carbon monoxide, carbon dioxide and light hydrocarbons. Also, the liquid oil can be directly used without any upgrading as a fuel oil in many combustion applications such as boilers. Upgrading is needed if the bio-oil shall be applied to a vehicle engine. The liquid oil is composed of a large variety of higher molecular weight species, organic acids, aldehydes, alcohols, phenols and other oxygenates. This oil is also known as a pyrolysis liquid, bio-oil or tar and has a lower heating value of about half that of conventional fuel oil [3]. The pyrolysis oil can undergo secondary reactions to be further broken down into gas, refractory tar and water [4,5]. The distribution and the yield of the pyrolysis products depend on several operating parameters including temperature, heating rate, types of biomass, biomass particle size, reaction condition, and reactor configuration, as well as the extraneous addition of catalysts [6].

At the CHEC research centre, a patented flash pyrolysis technology the pyrolysis centrifuge reactor (PCR) has been developed. In the present study the pyrolysis product yields of three biomasses, straw, wood and rice husk have been investigated on the PCR as a function of pyrolysis temperatures.

Specific Objectives
The main objective of the current study is to investigate the influence of biomass types on the flash pyrolysis products yield in the reactor temperature domain of 475-575 °C.

Experimental Section
Pyrolysis of wheat straw, pine wood and rice husk were carried out in a bench scale of Pyrolysis Centirfuge Reactor (PCR) developed at CHEC DTU, by employing flash pyrolysis principle as shown in Figure 1. The principle of the process is by tangentially feeding solid biomass particles into the horizontally oriented Ø 82 x 200 mm tubular reactor. The centrifugal force created by the rotation of three blade rotors keeps the particles

sliding on the heated wall while passing through the reactor. The solid particles transform to vapors by the high efficiency of heat transfer and while undergoing reaction, particles move down the reactor pipe before leaving suspended in the gas through the tangential outlet. Larger char particles were removed by a change-in-flow separator whereas fines were collected by the cyclone. Vapors were condensed in a direct water cooled condenser (bubble chamber) filled with previously produced bio-oil. Aerosols that were not retained by the condenser were collected in a coalescer filled with ROCKWOOL (fibers). The gas was pumped to the preheater and heated to 400 °C before it is recirculated to the reactor in order to maintain a desired gas residence time and avoid condensation of liquid products within the reactor. The amount of produced gas was measured by a temperature compensated gas meter and a sample was collected in a gas bag.

In this work, the biomass feedstock was fed to the reactor of approximately 20-23 g/min and with an approximately gas residence time of 0.3 s, a particle residence time of 180 s and initial heating rate of approximately 250-1000 °K/s. The performed measurements made it possible to determine the yield of char, gas, water and oil of the single measurements.

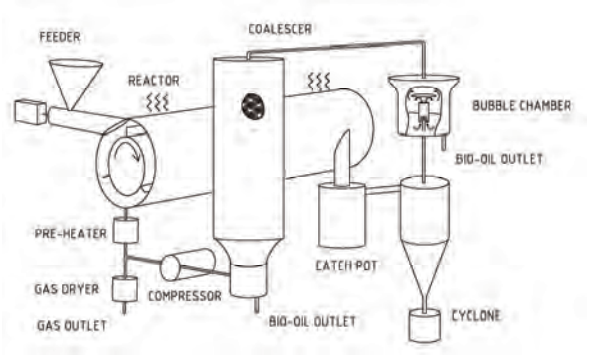

Figure 1: Schematic diagram of the developed ablative pyrolysis bench reactor system.

Results and Discussion

The chemical composition of a feedstock has a major influence on the flash pyrolysis products distribution. Figure 2 lists the chemical properties of wheat straw, rice husk, and pine wood to highlight the particular differences in feedstock. Rice husk is characterized by low volatile matter and high ash content compared to the wheat straw. Pine wood has the highest volatile matter and the lowest ash content.

The biomass ash mainly comprises of K, Ca, Mg, Si, Al, Fe, Ti, Na, and P. The ash content in straw, rice husk and pine wood were 6.02, 13.6 and 0.50 % wt db respectively. The straw ash is dominated by K, Mg and Na while rice husk ash is dominated by Si and pine wood ash has a high Ca content. Especially, alkali metals are known to catalyze the pyrolysis process such that a relatively high gas and char yield are obtained and a relatively low liquid organics yield [8].

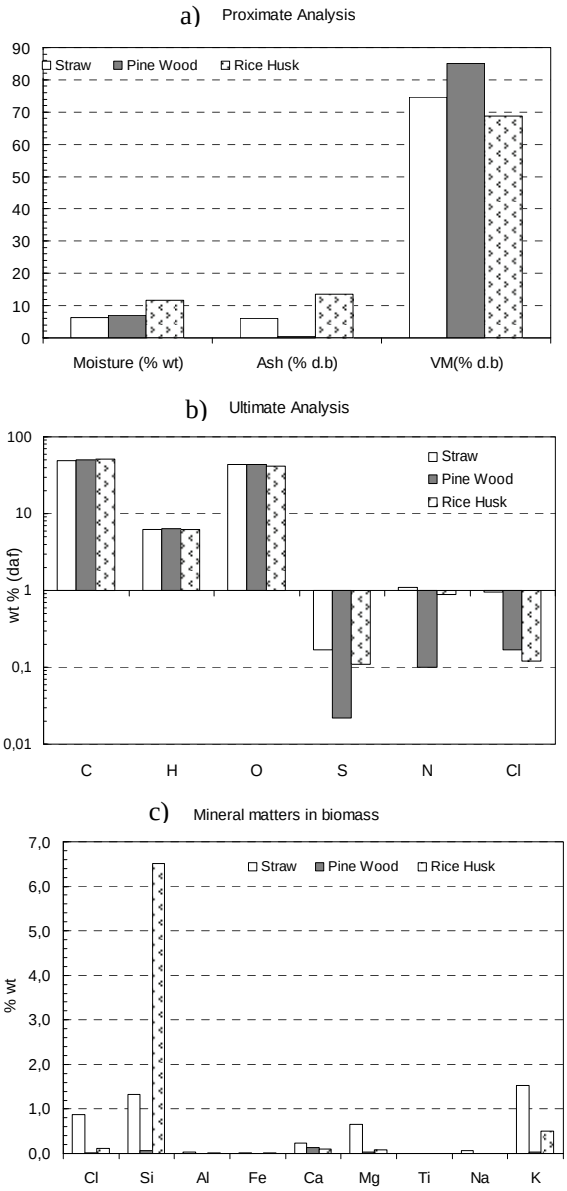

Figure 1. Chemical analysis of biomass a) Proximate analysis b) Ultimate analysis c) Mineral matters in biomass

Liquid Organics

Figure 2 shows the yields of liquid organics, char and gas + water generated from straw, wood and rice husk. In general, a maximum organics yield is obtained at an intermediate temperature. At high temperatures, a part of the tar decomposes and larger amounts of gas are formed.

The liquid organics yield from straw attained a maximum level at a reactor temperature of 525 °C (see Figure 2a). The maximum liquid organics yield from pine wood and rice husk was observed at 550 °C. The

lower maximum yield temperature of straw is probably caused by the high potassium straw content that shifted the cellulose and hemicellulose decomposition to a lower temperature. Previous study showed that the addition of KCl to the washed straw moved the cellulose decomposition to lower temperature by about 8 % [8].

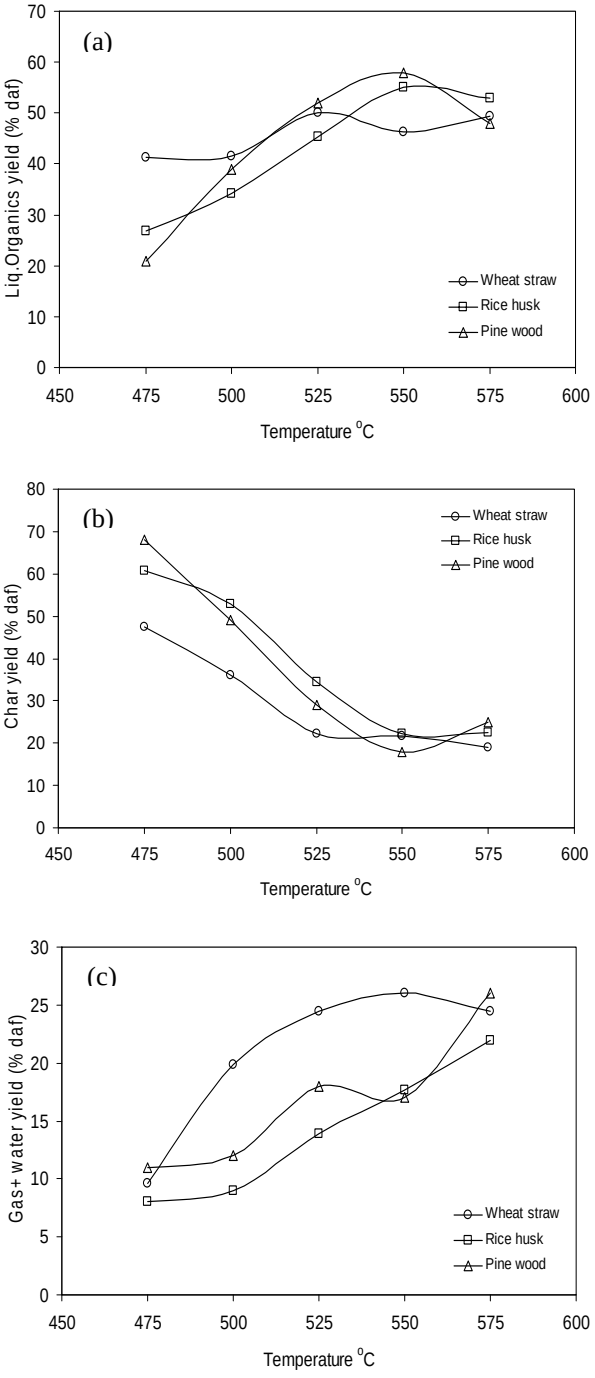

Figure 2. Flash pyrolysis product yields as a function of pyrolysis temperature

At optimum temperature, pine wood has the highest liquid organics yield followed by rice husk and finally straw. The maximum liquid organics yields for pine wood, rice husk and straw were 58, 55 and 50 % wt daf, respectively. The higher amount of Ca content in pine wood results in a higher liquid yield. The lower organics maximum yields of rice husk and straw compared to wood at temperature above 500 °C are probably caused by the alkali metals that catalyze a conversion of tar and fed to gas.

Char

The char yields for all biomasses types show a declining trend with increasing temperatures (see Figure 2b). Overall, the highest char yield is obtained from rice husk followed by pine wood and finally wheat straw. This can be explained by the high ash content in rice husk that is dominated by Si (> 85 % wt) that is retained in the char. The lowest char yield for straw is due to the high potassium content that catalyzed the pyrolysis process, to form more gasses and thus reducing char yield.

Gas + Water

The formation of gas and water during pyrolysis is shown in Figure 2c. The yield of gas + water kept increasing with pyrolysis temperatures. The high yield at high temperatures is causes by the pyrolysis oil vapor being converted into gases and water through secondary cracking of tar. It can be seen that straw produces high yield of gas+ water compared to others and this result is in good agreement with other findings [9]. The higher gas + water yield for wheat straw is mainly due to high potassium content in straw and thereby decreasing the char yield and it is simultaneously explain why straw char is the lowest compared to others.

Conclusion

The variation of alkali metals in wheat straw, rice husk and pine wood were investigated by pyrolyzed these feedstock materials by means of a pyrolysis centrifuge reactor. Potassium, magnesium, calcium and sodium, are the major alkali metals in biomass ash that can significantly affect the pyrolysis products yield and pyrolysis behavior. The maximum organics yield for straw occurred at 525 °C and at 550 °C for both rice husk and pine wood. At these optimum temperatures the yield of liquid organics were 50, 55 and 58 % daf for straw, rice husk and pine wood. The optimum yield temperature of straw is slightly lower than of wood and rice husk. However the gas + water formation for straw was higher compared to others and the amount kept increasing with temperatures due to the secondary reaction take places at higher temperatures.

The presence of alkali matters in biomass ash especially potassium, magnesium reduce the yield of liquid organics by catalytic decomposition of tar and also lowering the optimum yield temperature.

Acknowledgement
CHEC is financially supported by the Technical University of Denmark, DONG Energy A/S, Vattenfall A/S, FLSmidth A/S, Hempel A/S, Energinet.dk, the Danish Research Council for Technology Sciences, the Danish Energy Research Program, the Nordic Energy Research Program, and EU. The author acknowledges the financial support of the Ministry of Higher Education (MOHE) of Malaysia, Universiti Teknologi Malaysia (UTM), the Nordic Energy Research Program and the DTU-BIOCHAR project.

References

1. J.L. Gaunt and J. Lehmann, Environ.Sci.Techno, 2008, 42 4152.
2. J.A. Mathews, Energy Policy, 2008, 26, 940.
3. A.V. Bridgwater, and G.V.C. Peacocke, Renewable & Sustainable Energy Reviews, 2000, 41
4. N. Bech, M.B. Larsen, P.A.Jensen, K. Dam Johansen, Biomass and Bioenergy, 2009, 33 , 999.
5. M.J. Antal, Ind Eng Prod Res Dev, 1983, 22, 66.
6. M.J.Antal, Fundamentals of biomass thermochemical conversion, Elsevier, London, 1985, 511.
7. A.V. Bridgwater, Applied Catalysis, 1994, 5.
8. A.Jensen and K.Dam- Johansen, Energy & Fuels, 1998, 12,929.
9. L. Fagbemi, L. Khezami, and R. Capart, Pyrolysis products from different biomasses: Application to the thermal cracking of tar, Applied Energy. 69 (2001) 293-306.

Priyanka Jain
Phone: +45 4525 2876
Fax: +45 4588 2258
E-mail: pja@kt.dtu.dk
WWW: http:// www.cere.dtu.dk
Supervisors: Erling H. Stenby
Nicolas von Solms

PhD Study
Started: January 2009
To be completed: December 2011

Compositional Simulation of In-Situ Combustion EOR

Abstract
Modeling of a thermal process as complex as In-situ combustion requires in-depth understanding of detailed reaction kinetics and multidisciplinary process data. In order to facilitate the study of the influence of reservoir process characteristics in In-Situ combustion modeling a fully compositional In-situ combustion (ISC) model of Virtual Kinetic Cell (VKC; single-cell model) for laboratory scale combustion simulation is used .The VKC model based on In-situ combustion kinetics is employed to study the oxidation kinetics of the fractions of crude oil during In-situ combustion. The intention is to combine the results with a blend of analytical and numerical methods to define and implement an optimal simulation strategy for reactive transport processes, leading towards developing improved oil recovery methodologies

Introduction
In-situ combustion (ISC), also known as high pressure air injection or fire-flooding, is receiving strong renewed interest in the petroleum industry because of the depleting oil reserves. A thermal recovery process like ISC can be effective in improving recovery of existing reservoirs as well as unlocking the vast reserves of heavy oil in the world; in an environmentally sound manner. ISC is the process of injecting air (or air enriched with oxygen) into oil reservoirs to oxidize a portion of crude oil and enhance recovery through heat and pressure produced. It is also a technically and economically viable process as the portion of crude burned is likely to be heaviest and least valuable. ISC is generally applied for heavy oils due to the dramatic reduction in the oil viscosity with temperature.

The thesis work, in order to facilitate the study of the influence of reservoir process characteristics in In-Situ combustion, relies on laboratory scale combustion simulation of a fully compositional In-situ combustion (ISC) model – a single-cell model of Virtual Kinetic Cell (VKC) .In VKC, each grid block is effectively treated as a small chemical reactor, or kinetic cell in which only chemical kinetics and phase behavior are taken into account Two VKC models - Minimal model (6 components, 4 reactions) and SARA model (14 components, 14 reactions) - based on combustion kinetics are employed to study the oxidation kinetics of the fractions of crude oil during In-situ combustion.
.

Specific Objectives
The preliminary objective of the thesis work is to verify and further enhance the approach of In-Situ Combustion Modeling tools such as the Virtual Kinetic Cell (VKC). The aim is to study in-depth the process characteristics by integrating the kinetics of the different reactive transport processes into efficient and accurate simulation results. The scope is extended further to use the model in order to combine a blend of analytical and numerical methods to define and implement an optimal simulation strategy for reactive transport processes

The “reactive cell” plays the same role for the simulation of reactive transport as does the equilibrium flash for compositional reservoir simulation. Without efficient solution procedures at the grid block (cell) level, where millions of individual calculations are required, the overall simulation becomes infeasible. A particular problem is that changes in the reactive zone take place over a time scale and a length scale that is much smaller than that for the overall process. An important scope of the thesis work is to develop enhanced understanding of the “reactive cell” model and the subsequent integration of this knowledge in the overall solution procedure.

Approach

To achieve the desired objectives, the approach that this thesis work maintains is to first study the influence of reservoir process characteristics on In-Situ combustion by designing different simulation scenarios. The approach here is to determine optimal experimental conditions by performing sensitivity analysis using the Virtual Kinetic Cell; where simulation data is generated using the Minimal model and SARA model. The data acquired is proposed to be used for validation of the model for field-level calculations and to locate and improve possible model deficiencies within the context.

Results and Discussions

The thesis work, in its first phase, analyzed the influence of changing oxygen-feed concentration and activation energy on Light and Heavy Oils during thermal recovery process of ISC. The Minimal Model of VKC is used to compare the Peng-Robinson equation of state with the Wilson K-Value correlation. Since no appreciable difference between the two was observed, the Peng-Robinson equation of state was then used to further study the influence of- characterization (critical pressure, critical temperature and acentric factor) of Light and Heavy Oils on different VKC simulation output parameters. The results within this context of comparing the Light Oil to Heavy Oil shows that it is the heavy oil critical properties which significantly influence the simulation of the minimal model.

As stated previously, the VKC model is then extended further to study the oxidation kinetics of the SARA fractions of crude oil during in-situ combustion. The influence of changing oxygen-feed concentration, activation energy, critical properties of different process components (critical pressure, critical temperature and acentric factor), air injection rate, rock porosity and rock heat capacity on improving oil recovery are analyzed; again in conjunction with phase behavior models of Peng-Robinson equation of state and the Wilson K-Value correlation. It can be interpreted from the results available that operating parameters like air injection rate, oxygen feed concentration and activation energy have significant influence on oil recovery.. Furthermore, change in rock specific heat shows no significant influence on the SARA model, while increase in rock porosity tends to decrease oil recovery.

Conclusion

A general framework for simulation of in-situ combustion induced enhanced oil recovery process is considered. The fundamental idea behind this framework is to study the influence of reservoir process characteristics by performing sensitivity analysis using the Virtual Kinetic Cell where simulation data is generated using the Minimal model and SARA model.

The work done under the thesis work till date has some interesting conclusions to share with both the research and the industrial community. Adapting the Minimal model of VKC it is found that increasing the critical pressure of heavy oil increases the concentration of heavy oil in the recovery flow which then cracks to result in increase of light oil concentration. In contrast, increase in critical temperature of heavy oil results in decrease of both heavy and light oil concentrations.

Adapting the SARA model, it is found that the increase in air injection rate leads to cooling of the combustion front thus decreasing oil recovery. Although, an increase in oxygen feed assists combustion and contributes towards improved oil recovery. Also, it is observed that in SARA model where the critical properties of the pseudo components are not determined experimentally, fluid characterization holds certain significance. The composition plays a significant role and this is due to the fact that asphaltenes are most resistant toward oxidation and saturates are the easiest oxidizable ones.

Future Work

The thesis work intends to encompass another one-dimensional thermal-reactive and compositional model, the Virtual Combustion Tube, of In-Situ combustion in its scope. The sensitivity analysis is already planned to be performed on similar lines as adapted in the case of VKC. The intention is to compare and validate both the compositional models, the VKC and the VCT, using experimental data for their feasibility in field trials.

References

[1] Partha S. Sarathi. In-situ combustion handbook – principles and practices. Technical report, U.S. Department of Energy, 1999. DOE/PC/91008-0374.114

[2] Freitag, N. P. and Exelby, D. R. (2006), 'A SARA-based model for simulating the pyrolysis reactions that occur in high-temperature EOR processes', Journal of Canadian Petroleum Technology 45(3), 38–44

[3] K. H. Coats. In-situ combustion model. Society of Petroleum Engineers Journal, 269:533–554, 1980

[4] Kristensen, M. R. (2008), Development of Models and Algorithms for the Study of Reactive Porous Media Processes, PhD thesis, Technical University of Denmark

Irakli Javakhishvili
Phone: +45 4525 6817
Fax: +45 4588 2161
E-mail: irj@kt.dtu.dk
WWW: www.polymers.dk
Supervisors: Prof. Søren Hvilsted

PhD Study
Started: September 2007
To be completed: August 2010

Accelerated Synthesis of Linear-dendritic Cholesteryl-poly(ε-caprolactone)-*b*-(L-lysine)$_{G2}$ by Thiol-ene and Azide-alkyne "Click" Reactions

Abstract
The construction of linear-dendritic block copolymer consisting of terminal cholesteryl moiety, poly(ε-caprolactone), and second generation L-lysine dendron has been accomplished by the combination of copper (I) catalyzed azide-alkyne and UV-triggered thiol-ene "click" reactions. Ring-opening polymerization of ε-caprolactone initiated by 5-hexyn-1-ol and Mitsunobu coupling with 4-pentenoic acid provide hetero-telechelic poly(ε-caprolactone) bearing terminal alkyne and alkene groups. It is then employed in the sequential "click" reactions with the azide-functionalized dendritic wedge and thiocholesterol. Near to quantitative functionalization of the intermediate and final products has been attained as confirmed by NMR spectroscopy and MALDI-TOF spectrometry.

Introduction
Amphiphilic linear-dendritic block copolymers have gained significant importance due to their peculiar properties that drive self-assembly into various shapes. Different combinations of the constituting blocks have been prepared, and their capacity of forming complex supramolecular architectures have been investigated.[1]

Hedrick *et al*. have designed linear-dendritic amphiphiles that resemble naturally occuring phospholipids.[2] The hydrophilic dendrons based on 2,2-bis(hydroxymethyl)propionic acid (A) were combined with the linear segment of the hydrophobic poly(ε-caprolactone) (PCL) (B) via ring-opening polymerization (ROP) of ε-caprolactone (ε-CL) initiated by the dendrons possessing multiple functionalities. The symmetric linear-dendritic triblock copolymer (ABA) was also prepared via the Mitsunobu coupling of the linear-dendritic block copolymer (AB) with the acid-functionalized dendrons.[2]

Cao *et al*. developed the route towards poly(L-lactide)-*b*-dendritic poly(L-lysine) based on the metal free ROP of the L-lactide initiated by the hydroxyl end-capped Boc-protected poly(L-lysine) dendrons.[3] The authors have pointed out the role of poly(L-lysine) as a functional vector for DNA transfection.[3]

Stupp *et al*. have reported about the synthesis of the amphiphilic rodcoil dendrons where the dendritic wedge was connected with the rigid moiety via the polyester spacer.[4] Preparation of these intricate structures involved ROP of L-lactide initiated by cholesterol, and substitution of the hydroxyl terminus of this cholesteryl-oligo(L-lactic acid) with the L-lysine dendron. While liquid chrystalline character of the cholesteryl moiety could drive self-assembly of the rodcoil dendron, the L-lysine wedge could provide sterics to direct the nanostructure formation. Furthermore, both cholesterol and L-lysine could interact with the cell membrane, and thus promote and facilitate cell adhesion.[4]

However, this synthetic procedure, though subtle, is quite tedious and demanding. With the advance of the copper (I) catalyzed azide-alkyne cycloaddition[5] (CuAAC) and UV initiated thiol-ene[6] "click" reactions, and their successful implementation in the field of the macromolecular chemistry,[7] we believe that the synthetic approach towards the rodcoil dendrons can be accelerated, and made more robust and versatile: all three constituent blocks can be coupled to avoid default presence of either cholesterol or L-lysine wedge as is the case in the strategies discussed above.[3,4] Herein, we present the synthetic layout for the preparation of the rodcoil dendron based on cholesterol, PCL, and dendritic L-lysine. Since Hawker *et al*. pointed out the efficiency and compatibility of these orthogonal "click" reactions,[8] we believe this is one of the first succeful attempts to employ this strategy in building such multifunctional macromolecular architecture alongside Haddleton *et al*., where CuAAC reaction has been coupled with thiol-ene Michael addition,[9] and Anseth *et*

al., where copper-free "click" chemistry has been conjugated with thiol-ene photocoupling.[10]

Results and Discussions

ROP of ε-CL initiated by 5-hexyn-1-ol and catalyzed by tin (II) octoate at elevated temperature in bulk has been reported by Schubert *et al*.[11] The polydispersity index (PDI) of 1.19 was achieved. We have shown that better control over the reaction can be gained by conducting it at moderate temperature with high catalyst concentration.[12] Thus, PCL with the PDI=1.11 and high end-group fidelity has been obtained. The degree of polymerization estimated by ^{1}H NMR was 20. Esterification of the hydroxyl chain end with 4-pentenoic acid, according to Mitsunobu protocol,[12] afforded hetero-telechelic PCL bearing alkyne and alkene functional groups. The α-alkenyl-ω-alkynyl-PCL had narrow molecular weight distribution (PDI=1.11), and near to quantitative functionality as confirmed by ^{1}H NMR and MALDI-TOF analysis.

The synthesis of the second generation dendron of L-lysine, (L-lysine)$_{G2}$ (**3**), with the azide functional group in the focal point was carried out according to Figure 1.

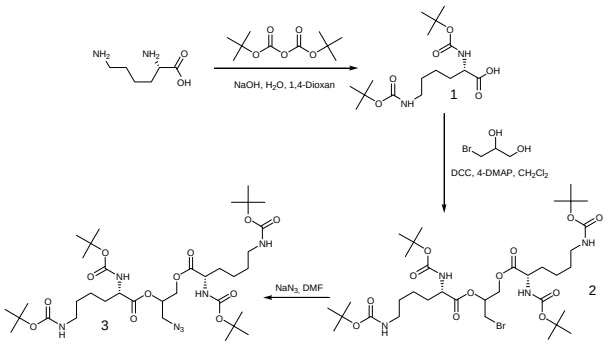

Figure 1: Preparation of bis-(di-Boc-L-lysine)-3-azido-1,2-propandiol

This approach allows immediate incorporation of the primary bromo function in the core. Therefore, it is not necessary to introduce bromoalkyl moiety by additional esterification reaction as would be the case in the standard procedure of building dendrons.[13] Subsequent nucleophilic substitution furnishes azide functional dendritic wedge of the second generation with high yield and purity. Thus, 3-bromo-1,2-propandiol was reacted with N_α,N_ε-di-Boc-L-lysine (1.1 eq) in the presence of *N*,*N*′-dicyclohexylcarbodiimide and 4-(dimethylamino)pyridine. The purification step did not require column chromatography, and sufficed with extractions. Afterward, **2** was converted to the corresponding azide by treating it with sodium azide (2 eq) at 40°C overnight. The heteronuclear single quantum coherence (HSQC) NMR experiment confirmed full conversion under these reaction conditions.

Azide-alkyne and UV initiated thiol-ene "click" reactions were conducted as depicted in Figure 2.

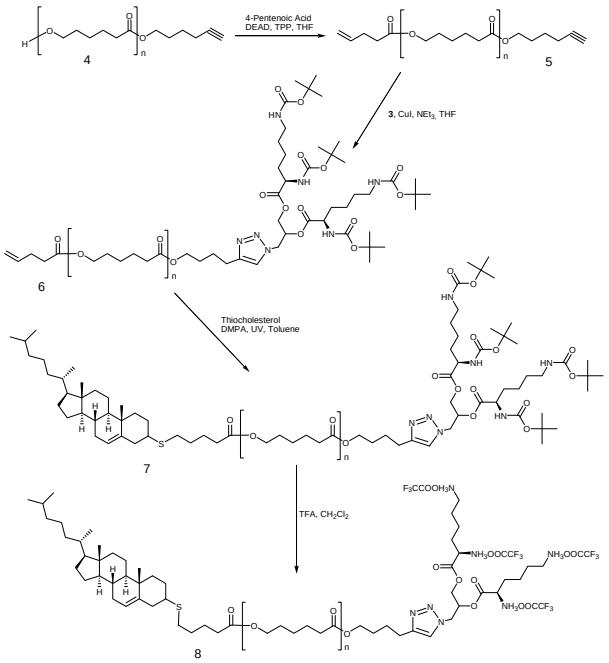

Figure 2: CuAAC and thiol-ene "click" reactions followed by the removal of Boc protecting groups

CuAAC reaction between α-alkenyl-ω-alkynyl-PCL **5** and bis-(di-Boc-L-lysine)-3-azido-1,2-propandiol **3** (2 eq) was catalyzed by CuI (1 eq in comparison to the alkyne). The "click" components were reacted in THF in the presence of NEt_3 at 35°C for 24 h.[14] The excess of **3** was removed by precipitation in MeOH:H_2O mixture. The product was analyzed by SEC, NMR, and MALDI-TOF.

SEC revealed monomodal, symmetrical trace, which was shifted to the higher molecular weight (Figure 3), and low PDI of 1.10. This implies that no chain scission took place nor did the polymer chains remain unreacted.

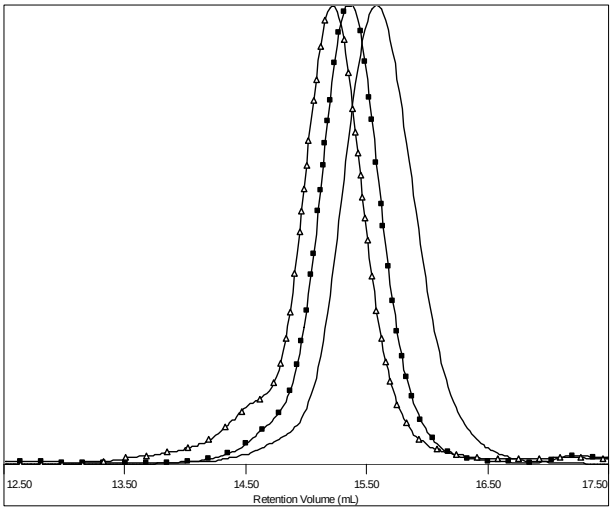

Figure 3: Normalized SEC traces of α-alkenyl-ω-alkynyl-PCL (**5**) (M_n=4100 Da, M_w/M_n=1.11) ——, alkenyl-PCL-*b*-(di-Boc-L-lysine)$_{G2}$ (**6**) (M_n=5100 Da, M_w/M_n=1.10) – – –, Cholesteryl-PCL-*b*-(di-Boc-L-lysine)$_{G2}$ (**7**) (M_n=5900 Da, M_w/M_n=1.15) –·–·–.

Near to quantitative functionalization was attained as judged from NMR experiments. Both ^{1}H and HSQC

NMR data indicated almost full conversion as the resonances corresponding to the alkyne functional group could no longer be detected. Furthermore, the peaks ascribed to the dendritic wedge and triazol ring (**h**) emerged (Figure 4). The signals assigned to the alkene moiety were observed at 5.00 ppm and 5.80 ppm (**p** and **o**). The integrals of the resonances from the alkene end-group (5.80 ppm, **o**) and C*H*$_2$NHBoc (2.93-3.22, **c**) were in good agreement with the theoretical values.

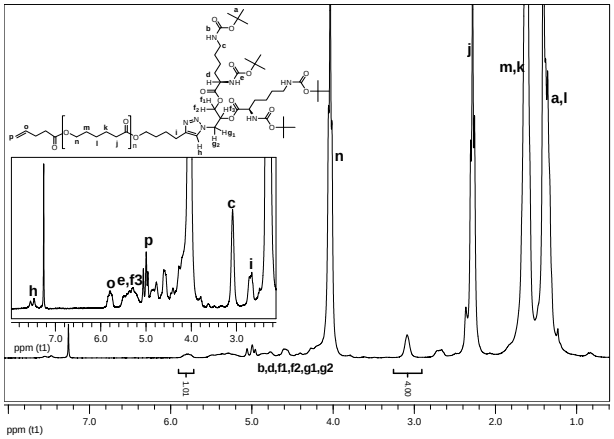

Figure 4: ^{1}H NMR spectrum of alkenyl-PCL-*b*-(di-Boc-L-lysine)$_{G2}$ (**6**). The spectrum was recorded in $CDCl_3$.

The MALDI-TOF analysis produced a spectrum with the signal spacing of approximately 114 Da, corresponding to the molecular weight of one repeating unit in the PCL chain. Two series were observed: one fitting the experimental molecular weight of the alkenyl-PCL-*b*-(di-Boc-L-lysine)$_{G2}$ (**6**) as the M-Na+-series, while the other minor series being assignable to the M-Li+-series with the loss of two of the Boc groups during the ionization process.

The cholesteryl moiety was introduced via the thiol-ene "click" reaction between the alkenyl-PCL-*b*-(di-Boc-L-lysine)$_{G2}$ and thiocholesterol (Figure 2). The solution of **6**, thiocholesterol, and 2,2-dimethoxy-2-phenylacetophenone (1:10:3.5 molar ratio) in toluene was stirred and irridiated at 365 nm in the presence of oxygen. Large excess of the thiol and the photoinitiator were taken to overcome the obstacles posed by rigid structure and hindered mobility of thiocholesterol,[15] and to achieve near to quantitative functionalization as concluded after investigations by NMR and MALDI-TOF. In the ^{1}H NMR spectrum (Figure 5) the signals from the alkene chain end disappeared completely, and the resonances originating from the cholesteryl moiety (**q**, **r**, and **s**) could be observed.

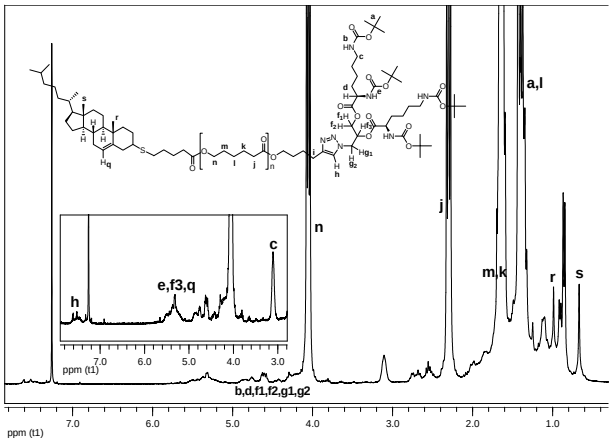

Figure 5: ^{1}H NMR spectrum of Cholesteryl -PCL-*b*-(di-Boc-L-lysine)$_{G2}$ (**7**). The spectrum was recorded in $CDCl_3$.

The MALDI-TOF analysis revealed the species of the molecular weight that correspond to **7**. The signal spacing of 114 Da indicative of the repeating unit of the PCL was again observed. In total, three series were observed as M-Na+-adducts with the main series being the M-Na+-series of **7**, while the other two series indicating again the loss of either one or two Boc moieties (Figure 6). However, the SEC trace had a small shoulder (Figure 3), though PDI was still fairly low (1.15). The appearance of the shoulder could tentatively be ascribed to the intramolecular side reactions of radical nature that could take place during the thiol-ene "click" reaction.

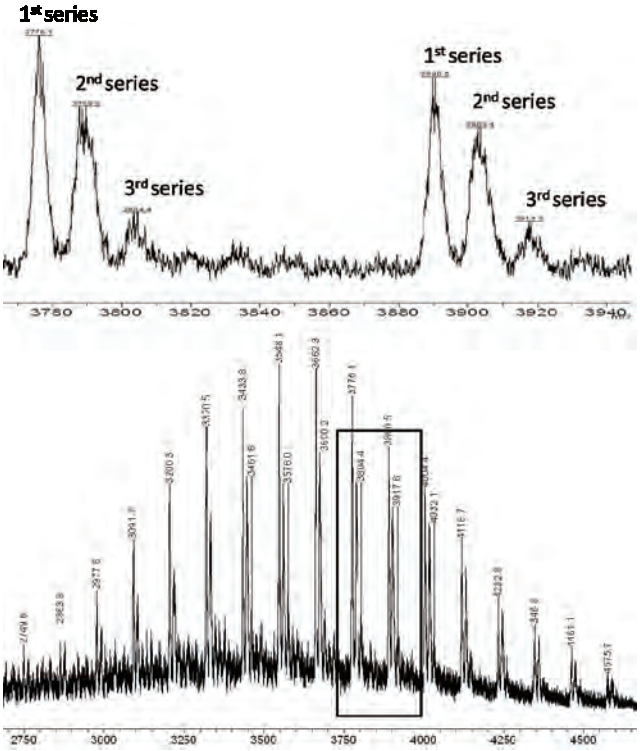

Figure 6: MALDI-TOF of Cholesteryl -PCL-*b*-(di-Boc-L-lysine)$_{G2}$ (**7**), bottom: full spectrum; top: expansion of the indicated region.

The final step involved deblocking of the amine functionalities. **7** was treated with trifluoroacetic acid in CH_2Cl_2. The solvent and the excess of the acid were removed *in vacuo*, and the product was analyzed by NMR and MALDI-TOF. In ^{1}H NMR spectrum (Figure 7) the signal corresponding to *tert*-butyl group was not observed, while the broad peaks related to the free amine groups were detected at 8.30-8.80 ppm and 7.65-8.05 ppm. The triazol proton resonated at 7.94 ppm.

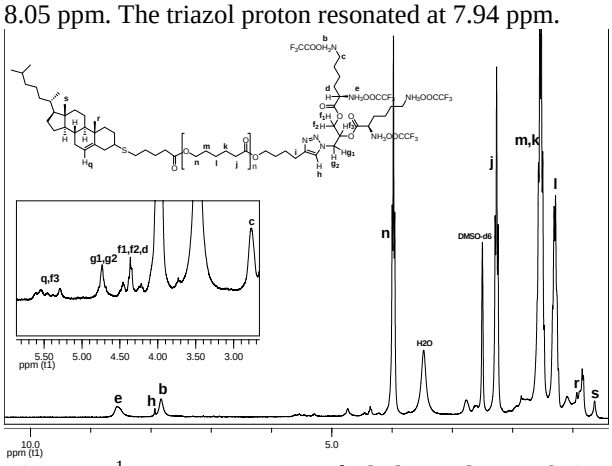

Figure 7: ^{1}H NMR spectrum of Cholesteryl -PCL-*b*-(L-lysine)$_{G2}$ (**8**). The spectrum was recorded in DMSO-d_6.

Such a dramatic shift could be explained by the cardinal changes in solubility of the macromolecule (the spectrum was recorded in DMSO-d_6). MALDI-TOF mass spectrometry (Figure 8) showed several series, proving the final structure with sequential loss of the trifluoroacetate moieties during the ionization process.

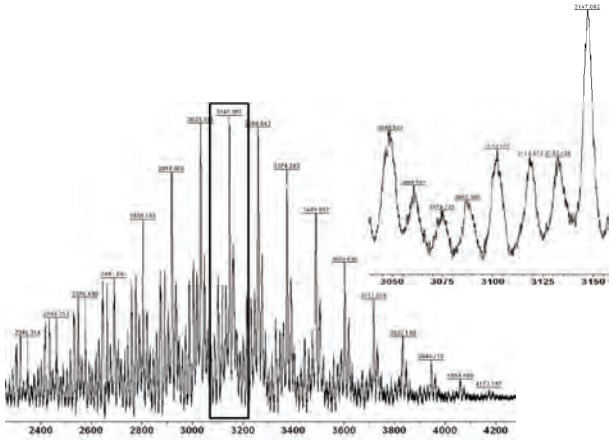

Figure 8: MALDI-TOF spectrum of Cholesteryl-PCL-*b*-(L-lysine)$_{G2}$ (**8**).

Conclusions

In conclusion, we have demonstrated the effectiveness and flexibility of the orthogonal azide-alkyne and thiol-ene "click" reactions in preparation of the rodcoil dendron cholesteryl-PCL-*b*-(L-lysine)$_{G2}$. The "click" reactions considerably shorten the synthetic cascade for building such macromolecules compared to the conventional esterification reactions. Moreover, the versatility of the heterofunctional PCL in combination with these orthogonal "click" reactions provides greater degree of freedom for incorporation of different structural elements, and thus opens new avenues to much larger library of complex amphiphilic architectures.

Acknowledgements

Professor W. H. Binder from Martin-Luther University Halle-Wittenberg is acknowledged for carrying out MALDI-TOF characterization.

References

1. I. Gitsov, J. Polym. Sci.: Part A: Polym. Chem. 46 (2008) 5295-5314.
2. A. Würsch, M. Möller, T. Glauser, L. S. Lim, S. B. Voytek, J. L. Hedrick, C. W. Frank, J. G. Hilborn, Macromolecules 34 (2001) 6601-6615.
3. Y. Li, Q. Li, F. Li, H. Zhang, L. Jia, J. Yu, Q. Fang, A. Cao, Biomacromolecules 7 (2006) 224-231.
4. H.-A. Klok, J. J. Hwang, J. D. Hartgerink, S. I. Stupp, Macromolecules 35 (2002) 6101-6111.
5. (a) V. V. Rostovtsev, L. G. Green, V. V. Fokin, K. B. Sharpless, Angew. Chem. Int. Ed. 41 (2002) 2596-2599; (b) C. W. Tornøe, C. Christensen, M. Meldal, J. Org. Chem. 67 (2002) 3057-3064.
6. K. L. Killops, L. M. Campos, C. J. Hawker, J. Am. Chem. Soc. 130 (2008) 5062-5064.
7. (a) W. H. Binder, R. Sachsenhofer, Macromol. Rapid Commun. 29 (2008) 952-981; (b) R. K. Iha, K. L. Wooley, A. M. Nyström, D. J. Burke, M. J. Kade, C. J. Hawker, Chem. Rev. 109 (2009) 5620-5686.
8. L. M. Campos, K. L. Killops, R. Sakai, J. M. J. Paulusse, D. Damiron, E. Drockenmuller, B. W. Messmore, C. J. Hawker, Macromolecules 41 (2008) 7063-7070.
9. L. Nurmi, J. Lindqvist, R. Randev, J. Syrett, D. M. Haddleton, Chem. Commun. (2009) 2727-2729.
10. C. A. DeForest, B. D. Polizzotti, K. S. Anseth, Nature Materials 8 (2009) 659-664.
11. R. Hoogenboom, B. C. Moore, U. S. Schubert, Chem. Commun. (2006) 4010-4012.
12. I. Javakhishvili, S. Hvilsted, Biomacromolecules 10 (2009) 74-81.
13. P. Wu, M. Malkoch, J. N. Hunt, R. Vestberg, E. Kaltgrad, M. G. Finn, V. V. Fokin, K. B. Sharpless, C. J. Hawker, Chem. Commun. (2005) 5775-5777.
14. R. Riva, S. Schmeits, F. Stoffelbach, C. Jérôme, R. Jérôme, Ph. Lecomte, Chem. Commun. (2005) 5334-5336.
15. N. ten Brummelhuis, C. Diehl, H. Schlaad, Macromolecules 41 (2008) 9946-9947.

List of Publications

I. Javakhishvili, S. Hvilsted, Biomacromolecules 10 (2009) 74-81.

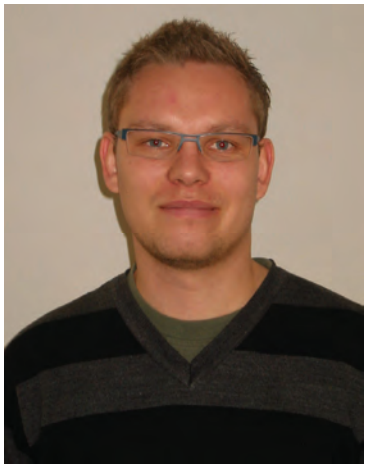

Lars Jensen

Phone: +45 4525 2858
Fax: +45 4588 2258
E-mail: lje@kt.dtu.dk
WWW: (no personal page)
Supervisors: Nicolas von Solms
Kaj Thomsen

PhD Study
Started: March 2007
To be completed: June 2010

Inhibition of Gas Hydrate Formation by Low-Dosage, Environmentally Benign Inhibitors

Abstract

Ice-structuring proteins (ISPs) have been considered as an environmentally-friendly alternative to commercial kinetic inhibitors of hydrate formation. ISPs obtained from certain species of pout (a cold-water fish) have been tested in the literature and in our laboratories and the results are promising. However, insect-based ISPs have been shown to be much more active than fish-based ISPs for freezing point depression. We have done initial testing with insect and fish ISPs in our labs for activity in hydrate inhibition and results are promising.

Introduction

Gas hydrates are crystalline compounds formed as a result of combination of water and suitably sized guest molecules at elevated pressure and low temperature. Light hydrocarbons; methane-pentane, carbon dioxide and hydrogen sulphide are the guest molecules of interest to the oil and natural gas industry [1]. Depending on the pressure and gas composition, gas hydrates may build up where water coexists with natural gas at temperatures as high as 300 K. Especially long gas transmission lines at cold weather conditions and process equipment are vulnerable to being blocked by hydrate formation causing potential hazards or economical loss.

Inhibition of gas hydrates is a necessity in the oil and gas industry in order to assure a continuous flow of reservoir fluids from the production well to the platform. Traditionally methanol or glycol has been used to inhibit the formation of gas hydrates by shifting the hydrate equilibrium to lower temperatures and higher pressures. Due to the relative large amounts (10-50 wt%) of methanol or glycol needed in the process of hydrate prevention [2] other chemicals capable of inhibiting hydrate formation at much lower doses (<1 wt%) have gained interest [3]. These impact the kinetics of hydrate formation, in contrast to the thermodynamic inhibitors, thus the chemicals are known as kinetic inhibitors.

Kinetic information of hydrate formation is very important if kinetic inhibition is applied as a mean of preventing hydrate formation in transmission lines, valves etc.

Ice-structuring proteins (ISPs) found in animals living at sub-cooling conditions and known to retard the nucleation and growth of ice might have the potential to work as kinetic inhibitors of gas hydrates.

In this work the effect of TmISP on the growth of methane hydrate has been investigated. The effect of type III ISP from ocean pout on the nucleation of methane hydrate has also been investigated.

Methods and Equipment

The growth of hydrate was investigated in a high-pressure stainless steel cell. This was done by stirring water and gas at high pressure and low temperature. Formation of gas hydrate will cause the pressure in the cell to drop. The cell has for this reason been attached with a pressure transducer and an electronic mass flow meter which in combination work as a backpressure control system. This will assure that the pressure in the cell will maintain constant during the experiment and monitor the amount of gas supplied to the cell to maintain pressure. The temperature of the cell was controlled by circulating coolant in a jacket surrounding the cell. The temperature was monitored by a platinum resistance probe. The cell was placed on a stir plate thereby allowing a magnet bar
to rotate within the cell. Data (P, T and ml gas injected to the cell) was recorded continuously on a computer. In figure 1 a schematic of the experimental set-up is shown.
For the nucleation experiments we have used the methodology reported by Dicharry et al. since that has

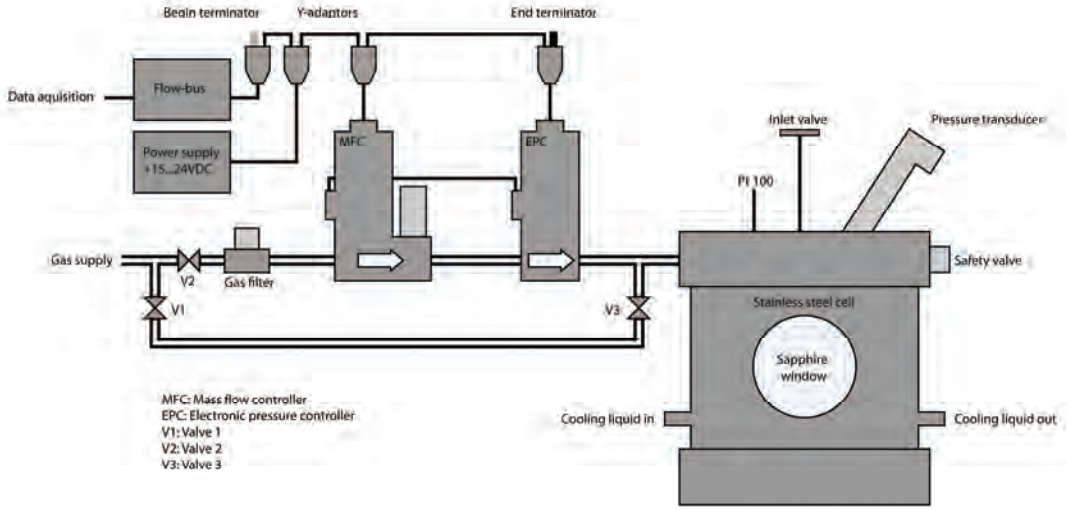

Figure 1: Experimental set-up showing the hydrate cell and the back pressure control and flow measurement system.

shown to increase experimental reproducibility [4].

Results

All the experiments were carried out under constant pressure. The maximum deviation between the experimental pressure and the set-point pressure during an experimental run was never more than 1%. The growth kinetics of methane hydrate was investigated at 277.15 K and at three different pressures. The result can be seen in Figure 2. In all three cases a linear growth pattern, in terms of total moles of methane consumed over time, can be observed. At higher pressure, i.e. higher driving force, the growth rate is seen to increase.

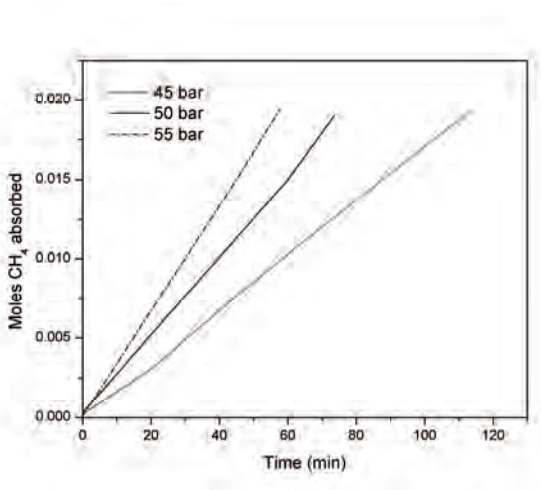

Figure 2. Growth kinetics of methane hydrate at pressures of 55, 50 and 45 bars and a temperature of 277.15 K. The growth kinetics is represented as the total number of moles accumulated in the hydrate as a function of time.

In order to assess the growth rate a simple rate expression similar to the one proposed by Skovborg and Rasmussen [5] however using the solubility, $x_{H\text{-}L}$, of the hydrate former in the liquid phase at the hydrate-liquid interface under H-L_w equilibrium at T_{exp} and P_{eq} instead of x_b which is the mole fraction of gas in the bulk water phase in equilibrium with the hydrate phase
at system P and T. The rate of mass transfer and thus the total gas consumption can be described using the following equation:

$$\frac{dn}{dt} = k_L A_{g\text{-}l} C_{w0} (x_{L\text{-}V} - x_{H\text{-}L}) \quad (1)$$

Where $k_L$is the mass transfer coefficient in the liquid film, $A_{g\text{-}l}$ is the gas liquid interfacial area, C_{w0} is the initial concentration of water (mol/m^3), $x_{L\text{-}V}$ is the mole fraction of gas in the water phase at system P and T and $x_{H\text{-}V}$ and $x_{H\text{-}L}$ as described before. The mole fraction of gas in water is found using Henry's law:

$$x_{L\text{-}V} = \frac{f(P_{exp}, T_{exp})}{H} \quad (2)$$

And $x_{H\text{-}L}$ is found as:

$$x_{H\text{-}L} = \frac{f(P_{eq}, T_{exp})}{H} \quad (3)$$

Henry's constant has been calculated using the relation (Carol and Mather, 1997):

$$\ln H_{iw} = 5.1345 + 7837/T - 1.5090\times10^{6}/T^{2} + 2.060\times10^{7}/T^{3}$$

The fugacities have been calculated using the SRK equation of state. The equilibrium P and T is found

using CSMGem [6]. As the gas liquid interfacial area is not known we substitute k_LA_{g-l} with K. dn/dt in (2) is obtained by making a linear regression of the experimental data presented in Figure 2. As seen the linearity of the experimental data is high thus good estimates of the slope is obtained. In table 1 the calculated mass transfer coefficients are provided. The mass transfer coefficients found are quite similar which would also be expected as primarily the driving force in (1) should compensate for the faster growth rate.

Table 1. Calculated mass transfer coefficients for 3 different pressures at 277.15 K.

T	P	System	K_LA_{g-l} $(m^3/s) \cdot 10^8$
277.15	45	No inhibitors	7.96
	50		6.58
	55		5.97
	55	0.1 wt% PVP	3.42
	55	0.004 wt% TmISP	3.78

The growth rate of methane hydrate when adding 0.004 wt% TmISP has been investigated. In Figure 3 the growth curve at 55bar is shown. As seen the TmISP causes the growth rate to decrease. The same is found for PVP however to obtain the same level of inhibition a concentration of 0.1 wt% is required. This suggests that TmISP is a stronger kinetic inhibitor than PVP. The mass transfer coefficients are also provided in Table 1.

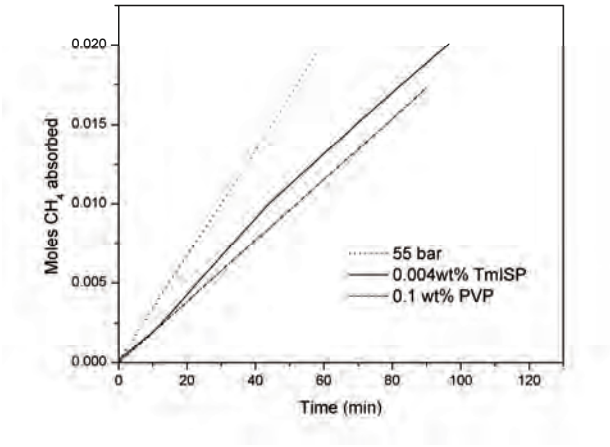

Figure 3. Growth kinetics of methane hydrate in the presence of 0.004wt% TmISP and 0.1wt% PVP at 277.15 K and 55 bar.

The nucleation periods has likewise been investigated to see if ISPs are also capable of inhibiting the induction period of hydrate formation. The induction times found is seen in table 2.

Table 2. Results of nucleation experiments for methane hydrate with and without inhibitors. The induction time listed is based on the average of 7 experiments. The number in parenthesis is the standard deviation.

T (K)	System	P (bar)	Nucleation period (h)
277.15	No inhibitor	54	1.15 (0.28)
	0.1 wt% OpISP	60	10.49 (2.41)

As seen the induction period is relatively short at 54 bar. A standard deviation of 0.28 for a hydrate forming system is considered relatively short considering the stochastic nature of hydrate nucleation. This is attributed to the experimental method applied. When adding the OpISP the nucleation period of methane hydrate is prolonged noteworthy even though that the pressure is increased by 6 bar compared to the first experiments with no inhibitor. Relatively the standard deviations in the two experiments are in the same order. The reason that nucleation periods of hydrate formation can be prolonged can be numerous. Previously studies have showed that nucleation of gas hydrates as in the case of ice is heterogeneous and therefore highly affected by the presence of impurities [7]. A recent study has revealed that nucleation inhibition using polymers like PVP is mainly due to adsorption of these molecules on impurities like dust particles causing a change in the hydrate-substrate contact angle [8]. The same observations have been made for the nucleation of ice when ISP III was added to the water [9]. With this in mind it seems reasonable to assume that OpISP inhibits the nucleation of methane hydrate by a similar mechanism.

While it is not likely that the nucleation prolongation is due to adsorption of ISPs on the nucleus surface, it is however likely that the growth decrease is caused by such an effect. Studies on ice growth inhibition by ISPs have shown that irreversible adsorption of ISP molecules on the ice surfaces are the primary mechanism by which growth is retarded [10]. The exact mechanism is however not well defined but one suggestion is that the ISP induces a dense ISP-water layer, which can significantly decrease the mole fraction of the interfacial water and, thus, lower the temperature for a seed ice crystal to grow in a super-cooled ISP solution [11]. Another theory suggests that ISP binding to ice results in facet formation due to the inhibition of growth on the binding plane. Such inhibition is thought to result from the Kelvin effect, whereby the ice surface is pinned by distantly spaced, bound ISP molecules, causing the ice front to grow with local positive curvature, which is less thermodynamically favorable [12]. Whether the TmISP is capable of modifying the crystal shape of methane hydrate during growth has not been possible to investigate in this work however the results indicates that the TmISP is somehow affecting the growth mechanism.

Future work

In our current work we are planning to increase the potency of these insect ISPs by genetic manipulation as well as bring down the production cost by producing them in bacterial fermentations. Also the ISPs will be tested on sII hydrate formers.

Acknowledgements

The authors would like to thank the Danish Research Council for Technology and Production Sciences for financial support through the project "Gas Hydrates-from Threat to Opportunity" and the Technical University of Denmark for financial support through a Ph.D. scholarship.

References

1. E.D. Sloan, Clathrate hydrates of natural gases, Marcel Dekker, New York, 1998.
2. Kelland, M., (1995). Studies on New Gas Hydrate Inhibitors, SPE 30420, 531-539.
3. Sloan, E.D., Lederhos, J.P., Long, J.P., Sum, A., Christiansen, R.L. (1996). Effective Kinetic Inhibitors for Natural Gas Hydrates, Chem. Eng. Sci., 51, 1221-1229.
4. Dicharry, C., Duchateau, C., Glénat, P., Hidalgo, M., Peytavy, J.L., Pou, T.E., Proceedings of the 6th International Conference on Gas Hydrates, Vancouver, British Columbia, CANADA, July 6-10, 2008.
5. Skovborg, P. Rasmussen, P. (1994). A mass transport limited model for the growth of methane and ethane gas hydrates, *Chem. Eng. Sci., 49*, 1131-1143.
6. M. D. Jager, A. L. Ballard , E. D. Sloan, Jr. The next generation of hydrate prediction: II. Dedicated aqueous phase fugacity model for hydrate prediction Fluid Phase Equilibria, Volume 211, Issue 1, 2003, 85-107.
7. Bishnoi, P.R., Natarajan, V., 1996. Formation and decomposition of gas hydrates. Fluid Phase Equilibria 117, 168--177.
8. Jensen, L., Thomsen, K., von Solms, N. (2008). Propane hydrate nucleation: experimental investigation and correlation, Chem. Eng. Sci., 63, 3069-3080.
9. Du , Ning, Liu,. Xiang Y., Hew, Choy L. (2003). Ice nucleation inhibition, The Journal of Biological Chemistry, 278 (38), 36000-36004.
10. Pertaya, N., Marshall, C.B., DiPrinzio, C.L., Wilen, L., Thomson, E.S., Wettlaufer, J.S., Davies, P.L., Braslavsky, I. (2007). Fluorescence Microscopy Evidence for Quasi-Permanent Attachment of Antifreeze Proteins to Ice Surfaces, Biophysical Journal (92), 3663–3673.
11. Mao, Y., Ba, Y. (2006). Ice-surface adsorption enhanced colligative effect of antifreeze proteins in ice growth inhibition, The Journal of Chemical Physics, 125.
12. Knight, C.A. (2000). Structural biology. Adding to the antifreeze agenda, Nature (406), 249–251.

Benedicte Mai Lerche

Phone: +45 4525 2821
Fax: +45 4588 2258
E-mail: bml@kt.dtu.dk
WWW: http://www.cere.dtu.dk/
Supervisors: Erling H. Stenby
Kaj Thomsen

PhD Study
Started: December 2008
To be completed: December 2011

CO_2 Capture from Flue Gas using Amino Acid Salt Solutions

Abstract
The reversible absorption of CO_2 into a chemical solvent is currently the leading CO_2 capture technology. Available solvents are almost exclusively based on aqueous alkanolamine solutions, which entail both economic and environmental complications. A new type of solvents based on the salts of amino acids have emerged as an alternative to the alkanolamine solutions. A number of advantages make amino acid salt solutions attractive solvents for CO_2 capture. The goal of this project is to find the optimal amino acid salt solution for CO_2 capture from flue gas.

Introduction
The leading technology for CO_2 capture is chemical absorption, which is a technique where a chemical solvent reacts reversibly with the CO_2 in flue gas. During contact with the flue gas, the solvent chemically absorbs the CO_2. Heating of the CO_2 rich solvent leads to release of the CO_2 from the solvent, which is hereby regenerated and ready for another round of absorption. The captured CO_2 can now be compressed and transported to a storage location.[1] Available solvents for the chemical absorption process are almost exclusively based on aqueous alkanolamine solutions. Unfortunately CO_2 capture using alkanolamine solutions entails economic drawbacks as well as environmental complications, making the large scale implementation of the technology difficult.[2]

Disadvantages of alkanolamine solutions
CO_2 capture using alkanolamine solutions is very energy intensive, mostly due to the large amount of heat/energy needed to release the CO_2 form the solution, but also due to loss of solvent caused by its degradation and evaporation. It has been widely reported that alkanolamines undergo degradation in oxygen-rich atmospheres, such as those typically encountered in the treatment of flue gases, resulting in very toxic degradation products.[2] Besides the economical problem this creates with loss of solvent, there is an increasing environmental concern, due to the possible emission of small amounts of these toxic degradation products to the air.[3] Because the desire to capture CO_2 is gaining momentum, there is an urgent need for the development of new solvents that have the ability to capture CO_2 in both a cost efficient and environmental safe manner.[4]

Amino acids salt solutions as CO_2 absorbents
In comparison to alkanolamines amino acid salt solutions have several desirable properties for CO_2 capture from flue gas. Their ionic nature makes them more stable to oxidative degradation and also gives them certain other desirable physical properties such as low volatility.[2][4] A further advantage can be achieved by the interesting feature of several amino acid salts solutions to form solid precipitates when absorbing CO_2.[5] It has been found that the driving force for absorption can be maintained at a high level even at high CO_2 loadings as a result of precipitation, significantly improving the absorber performance.[2] In addition some amino acid salt solutions have been shown to react with CO_2 with fast reaction kinetics. [4] [6] Despite the rising interest, few studies have been performed so far on amino acids as CO_2 absorbents. When a pure amino acid, with the overall formula $HOOC\text{-}R\text{-}NH_2$, is dissolved in water, the following equilibriums are established. [6]

$$\underset{\text{I}}{HOOC\text{-}R\text{-}NH_3^+} \xrightleftharpoons{-H^+} \underset{\text{II}}{^-OOC\text{-}R\text{-}NH_3^+} \xrightleftharpoons{-H^+} \underset{\text{III}}{^-OOC\text{-}R\text{-}NH_2}$$

The amino acid is predominantly on its zwitterionic form (II), where the carboxylic acid group has lost a proton while the amine group is protonated, and the pH of the solution is equivalent to the isoelectric point of the given amino acid. As CO_2 reacts only with

deprotonated amines, the zwitterionic form of the amino acid is incapable of reaction with CO_2. Hence it is necessary to add an equivalent amount of strong base to deprotonate the amine group and produce the negatively charged form of the amino acid (III). The base which is used for this purpose is usually potassium hydroxide, with the potassium salt of the amino acid becoming the active component, which reacts with CO_2. In the case of the amino acid glycine, the active component becomes the potassium salt of glycine (potassium glycinate), shown in Figure 1.[6]

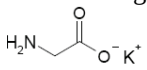

Figure 1: Potassium glycinate

It is generally agreed that alkaline salt solutions of amino acids react with CO_2 similar to alkanolamines having primary or secondary amine functionalities. The reactions that occur in the liquid phase are thus as follows (with the amino acid salt represented as AmA). [4]

$$CO_2 + 2AmA \rightarrow AmACOO^- + AmAH^+ \quad (1)$$

$$CO_2 + OH^- \rightarrow HCO_3^- \quad (2)$$

$$H_2O \rightarrow H^+ + OH^- \quad (3)$$

As seen CO_2 absorption can either take place by carbamate formation (Eq. 1) or bicarbonate formation (Eq. 2). There have been conflicting chemical mechanisms proposed to describe the absorption process. However, it is clear from the reaction rates that the initial absorption reaction is the formation of the carbamate. [4]

Specific objective of the project

The objective of the project is to establish a better scientific knowledge about the reaction between CO_2 and amino acid salt solutions, with the purpose of evaluating their potential as solvents for CO_2 capture from flue gas. The work is focused on finding a link between the CO_2 absorption capacity of the amino acids and their pKa values, water solubility, as well as chemical structure. In addition the connection between precipitation and CO_2 loading capacity of the solution is sought clarified.

Experimental work:

Selected amino acid salt solutions are presently being studied in regard to their CO_2 capturing ability, using a laboratory scale experimental set-up called a stirred cell shown in Figure 2. Synthetic flue gas (meaning 10% CO_2 and 90% N_2) is bubbled into the amino acid salt solution. The CO_2 absorption process is followed by measuring the % CO_2 in the outlet gas using a CO_2 analyzer. Also the temperature and pH in the solution is measured during the absorption. All data is collected as a function of time. The whole set-up is situated in a water bath, to keep a constant temperature (either 25 or 50 degrees Celsius).

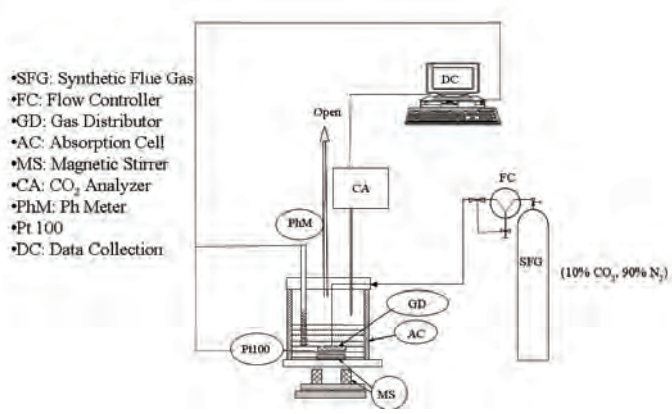

Figure 2: Representation of the stirred cell set-up

The CO_2 loading capacity of the solution is obtained by integrating the CO_2 signal (CO_2 in the inlet gas minus the CO_2 in the outlet gas) over time. Similar experiments are performed on mono-ethanolamine (MEA), which is the alkanolamine most widely used for CO_2 capture, thus representing a benchmark to which all new solvents will be compared. Analytical methods inculcating X-ray diffraction (XRD) Carbon 13 nuclear magnetic resonance (^{13}CNMR), and raman spectroscopy are applied in the study of the chemical composition of the lean and loaded solutions as well as the precipitates. The results of the laboratory scale studies provide data for the direct comparison of the performance of the amino acid salt solutions with that of MEA.

Future work

Apart from continuation of the described work other laboratory scale experiments including vapour liquid-equilibrium (VLE) experiments will be performed, in order to evaluate important solvent properties of the amino acid salt solutions. The aim is to test the amino acid salt solutions showing high performance in the laboratory scale studies on a pilot plant scale.

Acknowledgements

This project is sponsored by DONG Energy and Vattenfall A/S Heat Nordic.

References

1. IPCC Special Report on Carbon Dioxide Capture and storage. (2005)
2. P.S. Kumar et al. Ind. Eng. Chem. Res. 42 (2003) 2832-2840.
3. J. Gabrielsen Ph.D. Thesis, IVC-SEP, DTU. (2007)
4. J. van Holst et al. GHGT8 Trondheim. CATO publications(2006)
5. M. Majchrowicz et al. GHGT8 Trondheim. CATO publications(2006)
6. A.F. Portugal et al. Chem. Eng. Sci, 62 (2007) 6534–6547.

Publications

Benedicte Mai Lerche, Erling H. Stenby and Kaj Thomsen "CO_2 Capture from Flue Gas using Amino Acid Salt Solutions". *Proceedings from Risoe International Energy Conference 2009.*

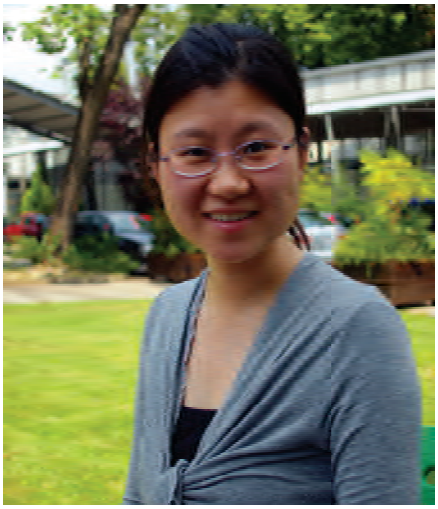

Li Li

Phone: +45 4525 2974
Fax: +45 4588 2161
E-mail: li@kt.dtu.dk
WWW: http://dpc.kt.dtu.dk
Supervisors Gunnar Eigil Jonsson
Sokol Ndoni, DTU Nanotech
Lydia D. Clausen, Radiometer Medical ApS
Kristian M. Hansen, Radiometer Medical ApS

Started: Feb 2008
To be completed: Jan 2011

Preparation, Characterization and Study of Transport Property of Nanoporous Polymer Membranes for Glucose Biosensors

Abstract
In the current work we investigated the glucose permeability of nanoporous 1,2-polybutadiene (1,2-PB) membranes. The nanoporous membranes were fabricated in form of flat sheets on a pneumatic-drive compressing setup. The roughness and thickness were examined by a stylus profiler. Characterizations by Atomic Force Microscope (AFM) revealed that two types of membranes existed in the whole batch of samples. Type 1 exhibited the 'close' structure on one side and 'open' structure on the opposite side; type 2 showed the same 'close' structure on both sides of the membrane. The reason of causing unrepeatable surface structure is uncertain. Glucose diffusion through these membranes strongly depended on the surface structure; type 2 showed a lower permeation rate than type 1 by a factor of ~ 10.

Introduction
Nanoporous membranes can be used as molecular or ionic separators for various applications, including medical devices.[Ref 1-3] Many nanoporous membranes have been tested in glucose biosensors. Biocompatibility, functional stability, and durability are necessary considerations; whereas glucose separation and diffusion control are critical functions for the glucose biosensors.[Ref 4-5] Biological fluids are often complex mixtures of proteins, electrolytes and cells etc. The unexpected molecules interfere the detection process, which negatively influences the desired biochemical and electrochemical reactions. Therefore, it is important to separate the interfering components from the targeted components to avoid the interference. Selectivity and permeation rate are two important parameters in terms of the performance of a given membrane.
Various techniques have been tried to prepare polymeric nanoporous membranes.[Ref 6-8] Deriving nanoporous membranes from self-organized block copolymers is one of the approaches, due to its highly ordered structure, uniform and controllable pore size, etc. Block copolymers consist of two or more chemically incompatible polymer chains connected via covalent bonds. If the respective blocks are sufficiently long, they tend to phase separate on the nano-scale due to entropic reason, similar to self-assembly of amphiphilic molecules.[Ref 9] Various morphologies can be formed depending on molecular weight, temperature, and degree of incompatibility of different polymer blocks. In thermodynamic equilibrium, such block copolymer samples are generally terminated by a thin layer of the lower surface energy block.[Ref 10, 11] The nanopores can be created by selectively etching one of the blocks.
In this study, we prepared nanoporous 1,2-PB membranes from 1,2-polybutadiene-*b*-polydimethylsiloxane (1,2-PB-*b*-PDMS). For this particular block copolymer, we expected that a skin layer of PDMS was present on the surface regime to minimize the air-polymer interfacial free energy, consistent with the lower surface tension of PDMS relative to that of PB.[Ref 12] For the final nanoporous membrane, the polymer-air interface will have a structure different from that of the bulk. For an asymmetric membrane, the resistance to mass transfer is determined largely or completely by the dense top layer. Therefore it is crucial to characterize the surface morphology of the membrane prepared and accordingly understand the effects on the transport property.
This work describes the preparation of nanoporous 1,2-PB membranes, and the evaluation as potential retaining and protection membranes for a glucose sensor. Flat sheet membranes were prepared in a pneumatic-drive compressing setup. A series of membranes were characterized by AFM. The effect of different surface morphologies on glucose diffusion was investigated.

Experimental

Membrane preparation

The material used was 1,2-PB-*b*-PDMS synthesized by living anionic polymerization. They were provided by the Self-Organized Nanoporous Materials group at DTU-Nanotech. 1,2-PB-*b*-PDMS was dissolved in tetrahydrofuran (THF, Sigma-Aldrich) with a concentration of ~ 688 mg/ml. Meantime, the cross-linker dicumyl peroxide (DCP, Sigma-Aldrich) was added into the polymer solution. The amount of DCP was 1% relative to the molar amount of repeating units of 1,2-PB in the block copolymer. For each polymer film to be fabricated, 50 µl of the solution was dispensed on the center of a teflon-coated borofloat glass wafer (ϕ= 10 cm), followed by drying at room temperature in air for 30 min and then in vacuum for 1 h. Next, the sample was covered with a borosilicate plate. Three pieces of aluminum (Al) foil (10 µm in thickness) were placed between the wafer and plate to control the thickness of the film to be prepared. Immediately the 'sandwich' was pressed in a pneumatic-drive compressing setup. The compressing process was performed under 4 bars in vacuum at room temperature for 1 h. Then the sample was cross-linked at 140 °C for 2 hours. After cross-linking, the sample on the borosilicate plate was separated from the teflon-coated glass wafer; separation was readily achieved because of the poor adhesion to teflon. Further, the cross-linked film was peeled off from the plate using razor blade.

Before etching, we cut the cross-linked samples into circular pieces with 9 mm in diameter. The etching agent was tetra-n-butylammonium fluoride (TBAF, Sigma-Aldrich) and the molar amount of TBAF was twice molar amount of Si-O bonds in PDMS. Selective and quantitative etching of PDMS in the cross-linked 1,2-PB-b-PDMS films was performed for 36 h at room temperature. The resultant nanoporous 1,2-PB membranes were washed in a mixture of methanol and acetone.

Membrane characterization

The thickness of the prepared nanoporous membranes was examined with an ID-H micrometer purchased from Mitutoyo. Resolution of the measurement is 0.5 µm and accuracy is 1.5 µm. The roughness of the membrane was checked on a stylus profiler, Dektak 8. The diamond stylus is 5 µm in radius. The membrane samples were pressed on a silicon wafer for scanning. Two perpendicular directions were scanned for each tested sample.

Surface morphology of the nanoporous membranes was observed by using NanoMan AFM in tapping mode. The sample to be measured was placed on a silicon wafer. All the images were obtained at ambient conditions. The scan area was 1 µm x 1 µm, and 512 x 512 pixels.

Glucose diffusion test

The diffusion set-up contains two chambers separated by the nanoporous membrane to be tested (Figure 1). The membrane with an active diameter of 4 mm was clamped between two chambers as shown in Figure 1. In order to avoid leakage of the solution, the membrane was put onto an O-ring, and the

Abstract two chambers were screwed together. We used a piece of PTFE seal tape as a support, and placed it between the membrane and the wall of permeate chamber. The surface of the prepared nanoporous 1,2-PB membrane was hydrophobic. Before the diffusion tests, the feed chamber was filled with ethanol to wet the surface and nanopores of the tested sample for 1.5 hours, then we filled both sides with pure DI water for another 1 hour.

5 ml of 100 mM glucose solution in deionized (DI) water was set in the feed side; the permeate side was filled with 5 ml pure DI water. Both chambers were stirred by standard Teflon magnetic stirrers at 320 rpm throughout the entire test. All the diffusion tests were conducted at room temperature.

For a certain interval, 50 µl of liquid was extracted from each side and the glucose concentration of the liquid in permeate chamber was analyzed with a reference analyzer provided by Radiometer Medical ApS.

The equations of mass transfer and flux are used to derive the equation which determines the effective diffusion coefficient of the measured membranes.

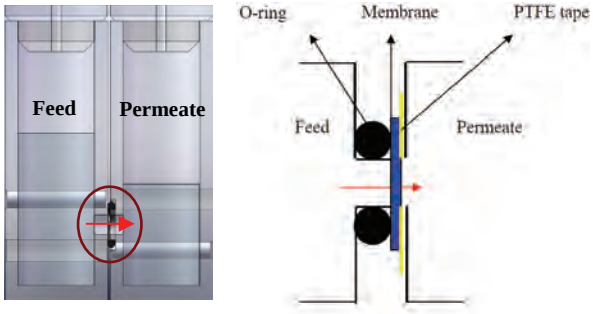

Figure 1: The schematic drawing of the diffusion setup (left). The membrane (blue) was clamped between two cells. The rubber ring was used for sealing and the PTFE was a support. Four screws were used to tighten the two chambers.

Results and Discussion

Membrane characterization

Figure 2 presents a thickness distribution of the final membranes prepared in the same batch. All these samples (ϕ= 9 mm) were cut from the cross-linked films (ϕ= 3~ 4 cm) before the etching step. We can see that the thickness was not uniform in the whole batch. Most samples were thicker than the Al spacer (10 µm) and mainly distributed from 12~ 22 µm. Currently, we found that the surface of the steel plate for compressing was not flat; it was convex, around 100 um outward. This probably led to the wide distribution of thickness. We also checked the roughness of the same batch of membranes. The results can also reflect the variation in the thickness of each membrane. Figure 3 gives the scanning curves of one representative sample. Two perpendicular directions (X direction and Y direction)

were scanned on the surface. At each direction, the scan started from the substrate (silicon wafer), moved onto the sample and through all the way down to the substrate at the end. The scanning curves showed smooth surfaces of the membranes. Appearance of some peaks or bumps might be due to either dirt on the scanned surface or air bubbles formed between the sample and the substrate. However, the curve in the lower figure in fig.3 was leaning all the way. This means the thickness of the membrane is not even along the Y direction and the difference in the thickness of two ends was ~ 3 μm. We found that the leaning surface existed commonly in most of the membranes prepared. This might be attributed to the bad quality of the compressing plate as mentioned above.

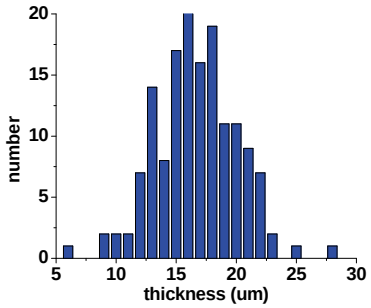

Figure 2: Thickness distribution of the entire batch of membrane samples. Each sample is 9 μm in diameter. Thickness was determined by measuring the central point of the sample with ID-H micrometer (resolution 0.5 μm, accuracy 1.5 μm).

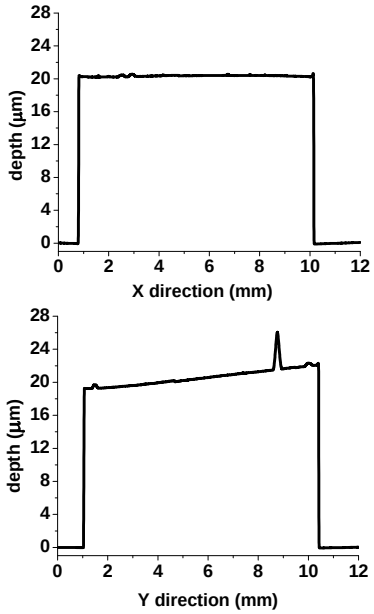

Figure 3: Stylus profile of roughness of one nanoporous membrane as a representative of the entire batch. One direction (X direction) and its perpendicular direction (Y) direction were scanned.

Thickness is one of the important parameters regarding the permeation rate of a given membrane. An increase in thickness causes a relevant increase in membrane resistance, therefore a decrease in permeation rate. Uniform thickness is necessary for well understanding and controlling the transport property of a given membrane.

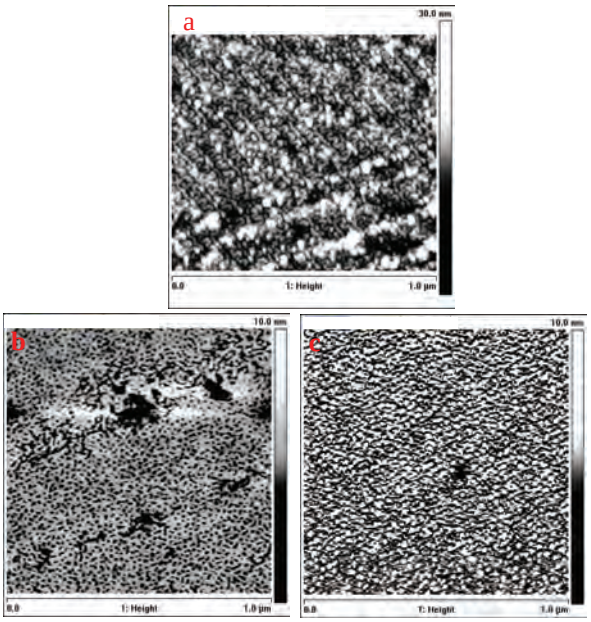

Figure 4: AFM images (acquired in tapping mode) showing (a) the cross-section of a thick membrane (500 μm), (b) and (c) two different surface morphologies found in the thin membranes (20 μm)

The surface and the bulk morphologies of the nanoporous 1,2-PB membranes were investigated by performing AFM in tapping mode, as depicted in Figure 4. Fig. 4a shows the typical knitting view of the gyroid structure in the bulk of a thick sample (500 μm) prepared in previous work, consistent with the reported results of SEM measurements [Ref 13]. Fig. 4b and 4c revealed surface characteristics of the thin membranes fabricated in this study, illustrating two different surface morphologies. In fig.4b a large number of pores randomly distributed on the entire surface measured. The diameter of the pores is approximately 10 nm and the surface porosity was around 45%. Some dark parts with a larger area than the pore size might be the surface defects. Here we referred this structure as ‘open’ structure. The surface shown in fig. 4c was close, and there were bump-like structures projecting out of the surroundings on the surface. We referred it as ‘close’ structure in this work. The formation of these two surface morphologies can be explained in terms of surface energy. Since the film was squeezed and cross-linked between the teflon-coated glass wafer and glass plate, the lower surface energy component (PDMS) would enrich in the surface region to minimize the Teflon-polymer interfacial free energy, whereas either

PDMS or 1,2-PB block shows no preference to the glass plate. Therefore in the nanoporous membrane, a relative denser skin layer (‘close’ structure) formed on the side contacting with teflon and a porous surface (‘open’ structure) on the glass side.
30 samples were selected out of the same batch and AFM was performed on both surfaces of each sample. We found that 13 samples showed the dense surface on one side and porous surface on the opposite side, as shown in fig. 4b and 4c. However, the rest of them displayed both surfaces with ‘close’ structure,. At present, the reason to form the two different types of membranes formed in the same batch is unexplained. In order to investigate the effect of the skin layer on the glucose diffusion, we decided to classify the membranes to be tested into two groups, referred to type 1 and type 2. Type 1 is the sample with one dense skin layer and one porous surface. Type 2 is the sample with ‘close’ skin layer on both sides.

Glucose diffusion tests

We evaluated glucose transport of the nanoprous 1,2-PB membranes with thickness of 20 μm, type 1 and type 2 respectively. A certain range of variation existed in the data in each group; the maximum variation was by a factor of 5. Figure 5 plots the average glucose concentrations in permeate chamber as function of time. Both types can effectively transport the glucose molecules with time, but glucose permeation rate across type 1 membrane was faster than the type 2 by a factor of 10. This remarkable difference can be attributed to the dense skin layer determining the glucose diffusion. Type 2 membranes with ‘close’ structure on both sides therefore showed much higher resistance to flux.

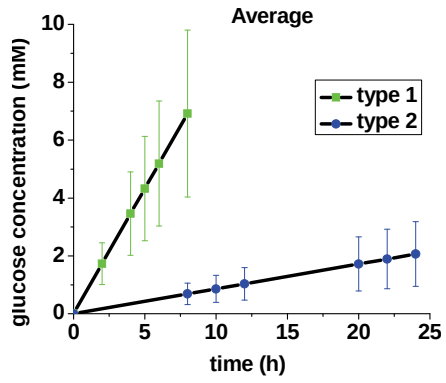

Figure 5: Glucose diffusion through nanoprous 1,2-PB membranes with different surface morphologies, type 1 (green) and type 2 (blue).

The effective diffusion coefficient is ~ 10^{-7} cm^2/s for type 1 and ~ 10^{-8} cm^2/s for type 2. The diffusion tests were run in 2~3 cycles to show a good reproducibility and stability of the membranes.

Conclusions

In the current work, membrane characterizations and glucose diffusion across two types of nanoporous membranes were investigated. Type 1 showed much faster diffusion than type 2. It is conclusive that the dense skin layer is the diffusion-limiting structure in the nanoporous membranes; however, the reason of forming the ‘close’ structure on both sides is uncertain.
In addition, compared with the reference membrane reported elsewhere [Ref 14], the effective diffusion coefficient of glucose across both types of nanoprous membranes were considerable larger than the desired value ~ 10^{-9} cm^2/s. In order to decrease the permeation rate for the studied membranes, the possible solutions are as follows, (1) different etching levels to adjust the volume porosity; (2) different UV exposure area to achieve various active porosities; (3) different thickness of the entire membrane to probably form different thickness of the dense skin layer. All these solutions will be studied in the future work.

Acknowledgements

The author acknowledges the workshop at DTU-KT for preparing the pneumatic-drive compressing setup and the diffusion setup.

References

[1] S.Zhang, G.Wright and Y.Yang, Biosensors & Bioelectronics 15 (2000) 273-282.
[2] Hillmyer, M. A., Adv Polym Sci 190 (2005) 137–181.
[3] Adiga, P.S., Curtiss, L.A., Elam, J.W., JOM 60 (2008) 26-32.
[4] Maines, A., Ashworth, D., Vadgama, P., Analytica Chimica Acta 333 (1996) 223-231.
[5] Lin, L., Guthrie, J.T., Journal of Membrane Science 173 (2000) 73-85.
[6] William A. Phillip, Javid R., Jounal of Membrane Science 286 (2006) 144-152.
[7] Olson, D.A., Chen, L., Hillmyer, M.A., Chem.Mater. 20 (2008) 869-890.
[8] Lee, S.B., Mitchell, D.T., Trofin, L., Nevanen, T.K., Soderland, H., Martin, C.R., Science 296 (2002) 2198–2200.
[9] F. S. Bates and G. H. Frederickson, Annu. Rev. Phys.Chem. 41(1990) 525.

[10] Jones, R.A.L., Kramer, E.J., Polymer 34 (1993) 115-118.
[11] Feng, C. L., Vancso, G. J., Schnherr, H., Langmuir 21 (2005) 2356-2363.
[12] Mark, J. E. Polymer Data Handbook, Oxford University Press, 1999.
[13] Szewczykowski, P. P. Nano-porous Materials from Diblock Copolymers and its Membrane Application, Ph.D. Thesis, Technical University of Denmark, 2009.
[14] Li Li, Yearbook contribution, DTU-KT, 2008.

Rasmus Lundsgaard

Phone: +45 4525 2869
Fax: +45 4525 2258
E-mail: RAL@kt.dtu.dk
WWW: http://www.cere.dtu.dk
Supervisors: Georgios M. Kontogeorgis
Bjarne Nielsen, Danisco A/S
Ulrik Aunskjær, Danisco A/S

PhD Study
Started: July 2007
To be completed: July 2010

Modeling of partition coefficients of additives in polymer/polymer and polymer/solvent systems by free energy calculations

Abstract
In the later years it has been approved by EU to estimate migration of additives from a monolayer polymer into a solvent utilizing the generally recognized migration model by EU[1] or even from multilayer polymer systems into a solvent utilizing finite element method (FEM). These models are though only as good as the parameters used, i.e. diffusion coefficients and partition coefficients. The semi-empirical model proposed by Piringer[2] for estimation of diffusion coefficients has been approved by EU, when no or only very little data exist. On the other hand, for partition coefficients, there is currently no approved consistent model.

Free energy of solvation from thermodynamic integration
It have been shown by Essex et al.[3] that from the free energy of solvation in solvent A and B (solvA and solvB in equation 1) it is possible to estimate the partition coefficient between the two solvents.

$$\log K_{solvA/solvB} = \frac{\Delta_{solvB}G - \Delta_{solvA}G}{2.303RT} \qquad (1)$$

But calculating the free energy of solvation by thermodynamic integration from molecular dynamics is not completely straight forward, as slowly stepwise elimination of all the solvent molecules is not possible. Instead the thermodynamic cycle shown below can be used to calculate this change, by calculating the other steps:

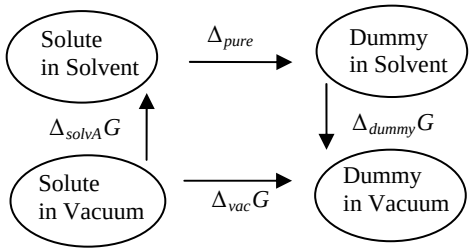

Calculations can be done knowing:
1. Decoupling of all interactions from solute to solvent gives $\Delta_{pure}G$
2. Decoupling of all interactions from solute in vacuum gives $\Delta_{vac}G$
3. The change from a dummy molecule in solvent into vacuum is zero

Thus:

$$\Delta_{solvA}G = \int_0^1 \left\langle \frac{\partial H}{\partial \lambda} \right\rangle_{\lambda}^{vac} d\lambda - \int_0^1 \left\langle \frac{\partial H}{\partial \lambda} \right\rangle_{\lambda}^{pure} d\lambda \qquad (2)$$

In equation 2 is H the Hamiltonian, and λ is the decoupling parameter going from 0 to 1. The solvent has complete coupling to the solute when λ =0, and is completely decoupled at λ =1.
It has though been shown by Shirts et al. [4], that splitting this approach up into two steps, first decoupling of electrostatic interactions and then the Lennard-Jones interactions, gives more accurate results and a more well-behaved function of the total decoupling of interactions.

Experimental
All the calculations were done using the Gromacs 4.0.3 software [5] on either an Ubuntu Linux workstation (Intel Quad-core 3.00GHz) or on an Apple OSX workstation (Intel Xeon Quad-core 2.80 GHz).
For each λ value the simulation procedure was as follows: Energy minimization using two minimization procedures (L-BFGS algorithm of Nocedal, for 5000 steps, then steepest descent minimization for 500 steps). Then a constant volume equilibration of 10 ps and a

constant pressure equilibration for 100 ps, and finally the 5 ns long NPT production run. This cycle on these types of systems takes approximately 50 min. which means a whole system can be calculated in approximately 20 × 50 min = 17 hours.
Simulations were done with 3 different force fields, to find the optimal force field for these types of calculations. The tested force fields were:

- Gromos Force field [6]
- TraPPE Force field [7]
- OPLS-AA Force field [8]

As the OPLS-AA is an All-Atom force field, it was chosen only to calculate the solute molecule with this force field, and all the solvent molecules by TraPPE as this was expected to give the best results.

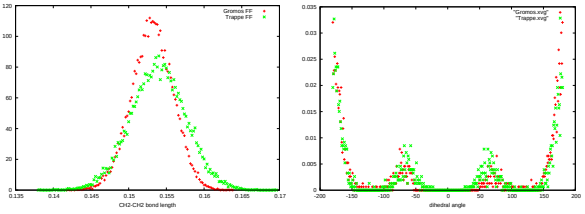

Figure 1: Statistical occupancy of the -CH_2−CH_2- bond length (left) and dihedral angle (right). The red dots are with the Gromos force field, and the green dots are with the TraPPE force field.

Results

Bond lengths and angles are plotted for solvent molecules to verify the correct use of the force fields, and as shown in figure 1 TraPPE and Gromos force fields give almost the same results. Figure 2 shows a plot of the function used for the same dihedral angle as in figure 1.

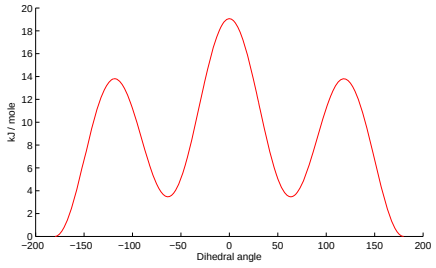

Figure 2: Plot of the function used to calculate the dihedral angle. The lowest energy state is at 180º, and two local minima at 60º.

From the calculated solvation free energies in Squalane and SPCE water (SPCE is a commonly used water model), it should be possible to calculate the partition coefficient of Ethyl butyrate between LDPE (Squalane) and water. The decoupling of the Lennard-Jones (LJ) intermolecular interactions from the solvent to the solute is shown in figure 3. Each data point is a 50 min MD simulation.

The area under the final function for the LJ (figure 3, right) and the Coloumb (not shown here) intermolecular interaction decoupling, gives the free energy of solvation for the solvent in the solute. From this solvation free energy the partition coefficient can be calculated as shown in equation 1.

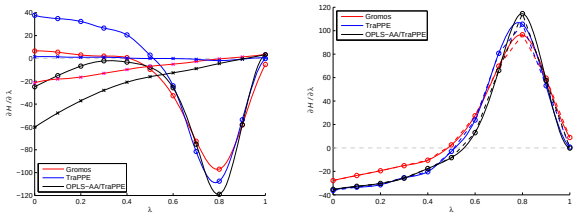

Figure 3: Ethyl butyrate in SPCE water (only LJ interactions). Left plot is the decoupling from vacuum and from solvent, right plot is the difference between the two graphs giving the decoupling of intermolecular LJ interactions of the solute molecule to the solvent

Table 1: The free energy of solvation of Ethyl butyrate into water and Squalane, and the partition coefficient between the two.

	$\Delta_{solv}G$ in water	$\Delta_{solv}G$ in Squalane	log $K_{P/L}$
Gromos	1.12	-30.82	5.597
TraPPE	-8.06	-19.73	2.045
OPLS-AA	-10.83	-25.13	2.506
Exp	-10.59 *[KJ/mol]*	*[KJ/mol]*	1.6-2.76

Conclusion

As shown in table 1, the calculated solvation free energies into water by this method was very close to the experimental results when using the TraPPE force field and even better with the OPLS-AA force field. The Gromos force field can for the moment not be used for polar molecules because of no consistent way of setting the atomic charges, even the best setup gives a high deviation from the experimental value as seen in table 1.

Acknowledgement

Dr. Ioannis Economou for help and guidance; Danisco A/S, MP_2T and DTU for the funding of this project.

References

[1]D. Byrne; Official Journal of the European Union, 220 (2002), 18-58
[2]O. Piringer, A.L. Baner: Plastic packaging - Interactions with food and pharmaceuticals; Weinheim Wiley-VCH, 2008
[3]J.W. Essex, C.A. Reynolds, W.G. Richards, J. Chem. Soc., Chem. Commun., 1989, 1152-1154
[4]M.R. Shirts, J.W. Pitera, W.C. Swope´, V.S. Pande; J. Chem. Phys., 119 (2003), 5740-5761
[5] B. Hess, C. Kutzner, D. van der Spoel, E. Lindahl; J. Chem. Theory Comput., 4 (2008), 435-447
[6]C. Oostenbrink, A. Villa, A.E. Mark, W.F. Van Gunsteren; J. Comput. Chem., 25(2004), 1656-1676
[7]M.G. Martin, J.I. Siepmann; J. Phys. Chem. B, 102 (1998), 2569-2577
[8]W.L. Jorgensen, D.S. Maxwell, J. Tirado-Rives; J. Am. Chem. Soc., 118 (1996), 11225-11236.

Philip Lutze
Phone: +45 4525 2960
Fax: +45 4588 2258
E-mail: PiL@kt.dtu.dk
WWW: http://www.kt.dtu.dk
Supervisors: John M Woodley
Rafiqul Gani

PhD Study
Started: December 2008
To be completed: November 2011

Development of a Systematic Synthesis/ Design Methodology to Achieve Process Intensification

Abstract
The chemical, biochemical and pharmaceutical industries are facing new challenges which need improvements in manufacturing processes. Process intensification (PI) has the potential to improve existing processes or create new process options which are needed in order to produce products using more sustainable methods. PI creates an enormous number of process options. In order to manage the complexity of options in which a feasible and optimal process solution may exist, the application of process synthesis tools results in the development of a systematic methodology to implement PI. Starting from an analysis of existing processes, this methodology generates a set of feasible process options and reduces their number through a sequence of screening steps until the optimal is found. The developed methodology will be tested and verified with case studies from the chemical, biochemical and pharmaceutical sectors.

Introduction
Process intensification (PI) provides opportunities, as well as challenges, to satisfy the needs for significant improvement or development of new process options in the (bio) chemical industry in order to achieve more sustainable production. Process intensification can be defined as the improvement of a process by adding/enhancing phenomena in a process through the integration of operations, integration of functions, integration of phenomena or alternatively through the sole enhancement of phenomena in a given operation (Arizmendi-Sánchez and Sharratt, 2008). Examples of already developed PI equipment are given in the following table 1.

Table 1: Examples for PI equipment with respect to the definition of PI.

Principle	PI Equipment
Integration of operation	Reactive Distillation, Distillation-Pervaporation,…
Integration of function	Heat-Exchanger reactor, static mixer reactor,…
Integration of phenomena	Spinning disc reactor, static mixer, …
Sole enhancement of phenomena	Microreactor, …

Using the above definition, PI potentially creates a large set of alternative process options. Hence, obtaining a feasible intensified process option that optimally improves the process is difficult.

Process synthesis is the systematic strategy to identify the optimal path to reach a given product in the desired quality and quantity with respect to defined constraints on the process. Therefore, application of process synthesis tools to achieve PI leads to the development of a PI synthesis/design methodology in which redundant intensified process options are systematically removed by checking against predefined constraints.

Specific Objectives
The specific objectives of this project are:

- Development of a general systematic synthesis/ design methodology to achieve PI together with associated tools and algorithms
- Development/ Implementation of the computer-aided methodology into a software environment
- Test/ validate methodology through several case studies

Methodology
The focus of the methodology is two-fold. First, all intensified options are generated and second, through

screening with respect to feasibility and performance, the search space is reduced in order to locate candidate process options from which the optimal improved process is found. Therefore, in the proposed methodology for PI, the search space for locating feasible intensified process options is reduced stepwise by employing a hierarchical sequence of steps where the lower level steps employ simple and easy calculations, while the higher level steps employ more rigorous and detailed calculations, as shown in Figure 1. In this way, as in the techniques for computer aided molecular design (Harper and Gani, 2000), large numbers of infeasible options are screened out early and the remaining are gradually removed through further (more detailed) analysis. Such a methodology is reliant on structured knowledge, which is provided in this work through a knowledge base where relevant information is classified in terms of known intensified processes and the principles on which the intensification are based, different methods for achieving PI and the tools employed to achieve them.

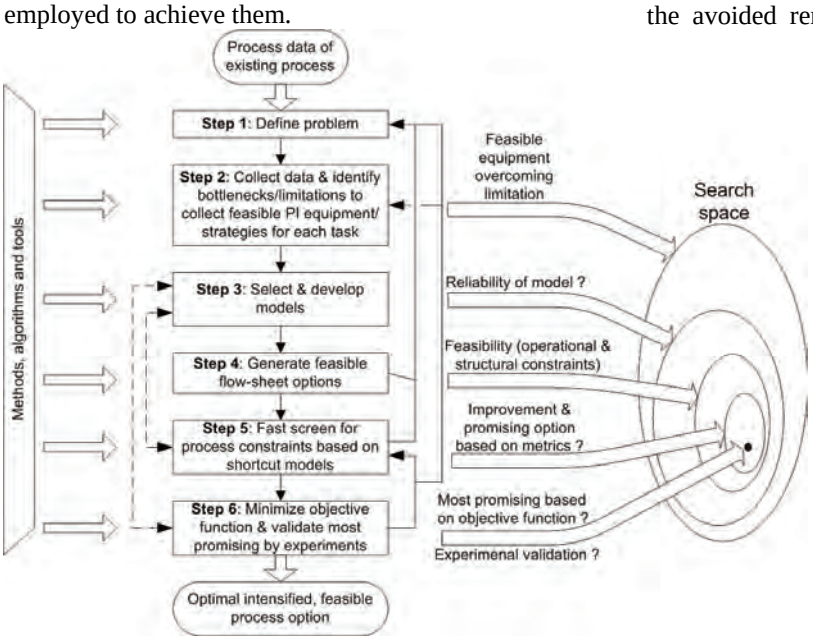

Figure 1: Systematic Methodology

The input to the methodology (and the specific synthesis methods) is information about an existing or a conceptual process. Subsequently, the PI-synthesis/design problem is defined and the metrics for evaluation and the objective function are selected based on sustainability requirements such as operational costs, capital costs, safety, energy consumption, waste generation, efficiency and development time, as well as intensified metrics, such as simplification, residence time, volume and flexibility.

Results and Discussion

The (so far) developed methodology has been applied to a case study of a batch production of isopropyl acetate (and water) from isopropanol and ethyl acetate. First, the objective has been defined to increase the yield of the process, currently 74.4%, without sacrificing the other metrics. The production is constrained to the amount of product per time and only the reaction step is under investigation. In the next step, the process has been thoroughly analyzed in order to identify the limitation which is the unfavorable equilibrium. A developed knowledge base, containing structured (ontology-based) published information about PI, has been consulted to identify possible PI strategies/ equipment which potentially overcome the observed limitation of the process. The search has been restricted only to the first principle of PI, so two possible strategies are identified, reaction-separation and the integration of two reactions. Only the first strategy is promising which leads to twenty different PI equipment options. After screening with respect to the necessary conditions obtained in the analysis, the search space is reduced to six intensified PI-equipments. From a superstructure of a generic model, developed in step 3, and taking structural constraints into account, such as the avoided removal of reactant and consideration of only one solvent per option, 100 different process options has been synthesized in step 4 from the equipment options obtained earlier. Through screening with respect to additional structural and operational constraints, such as waste metrics, the search space can be successful reduced to two process options.

After fast screening for process constraints in step 5 and minimization of the objective function (step 6) which is defined as the inverse of the yield, the most promising option is the internal integration of a reactor and a pervaporation to remove water in-situ to shift the equilibrium. The yield has been optimized to 96.1%.

Conclusions

The development of a systematic synthesis/design methodology to achieve PI is important to handle the complexity of PI process options. The application of the so far developed methodology to a case study shows promising results. Future work will be to refine the steps of the methodology to ensure applicability to a large number of processes and enlarge the number of computer-aided tools and algorithms such as a model library.

Acknowledgements

The author wishes to thank the Technical University of Denmark for financial support.

References

J. Arizmendi-Sanchez, P. Sharratt, Chemical Engineering Journal 135 (2008) 83-94.

P. M. Harper, R. Gani, Computers and Chemical Engineering 24 (2000) 677-683.

Karin Madsen
Phone: +45 4525 2826
Fax:
E-mail: kam@kt.dtu.dk
WWW: http://www.kt.dtu.dk
Supervisors: Anker Degn Jensen
Flemming Frandsen
Joakim Reimer Thøgersen, Haldor Topsøe

Industrial PhD Study
Started: May 2008
To be completed: May 2011

Mercury Chemistry in Flue Gas

Abstract
The speciation of mercury in flue gases from combustion processes is important to understand in order to optimize the mercury removal in the flue gas cleaning equipment. Mercury in oxidized form favors a high degree of removal, because $HgCl_2$ is soluble in water and is effectively removed in a wet scrubber.
The vanadium-based selective catalytic reduction (SCR) catalyst has been shown to have catalytic activity on mercury oxidation. This project is devoted to examining the catalytic oxidation of mercury across the SCR catalyst.

Introduction

Mercury emissions from coal-fired utility plants range from 1-20 µg/Nm^3 depending on the type of coal applied, the flue gas composition, operating conditions and the air pollution control devices (APCDs) [1].

Three mercury species are normally considered: elemental Hg^0, oxidized Hg^{2+} and particle bound Hg^p. It is important to understand the speciation of mercury in flue gasses in order to optimize the mercury removal in the flue gas cleaning equipment. Oxidized mercury is soluble in water and is effectively removed in a wet scrubber or by adsorption on fly ash in fabric filters. Elemental mercury is in contrast difficult to capture in existing APCDs due to its high volatility and low solubility.

Figure 1 shows the average partitioning of mercury in different process streams based on studies of power plants in the Netherlands.

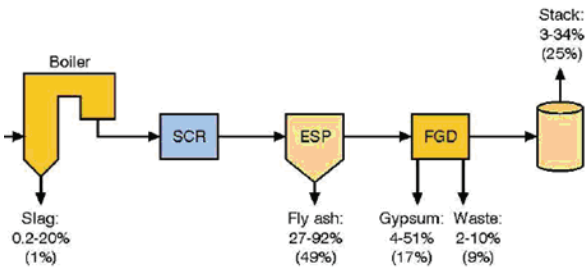

Figure 1: Typical partitioning of mercury in process streams from power plants [2].

Coal mercury is converted to gaseous Hg^0 in the combustion flame and is subsequently partially oxidized as the combustion gas cool. According to thermodynamic calculations all mercury should exist in the oxidized form for temperatures lower than 400°C [3]. Various full-scale and laboratory measurements show that the fraction of oxidized mercury ranges from 35-95%, which indicates that the conversion is kinetically controlled [1].

Mercury chlorination ($HgCl_2$) is generally considered to be the most dominating mercury transformation mechanism. The degree of mercury oxidation is also strongly correlated with the chlorine content in the coal, but many other parameters have been demonstrated to influence the mercury speciation. A fundamental understanding of the reactions taking place in the flue gas is needed in order to predict the mercury speciation.

International research of this type is under way and can generally be broken down into the study of homogeneous gas-phase reaction during quenching of the flue gas and heterogeneous gas/solid reactions with the fly ash. Furthermore, the vanadium-based selective catalytic reduction catalyst (SCR) has been shown to have catalytic activity on the mercury oxidation [4,5].

Specific Objectives

This project is devoted to examining the mercury oxidation across the SCR.

The SCR catalyst in lab-scale experiments has the effect of rendering the mercury speciation at the outlet close to equilibrium. Yet in full scale experiments, mercury in

the flue gas does not appear to come as close to equilibrium [6].

The mechanism for the catalytic oxidation across the SCR is not fully understood. In both lab- and full-scale experiments, a positive effect of chlorine and an inhibitory effect from ammonia has been reported [4,5,6]. However, the influence of other flue gas constituents and also of operating conditions is not as unambiguously reported in literature. A better understanding of this complex interplay is needed in order to optimize the oxidation.

Methodology

The catalytic reaction is being studied in a laboratory setup at Haldor Topsøe A/S. Here a simulated flue gas containing elemental mercury is passed through a SCR-reactor. The influence of flue gas constituents (such as HCl, SO_2, NO, NH_3, O2 and H_2O) and also operating conditions (such as temperature, space velocity and catalyst age) will be examined.

Full-scale experiments have been carried out at Plant Crist in Pensacola, Fl, where the mercury conversion across an SCR catalyst was measured in a slipstream.

Kinetic and thermodynamic modeling is being performed based on this data in order to get a better understanding of the mechanism for mercury oxidation on the catalyst.

Figure 2 shows the Mercury Research Center at Plant Crist, which functions as a research platform for various air pollution control devices.

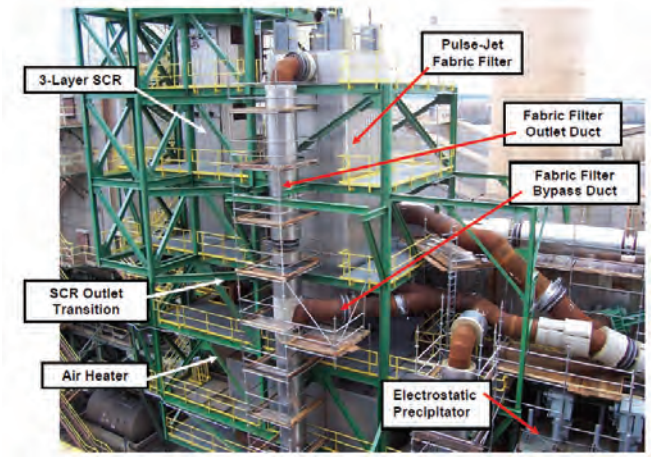

Figure 2: The Mercury Research Center is a 5 MW-equivalent slipstream facility.

Conclusions

An increased understanding of the mercury oxidation across the SCR catalyst can potentially be a means of optimizing the mercury removal from flue gasses in existing air pollution control devices.

References

1. J.H Pavlish, E.A. Sondreal, M.D. Mann, E.S. Olson, K. C. Galbreath , D.L. Laudal, S.A. Benson, Fuel Processing Technology 82 (2003) 89-165.
2. R. Meij, H. Winkel, Sci. Total Environment (2006), 368-393.
3. F. Frandsen, K. Dam-Johansen, P. Rasmussen, Prog. Energy Combustion Science 20 (1994), 115-138.
4. R. Mei, L.H.J Vredenbregt, H. te Winkel, Air & Waste Management Association 52 (2002), 912-917.
5. Pilot-scale screening evaluation of the impact of selective catalytic reduction for NOx on mercury speciation, EPRI, Palo Alto, U.S. Department of Energy, Morgantown, Wv, and U.S. Environmental Protection Agency, Raleigh, NC: 2000. 1000755.
6. Communication with C. Senior (2004), Reaction Engineering International, Salt Lake City, UT.

Malwina Michalak
Phone: +45 4525 2979
Fax: +45 4593 2906
E-mail: mmi@kt.dtu.dk
WWW: http://www.bioeng.kt.dtu.dk
Supervisors: Jørn Dalgaard Mikkelsen
Gunnar Jonson
Manuel Pinelo

PhD Study
Started: November 2008
To be completed: September 2012

Production and Purification of Prebiotic Oligosaccharides by Chromatography and Membrane Systems

Abstract
Prebiotics are non-digestable food ingredients that have beneficial effect on the host microbiota. Known examples of prebiotic food ingredients are oligosaccharides, e.g. fructans and fructooligosaccharides from Jerusalem artichokes, glactooligosaccharides obtained from lactose and maltooligosaccharides from starch. A large number of oligosaccharides with potential prebiotic effects can be obtained by degradation of side streams form the agricultural industry. This requires a number of specific enzymes which can be obtained by cloning and expression in the yeast *Pichia pastoris*. The oligosaccharides produced by the enzymatic catalyses may be purified by membranes and chromatography. The prebiotic potential of the oligosaccharides will be elucidated by functionality tests.

Introduction
Functional food ingredients possessing potential health benefits have become popular nowadays. Some of compounds displaying capability to improve the food are prebiotics. Prebiotics are non-digestable substances, which provide a beneficial effect on the host by selective stimulation of growth of a limited number of indigenous bacteria. The growth of such bacteria can be promoted by, for example, provision of oligosaccharides. Oligosaccharides could be obtained as products of hydrolysis of polysaccharides, like food hydrocolloids. Performing the hydrolysis by means of enzymes would make it selective and sustainable.

Specific objectives
The idea of the project is to use selective enzyme catalysts to convert polysaccharides into oligomers. Only few of the commercial enzymes are available for this task. Most of the commercial enzymes in addition contain other enzyme activities which degrade the desired oligosaccharides. Mono-component enzymes can, however, be produced by cloning and expression of suitable enzymes in the yeast, *Pichia pastoris.* This process can be performed in the laboratory of Genetically Modified Orgamisms (GMO) located at our department.

Furthermore, the optimal conditions of enzymatically catalyzed reactions have to be worked out. This includes up-scaling of the enzymatic reaction in order to deliver sufficient amount of oligosaccharides with potential prebiotic activity for evaluation. Moreover, the separation and purification process comprising chromatography and membrane systems, has to be established and optimized.

Production of enzymes by fermentation of *Pichia pastoris*
In order to produce a desired enzyme, the gene has to be cloned and inserted into the genome of the host cell of *Pichia pastoris*. Subsequently, the recombinant product is expressed in the yeast. The genetically engineered strain of yeast is grown in a fermentor. During this process such parameters as pH, temperature, rate of aeration are maintained at optimal level. Glycerol is used as a carbon source both in the batch and fed-batch mode to generate high cell density. Methanol is used for induction of the enzyme expression. The enzymes are excreted into the media. Thus, in order to recover the enzymes, the yeast cells are collected by centrifugation. The supernatant is subjected to sterile –and ultrafiltration.

The harvested enzyme is subjected to a number of analysis and purification processes. This comprises determination of protein concentration, SDS-PAGE, measurements of enzyme activity and determination of kinetic parameters. A typical result for the SDS-PAGE is shown in Figure 1. The molecular mass of the enzyme is 38,6 kDa. It can be seen that the harvested solution contains other protein bands with higher and lower molecular weigths than the desired enzyme.

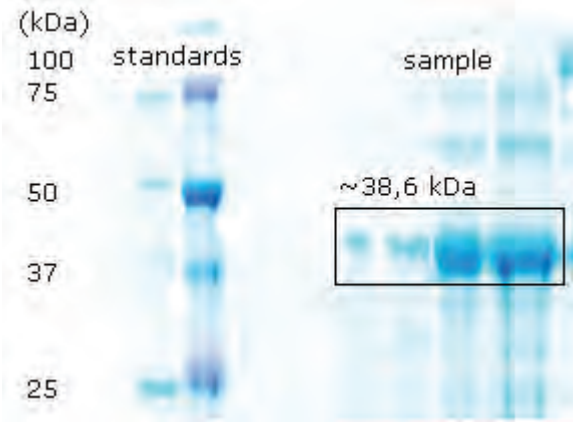

Figure 1: Example of SDS-PAGE of enzyme produced in the GMO laboratory. * The bands of the enzyme have different intensity due to different samples concentrations.

To purify the enzymes requires further methods, such as affinity chromatography (His-Tag), gel filtration and/or ion exchange chromatography (IEX). Our genetically engineered proteins contain a His-Tag tail, which comprise 6 histidines. This enables separation of the desired protein from other contaminating proteins. His-Tag protein is captured in a metal affinity column where Cu^{2+} or Ni^{2+} are used as the ligand. Contaminating proteins without the His-Tag are present in the run-off fraction of the column. His-Tag protein is eluted with solution of imidazole.

The activity of enzymes is assessed by different assays depending on the enzyme produced. But there is also a method universal for all enzymes hydrolyzing polymers, e.g. the reducing sugars assay. When the polymer is degraded the sugars with reducing ends are created.

Enzymatic hydrolysis and separation of products

The purified mono-component enzymes with the desired activity are used to catalyse the hydrolysis of polymeric substrates. The progress of the reaction can be monitored by reducing sugar analysis, high performance liquid chromatography (HPLC) or by thin layer chromatography (TLC). Among these methods, TLC is the fastest, the cheapest and the most reliable technology. TLC enables separation of oligosaccharides of different degree of polymerization, as is depicted in Figure 2. The reaction samples E1 comprise more oligomers than samples E2. It is due to the use of two different enzymes in samples E1 and E2.

Oligosaccharides, if obtained in a bigger scale, can be separated from the polymeric substrate by membrane filtration. Furthermore, single oligomers may be obtained by performing HPLC or TLC in a preparative scale.

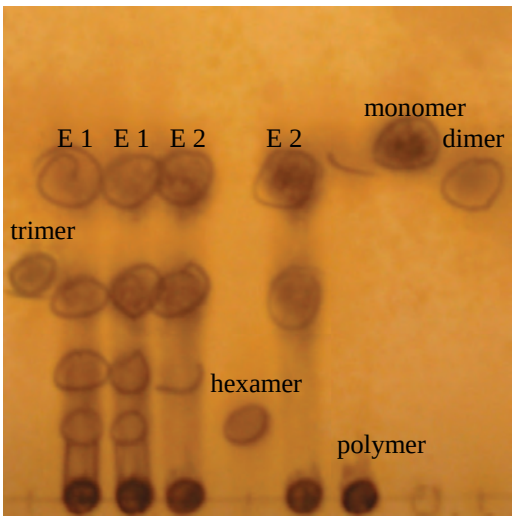

Figure 2: Example of TLC analysis of post-reaction mixture of enzymatic hydrolysis of polysaccharide.

Acknowledgements

The project is carried out within the Center for Biological Production of Dietary Fibers and Prebiotics at DTU ("Prebiotics Center").

David Mogensen

Phone: +45 4525 2922
Fax: +45 4588 2258
E-mail: dam@kt.dtu.dk
WWW: http://www.kt.dtu.dk (no personal page)
Supervisors: Prof. Kim Dam-Johansen
Prof. Jan-Dierk Grunwaldt
Jens U. Nielsen, Topsøe Fuel Cell A/S
Peter Vang Hendriksen, Risø

PhD Study
Started: November 2007
To be completed: October 2010

Mathematical Modeling of Solid Oxide Fuel Cells

Abstract

Solid Oxide Fuel Cells (SOFC) is a technology that potentially allows an increase of the efficiency of electricity production. Furthermore it has the advantage that even small units can be operated at high efficiency, which allows a decentralized power supply and thereby an increased utilization of local energy sources.
To achieve an optimal design and operation of an SOFC fueled by natural gas, kinetic expressions are required which are able to accurately describe the steam reforming rate. There are significant differences in the reported kinetic expressions over the anode material Ni-YSZ. The primary goal of this project is to determine both the intrinsic kinetics and the kinetics in an SOFC anode structure.

Introduction

The fossil fuel reserves are limited and because of this, it is necessary to investigate technologies that can be used to make our society independent of fossil fuels [1]. SOFC technology is highly versatile since it can use a large number of different fuels either from fossil or renewable sources, such as H_2, CH_4 and NH_3, methanol, dimethylether and diesel [2].

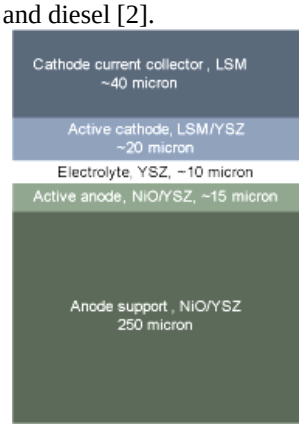

Figure 1: A schematic illustration of an SOFC as produced by Topsøe Fuel Cell A/S [8].

An SOFC is an electrochemical cell, which is continuously supplied with separated streams of gaseous fuel and air/oxygen. The species that is transported through the solid electrolyte is O^{2-}.
Both electrolyte and electrodes in the cell are made of ceramic materials and in order to obtain a sufficient rate of oxygen ion transport through the electrolyte a temperature in the range 600 K to 1000 K is needed. The configuration and materials of an SOFC are shown schematically in Figure 1. In this case the cathode is composed of strontium doped $LaMnO_3$ (LSM) and LSM on yttria-stabilized zicronia (YSZ), the electrolyte of YSZ, and the anode of NiO/YSZ [3].
The main electrode reactions taking place in the cell are:
Anode:

$$H_2 + O^{2-} \rightarrow H_2O + 2e^-$$

Cathode:

$$\tfrac{1}{2}O_2 + 2e^- \rightarrow O^{2-}$$

If methane is used directly as the fuel, it is catalytically converted into hydrogen by the Ni present in the anode material [6]. The overall steam reforming reaction is:

$$CH_4 + 2H_2O \rightleftarrows 4H_2 + CO_2$$

At the high temperatures that have typically been used in SOFCs the steam reforming reaction is very rapid (> 750 ºC), which means that little interest has been paid to the exact kinetics. Recent research has been focused on lowering operating temperature of an SOFC. Hence, it is now possible to tune the degree of internal reforming by carefully controlling the rate.
There are, however, big differences in the kinetic expressions that have been reported for steam reforming over Ni-YSZ [5-7]. Therefore a more thorough examination of the kinetics is necessary before optimization is possible.

Results and Discussion

The experiments where conducted in a packed bed reactor in differential conversion. The bed consisted of powder from a crushed industrial SOFC anode diluted with Mg-Al-spinel powder. The setup was tested for mass transport effects by varying total flow rate and the particle size of the catalyst powder.

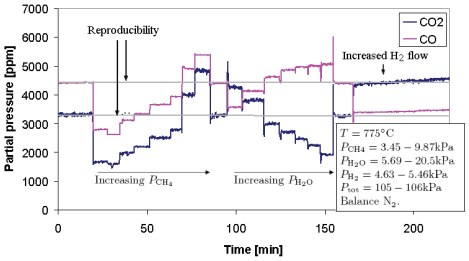

Figure 2: Rate determination experiment.

Figure 2 shows the concentrations of CO and CO_2 at the outlet of the reactor for a typical rate determination experiment. The grey lines indicate the standard conditions that are used as reference between each set of concentration variations and are therefore called "reference lines" (give exact conditions).
These experiments have been used to determine an expression for the steam reforming kinetics similarly as suggested by Wei & Iglesia [10], for Ni on Mg-Al-spinel, see equation 1.

(1) $$r = kP_{CH_4}^{\alpha} P_{H_2O}^{\beta} \cdot \left(1 - \frac{Q}{K}\right)$$

Where k is the rate constant K is the equilibrium constant and Q is the reaction quotient for the steam reforming reaction. The factor (1-Q/K) accounts for the distance from equilibrium. The rate constant is described by an Arrhenius type expression and Table 1 shows the values of the activation energy and the pre exponential factor, both for a best fit, and for α=1 and β=0.

Table 1: two possible sets of values of the constants for the kinetic expression

α	β	E_a	A
1	0	$124 \pm 6 kJ/mol$	$0.0115 \frac{mol}{g\,Pa\,s}$
0.899	-0.155	$123 \pm 3 kJ/mol$	$0.102 \frac{mol}{g\,Pa\,s}$

It should be noted that a dependence on the hydrogen partial pressure was also observed, this has not yet been fully investigated since a long term dynamic effect occurs after a change in hydrogen partial pressure. This can be seen in the right part of Figure 2 (170 - 220 min, slight increase). Another dynamic effect was observed during startup, as shown in Figure 3, and after temperature changes.
The two graphs in Figure 3 show the same results, but on different time scales. Figure 3 (a) shows that the catalyst reactivates over several hours. In addition, it seems that there is an equilibration period in the beginning until the reactivation starts.
This behavior has not previously been reported. The majority of the studies concerning the catalytic activity of Ni with regard to steam reforming, did, however, not use YSZ as the support material and the nickel particle size was much smaller [11, 12]. Because of this, we expect that the observed dynamic behavior is caused by YSZ and experiments are currently being conducted in order to investigate this in more detail.

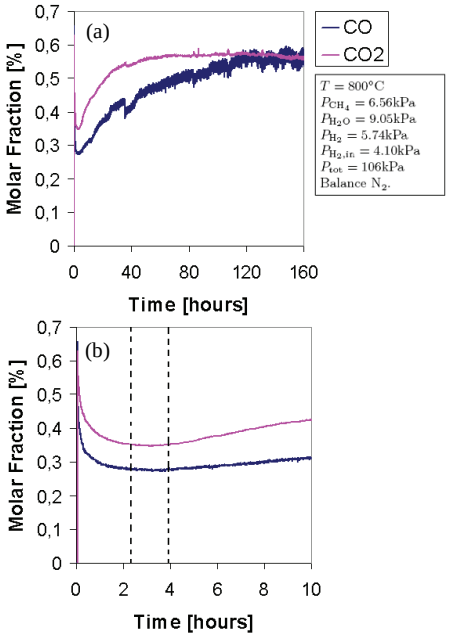

Figure 3: (a): CO and CO2 molar fraction in the outlet. (b): smaller time scale.

In summary, the present study aims at determining the kinetics of internal stem reforming over Ni-YSZ, that will be later used to model an SOFC and optimize its performance.

Acknowledgments

The work was carried out in collaboration between the Combustion and Harmful Emission Control (CHEC) Research Centre at the Technical University of Denmark, Topsøe Fuel Cell A/S, and the Graduate School in Chemical Engineering: MP_2T. Furthermore, several persons at Risø-DTU are strongly involved in the work and have given valuable help. The CHEC research Centre is co-founded by the Technical University of Denmark, Dong Energy, FLSmidth, Hempel's Fond, Vattenfall, Haldor Topsøe, Energinet.dk, The Danish Technical Research Council, The Danish Energy Research Programme, Nordic Energy Research, the European Union and several other industrial partners.

References

1. M. Asif, T. Muneer, Renewable and Sustainable Energy Reviews 11 (2007) 1388-1413.
2. N.Christiansen, J. B. Hansen, H. Holm-Larsen, S. Linderoth, P.H. Larsen, P.V. Hendriksen, M. Mogensen, Fuel Cells bulletin 8 (2006) 12-15.
3. http://www.topsoefuelcell.com/, 27/11-2007.
4. W. Vielstich et al., Handbook of Fuel Cells, John Wiley & Sons Ltd, 2003 ISBN: 0-471-49926-9.
5. J. Wei, E. Iglesia, Journal of Catalysis 224 (2004) 370-383
6. S. H. Clarke et al., Catalysis Today 38 (1997) 411-423
7. J. R. Rostrup-Nielsen, J. Sehested, and J. K. Nørskov., Advances in Catalysis 47 (2002) 65–139

Merlin Alvarado-Morales

Phone: +45 4525 2981
Fax: +45 4593 2906
E-mail: mal@kt.dtu.dk
WWW: http://www.capec.dtu.dk
Supervisors: Rafiqul Gani
John M. Woodley
Krist V. Gernaey

PhD Study
Started: April 2007
To be completed: March 2010

Synthesis, Design and Analysis of Downstream Separation in Bio-refinery Process through a Group-Contribution Approach

Abstract
There is an urgent need to bring commercially viable and technically effective bio-refineries in order to supply the chemical and energy needs of society and mitigate the environmental effects of fossil fuels and their rapid depletion. The use of a systematic approach to identify, analyze and improve processing routes for a specific bio-refinery product or products, is therefore a useful first step in the evaluation of the bio-refinery product tree. A novel systematic approach to simultaneously model, design, and synthesize chemical and biochemical processes is proposed. This approach is based on applying the principles of the group-contribution approach for pure component property prediction to the synthesis and design of chemical process flowsheets. The method is highlighted through a biorifinery case study to produce three commercial products.

Introduction
In the group-contribution method for pure component/mixture property prediction, a molecular identity is described by means of a set of groups bonded together to form a specified molecular structure. By analogy, for flowsheet property prediction, a process flowsheet can be described by means of a set of process-groups bonded together to represent a specified flowsheet structure. The process-groups can represent either a single unit operation (such as a reactor, distillation, crystallization, etc.) or a set of unit operations (such as extractive distillation, pressure swing distillation, etc). The bonds among the process-groups represent the streams and/or recycles, in analogous manner to the bonds that link molecular groups. Consequently, each process-group provides a contribution to the properties of the flowsheet. The properties can be the performance in terms of energy consumption, operating cost, profit, environmental impact, etc. In this way, once the process flowsheet is described by the process-groups, the property of interest can be calculated. Therefore, based on this premise we have applied the group-contribution approach to systematically model, synthesize/design and analyze downstream separation from chemical and biochemical processes. The main idea of the approach is based on the process-group approach [1] to solve synthesis/design problems related to chemical processes. In order to represent an extended set of unit operations, an extended set of corresponding process-groups have been developed. The application range of the new set of process-groups is illustrated by means of a bio-refinery case study involving the production of three commercial products: bioethanol (bioEtOH), succinic acid (SA), and diethyl succinate (DES), for which, energy efficient processing options have been identified.

Overview of the method
The process-group contribution based method consists of the following seven steps: (1) synthesis problem definition, (2) synthesis problem analysis, (3) process-group selection, (4) generation of flowsheet candidates, (5) ranking/selection of flowsheet candidates, (6) reverse simulation, and (7) final verification. Step 1 involves two tasks as objectives: i) the definition of structural constrains, which are related to the raw materials (inputs) and desired products (outputs) of the process flowsheet and ii) the selection of the flowsheet target property. In Step 2 the objective is to generate information for the subsequent steps. This step involves two tasks: i) reaction analysis and ii) pure component/mixture analysis. The reaction analysis is performed with the objective of identifying the reaction tasks needed to produce the desired product through a database search to find the chemical reactions yielding the desired product. The pure component/mixture analysis is performed by means of the thermodynamic insights based method [2] to identified the feasible

separation techniques to be used in the synthesis problem. In step 3, the process-groups are matched with the separation techniques identified in step 2. The objective in step 4 is to combine the process-groups selected in step 3 according to a set of connectivity rules and specifications [1] to generate flowsheet structures. In step 5 the generated flowsheet structure candidates are tested with respect to their target property values defined in step 1, using the corresponding flowsheet property model. Step 6 involves two tasks i) the resolution of the mass balance through each process-group in a process flowsheet structure and ii) the calculation of the flowsheet design parameters of the process unit operations through reverse simulation [1] in the flowsheet structure. The reverse simulation for separation process-groups (distillation, extractive distillation, flash) is based on driving force (*DF*) concept [3]. For the reactor process-group, it is based on identifying the highest point in the *AR* diagram [4] and using this point (reactant-product concentration) as the reference to determine all other reactor design parameters. In step 7, all the necessary information to perform the final verification through rigorous simulation is available. The use of a commercial simulator allows further fine-tuning of the flowsheet candidates and the possibility to perform optimization of the design parameters for the most promising design candidates.

Application of the method

Case study: The starting point of the case study is a slurry generated by a saccharification process where the conversion of cellulose to glucose is catalyzed by a cocktail of enzymes. The available glucose in the slurry to be converted into bioEtOH and SA is equal to 32110 *kg*/*h*. In order to calculate the amount of glucose that should be converted into SA, a mass balance is done based on a SA production capacity of 190.34 kg_{SA}/h and an annual load equal to 8406 *h*/*yr*. This SA production capacity corresponds to 10% of the current worldwide SA production [5]. Assuming a SA yield on glucose equal to 0.775 [6], the amount of glucose needed to produce this amount of SA is equal to 246 *kg*/*h*. From mass balance calculations, the amount of saccharified slurry containing this amount of glucose corresponds to 2811.6 *kg*/*h*. The remaining slurry is sent to the bioEtOH production plant where bioEtOH is produced by fermentation.

Step 1-Synthesis problem definition: Based on the above analysis, the structural definition of the synthesis problem related to the downstream separation of bioEtOH from the effluent of the fermentor is formulated as follows: 1 input process-group initialized with the mixture coming out of the fermentor and 1 output process-group initialized with the desired product, bioEtOH. The flowsheet property is the energy consumption of the process and the design objective (target) is to minimize this value. The structural definition of the synthesis problem related to SA production is formulated as follows: 1 input process-group initialized with mixture produced by the saccharification reactor, and 1 output process-group initialized with the desired product, SA. The flowsheet property is the energy consumption of the process and the design objective (target) is to minimize this value. For the DES production process the structural definition is formulated as follows: 1 input process-group initialized with the bioEtOH and SA streams resulting from their respective production process, and 1 output process-group initialized with the DES. Figure 1 depicts a schematic representation of the synthesis problem.

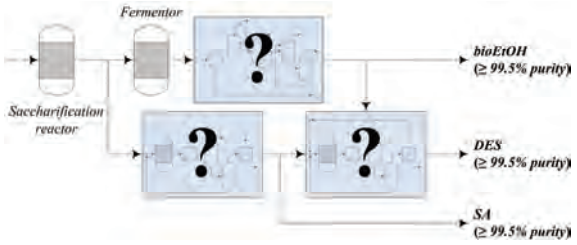

Figure 1: Schematic representation of the synthesis problem.

Step 2-Synthesis problem analysis: Based on the reaction analysis and performing a search database, the corresponding sets of reactions to produce SA by fermentation [6] and DES [7] have been identified. From the pure component/mixture property analysis for the bioEtOH process, flash separation has been identified to separate CO_2 and O_2 from the others components. Flash/evaporation and distillation were identified as alternatives to perform the separation of water of the rest of the components, except for the ethanol/water binary pair, which forms an azeotrope. Further analysis of this binary azeotrope indicated that ethanol can be recovered by using liquid membrane, pervaporation, gas adsorption or extractive distillation. For the SA process, formic acid, pyruvic acid, CO_2, H_2 O_2, ammonia and microbial cells were found to be either products and/or reactants in the reactions. Crystallization has been identified to separate SA from the rest of the components. However, due to the highly dilute nature of the mixture, liquid-liquid extraction has also been identified as suitable for the separation of water form the others components in the mixture. As DES is produced form SA via the intermediate formation of MES, this component was also taken into account for the component/mixture analysis. Flash/evaporation, liquid membrane, and pervaporation, were identified to perform the separation of water and ethanol from the others components in the DES synthesis problem. Crystallization has been found as a feasible separation technique to separate SA from DES and MES, while liquid adsorption, liquid membrane, and pervaporation have been identified to perform the separation of DES and MES.

Step 3-Process-group selection: The corresponding process-groups are selected from the process-group

database matching the separation techniques identified in step 2.

Step 4-Generation of flowsheet candidates: By combining the process-groups selected in step 3, 360 feasible flowsheet design candidates have been generated. Out of theses 360 flowsheet design candidates, 5 process flowsheet candidates are of interest to perform further analysis, as they are most likely with respect to minimum energy consumption. For SA production process, 65 flowsheet design candidates have been generated and 16 were found to be most likely with respect to property flowsheet target. For DES 54 feasible process flowsheet candidates have been generated.

Step 5-Ranking/selection of flowsheet candidates: The design candidate using solvent-based azeotropic separation process-group in the downstream separation design for the bioEtOH process is considered to highlight the workflow in this step of the method. There is one alternative to initialize the solvent-based azeotropic separation process-group, either by using organic solvents or ionic liquids. In spite of the alternative, that uses ionic liquid (IL) has a better performance in terms of energy consumption [10], due to environmental concerns, the alternative that uses organic solvent as entrainer is selected for further analysis. In the case of SA production process, the design candidate using liquid-liquid extraction process group is selected due to this unit operation the energy supply is not necessary. ProCAMD software [8] has been used to find the solvent to be used as extractant agent for liquid-liquid extraction process group. The following two solvents have been identified as potential candidates: *n*-butyl acetate and *n*-decyl acetate. The verification of the creation of two liquid phases at room temperature is confirmed through the liquid-liquid equilibrium (LLE) ternary phase diagram calculation for both solvents using ICAS [9] (see Figure 2).

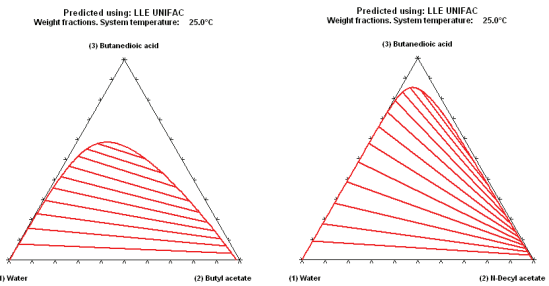

Figure 2: LLE ternary diagrams for the system succinic acid-water-solvent.

The ranking of the design alternatives is performed with respect to the performance of the solvent to be used as the extractive agent, but in this case, with respect to its *DF*. In this case, *n*-decyl acetate is selected as extractive agent since it is immiscible with water and can promote a higher *DF* than *n*-butyl acetate as shown in Figure 3.

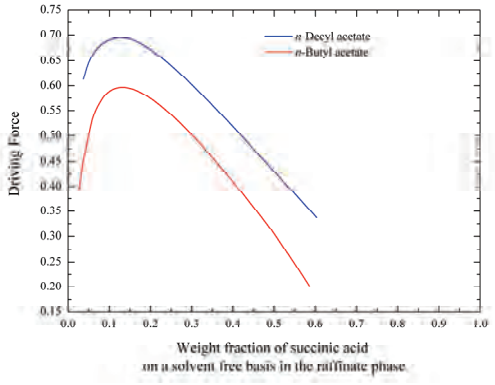

Figure 3: Driving force diagram for the system succinic acid-water-solvent on a solvent free basis.

Since the solvent needs to be recovered (for recycle), crystallization has been identified to separate the solvent from SA. In the case of DES production process, the one flowsheet candidate using pervaporation process-group is selected for further analysis.

Step 6-Reverse simulation: The final process flowsheet shown in Figure 4 is considered for the reverse simulation step. In Figure 4 each process unit operation is represented by its corresponding process-group. Once the solvent identity is known either for solvent based azeotropic distillation process-group as for the liquid-liquid extraction process-group, the respective solvent flowrate is calculated by mass balance. The mass balance was performed for each process-group in Figure 4. The downstream separation in the bioEtOH process using organic solvent (ethylene glycol) and the downstream separation in the SA process using *n*-decyl acetate as extractive agent were considered for reverse simulation. The reverse simulation of the flash and distillation process-groups was performed using the *DF*-based method [3] and the results are given in Table 1 (*NS*: number of stages; *FS*: feed stage; *RR*: reflux ratio).

Table 1: Design parameters of the distillation columns.

	Distillation column	Extractive column	Recovery column
NS	32	30	15
FS	17	22	5
RR	3.2	0.52	0.54
DF_{max}	0.35	0.48	0.59

In the case of the liquid-liquid based separation process-group, the number of stages can be determined by using the phase diagram, plotting *X* ($kg_{solute}/kg_{carrier}$) versus *Y* ($kg_{solute}/kg_{solvent}$) as illustrated in Figure 5.

Step 7-Final verification: The flowsheet candidates with bets performance in terms of energy consumption were verified through rigorous simulation using an appropriate simulator. The optimal integrated sequence

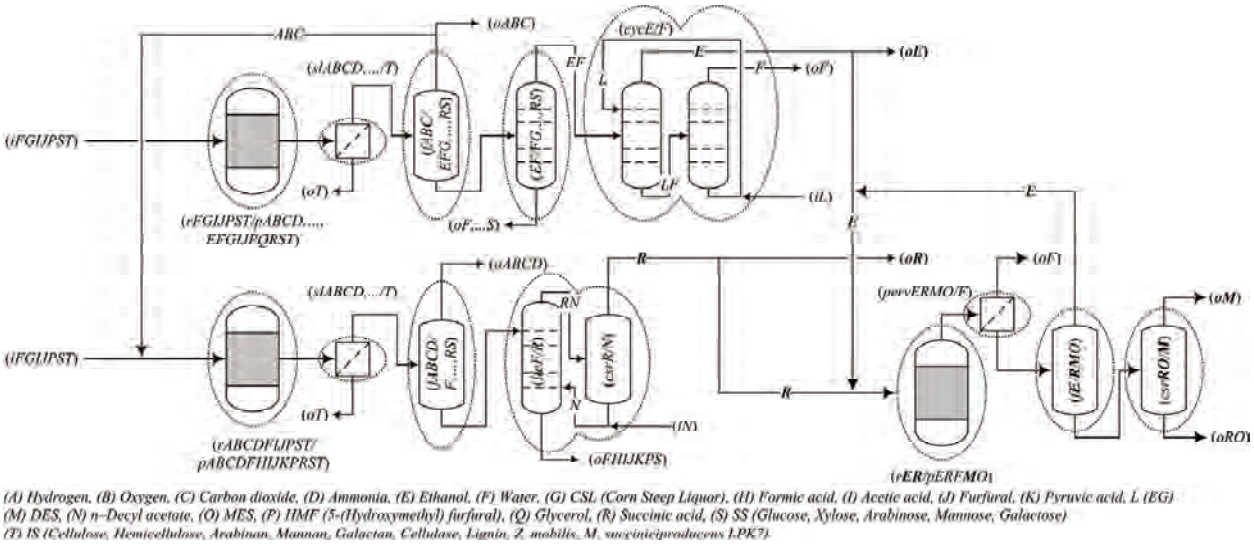

Figure 4: Process flowsheet represented by process-groups.

uses extractive distillation with IL for bioEtOH recovery, liquid-liquid extraction and crystallization for SA recovery and pervaporation for DES recovery. The total predicted energy consumption is equal to 0.329 *MkJ/h/kmole*.

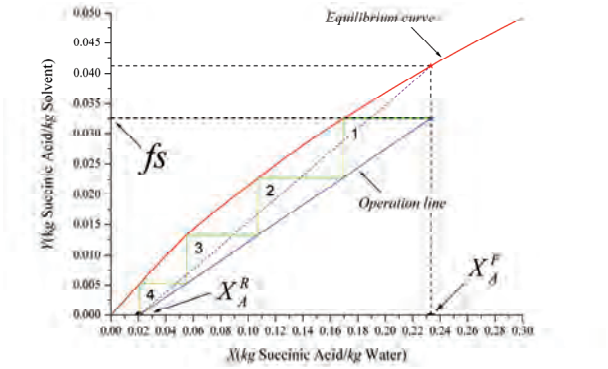

Figure 5: Graphical determination of the number of equilibrium stages for the liquid-liquid extraction based separation process-group.

Conclusions

A novel systematic approach based on the group-contribution concept has been presented. One important feature of the method is its versatility, since it can be extended by adding new process-groups representing all types of process unit operations. Thus, it is possible to simultaneously model, design, and synthesize novel products and processes as is demonstrated in this paper. On the other hand, the ability to predict a flowsheet property − energy consumption − without the need for rigorous simulation offers a lot of advantages as it opens the possibility to screen a lot of process options very quickly and with high accuracy, a feature which has been demonstrated for downstream separation from the bioEtOH and SA processes. Finally, the results also show that the method provides a fast, efficient, and systematic process design approach by first solving the mass balance based on the process-group specifications, followed by calculation of the design parameters of the unit operations through reverse simulation.

References

[1] L. d' Anterroches, R. Gani, Fluid Phase Equilib., 228-229 (2005) 141–146.

[2] C. Jaksland, PhD Thesis, Department of Chemical and Biochemical Engineering, DTU, Denmark, 1996.

[3] E. Bek-Pedersen, R. Gani, Chem. Eng. Process., 43 (2004) 251.

[4] F. Horn, (eds.), In Proc. 3rd Eur. Symp. On Chemical Reaction Engineering, 1964.

[5] M. Patel, The BREW Project, Final report, Utrecht University, 2006.

[6] H. Song, Y.S. Huh, S.Y. Lee, H.W. Hong, Y.K. Hong, J. Biotechnol., 132 (2007) 445.

[7] A.K. Kolah, N.S. Asthana, D.T. Vu, C.T. Lira, D.J. Miller, Ind. Eng. Chem. Res., 47 (2008) 5313.

[8] P.M. Harper, R. Gani, 2000, Comput. Chem. Eng., 24(2), 667-683.

[9] R. Gani, 2002, ICAS documentation. CAPEC, Technical University Of Denmark

List of Publications

[10] M. Alvarado-Morales, J. Terra, K.V. Gernaey, J.M. Woodley, R. Gani, Chem. Eng. Res. Des., 87(9) (2009) 1171-1183.

[11] M. Alvarado-Morales, M. Kamaruddin Abd Hamid, G. Sin, K.V. Gernaey, J.M. Woodley, R. Gani, PSE, Salvador Bahia, Brazil, 2009.

[12] M. Alvarado-Morales, N. Al-Haque, K. V. Gernaey, J. M. Woodley, R. Gani, ESCAPE 18, Lyon, France, 2008.

Nikolai E. Musko

Phone: +45 4525 2923
Fax: +45 4588 2258
E-mail: nm@kt.dtu.dk
WWW: http://www.chec.kt.dtu.dk
Supervisors: Prof. Jan-Dierk Grunwaldt
Prof. Georgios M. Kontogeorgis

PhD Study
Started: October 2009
To be completed: October 2012

Heterogeneously Catalyzed Selective Hydrogenation Reactions in Supercritical Carbon Dioxide

Abstract
Hydrogenation reactions over heterogeneous catalysts provide access to a wide variety of bulk and fine chemicals. This PhD project aims at the investigation of new types of bifunctional heterogeneous catalysts for selective hydrogenation of unsaturated aldehydes towards saturated aldehydes and subsequent aldol condensation of the latter both in conventional solvents and supercritical CO_2. Palladium on different types of supports has been tested in the process with different unsaturated aldehydes. Phase behavior has been studied as well to optimize the reaction conditions.

Introduction
Hydrogenation reactions in supercritical carbon dioxide are widely used for obtaining different chemicals which can be applied in a variety of ways [1]. Heterogeneous catalysis combined with the use of $scCO_2$ gives a number of opportunities [2]. Gas-like properties of $scCO_2$ significantly decrease heat and mass transfer limitations in the process and relatively high density and solubility (liquid-like properties) allow using it instead of conventional solvents. Liquid-like properties of CO_2 depend on pressure and temperature which makes both the chemical and separation processes quite tuneable. Moreover, carbon dioxide is a cheap, non-flammable and environmentally benign chemical. The amount of hydrogen can further be often reduced in case of hydrogenation processes with $scCO_2$ compared to those with conventional solvents. However, hydrogen decreases the density and thereby the dissolution power of carbon dioxide.
Hydrogenation of C-C double bond in unsaturated aldehydes gives industrially important saturated aldehydes which are frequently used as chemicals in different reactions. One of the most interesting is an aldol condensation reaction which provides chemicals used as solvents, flavours, additives for different purposes [3]. Conventional aldol condensation processes have lots of drawbacks, e.g., the use of strongly basic solutions, low conversion and selectivity. An interesting way of performing these two steps in one reactor over 1%Pd/Amberlyst-15 was found by Seki et. al. [4]. Moreover, the aldol condensation step has been studied in more detail [3]. All the reactions have been investigated in a continuous-flow system and it also has been found that palladium is the best metal for the hydrogenation step and Amberlyst-15 shows the best results in aldol condensation [3, 4].
For these types of reactions a bifunctional catalyst is necessary. Palladium and platinum are very active catalysts for hydrogenation processes, but palladium species work at milder conditions and give higher selectivity towards saturated aldehydes [5, 6]. Aldol condensation reactions are possible in both base and acidic conditions. Therefore, different kinds of support have been studied [3]. Among alumina oxide, supported NaOH, magnesium oxide and ion-exchanged resins, Amberlyst-15 was found to work at mildest conditions with highest conversion and selectivity in reactions with propionaldehyde and butyraldehyde.

Specific Objectives
The aim of this thesis is to find and investigate bifunctional catalysts for selective hydrogenation and aldol condensation as well as related reactions (Fig. 1).

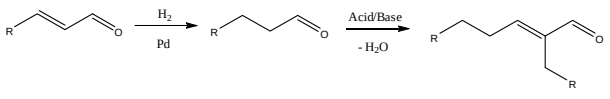

Figure 1: The reaction scheme.

Crucial is the optimization of the reaction conditions to gain maximum yields of the products. The conversion and selectivity strongly depend on the phase equilibria in the system which is mostly determined by

temperature and pressure. A little change in a parameter can cause significant changes in the process. For example, the system can become two phase instead of one. Tuneability of the systems with carbon dioxide as reaction medium is a very attractive tool for improving their performance. Therefore, phase modeling and theoretical calculations are to be done for better understanding of the process. Advanced association models, e.g. PC-SAFT or CPA, which can describe sc CO_2 and polar hydrogen bonding compound will be used [7].

Main Strategy

The whole project can be split up into several main parts. At first, different types of the carriers are to be tested in aldol condensation reactions with different saturated aldehydes (propanal, n-butanal, n-pentanal, n-hexanal, etc.) both in conventional solvents and scCO_2. All the experiments are supposed to be carried out in the batch cell together with phase behavior observations.

The catalysts that showed the best results are supposed to be tested in a continuous-flow setup. These best carriers will be used for the preparation of the palladium catalysts for conversion of unsaturated aldehydes into aldol condensation products in one step process (Fig. 1). Hydrogenation ability of the catalysts is to be studied with unsaturated aldehydes. Characterization techniques, such as X-ray diffraction (XRD), X-ray absorption spectroscopy (XAS), transmission electron spectroscopy (TEM), thermal programmed desorption (TPD), etc. will be used to give insight into the catalyst structure throughout the project. *Ex-situ* and *in-situ* measurements are planned. XRD and TPD analyses are crucial for the catalysts as the information on palladium particle size and acidic/base properties of the carriers is necessary for the process understanding and its subsequent improvement.

For the reactions with the best performance phase equilibria and thermodynamic calculations will be performed to rationally improve the reaction conditions.

Experimental Setups

Catalyst testing is supposed to be carried out both in a batch reactor and a continuous-flow system with a bed of the catalyst (NWA Analytics, Lörrach, Germany). The results obtained on the latter setup are more convenient for industrial applications.

Since the batch reactor is easier to handle with small catalyst quantities it is supposed to be used for investigation of the catalytic activity of the catalysts in general. It is also useful for obtaining information on the phase behavior during the progress of the reaction. Catalyst testing in the continuous flow system is not only necessary because the results are more applicable to industry, but also to vary the conditions continuously and thereby gaining insight into the mechanism and the reaction kinetics.

Both the setups are equipped with compressors for H_2 and CO_2. Reactants and products are analyzed by means of gas chromatography.

Screening Studies

Different types of neutral, acidic and base carriers have been obtained both commercially and by synthesis from literature). In particular, carriers as hydrotalcite, $NaOH/SiO_2$, sulfated zirconia, $H_4SiW_{12}O_{40}/SiO_2$ have been recently synthesized. Now they are being tested in aldol condensation reactions with propional and butanal. Furthermore, palladium based catalysts with 1% wt. and 5% wt. of Pd on carbon, alumina oxide and Amberlyst-15 have been prepared. Hydrogenation of unsaturated aldehydes has been carried out.

So far only the batch cell has been used for the experiments. Phase equilibria and behavior were directly observed during the experiments and the continuous-flow setup is built up.

Conclusions

The project aims at the development of new catalysts for two step hydrogenation reactions of unsaturated aldehydes into their aldol condensation products. *Ex-situ* and *in-situ* catalysts characterization combined with theoretical thermodynamic modeling of the phase behavior are expected to help the understanding and thereby to improve performance of selective hydrogenation reactions in supercritical carbon dioxide.

References

1. T. Seki, J.-D. Grunwaldt, A. Baiker. Heterogeneous Catalytic Hydrogenation in Supercritical Fluids: Potential and Limitations. *Ind. Eng. Chem. Res. 2008, 47, 4561 – 4585.*
2. J.-D. Grunwaldt, R. Wandeler, A. Baiker. *Catal. Rev. – Sci. Eng. 45 (2003) 1.*
3. J. G. Stevens, R.A. Bourne, M. Poliakoff. The continuous self aldol condensation of propionaldehyde in supercritical carbon dioxide: a highly selective catalytic route to 2-methylpentenal. *Green Chem., 2009, 11, 409 – 416.*
4. T. Seki; J.-D. Grunwaldt; A. Baiker. Continuous catalytic "one-pot" multi-step synthesis of 2-ethylhexanal from crotonaldehyde. *Chem. Commun., 2007, 3562 – 3564; Adv. Synth. Catal. 350 (2008) 691.*
5. F. Zhao, Y. Ikushima, M. Chatterjee, M. Shirai, M. Arai. An effective and recyclable catalyst for hydrogenation of α,β-unsaturated aldehydes to saturated aldehydes in supercritical carbon dioxide. *Green Chem., 2003, 5 (1), 76 – 79.*
6. B. M. Bhanage, Y. Ikushima, M. Shirai, M. Arai. The selective formation of unsaturated alcohols by hydrogenation of α,β-unsaturated aldehydes in supercritical carbon dioxide using unpromoted Pt/Al_2O_3. *Catalysis Letters, 1999, 62 (2 - 4), 175 – 177.*
7. N. van Solms, I. A. Kouskoumvekaki, M. L. Michelsen, G.M. Kontogeorgis, *Fluid Phase Equil., 241 – 344, 2006.*

Azizul Azri Bin Mustaffa
Phone: +45 4525 2811
Fax: +45 4593 2906
E-mail: azm@kt.dtu.dk
WWW: http://www.capec.kt.dtu.dk
Supervisors: Prof. Rafiqul Gani
Prof. Georgios Kontogeorgis

PhD Study
Started: April 2009
To be completed: March 2012

Development and Analysis of Group Contribution^{Plus} Models for Property Prediction of Organic Chemical Systems

Abstract
The prediction of properties in chemical process and product design is important and the implementation of a property model that can estimate the needed properties efficiently and reliably is the most wanted solution. However, due to the increased complexity of chemical molecular structures, wider range of chemicals and accuracy, hybrid models that combines molecular descriptors and group contribution theories have been developed using the Group Contribution Plus (GC^{Plus}) approach. In this work, the performance and accuracy of the hybrid models will be investigated and suggestions for improvement will be provided.

Introduction
The work on the GC^{Plus} approach was first documented by Gani and coworkers [1] through the establishment of a methodology for predicting missing group contributions for the Marrero and Gani group contribution method for pure component property estimation with the aid of valence connectivity indices. Since then, several works implementing the same methodology have been done to predict properties of polymers [2], surface tension and viscosity [3].

Recently, GC^{Plus} models for predicting mixture properties have been developed by combining the UNIFAC group contribution based activity coefficient model with valence connectivity indices developed by Kier and Hall [4], to be called UNIFAC-CI [5]. Group interaction parameters (GIPs) are needed for vapour liquid equilibrium (VLE) calculations and are regressed from experimental data. There are, however many gaps in the UNIFAC parameter table due to lack of data. Alternatively to performing measurements, the missing GIPs can be predicted through the GC^{Plus} approach using connectivity indices (CI) which uses information on the atoms and their connections. Connectivity indices are formalisms defined via graph theoretical concepts intended to describe the topological characteristics of molecular structures. The main idea is the use of connectivity indices to describe the molecular fragmentation that relates properties which is the molecular interactions with the molecular structures. The predicted GIPs are then used in the UNIFAC method to calculate activity coefficients. This approach can increase the application range of UNIFAC providing a reliable predictive model towards fast, cheap and efficient product development.

In the developed UNIFAC-CI model, an expression was developed by relating the GIPs to the number of atoms involved in the UNIFAC groups, CI and also atom interaction parameters (AIPs). The atom stoichiometry and the values of the CIs can be obtained directly from the group definition but the AIPs need to be regressed using available experimental data [5].

However, the UNIFAC-CI models does not work very well in certain systems and therefore further analysis of the UNIFAC-CI models in terms of its performance and accuracy must be done to increase its reliability and flexibility. Through the work done by Gonzalez et al. [5], model parameters for using the GC^{Plus} approach to the original UNIFAC [6] are available for groups formed by C, H, O, N, Cl atoms. Other than that GC^{Plus} approach has been also implemented for Modified UNIFAC (Dortmund) [7] for group containing C, H, O, N atoms.

Specific Objectives
The main objectives of this project is first to analyze the performance and accuracy of the developed UNIFAC-CI models. The systems which are not well predicted by this model will be further investigated and suggestions for improvement will be provided. Moreover, the second objective of this project is the development and

further investigation of the GC^{Plus} model in an industrial problem which involves SLE calculations and also in chemical product design where an industrial case study which involves edible oil processing will be selected. Finally the Modified UNIFAC-CI (Dortmund) will be further developed. Currently the model parameters (AIPs) are regressed by using only VLE experimental data. In this project, model parameters will be refitted by taking into account the activity coefficients at infinite dilution experimental data when regressing the parameters to improve predictions at infinite dilution.

Model Analysis

The model analysis started by initially analyzing the systems which involves atoms C, H and O. The AIPs which involves those groups were regressed using 228 data systems [5]. There are 43 types of systems used in the regression mainly alkane-alcohol with 21 systems followed by ketone-aromatic and alkane-aromatic both with 19 systems and cyclic alkane-aromatic with 16 systems. When regressing the experimental data, a measure of the error was chosen to be the average absolute relative deviation (AARD) for both reference UNIFAC and UNIFAC-CI defined in Equation 1.

$$AARD(\%) = \frac{1}{N}\sum_{i=1}^{N}\left|\frac{P_{\exp} - P_{calc}}{P_{\exp}}\right| \times 100 \qquad (1)$$

where N is the number of data points in the whole set of data, P_{exp} is the experimental pressure and P_{calc} is the calculated pressure. These AARD values which were obtained for each 228 dataset were then illustrated in Figure 1 with ascending order with respect to UNIFAC-CI.

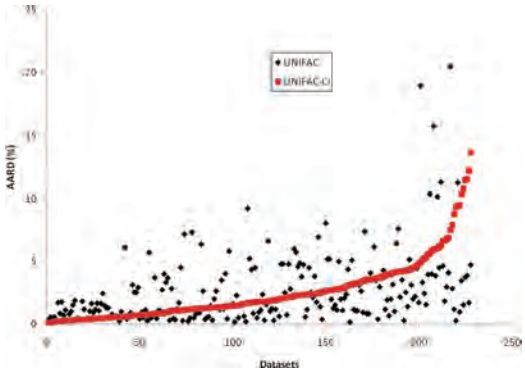

Figure 1: AARD (%) for each individual dataset between reference UNIFAC and UNIFAC-CI (COH systems)

From Figure 1, it can be seen that for some datasets UNIFAC-CI performs better than the reference UNIFAC. However, there many datasets which the reference UNIFAC works better. For further analysis, a limit of 5 % AARD was assumed to be an acceptable value and the datasets which have higher AARD with respect to UNIFAC-CI were further extracted and shown in Figure 2.

From Figure 2, 5 alkane-aldehyde systems (1-Butanal-n-Heptane at 343 K, 1-Butanal-n-Heptane at 318 K, 1-Pentanal-n-Heptane at 348 K, 2-Methylpropanal-n-Heptane at 335 K and 2-Methylpropanal-n-Heptane at 318 K) were identified to be the systems which have the highest AARD values between 10.3516 to 12.1783 % and further analyzed.

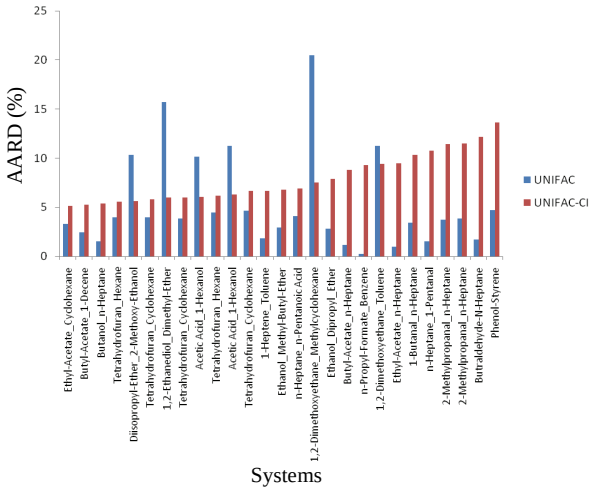

Figure 2: Systems with AARD (%) of more than 5 % with respect to reference UNIFAC compared with UNIFAC-CI (COH systems)

These 5 systems were the only alkane-aldehyde systems used in the parameter regression step. To analyze these alkane-aldehyde systems, first an investigation was done to see whether there are any AIPs which uniquely represent these systems and not others. However, Table 1 shows that the AIPs used by the alkane-aldehyde systems are also used by other systems. Therefore, new unique CI parameters that only affect those alkane-aldehyde systems and not others may need to be added.

Table 1: AIPs used by several systems

Systems	AIPs used
Alkane-Aldehyde	$b_{C\text{-}C}$, $b_{C\text{-}O}$, $c_{C\text{-}C}$, $c_{C\text{-}O}$, $bh_{C\text{-}C}$, $bh_{C\text{-}O}$
Alkane-Alcohol	$b_{C\text{-}C}$, $b_{C\text{-}O}$, $bh_{C\text{-}C}$, $bh_{C\text{-}O}$
Alkane-Ether	$b_{C\text{-}C}$, $b_{C\text{-}O}$, $c_{C\text{-}C}$, $c_{C\text{-}O}$, $bh_{C\text{-}C}$, $bh_{C\text{-}O}$

Furthermore, it is intended to analyze the model equation to investigate the source of the problem. First, activity coefficients were calculated using the reference UNIFAC and UNIFAC-CI for the alkane-aldehyde systems and compared with experimental data and the results are shown in Figure 3 for 1-Butanal-n-Heptane system at 318 K. All 5 systems show the same trends.

Figure 3 shows that the predicted activity coefficients by reference UNIFAC conform closely to the experimental values and not UNIFAC-CI.

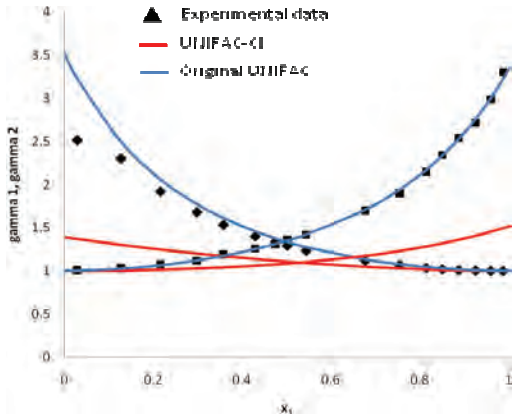

Figure 3: Comparison of the activity coefficients calculated using the reference UNIFAC and UNIFAC-CI with experimental data (pseudo) for 1-Butanal-n-Heptane at 318 K.

Then the UNIFAC equations are analyzed. UNIFAC model (Equation 2) are consists of the combinatorial part (Equation 3) which accounts for differences in molecular size and shape and the residual part (Equation 4) which accounts for the molecular interactions.

$$\ln \gamma_i = \ln \gamma_i^C + \ln \gamma_i^R \tag{2}$$

$$\ln \gamma_i^C = 1 - J_i + \ln J_i - 5q_i\left(1 - \frac{J_i}{L_i} + \ln \frac{J_i}{L_i}\right) \tag{3}$$

$$\ln \gamma_i^R = q_i\left[1 - \sum_k \left(\theta_k \frac{\beta_{ik}}{s_k} - e_{ki} \ln \frac{\beta_{ik}}{s_k}\right)\right] \tag{4}$$

The values for the combinatorial part (Equation 3) for both reference UNIFAC and UNIFAC-CI should be the same since it only contains the values of each UNIFAC group. Therefore the difference of the predicted activity coefficients is caused by the residual part (Equation 4). This part is a function of the GIPs which values are different for both reference UNIFAC and UNIFAC-CI. Next is to find the contribution from each UNIFAC group involved in the alkane-aldehyde system from this residual term. 2 UNIFAC main groups involve are CH_3 and CHO. From Equation 4, subscript k represents subgroups. Therefore, Equation 5 was extracted from Equation 4 to identify the contributions from each subgroup.

$$F = \sum_k \left(\theta_k \frac{\beta_{ik}}{s_k} - e_{ki} \ln \frac{\beta_{ik}}{s_k}\right) \tag{5}$$

By analyzing Equation 4, we can see that the higher the value of Equation 5 for a certain group, the less contribution from that specific group. Figure 4 were then constructed for 2-Methylpropanal-n-Heptane at 318 K systems showing the values of F (Equation 5) with respect to the compositions of both compounds.

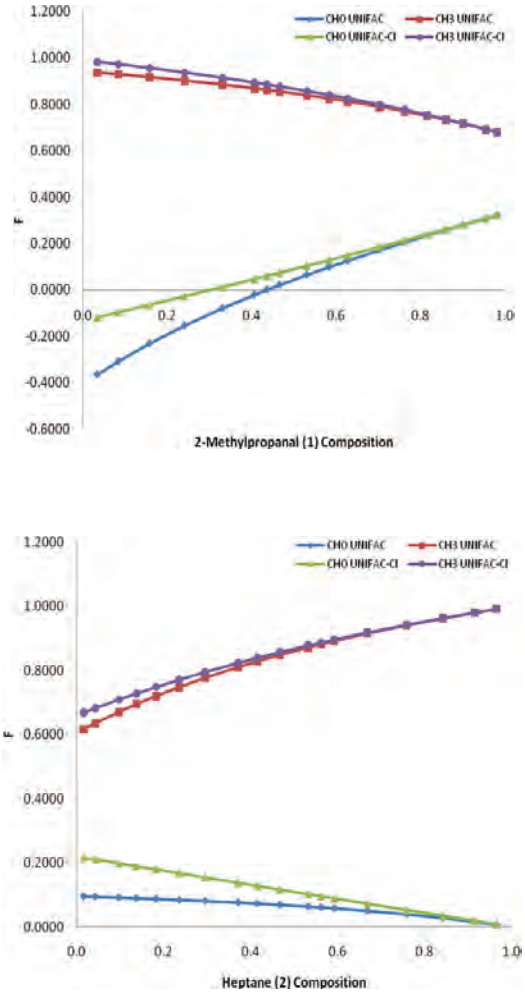

Figure 4: Values of F with respect to composition for 2-Methylpropanal-n-Heptane systems

Figure 4 shows that the contributions of the CHO group are higher compared to the CH_3 group for both reference UNIFAC and UNIFAC-CI. Contribution from group CH_3 are almost the same for both reference UNIFAC and UNIFAC-CI but slightly different for group CHO suggesting that the problem might be from the CHO group. The figure also shows that there are problems at lower concentrations.

Possible Solutions

From the analysis, several possible solutions were identified to improve the performance of the UNIFAC-CI model. First, more weights can be added in the objective function (for regressing the parameters) for those systems at lower concentrations and refit. Next possible solution is to introduce a new unique CI parameter only for the alkane-aldehyde systems for the interaction which involves C-O atom interaction. Other solution might be to add an activity coefficient at infinite dilution in the objective functions and refit using those related experimental data.

Future Works

All possible solutions suggested by the author as stated in the previous section will be implemented to further analyze the model in order to improve the model performance. If one solution is found to improve the performance, the analysis will be further extended for other problematic systems. Besides these VLE systems, the performance of UNIFAC-CI for SLE systems (extrapolating GIPs obtained from regression of VLE data for SLE systems) in a case study will also be analyzed and applied.

Conclusion

From the current work, it can be concluded that UNIFAC-CI is a powerful predictive model which can be used in cases where UNIFAC parameters are missing. However, UNIFAC-CI does not always perform well in certain systems. Therefore an analysis has been done and it is found that there might be a problem from the CHO group or at lower concentrations.

Acknowledgement

The author gratefully acknowledges the financial support from the Ministry of Higher Education of Malaysia (MoHE) and Universiti Teknologi Malaysia (UTM).

References

1. Gani R., Harper P., and Hostrup M. Automatic Creation of Missing Groups through Connectivity Indices for Pure-Compound Property Prediction, Ind. Eng. Chem. Res., 44, 7262 (2005).
2. Satyanarayana K. C., Gani R., and Abildskov J. Polymer Property Modeling using Grid Technology for Design of Structured Products, Fluid Phase Equilibria, 261, 58 (2007).
3. Conte E., Martinho A., Matos H., and Gani R. Combined Group Contribution and Atom Connectivity Index based Methods for Estimation of Surface Tension and Viscosity", Ind. Eng. Chem. Res., 47, 5751 (2008).
4. Kier L. B., and Hall L. H. Derivation and Significance of Valence Molecular Connectivity, Journal of Pharmaceutical Sciences, 70, 583 (1981).
5. González H.E., Abildskov J., Gani R., Rosseaux P., Le Bert B. A Method for Prediction of UNIFAC Group Interaction Parameters, AIChE J. 2007; 53, 6, 1393-1634.
6. Hansen H., Rasmussen P., Fredenslund A., Schiller M., Gmehling J. Vapor-Liquid Equilibria by UNIFAC Group Contribution. 5. Revision and Extension. Ind. Eng. Chem. Res. 1991, 30, 2352-2355.
7. Gmehling J., Li J., and Schiller M. A Modified UNIFAC Model. 2. Present Parameter Matrix and Results for Different Thermodynamic Properties", Ind. Eng. Chem. Res., 32, 178 (1993).

Tatyana Nesterova

Phone: +45 4525 2848
Fax: +45 4525 2258
E-mail: tan@kt.dtu.dk
WWW: http://www.kt.dtu.dk
Supervisors: Søren Kiil
Kim Dam-Johansen

PhD Study
Started: 1st January 2009
To be completed: 31st December 2011

Self-Healing Anticorrosive Coatings

Abstract
Self-healing anticorrosive coatings is a new and intelligent approach to anticorrosion protection. They have a built in capability to restore autonomically their structural integrity after mechanical damage and retain anticorrosive functions for longer time. This Ph. D. project is dedicated to design of such a coating for heavy-duty anticorrosion protection and investigation of its properties and performance.

Introduction

Anticorrosive coatings are an important type of industrial coatings used to protect steel structures from corrosion or rusting. They are widely used all over the world for protection of offshore rigs, buried pipelines, wind turbines, ships and many other industrial objects. Although a good performance of these materials can be now achieved, various mechanical, chemical, or thermal impacts, experienced by the products during service life, lead to formation of microcracks at the surface or within the product structure (figure 1a), to a damage of materials functionality and, eventually, to such unwanted premature failure.

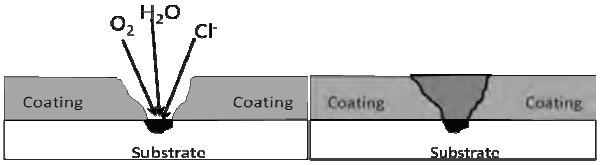

Figure 1: Schematic illustration of a generalized self-healing concept: a) microcrack formation, b) healing.

Self-healing polymeric materials is a new and intelligent approach to anticorrosion protection, being developed to prolong service life of coatings and thereby provide significant cost reductions. Different approaches to self-healing of thermoset composites and polymers have been developed to nowadays.

The work in this area has been initiated in application to composites in 1994 by American researcher Carolyn Dry, who developed a system of hollow fibers containing a reactive fluid, which released into the damage sites upon a fracture, reacted and healed the crack [1]. Other approaches utilize physical cross-linking of the chain ends at the crack surface [1, 2] and incorporation of thermally reversible polymers [1, 3] and thermoplastic additives [1, 4] into a thermoset matrix. Such systems require external trigger, heating or UV-light, to start healing, and therefore cannot be considered as truly autonomic self-healing materials.

An autonomic approach, based on pH-dependent release of corrosion inhibitor, has been proposed by D. Andreeva [5]. The coating obtained showed a good anticorrosion performance at the laboratory experiments but its use for industrial application can be problematic.

Microcapsules based self-healing approach utilizes chemical reaction of species, embedded into the polymer matrix and currently is the most studied method for production of self-healing materials owing to its versatility and applicability to industrial purposes [6].

Specific Objectives

This Ph.D. project aims to construct a "smart" coating with a built-in capacity to substantially recover properties - tensile strength and barrier properties - after a microcrack has occurred without any manual intervention. That will be reached through incorporation into the coating of two kinds of microcapsules filled with chemically reactive compounds (healing agents). Once a microcrack occurs within the coating, the healing agents are released and react forming a polymer at the fracture plane. This new formed polymer binds the sides of the crack together preventing propagation of chemical, corrosively active species down to the substrate (figure 1b) and prolonging the coating's service life.

The project consists of two main parts. First of them deals with preparation of microcapsules and include a choice of materials for encapsulation, development of experimental procedures and optimisation of their conditions. The aim is to synthesize microcapsules, which remain intact during coating formulation and application but rupture readily when a coating is damaged, are compatible with polymer matrix and exhibit good adhesion, are chemically stable and filled with reagents possessing fast reaction kinetics to allow formation of the healing film at the -10 – 35 ^{0}C temperature range at a reasonably short time. Once microcapsules are synthesized, formulation and application of the self-healing coating will become possible along with verification of self-healing ability of the created coating.

Results and Discussion

Polyepoxide barrier coating has been chosen as a model system for modification and further investigation. For the maximum materials compatibility and cross-linking at the application temperature interval a known epoxy-amine pair was chosen as a self-healing system. The generalized reaction scheme is shown at figure 2.

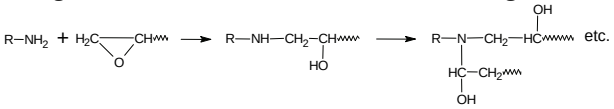

Figure 2: Scheme of reaction between amine and epoxide.

Poly(urea-forlmaldehyde) (PUF) and poly(melamine-formaldehyde) (MUF) were considered as possible options for microcapsules shell formation. The figure 3 illustrates interaction scheme of urea and formaldehyde in the two-steps conventional procedure. A dense, highly cross/linked polymer should be formed at the end of reaction in order to provide the necessary mechanical strength and stability to the capsules shells.

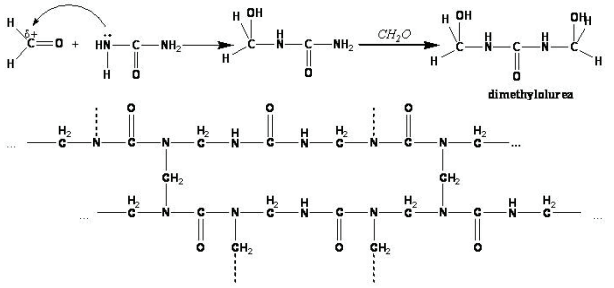

Figure 3: Poly(urea-formaldehyde) formation.

Three different encapsulation procedures were followed by in order to choose one, providing the best results. One of them dealt with encapsulation of bisphenol-A epoxidised resin into PUF shell via 2 steps (basic-acidic) procedure [7]. By this method no successful results were obtained. Another one [6] used only acidic stage of urea-formaldehyde polymerization reaction in order to decrease the formation of nanoparticles in solution and change the structure of resulting polymer. Application of this procedure to encapsulation of the epoxy resin was more successful but the capsules obtained were still not enough durable. The third procedure [8] was not pH-dependent and gave a better result. The micrograph of capsules, prepared through this procedure, is shown at figure 4.

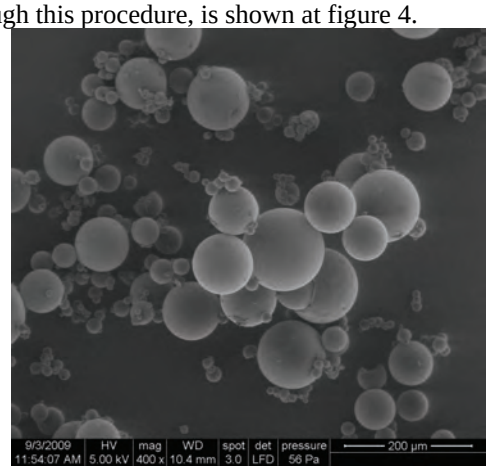

Figure 4: SEM micrograph of poly(urea-melamine-formaldehyde) microcapsules filled with alkylglycidylether.

Conclusions

Self-healing anticorrosive coating is a perspective tool for long-lasting protection of steel structures again heavy-duty corrosion. Although many attempts have been done to design such a coating during last 10 years, one, working in realistic conditions, has not been developed yet.

This Ph. D. project aims to investigate possibilities of creation of self-healing system, to implement it at the real anticorrosive coating, and to investigate its influence on the overall coating's performance.

To the time being, methods of capsules preparation and factors influencing the properties of the capsules have been assessed, and the main conclusion drawn was that the nature of encapsulated healing agents affected significantly stability and performance of microcapsules. It was confirmed, that an experimental procedure designed for encapsulation of a certain core agent could not be used without modification for encapsulation of others [8].

Acknowledgements

Author thanks Berit Wenzell for assistance at performing SEM analysis.

References

1. D.Y. Wu, S. Meure, D. Solomon, Prog. Polym. Sci. 33 (2008) 479-522.
2. R. Wool, Soft Matter 4 (2008) 400-418
3. X. Chen et al., Macromol. 36 (2003) 1802-1807
4. S.A. Hayes, J. R. Soc. Interface 4 (2007) 381-387.
5. D.V. Andreeva, D.G. Shchukin, Materials today 11 (10) (2008) 24-30
6. S. White et al., Nature 409 (2001) 794-797
7. L. Yuan et al., Polymer 47 (2006) 5338-5349
8. X. Liu et al., Macromol. Mater. Eng. 294 (2009) 389-395

Anders Rooma Nielsen

Phone: +45 4525 2831
Fax: +45 4588 2258
E-mail: arn@kt.dtu.dk
WWW: http://www.kt.dtu.dk
Supervisors: Kim Dam-Johansen
Peter Glarborg
Morten Boberg Larsen, FLSmidth A/S

Industrial PhD Study in corporation with FLSmidth A/S
Started: April 2008
To be completed: June 2011

Fuel Flexible Rotary Kilns For Cement Production

Abstract
The aim of this PhD project is to develop scientific based knowledge for precise prediction of the use of different alternative fuels in the material inlet end of cement rotary kilns. An important goal is to identify optimal rotary kiln design(s) for combustion of coarse, solid alternative fuels and at the same time maintain optimal conditions for cement clinker burning. This requires a solid understanding of how solid fuel combustion may affect the process stability in the rotary kiln system.

Introduction
Cement production is highly energy intensive. The global energy consumption by the cement industry is about 10 times the total energy consumption of Denmark [1, 2]. Coal and coke have traditionally been the primary fuels in the industry, but increasing fossil fuel prices and environmental concerns make other fuels attractive. Since energy costs accounts for 30-40% of the total costs of cement production, there is a great potential to reduce the overall production costs by replacing fossil fuels with alternative fuels[1]. Alternative fuels are typically cheaper than fossil fuels and in some cases the cement producer may even be paid to receive the alternative fuels.

Substitution of fossil fuels with alternative fuels offers the following major advantages:

1. Alternative fuels may be CO_2 neutral.
2. Fuel costs are typically reduced.
3. Solid residues from the alternative fuels are incorporated into the cement.
4. High flame temperatures and residence times provide good conditions for destruction of organic compounds.

In the recent years the use of alternative fuels has increased. In Germany, for example, the share of alternative fuels is today higher than 54%, while it was only 4% in 1987 [3, 4]. It is expected that the share of alternative fuels will continue to increase in the coming years, which will create a need for new technology to handle, treat and combust these fuel types [5].

Many types of alternative fuels are applied in the cement industry. The majority of the alternative fuels are on solid form, while liquids and gasses are less common. Some of the most common alternative fuels are refuse derived fuels (RDF, a mixture of house hold waste and industrial waste), tyre derived fuels (TDF), meat and bone meal (MBM) and waste wood. Technical feasibility, public acceptance, price and availability are typically the determining parameters for the type of alternative fuel that will be utilised at a specific cement plant.

It is attractive to fire coarse, solid alternative fuels into the material inlet end of cement rotary kilns in order to save expenses for shredding of the fuels to smaller particles and to increase flexibility. High temperatures in the rotary kiln and material retention times of 15-25 minutes provide good conditions for fuel burnout.
The main challenge is, however, that the solid fuel particles will be in physical contact with the cement raw materials: If the fuel particles are fully or partly covered by cement raw materials, mass transfer of oxygen to the fuel char will be hindered. Lean amounts of oxygen will lead to incomplete oxidation of the fuel char, forming reducing agents such as CO.

[1] In this context ”alternative fuels” refers to all non-fossil fuels and waste from other industries. Secondary, waste or replacement fuels are often used as synonyms for alternative fuels.

Local reducing conditions in the raw material charge are known to affect the product quality and process stability of the kiln system. The product quality can be influenced by raw material components such as Fe(III) being reduced to Fe(II). Fe(II) affects the formation of belite ($2CaO \cdot SiO_2$) and alite ($3CaO \cdot SiO_2$), the two strength-giving components in cement. The process stability is affected by increased release of sulphur from the raw materials, mainly by decomposition of $CaSO_4$:

$$CaSO_4\ (s) + CO\ (g) \rightarrow CaO\ (s) + CO_2\ (g) + SO_2\ (g)$$

SO_2 may react with alkali salts, forming eutectic salt mixtures which stick to the walls. Dust can adhere to this sticky layer and lead to deposit build-ups. These deposit build-ups accumulates typically in the material inlet end of the rotary kiln, or in the riser duct between the calciner and rotary kiln, where they lead to blockages that requires temporarily plant shut-down to remove.

Specific Objectives

The specific objective of this PhD project is to investigate how cement raw materials are affected by combustion of different alternative fuels under process conditions similar to those in the material inlet end of rotary kilns. The project should also clarify how fuel-air mixing may be optimized in order to minimize the risk of local reducing conditions in the kiln system.

The investigations are so far based on a combination of theoretical studies, experimental work in a rotary drum at FLSmidth and experimental work in a fixed bed reactor at CHEC. A new rotary drum is currently being constructed in order to study fuel/raw material interactions during fuel combustion.

Results and discussion

Mixing experiments have been made in a steel/plexi glass rotary drum with a diameter of 0.5 m. In these experiments, mixing of solid fuel particles and cement raw materials have been studied in order to clarify the influence of fuel particle size and shape,
rotary drum filling degree and rotational velocity on the way the fuel particles distribute in the material charge. The results indicate that even large fuel particles will quickly be fully or partly covered by raw materials in a rotary kiln. This is illustrated on Figure 1 with three different particle sizes. The largest particle size is observed to stabilize in a level with 30-50% visible particles while the smallest particle stabilizes in a significantly lower level with 0-5% visible particles. This has consequences for the heat up and burn out time of the fuels: Fuel particles will mainly be heated by conduction from the raw materials and the combustion will be diffusion limited due to poor oxygen mass transfer.
A clear tendency was observed that large fuel particles were less covered by raw materials than smaller fuel particles.

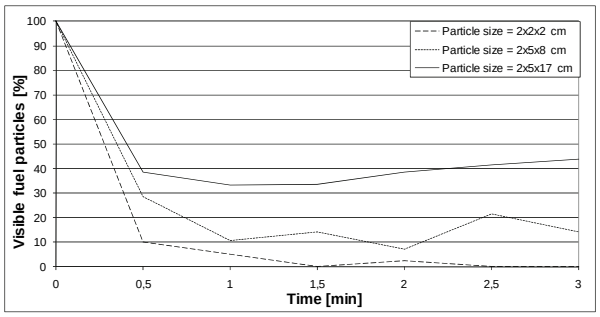

Figure 1: Percentage of particles visible as a function of time (13 rpm, 10% fill degree).

Experiments are currently being made to clarify the influence of gas atmosphere on the release of sulphur from cement raw materials. These experiments are being made in a fixed bed reactor at CHEC. Results obtained so far shows a clear tendency for increased sulphur release during alternating oxidizing and reducing atmospheres.

Conclusion

This industrial PhD project deals with combustion of solid, alternative fuels, fired into the material inlet of cement rotary kilns. The goal is to clarify how the combustion at this location may be optimized without negative impact on product quality or process stability. Experiments made so far indicate that particularly small fuel particles are likely to sink into the raw material charge in rotary kilns and create problematic, local reducing conditions.

Acknowledgements

This project is part of a research platform on future cement technology financed by The Danish National Advanced Technology Foundation, DTU and FLSmidth A/S.

References

1. Cembureau, Activity Report 2008, http://www.cembureau.be/.
2. Energistyrelsen, energistatistik 2008, http://www.ens.dk.
3. Schneider, M; Activity Report 2005-2007, Verein Deutscher Zementwerke, 2007. http://www.vdz-online.de.
4. Verein Deutscher Zementwerke, Environmental data for the German Cement Industry 2008. http://www.vdz-online.de.
5. J. H. Rasmussen, FLS skruer op for alternativ energi (2008), http://borsen.dk/nyhed/145258/. 18/11 2008.

Sidsel Marie Nielsen
Phone: +45 4525 2983
Fax: +45 4588 2258
E-mail: sa@kt.dtu.dk
WWW: www.cere.dtu.dk
Supervisors: Erling H. Stenby
Alexander Shapiro
Michael L. Michelsen

PhD Study financed through MP_2T; partly by DONG Energy
Started: September 2006
To be completed: July 2010

Modeling Microbial Enhanced Oil Recovery

Abstract
A potential method for enhancing oil recovery is to utilize the activity of microorganisms which are either present in or injected into the oil reservoirs. Microbial enhanced oil recovery is an emerging method for further exploitation of existing but non-productive oil fields to mobilize more residual oil. One of the important effects is reduction of viscosity. In order to mobilize residual oil, the effect of surfactant has been implemented in 1D. The reduction of residual oil affects the relative permeability curves, where different methods have been investigated and interpolation methods are mostly the case. Finally, this project is concerned with inclusion of a generic model for microbial activity into an existing streamline simulator and a finite difference simulator.

Introduction
The principle source of fluid fuels is the hydrocarbon resources. The finite nature of our hydrocarbon reserves has been discussed as discoveries of new oil reservoirs decrease. For the present techniques of oil recovery, a large amount of oil remains in the reservoir after water flooding, but the oil reservoirs must be abandoned as the production is no longer economically feasible. Methods of enhanced oil recovery (EOR) have been developed, but in many cases they are economically unattractive.

The biotechnology research has advanced and the oil industry has matured to consider microorganisms in the context of oil production. The oil reservoir may already contain indigenous microorganisms, which can be used for MEOR. Both indigenous and injected microorganisms are used and it depends on their applicability of the specific reservoirs. In MEOR, bacteria are often used as they are small and have different useful features. For bacterial growth and metabolite production, the requirements are different nutrients, which are led to the reservoir. In some cases, the carbon source is residual oil.

The MEOR purpose is, like other EOR methods, to mobilize the residual oil and thus reduce its content and/or increase the recovery efficiency. MEOR addresses the same physical parameters as chemical EOR, where they are subject to the same *in situ* technical difficulties. The essential difference between MEOR and chemical EOR resides in the method of introducing the recovery enhancing chemicals into the reservoir. Enhancement of the oil recovery through microbial action can be performed through several mechanisms as follows:

- Reduction of oil-water interfacial tension and alteration of wettability by surfactant production and bacterial presence.
- Viscosity reduction by gas production or degradation of long-chain saturated hydrocarbons.
- Selective plugging by bacteria and their metabolites.
- Generation of acids that dissolve rock improving absolute permeability.

MEOR is considered a potential ‘high risk, high reward’ process, where the high risk originates from the many performance constraints of the process. The reward is that the implementation difficulties and the cost resemble those of water flooding rather than those of the chemical EOR.

An oil reservoir is a harsh environment, which can have high temperature, high salinity and low pH (3-7). In general, this extreme environment should be taken into account, when selecting bacteria and nutrient media. As the reservoir conditions are specific, an extra effort has to be put on selecting and developing suitable bacteria and nutrient media for each reservoir to avoid undermining of MEOR economic viability.

Specific Objectives

The specific objective of the project is the investigation of the MEOR method through modeling. A 1D MEOR flow and reaction model is setup and solved numerically. The most important effects should be incorporated in several ways in order to explore these MEOR effects. After investigation and analysis of the MEOR effects, the MEOR should be incorporated in an existing simulator.

Transport Equations for 1D Flow System

The reservoir is considered to be 1D with two flowing phases with a total of five components, which is also depicted in Figure 1.

- Water phase
  - Water
  - Bacteria
  - Substrate
  - Metabolite (surfactant)
- Oil phase
  - Oil
  - Metabolite (surfactant)

The transport equations are given as below consisting of an accumulation, convection and reaction term. This is the mass conservation balance for each component:

$$\frac{\partial}{\partial t}(\phi\sum_{j=1}^{np}\omega_{ij}\rho_j s_j)+\frac{\partial}{\partial x}(v\sum_{j=1}^{np}\omega_{ij}\rho_j f_j)=\phi q_i \quad (1)$$

for i=1…nc.

where j is the phase, i is component, nc is number of components, ω_{ij} is mass fraction for component i in phase j, s_j is saturation of phase j, np is number of phases, v is linear velocity, ρ_j is density of phase j, f_j is fractional flow function of phase j, x is length variable, t is time, p is porosity, and q_i is the source term for component i. The volumes when mixing the components of the model is considered as *no volume change on mixing*.

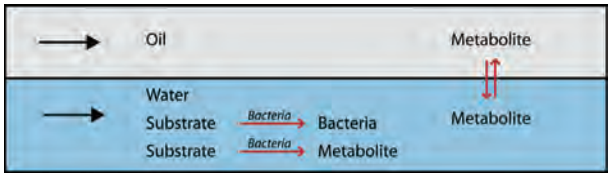

Figure 1. Sketch of the flow system, where a water phase and an oil phase exist. Substrate and bacteria exist only in the water phase, where bacteria convert substrate to metabolite and more bacteria. The metabolite can be distributed between both phases according to the distribution coefficient.

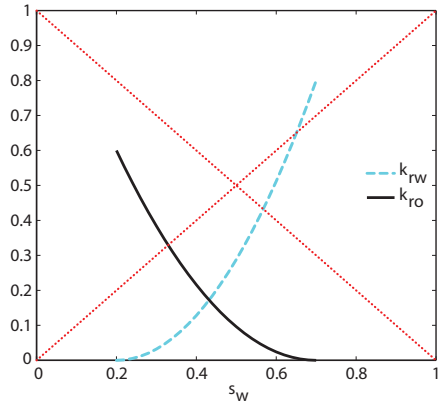

Figure 2. Relative permeability curve for water and oil with s_{wi}=0.2, s_{or}=0.3, k_{rowi}=0.6. and k_{rwor}=0.8. Decreasing interfacial tension make the curves go toward the red dotted lines as the curves become more linear and the residual saturations decrease.

As shown in Figure 1, two autocatalytic reactions occur, where bacteria convert substrate to metabolite and more bacteria. The rate expression is e.g. a Monod type with one or two limiting substrates and possibly with inhibition of substrates and products.

In this case, metabolite is surfactant. Metabolite can be distributed between both phases, where a coefficient K_i determines the distribution in relation to masses of water and oil.

The fractional flow function describes the flow of the phase j and is dependent on the saturation of phase j. Generally, the larger water saturation, the larger a fractional water flow. However, f_j depends on the relative permeability curves for water and oil, k_{rw} and k_{ro}, and their phase viscosities, μ_w and μ_o.

The relative permeabilities describe the ease of a fluid to pass through the porous media. Figure 2 shows the relative permeability curves. The relative permeability curves used are the Corey type, which is a polynomial in the water saturation s_w. Here, s_{wi} is the irreducible water saturation and s_{or} is the residual oil saturation, a scaled saturation value can be defined:

$$s^* = \frac{s_w - s_{wi}}{1 - s_{wi} - s_{or}} \quad (2)$$

and the approximations of Corey type of relative permeabilities of water and oil then becomes;

$$k_{rw} = k_{rwor}(s^*)^{pw} \quad \text{and} \quad k_{ro} = k_{rowi}(1-s^*)^{po} \quad (3)$$

where pw and pw can be obtained from measured data. Often p_j=2 is a suitable value.

Numerical Solution Procedure

The mathematical model developed is solved numerically using an implicit finite difference technique, where component mass balances and the total volume balance are satisfied. Application of fractional flow functions excludes solution of the pressure equations, which ease calculations.

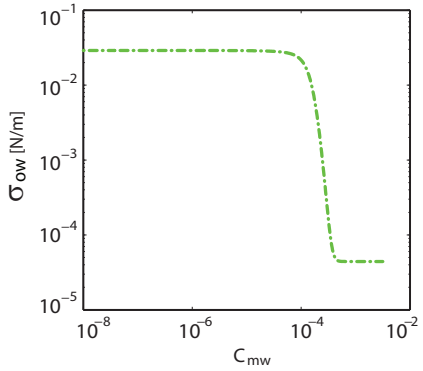

Figure 3. Typical correlation between metabolite mass concentration in the water phase C_m and IFT (interfacial tension).

Surfactant Effect

One of the most important effects is *in situ* production of surfactants, which can enhance the oil recovery. Surfactant decreases the interfacial tension between water and oil. As a result, the residual oil can to some extent become mobilized and thus displaced by the injected fluid.

An interesting approach is that surfactant is distributed between both phases. The surfactant effect depends on the actual concentration in the water. Therefore, the surfactant going into the oil phase can be considered 'disappearance' of surfactant reducing the surfactant effect.

Relative Permeability Curves

In the model, the surfactant decreases interfacial tension. A correlation between surfactant concentration and interfacial tension is used, but the correlations are very much dependent on the type of surfactant. The correlation type applied is shown in Figure 3. The lowered interfacial tension affect the shape of the relative permeability curves, where it is generally assumed that the curves become linear and residual water and oil saturations decrease.

Different methods have been proposed by different researchers, but they use the same general idea, where the interpolation between two curves at different interfacial tension using an interpolation function $g(\sigma)$.

$$k_{rj} = g(\sigma)k_{rj(base)} + [1 - g(\sigma)]k_{rj(misc)} \quad (4)$$

$$s_{or} = g(\sigma)s_{or(base)} \quad (5)$$

$$s_{wi} = g(\sigma)s_{wi(base)} \quad (6)$$

where $j=\{w,o\}$. The base curve is at the case with the highest interfacial tension, $\sigma_{(base)}$, and the miscellaneous curve often being straight line curves from corner to corner in the plot (cf. Figure 2).

A common interpolation function is a function of the capillary number, which is a function of water viscosity μ_w, linear velocity v and interfacial tension σ_{ow} between oil and water:

$$N_{CA} = \frac{\mu_w v}{\sigma_{ow}} \quad (7)$$

There exist many versions of the capillary number interpolation function reasoning that it is not shown here. Another function is a simple interpolation function of the interfacial tension.

$$g(\sigma) = \left(\frac{\sigma}{\sigma_{(base)}} \right)^{\frac{1}{n}} \quad (8)$$

1D Simulations

Different cases have been investigated at the 1D simulator. We inject a solution containing bacteria and substrates and no surfactant (metabolite). A prime example of the water phase saturation profile can be seen in Figure 4, where the capillary number method is used to introduce the surfactant effect.

The MEOR solution is injected, producing a water front like during waterflooding. As bacteria and substrate penetrate the reservoir, more bacteria and surfactant are produced. When enough surfactant is produced, the interfacial tension reduces significantly affecting the relative permeabilities. The interfacial tension reduction mobilizes oil creating *the oil mobilization point*. More water will accumulate instead producing a second water front with surfactant. This results in a traveling oil bank, which occasionally will catch up with the first front as a consequence of different front velocities. If the oil bank catches up with the first front, the water front now having a new saturation will be slowed down. On the other hand, as long as the oil bank does not catch up, the water front will be located at the position of the front for pure waterflooding and breakthrough occurs at the time for pure waterflooding breakthrough.

The recovery curve is also shown in Figure 4. When the oil bank catches up with the waterfront, it results in production with steepest recovery slope for an extra period of time (I), as water breakthrough occurs later. The second part of the curve (II) has a smaller inclination than the first part (I), which results from a larger water cut relative to the first part of the recovery curve. The water saturation is lower until breakthrough of the surfactant water front, where the recovery curve levels off (III). If the oil bank does not catch up with the water front, the recovery curve follows the waterflooding recovery curve until the oil bank breakthrough. Our incremental recovery is around 40%, when the current correlation between surfactant concentration and interfacial tension is used. It should be emphasized, that the incremental recovery depends on the specific surfactant and the actual reservoirs.

The recovery has been found to be markedly sensitive to bacterial growth rate and thus also the injection concentrations of bacteria and substrate. The partitioning of surfactant is found to determine the time

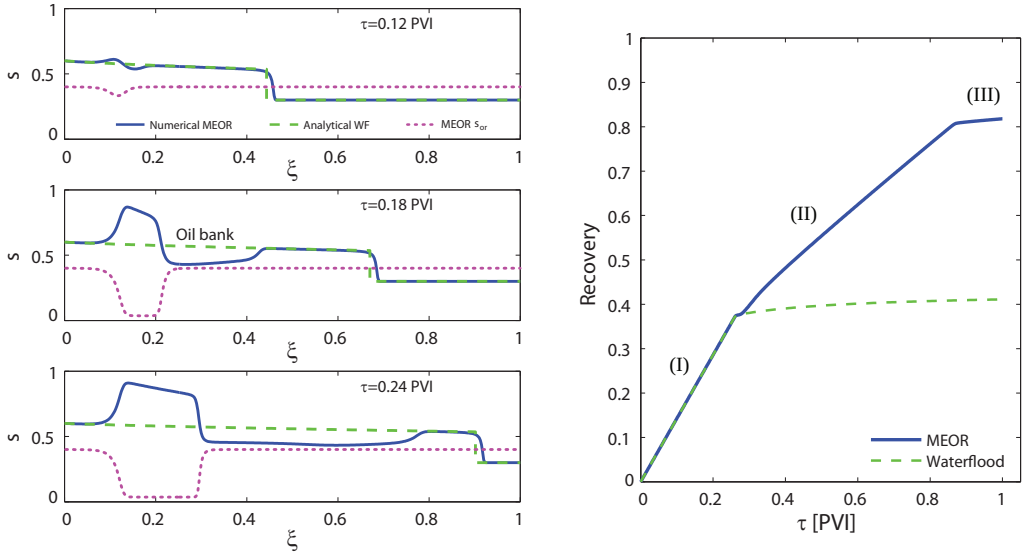

Figure 4. Saturation profiles at different dimensionless times τ (pore volumes injected). The dimensionless reservoir length is ξ. The capillary number is used as the interpolation function. The curves are the analytical Buckley-Leverett solution for pure waterflood, numerical MEOR water phase saturation, and the corresponding MEOR residual oil saturation s_{or}. Recovery curves are for MEOR and waterflooding

lag before residual oil mobilization takes place as sufficient amount of surfactant in the water phase has to be produced.

MEOR Streamline Simulator

The MEOR model for 1D has been implemented into an existing streamline simulator in order to perform simulations in 2D and 3D where also gravity comes into play. To compare the streamline simulations, the MEOR system has also been implemented into finite difference simulator using the IMPEC approach (implicit pressure explicit composition). The result should become very similar when convective dominated systems like MEOR is considered.

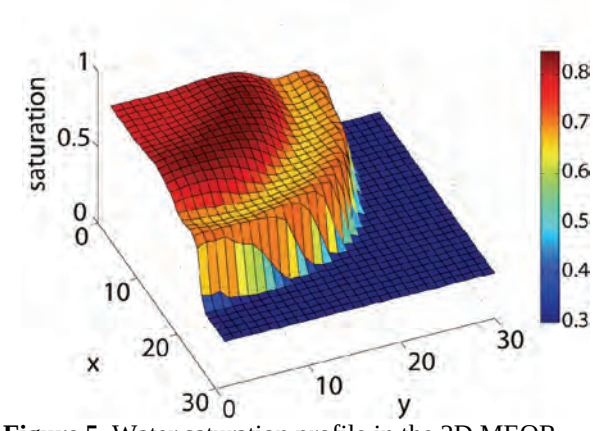

Figure 5. Water saturation profile in the 2D MEOR simulation using the interpolation function equation (8) in order to apply the surfactant effect. The permeability field is homogenous.

The streamline simulator uses the pressures at each grid point to calculate the velocity field of the reservoir. Based on the velocity field, the streamlines are tracked. Along each streamline the 1D solution is solved, which decouples the large 2D or 3D problem into multiple 1D solutions. One advantage with streamline simulators is that the calculation load is less, significantly reducing simulation time compared to a regular finite difference simulator.

The specific features that are seen in 1D are also seen in streamline simulator in 2D and 3D, which becomes very clear for a homogenous permeability field (see Figure 5).

Future Work

Further simulations are to be conducted using the MEOR Streamline Simulator. We investigate the displacement efficiency in 1D, 2D and 3D, when homogenous and heterogonous permeability fields are applied. In 1D, the MEOR system was found sensitive to e.g. bacterial growth rate. This will also be an issue to study in more dimensions.

Other effects were mentioned to be important in the context of MEOR. The next step is to implement the possibility of bacterial adsorption, which will affect porosity and thus permeability.

Acknowledgement

I would like to thank the research school MP²T for sponsoring my PhD. study and Associate Professor Kristian Jessen, University of Southern California, USA, for qualified advice and supervision during my external stay.

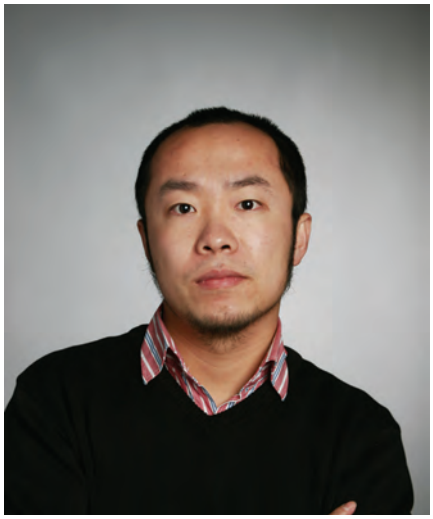

Ben Niu

Address: Building 229
Phone: +45 4525 2895
Fax: +45 4588 2258
e-mail: ben@kt.dtu.dk
www: www.ivc-sep.kt.dtu.dk
Supervisors: Alexander Shapiro
Erling H. Stenby
Wei Yan

Ph.D. Study
Started: September 2006
To be completed: March 2010

Carbon Dioxide Injection in the Carbonate Reservoir

Abstract

Carbon dioxide injection is a widely used EOR (Enhanced Oil Recovery) method. During the injection of carbon dioxide into reservoir at the MMP (Minimum Miscible Pressure), it will be become miscible with original oil. The compositional simulation including the reaction between carbon dioxide and carbonate matrix will also be investigated. The experiments will be conducted with CT scanner and ROP flooding rig under high temperature and high pressure conditions.

Introduction

Today's largest global challenges are climate changes and security of energy supply. With its efficient power plants located near the coast and the North Sea Denmark has a unique position to enable the development of methods to combine the utilization of CO_2 with enhanced oil recovery (EOR). This project is a part of the main project, "Enhanced Oil Recovery through CO_2 utilization" which is to ensure the build-up of knowledge within EOR in Denmark.

During laboratory and field studies, several problems become significantly important. The thermodynamic equilibrium under the circumstance of chemical reaction and the appearance of different ions in the saline water has a direct relationship with the prediction of various parameters in the oil production. The relative permeability between different phases could influence the breakthrough time of different zones, and further the longevity and cost of the whole project. The reaction between carbon dioxide and carbonate matrix will change the porosity and permeability of rock matrix, and further influence the injectivity, and finally limit the longevity of the whole project. The numerical method and algorithm varies with the different dimensions and the complexity of the model, which has significant influence on the robustness, efficiency and accuracy of the model.

The aim of this project is to investigate problems induced by carbon dioxide injection. The current research is focused on the experimental and modeling work.

Process description

The injection of CO_2 into a petroleum reservoir will result in either a miscible or immiscible displacement. If under the prevailing reservoir temperature and pressure, the injected gas is miscible with the reservoir fluid in all proportions, this type of displacement is called first – contact miscible (FCM)[1]. If the injected gas is enriched enough to be completely miscible with reservoir fluid at the front, this kind of displacement is referred as multicontact miscible flood (MCM)[1]. The last type of displacement is in which phases at the gas-oil front can not be miscible. Because the first two kinds of displacement finally achieve similar high recovery efficiency, the MMP has become an important optimization parameter in CO_2 injection.

Experimental Work

The experimental work is mainly conducted with CT scanner (figure 1) and ROP rig (figure 3) in IVC-SEP. In the oil industry, x-ray computed tomography (CT) has been accepted as a routine core analysis tool and mainly used to fundamental studies and recovery mechanisms, like saturation studies, improved recovery, hydrated studies, recovery of viscous oil, formation damage studies, acid treatment and stimulation[2].The saturation distribution of different phases during or after the flooding can be calculated based on the images from CT scanning.

Figure 1: CT scanner

In the recent experiment, three phases flooding in chalk sample is conducted by using CO_2, doped isopar-L and doped water under medium pressure, 6.5Mpa and room temperature 37C. In figure 2, Adsorption of the dopant at the inlet of the core is detected. Light color represents high density zone, which is filled with dopant. This result suggests the sensitivity of chalk sample to different dopants, which is not well-studied yet.

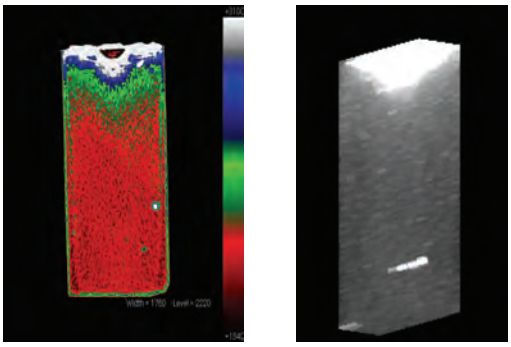

Figure 2: Adsorption of the dopant at inlet

With the analysis of CT images and mass conservation calculation, the experimental results indicate that the three phase experiments with two doped phases are difficult and complex and need further attentions. The choice of dopant is the key to success.

ROP flooding rig is an effective tool for the measurement of multiphase permeability. As in figure 3, the most important and sensitive part of the equipment is the three phase optical separator, which can separate three phases under medium pressure up to 11.5Mpa.

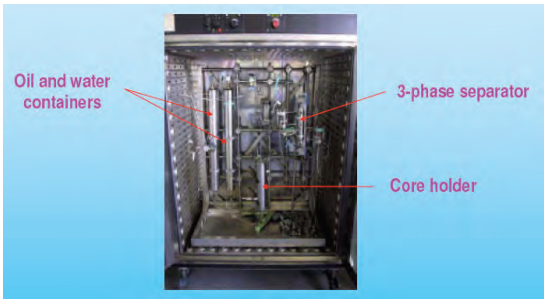

Figure 3: ROP flooding rig

The test experiment with ROP rig reveals that the wettability of glass tube in 3-phase separator can probably change from water wet to oil wet, which affects the final results.

Modeling work

The chemical reactions and multiphase flow in CO_2 flooding are considered in the model, which will be updated step by step.

For a carbonate system the kinetically controlled reactions is[3]:

$$H_2O + CO_2 + CaCO_3 \leftrightarrow Ca(HCO_3)_2$$

The reaction can change the porosity and permeability at the same time, and correspondingly the mechanical properties of the whole reservoir. The change is complex due to its dependence on rock type and the injection scheme. Suitable amount of icons and reactions will be chosen based on the time scale of the whole process and their individual importance.

Multiphase flow in CO_2 flooding could contain four phases, gas, two liquid hydrocarbon phases, and water. The importance of the second liquid hydrocarbon phase is still not fully clear, as mentioned many literatures[4, 5, 6]. This mechanism will be considered in the model.

At current stage, one dimension model has been proposed and in updating.

Future Work

Future research will be focused on multiphase flow and chemical reaction in carbonate reservoir. Flooding experiment will be mainly conducted under high pressure and high temperature conditions with CT scanner. Numerical simulation will mainly focus on the chemical reaction and the corresponding changes in petro-physical properties.

References

1. S. Haynes Jr. and R.B. Alston, SPE/DOE 20190 presented at SPE/DOE Seventh Symposium on Enhanced Oil Recovery, Tulsa, Oklahoma, 1990
2. E.M. Withjack, C. Devier, and G. Michael, SPE 83467 presented at SPE Western Regional/AAPG Pacific Section Joint Meeting, Long Beach, California, 19-24 May 2003
3. O. Izgec, B. Demiral, H. Bertin and S. Akin, SPE 100809 presented at the SPE Annual Technical Conference and Exhibition, San Antonio, Texas, USA, 2006
4. Nghiem, L.X., and Li, Y.K., SPE Reservoir Engineering, Volume 1, Number 4, 414-422, July 1986
5. Fanchi, J.R., SPE Annual Technical Conference and Exhibition, Dallas, Texas, 27-30 September 1987
6. K.K. Mohanty, W.H. Masino Jr., T.D. Ma, and L.J. Nash, SPE Reservoir Engineering, Volume 10, Number 3, 214-221, August 1995

Linda Nørskov
Phone: +45 4525 2952
Fax: +45 4588 2258
E-mail: lin@kt.dtu.dk
WWW: http://www.kt.dtu.dk
Supervisors: Kim Dam-Johansen, Peter Glarborg
Peter Arendt Jensen
Morten Boberg Larsen, FLSmidth A/S

Industrial PhD Study
Started: January 2009
To be completed: December 2011

Fuel Flexible Burners for Cement and Mineral Industry

Abstract
In cement production there is an increasing environmental and financial motivation for substituting fossil fuels for alternative fuels; waste and biomass. The alternative fuels introduce new challenges in the combustion processes. The present Industrial PhD project focuses on combustion of alternative fuels in the cement rotary kiln burner. Initial one-dimensional models are being developed with the aim of predicting flame properties and the possible effects on product quality, production stability, and emissions from information on physical and chemical characteristics of the fuel.

Introduction
5% of the global CO_2 emissions come from the cement industry [1], of which 54% is from the limestone calcination, 34% is from fossil fuel combustion, and the remaining 12% is from the electricity consumption [2].

During the last decades an increasingly share of the fossil fuels have been substituted with alternative fuels, i.e. biofuel or waste. The substitution is mainly motivated by the following reasons:

- Low fuel cost.
- The fossil fuel resources are saved.
- The alternative fuels may be partly or fully CO_2-neutral.
- Waste is effectively utilised as energy and the ash residue is incorporated into the cement product.

Alternative fuels cover a large range of fuels with different chemical and physical properties. The combustion process of alternative fuels may differ significant from the combustion of fossil fuel mainly due to the alternative fuels generally have larger particle sizes. Also, the alternative fuels often have a lower specific heating value, and a higher ash and moisture content. An additional challenge concerning alternative fuels is the varying and inhomogeneous physical and chemical properties resulting in a fluctuating thermal energy input.

Specific Objectives
The objective of this project is to develop a novel scientific framework for effective utilisation of alternative fuels in the main burner of cement and mineral rotary kilns. This will be achieved through studies of physical and chemical phenomena in the combustion process of alternative fuels in the rotary kiln and kiln burner.

The studies involve literature studies, experimental investigations at pilot plant set-ups, and full scale measurements at operating industrial sites, coupled with mathematical modelling eg. simplified one-dimensional engineering models and Computational Fluid Dynamics (CFD) .

The increased understanding of the combustion processes of alternative fuels will be used for optimising and redesigning fuel flexible burners and burner process settings. The goal is to develop a kiln burner that allow for complete substitution of fossil fuels without compromising the clinker quality, production stability, and pollutant emissions.

Results and Discussion
Initial one-dimensional mathematical models for the combustion process in the rotary kiln are being developed. The models should simulate the key processes and provide initial estimations of the time for complete combustion, the temperature profile in the flame, the heat transfer (radiation and convection) from

the flame to the surroundings, and thermal NO_x formation.

The controlling parameters for the combustion process, flame formation, heat transfer and the resulting influence on the cement clinker formation will be investigated and described by mathematical models. The goal is to develop simple mathematical models of the complicated system of coupled processes occurring in the cement rotary kiln.

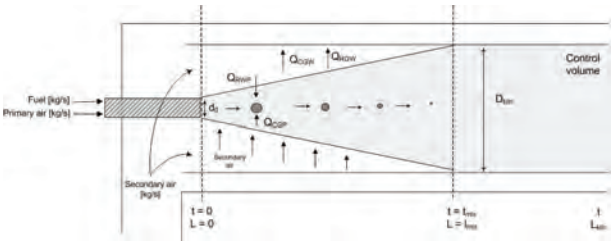

Figure 1: The model system simulating a rotary kiln flame.

Figure 1 shows a sketch of the simplified model system and control volume for the combustion calculations simulating a rotary kiln flame. Fuel particles and cold primary air is injected through a burner placed in a rotary kiln. Along the kiln length hot secondary air from cement clinker cooling is mixed into the reaction zone. The kiln length at which all secondary is mixed into the flame is defined as l_{mix}. The fuel particles are heated by thermal radiation from the hot kiln walls. The combustion gas is heated by the energy released by combustion. In return, the hot combustion gas transfers heat to the surrounding kiln walls and the cement clinker bed mainly by thermal radiation. The model consists of coupled differential equations of gas temperature, particle temperature, and combustion rates for the specific fuel.

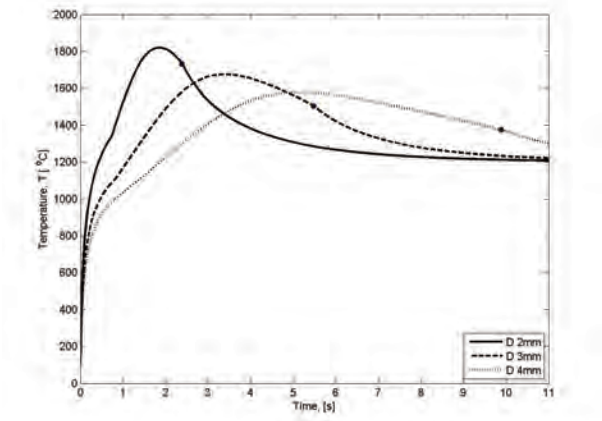

Figure 2: Gas temperature calculations as a function of time for polyethylene combustion with initial particle diameter of 2mm, 3mm and 4mm.

Figure 2 shows an example of the model calculations for combustion of polyethylene, a major component of refuse derived fuel (RDF) which is a possible alternative fuel for cement industry. One of the largest challenges of the alternative fuels compared to traditional fossil fuels is the cost of particle down sizing. This means that the alternative fuel particles often are significantly larger than in the typical coal combustion. Figure 2 shows three gas temperature curves for three fuel particle sizes with initial diameters of 2mm, 3mm, and 4mm. The bullets in the temperature curves indicate the point where complete combustion of the individual particle size is reached. It is seen that the particle size has a significant effect on the time for complete combustion. Typical fuel residence time in a rotary kiln flame is around 2-3s and the large fuel particle may not have sufficient time for complete combustion with the present burner operation settings. This can result in ineffective heat transfer to the cement clinker charge and the unwanted situation of fuel particles falling out of the flame and continuing combustion in the cement clinker bed in the rotary kiln.

Conclusions

The combustion process of alternative fuel differs from combustion of fossil fuel due to different physical and chemical characteristics. Simplified mathematical models of the combustion process are being developed in the present PhD-project. It is essential that these models later in the project are validated against well-defined pilot-scale experiments, and full-scale measurements at operating cement plants.

Acknowledgements

This project is an Industrial PhD project performed in corporation between FLSmidth A/S and the CHEC research Centre with co-funding from The Danish Agency for Science, Technology and Innovation. The project is a part of the research platform ‘New Cement Production Technology’, funded by the Danish National Advanced Technology Foundation, the Technical University of Denmark, and FLSmidth A/S.

References

[1] Mahasenan, N. et al., The cement industry and global climate change: current and potential future cement industry CO2 emissions, Presented at the 6th international conference on greenhouse gas control technologies (GHGT-6), Japan, 2002

[2] Smith, I.M., Potential for economic greenhouse gas reduction in coal-fired power generation. CCC/49, UK, IEA Coal Research, 2001

Mads Pedersen

Phone: +45 4525 2943
Fax: +45 4593 2906
E-mail: map@kt.dtu.dk
WWW: http://www.bioeng.kt.dtu.dk
Supervisors: Anne S. Meyer
Katja S. Johansen, Novozymes A/S

PhD Study
Started: April 2007
To be completed: April 2010

Lignocellulose Pretreatment for Maximal Enzymatic (Ligno)cellulose Degradation

Abstract
Pretreatment of lignocellulose is an important step in the production of second generation bioethanol. Without pretreatment of lignocellulosic biomass the yield of fermentable monosaccharides, and thereby the yield of ethanol, is too low to make bioethanol production cost-effective. However, pretreatment uses huge amounts of energy, and too harsh pretreatment may moreover induce losses by production of inhibitors. The main objectives of this project are therefore to develop new strategies for pretreatment of wheat straw by assessing the influence of pretreatment factors such as grinding of the straw, pretreatment pH and temperature on the enzymatic hydrolysis yields.

Introduction
Degradation of lignocellulosic materials such as straw to monosaccharides that are fermented to ethanol can with time become an environmentally friendly alternative liquid fuel production route, thereby reducing the dependency of fossil fuel sources and reduce the release of green house gasses [1]. A part of the process is the pretreatment of the plant material which is an important step in making the production of bioethanol economically feasible. The purpose of the pretreatment is to make the cellulose (and hemicelluloses) more susceptible to enzymatic hydrolysis for production of fermentable monosaccharides [2], see Figure 1. Different strategies are used for pretreating the plant material, but they often show to be energy, chemical and time consuming, thereby making the process expensive. Among the used methods are steam explosion and wet oxidation which use high pressure and high temperature to make the polymers degradable [3,4]. Strong acids and bases are also used for pretreating the plant material, but reduce the yield due to production of infermentable sugars and inhibitors. To make the use of bioethanol feasible the pretreatment needs more attention regarding reduction of energy demand and reduction of the production of potential inhibitors. Therefore, more research is needed in the field of pretreatment of plant material and understanding the role of each polysaccharide forming the complex matrix of plant cell wall [5].

Specific objectives
The purpose of the project is to find possible improvements for the pretreatment of lignocellulose which can make the production of bioethanol feasible.
Attention will be given to the presently used methods and issues resulting in expensive processes and low yields. To gain higher yields factors such as size of particles, surface and crystallinity need to be drawn into consideration. Another important part is the removal of lignin, which may cause nonproductive adsorption of the enzymes hydrolyzing the biomass.

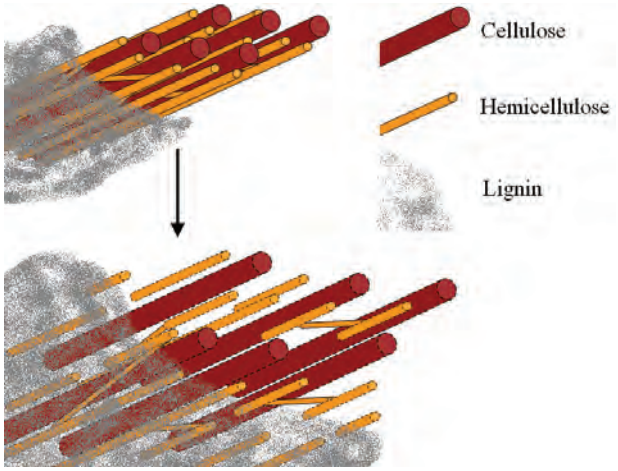

Figure 1: First proposed model of the effect of pretreatment.

Experimental work

Microbial pretreatment took place at DTU Systems Biology with the fungi *Schizophyllum commune*, *Phanerochaete chrysosporium* and *Cyathus stercoreus* incubated for 14 days at 25 °C, pH 5 in dark.

Wet oxidation was run at Risø DTU for pretreatment. This process was run at 195 °C for 10 minutes with 10 bar initial oxygen pressure [4]. Mild thermal pretreatment took place at DTU Chemical Engineering in a table autoclave at 140 °C with various catalysts.

Scanning Electron Microscopy (SEM) was used to analyze the physical alteration. SEM took place at DTU Mechanical Engineering.

Enzymatic hydrolyses of the untreated and pretreated wheat straw were made by the commercial enzymes Celluclast 1.5L (Novozymes A/S) and Novozym 188 (Novozymes A/S) to evaluate the pretreatment. The hydrolyses took place in eppendorf tubes at 50 °C in a thermomixer with 2 % dry matter for up to 24 hours [6].

Results and discussion

Particle size [7]

Particle size diminution will increase surface area and thereby increase the possible enzyme particle interaction. This was confirmed by improved glucose yields from enzymatic hydrolysis of wheat straw particles by cellulases (empty marks, Figure 2). With decreased particle size (from particle range 707-1000 μm to 53-149 μm) the effect more than doubled the yield of glucose. Hydrolysis of wet oxidized wheat straw showed the same pattern (filled marks, Figure 2), however, the effect decreased with continuation of particle size diminution. That is, pretreatment reduced the need of particle size diminution and will thereby reduce the amount of energy needed for grinding biomass prior to pretreatment and enzymatic hydrolysis.

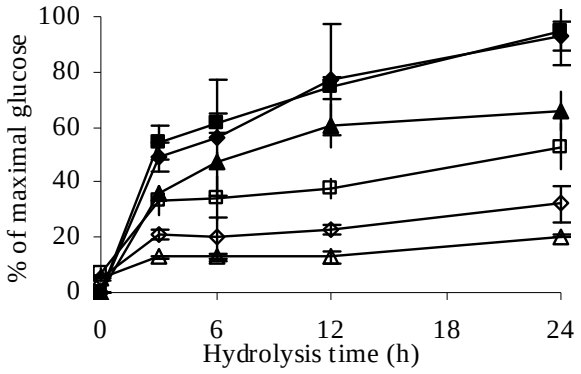

Figure 2: Percentage of maximal glucose release due to enzymatic hydrolysis of pretreated wheat straw (■: 53-149 μm, ♦: 250-500 μm, ▲: 707-1000 μm) and un-pretreated wheat straw (□: 53-149 μm, ◊: 250-500 μm, Δ: 707-1000 μm).

Visualization of the pretreatment effect [7]

To visualize the effect of pretreatment, samples from pretreatment was analyzed by SEM (Scanning Electron Microscopy). The images from the microscopy revealed a physical change of the wheat straw surface composition (see Figure 3). Before pretreatment the particles showed a clear line up of the fibers on the outer surface layer. However, when pretreated by wet oxidation the line up of the fibers seems disrupted. This disruption is thought to increase the accessibility of the hydrolyzing enzymes.

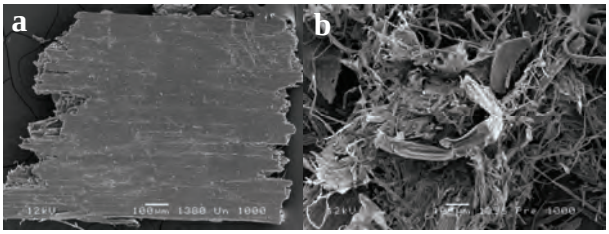

Figure 3: SEM images of wheat straw particle when (a) untreated and (b) pretreated.

Microbial treatment

The least energy consuming method is believed to be microbial pretreatment. Fungi produce enzymes degrading biomass [8,9]. The fungi used for this treatment are known as white rot fungi, which are able to degrade lignin and increase the digestibility of lignocellulose [10]. This treatment is accomplished at ambient temperatures, atmospheric pressure, low addition of chemicals, however, the process time is high. The treatment took 14 days and the fungi used some of the cellulose. This is shown in Figure 4, where three fungi were tested at 25 °C for 14 days growth in dark on wheat straw particles. The results showed that agitation lowers the lignin degradation, whereas, the glucose released from hydrolysis varies. *C. stercoreus* removed 20 % of the lignin and retained a high level of glucose in the biomass susceptible for enzymatic hydrolysis. Except for *P. chrysosprorium*, the fungi (nine fungi were tested) seemed to use more glucose for their growth when agitated.

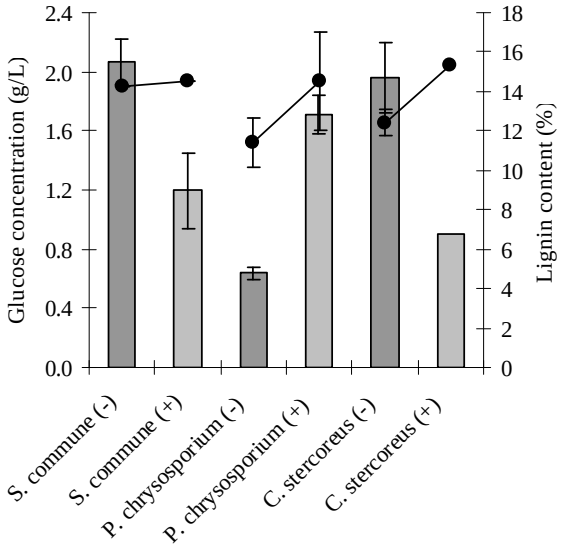

Figure 4: Microbial treatment of wheat straw. Glucose concentrations are read on the left hand axis, (●) lignin content on the right hand axis. (-): without agitation, (+): with agitation.

pH and catalysts in use [11]

Another important factor regarding pretreatment is the addition of catalysts. In the case with biomass pretreatment, different acids and bases are used as catalysts; e.g. hydrochloric acid, sulfuric acid, sodium hydroxide, sodium carbonate. These catalysts will change the initial pH, and also influence the final post treatment pH. The pH is found to affect the digestibility of cellulose and hemicellulose in different ways. The effect on glucose release related to change in pH is shown in Figure 5. Only acidic catalysts will release glucose during pretreatment. However, this enhanced the change of the production of degradation products (Figure 6). Alkaline catalysts did not release any monosaccharides, however, the solid fraction from pretreatment was found highly digestible.

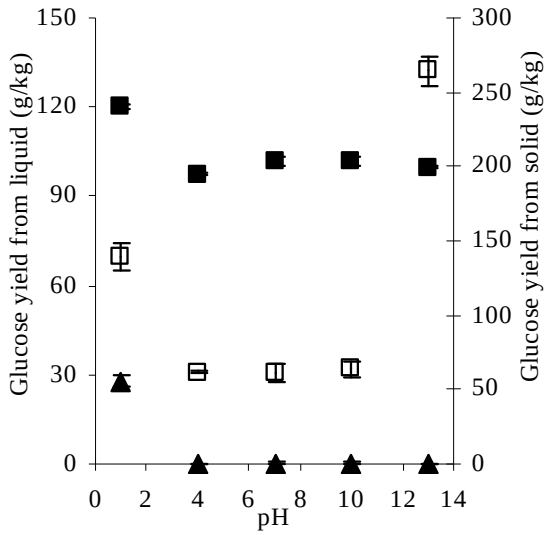

Figure 5. Effect of pH on enzymatically cellulose conversion. ▲: glucose from liquid fraction without enzymatic hydrolysis, ■: glucose from enzymatically hydrolyzed liquid fraction, □: enzymatically hydrolyzed solid fraction. Yields from the liquid fractions are read on the left hand Y-axis scale, while yields from the solid fractions are read on the right hand Y-axis scale.

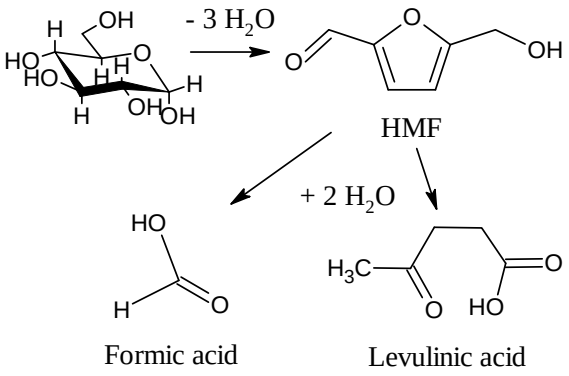

Figure 6. Production of formic acid and levulinic acid from glucose, via hydroxymethylfurfural (HMF) [12].

Pretreatment under mild conditions [11]

To lower the energy demand in the pretreatment of lignocellulosic biomass, a new strategy was tested. Wheat straw was pretreatment at 140 °C for 10 minutes twice (see Figure 7). The product was filtered after each pretreatment. After the first pretreatment, the liquid was collected for enzymatic hydrolysis, while the solid fraction was pretreated once more with a different type of catalyst. After the second pretreatment, the solid was collected for enzymatic hydrolysis, while the liquid fraction contained lignin from the biomass which was removed during the second pretreatment step. This new pretreatment strategy enabled an enzymatic release of glucose of 70 % and a total removal of acid insoluble lignin from the biomass.

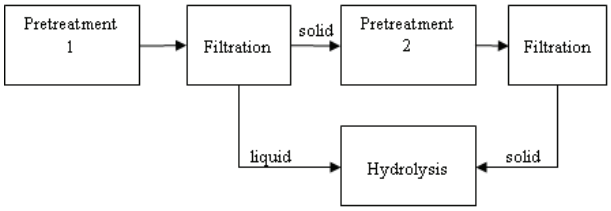

Figure 7. Pretreatment strategy to remove lignin while maintaining a high level of glucose.

The advantage of this strategy with respect to energy use is the low temperature (140 °C compared to 230 °C [5]). Furthermore, the removal of most of the acid insoluble lignin might increase the economical feasibility due to the possible recovery and utilization of lignin. The removal of lignin is carried out with only minor loss of fermentable monosaccharides. Additionally, the production of degradation products was found to be lower than the levels normally inhibiting the enzymes used in the enzymatic hydrolysis and the fermenting microorganisms used in the fermentation process. This pretreatment strategy is now prepared for scale up to large lab-scale (see Figure 8). With time, the process shall be run continuously in stead of batch wise, which will make this pretreatment strategy more applicable for industrial pretreatment processes.

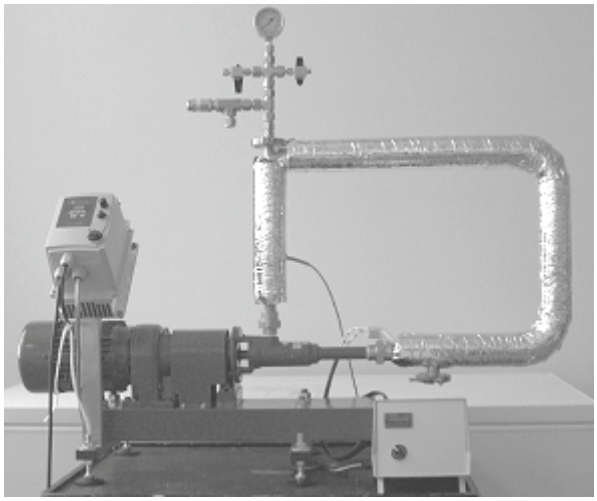

Figure 8. The pretreatment reactor.

Severity factor [4]
The severity factor is used to compare different pretreatment strategies. First, the factor was calculated by the equation proposed by Overend and Chornet in 1987 (Equation 1, [13]).

$$R_o = \int_a^b exp(\frac{T(t) - 100}{14.75})dt = exp(\frac{T(t) - 100}{14.75})t \quad (1)$$

Later on, the combined severity factor was proposed by Abatzoglou *et al*. in 1992 (Equation 2, [14]), where the addition of catalyst was taken into consideration.

$$R' = R_o[H^+] \quad (2)$$

These equations were proposed from work with acidic treatment of biomass, thus, they did not take into consideration that alkaline catalysts increase the digestibility of biomass. Therefore, we tested the combined severity factor as a result of changing initial pH. Depending on the catalyst used and the initial pH, the final pH (which is used in Equation 2) changed. However, as shown in Figure 9, there does not seem to be a linear correlation between the combined severity factor and the yields of glucose and xylose, and removal of lignin. Thus, we are working on a new equation which can predict the digestibility due to thermal pretreatment in a better way, taking temperature, pH and pretreatment time into consideration.

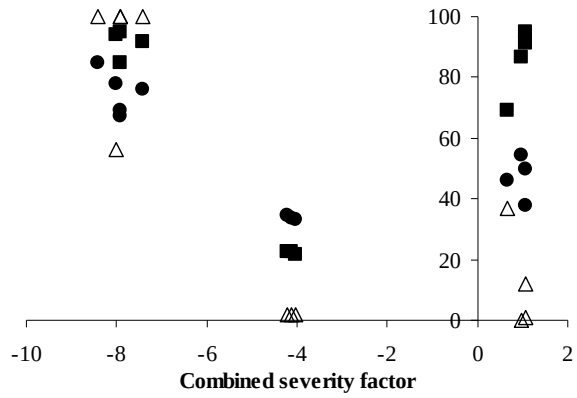

Figure 9. Release of glucose (●) and xylose (■), and the removal of lignin (Δ) from biomass as a result of changed combined severity factor [11].

Conclusion and future work
This project has revealed information on how different factors affect the digestibility of wheat straw. With our newly proposed two-step pretreatment strategy, we are now able to obtain high yields of fermentable monosaccharides, while removing lignin from the biomass. The removal of lignin from the biomass might turn out to be crucial due to the possible utilization in organic chemical production. The project will now focus on the new reactor setup and to make the new strategy a continuous process.

Acknowledgements
We thank Anne Belinda Thomsen and Tomas Fernqvist from Risø DTU for assistance with wet oxidation, Leila Leth from DTU Mechanical Engineering for help with SEM and Jørn Erik Pedersen (DLG) for wheat straw supply.
We acknowledge Novozymes A/S and Novozymes Bioprocess Academy for supporting this project.

References
1. M.A. Kabel, G. Bos, J. Zeevalking, A.G.J. Voragen, H.A. Schols, Bioresource Technology 98 (2007) 2034-2042.
2. H.R. Sørensen, S. Pedersen, A. Viksø-Nielsen, A.S. Meyer, Enzyme Microb. Tech. 36 (2005) 773-784.
3. T.A. Hsu, M.R. Ladisch, G.T. Tsao, Chemical Technology 10 (5) (1980) 315-319.
4. A.B. Bjerre, A.B. Olesen, T. Fernqvist, A. Plöger, A.S. Schmidt, Biotechnology and Bioengineering 49 (1996) 568-577.
5. M. Pedersen, A.S. Meyer, New Biotechnology (submitted, 2009).
6. L. Rosgaard, S. Pedersen, J.R. Cherry, P. Harris, A.S. Meyer, Biotechnology Progress 22 (2006) 493-498.
7. M. Pedersen, A.S. Meyer, Biotechnology Progress 25 (2009) 399-408.
8. M. Pedersen, M. Hollensted, L. Lange, B. Andersen, International Biodeterioration and Biodegradation 63 (2009) 484-489.
9. M. Pedersen, H.K. Lauritzen, J.C. Frisvad, A.S. Meyer, Biotechnology Letters 29 (2007) 743-748.
10. F. Keller, J.E. Hamilton, Q.A. Nguyen, Applied Biochemistry and Biotechnology 105 (2003) 27-41.
11. M. Pedersen, A. Viksø-Nielsen, A.S. Meyer, Process Biochemistry (submitted, 2009).
12. B.F.M. Kuster, Starch 42 (1990) 314-321.
13. R.P. Overend, E. Chornet, Philosophical Transactions of the Royal Society of London Series A 321 (1987) 523-536.
14. N. Abatzoglou, E. Chornet, K. Belkacemi, R.P. Overend, Chemical Engineering Science 47 (1992) 1109-1122.

List of publications
1. M. Pedersen, A.S. Meyer, Biotechnology Progress 25 (2009) 399-408.
2. M. Pedersen, A. Viksø-Nielsen, A.S. Meyer, Process Biochemistry (submitted, 2009).
3. M. Pedersen, A.S. Meyer, New Biotechnology (submitted, 2009).

Conference contributions
1. M. Pedersen, A. Viksø-Nielsen, A.S. Meyer, 7th European Symposium on Biochemical Engineering Science, Faro, Portugal (2008).

Nanna Petersen
Phone: +45 4525 2861
Fax: +45 4593 2906
E-mail: nap@kt.dtu.dk
WWW: http://www.kt.dtu.dk (no personal page)
Supervisors: Krist V. Gernaey
Anna Eliasson Lantz, DTU Systembiologi
Stuart Stocks, Novozymes A/S

PhD Study
Started: October 2006
To be completed: June 2010

In-situ NIR Spectroscopy for Analyte Specific Monitoring of Glucose and Ammonium in *Streptomyces coelicolor* Fermentations

Abstract
Over the past decades there has been a great effort in developing methods for real-time monitoring of fermentation processes using various advanced sensors such as Near Infrared (NIR) spectroscopy. In this study, NIR spectra were collected *in-situ* in *Streptomyces coelicolor* fermentations and subsequently used for prediction of the two important analytes glucose and ammonium. The prediction of glucose was highly satisfactory resulting in a RMSEP of 1.1 g/L whereas the quality of the ammonium predictions was greatly reduced compared to models calibrated based on offline NIR.

Introduction

Fermentation processes are widely used in the production of food and food ingredients, pharmaceuticals, enzymes, and a number of bulk chemicals. Efficient control of fermentation processes is often essential for obtaining a high yield, and relies on timely and accurate information concerning the physical, chemical, and biological conditions in the bioreactor. Today physical and chemical parameters such as for example the pH, temperature, dissolved oxygen concentration, and carbon dioxide evolution rate are measured reliably on-line whereas information concerning biologically important variables such as the concentration of different nutrients, metabolites, and the biomass is mainly available via laborious off-line analyses. Over the past decades there has been a great effort in developing methods for real-time monitoring of fermentation processes using various advanced sensors. The formulation of the Process Analytical Technology (PAT) guidance, launched by the U.S. Food and Drug Administration in 2004 (http://www.fda.gov/Cder /OPS/ PAT.htm) has resulted in an increased activity in this research area.

Near Infrared (NIR) spectroscopy has a large potential for monitoring fermentation processes and several studies have been published on the subject [1,2]. Most of the published studies discuss off-line and at-line NIR spectroscopy applications and can report low prediction errors for many nutrients such as glucose, glycerol, ammonium as well as biomass and various products. However, if the aim is *automatic* control, the measurements should be made on-line. On-line collection of NIR spectra poses a challenge as it does not allow for any sample pre-treatment e.g. the separation of biomass from the broth. Different on-line setups for collection of NIR spectra in fermentation processes have been tested and reported in the literature such as a by-pass loop, a reflectance probe outside a glass window, and reflectance and transmission probes immersed in the fermentation broth. Probes placed inside the fermenter, here referred to as *in-situ* setups, are subject to disturbances from agitation, air bubbles, solid particles (e.g. biomass or insoluble medium components), temperature, pH changes etc. Despite the large number of potential disturbances, successful studies have been reported for different cell cultures with probes placed inside the fermenter. In these studies, the processes under investigation are typically characterized by a low agitation rate and a low biomass concentration, which make these systems attractive for *in-situ* NIR monitoring. *In-situ* monitoring of various unicellular microbial systems such as yeast and *E. coli* run under more 'challenging' conditions, i.e. high aeration and stirring rates, have also been reported in the literature. From a comparative study of *in-situ* and at-

line measurements of biomass in an *E. coli* cultivation, Arnold et al. [3] have concluded on a number of challenges with *in-situ* monitoring such as loss of wavelength regions (potentially above 2000 nm) due to adverse signal to noise ratio, loss of light intensity, gas phase effects, and mechanical vibration of equipment.

A major challenge in the calibration of chemometric models for NIR monitoring of fermentations is the inherent correlation between the different analytes. A typical batch process will start with low biomass and product concentrations and high nutrient concentrations. As the fermentation progresses, the biomass and product concentrations will increase while the nutrients are taken up. This results in negative correlations between biomass and nutrient concentrations and positive correlations between the concentrations of different nutrients. If concentrations of nutrients, biomass and product are highly correlated it is possible to calibrate chemometric models for prediction of both nutrients and product based for example on the signal originating from biomass alone, so-called correlated models. This may be acceptable if the yields are constant during the fermentation. However, in abnormal situations – or actually as soon as the yields change – the predictions will not be accurate. Different solutions have been proposed in the literature to overcome this problem, including: (a) the use of purely synthetic samples; (b) semi-synthetic samples (fermentation samples that have been altered by addition of different compounds of interest); (c) samples from multiple fermentations in which for example the media composition is changed to introduce variations between batches; and (d) combinations of the above.

Specific objectives

The purpose of the present study was to critically evaluate the ability of NIR spectroscopy to measure important analytes in low concentrations *in-situ* in a filamentous fermentation broth. Addressing the problem of correlations between analytes in the model building *in-situ* was a central part of the evaluation since results cannot be transferred directly from the off-line setting. This study used a combination of standard batch samples and semi-synthetic samples to break the correlations between analytes and calibrate *analyte specific* models for glucose and ammonium. To highlight the specific challenges of collection of NIR spectra *in-situ*, the samples were also measured using off-line NIR spectroscopy.

Materials and methods

In-situ and off-line NIR spectra were collected in two standard batch fermentations (ST-1:2) with *Streptomyces coelicolor*. This data set was complemented with semi-synthetic samples (SS-1:5) from five batch fermentations. The procedure for the generation of the semi-synthetic samples is illustrated in Figure 1. Subsequently, Partial Least Squares (PLS) regression models were calibrated for prediction of glucose and ammonium based on the NIR spectra. For further details the reader is referred to [4].

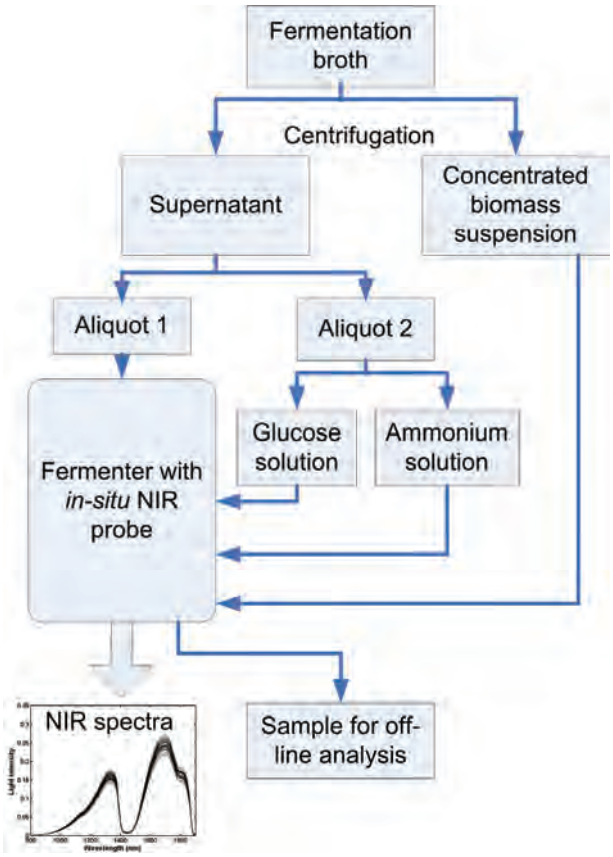

Figure 1: Experimental procedure for the generation of the semi-synthetic samples.

Results

PLS models were calibrated for the prediction of glucose based on the NIR spectra collected *in-situ* and off-line. The five sets of semi-synthetic samples (SS-1:5) and the standard batch 1 (ST-1) were used for model calibration. The pre-treatment, wavelength region, and the number of Latent Variables (LV) were determined by minimising the Root Mean Square Error of leave-one-batch-out Cross Validation (RMSECV). Following this, an independent data set (standard batch 2, ST-2) was used to validate the model thus providing the Root Mean Square Error of Prediction (RMSEP).

The RMSECV and the RMSEP for glucose were 1.9 g/L and 1.1 g/L respectively for the *in-situ* model compared to 1.4 g/L and 1.4 g/L respectively for the off-line model. Hence, the cross-validation and the validation errors were low and in the same range for both the off-line and the *in-situ* models. The prediction error of 1.1 g/L achieved by the *in-situ* model corresponds to 5.4% of the average glucose concentration in the validation set, which is in the same range as the reference method. For the semi-synthetic samples (Figure 2 top) the changes in glucose concentration were very well predicted, both during addition of biomass, ammonium, and glucose indicating that the models were indeed based on a signal from the glucose. Likewise, the plot of

the predictions of ST-2 (Figure 2 bottom) shows that the model was also able to capture the variation in the glucose concentration throughout a standard batch. Overall the model performed highly satisfactory.

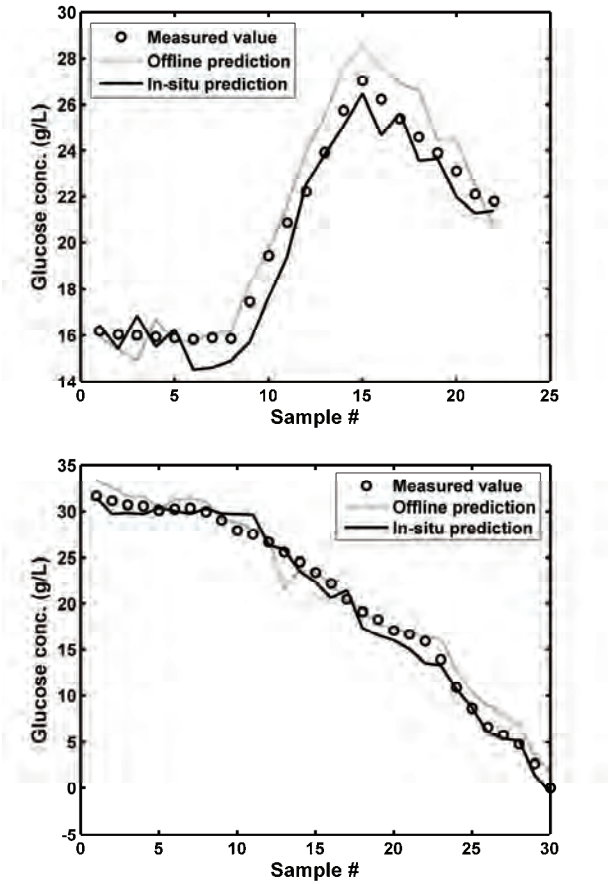

Figure 2: Prediction of the glucose concentration using the model calibrated based on the *in-situ* spectra (solid line) and the off-line spectra (dotted line). Top: Cross validation results for semi-synthetic sample set 3 (SS-3); Bottom: Validation results for the independent standard batch 2 (ST-2).

Models for prediction of ammonium were calibrated and validated following the same procedure as for glucose. The resulting RMSECV and the RMSEP for the *in-situ* model were 7.1 mM and 11 mM respectively. This corresponds to a prediction error of 16% of the mean value in the validation set, which is relatively high. The changes in ammonium concentration in the set of semi-synthetic (Figure 3 top) samples and the standard batch (Figure 3 bottom) were only partly captured by the model. Furthermore, the predictions of the standard batch were highly biased for the first 12 samples. Hence, the performance of the *in-situ* model for prediction of ammonium was not satisfactory.

For comparison, the ammonium prediction errors for the model based on spectra collected off-line were approximately half of the errors for the *in-situ* model. The off-line model was able to capture the variation of the ammonium concentration in both the semi-synthetic as well as the standard samples with the exception of one slightly outlying sample (Figure 3).

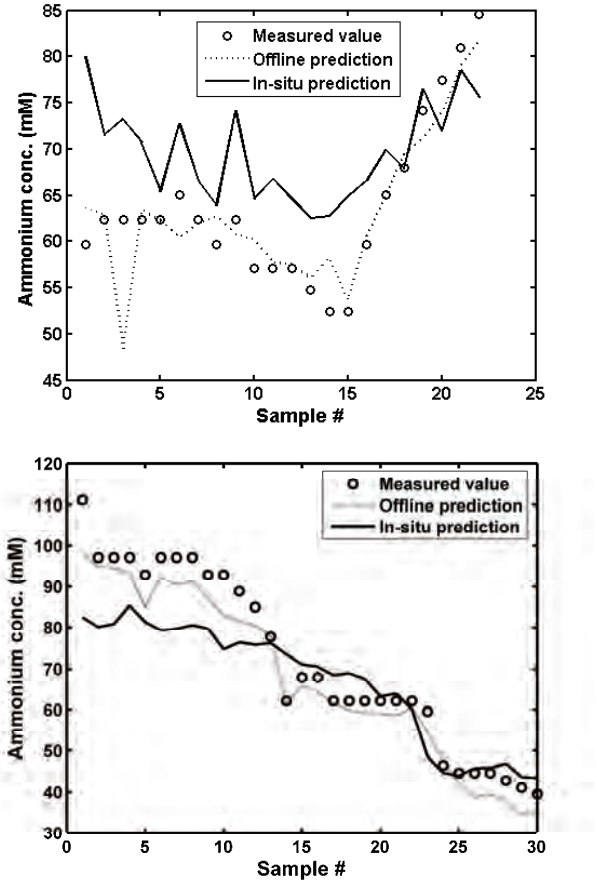

Figure 3: Prediction of the ammonium concentration using the model calibrated based on the *in-situ* spectra (solid line) and the off-line spectra (dotted line). Top: Cross validation results for semi-synthetic sample set 3 (SS-3); Bottom: Validation results for the independent standard batch 2 (ST-2).

Discussion

To ensure analyte specificity of the PLS models, it was crucial that the inherent correlation between biomass, glucose, and ammonium was reduced. This was achieved by measuring a large number of semi-synthetic samples in the fermenter using *in-situ* NIR spectroscopy. The inclusion of semi-synthetic samples successfully reduced the correlations between ammonium, glucose, and biomass from ±0.92-0.97 to ±0.77-0.79. This study thus presents an example of a strategy for implementation of NIR monitoring on a fermentation process by the use of semi-synthetic samples *in-situ* along with a thorough calibration and validation procedure, resulting in a critical and realistic estimate of the performance of NIR spectroscopy *in-situ*. We believe that such critical evaluations are necessary for the further development of NIR spectroscopy as part of PAT applications in the biotechnological industry.

The results showed that the glucose concentration could be predicted satisfactorily based on NIR spectra

collected *in-situ*. The prediction error for the *in-situ* model was 1.1 g/L corresponding to 5.4% of the average value in the validation set. In comparison Rodrigues et al. [5] achieved a relative error of 13% for the carbon source in the only other published study concerning *in-situ* NIR measurements in filamentous fermentations. The plots of the predicted glucose concentrations in both the semi-synthetic and the standard samples showed good predictions regardless of the concurrent increase or decrease in concentration of the other analytes in solution (Figure 2). These plots thus verified model specificity and constituted a visual check of the quality of the calibrated models. Real-time predictions of glucose will provide valuable insight into many fermentation processes and can for example be used for automatic control of glucose addition in fed-batch processes. Both process knowledge and implementation of automatic control to keep a process within its design space are important aspects of PAT.

For ammonium the validation of the *in-situ* model resulted in a relative RMSEP of 16% corresponding to a correlation coefficient of 0.73, which is very similar to the correlation coefficient of 0.716 obtained by Rodrigues et al. [5]. However, this is not considered satisfactory in this study – particularly since the correlation coefficient between biomass and ammonium was found to be 0.79 in the present data set, indicating that it was not possible to construct an analyte specific *in-situ* model for ammonium. A closer look at the PLS models for ammonium revealed that the *in-situ* model only used the wavelength region between 1500-1850 nm whereas as the off-line model also included the region between 2000-2200 nm. Ammonium has previously been predicted successfully in a number of studies using NIR spectroscopy. A literature survey revealed that the majority of the identified absorption peaks for ammonium are found above 2100 nm. Few studies report absorption peaks around 1680-1690 nm and at 900 nm. However, these peaks are placed within the overtone regions (first and third respectively) of the C-H stretch and cannot immediately be assigned to any of the theoretical absorption peaks of ammonium. This obviously presents some challenges for *in-situ* monitoring of ammonium, and highlights the importance of breaking inherent correlations when calibrating analyte specific prediction models. If monitoring of ammonium is required, it should be considered to optimize the signal in the region above 2100 nm. Using fluoride optical fibers instead of the standard glass fibers would be one way to improve the signal to noise ratio in that important wavelength region.

Conclusions

The main objective of the present study was to provide a critical and realistic evaluation of *in-situ* NIR spectroscopy for measurement of glucose and ammonium in filamentous fermentations. This was achieved by using semi-synthetic samples *in-situ* to break correlations and ensure analyte specificity and by validating the resulting model on an independent batch. The results showed that glucose could be predicted satisfactorily based on *in-situ* NIR spectroscopy. On-line prediction of glucose will be of high value in many fermentation processes for example to control the glucose addition in fed-batch processes. The models calibrated for ammonium based on *in-situ* NIR were not satisfactory. This may be partly explained by signal attenuation in optical fibers above 2000 nm. Thus, if monitoring of ammonium is important, it is suggested to improve the signal in this region.

Acknowledgements

This Ph.D. project is supported by a grant from the Innovative BioProcess Technology Research Consortium financed by the Danish Research Council for Technology and Production Sciences, Chr. Hansen A/S, Danisco A/S, and Novozymes A/S.

References

1. M. Scarff, S. A. Arnold, L. M. Harvey, B. McNeil. Crit. Rev. Biotechnol. 26 (2006) 17-39.
2. A.E. Cervera, N. Petersen, A. Eliasson Lantz, A. Larsen, K.V. Gernaey. Biotechnol. Progr. 2009 (in press). (doi: 10.1021/bp.280)
3. S.A Arnold, R. Gaensakoo, L.M. Harvey, B. McNeil. Biotechnol. Bioeng. 80 (2002) 405-413.
4. N. Petersen, P. Ödman, A.E. Padrell, S. Stocks, A. Eliasson Lantz, K.V. Gernaey. Biotechnol Progr.. 2009 (in press). (doi: 10.1021/bp.288)
5. L.O. Rodrigues, L. Vieira, J.P. Cardoso, J.C. Menezes. Talanta. 75 (2008) 1356-1361.

List of publications

1. N. Petersen, S. Stocks, K. V. Gernaey. Biotechnol. Bioeng. 100 (2008) 61-71.
2. G. Sin, P. Ödman, N. Petersen, A. Eliasson Lantz, K.V. Gernaey. Biotechnol. Bioeng. 101 (2008) 153-171.
3. N. Petersen, P. Ödman, A.E. Padrell, S. Stocks, A. Eliasson Lantz, K.V. Gernaey. Biotechnol Progr. (2009 in press). (doi: 10.1021/bp.288)
4. A.E. Cervera, N. Petersen, A. Eliasson Lantz, A. Larsen and K.V. Gernaey. Biotechnol. Progr. (2009 in press). (doi: 10.1021/bp.280)

Hanne Hostrup Poulsen

Phone: +45 4525 2838
Fax: +45 4588 2258
E-mail: hhn@kt.dtu.dk
WWW: http://www.chec.dtu.dk
Supervisors: Peter Glarborg
Sønnik Clausen
Stefan Mayer, MAN Diesel SE

Industrial PhD Study
Started: March 2006
To be completed: August 2009

In-Situ Investigations of the Combustion in Large, Two-Stroke Diesel Engines

Abstract
Due to restrictions on the emission levels from marine engines, MAN Diesel SE is conducting thorough research in areas connected with combustion optimization and emission reduction. An important tool in the combustion investigations is numerical analysis of the various combustion phases, but a lack of reliable experimental data provides an obstacle in validation and optimization of the developed code. For years, various optical analysis methods have been applied for investigations of the combustion in smaller engines, but due to the more restricted access, extremely sooting combustion, and very high heat loads, similar investigations undertaken at larger engines under realistic combustion conditions are limited.
This project considers optical in-situ investigations on a large, two-stroke Diesel engine. The aim of the investigations is to provide experimental data for the combustion under realistic running conditions and to use these data for validation and optimization of an existing CFD-code.

Introduction
Large, marine engines are responsible for approximately 2 % of the total world fuel consumption, and many of these engines are two-stroke Diesel engines. Strong restrictions are expected to be imposed on the industry in near future, thereby forcing the leading engine manufactures to focus further on emission reduction and engine performance optimization in general.
The costs of performing physical tests on marine engines are very large, which makes numerical analysis a natural alternative. Obviously, experimental data are necessary for validation of the numerical codes, and the developments in optical methods within the areas of measurements of complex flows make these a natural choice. These methods have been used for several years in smaller engines, though the transient characters of the combustion and the large and fast variations in pressure and temperature have provided several challenges in the design of both optical accesses and experimental equipment.
Unfortunately, the results obtained on smaller engines cannot be scaled up to the conditions present in the larger engines. This is mainly due to large difference in both length and time scale of the engine processes and the use of different types of fuel.

Specific Objectives
The aim of the present Industrial Ph.D.- project is to develop an optical access to the test engine located in the Test Centre at MAN Diesel in Copenhagen, and with this to provide experimental data from the Diesel combustion for validation and optimization of the in-house developed numerical models.
As opposed to many of the investigations undertaken so far, this project focuses on in-situ measurements under realistic conditions, thereby enabling validations of local character for real-size, two-stroke, marine engines.

Diesel combustion
The combustion cycle in a two-stroke, marine Diesel engine is complex and consists of several different stages. The following paragraph will give a very short introduction to these, in order to demonstrate the many different aspects of the Diesel combustion.
During the compression of the last parts of the scavenging air from the former combustion cycle, pressure and temperature in the combustion chamber is increased considerably. Diesel fuel is sprayed into the combustion chamber at high pressure and, due to the conditions, quickly vaporizes. The fast vaporization and the swirling motion of the scavenging air ensures that fuel and oxygen is mixed, which causes the auto-ignition processes to proceed.

After ignition, the Diesel flame spreads to the remaining parts of evaporated fuel. During this premixed, turbulent combustion, more fuel is still being injected into the combustion chamber. The fuel being injected is now ignited, resulting in a non-premixed, turbulent flame. When the injection is stopped, the last parts of the spray is mixed with air and finally burned out. Subsequent scavenging with air removes the combustion gases from the cylinder.
The dynamic and complex manner of the Diesel combustion illustrates the troubles encountered when trying to either control the formation of unwanted components or describing it numerically. It also emphasizes the possible shortcomings of the data obtained from simplified laboratory equipment or ideal reference fuels, and hence confirms the need for reliable data recorded at real engines under realistic conditions.

Optical investigations in engines

The predominant method for optical investigations of the combustion in engines is by use of a laboratory 1-cylinder engine constructed with large parts of the cylinder walls made of a transparent material. Due to the very large heat stresses in the larger engines, this approach is impossible for large marine engines.
Alternatively, an endoscope can be used for looking into a more limited space of the engine. An endoscope can be introduced through an existing opening of the engine, but also limits the view of the combustion chamber, when comparing to an ideal laboratory cylinder. This can though partially be solved by the wide range of industrial endoscopes available today, allowing for various directions and angles of view. Further, using existing openings, the modifications of the engine from the standard set-up are minimized, thereby providing experimental data obtained under as realistic conditions as possible.
Establishing a useful and reliable optical access to a large, marine engine is rather troublesome, due to the very harsh environment inside the engine cylinder during the combustion cycle.
Challenges include:

- Heavy sooting, which causes:
  - intense radiation of heat
  - soot depositions on the window
- Low speed, which gives long periods of time with high heat loads
- Two-stroke engines have no cooling stroke, which could otherwise lower the thermal stresses.
- The safety risks connected with a window breaking during running of the engine are high, and considerable care must be taken during both the design phase and the experiments.

With a functional optical access, various optical methods of investigations are possible. A typical method for basic information on the combustion process is doing direct imaging of the combustion. This means high speed images of the natural combustion light, which in the case of the non-premixed turbulent flames of the Diesel combustion means images of the soot being formed during the combustion.
The surfaces of the soot particles emit Planck radiation continuously throughout parts of the UV, the visible and the near-IR spectral regions, with an intensity corresponding to the surface temperature.
Due to the direct injection of fuel, the soot formation is very intense during the non-premixed turbulent combustion phase. However, because of the large overall air excess values, the final engine out emissions of soot in heavy marine engines is relatively low, compared to smaller Diesel engines.

Experimental set-up

The investigations are undertaken at the MAN Diesel test engine in Copenhagen. This is a real engine, run under realistic conditions, but also heavily experimentally equipped. In Table 1, a few data for the test engine can be found

Table 1: Data for the MAN Diesel test engine used for investigations.

Characteristics	Data
Engine type	Diesel, 2-stoke
No. of cylinders	4
Cylinder diam. [cm]	50
Stroke [cm]	220
Power [MW]	~ 8
Power [hp]	~ 10.000
Max. speed [rpm]	123
Adiabatic. gas temp. [°C]	~ 2400
Max pressure [bar]	~ 180
Overall air excess ratio [-]	~ 2

In Figure 1, the optical set-up used in the investigations on the test engine is depicted. The optical access gives a view across the top of one of the four cylinders, and is constructed inside the starting air valve. As the engine can be started without starting air on this cylinder, the access minimizes the influence on the combustion conditions. The optical assess involves the following components:

- Sapphire window shielding the optics from the combustion environment
- Endoscope guiding the image from the inside of the window to the outside of the valve
- A mirror directing the image towards to capturing equipment
- A standard 50 mm. Nikon lens
- Photron APX High Speed Camera, capturing light with wave lengths in the 400-1050 nm spectral range (visible region).

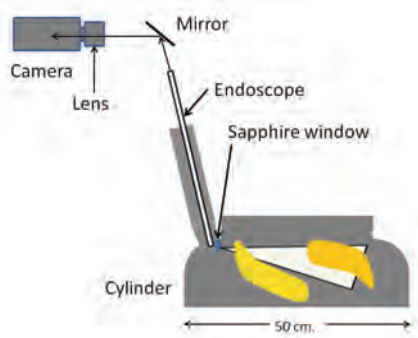

Figure 1: Sketch of the optical set-up for doing direct imaging of the combustion in the MAN Diesel test engine. The endoscope view covers approximately 53 degrees and looks across the top of the cylinder .

The choice of using the starting air valve for the optical access, along with the design of the cylinder cover and the optical access, pre-determines the view within the cylinder. The fuel is injected directly into the combustion chamber through a fuel nozzles, placed almost directly across from the optical access. This means, that when doing imaging of the sooting flame, the initial images will show the flame propagating from the fuel nozzle across the cylinder. Shortly into the combustion process, the swirling motion inside the cylinder will have developed the sooting flame into covering the entire field of view, giving a close-up image of a non-premixed turbulent flame, see Figure 2.

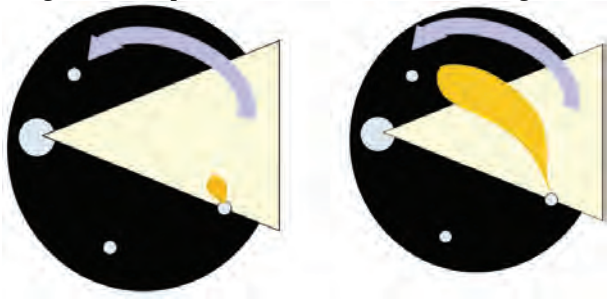

Figure 2: Top view of the flame development and optical field of view within the cylinder during combustion. The large triangle represents the field of view through the optical access, and the arrow the swirl direction.

The high speed camera has built-in functions for only using part of the chip (reducing field width) and triggering the camera for recording for a limited period of each cycle. This facilitates the recording of several cycles in a row without compromising the good temporal resolution. In Table 2, a typical set-up for high speed recordings of a 50 % load run with a single fuel nozzle are listed.

Table 2: Recording settings for direct high speed imaging of the combustion during a 75 % load run.

Recording parameter	Data
Engine speed [rpm]	97.5
Framing speed [fps]	18000
Image resolution [-]	384x352
Shutter speed [1/s]	1/252,000
Images pr. cycle	1000
Consecutive cycles recorded	14
Time covered pr. cycle [ms]	~60

Numerical calculations

Simulations of the combustion are performed with the KIVA CFD-code including a Flamelet model for extended soot formation modeling. Some selected data for the regular KIVA simulation set-up is given in Table 3.

Table 3: Selected parameters for the KIVA simulation set-up.

Recording parameter	Data
Initial number of cells	5300
Turbulence model	kε-RNG
Initial turbulence intensity	0.2
Initial temperature [K]	830
Initial pressure [bar]	74.7
Initial mass fraction, O_2 [-]	0.228
Initial mass fraction, N_2 [-]	0.750
Initial mass fraction, CO_2 [-]	0.0025
Initial mass fraction, H_2O [-]	0.0071

Compared to the regular Hiroyasu soot model, the Flamelet code for soot formation uses a more advanced mechanism for description of soot formation and oxidation. The mechanism includes the influence of:

- Particle inception
- Agglomeration
- Surface growth
- Soot oxidation

A thorough introduction to the soot formation mechanism can be found in references 1 and 2. The dynamics of given a soot particle ensemble is solved in each computational cell and each time step by the statistical approach of the Method of Moments, with a total of four moments included in the calculations. From the moments, averaged parameters of each of the soot particle ensembles can be determined, *e.g.*:

- Particle diameter
- Number density
- Volume fraction

The method of moments and the implications of this methodology is elaborated in references 3 and 4.

Results

In Figure 3, high speed images of the sooting par t of the combustion throughout the cycle are presented.

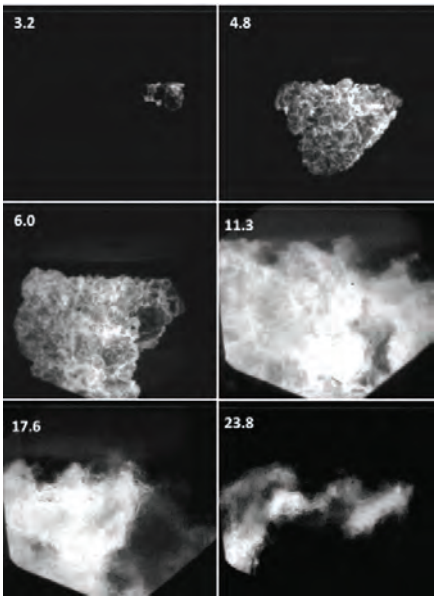

Figure 3: Development of sooting flame. Numbers in upper left corners represent the timing in CAD ATDC.

Results of the soot formation, as simulated by the KIVA code in connection with the Flamelet model, are to be compared to the high speed images. This is done within the post-processing tool, OpenDX, by simulating the soot luminescence distribution. The soot luminescence is simulated by multiplying the soot volume fraction with a factor representing the black body luminescence of solid soot within a given computational cell. The black body luminescence is calculated from the Planck distribution at the given temperature and is subsequently corrected with the spectral response of the high speed camera. Figure 4 shows an example of the black body curve for a temperature of 2100 K and the effect of including the camera response. The final soot luminescence is determined by summing up all contributions within the camera spectral response interval.

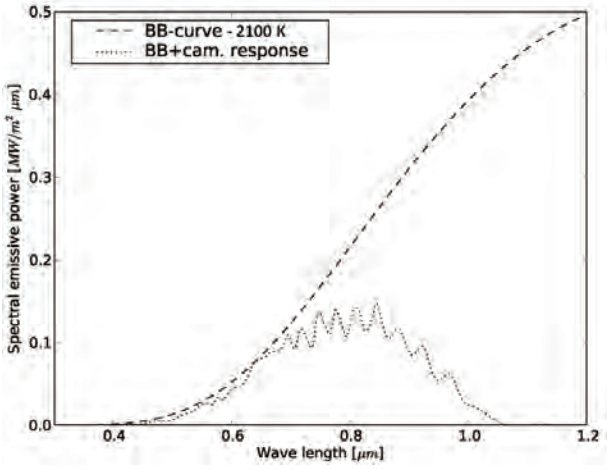

Figure 4: Planck curve for a Black Body at 2100 K, and the corresponding signal when including the influence of the spectral response of the high speed camera.

The resulting visualization of the Flamelet soot distribution and the comparison to the high speed images , can be seen in Figure 5. The images compare the recorded development of the sooting flame in the time span 4-6 CAD ATDC. Due to limitations in the post-processing software, the angle of view is not exactly the same in the two sets of images.

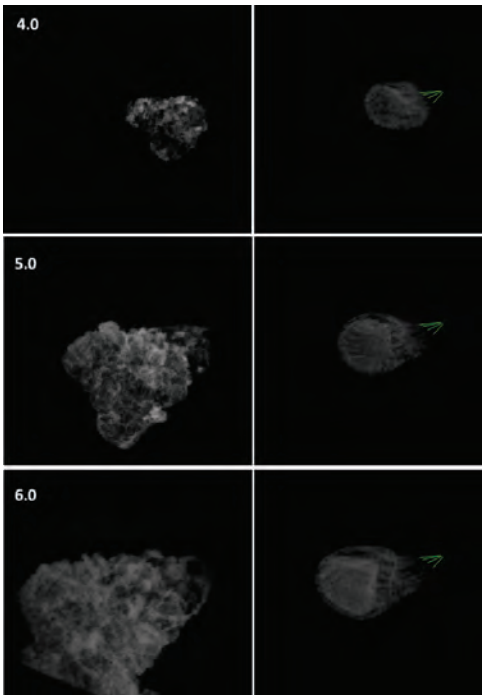

Figure 5: Comparison of images to luminescence simulations from OpenDX, based on Flamelet results. Green arrows indicate origin and direction of the fuel spray. Numbers in upper left corners represents the timing in CAD ATDC.

Conclusions

The work presented in this paper have shown the results obtained with in-situ optical investigations of the combustion in the cylinder of a large, two-stroke Diesel engine. The investigations have proven the applicability of the experimental set-up for doing robust, reliable and highly temporal resolved direct images of the soot luminescence during the Diesel combustion, even when running the engine under realistic conditions.

It is evident that the KIVA simulations, combined with the Flamelet model, are able to retrieve important features, both temporal and geometrical, of the developing flame.

References

1. F. Mauss and T. Schäfer in: H. Bockhorn (Ed.), Soot Formation in Combustion, Springer-Vorlag, Berlin, 1994
2. F. Mauss, K. Netzell, H. Lehtiniemi, Combust. Sci and Tech. 178 (2006) 1871-1885
3. M. Frenklach, S. Harris, Journal of Colloid and Interface Science 118 (1987) 154-164
4. A. Kazakov, M. Frenklach, Combustion and Flame 114 (1998) 484-501

Ke Qin

Phone: +45 4525 2890
Fax: +45 4588 2258
E-mail: ke@kt.dtu.dk
WWW: http://www.kt.dtu.dk
Supervisors: Anker Degn Jensen
Peter Arendt Jensen
Weigang Lin

PhD Study
Started: January 2009
To be completed: December 2011

Biomass Gasification in an Entrained Flow Reactor

Abstract
There is a world-wide interest in the use of biomass resources as feedstocks for producing power and fuels. The gasification of biomass plays an important role for the utilization of biomass. An entrained flow reactor was successfully employed for biomass gasification in entrained flow at atmosphere. In the present work, biomass gasification has been studied with a focus on the effects of temperature, excess air coefficient, steam to carbon molar ratio and biomass type on the gas composition, soot and tar in the producer gas.

Introduction
Among the renewable energy sources, biomass has a high potential [1]. Plant growth "recycles" carbon dioxide from the atmosphere, and the use of biomass resources for energy and chemicals results in low net emissions of carbon dioxide. Gasification is one of the key technologies for utilization of biomass, especially in the field of production of liquid fuels and chemicals. Of several gasification methods, the entrained flow gasifier has the advantage to produce a gas with low tar content and possibility to run at high temperature and pressure [2]
Systematic studies on gasification of biomass in entrained flow gasifiers are scarce. In addition the fundamental processes taking place during biomass gasification at temperatures relevant to entrained flow gasifiers are not fully understood. The production of synthetic liquid fuels for transportation from biomass has a large relevance for the near future [3]. In production of liquid fuels, it is important to control the syngas quality from gasification with respect to both the H_2/CO ratio and harmful impurities [4], such as tar.

Specific objectives
The objective of the project is to study entrained flow gasification of biomass to syngas. In the present work [5], gasification of biomass has been investigated under entrained flow reactor conditions with respect to main syngas composition (H_2/CO/CO_2/hydrocarbon), soot and tar as a function of operating conditions, such as temperature (T), excess air coefficient (λ), steam/carbon ratio (H_2O/C) and biomass type.

Results and Discussion
A reasonable carbon mass balance closure was achieved for all conditions (±9%) except one (22%). The largest deviation was observed at 1000ºC and may be caused by high yields of unmeasured tar and larger hydrocarbons.

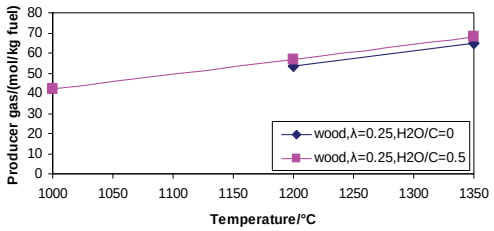

Figure 1: Effect of temperature on producer gas

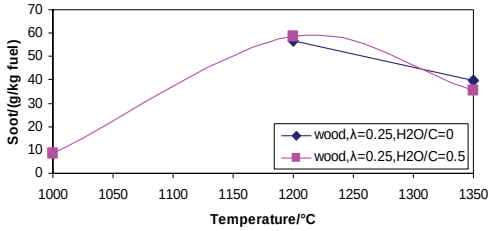

Figure 2: Effect of temperature on soot

Effect of temperature: The amount of producer gas (H_2, CO, CO_2 and hydrocarbon up to C_3 species) increases as the temperature increases, which is shown in Figure 1. The increased gas formation is caused by the conversion of tar and larger hydrocarbons into lighter gaseous products. The yields of H_2 and CO increase while CO_2 yield decreases with increasing temperature because char and soot gasification is endothermic. The yield of

C_xH_y (hydrocarbons up to C_3 species) decreases because it is converted to soot and light gases at higher temperature. From 1000°C to 1200°C, the soot yield increases, whereas from 1200°C to 1350°C, there is an opposite trend, which are shown in Figure 2. Soot is formed at high temperature and the increasing temperature favors soot formation. However, at higher temperature, soot has higher gasification reactivity. The amount of tar is highest at 1000°C (22%), whereas the yield of soot is lowest. At 1350°C, the tar content is very low, but significant soot was produced (7%). This shows that there is a trade off between tar and soot formation, which may result from soot formation by tar and hydrocarbons polymerization competing with soot gasification at high temperatures.

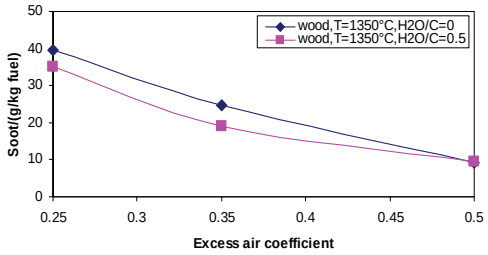

Figure 3: Effect of excess air coefficient on soot

Effect of excess air coefficient: The amount of producer gas nearly keeps constant with an increase of excess air coefficient. The H_2, CO and C_xH_y yields decrease with increasing excess air coefficient, whereas the yield of CO_2 increases due to oxidation of soot, CO and other gaseous species. It is observed that the amount of soot decreases with increasing excess air coefficient, which is shown in Figure 3, because a larger part of the soot is combusted as the excess air coefficient increases.

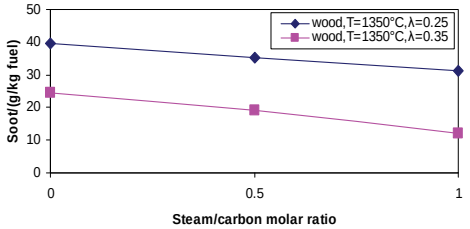

Figure 4: Effect of H_2O/C molar ratio on soot

Effect of steam/carbon molar ratio: As steam is introduced, the yield of the producer gas increases slightly due to the promotion of steam gasification of soot and larger hydrocarbons. However, even a high amount of steam injection only gives small changes in the gas composition. As the steam/carbon molar ratio increases, the H_2 and CO_2 yields increase, accompanied with a decrease of the CO yield, because the steam addition tends to promote the water gas shift reaction. The C_xH_y yield increases a little when steam is introduced, which is caused by the reformation of tar and larger hydrocarbons. The yield of soot decreases slightly with increasing steam/carbon molar ratio, which is shown in Figure 4, most likely due to steam gasification of the soot.

Effect of biomass type: Wood and straw gasification provide similar gas composition. Straw has high alkali content, but it does not change the gas composition significantly, probably because the char yield is negligible in all cases.

Conclusions

In all experiments, the char was completely converted. The amount of producer gas increases significantly when the temperature is increased from 1000°C to 1350°C. This is caused by the conversion of tar and larger hydrocarbons into lighter gaseous. The yields of hydrogen and carbon monoxide increase as the temperature is increased. It was found that at an excess air coefficient of 0.25 and a steam/carbon molar ratio of 0.5, the tar content is very low at 1350°C, but a significant level of soot (7%) was produced at this temperature. At 1000°C, the amount of tar is highest (22%), whereas the yield of soot is lowest. This trade off between tar and soot formation may result from the competition between soot formation by tar and hydrocarbons polymerization and soot oxidation at high temperatures. The yields of hydrogen and carbon monoxide decrease with increasing excess air coefficient. With addition of steam, the hydrogen yield increases while the carbon monoxide yield decreases due to the water gas shift reaction. The soot yield can be slightly reduced by addition of steam. The applied biomass type has little influence on the gas composition.

Acknowledgements

Danish Research Council for Technology and Production and the Danish Energy Agency are acknowledged.

References

1. World Energy Outlook 2004.
2. Higman C, van der Burgt M. Gasification. America, 2003.
3. Hamelinck CN, Faaij APC, den Uil H, Boerrigter H. Production of FT transportation fuels from biomass; technical options, process analysis and optimisation, and development potential. Energy 29(2004): 1743-1771.
4. Zwart RWR, Boerrigter H. High efficiency co-production of synthetic natural gas and Fischer-Tropsch transportation fuels from biomass. Energy & Fuels 19(2005): 591-597.
5. Qin K, Lin WL, Jensen PA, Jensen AD. Influence of operating conditions on gas composition, soot and tar in entrained flow gasification of biomass. International Conference on Polygeneration Strategies 09.

Louise Enggaard Rasmussen

Phone: +45 4525 2935
Fax: +45 4593 2906
E-mail: ler@kt.dtu.dk
WWW: http://bioeng.kt.dtu.dk
Supervisors: Anne S. Meyer
Jens F. Sørensen, Danisco A/S

PhD Study
Started: February 2007
To be completed: January 2011

Kinetics of Enzyme Catalyzed Heteropolysaccharide Degradation: Insoluble Arabinoxylan

Abstract

Examination of sensitivity of xylanases to ubiqutous inhibitors forms an integral part of understanding the kinetics of xylanase-catalyzed degradation of insoluble arabinoxylans.This study examined the kinetics and substrate selectivity of a GH11 *Bacillus subtilis* XynA xylanase (BsX) sensitive to inhibition by TAXI and an engineered variant which is much less inhibited by TAXI (BsX_{mut}). The main purpose of the work was to elucidate any influence of the structural point mutations on the kinetics and substrate selectivity of the enzyme. Three dimensional structures of both xylanases were superimposed to elucidate the structural basis for differences in their hydrolytic properties. The two xylanases were individually incubated with water-extractable arabinoxylan (WEAX), water-unextractable arabinoxylan (WUAX), birchwood xylan, and wheat bran, respectively. Both the BsX and the BsX_{mut} catalyzed the release of xylo-oligosaccharides with higher degree of polymerization from WUAX than from WEAX. At equimolar addition levels the activity of the BsX_{mut} was lower than that of the BsX with respect to both the initial rate and the product yields obtained after prolonged reaction on the xylan substrates. Most of the calculated substrate selectivity factors indicated that the BsX and the BsX_{mut} both had higher catalytic rate on WUAX than on WEAX. Addition of a 100:1 (TAXI:xylanase) molar ratio of inhibitor confirmed the significantly decreased inhibition of BsX_{mut} by TAXI. Addition of TAXI also influenced the xylanases' selectivity factor differently..

Introduction

Enzymatic hydrolysis of xylans is of considerable importance in several cereal processes ranging from food and biotechnological applications to exploitation of xylans as a carbohydrate source for fermentation of xylose to biofuels or as a base for development of novel prebiotic food ingredients. Xylan is a highly branched hetero-polysaccharide which varies in structure between different plant species. It consists of a backbone of β-1,4 linked D-xylopyranosyl residues and depending on the source of the xylan and the procedure used in its extraction, the xylose units can be substituted with L-arabinofuranose or 4-O-methyl glucuronic acid residues or they can be esterified with acetic acid. Furthermore, the L-arabinofuranosyl side chain residues can be esterified with ferulic and p-coumaric acid.

Endo-1,4-β-xylanases (xylanases, EC 3.2.1.8) catalyze the hydrolysis of the β-1,4 linkages in the arabinoxylan backbone, generating a mixture of xylo-oligosaccharides. Xylanases are mainly categorized in glycoside hydrolase (GH) families 10 and 11, although some xylanases are classified in GH5, GH8 and GH43. All reported structures of GH 11 xylanases have been described as a partially closed right hand consisting of only one domain folding into two β-sheets, which form a cleft on which the active site is situated. About 10 years ago, it was discovered that cereals such as wheat, durum wheat, barley and rye contained proteinaceous xylanase inhibitors which may affect the functionality of microbial xylanases, notably GH11 xylanases. *Triticum aestivum* xylanase inhibitors (TAXI) are proteins of ~40 kDa that specifically inhibit bacterial and fungal GH11 xylanases [1].

Because of the increased significance of microbial xylanases in baking and other cereal processing applications, a *Bacillus subtilis* XynA xylanase (BsX) (GH11) was recently modified to diminish the xylanase-inhibitor interaction [2]. Surface residues, D11 (residue 11, aspartic acid) and R122 (residue 122, arginine), surrounding the active site cleft were mutated to F (phenylalanine) and D (aspartic acid) respectively. The single R122D mutation was found to increase the activity of the xylanase, but did not induce resistance to inhibition by TAXI, whereas the D11F mutation produced significant resistance to inhibition by TAXI.

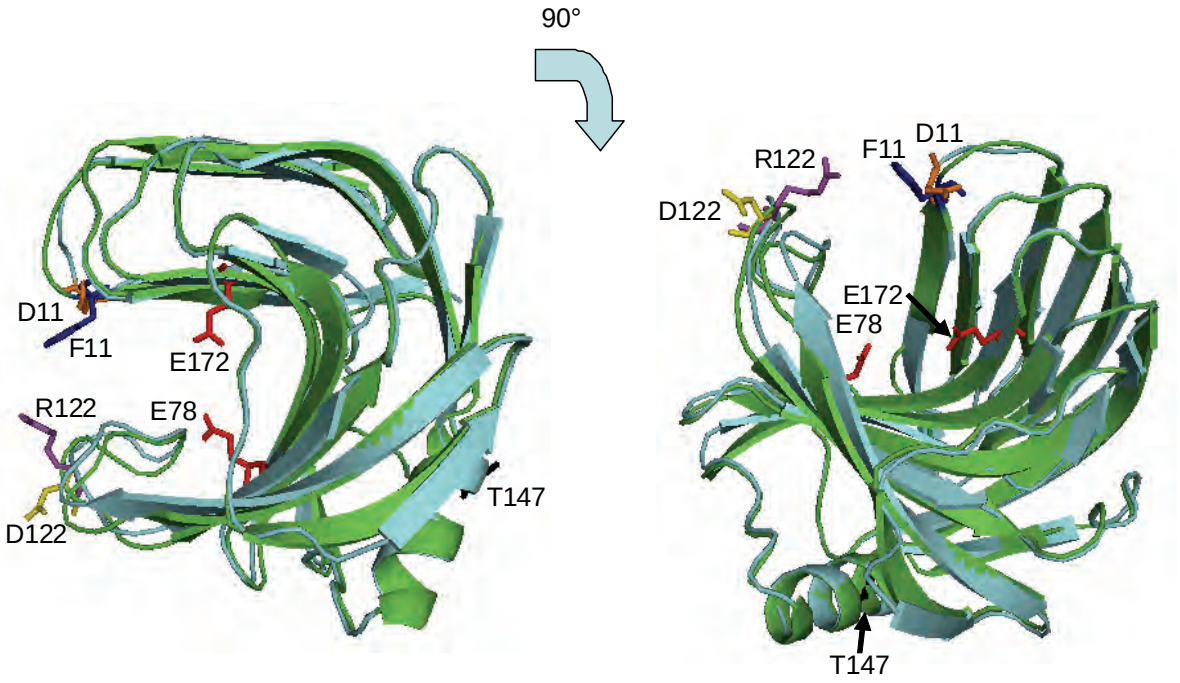

Figure 1: Superposition of the *B. subtilis* XynA xylanase wildtype (BsX) (green) and D11F/R122D variant (BsX_{mut}) (light blue) visualizing the mutation of the amino acid, D11 (orange) and R122 (puple) in BsX, which has been mutated to F (dark blue) and D122 (yellow) respectively in the variant BsX_{mut}. The two catalytic glutamic acid residues (E78 and E172) are highlighted in red. The residue highlighted in black (T147) is threonine in *B. circulans* xylanase but serine (S147) in BsX. This figure was drawn using PyMOL (v0.99) (DeLano Scientific, San Carlos, CA) based on the PDB-file 1NXB of *B. circulans* [3] and 2B45 of *B. subtilis* [4].

Specific objectives

The purpose of the present study was to evaluate the specificity and the TAXI resistance of this engineered TAXI resistant variant of the *Bacillus subtilis* XynA xylanase (BsX_{mut}) in comparison with the wildtype *Bacillus subtilis* XynA xylanase on different substrates. This was done by adding TAXI to various xylanolytic substrates in order to mimic the real conditions in genuine reaction media such as e.g. wheat dough where the xylanase will encounter the inhibitor. In order to elucidate the structural basis responsible for the different substrate specificities of the wildtype and recombinant xylanase, a comparison of 3D structures was also performed.

Experimental methods

Four substrates (water extractable arabinoxylan (WEAX), water unextractable arabinoxylan (WUAX), birch wood xylan and wheat bran) were hydrolyzed using BsX and BsX_{mut} respectively. For inhibition studies TAXI was preincubated with the substrates (WEAX and WUAX) prior to addition of the xylanases. The released hydrolysates were analyzed for xylo-oligosaccharides by High Performance Anion Exchange Chromatography (HPAEC) mainly focusing on the quantification of arabinose and xylo-oligosaccharides.

Results

Molecular modeling of the enzymes

To investigate the structural basis for differences in the catalytic properties of BsX and BsX_{mut}, the three dimensional structure of BsX was modeled using the *B. circulans* xylanase A (PDB ID: 1XNB) [3] as the search model. The model of BsX was superimposed onto the BsX_{mut} model (PDB ID: 2B45) [4] in order to elucidate the structural change of the D11F and R122D mutation. As seen in Figure 1, the D11F mutation appears to cause a slight narrowing of the entrance to the active site cleft because the phenylalanine is more bulky than the aspartic acid. Apparently the R122D mutation has the opposite effect since the change of arginine to aspartic acid causes a slight widening the entry to the active site cleft.

Enzymatic hydrolysis - Initial rates

For both enzymes the initial rates of the hydrolysis of the four substrates, WEAX, WUAX, birchwood xylan and wheat bran, were calculated and also for WEAX and WUAX respectively in the presence of TAXI (Table 1). Initial velocities were obtained directly from the initial slope of the progress curves showing a significant release of xylo-oligomers products during the first 30 min. The resulting catalytic efficiencies indicated that addition of TAXI to WEAX and WUAX decreased the initial rate of BsX significantly, namely by approximately 46% and 30%. The initial velocity of the hydrolysis of WEAX was more affected by addition

of TAXI than the initial velocity data on WUAX. For BsX_{mut}, no significant effect of TAXI on WEAX was observed. On WUAX, however, the catalytic efficiency was decreased by approximately 16%. For both enzymes the initial rates on birchwood xylan were the highest obtained (Table 1). This result may correlate to the relatively simple composition of this substrate. Analogously, the lowest initial rates were obtained on the wheat bran, which has a more complex composition. However, the initial rates for the hydrolysis of wheat bran were quite similar for BsX and BsX_{mut} and were similar to those obtained by BsX_{mut} on WEAX.

Table 1: Initial rates (v_i) [$\mu M\ min^{-1}$] from the hydrolysis of individual polymeric substrates by BsX and BsX_{mut} of various XOS. Coefficients of variation were all < 10.4%.

	WEAX	WEAX +TAXI	Inhibition [%]	WUAX	WUAX +TAXI	Inhibition [%]	Birchwood xylan	Wheat bran
BsX								
X2	7.23 ^{d,x}	4.01 ^{b,y}	44.5	5.93 ^{b,x}	3.99 ^{b,y}	32.8	12.75	1.21
X3	7.85 ^{e,x}	3.97 ^{d,y}	49.4	14.47 ^{d,x}	10.23 ^{d,y}	29.3	49.86	3.85
XOS	16.92 ^{f,x}	9.26 ^{f,y}	45.3	28.60 ^{f,x}	21.00 ^{f,y}	26.6	100.9	7.26
BsX_{mut}								
X2	1.38 ^{a,x}	1.36 ^{a,x}	1.4	2.39 ^{a,x}	2.07 ^{a,x}	13.4	3.88	1.00
X3	3.01 ^{b,x}	2.84 ^{c,x}	5.6	8.65 ^{c,x}	7.12 ^{c,x}	17.7	21.31	2.17
XOS	5.65 ^{c,x}	5.73 ^{e,x}	-1.5	17.40 ^{e,x}	14.29 ^{e,y}	17.9	60.05	5.49

Results in the same column followed by different roman superscript letters a-f are significantly different at P<0.05. Results in the same row, pair wise for SSF(Y_{MAX}) and SSF vi, followed by different roman superscript letters x, y are significantly different at P<0.05.

Discussion

The catalytic rates of both xylanases on substrates that differ in complexity may be related to the general structure of the active site for GH11 xylanases. In this family, the cleft-shaped active site results in a restricted catalytic behavior where substituents present a hindrance. Since birchwood xylan is a linear unbranched molecule, this substrate is better accommodated into the active site cleft than e.g. wheat bran which has a relative more complex composition.

The reduced activity of the BsX_{mut} compared to BsX on all four substrates (WEAX, WUAX, birchwood xylan and wheat bran) was in accordance with previous findings [2]. Whether this small difference in the product yield was due solely to the introduction of a more bulky amino acid at the entrance to the active site of the enzyme which thereby might retard the entrance of substrate to the active site or is a result of a truly different specificity in the attack mode of the BsX_{mut} requires further analysis.

Previous results have shown that a R122D mutation in BsX increased the activity by 31% [2]. Furthermore, crystallographic analysis of the structure of *B. subtilis* xylanase A mutants have showed that the thumb which contains residue R122 has a functional role in the catalysis since it is the most flexible part of this xylanase molecule [5]. The thumbs flexibility play a role in the open-close movements and therefore in the accessibility of the substrate to the enzyme. Therefore, the R122 mutation was combined with the D11F mutation in order to increase the activity of the less TAXI-inhibited xylanase (BsX_{mut}), which it did [2]. However, in the present study using different xylanolytic substrates the effect of this mutation on the activity of the enzyme was not apparent since the BsX_{mut} still had slightly lower activity than BsX (Table 1).

In this study approximately 110 nmole TAXI per nmole xylanase was used to assess the effect of TAXI on the catalyzed hydrolysis by the two xylanases. Typical inhibitor concentrations in wheat flour are in the range 110 mg kg^{-1} for TAXI. Generally, the molar xylanase inhibitor concentrations in wheat flours are much higher than the xylanase dosages used in biotechnological processes [6]. Since the xylanase and the inhibitor form a 1:1 complex [4], it is intriguing that despite high inhibitor concentrations, xylanases are still catalytically active and can be used in biotechnological processes. Firstly, a reason for this may be that the concentrations of both TAXI and xylanases are so low in genuine applications that there may be a delay in the complex formation as a result of the low probability that the TAXI and xylanase actually come in contact before the enzyme attacks the substrate; hence, the relative concentration of substrate to enzyme is much larger that the relative concentration of TAXI to enzyme, providing a favorable competitive advantage of the enzyme-to-substrate interaction as compared to the TAXI:xylanase complex formation. In addition, the inhibition by TAXI is reversible. Secondly, biotechnological applications of microbial xylanases do not fully resemble the biochemical *in vitro* experiments in regard to mobility, in many of the real applications water might be a limiting factor for enzyme and TAXI mobility.

Conclusion

This study established that the overall activity of the variant xylanase of *B. subtilis* XynA (BsX_{mut}) was significantly reduced on different polymeric xylan substrates. Based on the structure analysis, the reduced activity of BsX_{mut} might be due to the steric hindrance caused by the mutation D11F. The understanding of the changes in catalytic capabilities of mutant enzymes is very important for predicting dosages and outcome in genuine applications. The finding that one amino acid change at the entry to the active site did in fact alter the specificity may allow for new protein enzyme design that can promote the liberation of certain desirable product profiles in future applications.

Acknowledgements

This study was partly supported by the Innovative Bioprocess Technology Research Consortium financed by the Danish Research Council for Technology and

Production Sciences, Chr. Hansen A/S, Danisco A/S, Novozymes A/S. Financial support from the FOOD Denmark Graduate School, Center for Advanced Food Studies, Denmark, is also acknowledged.

References

1. Gebruers, K., Debyser, W., Goesaert, H., Proost, P., Van Damme, J., Delcour, J. A., 2001. Triticum aestivum L. endoxylanase inhibitor (TAXI) consists of two inhibitors, TAXI I and TAXI II, with different specificities. J. Biochem. 353, 239-244.
2. Sørensen, J.F., Sibbesen, O., 2006. Mapping of residues involved in the interaction between the *Bacillus subtilis* xylanase A and proteinaceous wheat xylanase inhibitors. Protein Eng. Des. Sel. 19, 205-210.
3. Campbell, G.L., Bedford, M.R., 1992. Enzyme applications for monogastric feeds: a review. Can. J. Anim. Sci. 72, 449-466.
4. Sansen, S., De Ranter, C.J., Gebruers, K., Brijs, K., Courtin, C.M., Delcour, J.A., Rabijns, A., 2004. Structural basis for inhibition of *Aspergillus niger* xylanase by *Triticum aestivum* xylanase inhibitor-I. J. Biol. Chem. 279, 36022-36028.
5. Pollet, A., Vandermarliere, E., Lammertyn, J., Strelkov, S.V., Delcour, J.A., Courtin, C. M., 2009. Crystallographic and activity-based evidence for thumb flexibility and its relevance in glycoside hydrolase family 11 xylanases. Proteins. 77, 395-403.
6. Gebruers, K., Courtin, C.M., Moers, K., Noots, I., Trogh, I., Delcour, J.A., 2005. The breadmaking potential of two Aspergillus niger xylanases is strongly dictated by their substrate selectivities and inhibitor sensitivities. Enzyme Microb. Technol. 417-425.

List of publications

1. Rasmussen, L. E., Meyer, A. S., 2010. Size exclusion chromatography for the quantitative profiling of the enzyme catalyzed hydrolysis of xylo-oligosaccharides. J. Sci. Food Agric. (in press).
2. Rasmussen, L. E., Sørensen, J. F., Meyer, A. S., 2010. Kinetics and substrate selectivity of a *Triticum aestivum* xylanase inhibitor (TAXI) resistant D11F/R122D variant of *Bacillus subtilis* XynA xylanase. J. Biotechnol. (subm.).

Martin Hagsted Rasmussen

Phone: +45 4525 2923
Fax: +45 4588 2258
E-mail: mhr@kt.dtu.dk
WWW: http://www.kt.dtu.dk
Supervisors: Professor Kim Dam-Johansen
Associate professor Stig Wedel
Kent Thomsen, FLSmidth A/S

PhD Study
Started: September 2007
To be completed: September 2010

Reduction of SO_2 Emission from Modern Cement Plants

Abstract

Co-absorption of CO_2 and SO_2 on CaO has been investigated. Absorption of SO_2 decreases with increasing CO_2 content for a fixed feed SO_2 concentration of 1000 ppm. At a CO_2 concentration of 20 %, CaO only absorbs 25 % of the SO_2 absorbed without CO_2 in the gas. CaO is much more reactive towards SO_2 than $CaCO_3$ under all conditions, even when CO_2 is present in high concentrations.

Introduction

Recently more attention has been given to the emission of SO_2 from cement plants due to tightened regulatory requirements, especially in the EU and northern America. The US Environmental Protection Agency in 2008 proposed a national limit of 0.6 kg SO_2/ton of clinker, which will increase the cost of clinker production with about 4 $ per ton if raw materials with a high sulphur content are used. For this reason it has become of interest to understand the processes that control the formation as well as the removal of SO_2 in cement plants.

The most common way to produce cement today is by the dry process, illustrated in figure 1. In the dry process raw meal, which mainly consist of limestone and clay, is fed to the preheater tower which typically consist of 4-6 cyclones. Through the cyclone tower the raw meal is, step by step and counter-currently, heat exchanged with the hot flue gas from the calciner/kiln.

The raw meal contains small amounts of sulfur, which is mostly found as pyrite (FeS_2). When pyrite is heated in an oxygen containing atmosphere, it will be oxidized to iron oxides and SO_2. This reaction takes place between 400 and 600 ºC [1].

SO_2 Capture Reactions

The SO_2 formed can leave the preheater as part of the gas phase or react with the limestone in the raw meal, according to Eq. 1.

$$CaCO_{3(s)} + SO_{2(g)} + \tfrac{1}{2}O_{2(g)} \rightarrow CaSO_{4(s)} + CO_{2(g)} \quad (1)$$

This reaction has been studied by Hu [2] under relevant conditions (relatively low temperatures and short residence times). In his experiments Hu [2] found a maximum conversion of the $CaCO_3$ particles of about 0.05 mole % at a particle-gas contact time of 0.35 s at 600ºC

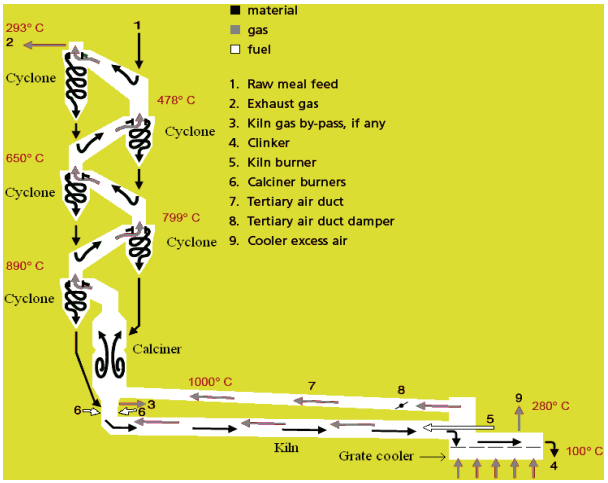

Figure 1: Illustration of the dry process for cement manufacturing.

It is also possible that SO_2 reacts with CaO formed in the calciner and transported upwards as part of the flue gas:

$$CaO_{(s)} + SO_{2(g)} + \tfrac{1}{2}O_{2(g)} \rightarrow CaSO_{4(s)} \quad (2)$$

The atmosphere inside a preheater tower contains about 30 vol% CO_2 which means that carbonatization of CaO will take place below 820 ºC. Therefore, CaO particles carried from the calciner to the upper cyclone stages will only be partly calcined, since some CaO reacts with CO_2 in the flue gas. Thus carbonatization and sulfation will be competitive reactions.

Objectives

The goal of the Ph.d. project is to provide scientific knowledge of the formation and absorption of SO_2 in the preheater, and to use that knowledge to diminish the SO_2 from our present and future kiln system.

Experimental Procedure

The CaO used for reaction with SO_2/CO_2 was prepared from Faxe Bryozo limestone by calcination in a fluidized bed for 50 minutes at 850 ºC. The lime became only partly calcined which means that the product still contained some $CaCO_3$. Next the CaO was reacted with SO_2/CO_2 in an entrained flow reactor, where it is possible to inject SO_2/CO_2 at four different locations in order to vary the contact time between particles and gas. All gases are preheated in order to ensure isothermal conditions when the reactions take place. The experiments were carried out with an SO_2 concentration of 1000 ppm and with CO_2 concentrations of 0.03 vol% (atmospheric air), 10 vol% or 20 vol%. The temperature setpoints used were 500 and 600 ºC (in practice the temperature is about 15 ºC lower) and the feed rate into the reactor was 200 g/hr of partly calcined limestone particles.

Results

In figure 2 the Ca conversion, calculated as mol SO_2 absorbed per mol of Ca injected, is shown as function of the CO_2 content in the reaction atmosphere.

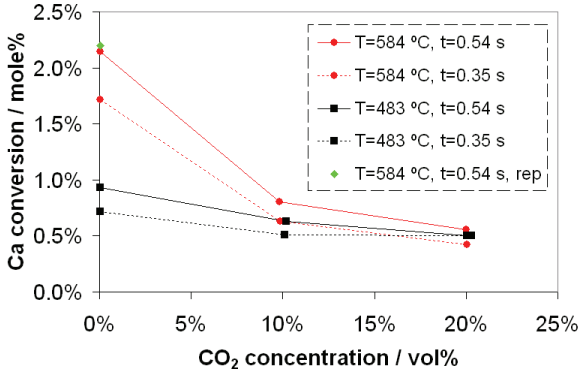

Figure 2: Ca conversion as function of CO_2 concentration at different temperatures and gas-solid contact time.

The figure shows that when no CO_2 is added to the gas, Ca conversion increases when the residence time increase and also increases with temperature as expected. It is also noticed (the point marked rep) that it is possible to reproduce data fairly well. On addition of 10 vol% CO_2 to the reaction atmosphere Ca conversion decreases significantly at the high reaction temperature while the decrease is less pronounced at the low temperature. A diminished influence of an increasing temperature is observed, while the effect of increasing the residence time seems to be unchanged. When adding 20 vol% CO_2 the decrease in Ca conversion levels off. At this CO_2 concentration increasing temperature has no effect on conversion at the longest gas-particle contact time. At the shortest residence time it even seems like the Ca conversion is smallest at the highest temperature, although this may not be significant.

Discussion and Conclusion

From the results presented here it is obvious that CO_2 have a negative effect on the reaction between CaO and SO_2 when the concentration of CO_2 is high and the temperature is lower than the equilibrium temperature of carbonatization. The reason is that CO_2 reacts with CaO and thereby inhibits the reaction between CaO and SO_2. At the same time the molar volume of the $CaCO_3$ formed is larger than the molar volume of CaO giving rise to a (partial) blockage of the small pores. This makes less CaO accessible for SO_2.

At higher CO_2 concentrations there is only a small to insignificant effect of increasing the temperature. Nearly the same conversion is observed at low and high temperatures. It also seems as if the conversion approaches an asymptotic level of about 0.5 mole% at high CO_2 concentrations. This behavior could be explained by a two site system, where the surface sites present in the partly calcined limestone can be divided into two types: one that reacts with both SO_2 and CO_2, and one that mainly reacts with SO_2. The sites that react with both SO_2 and CO_2 are easily inhibited by higher CO_2 concentrations and these sites' reactivity towards SO_2 is clearly affected by temperature. The second type of site reacts with SO_2 so fast that the gas-solid contact times used in these experiments are sufficiently large to give nearly complete conversion at both low and high temperatures.

The proposed two site mechanism is capable of explaining the results, but more research must be done in order to validate the specific mechanism.

However, even though addition of CO_2 significantly decreases the amount of SO_2 absorbed by the partly calcined lime (at the highest temperature the uptake is only 25 % of that observed with no CO_2), the uptake seen here at 584 ºC is still 10 times higher than that observed when using the non-calcined limestone under otherwise similar conditions [2]. Thus, small amounts of CaO that recirculates inside the preheater can still play an important role in abatement of SO_2 emissions from the top stage of the preheater tower.

Acknowledgements

This project is a part of a Research Platform on Future Cement Technology financed by Danish National Advanced Technology Foundation, FLSmidth A/S and DTU.

References

1. J.P. Hansen, SO_2 Emissions from Cement Production, Nørhaven Digital, Cph, Denmark, 2003.
2. G. Hu, Emission of SO_2 from Cement Production, DTU, Lyngby, Denmark, 2007.

Muhammad Riaz

Phone: +45 4525 2877
Fax: +45 4588 2258
E-mail: ria@kt.dtu.dk
WWW: http://www.cere.kt.dtu.dk
Supervisors: Georgios M. Kontogeorgis
Erling H. Stenby
Michael L. Michelsen

PhD Study
Started: April 2008
To be completed: July 2011

Distribution of Complex Chemicals in Oil-Water Systems

Abstract
Chemicals are added to the oil and gas value chain at different positions during the physical flow from well stream to traded product. A fraction of added chemical goes into oil and remaining is discharged to the sea via produced water. It is important to know accurately, how much of an added chemical will go to the water in order to report to the environmental authorities and how much of the chemical will go to the oil. This is becoming increasingly important for down stream processing. The objective of this project is to develop a predictive model for oil-water partition coefficients of complex chemicals, over a wide range of conditions and with minimum input of experimental information.

Introduction
As crude oil resources decrease, the oil industry demands sophisticated methods for the exploitation of natural resources. As a result, the use of oil field chemicals is becoming increasingly important [1,2]. These chemicals belong to families like alcohols, glycols, alkanolamines, ethers, imidazolium salts and polymers. They are added for various purposes such as gas hydrate inhibitors, corrosion and scale inhibitors defoamers, demulsifiers and drag reducers.

Over the last years, the use of chemicals has increased as shown in figure 1. Here the production chemicals used at Statoil operated fields is shown on annual basis.

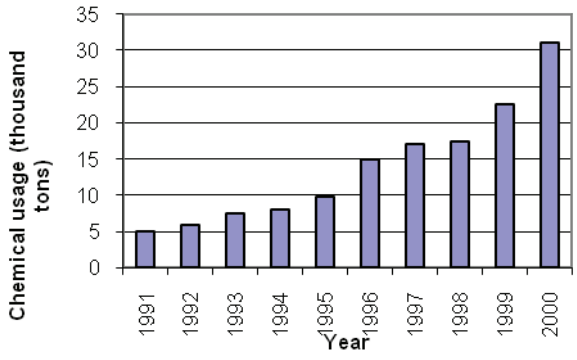

Figure 1: Trend in the use of production chemicals on Statoil operated fields [2].

In the past, calculation of oil-water partition coefficient (Koil) was based on octanol-water partition coefficient (Kow), but experiments have shown that oil-water partitioning does not always mimic well oil-water partitioning [1]. A well stream containing oil water and different chemicals is separated in a series of separators as shown in figure 2. These chemicals generally are added in such small quantities that direct detection by analysis is extremely difficult and in many cases impossible. It is therefore, of interest to establish a relationship between octanol-water and oil-water partition coefficients and modelling for oil-water partition coefficients to develop a predictive model.

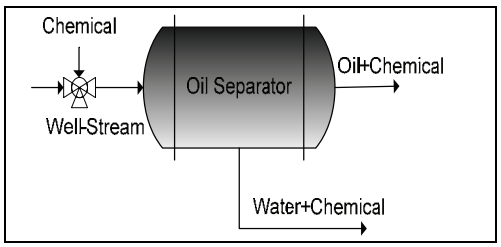

Figure 2: Addition and distribution of chemical in oil-water system

Oil-Water Partition Coefficient
The oil-water partition coefficient of a chemical *i* is the ratio of concentration of that chemical in the oil and

aqueous phases respectively. Concentration of a chemical can be measured and it can be represented in different units. When it is given in term of mole fraction, the partition coefficient can be expressed as illustrated in figure 3.

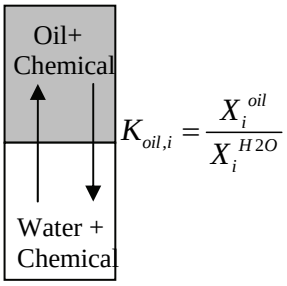

$$K_{oil,i} = \frac{X_i^{oil}}{X_i^{H2O}}$$

where

$K_{oil,i}$ = Oil water partition coefficient of chemical i

X_i^{oil} = mole fraction of chemical i in oil phase

X_i^{H2O} = mole fraction of chemical i in water phase

Figure 3: Oil-water equilibrium and definition of oil-water partition coefficient of a chemical

What is Oil?

Oil is a wider term with no specific general composition and usually mixture of thousands of hydrocarbon and other fractions like water, nitrogen etc. With existing chemical separation techniques we usually cannot identify the many hundreds or even thousands of components found in a reservoir fluid. Even if accurate separation were possible, the critical properties and equation of state (EoS) parameters of compounds heavier than C_{20} would not be known accurately. This problem can be solved by lumping, a number of heavier fractions into fewer fractions called oil characterization [3].

Thermodynamic Models

Cubic EoS such as Soave-Redlich-Kwong (SRK) and Peng-Robinson are the most widely used thermodynamic models for phase equilibrium calculations and physical property estimation in petroleum engineering. But in the presence of complex compounds such as water EoS do not perform very satisfactorily. To describe complex systems containing associating compounds, empirical/semi-empirical modifications of cubic EoS, or more rigorous EoS models explicitly accounting for association, are needed. The cubic plus association (CPA) EoS which is a combination of SRK and the Wertheim association term gives a better, more physical description of systems containing associating compounds compared with the empirical or semi-empirical modifications of cubic EoS. In addition, CPA has been successfully applied to water-light hydrocarbon systems and calculation of phase equilibrium between reservoir fluids, water, and methanol or monoethylene glycol [4].

Specific Objectives

The general research issues to be addressed are the following:

- To identify the most important chemicals of interest to Statoil applications, group them into families, collect experimental data of octanol-water (Kow) and oil-water (Koil) partition coefficient and investigate if correlations exist between them.
- To check different thermodynamic models and correlations against experimental values of Kow and Koil and select one to be used in the study, the model selected may be CPA or another SAFT-variant.
- Extension of CPA to reservoir and refinery fluids.
- To perform experiments for obtaining required phase equilibrium data, this will then be used in model development.
- To calculate octanol-water and oil-water partition coefficient of complex chemicals and evaluation of selected model.
- Possibly extend the study to ionic and polymeric materials.

Experimental Work

New experimental phase equilibrium data of binary MEG (monoethylene glycol)-reservoir fluids and ternary MEG-water-reservoir fluid at temperatures 2-53 ^oC and at atmospheric pressure is measured. Experimental work was carried out at Statoil Research and Development Center, Trondheim, Norway. The reservoir fluids used consist of two different gas condensates from Statoil operated gas fields in the North Sea. They are named as condensate 1 and condensate 2.

The experimental procedure consists of mixing of gas condensate, MEG and water in heating chamber at certain temperature. Mixed contents are then transferred to an equilibrium cylinder which contains holes and caps fitted with septum for sampling. At equilibrium, the contents of cylinder are splitted into two phases which are analyzed by gas-liquid chromatography, while the water content in the hydrocarbon phase is analyzed using Karl Fischer Coulometer as shown in figure 4. The direct analysis of both phases is not possible due to different limitations. Therefore hydrocarbons present in polar phase are extracted in carbon disulphide whereas MEG present in hydrocarbon phase is extracted in water.

Composition analysis for condensate 1 is given in table 1. Overall density and molecular weight of condensate are experimental whereas for individual components of hydrocarbon phase, simulated density and molecular weight are used.

Table 1: Composition analysis for condensate 1

Component	Mole %	Weight %	Molecular weight	Density kg/m³
Methane	0.000	0.000	16.04	300.0
Ethane	0.004	0.001	30.07	356.7
Propane	0.896	0.351	44.09	506.7
iso-Butane	2.382	1.229	58.12	562.1
n-Butane	7.813	4.031	58.12	583.1
Neopentane	0.046	0.030	72.15	597.0
iso-Pentane	5.456	3.494	72.15	623.3
n-Pentane	7.275	4.659	72.15	629.9
Hexanes, C6 total	**10.292**	**7.770**	**85.0**	**666.2**
n-Hexane	*4.705*	*3.599*	*86.2*	*662.7*
iso-Paraffins (C6)	*4.867*	*3.722*	*86.2*	*660.8*
Naphtenes (C6)	*0.720*	*0.448*	*70.1*	*748.1*
Heptanes, C7 total	**16.046**	**13.016**	**91.4**	**736.2**
n-Heptane	*3.273*	*2.911*	*100.2*	*686.9*
iso-Paraffins (C7)	*3.612*	*3.213*	*100.2*	*690.5*
Naphtenes (C7)	*7.601*	*5.811*	*86.1*	*768.1*
Aromatics (C7)	*1.559*	*1.081*	*78.1*	*883.1*
Octanes, C8 total	16.632	15.293	103.6	768.6
n-Octane	*2.167*	*2.197*	*114.2*	*707.0*
iso-Paraffins (C8)	*2.104*	*2.146*	*114.9*	*706.8*
Naphtenes (C8)	*8.715*	*7.968*	*103.0*	*771.1*
Aromatics (C8)	*3.646*	*2.982*	*92.1*	*872.0*
Nonanes, C9 total	**8.903**	**9.363**	**118.5**	**780.6**
n-Nonane	*1.664*	*1.894*	*128.3*	*723.0*
iso-Paraffins (C9)	*2.176*	*2.479*	*128.3*	*722.9*
Naphtenes (C9)	*1.889*	*1.999*	*119.2*	*794.4*
Aromatics (C9)	*3.174*	*2.991*	*106.2*	*872.1*
Decanes plus, C10+	**24.254**	**40.766**	**189.4**	**846.4**
Sum	100.000	100.000		
Mean molecular weight:			112.7	
Gas gravity:				756.2

Results for solubility of hydrocarbon in polar phase are given in table 2. The feed consists of 50% (mass) condensate and 50% polar phase. The polar phase consists of varying composition of monoethylene glycol (MEG) and water. The solubility results for hydrocarbon in polar phase are given in mass ppm (part per million). Results show that solubility of hydrocarbon contents decreses with decreasing MEG content in polar phase at given temperature and feed composition. The solubililty of of aromatic hydrocarbon is higher as comapred to nephthenic and parafinic. Such data is therefore, very important in gas processing plants as well as to follow the environmental regulations which permit the discharge of aromatic hydrocarbon in sea water upto a cerntain level. Data given in table 2 is ploted in figure 5.

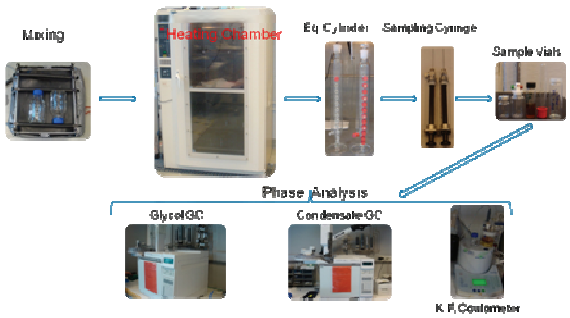

Figure 4: An overview of the experimental setup

Table 2: Solubility of condensate 1 in polar phase (MEG + water)

Comp. No.	Condensate 1 at 50 C Component Name	10% H2O 90% MEG	30% H2O 70% MEG	60% H2O 40% MEG
1	Propane	11.9	5.2	1.9
2	i-butane	34.6	11.7	4.0
3	n-butane	134.8	43.8	13.6
4	i-pentane	84.2	21.4	6.9
5	n-pentane	104.4	25.4	7.8
6	2,2-DM-butane	21.0	14.2	13.7
7	cy-Pentaen	39.7	9.7	1.9
8	2,3, DM-Butane	31.4	6.2	2.1
9	2-M-Pentane	0.0	0.0	0.0
10	3-M-Pentane	21.6	4.4	1.4
11	n-Hexane	50.3	8.9	2.7
12	M-cy-Pentane	85.9	20.0	3.3
13	2,2,3-TM-Butane	63.7	42.2	13.1
14	Benzene	631.0	280.9	82.6
15	cy-Hexane	143.0	34.6	5.8
16	2-M-Hexane	7.3	6.5	0.0
17	2-3-DM-C5	2.4	0.0	0.0
18	1,1-DM-cy-C5	3.6	0.0	0.0
19	3-M-C6	9.9	0.0	0.0
20	cis-1,3-DM-cy-C5	7.8	0.0	0.0
21	trans-1,3-DM-cy-C5	7.0	0.0	0.0
22	trans-1,2-DM-cy-C5	13.6	0.0	0.0
23	n-Heptane	22.6	0.0	0.0
24	M-cy-C6+cis-1,2-DM-cy-C5	123.4	23.6	0.0
25	Toluene+2,3,3,TM-C5	874.0	306.9	62.9
26	cis-1,3-DM-cy-C6	0.0	0.0	0.0
27	trans-1,2-DM-cy-C6	0.0	0.0	0.0
28	unidentified C9	0.0	0.0	0.0
29	Ethylbenzen	64.0	15.8	2.2
30	m-Xylene	209.8	58.1	9.0
31	p-Xylene	62.3	15.7	3.0
32	o-Xylene	97.2	27.7	0.0
33	C10	108.9	0.0	0.0
34	C12	36.0	0.0	0.0
35	C13	51.9	0.0	0.0
	Total	**3159.2**	**982.8**	**237.9**

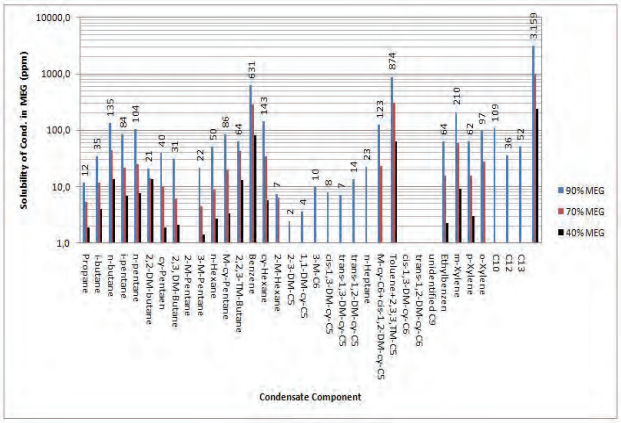

Figure 5: Solubility of hydrocarbon in polar phase at 50 ^{o}C and 1 atm.

Solubility of MEG and water in organic phase is also measured and is given in table 3 along with solubility of hydrocarbon in polar phase. The compositions in table 3 are given in mass fraction. Similar measurements are carried out for condensate 2 which contains both binary (MEG + Condenste) and ternary (MEG + Condenste + H2O) measurements.

Table 3: Ternary LLE data for MEG H2O and Condensate 1

Temp.	Feed			Polar Phase			Organic Phase		
(C)	MEG	Water	Cond.	MEG	Water	Cond.	MEG	Water	Cond.
50 C	X1	X2	X3	100X1	100X2	100X3	100X1	100X2	100X3
90% MEG	0.446912	0.049585	0.503502382	90	10	0.3159	0.020989	0.0064334	99.972577
70% MEG	0.344378	0.14745	0.508172363	70	30	0.0983	0.009468	0.0148715	99.975660
40% MEG	0.201137	0.297577	0.501285948	30	70	0.0238	0.003366	0.0194944	99.977140

Conclusions

A literature study has been carried out and investigation of correlations of Koil and Kow was also made. A preliminary calculation of Koil using CPA model was also made and compared with Statoil experimental data. After performing these tasks we have concluded.

1. Oil characterization is a useful tool to make phase equilibrium calculations of complex reservoir fluids
2. There is a real need for experimental Koil data and without it, correlation between Koil and Kow is not possible. Only very few Koil data sets were found in literature.
3. CPA has the capability to model complex associating fluids.

Future Work

1. Compare experimental data of Koil from Statoil to data from other sources for both reservoir fluid-water-chemical and well defined oil (alkane)-water-chemical system.
2. Investigate the effect of interaction parameter of model and characterization method on performance of CPA
3. Modeling of solubility of MEG-H2O and condensate using CPA with suitable characterization method.

Acknowledgements

We are grateful to StatoilHydro Norway, for funding the project.

References

1. N. Ass, B. Knudsen, J. O. Sæten, E. Nordstad., Society of Petroleum Engineering International 2002(SPE No. 74083)
2. J. Fink, GP Press, 2003, p. ix
3. K. S. Pedersen, P. S. Pedersen, Taylor Francis, 2007, p.81
4. W. Yan, G. M. Kontogeorgis, E. H. Stenby, SPE International, 2007(SPE No. 110009-PP

Alicia Roman-Martinez

Phone: +45 4525 2910
Fax: +45 4593 2906
E-mail: arm@kt.dtu.dk
WWW: http://capec.kt.dtu.dk
Supervisors: Rafiqul Gani
John M.Woodley

PhD Study
Started: August 2008
To be completed: July 2011

Design of Integrated Chemo-enzymatic Processes

Abstract
This project is about developing a general model-based framework for design and development of intengrated biochemical processes in their parts. The framework is made to be applied for processes that consist of the production of chemicals of low molecular weight made mainly by the enzymatic route in a maximum of two reaction steps. Hence, the framework is generic and provides the advantages of considering all possible feasible options in a process and reducing experimental efforts since the optimal feasible intensified option obtained from using this framework is subjected to experiments for final validation. The application of the framework is highlighted here through the case study of synthesis of N-Acetylneuraminic Acid since is an important intermediate pharmaceutical used for antiviral and anticancer purposes and the current processes present considerable drawbacks. Having as result the optimal process configuration is the one who uses a purification step of the intermediate product (N-Acetylanosamine Acid) and downstream processing by crystallization of the product with acetic acid to achieve the maximum product yield.

Introduction
The use of biocatalytic process technologies as a complement to conventional chemical synthesis has attracted particular attention in recent years since new options for sustainable and environmentally benign processes can be established. Biocatalysis offers numerous advantages for achieving 'green' chemistry, such as high yield, high selectivity under ambient temperature and pressure, in an aqueous environment. Through the avoidance of high temperatures and pressures, and large consumption of metals and organic solvents, the generation of mass and energy waste per unit of product is drastically reduced (Woodley, 2008). However, this kind of bioprocesses present several issues, like the unfavorable equilibrium and the product inhibition in the biotransformations, as well as the difficult downstream processing, which can be overcome by using the approaches of bioprocess intensification of one-pot synthesis and *in situ* product removal (ISPR). Also, the implementation of an industrial-scale bioprocess usually takes considerable time for development which can be reduced by using process synthesis techniques together with a systematic framework to intensify this kind of process. This work provides a general framework that combines the alternatives of bioprocess intensification together with a model-based methodology that can help the designer to find the optimal process option according to defined criteria like maximizing the yield or reducing the processing time and/or costs. This framework has the advantage of being of general applicability to different biotransformation systems.

Objective
In this project, the general objective is to develop and apply a systematic model-based generic methodology for design and development of intensified bio-chemical processes, considering all process options to select an optimal that provides a step change in productivity and/or reduction of processing time and/or costs.

The methodology uses model-based strategies for hybrid bio-chemical process design, like the use of a superstructure and a generic model, supported by computer -aided simulations and combined with *a priori* knowledge of data and constraints of the process defining the windows of operations to generate and evaluate all the possible synthesis routes including the options with ISPR and one-pot synthesis procedures to find and optimal bioprocess. Modeling is oriented at the optimization task to be solved and considers all the knowledge available about the biocatalytic system used.

Mathematical Formulation of the Optimization Problem

Since the objective for the general model-based framework is to find the optimal reaction(s) and separation(s) configuration, the basis is to have a mathematical formulation of the optimization problem.

The goal is to optimize the defined performance criteria (defined by an objective function) subject to a set of optimization variables (set of design, decision variables, parameters, etc.) and a set of constraint functions, which include process model, logical constraints, structural-operational constraints, etc. The problem is solved when the values of the optimization variables that satisfy the objective function and the constraints are found.

The mathematical formulation of the problem is given as:

Minimize (or maximize):

$$Z = \sum_{m=1}^{NF} f(Y_j^k, F_i^k, x, d, \vartheta) G_m \quad (1)$$

Subject to:

$$Y_j^k, F_i^k, x, d, \theta, G_m$$

and

$$\sum_{j=1}^{NK} Y_j^k \leq 1 \quad k = 1,2,3,\dots,k \quad j = 1,2,3,\dots,j \quad (2)$$

$$h_p(x, F_i^k, d, \theta) = 0 \quad (3)$$

$$g_1(Y_j^k, F_i^k, x, d, \theta) = 0 \quad (4)$$

$$g_2(Y_j^k, F_i^k, x, d, \theta) \leq 0 \quad (5)$$

Where equation (1) is the objective function, which is function of the binary variables Y_j^k, that can take the values of 0 or 1, and represents the existence of an option $j$in a different processing step k, F_i^k is the flow rate of compound i in a different processing step k, x represents other process variables, d are equipment parameters, θ represents specified process-product variables and $G_m$is a binary variable which indicates the different criteria for optimization (like product yield, enzyme load, etc.)

Equation (2) represents the logical constraints which represent the logical sequence of allowed operations in the processing steps, this leads to a generation of different flow sheet options. Equation (3) represents the process model which consists in the differential (balance) equations of mass and energy and constitutive equations. Equations (4) and (5) represent other interrelationships of the optimization variables (for example, allowed flow rates for selected processing routes). The solution of the problem is to find the values of the optimization variables that satisfy all the constraints and minimize (or maximize) the objective function. So, the general objective in optimization is to choose a set of values of the variables subject to the various constraints that produce the desired optimum response for the chosen objective function.

All the equations, (1) to (5), can be solved all together if the problem is of low complexity. In many cases, the problem is to complex that the solution has to be obtained by decomposition, this is, breaking the problem formulation up into manageable parts (sub-problems). These parts are shown in the steps of the methodology shown in figure 1.

Methodology

The solution technique of the optimization problem is reflected in a systematic methodology for design and development of intensified biochemical processes presented in Figure 1.

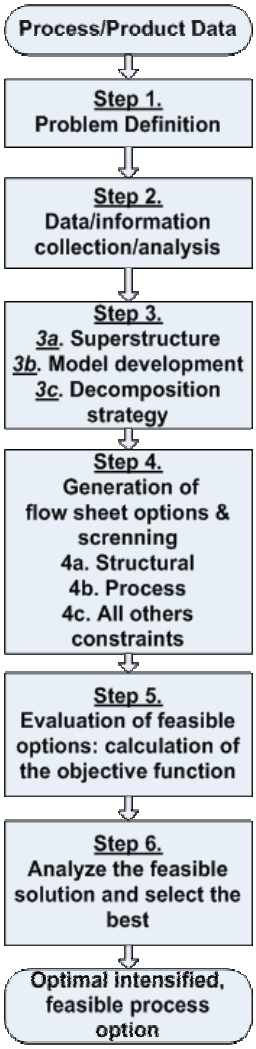

Figure 1: Systematic methodology for design and development of intensified biochemical processes

In Step 1 (Problem definition), an analysis of the process is done so that the process variables and specific characteristics of interest are defined, like the bottlenecks and difficulties of the process, to determine the criterion for intensification/optimization, and specify the objective function in terms of the defined variables at the beginning together. This step provides the performance model.

In Step 2 (Data/information collection and analysis) all data with respect to the variables and scenario defined at the first step is collected and analyzed. Examples of data are enzyme activities, charges, solubility, kinetic constants, etc. The reported process/equipment options from knowledge-base are collected together with the information related to the different limitations that must be overcome.

In Step 3 (Model development and validation) a valid process model that relates the input-output variables of the process is developed. Because process intensification creates an enormous number of process options, a generic model is developed. The generic model represents the mass an energy balances derived from a superstructure in which all the possible synthesis routes can be derived.

In Step 4 (Generation of flow sheet options and screening), we use the superstructure and equation (2) of the problem formulation to generate the options connecting all the process/equipment tasks collected from the literature in step 2. For each process task several choices are available. For example, for the separation step we can have crystallization, chromatography, liquid-liquid extraction, adsorption, etc. The screening can be done in three parts, first for structural constraints (equation (2), Step 4a) second by process constraints (equation (3), Step 4b), followed by other constraints (equations (4) and (5), Step 4c). The screening leads to a reduced number of options.

In Step 5, calculation of equation (1) is done for the reduced number of options in step 4. This will lead to an optimal option that needs to be validated by experiments to finally obtain an optimal, intensified feasible process option (Step 6).

Superstructure

A superstructure representing all intensified bioprocess options (Figure 2) has been developed. A generic model has been derived from this superstructure consisting of mass and energy balance equations and connection equations. From this generic model different specific process\operation sub-models are generated from the identified options for the subsequent screening steps. Process options based on unreliable models are removed.

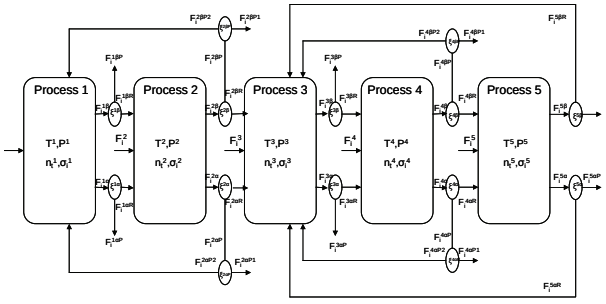

Figure 2: Superstructure for the integration of reaction with reaction/separation for bio-based processes.(Symbols: streams F [mol], temperature T [K], pressure P [bar], molar hold up's n [mol], separation factors σ [-], binary existence variable ξ [0,1]; Subscripts: Bottom flow α, top flow β, product P)

Case study: synthesis of N-Acetylneuraminic acid (Neu5Ac)

The methodology is highlighted through the production of Neu5Ac. The synthesis of Neu5Ac, an important pharmaceutical intermediate due to its anti-viral, anti-cancer and anti-inflammatory effect, is attracting growing attention due to increased need for this compound in the pharmaceutical industry. In spite of this growing need there has been almost no advancement of the synthesis routes during recent years, although a number of problems like, unfavorable equilibrium, high amount of waste per kilogram of product and difficult downstream processing are encountered (Zimmermann, 2007).

The chemical reactions for Neu5Ac synthesis are presented in Figure 3.

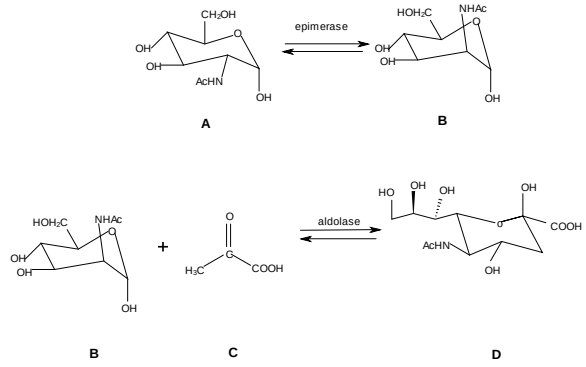

Figure 3: Synthesis of Neu5Ac from GlcNAc in two reaction steps;A: N-acetyl-D-glucosamine (GlcNAc); B: N-acetyl-D-manosamine (ManNAc); C: pyruvic acid (Pyr); D: N-acetylneuraminic acid (Neu5Ac); Epi: N-acylglucosamine-2-epimerase and Ald: N-acetylneuraminic acid aldolase

Starting from the methodology, in the first step the problem is defined .The objective function is set to maximize the product yield, defined as:

$$yield = \frac{n_{product,end} - n_{product,0}}{n_{substrate,0}} \quad (6)$$

In the second step, all data with respect to the process scenario, such as, enzyme properties, solubilities, charges, properties with respect to inhibition of the enzyme, are collected. The known limitations of the process are identified to be an unfavorable equilibrium, high amounts of waste per kilogram of product and difficult downstream processing. Searching the knowledge base for possible solutions indicated that, for these limitations, two possible strategies could be considered: the integration of both reaction steps in a single pot reactor and the integration of reaction/separation (in situ product removal, ISPR). Hence, all obtained data, the objective function and constraints defined in step 1 are delivered to the second step of the methodology.

Following the workflow of the methodology, the reported process options from knowledge-base are collected together with information related to the

different limitations that must be overcome. In step 3, the generic model is developed, represented by the superstructure in Figure 2, and validated based on experimental data for the one pot synthesis with a relative deviation in the product yield of less than 5%. In step 4, the options for the synthesis route are generated connecting all reported process equipment/tasks collected from the literature in step 2. For each process task several choices are available. For example, the number of process steps can vary according to the superstructure in Figure 2 between 5 process units (e.g. epimerization reaction, ManNAc enrichment, aldolase reaction, pyruvate treatment and downstream processing) and 2 process units (e.g. one-pot synthesis followed by downstream processing), In total 622 options are generated. The generated options are stepwise screened with respect to structural constraints and operational constraints based on the defined performance metrics. The result of the screening is presented in table 1. In this way, the number of feasible process options has now been reduced to 10.

Table 1. Results of the stepwise screening through a set of constraints

Constraint/ Metric	Number of redundant options	Example
Waste	104	Use of two different solvents for base catalysed epimerization
Energy	103	High energy use for evaporation for ManNAc enrichment
Efficiency	311	Enzyme in solution
Maturity	30	Difficult reported operation for whole-cell biotransformation
Operational cost	52	Chromatography discarded
Flexibility	12	Enzyme in solution

All remaining options are screened for process constraints based on their performance in step 4, through simulation with the generated models. The simulation results of two promising options, compared to an existing (conventional) configuration, are presented in Table 2.

Table 2. Simulation results of step 5 of the specific methodology. Conditions: Initial concentration of substrates: GlcNAc: 1.3 M, Pyr: 1.0 M. Enzyme concentrations: 12000 U/l for epimerase and aldolase. T=25^{o}C, pH=7.5

Process	Scenario	Process time [h]	Efficiency [%]	Number of processing units
Conventional	Epimerization+Aldolase Reaction Crystallization	10.45	37.8%	3
Intensified 1	Epimerization+ManNAc enrichment+Aldolase reaction+Crystallization	12.982	81.1	4
Intensified 2	One-pot synthesis ISPR by crystallization	8.27	75.7	2

In the next step 5, the most promising option is further optimized with respect to the objective function and process variables such as the enzyme concentration. At this point, all other performance and structural process option variables such as binary decision variables have already been fixed. Hence, only the process "Intensified 1" has been optimized by adjusting the enzyme loading at fixed temperature and pH as well as equimolar reactant concentration. The result is shown in figure 4, indicating that the most efficient process can be found at the upper bound of loading for both enzymes.

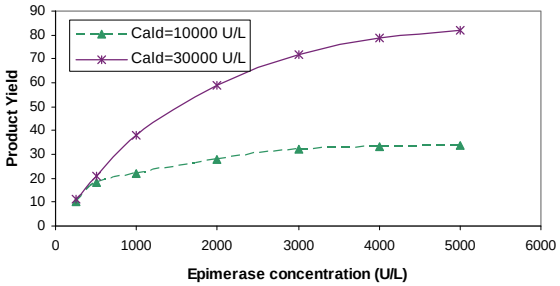

Figure 4: Product yield with respect to enzyme concentration; Initial concentration of substrates: GlcNAc: 1.0 M, Pyr: 1.0 M., T=25oC, pH=7.5

Conclusion

It has been shown that the methodology presented here has the potential to improve bio-based processes. The methodology provides the mean to generate, evaluate and identify intensified options, from which the optimal can be found. Hence, it is possible to manage the complexity associated with finding the optimal intensified process. The methodology has been successfully applied to a relevant case study involving a typical product from the pharma-sector.

References

1. Woodley J.M., (2008), Trends in Biotechnology, 26, 6, 321-327.
2. Zimmermann V., Hennemann H., Dauβmann T., Kragl U., (2007), Applied Microbiology and Biotechnology, 76, 597-605.

Oscar Andrés Prado Rubio
Phone: +45 4525 2801
Fax: +45 4593 2906
E-mail: oap@kt.dtu.dk
WWW: http://www.kt.dtu.dk
Supervisors: Gunnar Eigil Jonsson
Sten Bay Jørgensen

PhD Study
Started: June 2007
To be completed: May 2010

Bioreactor Modeling with an *in situ* Lactate Recovery through REED

Abstract
The present contribution is part of our efforts modeling a novel process for lactic acid production, where the fermentation and product removal are tightly integrated. The lactic acid production is intensified by the continuous lactate removal and the recycling of biomass and unconsumed substrate. An unstructured kinetic model is proposed to describe the lactate inhibition. The structure of the model is investigated and compared to a model previously proposed in the literature. The kinetic model parameters are regressed using experimental data available in literature. The model performance is validated on independent data. A degree of freedom analysis is performed for the individual system units as well as for the integrated system to reveal the handles for operational design.

Introduction
Previously, a dynamic model was derived to describe simultaneous ion transport across anion exchange membranes in a dialysis cell. Investigations were performed for operation without imposing current density, operation applying an external potential gradient and operation under current reversal conditions. These operation scenarios are referred to as Donnan Dialysis (DD), Electro-Enhanced Dialysis (EDD) and Reverse Electro-Enhanced Dialysis (REED) (Prado-Rubio e*t al*., 2009a, 2009b). The present contribution is focused on modeling lactic acid fermentation suitable for integration with the previously derived REED model. This type of intensified process can be used for a variety of applications in biotechnology, where the fermentation production rate is limited by ionic species. It is well know that lactic acid fermentation is impaired by product inhibition (Luedeking and Piret, 1959, Nielsen et al., 2003). Therefore, the production can be enhanced by the continuous removal of the biotoxic carboxylic anions from the cultivation broth and the recycling of biomass and unconsumed substrate. A sketch of the integrated fermenter and REED module is depicted in figure 1.
In order to further understand the interaction between the REED module and the bioreactor it is desirable to develop a dynamic model for the fermentation. This model should describe the lactate production rate as a function of key variables such as substrate, biomass and product concentrations. The paper is structured as follows: lactic acid fermentation is introduced and the kinetic model characteristics are described. Subsequently, the proposed kinetic model is depicted and the batch fermentation model is presented. Afterwards, the structure of the kinetic model is investigated and the relation with the original model from the literature is elucidated. The parameters in the developed model are regressed and validated. Finally, the operational design of the integrated bioreactor and REED module is discussed based upon a degree of freedom analysis of the model.

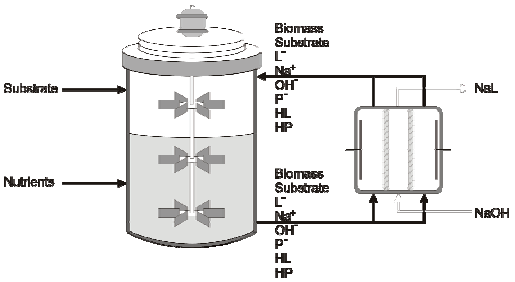

Figure 1: Sketch of the integrated bioreactor with the REED module for a batch/fed-batch fermentation

Bioreactor modeling
Lately, the tendency in bio-systems modeling is to exploit the increasing fond of knowledge of intracellular metabolism, and then substitute heuristic-based models by mechanistic representations of the cell behavior. As a consequence, the predictive power of the models is augmented. The complexity of the metabolism of a cell lies in the hundreds of reactions subject to regulatory

mechanisms. However the cellular control systems are not yet well understood, therefore it is necessary to employ different assumptions and modeling approaches according to the specific model purpose. Traditionally, fermentation processes have been modeled employing unstructured biomass models. The model parameters are estimated from measurements of extracellular metabolites and biomass concentrations. Even though these models do not provide insight into cellular physiology and thus their predictive power is limited, they have been widely used in engineering since they provide a simple representation of cell growth (Nielsen *et al*., 2003).

Kinetic model development

The kinetics is the core of a fermenter model. An appropriate description of the microorganism growth is vital for the bioprocess design. A variety of unstructured models have been applied, those models account the growth dependency on substrate concentration and product inhibition. The substrate concentration influence on the growth rate is usually modeled using Monod based kinetics, i.e. where the growth is inhibited at some concentration of the rate limiting substrate. The point where substrate inhibition occurs is very important, especially in batch cultivations. For the product inhibition, different types of linear and non linear functions have been investigated. A linear inhibition term has shown to be useful in several applications (Nielsen *et al*., 2003, Boonmee *et al*, 2003). However, for other cases the functionality of the product inhibition term is highly non linear, mainly exponential (Cachon and Divès, 1993, Amrane and Prigent, 1994, Åkerberg *et al*, 1998, Burgos-Rubio *et al*, 2000).

The growth kinetic that we are proposing for the prokaryote is based on the Luedeking-Piret model with inhibition proposed by Boonmee *et al*. (2003). The original growth model includes a linear product inhibition term and substrate inhibition at high concentrations. The substrate influence on the growth rate is modeled using a modified Monod expression, completely comparable to Haldane equation. Besides, lactate inhibition is considered to work within a concentration band. It means, there is a minimum lactate concentration (P_i) which is required to initiate the inhibition. On the other hand, there is a maximum lactate concentration (P_m) which provokes complete inhibition. Different values of P_i and P_m for growth and lactate production/lactose consumption were found by Boonmee *et al*, 2003.

Our contribution lies in the lactate inhibition functionality. The basic concept is preserved for the inhibition term, but the function describing it is substituted by a normalized Boltzmann two parameter sigmoid function. Boltzmann sigmoid functions are interesting since they are continuous and monotonically increasing/decreasing between 2 defined boundaries, therefore they have smooth derivatives. These characteristics make them useful in neural networks training and gradient based calculations (Baughman and Liu, 1995, Rutledge and Steward, 2008). The proposed growth model is:

$$q_x = \mu_{\max}\left(\frac{S}{K_{sx}+S}\right)\left(\frac{K_{ix}}{K_{ix}+S}\right)\left(1-\frac{1}{1+\exp\left(\frac{P_{½x}-P}{k}\right)}\right)X \quad (1)$$

Analogously, the substrate uptake is:

$$q_s = -q_{s,\max}\left(\frac{S}{K_{ss}+S}\right)\left(\frac{K_{is}}{K_{is}+S}\right)\left(1-\frac{1}{1+\exp\left(\frac{P_{½s}-P}{k}\right)}\right)X \quad (2)$$

The lactate production rate is given by the Luedeking-Piret model. When the product inhibition is low, the dominant lactic acid production rate has shown to be growth associated. However, at high lactate concentrations it follows a non growth associated pattern (Luedeking and Piret, 1959).

$$q_p = \alpha q_x + q_{p,\max}\left(\frac{S}{K_{sp}+S}\right)\left(\frac{K_{ip}}{K_{ip}+S}\right)\left(1-\frac{1}{1+\exp\left(\frac{P_{½p}-P}{k}\right)}\right)X \quad (3)$$

Based on Boonmee's *et al*. (2003) assumptions, the number of parameters in this model is slightly reduced. It is assumed that $K_{ss}= K_{sp}$, $K_{is}= K_{ip}$, $P_{½s}= P_{½p}$ and k is constant. This means that substrate uptake and lactate production are affected in the same way by substrate and product concentrations. The number of parameters to be regressed was reduced from 14 to 11. In the proposed model there is one parameter less than the original model. There is still one assumption which is questionable, the so called no biomass viability loss. A discussion on this issue is addressed in the results and discussion section.

Fermenter model

The main assumptions in the model development are:

FA1. The growth is influenced by carbon source limitation and lactate inhibition.

FA2. There is only one carbon source.

FA3. The cultivation broth contains the main carbon source. Phosphate, nitrogen source, salts and vitamins are assumed available.

FA4. The fermentation is considered homofermentative with lactate as product.

FA5. The modeled species are: biomass, carbon source and lactate.

Results and Discussion

Product inhibition term development

The motivation to propose the new kinetic functionality lies in how the no biomass viability loss assumption is handled in the original model. The assumption states

that when the maximum growth inhibiting lactate concentration (P_{mx}) is reached, the biomass concentration remains constant with no viability loss or cell lysis. The original growth model, as presented by Boonmee *et al*. (2003), is:

$$q_x = \mu_{\max}\left(\frac{S}{K_{sx}+S}\right)\left(\frac{K_{ix}}{K_{ix}+S}\right)\left(1-\frac{P-P_{ix}}{P_{mx}-P_{ix}}\right)X \quad (4)$$

It can be seen that when the product concentration is higher than P_{mx} the product inhibition term becomes negative. From a mathematical point of view, it means that the growth rate is negative. In other words, the model predicts biomass death. This contradicts the initial assumption of no viability loss. Another inconsistency is evident when the product concentration is lower than P_{ix}, since the product inhibition term in eq. (4) then is larger than 1. Under that condition, the model predicts that the biomass growth is enhanced by the presence of the product. That scenario should be supported by experimental evidence. In order to avoid the above listed situations, the growth must be saturated. It can be done using constraints in the product inhibition term, i.e. it must be between zero and one. However, simple saturation of the inhibition term is a potential problem for gradient based calculations, such as the parameter estimation procedure. For that reason, the normalized Boltzmann two parameter sigmoid function is very attractive. That function saturates between 2 defined boundaries and has smooth derivatives. When the function constraints are known, the number of parameters in the inhibition term are $P_{½}$ and k, as can be seen in equation (1). Where, $P_{½}$ is the inflexion point of the function and k is related to the slope at the inflexion point.

When an alternative black box function is proposed, the most important is to find the meaning of the model parameters. Using the parameters estimated by Boonmee *et al*. (2003), the Boltzmann function parameters were regressed. The results are depicted in figure 2.

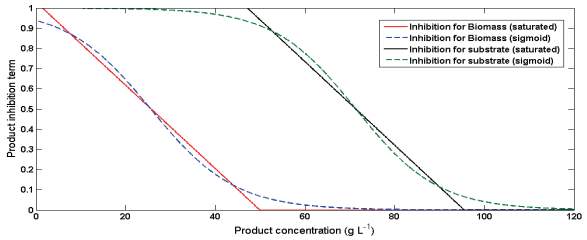

Figure 2: Saturated product inhibition term (solid lines) according to Boonmee *et al*. (2003) and the regressed Boltzmann sigmoid functions (dashed lines), for biomass and lactose/lactate inhibition.

It was found that the inflexion point of the Boltzmann function ($P_{½}$) can be considered as the average value between P_i and P_m for both biomass and lactate kinetics. Additionally, $-k$ is one fourth of the product inhibition term derivative evaluated at the inflexion point. The results also indicate that the differences between the slopes in the rate expression are small.

For that reason, k was considered to be constant in the three reaction rates. From the performed investigation, it is concluded that $P_{½}$ and k satisfactorily describe the location of the inhibition band.

Fermenter model regression

Boonmee *et al*, (2003) performed a series of batch and continuous fermentations using *Lactococcus lactis* NZ133. The cultivations were carried out in a 1l Quickfit fermenter with 400 ml working volume. The experiments took place at 30°C. The pH was controlled at 6.5 by adding 5M NaOH. The series of batch and continuous fermentations used a modified M17 medium with 20, 40, 60, 80 and 100 g/l of initial lactose. The data sets available were divided into two groups. The first is used for parameter estimation and the second for model validation. The data sets used for model regression are the ones containing 60 and 100 g/l of initial lactose and the continuous fermentations. The methodology used for parameter estimation is a numerical method for large scale optimization, this algorithm is a subspace trust region method based on the interior reflective Newton method for non linear minimization subject to bounds (Coleman and Li, 1994). The objective function to minimize is the sum of the squared residuals. The calculations are performed in MATLAB.

An identifiability analysis is emploied to reduce the parameter space search, thereby significately reducing the parameter correlations. As a result, the entire set of model parameters is identifiable using the above mentioned experimental data from both continuous and batch operation. The model fit to the experimental data is depicted in figure 3, corresponding to the model regression. Despite the satisfactory estimation results, it should be noticed that the parameter estimation procedure is quite sensitive to the initial parameter guesses. The estimated parameter values are: $\mu_{\max}$=1.1882 h^{-1}, K_{sx}=6.135 g/l, K_{ix}=300.0105 g/l, $P_{½x}$= 24 g/l, k= 7.8875 g/l, $q_{s,max}$= 6.3717 g/(g·h), K_{ss}= 4.6069 g/l, K_{is}= 145.1781 g/l, $P_{½s}$ = 64.4049 g/l, $q_{p,max}$=4.4563 g/(g·h) and α=2.1613 g/g.

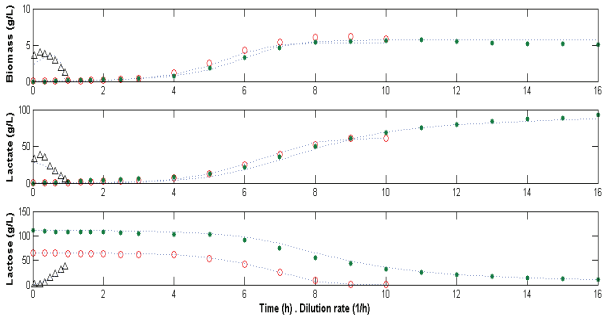

Figure 3: Experimental data for batch and steady state continuous fermentation (points) and regressed model (dashed lines). (○) 60 g/l lactose, (♦) 100 g/l lactose and (Δ) 40 g/l lactose - continuous.

Fermenter model validation

Using the estimated parameters, the model is validated against the remaining data sets. The predictions are shown in figure 4.

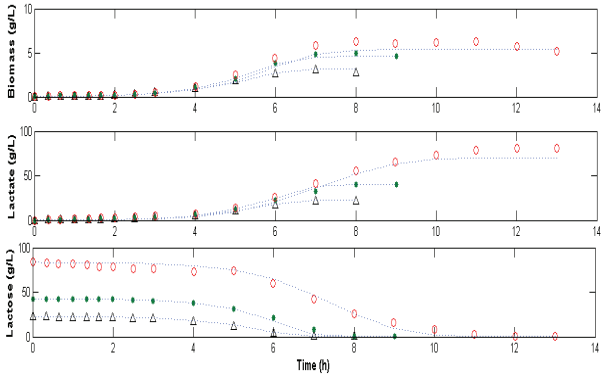

Figure 4: Experimental data for batch fermentation (points) and model validation (dashed lines). (○) 80 g/l lactose and (♦) 40 g/l lactose and (Δ) 20 g/l lactose.

Bioreactor and REED models integration

The degree of freedom (DOF) analysis is a general methodology used to identify the number of variables to be specified such that the system can be solved. A DOF analysis was performed for the REED module and the fermenter separately, and for the integrated system. In this analysis it is considered that the initial conditions, kinetic model parameters and equipment design are defined. The variables (DOFs) that must be specified have been identified. Some of these DOFs can be used as possible manipulated variables in order to achieve a desired operational goal. The remaining degrees of freedom are considered as disturbances. The introduction of a control law modifies the degrees of freedom since the controller relates the target state and the manipulated actuator variable by an additional equation, therefore the degrees of freedom are shifted to the sets points at the controllers.

Nomenclature

C_i	Concentration *S*, *X*, *P* (g L^{-1})
k	Inhibition term constant (g L^{-1})
K_i	Product inhibition constant (g L^{-1})
K_s	Substrate inhibition constant (g L^{-1})
P	Product concentration (g L^{-1})
$P_{½}$	Average product concentration in the threshold (g L^{-1})
P_i	Minimum lactate inhibiting concentration (g L^{-1})
P_m	Maximum lactate inhibiting concentration (g L^{-1})
q_i	Reaction rate of *i* (g L^{-1} h^{-1})
$q_{p,max}$	Maximum specific lactate production rate (g g^{-1} L^{-1})
$q_{s,max}$	Maximum specific lactose consumption rate (g g^{-1} L^{-1})
S	Substrate concentration (g L^{-1})
X	Biomass concentration (g L^{-1})
Greek symbols	
α	Growth associated constant (g g^{-1})
μ_{max}	Maximum specific growth rate (h^{-1})

References

Amrane, A. and Prigent, Y. (1994). Mathematical Model for Lactic Acid Production from Lactose in Batch Culture: Model Development and Simulation. *J. Chem. Tech. Biotechnol.* 60, 241-246.

Baughman, D.R. and Liu, Y.A. (1995). Neural Networks in Bioprocessing and Chemical Engineering. Academic Press.

Boonmee, M.; Leksawasdi, N.; Bridge, W. and Rogers, P. (2003). Batch and Continuous Culture of *Lactococcus lactis* NZ133: Experimental Data and Model Development. *Biochemical Engineering Journal*, 14, 127-135.

Burgos-Rubio, C.N., Okos, M.R., Wankat, P. C. (2000). Kinetic Study of the Conversion of Different substrates to Lactic Acid Using *Lactobacillus bulgaricus*. *Biotechnology progress*, 16, 305-314.

Cachon, R. and Divès, C. (1993) Modeling of Growth and Lactate Fermentation by *Lactococcus lactis* subsp. *lactis* biovar. *Diacetylactis* in Batch culture. *Appl. Microbiol. Biotechnol.*, 40, 28-33.

Coleman, T. and Li, Y. (1994). On the Convergence of Interior-Reflective Newton Methods for Nonlinear Minimization Subject to Bounds. *Mathematical Programming*, 67, 189–224.

Hongo, M.; Nomura, Y. and Iwahara, M. (1986). Novel Method of Lactic Acid Production by Electrodialysis Fermentation. *Applied and Environmental Microbiology*, 52(2), 314–319.

Luedeking, R. and Piret, E.L. (1959). A Kinetic Study of the Lactic Acid Fermentation. Batch Process at Controlled pH. *J. Biochem. Microbiol. Technolog. Eng.* 1(4), 431-459.

Prado-Rubio, O.A.; Jørgensen, S.B and Jonsson, G. (2009a). Lactic Acid Recovery in Electro-Enhanced Dialysis: Modelling and Validation. In Jeżowski, J. and Thullie, J., editors, 19th European Symposium on Computer Aided Process Engineering, volume 26, pages 773–779. Elsevier.

Prado-Rubio, O.A.; Jørgensen, S.B and Jonsson, G. (2009b). Tool for Optimizing the Design and Operation of Reverse Electro-Enhanced Dialysis of Monoprotic Carboxylic Acids. In Alves, B.; Nascimento, O. and Biscala, J., editors, 10th International Symposium on Process System Engineering. Volume 27, pages 663-668. Elsevier.

Rutledge, R. and Steward, D. (2008). A Kinetic-Based Sigmoidal Model for the Polymerase Chain Reaction and Its Application to High-Capacity Absolute Quantitative Real-Time PCR. *BMC Biotechnology*, 8, paper number 47.

Åkerberg, C., Hofvendahl, K. Zacchi, G., and Hahn-Hägerdal. (1998). Modelling the Influence of pH, Temperature, Glucose and Lactic Acid Concentrations on the Kinetics of Lactic Acid Production by *Lactococcus lactis* ssp. *Lactis* ATCC 19435 in Whole Wheat Flour. *Appl. Microbiol. Biothenol*, 49, 682-690.

List of publications

Contributions during the previous year:

Prado-Rubio, O.A.; Jørgensen, S.B and Jonsson, G. Lactic Acid Recovery in Electro-Enhanced Dialysis: Modelling and Validation. In Jeżowski, J. and Thullie, J., editors, 19th European Symposium on Computer Aided Process Engineering, volume 26, pages 773–779. Elsevier. 2009.

Prado-Rubio, O.A.; Jørgensen, S.B and Jonsson, G. (2009b). Tool for Optimizing the Design and Operation of Reverse Electro-Enhanced Dialysis of Monoprotic Carboxylic Acids. In Alves, B.; Nascimento, O. and Biscala, J., editors, 10th International Symposium on Process System Engineering. Volume 27, pages 663-668. Elsevier. 2009.

Prado-Rubio, O.A.; Jørgensen, S.B and Jonsson, G. Modeling Donnan Dialysis Separation for Carboxylic Anion Recovery. Computers and Chemical engineering. Submitted. 2009.

Prado-Rubio, O.A.; Jørgensen, S.B and Jonsson, G. Control System Development for Integrated Bioreactor and Membrane Separation Process. 20th European Symposium on Computer Aided Process Engineering, submitted. 2009.

Negar Sadegh
Phone: +45 4525 2821
Fax: +45 4588 2258
E-mail: nes@kt.dtu.dk
WWW: http://www.cere.dtu.dk
Supervisors: Kaj Thomsen
Erling H.Stenby
Georgios Kontogeorgis

PhD Study
Started: April 2009
To be completed: March 2012

Thermodynamic Modeling of Water-Acid Gases-Alkanolamine Systems

Abstract
This project is about thermodynamic modeling of natural gas cleaning process with alkanolamines as solvent. The research combines both experimental and thermodynamic modeling studies. Measuring high pressure VLE data for methane-water- acidic gases- MEA and MDEA as a solvent is planned for the experimental part. For the modeling part the Extended UNIQUAC model will be used for representation of the behavior of acid gas-alkanolamine mixtures over an extensive pressure range, with emphasis on mixed acid gases .

Introduction
The problem with thermodynamic modeling of acid gas treating plants is that the vapor–liquid equilibrium (VLE) data reported for these systems are not generally very consistent.
Moreover, other indispensable data such as binary VLE of alkanolamine–water system, excess enthalpy data and standard state properties of alkanolamines for both gas and liquid phases are scarce and those available from a handful of sources show discrepancies.
Thermodynamic modeling of these systems has been done through 3 different ways: empirical correlations, such as: Kent and Eisenberg (1976) for CO_2+MEA/DEA+H_2O systems and Gabrielsen et al. (2005) for CO_2+MEA/DEA/MDEA+H_2O systems; equations of State, such as: Chunxi and Fürst (2000), Huttenhuis (2008), Vrachnos et al. (2004) , Solbraa (2002) and activity coefficient models, such as: E-NRTL (Austgen et al. (1989)), Extended UNIQUAC (Faramarzi et al. (2009)), UNIQAC-NRF (Haghtalab and Dehghni (2007)), Modified Clegg-Pitzer (Kundu at al. (2003)).
Empirical correlations fail when being extrapolated to conditions other than what they are based on. Equations of state mostly are limited to certain conditions. For instance Solbraa EoS can only show good results at ambient temperature. Currently, the best approach for modeling the behavior of these systems is by activity coefficient models for electrolyte solutions.
The purpose of the present work is to apply the extended UNIQUAC model [1] to estimate various thermodynamic properties of the alkanolamine systems required for the design of natural gas treating units. The extended UNIQUAC model [1] was applied to the thermodynamic representation of carbon dioxide and hydrogen sulfide absorption in aqueous monoethanolamine (MEA), methyldiethanolamine (MDEA) and mixtures of the two alkanolamines (MEA–MDEA). All the essential parameters of the model are simultaneously regressed to a collective set of data on the single MEA and MDEA systems and mixed systems.

Specific Objectives
The purpose of this study is to get an accurate estimation of thermodynamic behavior of natural gas treating process. This will be done by gathering experimental VLE data on water-acid gases-alkanolamine systems and thermodynamic modeling of the system with Extended UNIQUAC.

Results and Discussion
Both acid gases are weak electrolytes and they partially dissociate in the aqueous phase to form a complex mixture of molecular and ionic species. In a closed system at constant temperature and pressure, physical equilibrium governs the distribution of molecular species between the liquid phase and the vapor phase. Simultaneously, in the liquid phase, alkanolamine reacts with CO_2 and H_2S, either through acid-base buffer mechanisms or through a direct reaction of CO_2 with primary or secondary alkanolamine to produce ionic species: physical and chemical equilibrium are highly coupled. Representation of the vapor-liquid equilibrium

(VLE) behavior of acid gas-alkanolamine-water systems is complex due to the large number of chemical reactions which occur in the systems. It requires that both physical and chemical equilibria be accounted for in a thermodynamically rigorous way.

Extended UNIQUAC Model:

The extended UNIQUAC model as presented by Thomsen and Rasmussen [1] is used for the thermodynamic calculations of this work. Extended UNIQUAC is the original UNIQUAC equation (Abramsand Prausnitz [2] and Maurer and Prausnitz [3]) combined with the Debye–Hückel term. The latter term is added to account for the electrostatic interactions caused by the presence of the ionic species in the solution. Therefore, the excess Gibbs energy is expressed as the combination of three terms: the entropic and enthalpic terms of the original UNIQUAC equation to consider the non-electrostatic interactions and, the electrostatic term (Debye–Hückel):

$$\frac{G^E}{RT} = \left(\frac{G^E}{RT}\right)_{UNIQUAC\ Entropic} + \left(\frac{G^E}{RT}\right)_{UNIQUAC\ Enthalpic} + \left(\frac{G^E}{RT}\right)_{Debye-Huckel}$$

Parameter Regression Database:

The modeling will be done by using around 4500 acid gas solubility data in alkanolamine aqueous mixtures. Some of the preliminary modeling results are shown in the following figures.

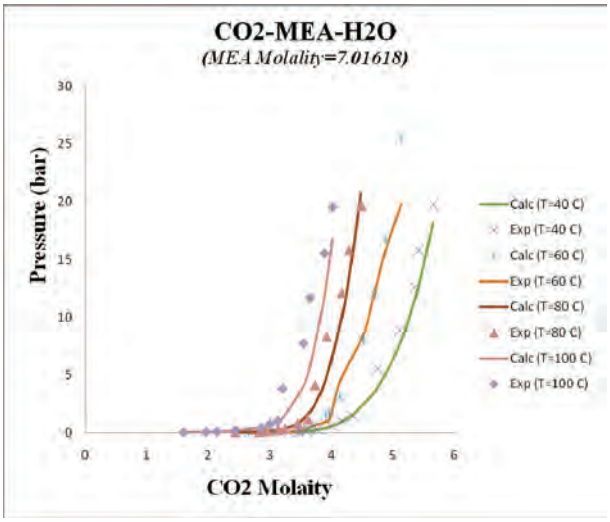

Figure 1: P-x diagram for MEA-Water-CO_2 system for solvent molality of 7.01 , between 40-100 C and 0-30 bar

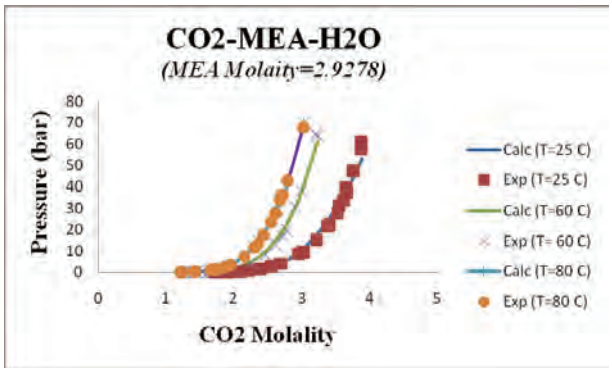

Figure 2: P-x diagram for MEA-Water-CO_2 system for solvent molality of 2.92 , between 25-80 C and 0-80 bar

As it is shown in the following figures the modeling results are in quiet agreement with the experimental data.

Conclusion:

In this work Extended UNIQUAC is used for thermodynamic representation of water-acidic gases-alkanolamine systems**.**

It has been shown that Extended-UNIQUAC can accurately represent phase behavior of the MEA-CO_2-H_2O system.

Acknowledgment:

We would like to thank Statoil for funding this PhD project.

References

1. K. Thomsen, P. Rasmussen, Chem. Eng. Sci. 54 (1999) 1787–1802.
2. D.S. Abrams, J.M. Prausnitz, AIChE J. 21 (1975) 116–128.
3. G. Maurer, J.M. Prausnitz, Fluid Phase Equilib. 2 (1978) 91–99.Conference

List of Publications

N. Sadegh, K. Thomsen, E. H. Stenby, G. Kontogeorgis, Thermodynamic modeling of water-acid gases-alkanolamine systems, oral presentation at the 9th AIChE annual meeting (2009)

Kaushal Shashikant Sagar
Phone: +45 4525 6825
Fax: +45 4525 2161
E-mail: kass@kt.dtu.dk
WWW: http://www.licort.dk
Supervisors: Professor Ole Hassager
Senior scientist Sokol Ndoni
Mads Brøkner Christiansen, Post Doc

Started: July 2008
To be completed: July 2011

Polymer Design and Processing for Liquid Core Waveguides

Abstract
Current social scenario demands an attention to the growing need of quick, simple and low cost diagnostics of issues related to health, pollution, food safety. Diagnostics for high sensitivity quantitative measurements are to a large extent based on optical sensors. A perfect scenario would thus be able to perform on-site measurement capability, which is miniaturized for lab-on-a chip applications. The present project intends perfect focus on a sensor application by using liquid core waveguide technology.

Introduction
Optically based detection systems are widely used in analytical systems because of their high sensitivity to extremely low quantities of materials. There is currently much interest in basing miniaturize sensing systems on optical detection where the matter of interest is confined to a micro channel. The use of optical waveguides on-chip with the liquid core technology has opened the way for more advanced detection systems with improved limits of detection.

This work mainly focuses on the processing development for devices used for the above applications. This is materialized using the clean room facilities at DTU DANCHIP. This will lead to fabrication of the liquid core waveguides based on nanoporous materials [1, 2].

Experimental work
Liquid core waveguide phenomenon can be seen in Figure 1. As the refractive index (RI) values plays a crucial role in waveguiding phenomenon, the initial block copolymer upon etching reduces the effective RI to a greater extent.

Here the nanoporous polymers are prepared by initially solvent casting the *polybutadiene-polydimethylsiloxane (PB-PDMS)* block copolymer in *tetrahydrofuran (THF)* with 1 mol % of the cross-linker *dicumyl peroxide* wit respect to the number of double bonds of the PB component.[3,4] This is further cross-linked at 140 ^{o}C in an argon/nitrogen atmosphere for 2 hours. The etching of the PMDS minority block is done by using *tetrabutyl ammonium fluoride (TBAF)* in 1:3 molar ratio of PDMS. The etching step lasts for 36 hours which is followed by the cleaning of etched matrix in THF and methanol for total 16 hours (Figure2)

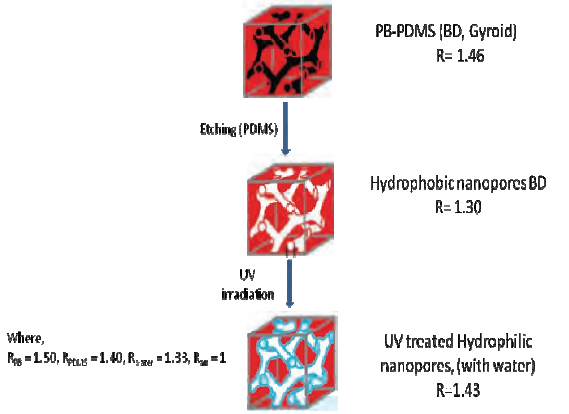

Figure 1. Schematic diagram illustrating the working principle of liquid core waveguide

The nanoporous material is further turned selectively hydrophilic by using appropriate mask under UV irradiation; λ= 320-350nm which means that the exposed volumes will then take up water upon submerging of the sample into water. This is ready for further optical testing part as the contrast in the refractive index is now feasible [5,6].

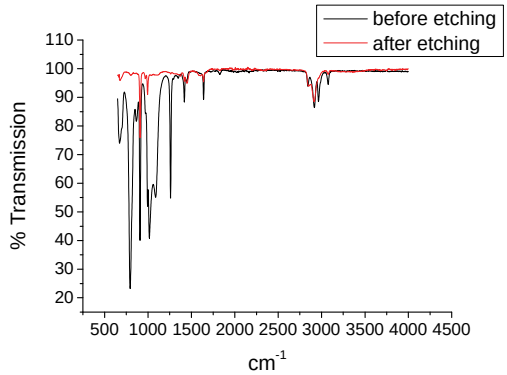

Figure 2. *Fourier Transform Infrared spectra of* nanoporous polymer, — unetched, — etched sample.

These samples are subjected to the optical testing set up. It consists of a laser light source of 655nm. Light at the other end of the curved hydrophilic waveguide is being collected by a spectrometer probe which shows the intensity of the out coming light signal (Figure 3).

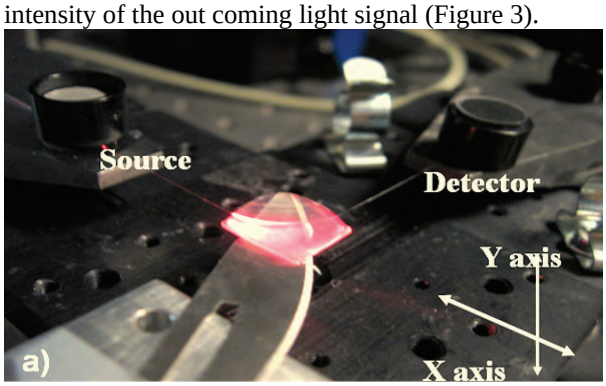

Figure 3 Setup for the optical testing of waveguide

Results and Discussion

As can be seen from the Figure 4, a dry sample does not exhibit any significant peak at the ingoing wavelength but scatters the beam of light. On the other hand, when the water filled waveguide is subjected to the laser source it guides the light due to higher refractive index of the core than the surrounding material. It thus bends the light in the curved waveguide.

Figure 4. Light guiding experiment demonstrating the waveguiding phenomenon.

Figure 5 demonstrates the light guiding profile in width and depth. As can be seen from the Y-axis translation, the depth of the waveguide is almost 400microns, which is also the thickness of the sample. This also means that the hydrophilisation has managed to cover the entire depth and can perform as the waveguide throughout the thickness. X-axis translation is slightly more than the width of the mask i.e.500 microns. This leads to the scattering of the signal and thus the tailing of the curve beyond the expected region where scattered light is being collected. This can be primarily attributed to the volume scattering of the microchanels. Currently much of the work is being carried out to overcome the scattering of propagating light.

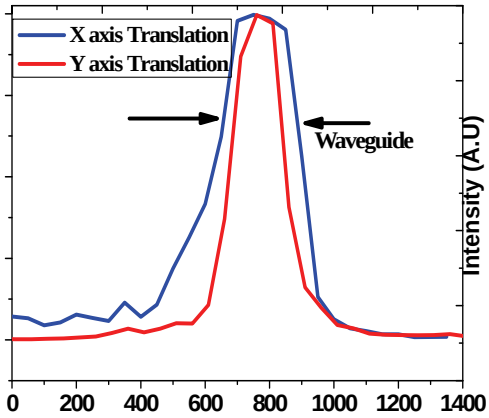

Figure 5. Light guiding profiles in translation mode to map scattering and size of the waveguide.

It is evident that light guiding is greatly influenced by the UV photo-oxidation step. It is thus essential to study the process of photo-oxidation macroscopically and microscopically-within the nanoporous and around to gain overall control on the entire process to optimize the performance of the liquid core devies.

The next section discusses qualitative aspects-photo products formation to understand the kind of hydrophilic groups formed imparting the hydrophilisation of the nanoporous system [6].

As can be seen from figure 2, after UV treatment, the distinct peaks appearing are –OH and carbonyl stretch. The rest of the spectra show massive overlap at lower wave number values and hence it is difficult to analyze it. It is essential in this case to further investigate the carbonyl infrared spectra which can be done by NaOH staining. From the reaction below

$$R\text{-}COOH + NaOH - R\text{-}COO^{-}Na^{+} + H_2O$$

NaOH staining transforms carboxylic acid groups into carboxylate ion. This group typically shows a peak at lower wavenumber than the carbonyl stretch peak. Figure 6 shows FTIR spectra whereupon NaOH staining majority of the peak is exhibiting a shift to the carboxylate ion peak. This is a good indication of presence of R-COOH groups which imparts hydrophilic nature of the polymer. This is further confirmed by obtaining solid state NMR spectra of the sample. Figure 7(a) shows C^{13} spectra of the treated sample where around 200ppm responsible for ketones peak and aldehydes is missing. In figure 7(b) after NaOH treatment the peak at 175ppm has shifted to 181ppm

due to formation of carboxylate ion leaving no signal at 175. This indicates most of the carbonyl groups formed are carboxylic and not esters. Upon NaOH staining, they are largely consumed and hence peak shifting at slightly higher ppm value is observed.

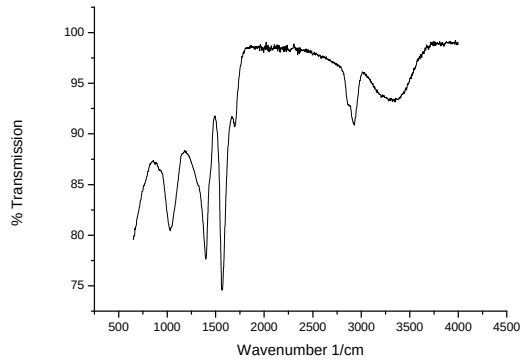

Figure 6. FTIR spectra of NaOH stained UV treated nanoporous polymer.

NMR also yield us important information that small amount of –OH peak indicating presence of hydroxyl groups as well.

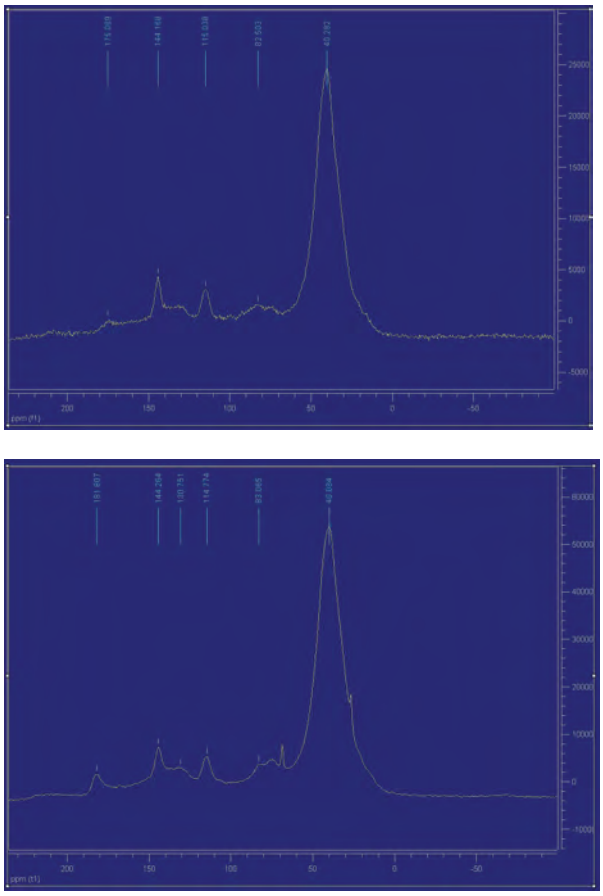

Figure 7. a) Solid state NMR of UV treated sample indicating presence of COOH based photoproducts. b) NaOH treated spectra of the sample indicating absence of other carbonyl groups presence.

Table 1. List of photoproducts in nanoporous system.

Photo product	FTIR peak	NMR peak	
Aliphatic Ketone	1715	190	X
Aliphatic Aldehyde	1730	190	X
Carboxylic acid	1710	175	√
Hydroxyl	3400	70	√
Unsaturated ketones	1640	-	-

Thus it helps us constructing a table wherein, we can list all the possible photo products possible from the carbonyl stretch. Tables 1 show all the photo products along with their position in FTIR and NMR spectra. It is important to note that the presence of α-β unsaturated ketones cannot be denied. Its presence is not yet proved experimentally, but yellowing of the polymer after UV treatment indicates the presence of extended conjugated photo products.

It is essential to locate above mentioned hydrophilic groups within the complex nanoporous system to quantify the process microscopically. This is done by NaOH staining using 3 different solvent systems; water, methanol and THF. The solvent systems are selected based on its affinity into the nanoporous system. After hydrophilisation, water can penetrate into the nanopores mainly. Methanol can either stay in the nanopores or penetrate into the matrix slightly. THF on the other had can occupy both-nanopores and matrix. Thus it can be a good contest to compare all 3 solvents with NaOH to check the carboxylic groups presence at different places in the porous system.

Table 2. Differential solvent staining for microscopic distribution of carboxylic acid groups.

Type of solvent	Volume uptake (%)	*Peak ratio
H_2O + NaOH	81	0.80
CH_3OH + NaOH	80	0.79
THF + NaOH	108	0.81

***Peak Ratio**: It is calculated by normalizing the carboxylate Ion peak value with the C-H peak SP^3 i.e.

Trasmission values in cm^{-1} at 1568/2917.

Table 2 shows solvent volume uptake % with reference to the original. Here the volume uptake can be related to the nanoporosity. As can be seen from uptake values of water and methanol which are similar indicating they are staying in the pores mainly and does not penetrate into the matrix. THF however, can occupy the matrix as well resulting in to higher volume uptake value. These samples are then washed with the consecutive solvents to remove excess of NaOH from the polymer and dried thoroughly. After this, FTIR spectra were recorded and the peak ratio was calculated based on the C-H sp^3 hybridized internal standard peak. It is interesting to note that despite of different volume uptake in the polymer system, concentration of carboxylate ion peak is identical in all 3 systems. This leads to an important conclusion that the photo-chemistry is mainly happening in the nanoporoes due to the abundance of oxygen and not in the amorphous regions of polybutadiene matrix (figure 8).

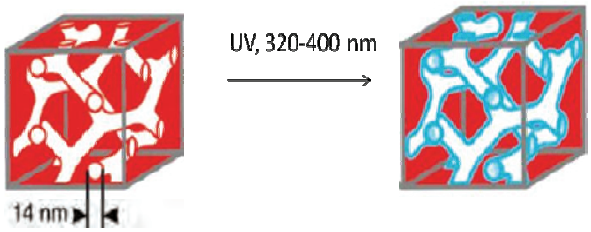

Figure 8. Schematic distribution of COOH groups in the nanopores system.

Acknowledgement
The present work was carried out in collaboration with Nimi Gopalakrishnan, PhD student at DTU Nanotech.

References

1. M.P. Duggan et al, A non- vasive analysis method for on-chip spectrometric detection using liquid-core waveguiding within a 3D architecture. Analyst 2003 128 1336-1340
2. M. Holtz et al, small volume Raman spectroscopy with liquid core waveguide. Anal. Chem,vol 71 pp 1999 2934-2939
3. S. Ndoni et al, Nanoporous materials with spherical and gyroid cavities created by quantitative etching of polydimethylsiloxane in polystyrene-polydimethylsoloxane block copolymer. J.AM. CHEM. SOC. 2003 125 13366-13367
4. M. Hansen et al, Nanoporous crosslinked polyisoprene from polyisoprene. Polydimethylsiloxane block copolymer. Polymer Bulletin 51 2004 403-409
5. S.Ndoni et al, Controlled Photooxidation of Nanoporous Polymers. Macromolecules 42 2009 3877-3880
6. J. Lucki et al, Comparative studies of reactions of comeercial polymers with molecular oxygen, singlet oxygen, atomic oxygen and ozone II, reactions with 1,2-Polybutadiene. European Polymer Journal 15 1979 1101- 1110

Noor Asma Fazli Bin Abdul Samad

Phone: +45 4525 2912
Fax: +45 4593 2906
E-mail: nas@kt.dtu.dk
WWW: http://www.kt.dtu.dk
Supervisors: Rafiqul Gani
Krist V. Gernaey
Gürkan Sin

PhD Study
Started: January 2009
To be completed: December 2011

A Generic Model-based Framework for Process Control and Monitoring of Product Qualities in Batch Cooling Crystallization

Abstract
A generic model-based framework has been developed for crystallization processes aiming at the control of process operations and the monitoring of product qualities. This generic model-based framework allows the systematic development of a wide range of crystallization models for different operational scenarios. This enables the design and control engineers to analyze various crystallization operations and conditions, thus facilitating the development of process control and monitoring systems (PAT) for crystallization processes. The generic framework has been implemented in the ICAS-PAT software which allows the user to design and validate PAT systems through a systematic computer-aided framework.

Introduction
Crystallization is an important operation when manufacturing fine chemicals or pharmaceuticals. It is a widely used technique in solid-liquid separation processes to obtain solid products of high purity at relatively low costs. Requirements for crystal products are usually high purity, a specific crystal size distribution and a desired crystal shape [1]. Consequently many efforts have been made to model the crystallization process to support the development of appropriate process operations and control scenarios to meet specific end product demands. Development of crystallization process models however is tedious and requires, among others, expertise in modeling, numerical methods as well as process engineering insights. So far the models of the crystallization processes have been problem specific, meaning that the models were developed with a certain crystal product in mind. Hence it is not surprising to notice that research on crystallization modeling emphasizes different issues such as crystal size distribution (CSD) or crystallization kinetics [1, 3]. Furthermore, specific models employ numerous underlying assumptions, for example, on agglomeration and crystal breakage factors. As a consequence, there are many specific models available in the literature with different degrees of complexity, which makes their selection and use for a specific problem difficult if not confusing. There is therefore a need for the development of a generic crystallization model to assist the systematic and efficient development of appropriate models for specific crystallization processes.
Once an appropriate crystallization model has been developed, it can be used as a tool for process design, control and monitoring systems to ensure the desired end product quality. Such a process control and monitoring system is expected for a pharmaceutical production process that is operated according to the Process Analytical Technology (PAT) guidance [2]. Therefore, the objective of this work is to develop a generic model-based framework that allows the study of different crystallization operational scenarios and through which the design of process control and product monitoring systems can also be developed, analyzed and validated. Since this framework will need to rely on process models, the framework will be extended with a tool to systematically develop crystallization models.

Generic Model-based Framework
An overview of the extended framework for design of process control and product monitoring systems is shown in Figure 1 where the generic model options have been added to the original [2, 4]. The starting point for the design methodology is the problem definition in terms of process specifications and product quality specifications that is usually provided by the manufacturer or PAT system designer. A model library and a knowledge base have been developed and act as the supporting tools for the design of the process control and product monitoring system.

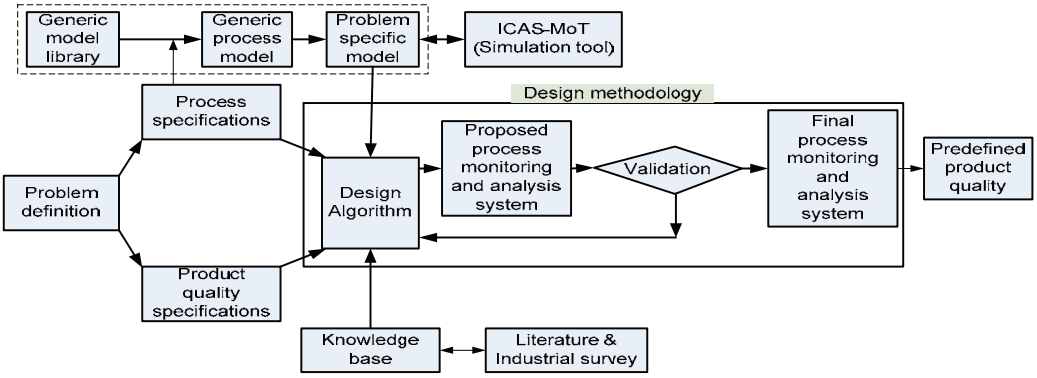

Figure 1: Extended schematic representation of the PAT design framework [2, 4]

A systematic modeling framework (see Figure 2) has been developed to create the various crystallization process/operation models from the generic batch cooling crystallization model methodology and implemented in the ICAS-PAT model library.

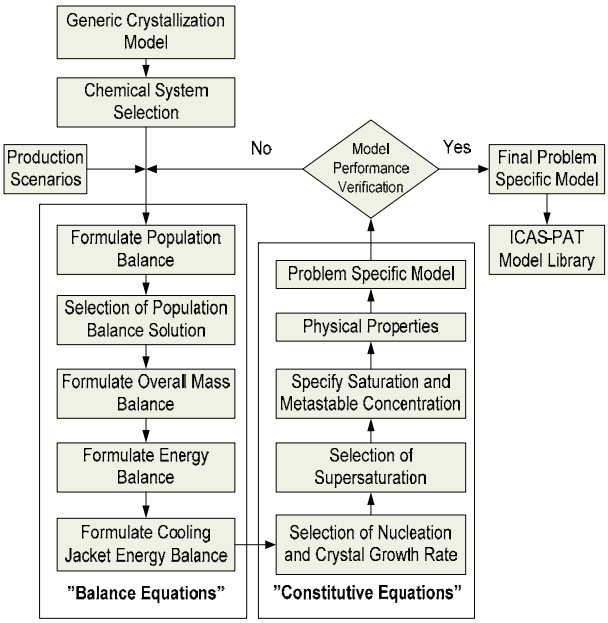

Figure 2: Generic crystallization modeling framework

This modeling framework starts with the selection of the chemical system that needs to be investigated and the associated known information about its production scenarios. Then, the necessary balance equations and constitutive equations are extracted from the generic model library. The balance equations consist of population balance, overall mass balance and energy balance equations for the defined crystallization volume plus energy balance equations for cooling jacket. The constitutive equations library contains a set of models of nucleation, crystal growth rate, supersaturation, saturation concentration, metastable concentration and physical properties corresponding to different type of crystallization processes. Subsequently a problem specific model is created which is verified through model analysis and solution. Finally the problem specific model is transferred to the ICAS-PAT model library through ICAS-MOT. In this way, based on the process and product quality specifications supplied by the user (see Figure 1), the generic model is adapted to reflect a specific case study and it allows the user to consider the necessary operational scenarios enabling thereby analysis of crystallization operations and conditions.

The developed design algorithm in the PAT design framework (see Figure 1) relates the product and process specifications to the available supporting tools and subsequently generates a design proposal for the process monitoring and analysis system. If the obtained PAT system satisfies the requirements then it is selected as the final design of the process control and product monitoring system, which can then be subsequently implemented and used in practice to obtain the predefined product quality consistently.

Conclusions

A generic model for crystallization process/operation has been developed and implemented in the ICAS-PAT software. This generic crystallization process model provided the means to generate the necessary crystallization process operational models for different production scenarios and thereby increased the (re)usability the generic model.

Acknowledgements

The author acknowledges the financial support of the Ministry of Higher Education (MoHE) of Malaysia and Universiti Malaysia Pahang (UMP).

References

[1] M. Fujiwara, Z.K. Nagy, J.W. Chew, R.D. Braatz, Journal of Process Control, 15(2005) 493-504.

[2] R. Singh, K. V. Gernaey, R. Gani, Computers & Chemical Engineering, 33(1) (2009) 22-42.

[3] Z.K. Nagy, J.W. Chew, M. Fujiwara, R.D. Braatz, Journal of Process Control, 18(2008) 399-407

[4] R. Singh, K. V. Gernaey, R. Gani, Computers & Chemical Engineering, (2009), doi:10.1016/j.compchemeng.2009.06.021

Sara Bülow Sandersen

Phone: +45 4525 2982
Fax: +45 4588 2258
E-mail: sbs@kt.dtu.dk
WWW: http://www.ivc-sep.kt.dtu.dk
Supervisors: Nicolas Smit von Solms
Erling Halfdan Stenby

PhD Study
Started: May 2008 (marternity leave from June 2009 to February 2010)
To be completed: January 2012

Enhanced Oil Recovery with Surfactant Flooding

Abstract
The aim of this Ph.D.-study is to investigate the phase behavior of single component surfactant systems at elevated temperatures and pressures for use in surfactant flooding for enhanced oil recovery. A literature study has been conducted to create a basis for the experimental work. Previously it has been common to use multi component systems for surfactant flooding, but as chromatographic separation takes place in the reservoir this is not a preferable approach. The mixed surfactant solution will then adsorb to the reservoir rock during flooding, which results in a surfactant blend that deviates from the optimal surfactant blend originally injected. Finally this results in poor oil recovery, which must be avoided.

Introduction
Many mature reservoirs still has about 50 % of the original oil in place despite that they are already using both primary and secondary oil recovery techniques.
One technique to attain higher oil recovery is chemical enhanced oil recovery (EOR), where surfactants are injected to the reservoir to reduce the interfacial tension (IFT) between oil and water. However, this technique encompasses several complex issues and the design of chemical EOR must be tailored to the reservoir rock and fluid. The principle of flooding is illustrated in figure 1.

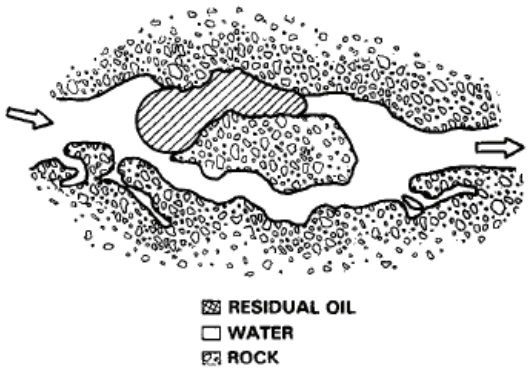

Figure 1: Principles of flooding, where residual oil is trapped in the reservoir, [1]. The residual oil trapped in narrow capillary pores is held back thanks to capillary forces and it is required to reduce the IFT between oil and water to 0.001 dynes/cm to mobilize the oil.

The primary goals in EOR operations are to displace or alter the mobility of the remaining oil, still present in the reservoir after conventional primary and secondary oil recovery techniques has been applied. Surfactant flooding EOR is a rather expensive technique and therefore it can only be justified when the oil price are relatively high. Usually the remaining oil is distributed in the pores in the reservoir, where the oil is trapped due to capillary and viscous forces. The mobilization of the residual oil is achieved through surfactants generating a sufficiently low oil/water IFT. Low IFT further gives capillary numbers large enough to overcome the capillary forces. The recovery efficiency is highly dependent on the capillary number which is defined as equation 1.

$$N_c = \frac{\mu_w \nu_w}{\varphi \gamma_{wo}} \quad (1)$$

Where N_c is capillary number, μ_w is viscosity of the aqueous or displacing phase in [Pa Sec], ν_w is flow rate of the displacing fluid in [cm/sec], φ is effective porosity of formation and γ_{wo} is interfacial tension between water and oil in [N/m].
It is not unusual that co-surfactants are blended into the liquid aqueous solution to improve the properties of the surfactant solution. Co-surfactants serve as a promoter or help the blend to meet optimal conditions with respect to reservoir temperature, pressure and salinity. It is experienced that due to chromatographic separation during flooding it is very complicated to design a surfactant/co-surfactant solution that can perform

optimal throughout the reservoir. During surfactant flooding there will be losses due to adsorption and trapping to the rock.
Also it is essential to assure stability of the surfactant solution, which must resist physical conditions such as high temperatures, high pressures and high salinities. [2]

Specific Objectives
In this Ph.D.-project it is the purpose to investigate the potential of single component surfactant systems in contrast to the more ordinary systems with surfactants and co-surfactants.

Surfactant Flooding
EOR with surfactant flooding has been investigated for many years. Unfortunately, the economic reality of the process is that the technique is very expensive and therefore it has not yet been commercial employed, as it has not been tested successfully in full scale yet. [3]
Chemical EOR is introduced as this can contribute to improve oil recovery efficiency. The process is the injection of one or more specific liquid chemicals, the so-called surfactants, that controls the phase behavior properties in the reservoir. Injecting surfactants should entail that the IFT between the injected liquid and oil is reduced to 0.001Dynes/cm, which will then overcome the existing capillary forces and thus mobilize the oil towards the production well.
There is a great potential of chemical EOR with surfactant flooding, as this technique encompasses the possibility of designing a process where the overall displacement efficiency can be increased. It is also expected that surfactant flooding could be designed to increase the economic productivity, as the economic productivity for some mature reservoirs nowadays are low despite having 50-70% of the original oil still in place. [4] Surfactants in their common form take structures as depicted in figure 2.

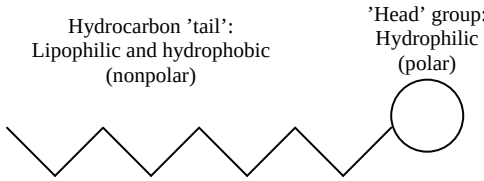

Figure 2: Surfactant molecule, whit the nonpolar hydrocarbon 'tail' to the left and the polar 'head' group to the right.

Surfactant flooding EOR involves microemulsions, where oil/water and water/oil micelles are formed. In the beginning of a surfactant flood the surfactant concentration is low and then the concentration increases as the amount of injected surfactant solution rises. At low surfactant concentrations the surfactant molecules are dispersed as monomers. As surfactant concentration is increased the surfactants molecules starts to aggregate and at some point the concentration will reach the critical micelle concentration (CMC). Any further addition of surfactants will form into micelles.

Surfactants are frequently classified by their ionic nature of the head group as anionic, cationic, nonionic or zwitterionic.
Anionic surfactants are the most widely used surfactants for surfactant flooding and according to Austad *et al.* (1996) [5] promising surfactants, for single component surfactant flooding, are branched ethoxylated sulfonates.

Phase Behavior
It is reported in literature that an increase in temperature increases the optimal salinity for the surfactant system.
Aside from the influence of temperature the effect of pressure on the phase behavior of the microemulsion is widely discussed as results from different researchers disagree. Reservoir conditions are typically at elevated pressures, why this is of importance.
Observing surfactant systems there are three types of systems to be considered.

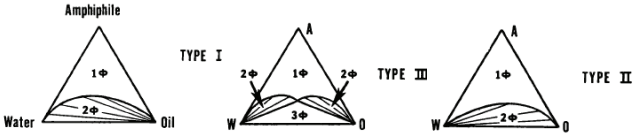

Figure 3: From left to right: multiphase region with lower-phase microemulsion with excess of oil, middle-phase microemulsion and upper-phase microemulsion with excess of water/brine.

Figure 3 represents the phase environment where surfactant/water/oil systems can equilibrate as either a single phase or as multiple phases. These generalized systems are often referred to as the so-called Winsor Type systems.

Experimental Work
Experimental activities regarding phase behavior has been conducted. Phase behavior of oil/ surfactant/ alcohol/ brine systems at elevated temperatures and pressures has been examined. The model system studied, heptane/ SDS/ 1-butanol/ brine, shows that both temperature and pressure has an effect on the equilibrium system and further studies are ongoing.

References
1. B.M. O'Brian, Journal of American Chemists' Society, 59(839a-852s), Houston, 1982
2. D.W. Green, G.P. Willhitw, Enhanced Oil Recovery, SPE Textbook Series, vol. 6, USA, 1998, p. 7
3. Y. Wu, P. Shuler, Y. Tang, W.A. Goddard, SPE 95404 presented at SPE Annual Technical Conference and Exhibition, Dallas, Texas, 2005
4. A.K. Flaaten, Q.P. Nguyen, G.A. Pope, J. Zhang, SPE 113469 presented Improved Oil Recovery Symposium, Tulsa, Oklahoma, 2008
5. T. Austad, H. Hodne, S. Starnd, K. Veggeland, Colloids and Surfaces, 108(253-262), Norway, 1996

Paloma Andrade Santacoloma

Phone: +45 4525 2804
Fax: +45 4593 2906
E-mail: psa@kt.dtu.dk
WWW: http://www.kt.dtu.dk
Supervisors: John M. Woodley
Krist V. Gernaey
Gürkan Sin

PhD Study
Started: October 2008
To be completed: September 2011

Systematic Framework for Multienzyme Process Modeling

Abstract

Biocatalysis has been attracting increasing interest in recent years. Nevertheless, most of the kinetic studies concerning biocatalysis have been carried out using isolated enzymes (soluble or immobilized). Nowadays multiple enzyme mixtures are attractive for many industrial applications. Therefore, a systematic framework is proposed to develop mathematical models which describe multienzyme processes. In this way, the best outcome of the process can be obtained by developing a thorough understanding of what modifications in the system and process design are required to optimize the use of the individual enzymes.

Introduction

Biocatalysis is now offering a range of new catalytic options for complex industrial syntheses. The use of enzymes in whole-cell, soluble or immobilized format is now widely applied in many processes for single step conversions[1]. A further opportunity arises where two or more sequential steps can be carried out by a mixture of enzymes in a single reactor[2]. Such multi-enzymatic systems are very well suited to be run in an integrated fashion since the conditions in each reaction (media, concentrations, pH and temperature) are typically well matched. An important advantage of single reactor multi-enzymatic systems is the elimination of separation and purification steps of intermediate products[3]. In this way, a substrate transformed to a product can be used by another enzyme and so on, in a cascade.

The work reported here shows a framework for mathematical modeling of such multi-catalytic syntheses. The framework provides a systematic method to build high quality models in an efficient manner. These models will then be used to evaluate and enable the potential of multi-enzymatic technology to be fully exploited, e.g., understanding the modifications required in the system to make optimal use of the individual enzymes. The framework is based on a hierarchical structure where a chain of strategic decisions is made at different levels.

Methodological framework

Mathematical models for multienzymatic reactions can be formulated considering a sequence of steps and feedback lines in order to obtain the best approximation of the real system. In this section, a systematic evolution of this iterative model formulation process is described in Figure 1. The scheme can be generalized for different mathematical model formulations, nonetheless the criteria are focused on a multienzyme approach.

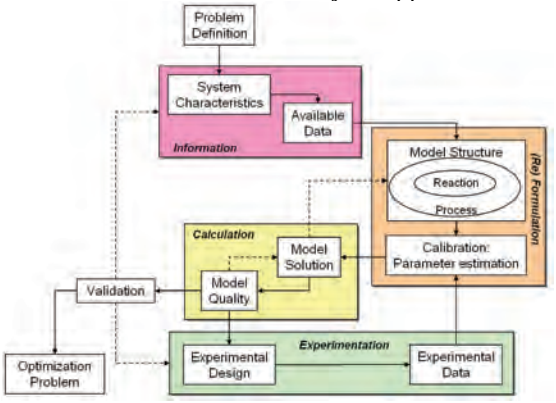

Figure 1. Schematic framework for multienzyme process modeling

According to Figure 1, four (4) general areas can be classified, thus:

1. *Information:* general information about the system such as properties and experimental data reported in the literature, which forms the base for the model formulation.
2. *(Re) Formulation:* selection of relevant information about the enzymatic reactions and the process operation, model structure selection and formulation of model equations.

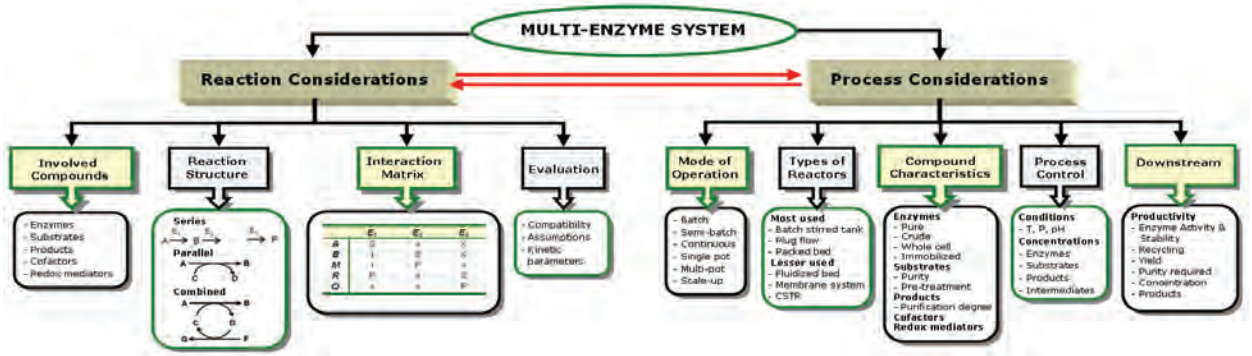

Figure 2. Considerations between reaction and process for multienzyme system modeling

Some considerations are given in Figure 2 and a brief description is provided in the following section. Thus, mathematical models are formulated based on first principles developing equations to describe reaction rates and mass balances for the desired system. A calibration of the model, i.e. parameter estimation, is performed if experimental data are available, otherwise the suggested model could be used as the basis to formulate a relevant experimental design which provides the required information for validation.

3. *Calculation:* evaluation of the model is required to study and understand dynamic behavior of the system when exposed to different changes in the inputs. In the same way, different types of tests can be applied in order to evaluate the model quality e.g. uncertainty and sensitivity analyses that identify critical factors affecting the system which may also give relevant information for experimental design, if required.
4. *Experimentation:* experimental data is always required for model validation, especially when models will be applied for prediction, optimization or process control. Experimental data obtained from literature is a good starting point for model analysis. However, a specific experimental design should be performed in order to meet the validation criteria.

Considerations for the Model Structure

Mathematical models are formulated and adapted according to the conditions where processes can be feasibly applied. Considerations between reactions and process characteristics define the structure of the mathematical model. Figure 2 shows the considerations that should be evaluated for better understanding the design and modeling of a multi-enzyme system. Hence, considerations for the reaction include the definition of the *involved compound*s i.e. substrates, enzymes, products, etc.. The *reaction structure* describes the pathway towards the desired product taking into account the series, parallel and combined reactions involved in the process. The *interaction matrix* shows the relationship between compounds and enzymes e.g. to analyze inhibitory effects. Finally, an e*valuation* is required to analyze the feasibility of the selected considerations in the other steps. In addition, process considerations are also required, and they are coupled with the considerations taken for the reaction stage. In this case, the *operating mode* is determined by the process objective i.e. to follow kinetics, to optimize yields, etc.; the *type of reactor* is selected according to media compatibility, and finally *compound characteristics*, includes specific information about enzymes and substrates. The quality of the desired products and the required *process control* drives the system to be kept at the optimal operating conditions to achieve control of the measured variables. Finally, the *downstream processes* are evaluated according to the required purity of the desired product and the productivity of the reaction which is directly related to the efficiency of the biocatalysts, yield, recycling, compound purities, etc. Defining the model, one can then proceed to the next step in the methodological framework as shown in Figure 1.

Challenges and Benefits of this approach

We believe that relevant conversions using multiple enzyme mixtures have a tremendous potential for industrial application. Furthermore, the modeling of these systems brings many benefits e.g. the interaction between enzyme, substrates, and products in a one-pot reactor can be understood, a large number of simulations of the process can be performed studying different scenarios and conditions of the process. Moreover, better experimental design can be formulated saving experimental time and effort. In the same way, optimal applicability in real plants can be improved. However before all these benefits are achieved, there are some challenges that must be faced first, e.g. how can we evaluate feasible multi-enzyme mixtures for the generation of desired products? How can we estimate and analyze kinetic parameters for multi-enzyme mixtures? How can we achieve optimal conditions for maintaining maximal activity of the multi-enzymatic system? How can we get reliable experimental data for higher accuracy in model validation? These questions among others will be answered in this project where different case studies are evaluated based on multi-enzyme systems reported in literature.

References

1. J.M. Woodley, Adv Biochem Eng Biotechnol, 2000, 70, 93.
2. D.Y. Murzin and R. Leino, ChERD, 2008, 86, 1002
3. A. Bruggink, R. Schoevaart and T. Kieboom, Org Process Rec Dev, 2003, 4, 622

Daniel Schäpper
Phone: +45 4525 2960
Fax: +45 4593 2906
e-mail: dsc@kt.dtu.dk
www: www.kt.dtu.dk
Supervisors: Krist V. Gernaey
Anna Eliasson Lantz
Stuart Stocks, Novozymes A/S

Ph.D. Study
Started:
To be completed: March 2010

Continuous Culture Microbioreactors

Abstract
The current microbioreactors mostly operate as fed-batch or continuous culture with *E. coli* as culture strain. This projects aims to design a microbioreactor running continuous cultures of *S. cerevisiae* in a reactor volume of approximately 100µL. The most important culture parameters can be measured on-line allowing for a high information-per-experiment ratio. Industrial relevance will be proven through comparisons of continuous culture microbioreactor experimental data with bench-scale experiments performed at the Department of Systems Biology.

Introduction

Biotechnology plays an increasingly important role in production processes in the food, the chemical and the pharmaceutical industry. Well-known examples of biotech-based products that have an important function in the life of many people are enzymes used in laundry detergents, pharmaceuticals such as insulin, etc.

However, starting up a new biotechnological production is usually preceded by a tremendous research effort in which for example the productivity of different candidate production strains is compared (=screening). Usually, such screening is done in shake flask cultures. In a later stage of production process development, experiments done in bench scale reactors are performed to investigate the influence of process conditions on productivity.

Experiments done in shake flasks (typically with a volume of 100 mL to 1 L) are easy to set up. However, shake flask cultures only allow batch experiments, and the information gained per experiment is limited: typically only end-point measurements of for example the product quality are performed. If additional measurements are needed, manual sampling is required, which additionally disturbs the culture. Compared to shake flasks, bench scale reactors (typically with a volume of 1 to 10 L) have the advantage that they allow on-line measurements. Moreover, bench scale reactors are flexible since they can be operated in batch or fed-batch, but also as a continuous culture. However, the work effort needed to prepare, operate and subsequently clean bench scale reactors is vast.

Summarizing, biotechnological process development is expensive, for example because both traditional cultivation methods work with substantial volumes that in turn then require preparation of the appropriate amount of expensive nutrient media.

Motivation

Microbioreactors (MBRs) offer the possibility to circumvent many of the above-mentioned problems: The production cost of the MBRs is low, since they can be produced from polymers; The working volumes are very small (in the µL/mL range), keeping costs for culture media low; On-line measurements are possible for the most important culture parameters (optical density (OD), dissolved oxygen (DO), pH); Batch, fed-batch and continuous culture conditions can be created in MBRs; The reactors are disposable after use and thus require no cleaning effort at all; Scaling out MBRs to systems with many parallel reactors allows for high-throughput screening, thus yielding a massive gain in information per experiment with continuously small working volumes.

The above advantages result in more-information-per-experiment (on-line measurements), financial savings (small volumes, less labor intensive) and the possibility to develop production schemes on the resource-saving micro-scale before scaling up a process.

Objectives

Currently, MBRs described in the literature are operated either as fed-batch or as continuous cultures, most often with *E. coli* as the culture strain. This project

aims at the development of a continuous culture MBR that can perform experiments with yeast (*S. cerevisiae*). Compared to a batch experiment, the continuous culture has the advantage that steady-state conditions can be achieved. Additionally, it should be possible to induce step changes in the dilution rate, forcing the culture from one steady-state to the other with continuous measurement of the important culture parameters, thus leading to dynamic information on the behavior of the culture under well-controlled experimental conditions.

The planned working volume is in the range of 100µL, which is smaller than most of the current reactors running continuous cultures.

In the first part of the project, a reactor with the above features is to be designed and fabricated, and a complete measurement and control setup is to be installed. The second step will then be to prove the industrial relevance through comparisons of MBR results with larger-scale data from the literature and from *S. cerevisiae* cultivations performed at the Department of Systems Biology (DTU).

Naturally, MBR construction also poses some challenges. Proper mixing for example is very essential for good cultivation results, since substrate gradients in the culture might otherwise lead to a varying (location dependent) metabolic state of the culture. In the projected volume range turbulent flow is difficult to achieve due to the small Reynolds numbers. On the other hand the volume is too large to be able to rely on diffusion alone. Therefore one of the challenges in the project is to find a mixing regime which efficiently reduces diffusion distances.

Another challenge is the mechanical integration of the various sensors, a mixing apparatus and the aeration system into the small volume in such a fashion that the device is easy to manufacture.

Microbioreactor Technology

The current reactor is designed to have a working volume of 100 µL which is sufficiently large to allow enough space for the sensors and actuators, but still small enough to considerably reduce the amount of media needed.

Contrary to conventional reactors which are mostly aerated by means of bubbles, microbioreactors are designed to work bubble-free. Aeration is done through a semi-permeable silicone membrane which allows both the incoming transport of oxygen and the outgoing transport of CO_2.

DO and pH are both measured with fluorescent sensor spots which change both the amplitude and the phase of the emitted light with a change in the sensitive parameter. A lock-in amplifier measures the phase difference and thus quantifies the measured variable.

Optical density is continuously measured both in the reactor itself and in the outflow channel. Light from a LED is guided into the reactor with optical fibers, sent through the substrate and then guided to a photo detector (**Figure 1**).

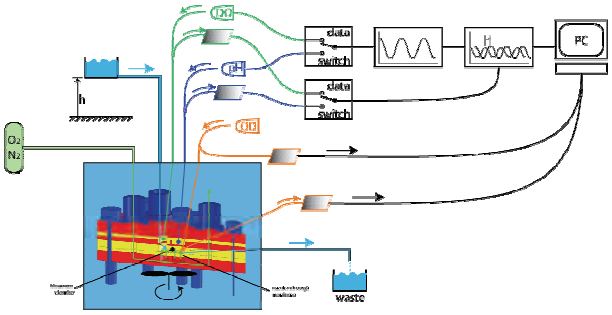

Figure 1: Schematic of a MBR setup

The flow rate is currently adjusted by a syringe drive. Both continuous and step changes in flow rate are possible which allows for various changes in dilution rates.

Temperature is measured with a Pt-100 element located under the reactor chamber and controlled with an on/off controller with a heating wire located under the reactor chamber in which an electrical current can flow. This allows us to maintain the temperature within ±0.3 ° of the setpoint.

pH is currently being controlled by gaseous means as addition of liquid to the reactor leads to an increase in volume. Thus either NH_3 or CO_2 are added to the aeration gas and then diffuse through the membrane into the reactor and change the pH accordingly. This allows to maintain pH at a certain setpoint; pH steps can also be forced onto the system if desired.

Mixing is done with a small freely spinning stirrer bar in the reactor chamber - this is sufficient to mix the contents and keep the cells in suspension.

The reactor is currently fabricated out of the polymers poly(methylmethacrylate) (PMMA) and poly(dimethylsiloxane) (PDMS), which both are cheap materials. Additionally, no clean room fabrication steps are necessary which allows for cheaper manufacturing. Indeed, it means that the final product can be mass-produced, sterilized and pre-packaged similar to syringes.

Next Steps

Currently cultivations of *S. cerevisiae* with controlled pH are being run, and these results will then be compared with results achieved from parallel cultivations done in bench-scale reactors.

Acknowledgements

The Novozymes Bioprocess Academy is acknowledged for the financial support of this project.

Also, I would like to thank all my supervisors for their continuing support.

List of Publications

Schäpper D., Muhd Nazrul Hisham Zainal Alam, Szita N., Eliasson Lantz A and Gernaey K.V. Application of microbioreactors in fermentation process development: a review. Analytical and Bioanalytical Chemistry, 395 (2009), 679-695

Inês Rodrigues da Silva

Phone: +45 4525 2979
Fax: +45 4588 2258
E-mail: ins@kt.dtu.dk
WWW: http://www.bioeng.kt.dtu.dk/
Supervisors: Jørn Dalgaard Mikkelsen
Anne S. Meyer

PhD Study
Started: February 2009
To be completed: January 2013

Enzymatic Production of Prebiotic Polysaccharides with Hydrophobic Decoration

Abstract
Prebiotics are non-digestible carbohydrates that beneficially affect the host by selectively stimulating the growth of a limited number of bacteria in the colon. Known examples of prebiotic food ingredients are oligosaccharides, e.g. fructans and fructooligosaccharides from Jerusalem artischokes, galactooligosaccharides from lactose and maltooligosaccharides from starch. The waste streams from agricultural industry are a large source of oligosaccharides with potential prebiotic effects. These streams comprise barley bran, sugar beet pulp and potato pulp from the brewing, sugar and starch industries. Modification of oligomers to achieve the desired prebiotic effect requires a number of specific enzymes which can be acquired by cloning and expression in the yeast *Pichia pastoris*. The oligosaccharides produced by the enzymatic catalyses may be purified and further modified by hydrophobic decoration.

Introduction

Functional food ingredients possessing potential health benefits have recently attracted strong attention. Some of the functional food ingredients are prebiotic oligosaccharides. Dietary fibers and prebiotics are non-digestible carbohydrates that beneficially affect the host by selectively stimulating the growth and/or activity of one or a limited number of bacteria in the colon. Oligosaccharides could be obtained as products of hydrolysis of plant derived polysaccharides, or directly from plant cell walls. Rational enzyme catalysed reactions are going to be develop to modify heterogeneous samples of substrates to create 'designer' oligosaccharides with defined structures and high prebiotic potential.

Specific objectives

The idea of the project is to use selective enzyme catalysts to convert polysaccharides into oligomers and furthermore decorate the oligomers by hydrophobic residues. Only few commercial enzymes are available for this task. Most of the commercial enzymes in addition contain other enzyme activities which degrade the desired oligosaccharides. Mono-component enzymes can, however, be produced by cloning and expression of suitable enzymes in the yeast, *P. pastoris.* This process can be performed in the laboratory at our department. Furthermore, the optimal conditions of enzymatically catalyzed reactions have to be worked out as well. This include up-scaling of the enzymatic reaction in order to deliver sufficient amount of oligosaccharides with potential prebiotic activity.

As an example we have expressed the enzyme of interests, Enzyme A, with a MW of 83 kDa in *P. pastoris*. *P. pastoris* has been used for production of GRAS (General Regarded As Safe) protein and enzyme products to food, feed and pharmaceutical applications. The methylotrophic yeast, *P. pastoris*, has been shown to be an outstanding host for high-level heterologous gene expression for both basic research and industrial use **[1**]. The recombinant proteins we want to produce are isolated by diversity screening or identified in genomic databases. The genes are inserted into *P. pastoris* under the control of the AOX1 (Alcohol Oxidase 1) promotor, in order to induce the gene of interest in the presence of methanol **[2, 3]**.

Results

The genetic engineered strain was grown in a 5L Sartorius Biostat Aplus fermentor using glycerol as the C-source and ammonia as the N-source. The production of the heterologous protein was followed by measuring the optical density (OD), determining the enzyme activity, and monitoring the MW by SDS-PAGE. The

OD (cell density) and the total level of enzyme are shown in Figure 1. The protein was also purified by Gel Filtration (PD-10 desalting columns) and by Immobilized Metal Affinity Chromatography (IMAC).

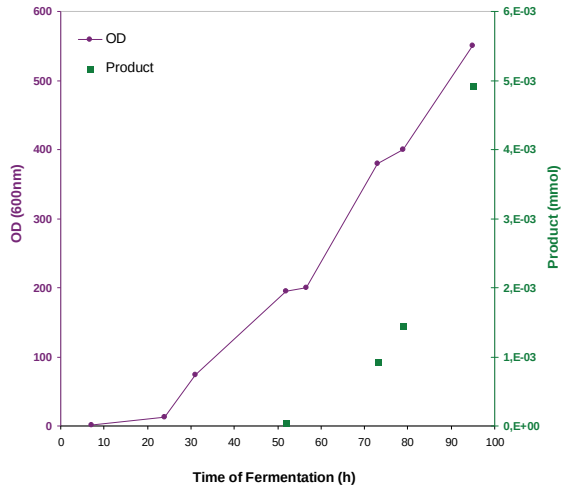

Figure 1: Cell density was followed at OD_{600} whereas the induction of Enzyme A was measured by the release of hydrolysed products.

The fermentation of Enzyme A was also followed by SDS–PAGE to verify the presence and yield of the enzyme. Except for the strong protein band of Enzyme A, only very few minor bands were present in the SDS-PAGE gel in Figure 2. The MW of Enzyme A was approx. 83kDa, which correspond to the theoretically molecular mass of the recombinant protein.

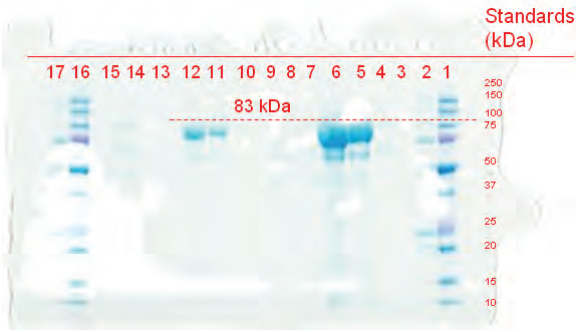

Figure 2: Protein samples from the methanol Fed Batch phase after analysis by SDS-PAGE. Wells were: 1. Standard - dual color; 2. Standard – unstained; 3.4. Enzyme A (52h) - 25 ul; 5. Enzyme A (73) - 25 ul; 6 Enzyme A (95h) - 25 ul; 10. Enzyme A (52h) - 5 ul; 11. Enzyme A (73h) - 5 ul; 12. Enzyme A (95) - 5ul;16 Standard - dual color; 17. Standard - unstained

The total activity of Enzyme A was also calculated and the fermentation results are sumarixed in Table I.

Table I: Activity of the enzyme of interests, Enzyme A, after induction with methanol

Time of Fermentation (h)	Average (U/mL)
52	0,2
73	4,2
79	9,5
95	42,3

Conclusions

It was possible to produce high level of the desired recombinant, Enzyme A, in a high density cell culture. The protein was expressed and identified positively by a specific enzyme assay. The expected MW was furthermore confirmed by SDS-PAGE. The activity of Enzyme A increased as expected in response to time and methanol induction. The Highest activity was detected after 95h of fermentation and the final amount was 42,3U/mL.

References

1. Cereghino, J. L. and Cregg, J. M. (2000). "Heterologous protein expression in the methylotrophic yeast Pichia pastoris." FEMS Microbiology Reviews 24(1): 45-66.
2. Cereghino, G. P. L.;Cereghino, J. L.;Ilgen, C. and Cregg, J. M. (2002). "Production of recombinant proteins in fermenter cultures of the yeast Pichia pastoris." Current Opinion in Biotechnology 13(4): 329-332.
3. Stratton, J.;Chiruvolu, V. and Meagher, M. (1998). High Cell Density Fermentation. Pichia Protocols. D. Higgins and J. Cregg. New Jersey, Humana Press. 103: 107-120.

Chutima Swangkotchakorn
Phone: +45 4525 2910
Fax: +45 4588 2258
E-mail: chs@kt.dtu.dk
WWW: http://www.capec.kt.dtu.dk
Supervisors: Rafiqul Gani
John M Woodley
Jan-Dierk Grunwaldt

PhD Study
Started: September 2008
To be completed: August 2011

Optimization of Tailor-Made Chemicals from Renewable Resources

Abstract
In the future, the chemical industry will need to be based on the conversion of renewable material, such as biomass and in particular lignocellulosic biomass. In order to meet the world's needs for industrial chemicals and liquid fuels, while minimizing the environmental impact, the economic and societal benefits would need to be maximized through the use of a new strategy. The objective of this strategy would be to develop a model biorefinery by matching a set of biomaterial feedstocks to an optimal set of end-point products (chemicals and fuels) through a range of sustainable processing routes. The optimal biorefinery model would be obtained by formulating and solving an optimization problem taking into account multiple criteria including biomaterial resources, product demands, processing routes and environmental impacts.

Introduction
The decrease in the world's crude oil reserves and environmental concerns have continuously driven the current chemical processes which are heavily reliant upon fuel from fossil-based resources to the use of renewable resources for the production of energy (needed, for example, in the transport and industrial sectors), as well as the production of a host of chemicals (needed, for example, to sustain chemicals-based consumer products). Industry based on conversion of material would preferentially use biomass, in particular lignocellulosic biomass, because it is a non-food feedstock and has desirable environmental and price attributes. The process for separation of biomass constituents and converting them to high value products is known as biorefining. The development of a model for an integrated biorefinery provides a good opportunity to develop new tools for application in the growing biorefinery manufacturing sector by creating new product streams [1].

In an initial conceptual study, two major pathways, hydrolytic and thermochemical, could be considered for lignocellulosic biorefineries. These processes include pyrolysis, gasification, thermochemical liquefaction, hydrolytic liquefaction, fermentation, and chemical synthesis. Because there are numerous ways to combine these operations, there is a need for a systematic methodology capable of generating, analyzing, and selecting the optimal sustainable processing routes for the conversion of a given set of raw materials into a defined set of desired tailor-made products. Bio-petrochemicals are those chemicals that are made to meet given specifications, by reducing and/or replacing non-renewable resources (such as petroleum) with appropriate bio-resources or a combination of both. In principle, economic and environmental impacts will be minimized through the optimal use of renewable and non-renewable feedstocks. Reliable optimization techniques will answer a number of important questions, such as:

- For a given set of product prices, what should be the optimal process configuration, i.e., what products should be produced, in what amounts and how?
- For a given product portfolio, can process integration methods be used to optimize production routes leading to a more sustainable alternative?

PhD-Project Objectives
The aim of this PhD project is to develop the optimal biorefinery model in systematic way. This biorefinery model will match a set of biomaterial feedstocks to an optimal set of end-point products (chemicals and fuels) and identify the potential routes for producing a set of precursor tailor-made chemicals. Environmental impacts will be minimized through the optimal use of renewable and non-renewable feedstocks, while the use of raw materials, utility chemicals, and energy resources

will be minimized to maximize economic and societal benefits.

Biorefinery model

1.1. Optimization problem

The problem for this biorefinery model is which process paths to select according to the defined objective function taking into account multiple criteria such as biomaterial resources, product demands, and cost of materials. The objective function is the function of binary variables (Y^{kk}), flowrates ($\overline{\overline{f}}_i^{kk}$), and known parameters (σ). The binary variables denote which process paths to use and what connection to make in order to obtain the desired product. The mathematical formulation of this problem is given as:

$$Maximize \quad z = \sum_{m}^{NF} f(Y^{kk}, \overline{\overline{f}}_i^{kk}, \sigma) W_m$$

Subject to Y^{kk}

Logical constraints

$$\sum_{kk}^{NF} Y_j^{kk} \le 1 \qquad \text{Eq.1}$$

Process models

$$h(\gamma_{i,kk,r}, \theta_{react,kk,r}, \alpha_i^{kk}, MW_i, SW_i^{kk}) = 0 \qquad \text{Eq.2}$$

Structural constraints

$$g_1(Y^{kk}, \overline{\overline{f}}_i^{kk}, \sigma) = 0 \qquad \text{Eq.3}$$

Structural constraints

$$g_2(Y^{kk}, \overline{\overline{f}}_i^{kk}, \sigma) \le 0 \qquad \text{Eq.4}$$

In the above optimization problem, the logical constraints represent the allowed operation in intervals (stages); the process models represent the mass balance for the processing paths; the structural constraints represent the allowed flowrates for selected processing paths.

1.2 Case study

Since ethanol is not only a fuel, but also a basic chemical for a lot of solvents, products and materials [2], it is therefore selected as a starting product for one model biorefinery. The production of ethanol by a hydrolytic pathway and an oil refinery process producing gasoline are considered here. The products of these two processes, ethanol and gasoline, will also be used as the feedstock for gasohol blending and for producing other chemicals. The ethanol production process is divided into six stages: size reduction [3], pretreatment [4], hydrolysis [3, 5], seed production [3], fermentation [3], and separation [6]. Lignocellulosic biomass is converted into sugars and solid lignin by either acid or enzymatic hydrolysis. Prior to the hydrolytic step, the biomass is pretreated to improve the overall sugar yields. Pretreatment includes both physical and chemical methods. The goal of pretreatment is to decrease the crystallinity of cellulose, increase the surface area of the biomass, remove hemicellulose and break the lignin seal. The various pretreatment methods considered in this study are (1) ammonia fiber explosion (AFEX), (2) dilute acid hydrolysis, (3) controlled-pH pretreatment, (4) aqueous ammonia recycle pretreatment (ARP), and (5) lime pretreatment. All the pretreatment technologies, except controlled-pH (which is a physical-chemical process) use chemicals such as dilute acids, ammonia, and lime. Two different operations are considered in the hydrolytic step to convert cellulose to glucose: (1) acid hydrolysis and/or (2) enzyme hydrolysis. For separation processes, three options are considered :(1) extraction (by ionic liquids or solvents), (2) with membranes, and (3) by adsorption.

1.3 Superstructure

The superstructure (see Fig. 1) representing all combinations of processing options for this case study consists of six different stages: thirty-three process steps; two source raw materials (biomass and crude oil); and three main sink products (ethanol, gasoline, and gasohol) and other valuable by-products e.g., acetic acid, furfural, 5-hydroxymethyl-2-furfural, lactic acid, glycerol, and succinic acid. The solution search space of the above optimization problem is also illustrated through this superstructure. Its configuration consists of stages representing (the principle process technologies) and different sub-processes (the operations) inside the stage. The source node represents the feedstocks while sink node represents the products. Chemical additives and utilities enter and leave in the vertical direction while chemical products move in the horizontal direction. Each of the process technologies is represented by an interval box (stage).

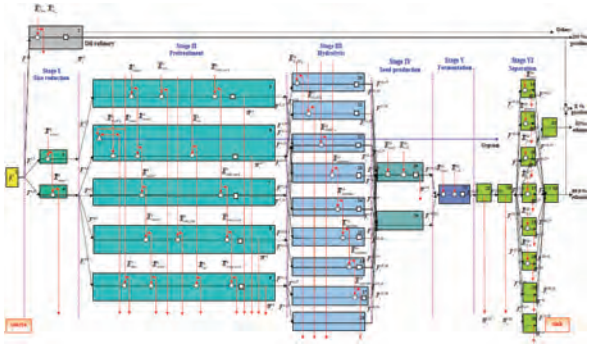

Figure 1: Superstructure for biorefinery model

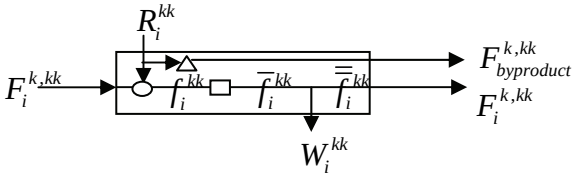

Figure 2: Flow pattern in a representative interval. Where O is mixing (chemicals being dissolved); Δ is vertical utilities (chemicals, waste) reacting to give by-products (by-products are horizontal); □ is horizontal raw material reacts to give main products; $\overline{\overline{\ }}$ is separation of utility chemicals

The operations within an interval are represented by symbols and their corresponding mass balance models. The transformation of the chemicals in an interval and the operations involved are shown in Fig. 2. There are three operating steps that can occur in one interval: chemical mixing, chemical reaction, and the utilities separation. The total model is obtained by collecting and connecting together the individual models for all the interval operations and connections. The model for this problem (considering ethanol and gasoline only) involves 19 block equations, 80867 single equations, 33 integer variables, 8 optimization block variables (including objective function and binary variables), 76927 single variables, 2 scalars and 8 matrix tables.

1.4 Model for processing steps

Chemical mixing $$f_i^{kk} = \sum_{i,k} F_i^{k,kk} + \alpha_i^{kk} \overline{R}_i^{kk} Y^{kk} \qquad \text{Eq.6}$$

In the chemical mixing operation represented by "Eq. 6", the mixed flow is obtained by combining the product chemicals (horizontal paths) and utility chemicals (vertical paths). $F_i^{k,kk}$ is the flow rate of chemical i coming to interval kk from interval k. $\overline{R}_i^{kk}$ is flow rate of utility chemical i coming to interval kk. The binary variable (Y^{kk}) indicates if utility mixing takes place or not. The consumption factor (α_i^{kk}) is used to state that only some parts of the chemicals are consumed.

Biomass reaction

$$\overline{f}_i^{kk} = f_i^{kk} + \left[\sum_r \gamma_{i,kk,r} \theta_{react,kk,r} \frac{f_{react}^{kk}}{MW_{react}} \right] MW_i \qquad \text{Eq.7}$$

When chemical reactions are taking place (represented by "Eq. 7"), the stoichiometric coefficients (γ) and conversion factors (θ) are used to calculate the flow of product after the reaction $(\overline{f}_i^{kk})$. These parameters are used to define how much the materials have been generated or consumed. The subscripts *r*, *react*, and *MW* indicate reaction number, reactant, and molecular weight, respectively.

Oil-refinery $$\overline{f}_i^{kk} = f_i^{kk} + \left(\sum_r \gamma_{i,kk,r} \theta_{react,kk,r} f_{react}^{kk} \right) \qquad \text{Eq.8}$$

For the oil refinery process, the model equation may be written in the form of chemical reactions. The right hand side term represents the generated or consumed chemical as in "Eq. 7". However, the γ and θ in this equation are used in mass proportions unlike in "Eq. 7" which is in mole. By using these parameters, "Eq. 8" can be used to calculate quantities such as the amount of products that can be produced with a given feed.

In separation process, the utilities and unwanted products are separated out in vertical direction by using separation factor (SW_i^{kk}). The flow after separation $(\overline{\overline{f}}_i^{kk})$ is the outlet flow of the interval. It will transform as the inlet flow $(F_i^{k,kk})$ of the next interval by connecting with connection link parameter that allow which interval can be match with another interval.

Utility chemical separation $$\overline{\overline{f}}_i^{kk} = \overline{f}_i^{kk} (1 - SW_i^{kk}) \qquad \text{Eq.9}$$

Results

In order to solve the optimization problem, there is a need to create a database containing values of the known parameters. In the case of chemical mixing, the amounts of chemicals coming in the vertical direction and used in specific process paths are required, while, stoichiometric coefficients, conversion factors, and molecular weights are needed for chemical reactions. The separation factors for every interval are also necessary to separate the utility chemicals, unwanted products, and by-products from the main products. The optimization problem ("Eqs. 1-9") is represented as an MILP problem, which is solved through GAMS/Cplex with the MIP option. That is, a set of linear constraints are solved and an objective function is maximized for specified sets of data from the database and subject to the process constraints, structural constraints, and optimization variables. Some of the data such as molecular weight, feed composition, and price of chemicals have 1-dimension while the connection links, consumption factors, and separation factors have 2-dimensions. The stoichiometric coefficients and conversion factors have 3-dimensions. Therefore, the known data are given as parameters in the form of vectors, matrices and tensors. As an example of the specified data, the (partial) table of $\gamma_{i,kk,r}$ (stoichiometric coefficients) is given in Table 1. It is for reaction number one (glucose production) that takes place in interval 6. Before this table is generated, all chemical reaction equations need to be listed in terms of reaction number and classified if they are going to be used in the interval. The minus sign indicates that this component is consumed in the reaction while plus is for generation. The zero value means that the compound does not take part in the reaction. The 2-dimentional parameters are also stored in this manner, where compounds are placed in the rows and the columns indicate the corresponding intervals, or, rows for the intervals and columns for the connection link parameters.

108 feasible solutions were generated from this MILP model. The maximization of the objective function, in this paper, considers four different scenarios. The first scenario maximizes the anhydrous ethanol production (case A). The second scenario maximizes the profit by including cost of material used (case B). The third scenario minimizes the waste water generated from the selected process (Case C). The last scenario maximizes ethanol, minimizes waste water and maximizes the profit (Case D). Table 2 summarizes the optimal

solutions corresponding to the four scenarios, where the X indicates the options used in the objective function.

Table 1: Stoichiometric coefficients table ($\gamma_{i,kk,r}$)

Component (i)	Interval(kk)	Reaction number(r)			
		1	2	3	4
glucan	6	-1	-1	-1	0
glucose	6	1	0	0	0
xylan	6	0	0	0	0

For cases A and B, the best processing route was found to consist of feed handling followed by size reduction with 35% moisture, dilute acid pretreatment, enzymatic hydrolysis, fermentation by *Z.mobilis*, ionic liquid [BMIM]Cl extraction. The optimal processing route corresponding to minimization of waste water (case C) was found to consist of the feed handling followed by size reduction with 35% moisture, APR pretreatment, enzymatic hydrolysis, fermentation by *Z.mobilis*, ethylene glycol extraction. However, the results from maximizing ethanol production, minimizing waste water and maximizing the profit at the same time showed that the processing route would be the feed handling followed by size reducing with 60% moisture, AFEX pretreatment, enzymatic hydrolysis, fermentation by *Z.mobilis*, ionic liquid [BMIM]Cl extraction. The ethanol in different purity will be used together with the gasoline product from oil refinery process as a feedstock of gasohol blending.

Table 2: Optimization results

Case	Max ethanol	Min waste H_2O	Max profit	Result/100 kg biomass		
				ethanol (kg)	H_2O (kg)	Profit ($)
A	X			**27.835**	484.390	22.309
B	X		X	**27.835**	484.390	**22.309**
C		X		21.101	**277.505**	9.936
D	X	X	X	**26.111**	**291.656**	**19.354**

Conclusions

We developed a biorefinery model for selecting processing routes subject to optimization of product yield, cost, and waste. The results show that this kind of long range planning model can be used to determine an optimal biorefinery model. As a proof of concept, ethanol was considered as one of the main products. The next stage of this work will investigate issues of blending of ethanol and gasoline to produce gasohol and diversion of glucose to produce the other chemicals. Using the current biorefinery model as a starting point, the full biorefinery model can now be easily be developed by extending in several directions. For example, adding more tailor-made chemical products, more processing path options and more starting materials, but keeping the same configuration of the superstructure. It is hoped that processing paths that need new technologies can be identified through this approach together with the optimal biorefinery. The current results with ethanol and gasoline, therefore, is a good starting point. Future work will address the processing cost of different routes to improve the accuracy.

Acknowledgements

The author acknowledges the financial support of the Technical University of Denmark.

References

1. A.V. Bridgwater, Chemical Engineering Journal, 91(2003) 87-102.
2. B.Kamm, M. Kamm, Applied Microbiology and Biotechnology, 64(2004) 137-145.
3. A. Aden, M. Ruth, K. Ibsen, J. Jechura, K. Neeves, J. Sheehan, and B. Wallace, NREL report TP-510-32438, (2002).
4. C.E. Wyman, B.E. Dale, R.T. Elander, M. Holtzapple, M.R. Ladisch, Y.Y. Lee, Bioresource Technology, 96(2005) 2026-2032.
5. C.N. Hamelinck, G.V. Hooijdonk, A. Faaij, Biomass and Bioenergy, 28(2005) 384-410.
6. M. Alvarado-Morales, J.Terra, K.V. Gernaey, J.M. Woodley, R. Gani, Chemical Engineering Research and Design, 87(2009) 1171-1183.

Conference presentations

1. C. Swangkotchakorn, J.D. Grunwaldt, J. M. Woodley, R.Gani, Biotrans 2009, Optimization of tailor-made chemicals from renewable and non-renewable sources, Bern, Switzerland, 2009.
2. C. Swangkotchakorn, J.D. Grunwaldt, J. M. Woodley, R.Gani, AIChe 2009, Sustainable bioprocess synthesis routes for tailor-made chemicals, Nashville, TN, USA, 2009.

List of Publications

1. C. Swangkotchakorn, J.D. Grunwaldt, J. M. Woodley, R.Gani, ESCAPR20, Optimization of long-term planning, supply chain and processing routes for tailor-made bio-chemicals, Naples, Italy, 2010

Per Aggerholm Sørensen

Phone: +45 4525 2927
Fax: +45 4588 2258
E-mail: pas@kt.dtu.dk
WWW: http://www.kt.dtu.dk
Supervisors: Søren Kiil
Kim Dam-Johansen
Claus Weinell, Hempel A/S

PhD Study
Started: February 2007
To be completed: January 2010

High Performance Anti-Corrosive Coatings

Abstract
One of the major modes of degradation of organic coatings immersed in sea water is called cathodic delamination. Cathodic delamination occurs on coating containing a defect, which allows corrosive species to react with the steel. Quantification of the most important steps responsible for cathodic delamination of organic coatings is an important step in indentifying the rate determining step. This knowledge may subsequently be used in the development of novel high performance anticorrosive coatings and lifetime predictions.

Introduction
The rapid oxidation of steel in aqueous environments necessitates the use of organic coatings to prevent corrosion. Despite significant improvement in existing coating technologies, problems continue to exist in the long-term protection of metal from aggressive environments because organic coatings are slowly degraded by the elements [1]. An example of coating failure leading to corrosion in a ballast tank is shown in figure 1.

Figure 1: Corrosion in ballast tank on cargo ship.

One of the main reasons for the lack of high performance anticorrosive coatings is the complexity of the coating-steel interfaced the number of factors affecting the performance and durability of anticorrosive coating systems. Besides the composition of the coating, which consists of binder, pigments, solvents, extenders and additives, the performance and service life of anticorrosive coatings depend on several different parameters such as type of substrate, pretreatment of substrate, curing, coating thickness, adhesion between the coating and substrate as well as several external environmental parameters [1].

Cathodic delamination
One of the major degradation modes for organic coating immersed in seawater is so-called "cathodic delamination". Cathodic delamination refers to the loss or weakening of the adhesion between a coating and the steel due to the reduction of oxygen, reaction 1.

$$2H_2O(l) + O_2(aq) + 4e^- \rightarrow 4OH^- \qquad (1)$$

The cathodic reaction is very complex and several reactive intermediates such as peroxides and free radicals may also be formed when oxygen is reduced on the steel surface.

The reduction of oxygen can occur on a corroding steel surface in which case it will be balanced by an anodic reaction (reaction 2), or under cathodic polarization by an external current.

$$Fe(s) \rightarrow Fe^{2+} + 2e^- \qquad (2)$$

The cathodic activity on the oxidized steel surface results in disruption of the bonds between the coating and the steel surface. Hence the bare steel is exposed to the surrounding environment, promoting corrosion and further degradation of the anticorrosive coating.

The reason for the cathodic delamination is proposed to be so-called polarization. The cathodic polarization of the steel arises when the anodic and cathodic reactions take place at a defect in the coating. The process moves forward under coatings due to continuous migration of water and oxygen (necessary for the cathodic reaction) and positive ions, necessary in order to locally balance the electric charge [2-4].

Results

The progress of the delamination front is proportional with the square root of time (see fig. 2). This suggests that interfacial diffusion along the coating-steel interface is likely to be the rate-determining step of the process of cathodic delamination because the mean diffusion length, $\bar{x}$, for a diffusion time, t, for linear isotropic and semi-infinite diffusion is given by

$$\bar{x}=2\cdot\sqrt{D\cdot t} \qquad (5)$$

Interfacial diffusion of cations may very well be the rate-determining step in cathodic delamination because of the observed inhibition of the delamination when the artificial defect was sealed with a molten mixture of bee wax and natural gum rosin after four weeks exposure. This procedure represses the transport of cations along the coating-steel interface from the defect to the delamination front without affecting the transport of cations perpendicular to the coating (i.e. through the intact or delaminated regions in the coating). Hence it is clear that the main route of the cations required for charge neutralization of the hydroxyl ions is along the coating-steel interface and not perpendicular to the coating system.

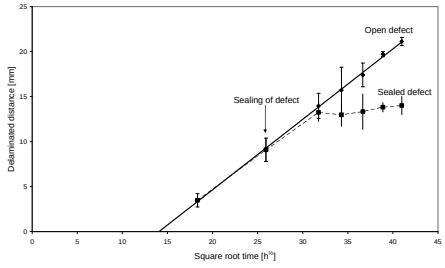

Figure 2: Delamination behavior for an inert pigmented epoxy coating in aerated 0.5 M NaCl solution at 25°C with an open defect and a sealed defect sealed after 4 weeks of exposure to seawater [3].

The inverse proportionality between the delamination rate and the tortuosity of the coating-steel interface given in figure 3 shows that cathodic delamination is a diffusion controlled process, where cations must migrate from a defect to the delamination front to neutralize the charge of hydroxyl ions generated by the cathodic reactions. This means that the migration of cations as well as the production and migration of hydroxyl ions along the coating-steel interface will determine the rate of cathodic delamination

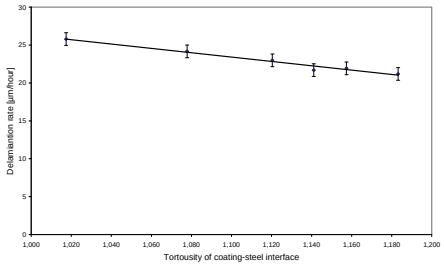

Figure 3: Effect of tortuosity of the coating-steel interface on the delamination rate of a commercial TiO_2 pigmented barrier coating [3].

Figure 4 shows that there is a strong relationship between cathodic delamination and the apparent diffusivity of sodium ions along a coating-steel interface. This confirms that the rate determining step for cathodic delamination of anticorrosive coatings is the transport of cations along the coating-steel interface.

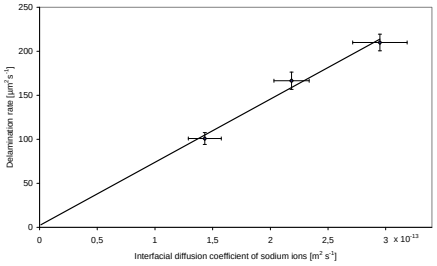

Figure 4: Relationship between cathodic delamination and the apparent diffusivity of sodium ions along the coating-steel interface for three commercial coatings [4].

Conclusions

The cathodic activity underneath a coating results in a highly alkaline environment with reactive intermediates, which destroy the adhesion between the coating and the steel. The rate determining step for cathodic delamination is the transport of cations along the coating-steel interface

Acknowledgments

The project is financially supported by the Technical University of Denmark and J. C. Hempel's foundation.

References

1. P. A. Sørensen, S. Kiil, K. Dam-Johansen, C. E. Weinell, "Anticorrosive coating – a review", J. Coat. Technol. Res., In Press.
2. H. Leidheiser, W. Wang, L. Igetoft, "The mechanism of cathodic delamination", Prog. Org. Coat. 11 (1) (1983) 19-40.
3. P. A. Sørensen, S. Kiil, K. Dam-Johansen, C. E. Weinell, "Influence of substrate topography on cathodic delamination of anticorrosive coatings", Prog. Org. Coat., 64 (2009) 142-149.
4. P. A. Sørensen, S. Kiil, K. Dam-Johansen, C. E. Weinell, "Cathodic delamination: quantification of ionic transport rates along coating-steel interfaces", Prog. Org. Coat., in press.

Samira Telschow

Phone: +45 4525 2952
Fax: +45 4588 2258
E-mail: ste@kt.dtu.dk
WWW: http://www.chec.kt.dtu.dk
Supervisors: Professor Kim Dam-Johansen
Associate professor Stig Wedel
Associate professor Flemming Frandsen
Kirsten Theisen, MSc. FLSmidth A/S

PhD Study
Started: March 2008
To be completed: February 2011

Investigation of the Reaction Mechanism and Kinetics During the Clinkerization of Cement Raw Meal at High Temperatures and Improvement of the Burning Technology

Abstract

In the cement manufacturing industry, reduction of the energy consumption and the CO_2 and NO_x emission levels while simultaneously increasing of the cement quality, is of great interest. The aim of this project is to investigate the development of the cement properties, depending on process conditions. Special focus is on the clinker properties: product composition, porosity and crystal/particle size distribution.

Introduction

Concrete is one of the most important materials in the construction industry world wide. The main component of concrete is cement, a hydraulic binder (characterized by its ability of hardening under water). The world production capacity of hydraulic cement was in 2006 3-5 Gt [1, 2]. One of the most common cement types is Portland cement, which consists of Portland cement clinker ground with ~5wt.% gypsum. By addition of granulated slag, pozzolan, sulfate or lime to Portland cement clinker, cement with special properties e.g. higher concrete strength or special resistance against aggressive agents is obtained. Examples are e.g. Blast-furnace cement, Pozzolan-lime cement or Supersulfated cement.

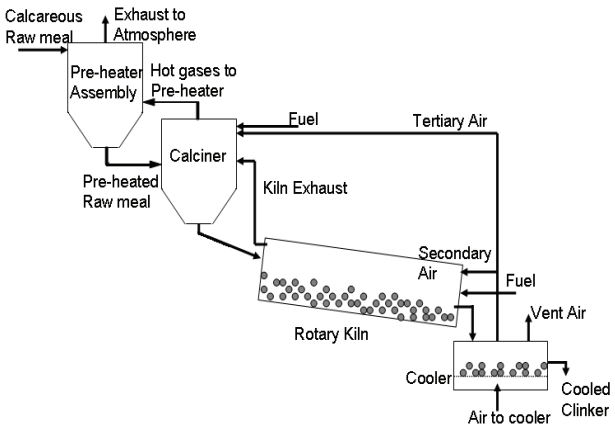

Fig. 1: A flow diagram of a cement kiln system [3].

A typical raw meal is composed of a mixture of calcareous material, such as limestone or marble, and SiO_2/Al_2O_3-rich clays (kaolinite, illite) or shale, as well as iron ore. Additionally, minor compounds e.g. Mg, Na, K, Ca as well as sulphates, phosphates, halogens etc. may also be present in the raw materials [4-6]. The crushed raw materials are blended and ground, before the raw meal is fed into the preheater section (a series of cyclones, see Fig. 1). There the materials are heated up to 800°C by hot gases from the calciner and kiln. Water, which is contained in the raw materials, is released. In the calciner most of the limestone is decomposed at ~900°C, i.e. CO_2 is removed and CaO is formed [7]. The degree of calcination is approximately 90-95%. In order to achieve the necessary temperatures in the calciner, fuel is burned there. Thereafter the material enters the rotary kiln. The material moves along the kiln to the lower end and is heated by hot gases from combustion of a secondary fuel at the outlet from the kiln. In the hot zone at the lower end of the kiln (gas temperatures of ~1800°C) the mixture reaches a temperature of ~1500°C, and melts partly [1, 7, 8]. In the kiln at temperatures of 1100-1500°C a series of reactions is occurring, resulting in the formation of the major crystal phases in the clinker product: Ca_2SiO_4 (belite), Ca_3SiO_5 (alite) and the so-called liquid phase (melt) $Ca_3Al_2O_6$ (aluminate) and $Ca_4Al_2Fe_2O_{10}$ (ferrite) [4, 7].

In the cooler, the hot clinker is rapidly cooled by heat exchange between the clinker solids and air, in order to

recover the heat. The clinker product is ground with gypsum and possibly other additives, stored, packed and sold.

The processes from drying of raw material to the clinkerization consumes an average thermal energy of 3.1-3.5 MJ/kg of produced clinker [2]. Additionally, ~100 kWh/t of electrical power is necessary e.g. for grinding of the raw material and the cement product [9]. The highest proportion of the electrical energy is attributed to cement grinding due to the clinker properties (the different clinker phases and other clinker characteristics).

Specific Objective

A critical product property is the clinker hardness, which is mainly influenced by the kind of crystal phases in clinker, the crystal/particle size distribution, and, the clinker porosity. Decreasing the clinker hardness facilitates the cement grinding and reduces the energy consumption of this process, as well as the material attrition of the mills. In general, the smaller the crystal sizes in clinker, the higher the grindability of clinker. The preferred crystal phase in clinker is alite, since it controls its setting and hardening of cement. Also, it forms more brittle crystals, containing micro-cracks, than belite, which eases the clinker grinding. Therefore, high alite and low belite concentrations in the clinker are desired. The distribution of the clinker phases influences greatly the grindability. Often, belite crystals are arranged in clusters (Fig. 2), which are harder to grind than belite crystals distributed between alite crystals.

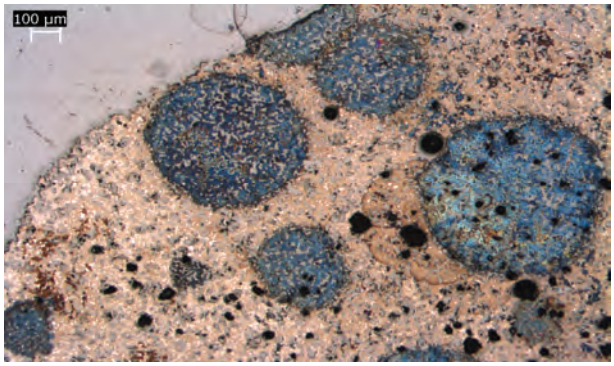

Fig. 2: Belite crystal cluster (blue areas) surrounded by alite crystals (brownish areas).

The focus in this project is on how the three properties (crystal phases, the crystal size distribution and the porosity) are developed as a function of different process conditions,

- Raw mix composition
- Raw mix particle size distribution
- Maximum burning temperature
- Heating rates
- Burning time
- Rotation velocity

The clinker formation experiments need to be automated as much possible, in order to study the influence of only one parameter at a time on the clinker property development. Therefore, a new setup is build (Fig. 3). It consists of two parts: 1) a horizontal heating furnace and 2) a pushing system. In the furnace, a temperature gradient along the horizontal axis from 900 to 1600 ^{o}C can be achieved. The sample is inserted into the ceramic tube of the pushing system (2c), which is pushed with a defined velocity into the furnace and thereby simulating different heating rates. Additional to the horizontal motion of the ceramic tube, it is rotating around its axis (up to 50rpm).

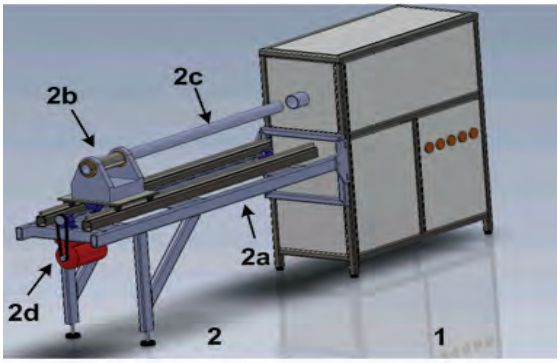

Fig. 3: Experimental set up. 1) The heating furnace; 2) the pushing system consists of a steal frame 2a) with two sliding bars, a sliding carriage 2b) holding a ceramic tube 2c), which carries the sample. The carriage is moved along this threat rod by a step motor 2d).

Acknowledgement

The Danish National Advanced Technology Foundation and FLSmidth A/S are acknowledged for financial support of this project.

References

[1] U.S. Environmental Protection Agency, Inventory of U.S. Greenhouse Gas emissions and Sinks: 1990-2006, 2008.

[2] Verein Deutscher Zementwerke e.V., Forschungsinstitute der Zementindustrie, VDZ Activity report 2005-2007, Verlag Bau + Technik GmBH, Duesseldorf, 2008, p. 26, 74.

[3] A. Z. Jensen; Master thesis; Institute of chemical and biochemical engineering at DTU; 2008.

[4] G.C. Bye, Portland Cement-Composition, Production and Properties, Pergamon Press, Oxford, 1983, 8pp.

[5] F.P. Glasser, J.I. Bhatty, F. McGregor, S.H. Kosmatka, Innovations in Portland Cement Manufacturing, Portland Cement Association, Skokie, Illinois, 2004, p. 332.

[6] F. Nishi, Y. Takéuchi, I. Maki; Zeit. Krist. 172 (1985) 297.

[7] H.F.W. Taylor, Cement Chemistry, Academic Press Thomas Telford, London; 1997, 55pp.

[8] J. Klauss, ZKG international 53 (3) (2000) 132-144.

[9] V. Johansen, T.V. Kouznetsova; 9th ICCC; New Delhi, 1992.

Lise Vestergaard Thomassen
Phone: +45 4525 2979
Fax: +45 4593 2906
E-mail: lvt@kt.dtu.dk
WWW: http://www.bioeng.kt.dtu.dk
Supervisor: Anne S. Meyer

PhD Study
Started: April 2008
To be completed: March 2011

Statistically Designed Optimisation of Enzyme Catalysed Starch Removal from Potato Pulp

Abstract
Potato pulp is a byproduct resulting from the industrial manufacture of potato starch. The pulp is a rich source of biologically functional dietary fibers, but the targeted valorisation of the fibers requires removal of the residual starch from the pulp. The objective of this study was to release the residual starch, making up 21-22% by weight of the dry matter, from the potato pulp in a rational way employing as few steps, as few enzyme activities, as low enzyme dosages, as low energy input, and as high pulp dry matter as possible. Statistically designed experiments were performed and the data demonstrated that all the starch could be released from potato pulp in one step when 8% w/w dry potato pulp was treated with 0.2% v/w (enzyme/substrate) of a thermostable *Bacillus licheniformis* α-amylase at 70 °C for at least 65 min. The study also indicated that the amount of other carbohydrates released from the pulp during the release of starch was less than using the AOAC Official Method 985.29 and another recently published starch release method employed as a pretreatment for enzymatic upgrading of a pectinaceous potato pulp fiber.

Introduction
Potato pulp consists mainly of disrupted tuber cell walls, potato skin fractions and residual intact cells. The pulp is primarily used as cattle feed but it is of interest to identify new alternative products and valorisation routes for the potato pulp.
Previous studies have examined the fermentability of enzymatically solubilised fibers from potato pulp. One study was in essence a small human intervention trial, involving seven healthy human volunteers. The results indicated that the fibers were fermented in the human gastrointestinal tract, confirming the dietary fiber properties of the soluble potato fiber [1]. Another study showed that rats fed with a similarly enzymatically solubilised dietary fiber fraction from potato pulp had significantly lower weight gain than control groups of rats that were fed with a cellulose fiber control or with an insoluble potato fiber fraction [2].
In general, procedures for production of dietary fiber always include removal of starch from the fiber fraction followed by some kind of extraction/solubilisation of the dietary fiber. The starch removal procedure employed is typically based on the methodology employed in the AOAC method 985.29 [1,2,3].
Starch removal to obtain dietary fibers is usually accomplished via a three step, sequential enzymatic treatment procedure involving the sequential application of different enzymes, α-amylase, protease, and amyloglucosidase, reacting at different temperatures and pH values for removal of starch.

Specific objectives
The classical starch removal procedure having origin in dietary fiber analysis methods is not necessarily optimal for large scale valorisation of potato pulp. This study was undertaken with the objective of assessing whether the enzymatic starch removal process on potato pulp could be rationalised. The influence of different reaction factors on the amount of starch released from potato pulp was therefore examined.

Experiments
The theoretical maximum amount of starch in pulp was determined via enzyme catalysed starch removal according two benchmark methods: The AOAC Method 985.29 [4] and the method described by Meyer *et al.* [3].
Statically designed experiments were performed to find the rationalised conditions under which the maximum amount of starch was released. First a screening experiment comprising different combinations of four factors was conducted: dry matter (0.8-8% w/w), α-amylase (Termamyl® SC) (0-1.6% v/w E/S), incubation temperature (70-95 °C) and incubation time (10-60

min). In the second design the amount of dry matter was kept at 8% w/w and the design comprised different combinations of three factors: α-amylase (0.2-2.4% v/w E/S), incubation temperature (70-95 °C) and incubation time (10-85 min). At last a time study was performed to find out if it was possible to decrease the incubation time (45-48 min).
The amount of starched released was determined by measuring the amount of glucose released applying a glucose oxidase assay. The amount of released and remaining carbohydrates in the potato pulp was determined by hydrolysis of the samples with 2 M TFA at 121 °C for 2 hours followed by analysis by HPAEC-PAD.

Results
The maximum amount of starch released from potato pulp was determined to 21-22% by weight by the AOAC method 985.29 (method 1) and the method used by Meyer *et al*. (method 2).
To assess the optimal procedure for starch removal from potato pulp two statistical experiments were designed. The first experiment showed that it was possible to release all the starch by applying only α-amylase to 8% w/w potato pulp. In figure 1 a typical response surface made from some of the data in this experiment is shown.

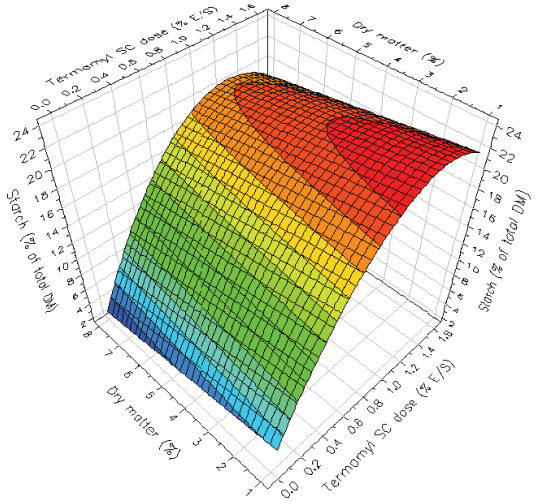

Figure 1: A three-dimensional response surface showing the starch yield (% by weight of dry matter) as function of dry matter (% w/w) and Termamyl® SC (% v/w E/S).

In the second experiment it was found that the maximum amount of starch could be released from potato pulp applying 8% w/w potato pulp and 0.2% v/w E/S α-amylase at 70 °C for 85 min (method 3). The following time study indicated that the incubation time could be decreased to 65 min and all the starch was released. Besides release of all the starch, other carbohydrates were also released (table 1).

Table 1: Carbohydrates removed from the potato pulp during release of starch.

% by weight of total dry matter	Method 1	2	3
Glucose	22.3 ± 0.6	21.0 ± 0.9	22.3 ± 1.0
Galacturonic acid	4.9	4.5	0.7
Rhamnose	0.4	0.4	0.0
Galactose	6.0	7.7	0.9
Arabinose	1.1	1.1	0.2
Non-solubilised	54.4 ± 6.5	51.1 ± 2.1	73.4 ± 4.8
Unknown	10.9	14.2	2.5

From table 1 it can be seen that the amount of starch released (as glucose) was the same applying the three different methods. Furthermore, it can be seen the amount of other carbohydrates released is less applying method 3 compared to method 1 and 2.

Conclusions
It was possible to identify a method by which the theoretically maximal amount of starch was released from potato pulp, i.e. with the theoretical maximum defined by starch removal used in AOAC method 985.29 [4] and the method applied by Meyer *et al*. [3]. The new method was rationalised by employing a higher level of pulp dry matter (8% w/w), less enzyme (0.2% v/w E/S Termamyl® SC), a lower temperature (70 °C), and less total reaction time. The results furthermore indicate that this new, rational starch removal method for potato pulp, leaves more remaining pectin in the pulp after release of starch.

Acknowledgments
This study was supported by the Danish Strategic Research Council's Committee on Food and Health (FøSu, Center for Biological Production of Dietary Fibres and Prebiotics). Financial support from the FOOD Denmark Graduate School, Center for Advanced Food Studies, Denmark, was also acknowledged and Lyckeby Stärkelsen, Kristianstad, Sweden for supplying the potato pulp.

References
1. Olesen M, Gudmand-Hoyer E, Norsker M, Kofod L, Adler-Nissen J. Eur J Clin Nutr 1998;52:110-4.
2. Lærke HN, Meyer AS, Kaack KV, Larsen T. Nutrition Research 2007;27:152-60.
3. Meyer AS, Dam BR, Lærke HN. Biochem Eng J 2009;43:106-12.
4. Prosky L, Asp NG, Furda I, DeVries JW, Schweizer TF, Harland BF. J Assoc Off Ana Chem 1984;67:1044-52.

List of Publications
1. L. V. Thomassen, A. S. Meyer, Enzyme and Microbial Technology (2009) In press.

Stuart R Tindal

Phone: +45 4525 2950
Fax: +45 4588 2258
E-mail: st@kt.dtu.dk
WWW: www.kt.dtu.dk
Supervisors: John M Woodley
Suzanne Farid, UCL
Helen C Hailes, UCL
Ian Archer, Ingenza Ltd

PhD Study
Started: September 2006
To be completed: August 2010

Experimental Toolbox for Assessment of Industrial Biocatalysts

Abstract

Biocatalysis is a rapidly developing area of biotechnology that offers novel and alternative synthetic strategies to a range of useful chemical products. In particular chiral intermediates represent a huge potential market for biocatalysis-based products. However, enzyme stability and therefore low productivity, has hindered the implementation of many enzymes including oxidases. Using 3 case studies each with a different form of D-amino acid oxidase (AAO) and reactor setup an assessment of the maximum productivity for the deracemisation of racemeric amino acids was made. An experimental toolbox was used generate modelling data which assessed the industrial application of these biocatalysts.

Introduction

Biocatalysis contributes to just over 2% of the total $27 billion market for basic, intermediate, fine and specialty chemicals and polymers [1]. The potential for this to grow is enormous, especially given the current pressures to reduce waste and increase process sustainability, atom efficiency and product quality. A key area in which biocatalysis can challenge chemical catalysis is in the production of chiral molecule building blocks for use in the chemical development of new and existing pharmaceuticals [2]. One such example is the deracemisation of chemically produced amino acid racemates into their corresponding optically pure forms. The chiral raw materials and synthetic intermediates market currently stands at $15 billion and is growing at 9.4% annually [1]. The high enantio- and regioselectivity of biocatalysis is well suited to chiral organic synthesis and the progress of techniques in bioinformatics and microbial genomics are broadening the capacity and availability of new biocatalysts. A promising prospect is the synthesis of optically pure amino acids in a process that incorporates a hybrid chemoenzymatic reaction to convert a racemate into an enantio-pure material.

Technology

The reaction case studies are based on the oxidation of D-amino acids into their corresponding α-keto acids for use in a deracemisation process [3]. Further, to improve the yield beyond 50%, a non-selective chemical reducing agent is coupled to the reaction to produce the desired enantiomer in excess of 99.5% as shown in Figure 1 [4]. The production of these key building blocks is essential in many important pharmaceutical products. Currently, the reaction has been scaled-up to an industrial level with some substrates and has shown potential to become a valuable biocatalytic synthetic process [5].

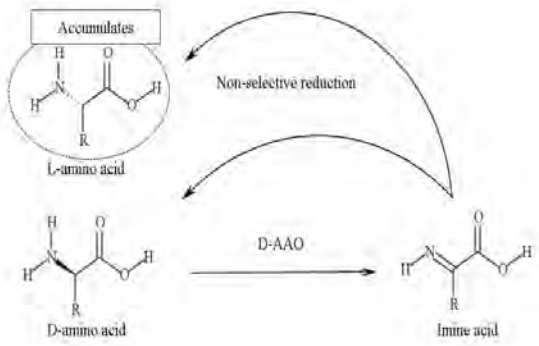

Figure 1: Generic deracemisation process using AAO. The AAO reacts much faster with one of the enantiomers oxidising it to the imine and the chemical reducing agent produces an equal amount of both enantiomers. Hence the non-reactive enantiomer accumulates resulting in an enantiomeric excess above 99.5% [3].

The objective of this project is to use experimental data collected in scale-down reactors to model the factors that affect the productivity of AAO. The detrimental variables uncovered will be used in a stability improvement study which models the need for changes in the process conditions, reactor design and biocatalyst. These models will be used to improve the biocatalyst industrial potential and predict the productivities at scale.

Biocatalyst testing

The aim of this project is to create and develop biocatalyst testing methods and create models that can be used to rapidly assess and predict its industrial potential. This data can be collected by testing for the maximum enzymatic turnover number (ToN) along with determining the limitations of the process. Developing these testing methods at industrially relevant conditions can highlight mechanisms and major factors responsible for low productivity. The models formed from the test's data can be used to intelligently redesign or further optimise the bioprocess. This method should significantly decrease the time and cost of implementation of a biocatalyst into an industrial process.

Toolbox

As there are a significant number of factors that affect the productivity (space time yield and maximum product concentration) a simplification in data collection is needed. Creating an experimental toolbox (Figure 2) that tests different facets of the biocatalyst's potential and provides modelling data that can be used to predict the process at scale will streamline that data collection. The first part of the experimental toolbox replaces the reactive substrates with chemical analogues and performs a mimic of the reaction by removing the dynamic changes resulting from the conversion. This experimental tool determines the reactor stability of the biocatalyst by incremental activity testing. The data and model from this method can be used in conjunction with the second part of the toolbox. This toolbox part uses conditions found at the end point of a reaction (fully converted substrate). This method examines the residual activity loss along with product stabilities. Monitoring changes in the biocatalyst physical and chemical form indicates mechanisms of deactivation and enables focused redesign.

The third experimental part of the toolbox performs batch reactions, varying the conditions to determine their response on productivity, space time yield and final product concentration/yield. Starting at an initial concentration of substrate that exceeds what a specific loading of biocatalyst is capable of converting gives the maximum ToN at those reactor conditions. Having weightings on the responses will allow the process to be optimised for a given set of industrial criteria.

Conclusions

Over the course of this project three enzyme forms of AAO have been tested in three different reactor setups. Two of these biocatalyst forms; soluble ammonium sulphate cut and a commercially immobilised AAO were found to have insufficient reactor stability. Both the deactivation routes of the two forms were found from part I and II of the toolbox. Optimised productivities calculated from the III part of the toolbox did not meet the desired criteria and therefore an intelligent redesign was implemented.

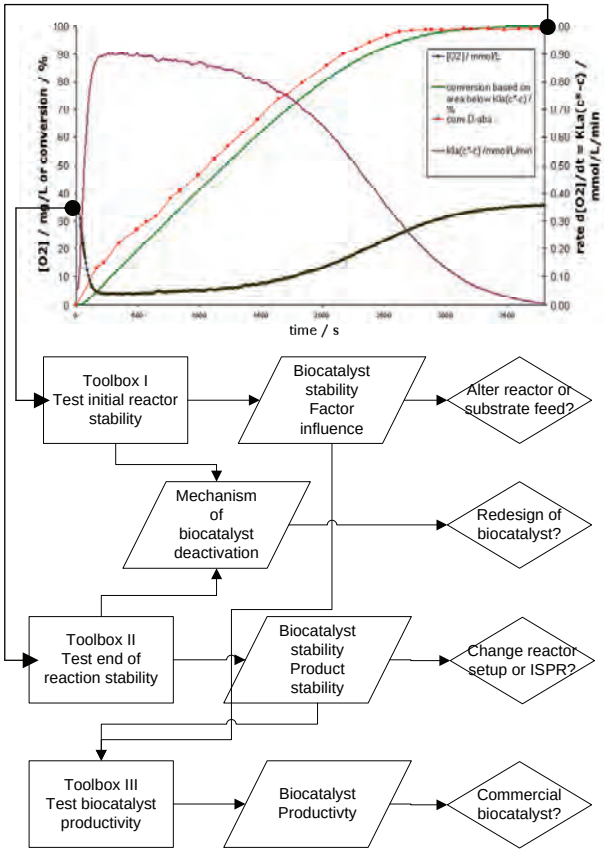

Figure 2: flow-sheet of data collection from experimental test toolbox. Toolbox I provides information on biocatalyst reactor stability. Toolbox II provides information on reaction solution stability. Toolbox III uses data from part I and II to assess the biocatalyst's productivity.

Current work on a third form of DAAO expresses the AAO in *Pichia pastoris*, freeze dried and permeabilized. The reactions are being performed in a pressurised biocatalyst reactor to alleviate negative interfacial effects as well as improving oxygen mass transfer. Initial studies have shown improved activity and stability giving enhanced productivities when compared to the two previous case studies.

Acknowledgements

I would like to thank the EPSRC, DTU and Ingenza Ltd for the funding of this project and DTU for hosting my laboratory studies.

References

[1]. Schmid A, Hollmann F, Park JB, Buhler B. 2002. *Current Opinion in Biotechnology* **13**:359-368.

[2]. Pollard DJ, Woodley JM. *Trends in Biotechnology*. 2007. **25**(2):66-73

[3]. Fotheringham, I.; Archer, IVJ; Carr, R.; Speight, R.; Turner, NJ. *2006. Biochem. Soc. Trans*, **34,** *287-290.*

[4]. Archer, IVJ; Fotheringham, I.; Carr, R.; Arnold, SA. *2008. World Intellectual Property Organization., WO2008080138*

[5]. Turner, NJ. *2004. Current Opinion in Chemical Biology.* **8,** *114-119.*

Maja Bøg Toftegaard

Phone: +45 4525 2830
Fax: +45 4588 2258
E-mail: mbt@kt.dtu.dk
WWW: http://www.kt.dtu.dk
Supervisors: Anker Degn Jensen
Peter Glarborg, Peter Arendt Jensen
Bo Sander, DONG Energy

Industrial PhD Study
Started: April 2007
To be completed: October 2010

Oxy-Fuel Combustion of Coal and Biomass

Abstract
A drastic decrease of the CO_2 emission from power production is necessary to limit global warming. One of the promising technologies which will enable almost complete capture of CO_2 from power plants burning fossil fuels is oxy-fuel combustion. There is a need for a more in-depth insight into the fundamental aspects of the effects of oxy-fuel combustion regarding combustion chemistry and the effects on especially ash quality in relation to cement and concrete production. The PhD study includes an experimental and theoretical investigation of these aspects.

Introduction
Several technologies have been proposed and are investigated for carbon capture and storage (CCS), i.e. the removal of CO_2 from exhaust gases from e.g. power plants or other fossil fuel fired processes. Oxy-fuel combustion is one of the more promising of these technologies [1]. Figure 1 shows the principle in an oxy-fuel power plant. The fuel, e.g. coal, biomass, or others, is burned in an atmosphere consisting of oxygen and recirculated flue gas (consisting primarily of CO_2 and water). The resulting flue gas has a CO_2 content of up to 95 % on a dry basis compared to about 14 % from a conventional plant. The CO_2 can be stored after cleanup and compression.

Generally, there is insufficient knowledge on many fundamental and practical aspects related to the change from the conventional to the oxyfuel combustion process. From a chemical engineering point of view this concerns among others the emission levels of CO, NO_x, and SO_2, the quality of the ash fractions, the risk of increased corrosion due to a change in the chemical composition of the combustion atmosphere and deposits, and the temperature and radiation in the boiler which are affected by the changed gas phase composition, i.e. the increased levels of CO_2 and water. Especially aspects regarding the effect of the flue gas cleaning strategy on fly ash quality and corrosion still need significant further investigations. Furthermore, the effect of using biomass as fuel in CCS has only been investigated experimentally by very few research groups [1]. This approach involves the possibility of operating power plants with negative CO_2 emissions.

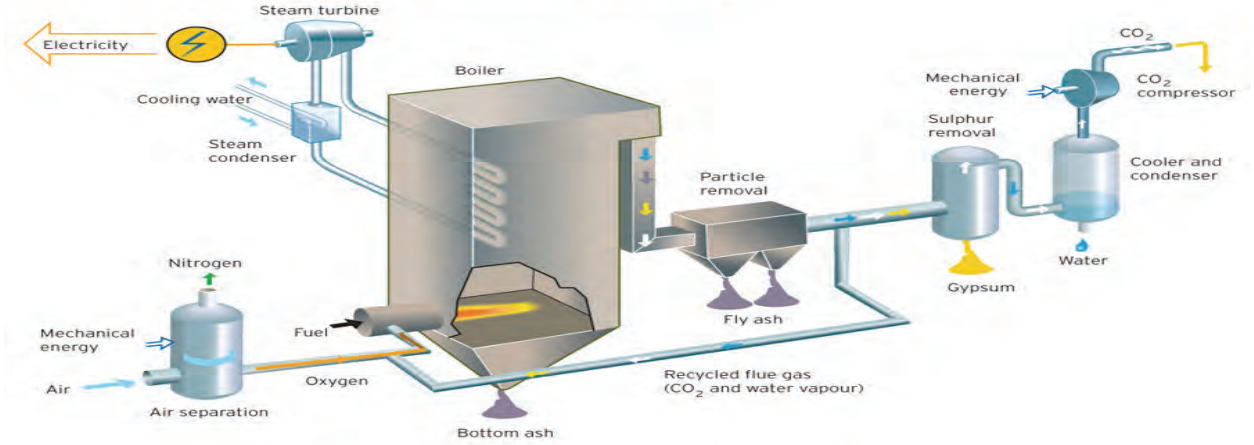

Figure 1: Possible layout of an oxy-fuel power plant showing the air separation, flue gas recirculation, and flue gas treatment new to the plant compared to a conventional air-fired power plant. Graphics: www.kjell-design.com

Specific Objectives

The aim of the PhD study is to strengthen the scientific basis for the development and application of the oxyfuel combustion technology to thermal power plants. Both experimental and theoretical investigations of the fundamental aspects of the combustion chemistry obtained when burning coal and biomass are performed. Specific topics addressed are:

- Ash composition and quality, especially related to sulphur retention – because of the application of fly ash in cement and concrete production this is a very important area of investigation.
- Deposits composition – the chemical composition is indicative of the risk of corrosion on heat transfer surfaces.
- Emissions of CO, NO_x, and SO_2 from the boiler – the recirculation of flue gas will play a role in the obtained levels of the emissive gas phase components together with the chosen strategy for flue gas cleaning.
- Necessary excess oxygen level – Oxygen is produced in a cryogenic air separation unit. Excess oxygen for combustion is thus associated with a significant economic penalty compared to air-firing.
- The effect of co-firing coal with wheat straw.

The results obtained in the experimental investigations will be applied in a validation of a Computational Fluid Dynamics (CFD) model for oxyfuel combustion. The CFD model will be built as part of the PhD study and should be applicable for design and process optimization in full scale boilers.

Experimental setup

An existing experimental setup is applied in the investigations, see Figure 2. The setup consists of a cylindrical reactor (inner diameter 30.5 cm) with a swirl burner. The setup is equipped with a solid fuel feeder, a fly ash sample system (not shown), and 8 measuring ports for temperature and gas phase composition measurements. The setup is run at a thermal input of approximately 30 kW.

As part of the project the setup has been rebuilt to be able to run at oxyfuel conditions. In full scale, flue gas will be recirculated to adjust the flame temperature, but in the pilot plant flue gas recirculation is not applied. Instead, synthetic flue gas consisting of pure CO_2 from gas cylinders is used. Pure oxygen is likewise delivered to the setup from gas cylinders and mixed with CO_2 in a special mixing panel. A system to enable addition of both N_2, NO and SO_2 to the CO_2 stream is likewise included in the setup.

Conclusions

The initial experiments are currently being performed and reference cases for air and oxy-fuel combustion are being established. It has been shown that it is possible to obtain stable combustion conditions with satisfactory burnout of coal in both air and the O_2/CO_2 atmosphere.

The different probes which have been manufactured as part of the project to enable the characterisation of the combustion process (FTIR probe for gas phase temperature and composition, IR CCD camera for particle temperatures, and a deposition probe) are being tested.

The work will continue with investigations of the areas of interest mentioned in the section Specific Objectives.

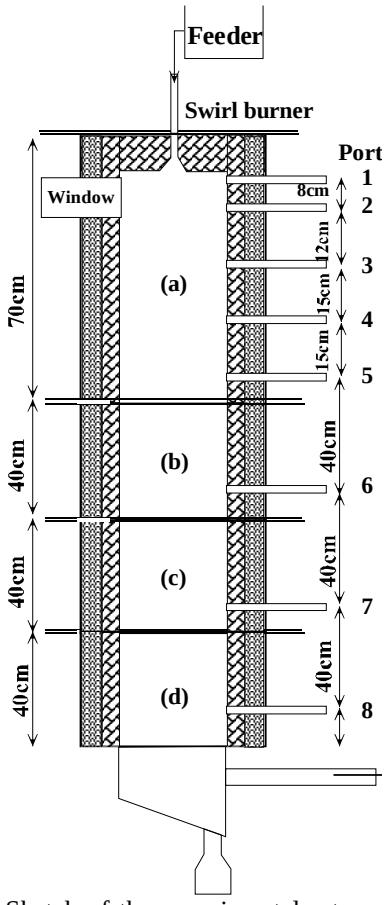

Figure 2: Sketch of the experimental setup – a 30 kW down-fired swirl burner.

Acknowledgements

The PhD study is part of PSO project 7171 (Oxy-fuel Combustion for below zero CO_2 emissions) which is carried out in collaboration between DONG Energy, Vattenfall A/S, the Combustion and Harmful Emission Control (CHEC) group at the Chemical Engineering department (KT), and department of Manufacturing Engineering and Management, DTU.

The PhD study is financially supported by PSO, DONG Energy, and the Ministry of Science Technology and Innovation (VTU).

References

1. M.B. Toftegaard, J. Brix, P. Glarborg, P.A. Jensen, A.D. Jensen. Oxy-Fuel Combustion of Solid Fuels. Prog Energy Combust Sci, *submitted*.

Carlos Axel Díaz Tovar
Phone: +45 4525 2808
Fax: +45 4593 2906
E-mail: adi@kt.dtu.dk
WWW: http://www.capec.dtu.dk
Supervisors: Rafiqul Gani
Bent Sarup, Alfa Laval

PhD Study
Started: May 2008
To be completed: April 2011

Systematic Methodology and Property Prediction of Fatty Systems for Process Design/Analysis in the Oil and Fat Industry

Abstract
The solvent recovery section of a soybean oil extraction process has been studied with special emphasis on the effect of design variables on the performance of the process. Two different sets of simulations were carried out to analyze their effects. The first set of simulations used the Plackett-Burman (PB) methodology to establish the parameters that make significant impact on the process. Meanwhile, the results of the second set of simulations were used to generate a reduced model for all the response variables. Results showed that with the PB methodology a reduction of 40% in the number of process variables to be considered in the performance analysis could be achieved. Even tough, the response surface pointed out that the process is already in the optimum zone, optimization the reduced model indicated that further improvement in the amount of hexane recovered could be obtained.

1. Introduction

Fats and oils are a source of energy and play an important role in human nutrition. The production of edible oils/fats involves a great variety of processing steps and unit operations, and state of the art in process modeling has only to a very limited extent penetrated this industry and part of the reason is the complex nature of the lipid systems involved. Lipid technology refers to products and processes (modification, purification, separation, etc.) that involve fatty acids, their derivatives, and related substances. This work develops computer aided methods and tools for the systematic design and analysis of a process that employs lipid technology, the solvent recovery section of the soybean oil extraction process.

It is known that the soybean oil is almost exclusively produced by solvent extraction and the most widely used solvent for extraction of oil from oilseeds is hexane, because it has high solubility for fats and oil, chemical stability and a suitable vapor pressure allowing for easy separation by flash and stripping operations [*1*]. The hexane recovery section (see **Figure 1**) includes four parts: An oil recovery, a condensation system, a mineral oil system and a water-solvent separation. After the "washing" of the soybean flakes, both the miscella (mixture of oil and solvent) and the white flakes (extracted flakes wet with solvent) are heated separately to remove the solvent. The flakes go to a desolventiser–toaster–drier–cooler (DTDC) unit and the miscella enters the first part of the solvent recovery section, the oil recovery system, where the oil is concentrated. Here the solvent is removed from the oil that is subsequently concentrated nearly to 100% (crude oil). All the recovered solvent vapors mixed with steam, including those coming from the DTDC facility, are retrieved by means of three sub-systems that make part of the solvent recovery system: the condensation, the MOS (mineral oil system), and the water–solvent separation. Therefore, vapors are condensed and the residual vapors are captured in the mineral oil system. The condensates from the condensation system enter a water–solvent separation section, where the solvent is recovered and after mixing with a make-up stream, is redirected to the extractor.

The aim of this work is to optimize the performance of the solvent recovery section of the soybean oil extraction process in terms of the important design variables. This is not an easy task since the number of design variables involved in the process (temperature, pressure, and number of stages) is quite large, and optimization of the process performance with a rigorous simulation model in this case, is quite complex. An alternative approach is to use techniques such as the Plackett-Burman and the Full Factorial Designs [2], which are useful tools to identify, observe, and analyze the critical parameters of the process and their effects on the process behavior subject to changes in the design variables; the objective here is to obtain a reduced

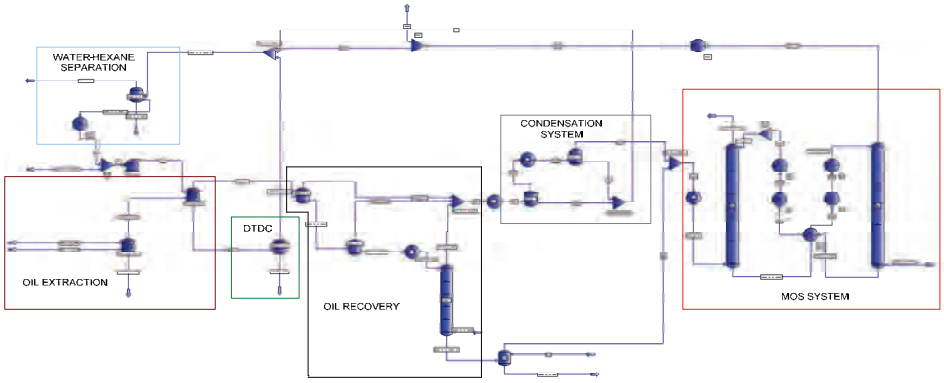

Figure 1: Solvent Recovery PRO II Model [*1*]

model. Two techniques are considered here: the first applies a screening procedure to discard design variables that do not affect the overall performance of the process; the second establishes the order to perturb the remaining design variables to observe their effect on the process performance defined in terms of the identified process parameters.

The solution procedure employed in this work consists of three main steps: Process simulation, process model reduction, and process optimization. The process simulation step consists of generation of the properties of the chemicals (lipid compounds: glycerides, fatty esters, and unsaponifiable compounds) present in the process and creating a database for use in process simulation models. The model reduction step applies design of experiments techniques to identify the most significant design variables, the parameters affecting the process performance, and creates a reduced "quadratic" model relating the design variables and the process parameters. The optimization step determines the design variables values corresponding to the optimal process performance.

2. Methods and tools used

2.1 Property prediction of lipid compounds

Oils and fats oils are complex chemical mixtures of compounds such as glycerides, fatty acids, fatty esters, sterols, and tocopherols. In this work, thirteen different types of the most widely used vegetable oils (soybean, sunflower, canola, etc.) and two different kinds of fats (lard and tallow) were reviewed in the literature in order to define their typical chemical composition.

The database created from this literature review includes a total of 28 fatty acids (from C6 to C24), 51 triacylglycerides (from C28 to C58), 44 diacylglycerides (from C14 to C40), 16 monoacylglycerides (from C8 to C22), 58 fatty esters (methyl and ethyl from C6 to C24), and 26 minor compounds (sterols, tocopherols, and tocotrienols). The database also includes predicted properties for the lipid compounds such as melting point (a new model has been developed); vapor pressure [3]; densities [4]; and critical properties that were calculated by means of the software ICAS™ ProPred [*5*].

2.2 Process simulation model

The solvent recovery section consists of several unit operations: flash, heath exchange, mixing, splitting, stripping, and absorption. In this work, the process section was simulated using the commercial software PRO II and the database of lipid compounds integrated to PRO II.

The process model describing the solvent recovery section is shown in **Figure 1** [*1*]. According to the flow sheet the streams where both the hexane solvent and vegetable oil can be lost are the following: Crude_Oil, Vap_Out, Solid_Out, S33 (Purge), Mos_Water, and Vap_Mos. The corresponding process design variables are listed below:

- Oil recovery section: Temperature and pressure of evaporator 1 (TEVAP1 & PEVAP1), temperature of evaporator 2 (TEVAP 2), and temperature and number of stages (NS) of the stripping column (TSTP1 & NSTP1).
- Condensation section: Pressure of the condenser 1 (PCOND1) and temperature of condenser 2 (TCOND2).
- Water-hexane separation section: temperature and pressure of the decanter (TDECANT & PDECANT).

Process parameters:

- Oil recovery section: Pressure of evaporator 2 (PEVAP 2), duty and pressure drop of evaporator 3 (QEVAP3 & DPEVAP3), and pressure of the stripping column (PSTP1).
- Condensation section: Temperature of the condenser 1 (TCOND1) and pressure of condenser 2 (PCOND2).
- MOS System: Temperature, pressure, and number of stages of the absorption and stripping columns (TABSPC, PABSPC, NTABSPC, TSTP2, PSTP2, & NSTP2).

2.3 Model Reduction

The Plackett-Burman method is a technique where only the main effects are considered to be significant,

achieving thereby a reduction in the number of design variables. The advantage of this technique is that it only requires a number of experimental runs that are a multiple of 4 instead of a power of 2 [2]. The full factorial design is a technique that is sufficient for evaluating many production processes because it considers not only individual effects but also non distinguishable effects on a response.

3 Case Study: Optimization of a Soybean Extraction Process

3.1The Optimization Problem

The goal of this optimization problem is to minimize the loss of hexane solvent and vegetable oil (product) in the solvent recovery process section.

Objective Function

$$\begin{aligned} OF = {} & Crude\_Oil(Hex) + Vap\_Out(Hex) \\ & + S33(Hex) + Solid\_Out(Hex) \\ & + Vap\_Mos(Hex) + Mos\_Water(Hex) \\ & + Vap\_Mos(Oil) + Mos\_Water(Oil) \end{aligned} \quad (1)$$

$$26.46 \le TCOND2(°C) \le 35.80 \quad (2)$$

$$25.51 \le TDECANT(°C) \le 28.19 \quad (3)$$

$$53.34 \le TEVAP1(°C) \le 72.16 \quad (4)$$

$$88.00 \le TEVAP2(°C) \le 132.00 \quad (5)$$

$$104.50 \le TSP1(°C) \le 115.50 \quad (6)$$

$$0.26 \le PCOND1(bar) \le 0.36 \quad (7)$$

$$0.18 \le PDECANT(bar) \le 0.42 \quad (8)$$

$$0.39 \le PEVAP1(bar) \le 0.73 \quad (9)$$

$$\text{Number of Stages} \ge 1 \quad (10)$$

3.2Results

3.2.1Process Simulation

Data related to the solvent recovery process was available, so it was possible to make a detailed analysis of the accuracy of the soybean oil extraction process simulation. The average relative deviation (ARD) between the industrial data and the simulated data for the crude oil and the overall loss of hexane was analyzed according to,

$$ARD = \frac{\sum \left| x_i^{\exp} - x_i^{\text{model}} / x_i^{\exp} \right|}{N} * 100 \quad (11)$$

Where $x_i^{\exp}$ is the plant data for vegetable oil and hexane mass compositions in stream i, and, x_i^{model} are the calculated data for the same variables for N different experimental (plant) runs. The ARD for the oil composition in the crude-oil stream is 0.31%, while the ARD for the loss of hexane in the process is 4.71%.

The analysis of the simulation results generated through the process simulation for various (perturbed) values of the design variables led to the following observations:

- Presence of hexane in the stream Solid_Out can be neglected because, according to the plant data, the DTDC process removes all hexane and water from the white flakes.
- The major loss of vegetable oil in the process is located in the solvent extraction process, where some oil may remain in the waste solid. Since a predictive model to calculate this variable was not available, the stream Solid_out was not considered in the model reduction step.
- The amount of oil in the streams S33 (Purge) and Mos_Water can be neglected as these values were found to be very small.
- Two liquid phases (water and hexane) are present in the vessel named DECANTER. Therefore, stream tagged as Vap_Mos in the flow sheet was neglected in the further solution steps.

Based on the above observations, the objective function (see Equation (1)) is reduced to

$$OF = Crude\_Oil(Hex) + Vap\_Out(Hex) + S33(Hex) \quad (12)$$

Equation (12) actually corresponds to the amount of hexane recovered in the process, which will now be maximized.

$$\text{Objective Function} = \text{Recovery of Hexane} \quad (13)$$

3.2.2Model Reduction

Plackett-Burman Design: The ±1 levels (perturbed values) used in the 16 simulations for each of the design variables are listed in Table 1. From analysis of the simulation results it was concluded that only five variables significantly affected the amount of hexane recovered in the process.

Full Factorial Design: Based on the results of the PB method a second set of 43 simulations (2^5+2*5+1) was performed using the full factorial technique. From a statistical analysis of the results, a quadratic model for the Hexane Recovery response was obtained. The model, Equation (14), for maximizing hexane recovery is given in terms of 3 design variables (TCOND2, TEVAP2, and TSP1) as only these variables affect the hexane content (see Table 2). The ARD value for the reduced model is 0.008%. Using Equation (14) the response surface for this model was generated (Figure 2).

$$\begin{aligned} \text{OF} = {} & -0.005T_{\text{EVAP2}}^2 + 0.013T_{\text{EVAP2}} + 0.0054\left(T_{\text{EVAP2}}\right)\left(T_{\text{SP1}}\right) \\ & - 0.0178T_{\text{SP1}} - 0.0047\left(T_{\text{SP1}}\right)\left(T_{\text{TCOND2}}\right) + 99.963 \end{aligned} \quad (14)$$

3.2.3Optimization

The optimization model of the solvent recovery process is represented by Equations (15)-(18). As stated before, the goal is to maximize the objective function

Max Objective Function = Hexane Recovery (15)

s.t.

$$26.46 \le T_{\text{TCOND2}}(°C) \le 35.80 \quad (16)$$

$$88.00 \le T_{\text{EVAP2}}(°C) \le 132.00 \quad (17)$$

$$104.50 \le T_{\text{STP1}}(°C) \le 115.50 \quad (18)$$

The optimal values of the design variables and the percentage of hexane recovered under the optimized condition are: $T_{COND2} = 35.80°C$, $T_{EVAP2} = 110.14°C$, $T_{STP1} = 104.50°C$, and Recovery = 99.98%.

Table 1 Perturbed values of the design variables for the Plackett-Burman design

DESIGN VARIABLE	LEVELS	
	-1	+1
TCOND2(°C)	26.46	35.8
PCOND1(bar)	0.26	0.36
TDECANT(°C)	25.51	28.19
PDECANT(bar)	0.18	0.42
TEVAP1(°C)	53.34	72.16
TEVAP2(°C)	88.00	132.00
TSTP1(bar)	104.50	115.50
NSTP1	4.00	6.00
PEVAP1(bar)	0.39	0.73

Table 2 Plackett-Burman design results

PROCESS	SIGNIFICANT DESIGN
Vap Out	TCOND2, PCOND1, TEVAP1
Crude Oil	TCOND2, TEVAP2, TEVAP1
Purge	TCOND2, TSTP1

4 Conclusions

The predicted properties of the lipid compounds included in the database have been validated by comparing the simulation of the process and the plant data. The first set of operational variables considered inthis work would have needed more than 500 simulations if the full factorial technique was used without any pre-analysis. Therefore, the Plackett-Burman method was helpful to significantly reduce the total number of simulations that needed to be performed. With the reduced set of design variables, the full factorial technique was applied and a reduced model correlating the selected design variables and the process parameters was obtained. The development of the reduced model allows the representation of the process in terms if the most important design variables. The response surface generated through the reduced model showed that the process is within the optimum zone, although improvements are possible. Therefore, optimal values of design variables where hexane recovery is maximum, was found. The results confirm that through a combination of property database and process modelling techniques, the operation and design of industrial lipid technologies can be optimized.

References

1 A. Martinho, H. A. Matos, R. Gani, B. Sarup, W. Yougreen, 2008, Modeling and Simulation of Vegetable Oil Processes, Food and Bioproducts Processing, 86, 87, 9.

2 D. C. Montgomery, 2005, Chapter 6: The 2^k Factorial Design, Design and Analysis of Experiments, 6^{th}, 51.

3 R. Ceriani, J. A. Meirelles, 2004, Predicting vapor-liquid equilibria of fatty systems, Fluid Phase Equilibria, 215, 2, 10.

4 J. D. Halvorsen, W.C. Mammel, Jr, L.D. Clements, 1993, Density estimation for fatty acids and vegetable oils based on their fatty acid composition, Journal of the American Oil Chemists' Society70, 9, 6.

5 J. Marrero, R. Gani, 2001, Group-contribution based estimation of pure component properties, Fluid Phase Equilibria, 183-184, 26.

Acknowledgements

The author wishes to thank the Technical University of Denmark and the Company Alfa Laval for founding this PhD project.

Also Professor Rafiqul Gani and Dr. Bent Sarup are to receive a grateful acknowledgement for their hard and helpful work on the development of this project.

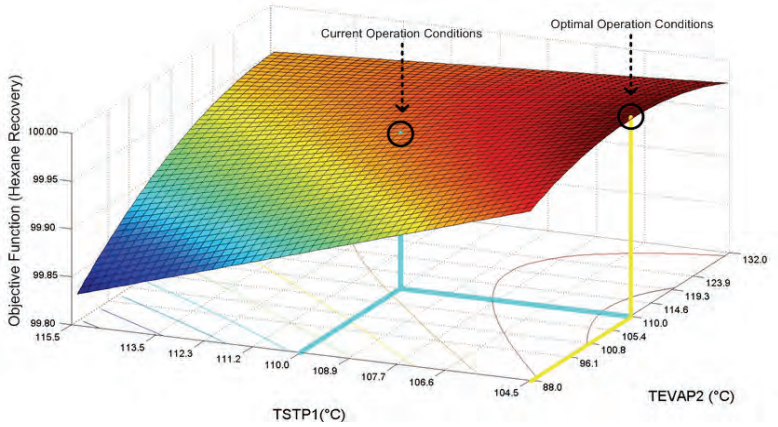

Figure 2: Hexane recovery surface response generated with the reduced second order process model

Chien-Tai Tsai
Phone: +45 4525 2943
Fax: +45 4593 2906
E-mail: ctt@kt.dtu.dk
WWW: http://www.dtu.dk/centre/BioEng.aspx
Supervisors: Anne S. Meyer
Anders Viksø Nielsen, Novozymes A/S

PhD Study
Started: May 2008
To be completed: April 2011

Physical and Chemical Properties of Pretreated Lignocellulose

Abstract

The project focuses on the chemical and physical properties of pretreated lignocellulose as well as the relation between these properties and enzyme hydrolysis efficiency. The information facilitates developing new strategies improving the efficiency of lignocellulose deriving bioethanol production process.

Introduction

Due to the increasing demand for energy but the decreasing petroleum, and the deteriorating environment, seeking for alternative energy is more and more important. Biofuel made from plant biomass, oil containing plants or starch and sugar rich crops are alternatives. However, under the pressure for food, optimal utilization of agricultural residuals to produce fuel is crucially important.

Plant biomass is mainly composed of lignocellulose. Cellulose is a polysaccharide with D-glucose as monomer. The hydrolysis of cellulose to release D-glucose monomers for down stream fermentation is one of the key steps for producing ethanol. However, due to the recalcitrant properties of the biomass, until now there is no satisfying pretreatment. Hence, as a base for developing better pretreatment and enzymatic hydrolysis schemes the fundamental objective of the present project is to provide an improved understanding of the chemical and physical properties of pretreated lignocellulose as well as the relation between these properties and enzyme hydrolysis efficiency. The information facilitates developing new strategies improving the efficiency of lignocellulose deriving bioethanol production process.

Specific objective

In chemical reactions, the reaction area affects the reaction rate. Hence, for a heterogeneous enzymatic catalysis system, the pore size of the substrates determine the diffusivity of enzymes into the interior part substrate, and a main hypothesis of this project is that the accessible substrate surface area and hydrolysis efficiency depend on the pore size distribution of the substrate. In this part we will characterize the pore size distribution of wheat straw after pretreatments and evaluate the hydrolysis efficiency.

Due to the multicomponent nature of lignocellulose (cellulose, hemicellulose and lignin etc.), which are mainly polymers, after pretreatment destroying the organized tissue structure, the conformational structures and the interaction of these components in water should be very complicated. Until now, there is no research directly visualizing the conformation and interaction of these components in water. The substrate conformational change may be an explanation to rheological property of the pretreated lignocellulose and the efficiency of hydrolysis of cellulose. The rheological behavior of pretreated lignocellulose may correlate to its interaction with water. The aim of the research is also investigating the interaction between water and pretreated lignocellulose.

The viscosity of pretreated plant biomass is too high to process. It is necessary to add a large quantity of water to lower the viscosity, resulting in the sizes of processing facilities have to be enlarged to adapt the material containing so much water. Besides, more energy has to be put in to distil ethanol from the end product. All this increases the cost of processing and waste energy.

The research mainly consists of the following parts:

- Characterize the Pore Size Distribution of Wheat Straw after Different Pretreatments
- Visualize the Conformation and Interaction of the Components in Pretreated Lignocellulose

- Interaction between Water and Pretreated Lignocellulose

References

1. Mads Pedersen, Anne S. Meyer. Influence of substrate particle size and wet oxidation on physical surface structures and enzymatic hydrolysis of wheat straw. Biotechnology Progress (In press)
2. Lisa Rosgaard., Sven Pedersen, Anne S. Meyer. Comparison of Different Pretreatment Strategies for Enzymatic Hydrolysis of Wheat and Barley Straw. Appl Biochem Biotechnol (2007) 143:284–296

Bodil Voss

Phone: +45 4525 2826
Fax: +45 4588 2258
E-mail: bov@kt.dtu.dk
WWW: http://www.kt.dtu.dk
Supervisors: John M Woodley
Simon Ivar Andersen (Haldor Topsøe A/S)
Jan-Dierk Grunwaldt

Industrial PhD Study
Started: May 2008
To be completed: May 2011

Catalytic Conversion of Bio-Ethanol on Heterogeneous Catalysts

Abstract
Bio-ethanol has attracted great interest due to its use as a gasoline supplement. For example, the development of second generation bio-ethanol technology will enable the sustainable use of biomass as a feedstock. There lies an even greater potential in catalytically producing chemicals from bio-ethanol, utilizing its chemical functionality, to produce value-added chemicals. If adequate selectivity is obtained for a catalyst, a shorter process route could form the basis for an economical viable alternative to existing technology.

Introduction
The climate meeting held in Copenhagen (COP15) during December 7-18 2009 reminded the public once more of sustainability issues and the negotiations taking place between the countries on climate matters were resumed again out of urgency: resources are running out and the globe is warming. The world has to consume fewer raw materials, while producing more chemical products. Scientists catching the essence of the political winds blowing are constantly working to obtain the scientific results which are needed to meet these challenges.
The utilization of renewable sources such as bio-ethanol is a hot topic. We advocate the use of bio-ethanol for the production of chemicals [1]. Possible value-added products from bio-ethanol comprise ethylene and acetic acid. The production routes from fossil oil or natural gas involve high energy inputs and/or long process routes [2]. An important feature of the production of chemicals from ethanol is the chemical functionality built into the ethanol molecule. In comparison oil and gas feedstocks have low functionality requiring the breaking down of the molecules into synthesis gas as intermediates in the course of conversion [3].
The conversion of bio-ethanol may take place over a wide range of catalysts leading to different products. An important aspect around bio-ethanol is that a tolerance to water in the feedstock of the catalyst will save on the preparation of the ethanol feedstock [4].

Project objective
The aim of this project is to find a catalyst capable of converting a biomass-based feed stream such as bio-ethanol to a value added product over a catalyst with the required selectivity to obtain a viable process alternative to the conventional.
In the present study bio-ethanol conversion has been selected as the biomass based feedstock. Numerous catalysts have been investigated with respect to their catalytic performance. Special focus has been laid on Cu and Pt based catalysts. In order to investigate the catalysts an experimental setup has been developed.
Furthermore interesting catalyst candidates have been characterized by several complementary characterization methods.

Experimental work
The experimental work has been carried out in a single-pellet-string reactor at Haldor Topsøe A/S. The characterization work has been partly made at the Department of Chemical and Biochemical Engineering at DTU. A diagram of the experimental set-up is shown in figure 1.

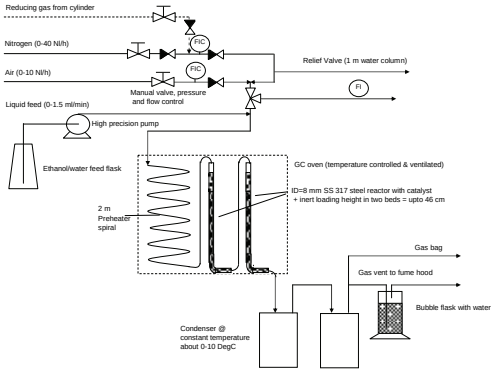

Figure 1: Experimental set-up.

The catalyst bed is contained in an ID=8 mm SS 316L temperature controlled steel reactor in a ventilated oven and with a thermocouple installed for the measurement of bed temperature. The individual catalyst pellets are separated by inert beads. The bio-ethanol is pumped and evaporated in a coil in the oven and nitrogen is added to the feed stream in order to improve the fluid dynamic properties. After conversion, the product is collected in a condenser being cooled to about 5°C. The liquid and the gaseous products are individually analyzed by GC and the results are recorded.
Characterizations of the catalysts have been made according to well-known techniques such as HBET, XRD, HGA, TPR and EXAFS.

Results and Discussion
While the conversion of ethanol over the catalyst to C_2-C_4 products was found to have relatively high initial space time yield, the catalyst activity tended to decrease over a few hours, and high-molecular by-products emerged deteriorating the catalyst. Under some of the catalytic conditions the Cu based catalysts are subjected to reduction. As the performance of the catalyst on a longer term seems to depend very much on the reduction method applied, special focus has been given to studying the reduction of the Cu catalysts. The reduction of a copper spinel catalyst has been followed *in-situ* both in a TEM microscope and in XAFS.

Figure 2 shows the TEM picture of a Cu depleted copper spinel structure.

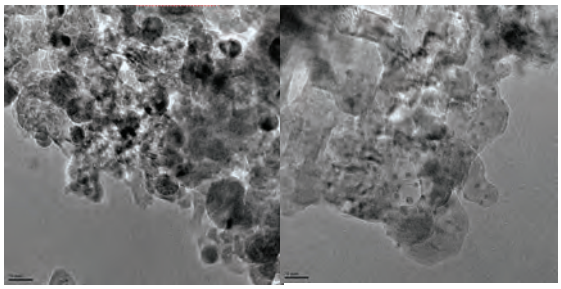

Figure 2: TEM picture showing the copper depleted spinel structure. Left: The spherical dark dots are nano-sized Cu particles being formed on the surface of the spinel structure. The light contrast starry spots are interpreted as vacancies in the spinel. Right: *In-situ* recording of Cu particle growth (dark spherical spots) on the alumina.

The spinel character of the catalyst fades over time leaving an alumina structure with distinct equally sized Cu particles on the surface.

Figure 3 shows some preliminary XANES data. Both the XANES and EXAFS spectra reveal the different Cu states during the reduction. From the XAFS spectra it is possible to follow the progress of the reduction of Cu from Cu(II) to Cu(0) as a function of temperature.

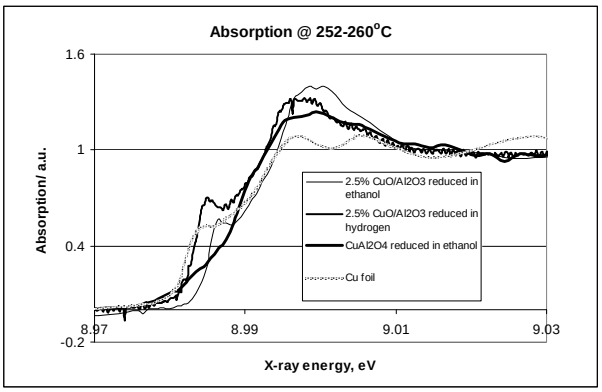

Figure 3: EXAFS spectra. The reduction of CuO/Al_2O_3 takes place via Cu(I). The reduction in hydrogen is faster than in ethanol. Copper spinel ($CuAl_2O_4$) is reduced faster than 2.5% CuO/Al_2O_3

The copper surface area seems to play an important role as mentioned above. The optimum copper surface area has been investigated in an HGA set-up using CO as the probe molecule. The optimum reduction temperature found was 340°C which was in accordance with an optimum degree of conversion of ethanol over the catalyst found at that temperature.

Conclusions
The synthesis of value-added chemicals from functionalized biomass based feed streams over heterogeneous catalysts may be viable if adequate selectivity and activity of the catalyst is obtained. The reduction of a Cu based catalyst for the conversion of bio-ethanol seems crucial to the performance of the catalyst under operation. Important information on reduction temperature and means for reduction has been found for such a catalyst through fundamental characterization methods.

Acknowledgements
This work is part of an industrial PhD study in collaboration with Haldor Topsøe A/S. The work is financed by Haldor Topsøe A/S and the Danish Ministry of Science, Technology and Innovation. Beam time at MAXLAB (Lund) amd HASYLAB (Hamburg) are gratefully acknowledged.

References

1. Bodil Voss et al, C-factors Pinpoint Resource Utilisation in Chemical Industrial Processes, accepted for publication by ChemSusChem December 2009.
2. William F. Banholzer et al, How might Biofuels Impact the Chemical Industry?, CEP, March 2008, S7-S14.
3. E. Taarning et al, ChemSusChem, 2008, 1(1-2), 75-78.
4. James Clark et al, Introduction to Chemicals from Biomass, Wiley, 2008, p. 168-174.

Rasmus Wedberg

Phone: +45 4525 2959
Fax: +45 4593 2906
E-mail: raw@kt.dtu.dk
WWW: http://www.kt.dtu.dk
Supervisors: Jens Abildskov
Günther H. Peters, DTU Chemistry

PhD Study
Started: November 2007
To be completed: October 2010

Fluctuation Solution Properties and Medium Effects on Enzyme Dynamics – Molecular Modeling Approaches

Abstract
The project deals with developing and improving the applicability of molecular modeling approaches to two different tasks, which turn out to be connected. The first task concerns prediction of fluctuation solution properties i.e. derivatives of thermodynamic properties via calculation of so-called Kirkwood-Buff integrals. The second task deals with solvent effects on protein dynamics, which has applications in medium engineering for biocatalysis.

Introduction
Molecular modeling methods have the potential to play an important role in Computer-Aided Molecular Design (CAMD). Though computationally expensive, such methods have proven to be of great value in situations where conventional property-prediction methods fall short [1].

A relevant example is the prediction of thermodynamic properties of solutions, in particular phase equilibria. Molecular modeling tools such as Gibbs-Ensemble Monte Carlo and COSMO-RS, are gaining popularity.

Molecular modeling is also frequently employed to study biomolecules. Predicting relative protein-ligand binding free energies and the effects of site-specific mutations are common tasks. However, molecular modeling approaches are not yet exploited for the task of selecting solvent for biocatalysis. Organic solvents are routinely used in industry for enzyme-catalyzed reactions [2]. However, in this context, solvent design is typically done on a 'trial-and-error' basis. The employment of CAMD methods to support the selection of solvent is thus desirable to practitioners in the field. Such an approach can benefit from the use of molecular dynamics (MD) simulations and quantum mechanical/molecular mechanics (QM/MM) simulations [3] which allows one to study the interactions between the enzyme and the solvent in great detail, and extract properties that can be correlated with activity, e.g. protein flexibility.

Specific Objectives
The project attempts to advance the fundamentals of molecular modeling approaches and bridge the gap between established CAMD and molecular modeling.

Fluctuation solution properties
The first sub-task of the project concerns the extraction of thermodynamic properties of solutions. We employ equations from fluctuation solution theory (FST) [4, 5], which relate derivatives of thermodynamic properties to the so-called Kirkwood-Buff (KB) integrals.

$$H_{ij} = \rho \int h_{ij}(\mathbf{r}) d\mathbf{r} \qquad (1)$$

where ρ and h_{ij} denote the density and the total correlation function (Fig. 1) of the molecular species i and j, respectively.

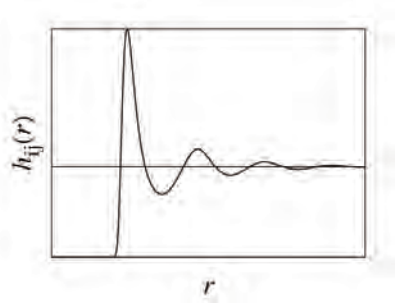

Figure 1: Total correlation function of a Lennard-Jones fluid.

Isothermal compressibility, partial molar volumes, and activity coefficient derivatives are examples of

properties that can be computed directly once the KB integrals are known. The total correlation functions are easily obtained from molecular simulations via the radial distribution function.

In previous studies, the evaluation of KB integrals from MD simulations data has been explored for predicting the excess Gibbs free energy of binary polar/non-polar mixtures [6-8], and the isothermal compressibility of pure alkane fluids (Wedberg et al, 2008). However, integrating the radial distribution functions obtained from simulations has turned out to be more challenging than expected. This is due to that the integral in Eq. 1 converges slowly, and therefore, it is necessary to extend $h_{ij}(r)$ beyond the range of r accessible to MD simulation.

A previously employed method for extension is to fit the tail of $h_{ij}(r)$ obtained from simulation to the empirical expression

$$h_{ij}(r) \propto ae^{-b(r-c)} \sin\left(d(r-c)\right) \tag{2}$$

which allows for extending $h_{ij}(r)$ so that the integral can be evaluated. Although this approach has yielded some good results, it is not certain that it works for all systems.

Our objective is to explore an alternative way to extend $h_{ij}(r)$, that is well-motivated by statistical mechanical theory. We utilize that the total correlation functions are connected to the corresponding direct correlation functions, $c_{ij}(r)$ (Fig 2.), that in contrast to $h_{ij}(r)$ have a simple and well-known behavior when r is large.

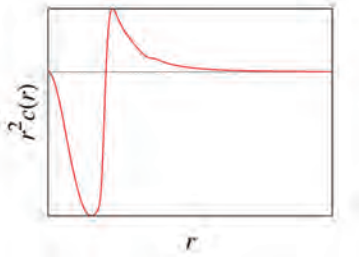

Figure 2: Direct correlation function of a Lennard-Jones fluid.

Protein Dynamics in Organic Solvents

The second sub-task of the project is concerned with molecular simulation of proteins for biotechnology applications. We are carrying out MD simulations of *Candida antarctica* Lipase B (CALB) in various organic solvents, and under varying hydration conditions. The purpose is to study the interactions between the enzyme and the medium. This includes medium-induced changes in enzyme structure and flexibility, and the local composition and dynamics of solvent around the enzyme surface.

The purpose of these studies is to gain a deeper understanding of the solvent effects at the molecular scale. It is also our intention to make comparisons with experimental measurements of the kinetics of CALB-catalyzed reactions in different solvents. By this, we wish to investigate what significance the molecular scale observations have for process-scale quantities, such as activity and selectivity.

A challenge for current simulation procedures is to set the simulations up so that the mixture of water and organic that surrounds the enzyme is kept at a specific water activity. This is useful, since experimental comparisons of enzymatic activity should be carried out at fixed water activity [9], which in turn controls the hydration level of the enzymes. We aim to establish an approach to control the water activity in molecular simulations of proteins, that makes use of the concept of Kirkwood-Buff integrals described above. Such an approach will allow for more proper comparisons between simulation and experiment.

Figure 3: The three dimensional structure of CALB, determined by x-ray crystallography [10].

Results and Discussion

Fluctuation solution properties

We have explored a method for extending the $h_{ij}(r)$ obtained from simulation which is based on an idea of Verlet [11]. The method utilizes that the total correlation function is related to the direct correlation function via the Ornstein-Zernike (OZ) equation, which for a pure fluid has the form

$$h(\mathbf{r}) = c(\mathbf{r}) + \rho \int c(\mathbf{r}-\mathbf{r}')h(\mathbf{r})\,d\mathbf{r} \tag{3}$$

The long-range behavior of c(r) is well approximated by the Mayer f-function, given by

$$f(r) = \exp\left(-\frac{u(r)}{k_B T}\right) - 1 \tag{4}$$

where $u(r)$ is the intermolecular potential and k_B and T denote the Boltzmann constant and temperature, respectively. In order to extend $h(r)$, we impose the constraints

$$\begin{cases} h(r) = h_{MD}(r), & r < R \\ c(r) = f(r), & r > R \end{cases} \tag{5}$$

where $h_{MD}(r)$ denotes the total correlation function obtained directly from MD simulation. We solve the OZ equation numerically under these constraints to obtain $h(r)$ for all values of r. The KB integrals are then easy to calculate using Eq. 1.

In order to assess the reliability of the extended correlation function and the accuracy of the computed thermodynamic properties, we carried out MD simulations of the pure Lennard-Jones (LJ) and

Stockmayer fluids. In the former, the particles interact via a spherically symmetric potential

$$u_{\mathrm{LJ}}(r) = 4\left(r^{-12} - r^{-6}\right) \tag{6}$$

while Stockmayer particles in addition have dipole-dipole interactions

$$u_{\mathrm{S}}(\mathbf{r}, \boldsymbol{\mu}_1, \boldsymbol{\mu}_2) = u_{\mathrm{LJ}}(r) + \frac{(\boldsymbol{\mu}_1 \cdot \boldsymbol{\mu}_2)}{r^3} - \frac{3(\boldsymbol{\mu}_1 \cdot \mathbf{r})(\boldsymbol{\mu}_2 \cdot \mathbf{r})}{r^5} \tag{7}$$

where $\boldsymbol{\mu}_1$ and $\boldsymbol{\mu}_2$ are dipole moment vectors.

The total correlation functions sampled in the simulations were extended as described, employing Eqns. 3-5, and the isothermal compressibility, κ_T, was obtained using the relation

$$k_{\mathrm{B}} T \rho \kappa_T = 1 + H = 1 + \rho \int h(\mathbf{r})\, d\mathbf{r} \tag{8}$$

We verified the approach by comparing the results with the equations of state (EOS) by Mecke et al. [12] and by Gross and Vrabec [13], which are based on correlations of data from simulations of the LJ and Stockmayer fluids, respectively. Representative results are shown in Figs. 4 and 5.

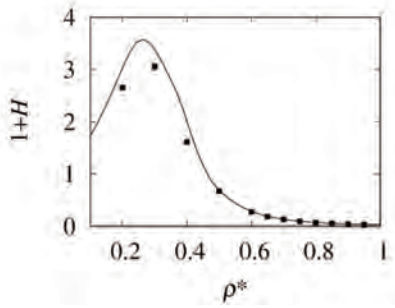

Figure 4: Comparing κ_T obtained from KB integration applied to LJ simulations (points) with the Mecke EOS [12] (line), at a supercritical isotherm.

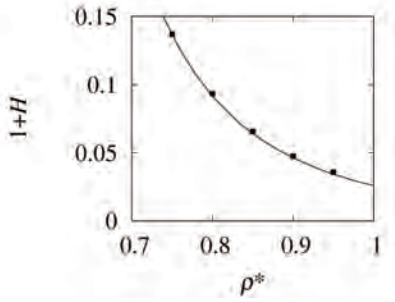

Figure 5: Comparing κ_T obtained from KB integration applied to Stockmayer (points) simulations (with $\mu^2 = 3$) with the Gross EOS [13] (line), at a subcritical isotherm.

Good agreement is achieved at high densities, at least as high as 1.5 times the critical density. Under those conditions, the compressibilities obtained from KB integration are within a few percent from the EOS. The agreement breaks down at low densities, and close to the critical point.

Our current efforts focus on extending the computational protocol of Eqns. 3-5 to mixtures. We are carrying out simulations of mixtures of LJ and Stockmayer particles, which is a simple model system resembling a mixture of polar and non-polar species. The applicability of KB integration is more appreciable for mixtures, since it allows for efficient calculation of activities.

Protein Dynamics in Organic Solvents

We have performed several MD simulations of CALB in four different solvents; water, hexane, acetone and tert-butanol. The simulations with water were carried out in order to have a reference, while acetone and hexane were studied in order to have one polar and one apolar organic solvent considered. Tert-butanol was included since it is commonly used as solvent, for example with lipase-catalyzed transesterification.

We used the coordinates from the x-ray resolved structure of CALB [10] in order to set up the initial configuration for the simulations. In the simulations using organic solvents, the 286 water molecules present in the coordinate file were also included in the simulation box. The simulations were carried out using the software NAMD [15], the CHARMM27 force field [16] and the TIP3P model for water.

In order to characterize the flexibility of the various parts of the protein, b-factors of the C_α atoms were calculated. The b-factor is defined as

$$\beta_i = \frac{8\pi^2}{3} \left\langle \left| \mathbf{r}_i - \langle \mathbf{r}_i \rangle \right|^2 \right\rangle \tag{9}$$

where $\mathbf{r}_i$ denotes the position of atom i and the angular brackets denote time average over the simulated trajectory. The calculation yields a plot showing the flexibility of the different parts of the protein. Results for one of the acetone simulations are shown in Fig. 6. In the acetone simulations, as well as in the water simulations, we observe the residues 140-150 and 250-300 to make up the flexible regions of the protein. Interestingly, these regions are two α-helices, located at the entrance to the active site pocket. In the tert-butanol and hexane simulations, these helices do not exhibit the same flexible behavior as in water or acetone.

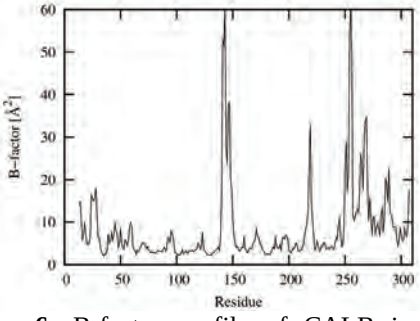

Figure 6: B-factor profile of CALB in acetone as obtained from MD simulation. Residues 140-150 and 250-300 constitute the more flexible parts of the protein in this simulation.

A characteristic measure of the overall flexibility is the sum of the b-factors of all C_α atoms. This number is reported for the four different solvents in Table 1. We observed the highest flexibility of CALB in water,

followed by acetone, while tert-butanol and hexane yielded the most stable behavior of CALB. The first important conclusion is that medium effects on CALB flexibility can be observed and quantified by MD simulations. The second is that the protein seems to be less flexible in organics, as compared to water. This is expected due to the lower dielectric constant of the medium, and the lower abundance of protein-solvent hydrogen bonds.

Table 1: Total flexibility and hydration level of CALB in four simulations using different media.

Medium	B-factor sum [Å^2]	#H_2O at surface
Water	3609	595
Acetone	2442	98
Tert-butanol	1572	175
Hexane	1684	241

Another observation concerns the behavior of the 286 water molecules included in the organic simulations. In hexane, all these molecules stay on the protein surface, while in acetone and tert-butanol, some are stripped off during the course of simulation (Fig. 7). A steady state is reached after about 10 ns, where the water molecules are distributed between the CALB surface and solvent.

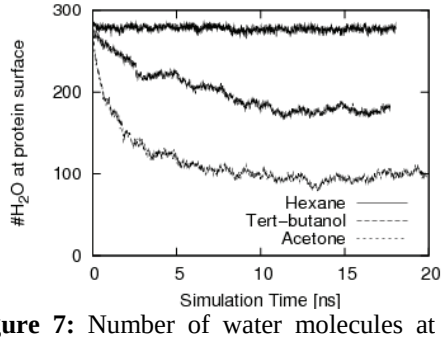

Figure 7: Number of water molecules at the protein surface vs. simulation time in three simulations using different organic solvents.

The fact that the simulations in different solvents result in different hydration levels for CALB could complicate the comparison of flexibility shown in Table 1. This is due to that the flexibility might not only be affected by the solvent species, but also by the hydration level. In order to investigate whether this is the case, we carried out several simulations of CALB in acetone, with varying amounts of water present. The resulting b-factor sums are on display in Fig. 8. Seemingly, flexibility increases with the hydration level. When we compare solvent effects on flexibility or other molecular properties, it is essential to maintain similar hydration levels in the different solvents. How this can be achieved is the focus of our current efforts.

A common approach taken in experimental kinetics measurements is to fix the thermodynamic activity of water in the medium [9]. This can in principle be done in simulations as well. Calculating thermodynamic activities from molecular simulations can however be tricky. We are currently exploring a strategy based on computing activities via the KB integrals.

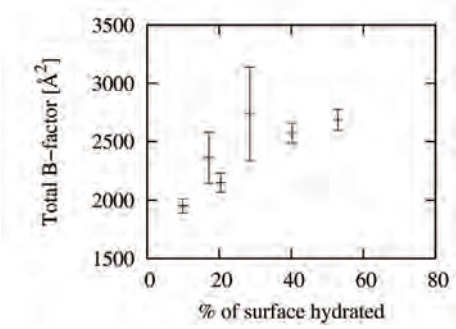

Figure 8: Average B-factor sums for simulations of CALB in acetone under various hydration conditions.

Acknowledgements
The author gratefully acknowledges IP Bioproduction within the European Union Sixth Framework Programme, for financial support. Our collaborator, John P. O'Connell from University of Virginia, is also acknowledged for his valuable contributions.

References

1. J.J. Pablo, F.A. Escobedo, AIChE J. 48 (12) (2002) 2716-2721.
2. G. Carrea, S. Riva, Angew. Chem. Int. Ed. Eng. 39 (13) (2000) 2226-2254.
3. G. Colombo, G. Carrea, J. Biotechnol. 96 (1) (2002) 23-33.
4. J.G. Kirkwood, F.P. Buff, J. Chem. Phys. 19 (6) (1951) 774-777.
5. J.P. O'Connell, Mol. Phys. 20 (1) (1971) 27-33.
6. S. Christensen, G.H. Peters, F.Y. Hansen, J. Abildskov, Fluid Phase Equilibr. 261 (1-2) (2007) 185-190.
7. S. Christensen, G.H. Peters, F.Y. Hansen, J.P. O'Connell, J. Abildskov, Fluid Phase Equilibr. 260 (2) (2007) 169-176.
8. S. Christensen, G.H. Peters, F.Y. Hansen, J.P. O'Connell, J. Abildskov, Mol. Simulat. 33 (4-5) (2007) 449-457.
9. R.H. Valivety, P.J. Halling, A.R. Macrae, Biochim. Biophys. Acta 1118 (3) (1992) 218-222.
10. J. Uppenberg, M.T. Hansen, S. Patkar, T.A. Jones, Structure 2 (4) (1994) 293-308.
11. L. Verlet, Phys. Rev. 165 (1) (1968) 201-214.
12. M. Mecke, A. Müller, J. Winkelmann, J. Vrabec, J. Fischer, R. Span, W. Wagner, Int. J. Thermophys. 17 (2) (1996) 391-404.
13. J. Gross, J. Vrabec, AIChE J. 52 (3) (2006) 1194-1204.
14. J.C. Phillips *et al*, J. Comput. Chem. 26 (16) (2005) 1781-1802.
15. A.D. MacKerell Jr. *et al*, J. Phys. Chem. B 102 (18) (1998) 3586-3616.

List of Publications

R. Wedberg, G.H. Peters, J. Abildskov, Fluid Phase Equilibr. 273 (1-2) (2008) 1-10.
R. Wedberg, J.P. O'Connell, G.H. Peters, J. Abildskov, Mol. Simulat. (2009) (*Accepted*).

Hao Wu

Phone: +45 4525 2927
Fax: +45 4588 2258
E-mail: haw@kt.dtu.dk
WWW: http://www.chec.dtu.dk
Supervisors: Peter Glarborg
Kim Dam-Johansen
Flemming J. Frandsen

PhD Study
Started: November 2007
To be completed: January 2011

Co-Combustion of Fossil Fuel and Waste

Abstract
Co-combustion of coal and solid recovered fuel (SRF) has been studied both by lab-scale experiments in an entrained flow reactor and full-scale particle measurement in a pulverized coal-fired power station. The results indicate that co-combustion of coal and SRF may not cause significant ash deposition and corrosion problems in the boiler. Although SRF usually contains higher chlorine and alkali contents than coal, the alkalis may mostly react to aluminosilicates and the chlorine may primarily release to gas phase as HCl during co-combustion. In addition, full scale results indicate the formation of ultrafine particles is increased in co-combustion of coal and SRF.

Introduction
With the target of reducing the CO_2 emission, replacing part of the fossil fuel consumption by biomass or waste which is usually considered to be CO_2 neutral has become an attractive option. Among the various technologies that utilize biomass or waste as an energy source, one of the most simple and promising methods is to co-fire biomass or waste together with coal in existing coal-fired power stations.

Solid recovered fuel (SRF) commonly refers to non-hazardous waste streams usable for energy recovery in waste incineration or co-incineration plants. In comparison with combustion in waste incineration plants, co-combustion of SRF and coal in pulverized coal-fired boilers may offer several advantages. For example, co-combustion is a cheap approach to treating the increasing amount of waste, since the capital cost for co-combustion in an existing coal-fired boiler is lower than building a new dedicated incineration plant. The electrical efficiency in a pulverized coal-fired boiler is generally higher than that in a waste incineration plant. Therefore, co-combustion can have the potential to increase the efficiency of utilizing waste energy. The NO_x and/or SO_x emissions from power plants may be reduced by co-combustion, since combustible waste usually contains lower nitrogen and sulphur contents than coals, and the synergy effects between coal and waste may also lead to the reduction of NO_x and/or SO_x emissions. Moreover, compared to the fly ashes from dedicated waste incineration plants which are mostly landfilled, co-combustion of coal and waste may generate more valuable fly ashes that may be usable in cement or concrete production.

Besides advantages, problems and challenges may be associated with co-combustion of coal and SRF. For example, SRF often contains higher alkali and chlorine contents than coals. When a secondary fuel with high alkali and chlorine contents is co-fired with coal, the ash deposition and corrosion problems in the boilers may become more severe, the fly ash quality may be lower, and the deactivation of the SCR catalysts may happen faster. In addition, combustible waste from industrial or household often contains much higher trace element contents than coals. Thus, the emissions of trace elements may become a concern for co-combustion of coal and SRF.

Specific objective
The objective of this PhD-project is to identify suitable waste types, fraction and particle size that can be co-combusted in pulverized coal-fired power stations, and to optimize the co-combustion of coal and waste through laboratory, pilot- and full-scale experiments, supplemental by modeling work. The impacts of co-firing on deposit formation, fly ash quality, and trace element partitions will be the main focus. The mechanism governing the transformation and the partition of major- and trace elements during co-combustion of coal and waste will be studied through experiments and modeling.

Entrained flow reactor

The entrained flow reactor (EFR) shown in Fig. 1 is designed to simulate the combustion environment of a suspension fired boiler. The setup consists of a vertical reactor, equipment for data acquisition, a particle feeder, a gas supply system, a gas preheater, a deposition probe system, and a controlled gas and particle extraction system. During a co-firing experiment, coal and SRF are premixed and combusted in the reactor. The flue gas composition is measured continuously by two gas analyzers. Fly ash from combustion is sampled by a cyclone and an aerosol filter, and deposit samples which represent superheater deposits in the boiler are collected by an air-cooled probe. Through analyzing the chemical composition and weight of the collected deposit samples, effects of co-combustion on ash deposition and corrosion in superheater region can be studied.

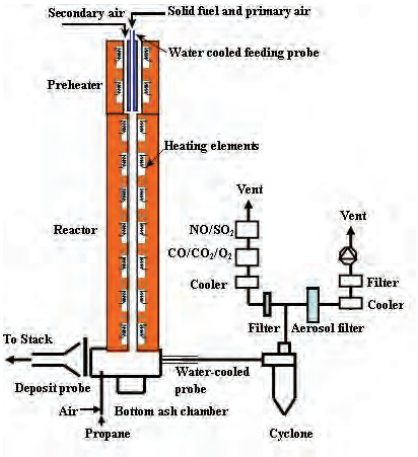

Fig. 1. Schematic diagram of the entrained flow reactor.

Full-scale aerosol measurement

Full-scale tests on co-combustion of coal and SRF were carried out by DONG Energy A/S at the 400MW Esbjerg Power Station in December 2008 and January 2009. During the campaign, the SRF type, share and injection position were varied, and a comprehensive measuring program was carried out. As part of the measuring program, a low-pressure cascade impactor was applied to sample the particles in the flue gas, and the collected particles were analyzed by SEM-EDS.

Selected results from EFR experiments

For the combustion experiments carried out in the EFR, the parameter "deposition flux/ash flux" is used as an indication of fly ash deposition propensity. As shown in Fig. 2, when coal is co-fired with SRF, the deposition propensity of the fly ashes generally decreases with increasing share of SRF. It indicates that the alkalis in the SRF may mostly react to high melting point aluminosilicates during co-combustion thus do not create severe ash deposition problems. Besides, the relatively high Ca content in the SRF may be beneficial to the melting point of fly ashes and result in the decreased ash deposition propensity during co-combustion.

The effects of different additives on the deposition propensities of fly ashes from co-combustion of coal and SRF are also presented in Fig. 2. It shows that the addition of 2wt% PVC and 1wt% NaCl slightly increases the deposition propensity of the fly ashes. However, the deposition propensities of the fly ashes in these two cases are not much higher than in dedicated coal combustion. It may imply the added sodium is primarily combined to aluminosilicates and the added chlorine is mainly released to the gas phase as HCl. The formation of alkali chlorides, which act as glue to enhance the deposit formation, may not be significantly increased.

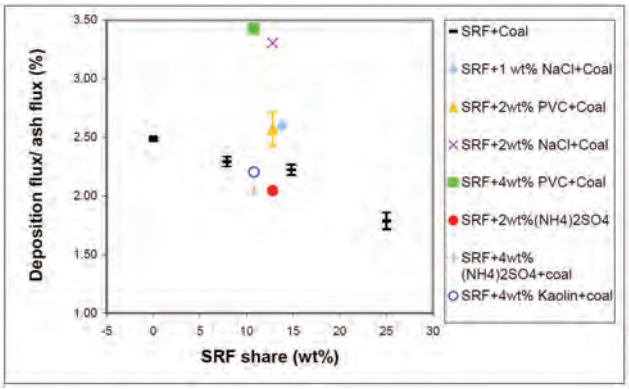

Fig. 2. Deposition flux/ash flux (%) from co-combustion experiments in the EFR.

With the addition of 4wt% PVC or 2wt% NaCl, the deposition propensity of the fly ash increases significantly. It indicates the presence of chlorides may be significant in these two cases. Addition of $(NH_4)_2SO_4$ slightly decreases the deposition propensity of the fly ash from co-combustion, probably due to the sulphation reaction which can form alkali sulphates. In contrast to NaCl or PVC, addition of more $(NH_4)_2SO_4$ (from 2wt% to 4wt%) almost has no further effect to the deposition propensity of the fly ash. The addition of Kaolin almost does not affect the deposition propensity of the fly ash. This indicates that the coal used in the experiments probably contain enough Al and Si for the reactions with Na and K. The addition of Kaolin would not promote these reactions any further.

Selected results from full-scale measurements

The full-scale results presented here are based on COCERR coal combustion and co-combustion of 7th% SRF and coal. Fig. 3 shows the average mass-based particle size distribution obtained from impactor stage 1-7. The standard deviations shown in the figure indicate that the measurement uncertainties are not very significant, especially for submicron particles. In Fig. 3, a peak particle size distribution can be seen at average aerodynamic diameter (d_{ae}) around 0.1 µm. This peak is evident both for the results from coal reference case and co-combustion case. The obtained results are in general consistent with a number of full-scale and lab-scale

experiments which found that fine particles from pulverized coal combustion contained an ultrafine mode centered at approximately 0.1 µm.

Fig. 3 shows that co-combustion of coal and SRF has an impact on the formation of fine particles. When coal is co-fired with 7th% SRF, the mass concentrations of the fine particles below 0.2µm are increased. This tendency may be further supported by the increased amount of dusts sampled in the stack of the plant during co-combustion. Compared to coal reference case, the amount of particles collected on impactor stage 7 (mean d_{ae}=1.32µm) is reduced in co-combustion.

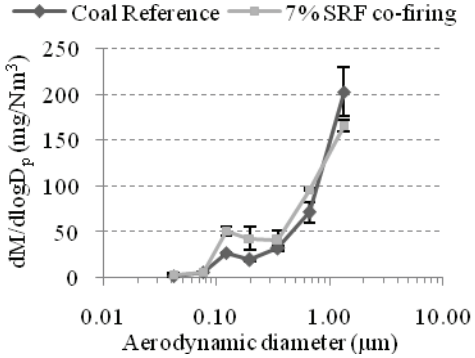

Fig. 3. Mass-based particle size distribution from coal combustion and co-firing of coal and 7th% SRF.

The morphology of the fine particles collected from the plant is characterized by SEM. It is found that there is no noticeable morphology difference between the particles from co-combustion and dedicated coal combustion. The SEM pictures of the fine particles collected from co-combustion of coal and 7th% SRF are shown in Fig. 4. Those morphologies are also representive for the particles from COCERR coal combustion.

Fig. 4a shows the particles collected on impactor stage 8. It is seen that those supermicron particles primarily consist of individual spherical particles which are in agreement with the observed morphology of supermicron particles from pulverized coal combustion. The perfect spherical appearance of the particles implies that the minerals in coal or SRF are almost completely melted during the combustion. Although small aggregates exist, the surfaces of those particles are in general quite smooth which indicates that the condensation and aggregation of vaporized species are not significant for the formation of supermicron particles. In contrast, the supermicron particles are primarily generated from the minerals in coal and SRF that are melted during the combustion in the boiler. The detailed formation mechanisms may involve coalescence of inherent minerals, fragmentation of chars, and the melting of excluded minerals. The contribution of different detailed mechanism to the formation of supermicron particles is difficult to distinguish from the present results.

Fig. 4b shows the morphology of particles collected on impactor stage 7, which contain both supermicron and submicron particles. From the figure, it is seen that the particles on this stage are also dominant by individual spherical particles. However, different from the particles collected on stage 8, it is shown in Fig. 4b that the surfaces of majority of submicron particles are to a large extent covered by small aggregates. Those small aggregates may either from direct condensation of vapor phase species or aggregation of nucleates formed from inorganic vapors.

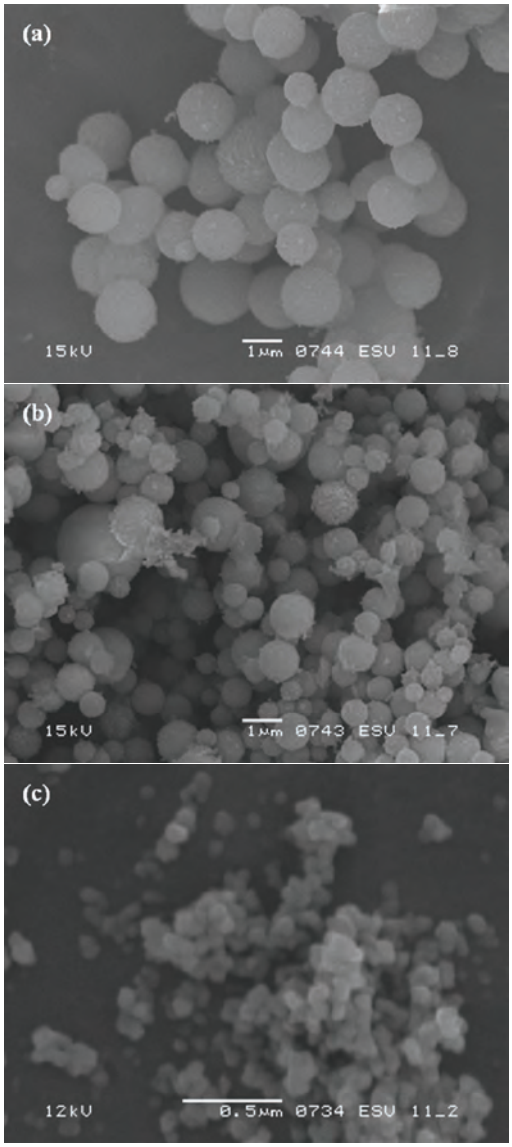

Fig. 4. Morphology of the particles collected from co-combustion of coal and 7% SRF, (a) LPI stage 8 (mean d_{ae}=2.61µm), (b) LPI stage 7 (mean d_{ae}=1.32µm), and (c) LPI stage 2 (mean d_{ae}=0.075µm).

The morphology of the particles shown in Fig. 4b indicates that for particles in between supermicron and ultrafine particles, condensation of vapor phase species or aggregation of the particles from homogeneous nucleation on the surfaces of existing spherical submicron particles may be an important formation mechanism. This mechanism would be closely related with the surface area of the particles. For spherical particles, the specific surface area of the particle

increases with decreasing particle diameter. As a result, this mechanism would be more pronounced for smaller particles i.e. the contribution of vaporized species/nucleates would be more significant for the formation of smaller particles. It should be aware that some of the particles formed from homogeneous nucleation may coagulate and grow to a particle larger than 0.1µm. Those particles may also contribute to the formation of particles between supermicron and ultrafine modes. However, the contributions of those particles are likely negligible for large particles close to 1 µm, as indicated by the particle morphologies shown in Fig. 4b.

The morphology of the ultrafine particles collected on stage 2 of the impactor are presented in Fig. 4c. It is obvious that the morphology of the ultrafine particles differ significantly from the particles shown in Fig. 4a and Fig. 4b. The observed ultrafine particles primarily consist of irregular shape particles with a characteristic size around 50-100nm. The remarkable difference between the morphology of ultrafine particles and supermicron particles suggest that their formation mechanism is different. The observed ultrafine particles with irregular shapes are believed to be a result of the collision and partial fusion of tiny particles below 10nm from homogeneous nucleation.

Elemental compositions of the fine particles from COCERR coal combustion have been analyzed by EDS and the results are given in Fig. 5. The oxygen and carbon contents in the particles are not included in the results, as the measurement uncertainties on these two elements are larger than other elements and the carbon content may be influenced by carbon coating used in sample preparation. From the figure, it can be seen that the supermicron particles are dominant by Si and Al, with an approximate content of 50wt% and 20wt% respectively. With decreasing particle size, the contents of Si and Al in the particles decrease. For ultrafine particles collected on impactor stage 2, the content of Si and Al becomes about 24wt% and 11wt% respectively. K content also shows a reducing tendency with decreasing particle size .The K content in the supermicron particles is around 6wt%, while its content in the ultrafine particles is decreased to about 1wt%.

Different from Si, Al and K, the contents of Ca, S and P in the particles generally increase with decreasing particle size. For supermicron particles collected on impactor stage 8, the content of Ca, S and P is approximately 4wt%, 1wt% and 1.5wt% respectively. However, for ultrafine particles collected on impactor stage 2, the content of Ca, S and P increases to about 23wt%, 18wt% and 5wt% respectively. Compared with supermicron particles, the enrichments of Ca and S in ultrafine particles are significant, with an approximate factor of 6 and 18 respectively. The enrichment of P in ultrafine particles is by a factor of 3-4, which is slightly lower than those of Ca and S. Small increase of Na content is also seen with decreasing particle size in Fig. 5. However, the general low Na contents in the particles indicate that the contribution of Na is not significant for the formation of fine particles.

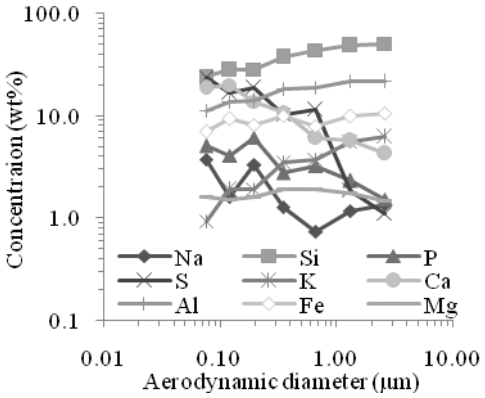

Fig. 5. Elemental composition of the particles from COCERR coal combustion.

Compared to other elements shown in Fig. 5, the contents of Fe and Mg are more evenly distributed over different particle size. The Fe content is around 9wt% for all of the particles and content of Mg is close to 2wt%. In addition to the elements shown in the Fig. 5, Ti and Cu have been detected in the particles collected on different impactor stages, and Mn and Cl are observed on some impactor stages. However, the contributions of those elements to the formation of particles are less significant, in comparison with the elements shown in Fig. 5.

Conclusion

Studies on co-combustion of coal and SRF have been carried out through experiments in an entrained flower reaction and full-scale particle measurement. The results indicate that co-combustion of coal and SRF would not cause severe ash deposition and corrosion problems in the boiler. Although SRF usually contains higher chlorine and alkali contents than coal, the alkalis may mostly react to aluminosilicates and the chlorine may primarily release to gas phase as HCl in co-combustion. However, a potential problem is that the formation of ultrafine particles would be increased in co-combustion of coal and SRF.

Acknowledgments

The work is part of the CHEC (Combustion and Harmful Emission Control) Research Center. The present work is sponsored by the Technical University of Denmark and co-funded by the Energinet.dk. DONG Energy A/S is acknowledged for giving the opportunity to perform the experiment.

Cheng Xu

Phone: +45 4525 2935
Fax: +45 4588 2258
E-mail: cxu@kt.dtu.dk
WWW: http://www.kt.dtu.dk
Supervisors: Anne Meyer, DTU
Jens Sørensen, Danisco A/S

PhD Study
Started: March 2007
To be completed: Feb 2010

Kinetic Models Describing Enzyme Catalyzed Degradation of Water Soluble Arabinoxylan

Abstract

The project focuses on modelling of the cooperative and synergistic action of the enzymes during modification, debranching and depolymerisation of differently substituted, water soluble arabino-xylooligosaccharides. The main purposes are to study the kinetics model of degradation with pure enzymes and to design a process in order to obtain target xylo-oligosaccharides with high prebiotics activity

Introduction

Native arabinoxylans are abundant in cereal plant cell walls and are composed of a backbone of (1,4)-linked-D-xylose residues having α-arabinose substituents. Recent findings indicate that xylooligosaccharides stimulate the growth of probiotic, cecal bifidobacteria in vivo and exert inhibitory effects on precancerous colon lesions in rats. An overall aim of the PhD project is to use specific enzymes to design biofunctional xylooligosaccharides with defined substitution patterns and chain lengths, and in particular to quantify the rates of the different events by developing enzyme kinetic models. The hypothesis behind the project is that provision of a better quantitative understanding of the events by modelling of the reactions is a prerequisite for optimally exploiting the complex, sequential enzyme reactions in new food and ingredient processes and development. With arabinoxylan, the results are particularly relevant in baking, brewing, prebiotics design, and in non-food cereal based processes.

The enzymatic hydrolysis of arabinoxylan is a complicated process which requires the action of different enzyme activities for complete hydrolysis; These are first and foremost various α-L-arabinofuranosidases, endo-1,4-β-xylanase and β-xylosidase [1]. Arabinoxylan consist of (1,4)-β-linked D-xylopyranosyl residues to which α-L-arabinofuranosyl residues can be single substituted at α-1,3 or α-1,2 and double-substituted at α-1,3 and α-1,2, [2]. The enzymatic degradation of arabinoxylan, can be expected to depend on the degree of arabinose substitution, the position of glycosidic bonds and their distribution along the xylan backbone [3].

This study investigated the kinetics of enzymatic degradation of soluble wheat arabinoxylan by monitoring the release of xylose and arabinose during designed treatments with selected monoactive enzymes [4,5] at different substrate concentrations. The results of different combinations of α-L-arabinofuranosidases (EC 3.2.1.55), one derived from Aspergillus niger (Abf A.niger) and one from Bifidobacterium adolescentis (Abf Bifido), respectively, a β-xylosidase (EC 3.2.1.37) from Trichoderma reesei [6], and an endo-1,4-β-xylanase (EC 3.2.1.8) from Bacillus subtilis were examined. The selected α-L-arabinofuranosidases catalyze liberation of arabinose residues linked 1→3 to singly (Abf A.niger) or doubly (Abf Bifido) substituted xyloses in arabinoxylan, respectively.

Objectives

The purpose of current study is to understand the enzyme kinetics in arabinoxylan degradation. The overall aim is that we can design and control the reaction optimally; a particular purpose of this study is to control the hydrolysis in order to produce specific xylo-oligsacchrides with high prebiotics activity.

Results

The data obtained (Fig. 1,2) demonstrated that the endo-1,4-β-xylanase activity is the dominating rate-limiting enzyme activity for xylose release during enzymatic hydrolysis of water soluble arabinoxylan by the cooperative action of α-L-arabinofuranosidases having different specificities, together with endo-1,4-β-xylanase and β-xylosidase. Endo-1,4-β-xylanase exhibited a significant synergistic effect on xylose release when acting together with β-xylosidase.

Comparably, the arabinofuranosidases, including the Abf A. niger releasing (1→3) bonded arabinofuranosyls from singly substituted xyloses, exerted lower synergistic effects with β-xylosidase on xylose release. The data confirmed the different actions and the different arabinoxylan hydrolysis consequences of the two α-L-arabinofuranosidases: Although the Abf Bifido had higher specific molar catalytic activity on the arabinoxylan, the Abf A.niger exhibited better synergy with β-xylosidase to release xylose. Doubling of the β-xylosidase enzyme dosage did not increase either xylose or arabinose release, rather did the surplus of β-xylosidase decrease the yields of both arabinose and xylose, presumably as a result of competitive non-productive binding of the surplus β-xylosidase to the substrate, which blocked the access of the other enzymes.

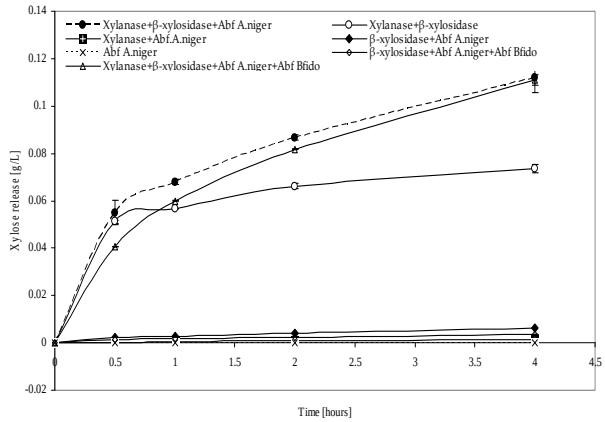

Figure 1: Xylose release from the hydrolysis by β-xylosidase and α-L-arabinofuranosidases.

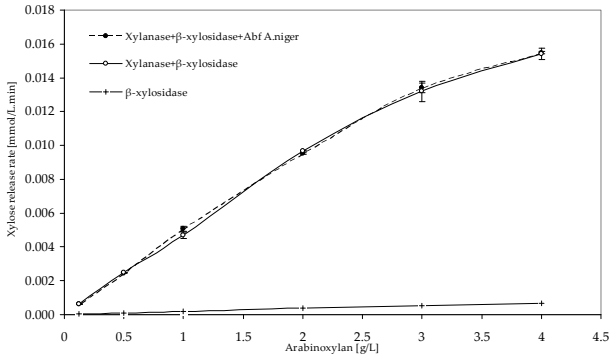

Figure 2: Reaction rates (xylose) on different substrate concentrations.

Acknowledgement
I would like to thank Danisco A/S for delivering enzymes for the experimental work.

References

1. Rasmussen LE, Sørensen HR, Vind J, Viksø-Nielsen A (2006) Mode of action and properties of the β-xylosidase from Taleromyces emersonii and Trichoderma reesei. Biotechnol Bioeng 94:869-876
2. Izydorezynk MS, Biliaderis CG (1995). Cereal arabinoxylans: advances in structure and physicochemical properties. Carbohyd. Polym. 28: 33-48.
3. Dervilly-Pinel G, Tran V, Saulnier L (2004). Investigation of the distribution of arabinose residues on the xylan backbone of water-soluble arabinoxylans from wheat flour. Carbohyd. Polym. 55: 171-177..
4. De Vries RP, Visser J (2001). Aspergillus enzymes involved in degradation of plant cell wall polysaccharides. Microbiol. Mol. Biol. R. 65: 497-522.
5. Sørensen HR, Meyer AS, Pedersen S (2003) Enzymatic hydrolysis of water-soluble wheat arabinoxylan. 1. synergy between α-L-arabinofuranosidases, endo-1,4-β-xylanases, and β-xylosidase activities. Biotechnol Bioeng 81:726-731
6. Poutanen K and Puls J (1988). Characteristics of Trichoderma reesei β-xylosidase and its use in the hydrolysis of solubilized xylans. Appl Microbiol Biotechnol. 28: 425-432.

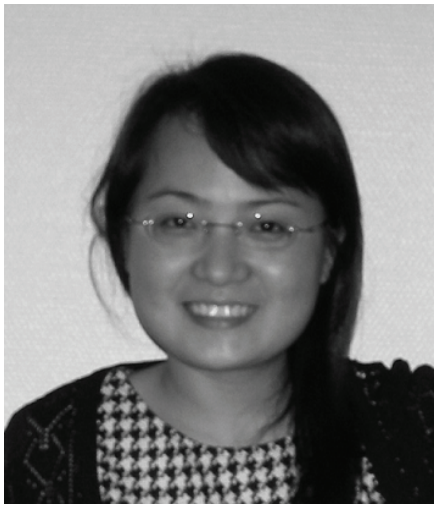

Yuan Xu

Phone: +45 4525 2960
Fax: +45 4593 2906
E-mail: xuy@kt.dtu.dk
WWW: http://www.kt.dtu.dk
Supervisors: John M. Woodley
Mathias Nordblad

PhD Study
Started: March 2009
To be completed: February 2012

Process Technology for Lipase-Catalyzed Reactions

Abstract

As one of the products from lipase-catalyzed reactions, biodiesel is one of the most promising renewable energy alternatives. The chemical process of biodiesel production has been well developed but the enzymatic process is still in its infancy. In this project lipase-catalyzed biodiesel production is taken as an example for the next generation of process technology. The reactor and separation technology will be the core considerations to improve the process efficiency. The scope of this project is to establish a suitable scale-down methodology to test and accurately predict the performance of a process for effective conversion of oils into biodiesel.

Introduction

Lipase-catalyzed reactions have been widely applied in the field of food technology, pharmaceutical industry, chemical and detergent industries. However, the lipases are costly, especially when they are immobilized. An effective process should improve the catalytic activity and stability of the enzyme and thus offer the possibility for a cost-efficient application of lipase in low-value products. One such product is biodiesel, which is produced via transesterifications of fats and oils (Figure 1).

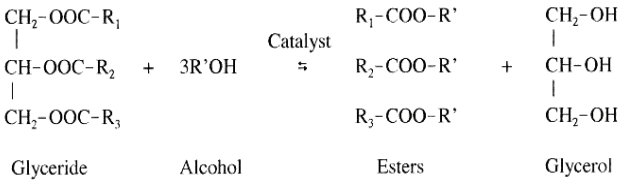

Figure 1: Transesterification of triglycerides with alcohol [1]

The depletion of fossil fuels and the associated pollution problems make it increasingly necessary to develop renewable energy alternatives that have smaller environmental impact than the traditional ones. Biodiesel shows great promise as a fuel and with respect to sustainability[2].

Biodiesel produced from vegetable oils or their blends has the following advantages over conventional diesel or petroleum: it is renewable, biodegradable, oxygenated and less toxic; it has higher cetane number; produces less smoke and particulates; and produces lower CO_2 and less SO_2 emission; it also has a low aromatic content and high heat content; it is less volatile and safer to transport or handle due to its high flash point (150 ^{o}C)[3,4].

Compared to the conventional base-catalyzed biodiesel process, the enzymatic process requires less energy and is also highly selective producing less byproducts or waste. Using immobilized lipases also makes it easy to remove and reuse the catalysts. The biodiesel production catalyzed by lipases is considered as a "green reaction". Involving ethanol turns the biodiesel even "greener", because ethanol can be obtained from agricultural products and hence is more environmentally friendly and renewable than methanol, which is commonly used in chemical biodiesel production. Additionally, the extra carbon brought by the ethanol molecule slightly increases the mass yield as well as the heat content and the cetane number[3,5].

Although lipase-catalyzed biodiesel production has a number of potential benefits, it is not sufficiently developed technically to implement commercially. Those reported studies which have been conducted with enzymatic biodiesel production to date are at a modest scale and have been focused on the effects of concentrations of enzyme, alcohol and water with a variety of oils containing differing amounts of FFAs. The few studies that have addressed scale-up issues have been focused on acid or alkali based catalysis. In this respect this work will provide an important contribution to the development of new process technology by taking the scale-up of enzymatic

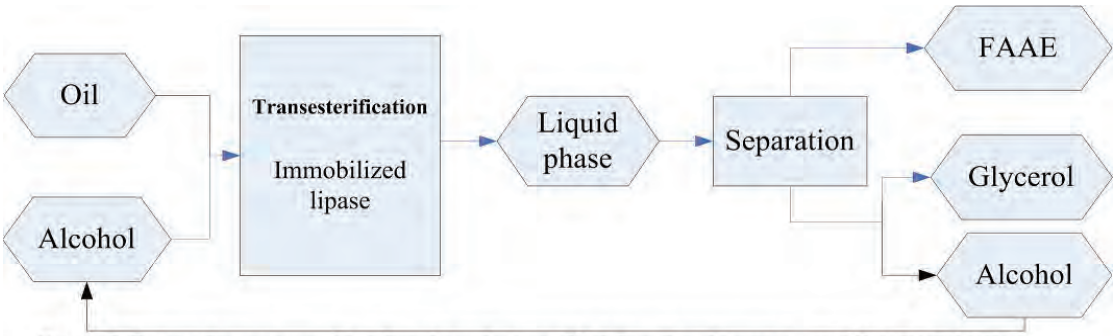

Figure 2 Enzymatic process of biodiesel production (FAAE is the abbreviation of Fatty Acid Alkyl Ester, usually FAME ore FAEE)

biodiesel production as an example. The general immobilized lipase involved biodiesel process is shown in Figure 2. To maximize the process efficiency, emphasis will be put on the reaction and on reactor design, removal of catalyst inhibitor and separation of products.

This work is conducted within the framework of the Danish National Advanced Technology Foundation program on Sustainable Biodiesel. A close working relationship with the other members of the program will ensure targets and milestones are evaluated in an industrial context. The project will also consider environmental performance of the process design to increase the environmental sustainability of the biodiesel production.

Specific objectives

- ✧ Select and design an effective reactor for lipase-catalyzed biodiesel reactions
- ✧ Integrate the separation technology of glycerol and water to the whole process and evaluate its efficiency
- ✧ Establish a methodology for evaluating alternative enzymes and oils in a scale-down version of this process

The milestones of this project:

- ➢ Develop suitable analytical method for the project
- ➢ Define and evaluate experimental separation methods and in particular methods for the separation of glycerol and water
- ➢ Investigate catalyst stability / activity under process conditions using a scale-down version of the chosen process(es)
- ➢ Evaluate the feasibility and efficiency of alternative reactors for carrying out the chosen process

The project goal will be achieved by fulfilling the tasks through four stages:

Stage 1: Fundamental study

The study will focus on the phase behaviour study and catalyst properties. The affinity of glycerol for different biocatalysts is a focus.

Stage 2: Glycerol separation

Solutions for separating glycerol from biodiesel, glycerides and catalyst will be provided and evaluated by experimental study. One of the highlights of this stage will be the solutions for glycerol separation in situ.

Stage 3: Reactor evaluation and innovation

The lipase-catalyzed reaction will be applied in various reactors. The feasibility and efficiency of reactor candidates will be evaluated. One aim is to design a novel reactor specially adapted to this type of reaction.

Stage 4: Process design, integration and demonstration in a pilot plant (not a focus of this Ph.D project)

Based on the selection of optimum reactor and evaluation of kinetic data a process model will be devised to enable the simulation of alternative process schemes. A mini pilot-plant (50L) scale will be designed and built based on the results of the reactor selection and simulation of process options. One of the purposes of the plant is to demonstrate the feasibility and the robustness of the chosen design.

Acknowledgements
The project is funded by Danish National Advanced Technology Foundation, Novozymes A/S, Emmelev A/S and DTU.

References

1. F. Ma, M. A. Hanna, Bioresource Technology 70 (1999) 1-15.
2. Nielsen, P.M., Brask, J., Fjerbæk, L., European Journal of Lipid Science and Technology, 110(2008), 692.
3. Akoh, C.C., Chang, S., Lee, G., Shaw, J., Journal of Agricultural and Food Chemistry 55 (2007), 8995-9005.
4. Frondel, M., Peters, J., Energy Policy 35(2007), 1675–1684.
5. Bouaid, A., Martinez, M., Aracil, J., Chemical Engineering Journal 134(2007), 93-99.

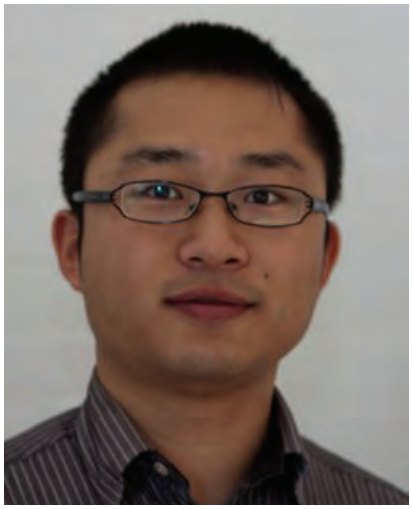

Hao Yuan

Phone: +45 4525 2960
Fax: +45 4588 2258
E-mail: hy@kt.dtu.dk
WWW: http://www.ivc-sep.kt.dtu.dk/
Supervisors: Alexander Shapiro
Erling Stenby

PhD Study
Started: Oct. 2009
To be completed: Oct. 2012

ParPor: Particles in Pores. Stochastic Modeling of Polydisperse Transport

Abstract

Liquid flow containing particles in the different types of porous media appear in a large variety of practically important industrial and natural processes. The project aims at developing a stochastic model for the deep bed filtration process in which the polydisperse suspension flow in the polydisperse porous media. Instead of the traditional parabolic Advection-Dispersion Equation (ADE) the novel elliptic PDE based on the Continuous Time Random Walk is adopted for the particle size kinetics [1, 2]. The pore kinetics is either described by the stochastic size exclusion mechanism or the incomplete pore plugging model[3, 4]. In the current phase of the project the computation is only performed for the polydisperse suspension flow in monodisperse porous media. The slower transport speed of the peak and larger tail indicates that the elliptic model is more adaptable for anomalous diffusion. Porosity decline of the porous media and convection acceleration of the flow are observed from the modeling results which agree with the general experimental observation.

Introduction

Liquid flow containing particles in the different types of porous media appear in a large variety of practically important industrial and natural processes. A large body of applications has resulted in a large body of research; the researchers from the different areas have scarcely exchanged results and ideas though. The studies may roughly be classified into the two categories: Microscopic, detailed analysis of the particle-pore interactions and of the individual or collective particle behavior on the pore level; and modeling of the particle suspension flows in porous media on the macroscopic level, in the volume larger than REV containing a number of particles and pores. The latter is being focused on in the project.

Macroscopic modeling of the suspension flows in porous media is often based on a hydrodynamic model of the advection-dispersion type, which typically takes the parabolic PDE form (ADE). Particle deposition is modeled similar to “the first order chemical reaction”. Such approach does not account for polydispersity: both particles and pores may be of different sizes and possess different properties, which strongly affects both transport and deposition. Several discrepancies between predicted and observed pictures of filtration were observed in the experiments [5, 6]. These discrepancies are important for practice: for example, porous media lead to separation of the different particles. The particles of the different sizes move with the different microscopic velocities and may be dispersed in the different ways, which leads to the different kind of transport than the classical “diffusion-like” evolution. This may happen even with the particles of the same size (and even with the molecules of a tracer). They may be delayed indefinitely in the pores and then move further. Variability on the pore level leads to dispersion of the particle flight times and to non-conventional transport equations.

The process of suspension flow in porous media is stochastic in nature, and it calls for stochastic modeling. Several stochastic models emerged recently. The continuous-time random walks (CTRW) approach [7, 8]has been applied suspension and tracer flows [6, 9]with effectively monodisperse, but randomly “walking” particles. This approach has managed to explain some (but not all the) experimental results relevant to time dispersion of the particle flights. Based on this theory Pavel and Shapiro developed a novel elliptic model differing from the conventional parabolic ADE [1, 2].

The pore kinetics is either described by the size exclusion mechanism, adsorption, bridging, or other mechanisms which may cause incomplete pore plugging[3, 10]. The porosity decline leads to the convection acceleration of local fluid velocity. This leads to the non-linearity of the elliptic PDE which requires special technique to implement fast computation.

Particle size kinetics

The equation of particle size kinetics should be obtained from a microscopic and stochastic point of view. Following a similar procedure to that in Ref[2], we start with a so-called continuous-time random walker which represents a particle carried by the advection flux from one pore to another, as seen in **Figure 1**.

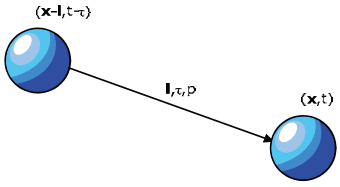

Figure 1: an arbitrary continuous-time random walker's step

As mentioned above the particle may pass through the same pore along different paths. The portion of particles along one path is denoted by c(**l**,τ,r_s,**x**,t), in which the flow direction and the flight time reflect the particle velocity. c(**l**,τ,r_s,**x**,t) is better to be understood as the probability of the condition (**l**,τ,r_s,**x**,t) to happen. p is the probability for the particle to pass the pore under the condition (**l**,τ,r_s,**x**,t), p ranges from 0 to 1.

$$P(\mathbf{l},\tau,p,r_s,\mathbf{x},t)=f(p\,|\,\mathbf{l},\tau,r_s,\mathbf{x},t)c(\mathbf{l},\tau,r_s,\mathbf{x},t)$$

The probability distribution for the walker to appear at (**x,** t) is associated with the PDF for walker to appear at (**x-l,** t-τ) by the convolution law:

$$\begin{aligned}&\phi(\mathbf{x},t,r_s)C(\mathbf{x},t,r_s)\\&=pP(\mathbf{l},\tau,p,r_s,\mathbf{x},t)*\left[\phi(\mathbf{x}-\mathbf{l},t-\tau)C(\mathbf{x}-\mathbf{l},t-\tau,r_s)\right]\\&=\int_0^\infty\int_0^\infty\int_0^1 d^d\mathbf{l}\,d\tau\,dp\left\{\begin{matrix}pf(p\,|\,\mathbf{l},\tau,r_s,\mathbf{x},t)c(\mathbf{l},\tau,r_s,\mathbf{x},t)\times\\\left[\phi(\mathbf{x}-\mathbf{l},t-\tau)C(\mathbf{x}-\mathbf{l},t-\tau,r_s)\right]\end{matrix}\right\}\end{aligned}$$

where the superscript 'd' represents the number of dimensions. C(x,t,r_s) is the number of particles of r_s at (x,t). c(**l**,τ,r_s,x,t) is the PDF for the particles of r_s randomly walking along the vector **l**. Further reformations of the equation above lead to the following elliptic PDE for one particle size finally:

$$\begin{aligned}&\partial(\phi C)/\partial t+\mathbf{u}\cdot\nabla(\phi C)\\&=D_{\mathbf{x}}\nabla^2(\phi C)+D_t\frac{\partial^2(\phi C)}{\partial t^2}+D_{\mathbf{x}t}\frac{\partial(\nabla\phi C)}{\partial t}-\Lambda(\phi C)\end{aligned}$$

where the detailed coefficients and moments, when time interval is infinitesimal, are:

$$\mathbf{u}(r_s,\mathbf{x},t)=\langle\mathbf{l}\rangle_p/\langle\tau\rangle_p;\ D_t(r_s,\mathbf{x},t)=\langle\tau^2\rangle_p/2\langle\tau\rangle_p$$

$$D_{\mathbf{x}}(r_s,\mathbf{x},t)=\langle\mathbf{l}^2\rangle_p/2\langle\tau\rangle_p;\quad D_{\mathbf{x}t}(r_s,\mathbf{x},t)=\langle\mathbf{l}\tau\rangle_p/2\langle\tau\rangle_p$$

$$\Lambda(r_s,\mathbf{x},t))=(1-P(r_s,\mathbf{x},t))/\langle\tau\rangle_p$$

$$\langle\mathbf{l}\rangle_p=\int_0^\infty\int_0^\infty\int_0^1 d^d\mathbf{l}\,d\tau\,dp\{\mathbf{l}pf(\mathbf{l},\tau,p\,|\,r_s,\mathbf{x},t)\};$$

$$\langle\mathbf{l}^2\rangle_p=\int_0^\infty\int_0^\infty\int_0^1 d^d\mathbf{l}\,d\tau\,dp\{\mathbf{l}^2pf(\mathbf{l},\tau,p\,|\,r_s,\mathbf{x},t)\};$$

$$\langle\tau\rangle_p=\int_0^\infty\int_0^\infty\int_0^1 d^d\mathbf{l}\,d\tau\,dp\{\tau pf(\mathbf{l},\tau,p\,|\,r_s,\mathbf{x},t)\};$$

$$\langle\tau^2\rangle_p=\int_0^\infty\int_0^\infty\int_0^1 d^d\mathbf{l}\,d\tau\,dp\{\tau^2pf(\mathbf{l},\tau,p\,|\,r_s,\mathbf{x},t)\};$$

$$\langle\mathbf{l}\tau\rangle_p=\int_0^\infty\int_0^\infty\int_0^1 d^d\mathbf{l}\,d\tau\,dp\{\mathbf{l}\tau pf(\mathbf{l},\tau,p\,|\,r_s,\mathbf{x},t)\};$$

The last sink term in represents the retention rate which reflects the capture probability (1-p) on the microscopic level, and this coefficient physically represents the retention probability per unit length of porous media and per unit time. The first coefficient **u** which is the average of step length divided by the average of waiting time is actually the average particle velocity in the pore.

Pore kinetics

The pore structure is changed only when the particles are captured by the pores. To reveal the random process the introduction of a probability for the pore size change is convenient and also necessary for the case of incomplete pore plugging[3]. Let us introduce such a probability ($r_p\rightarrow r_p$') as the probability of the pore radius changing from r_p to r_p' while capturing a particle of r_s, i.e. when a particle of r_s is captured at **x**,t the pore radius is changed from r_p into r_p', the distribution of r_p is f(r_p|r_s,**x**,t), the distribution of r_p' is f(r_p'|r_s,**x**,t), the total probability is:

$$P_d(r_s,\mathbf{x},t,r_p\rightarrow r_p')=P_d(r_s,\mathbf{x},t)f(r_p\,|\,r_s,\mathbf{x},t)f(r_p'\,|\,r_s,\mathbf{x},t);$$

$$P_d(r_s,\mathbf{x},t,r_p\rightarrow r_p')=0:\ r_p\le r_p';$$

$$f(r_p'\,|\,r_s,\mathbf{x},t)=0:\ r_p\le r_p';$$

$$\int_0^\infty P_d(r_s,\mathbf{x},t,r_p\rightarrow r_p')dr_p'=P_d(r_s,\mathbf{x},t)f(r_p\,|\,r_s,\mathbf{x},t);$$

$$\int_0^{r_p} P_d(r_s,\mathbf{x},t,r_p\rightarrow r_p')dr_p'=P_d(r_s,\mathbf{x},t)f(r_p\,|\,r_s,\mathbf{x},t);$$

The second equation above corresponds reflects the fact that the particle will and can only decrease the size of the pore. The resulted integration p_d (r_s,r_p,**x**,t) the total probability for the particles of r_s being captured by the pores of r_p at (**x**,t). The introduction of such a probability is nontrivial in the following sense. The pore kinetics is described on the premise of the pore of r_p capturing a particle of r_s; both of the pore and particle shape parameters are known. Nonetheless the pore size change is still random. This can be illustrated by **Figure 2**, in which the resulted pore shape parameter is random due to the random capture process.

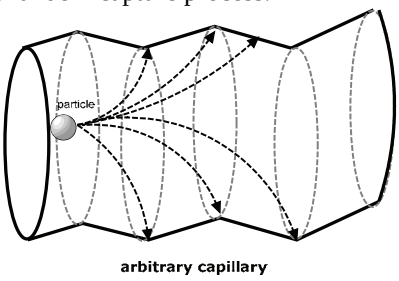

Figure 2: the random capture process of a particle smaller than the pore

Here the governing equations for the pore evolution are obtained following a similar procedure as in Ref[3]. The change of the pore distribution of r_p is revealed by the increasing term and a decreasing term. Larger pores than those of r_p capturing particles may increase the number the pores of r_p. Pores of r_p capturing particles leads to decreasing the number of pores of r_p.

$$\mathrm{H}(\mathbf{x},t,r_s,r_p)\text{-}\mathrm{H}(\mathbf{x},t\text{-}\tau,r_s,r_p)=I(\mathbf{x},t,r_s,r_p)-D(\mathbf{x},t,r_s,r_p)$$

where I represent the increase rate and D represents the decrease rate of the number of pores of r_p during the time τ. Since the particle capture does not influence the pore length, the pore distribution adopted here does not depend on the pore length. Define the probability to have 1-p for a particle to be captured simultaneously with the setting (l,τ,r_s,p,x,t):

$$P_d(\mathbf{l},\tau,p,r_s,\mathbf{x},t) = P_d(r_s,\mathbf{x},t)\, f(\mathbf{l},\tau,p \mid r_s,\mathbf{x},t)$$

where $P_d(r_s,\mathbf{x},t)$ is total probability for a particle of r_s being captured, this is defined in the same fashion as regarding the particle passing the pore. The probability for a particle to be captured with the setting (l,τ,r_s,p,x,t):

$$(1-p)P_d(\mathbf{l},\tau,p,r_s,\mathbf{x},t) = \left(1-pf(p \mid \mathbf{l},\tau,r_s,\mathbf{x},t)\right)c(\mathbf{l},\tau,r_s,\mathbf{x},t)$$

According to definition of microscopic p_d the probability for the particle of r_s being captured, with the particle flight as (l,τ,p) and the pore of r_p to be changed into r_p':

$$P_d(\mathbf{l},\tau,p,r_s,\mathbf{x},t,r_p \to r_p') = P_d(\mathbf{l},\tau,p,r_s,\mathbf{x},t)\, f\left(r_p \mid \mathbf{l},\tau,p,r_s,\mathbf{x},t\right) f\left(r_p' \mid \mathbf{l},\tau,p,r_s,\mathbf{x},t\right)$$

With the obtained probability above the decreasing term can be formulated as:

$$D(\mathbf{x},t,r_s,r_p) = \int_0^1\int_0^{r_p} dp\,dr_p' \left\{\begin{matrix}(1-p)P_d(\mathbf{l},\tau,p,r_s,\mathbf{x},t,r_p \to r_p')* \\ \left[\phi(\mathbf{x}-\mathbf{l},t-\tau)C(\mathbf{x}-\mathbf{l},t-\tau,r_s)\right]\end{matrix}\right\}$$

$$= \int_0^\infty\int_0^\infty\int_0^1\int_0^{r_p} d\mathbf{l}\,d\tau\,dp\,dr_p' \left\{\begin{matrix}(1-p)P_d(\mathbf{l},\tau,p,r_s,\mathbf{x},t)\, f\left(r_p \mid \mathbf{l},\tau,p,r_s,\mathbf{x},t\right)\times \\ f\left(r_p' \mid \mathbf{l},\tau,p,r_s,\mathbf{x},t\right)\left[\phi(\mathbf{x}-\mathbf{l},t-\tau)C(\mathbf{x}-\mathbf{l},t-\tau,r_s)\right]\end{matrix}\right\}$$

According to the property of p_d the integral for r_p' can be reduced to:

$$D(\mathbf{x},t,r_s,r_p) = \int_0^\infty\int_0^\infty\int_0^1 d\mathbf{l}\,d\tau\,dp \left\{\begin{matrix}(1-p)P_d(\mathbf{l},\tau,p,r_s,\mathbf{x},t)\, f(r_p \mid \mathbf{l},\tau,p,r_s,\mathbf{x},t)\times \\ \left[\phi(\mathbf{x}-\mathbf{l},t-\tau)C(\mathbf{x}-\mathbf{l},t-\tau,r_s)\right]\end{matrix}\right\}$$

Taylor expansion of the inside of the integral leads to the total equation for the pore kinetics:

$$D(\mathbf{x},t,r_s,r_p) = \int_0^\infty\int_0^\infty\int_0^1 d\mathbf{l}\,d\tau\,dp \left\{\begin{matrix}(1-p)P_d(\mathbf{l},\tau,p,r_s,\mathbf{x},t)\, f(r_p \mid \mathbf{l},\tau,p,r_s,\mathbf{x},t)\times \\ \left(\begin{matrix}\phi(\mathbf{x},t)C(\mathbf{x},t,r_s) - \mathbf{l}\dfrac{\partial(\phi C)}{\partial\mathbf{x}} - \tau\dfrac{\partial(\phi C)}{\partial t} \\ -\mathbf{l}^2\dfrac{\partial^2(\phi C)}{\partial\mathbf{x}^2} - \tau^2\dfrac{\partial^2(\phi C)}{\partial t^2} - \mathbf{l}\tau\dfrac{\partial^2\phi C}{\partial t\partial\mathbf{x}}\end{matrix}\right)\end{matrix}\right\}$$

Further reformations lead to the following elliptic PDE form inside the integral:

$$\frac{\partial H(\mathbf{x},t,r_s,r_p)}{\partial t} = P_d(r_s,\mathbf{x},t)\, f(r_p \mid r_s,\mathbf{x},t)\times\left[1-\int_{r_p}^\infty dr_p' f\left(r_p' \mid r_s,\mathbf{x},t\right)\right] \left\{\begin{matrix}\dfrac{\partial(\phi C)}{\partial t} + \mathbf{u}_d(r_s,\mathbf{x},t)\dfrac{\partial(\phi C)}{\partial\mathbf{x}} + D_{xd}(r_s,\mathbf{x},t)\dfrac{\partial^2(\phi C)}{\partial\mathbf{x}^2} \\ +D_{td}(r_s,\mathbf{x},t)\dfrac{\partial^2(\phi C)}{\partial t^2} + D_{xtd}(r_s,\mathbf{x},t)\dfrac{\partial^2\phi C}{\partial t\partial\mathbf{x}}\end{matrix}\right\}$$

where the coefficients with the subscript 'd' possess almost the same definitions as in the particle kinetics, only the probability for the moments calculation is p_d.

CFD implementation

The numerical solution to this non-linear problem is non-trivial. The present computation is confined to the mechanism of size exclusion, in which the increasing term I in the equation above disappear (one particle remains, one pore dies). Setting the constant flow the fluid is accelerated due to convection. We adopt the matrix form of the elliptic PDE for the particle kinetics, where the four boundary conditions are set as: inject suspension for one fifth of the total injection time then inject water to 'wash away' the particles, so that at the end of time the suspension concentration is zero. After solving once the concentration profile we solve the equations of porosity evolution and the velocity profile with convection acceleration. The iteration with this pattern of calculation continues until converge.

Results

The behavior of the elliptic PDE for the particle kinetics is shown in Figure 3. It can be observed that the velocity of the peak is slower and the tail at the outlet is larger in the elliptic model than those in the parabolic ADE.

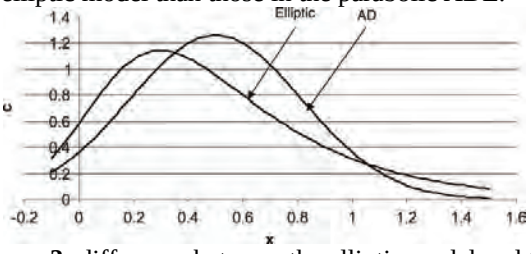

Figure 3: difference between the elliptic model and the parabolic ADE[2]

The concentration profile for the particles of a certain size can be found in Figure 4, in which at the end of injection time all particles are washed away. For particles of n sizes there are n similar profiles like this. The porosity profile in Figure 5 shows that the porosity decline is most dramatic at the inlet. The velocity profile shows that the fluid is accelerated due to convection as in Figure 6. The deposition profile shows that the deposition accumulates mostly at the inlet as seen in Figure 7. This corresponds to the porosity decline profile and the velocity profile.

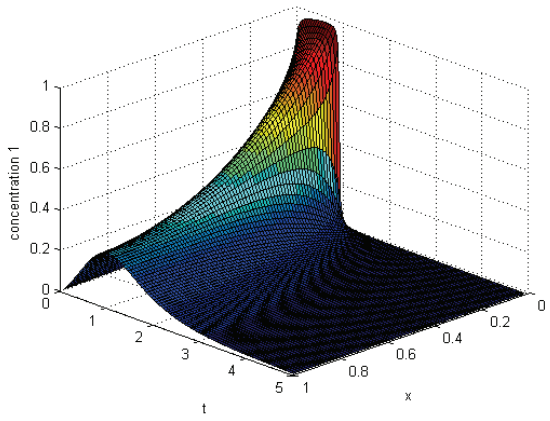

Figure 4: suspension concentration profile

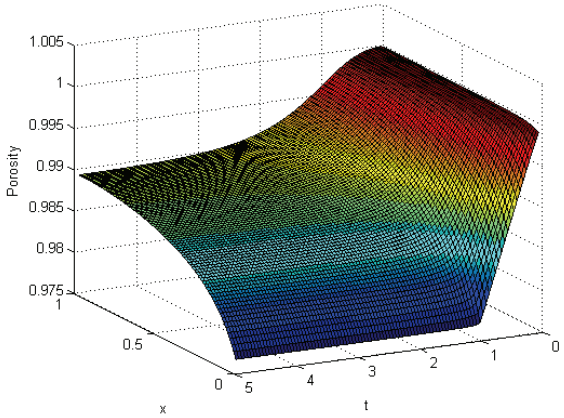

Figure 5: porosity decline profile

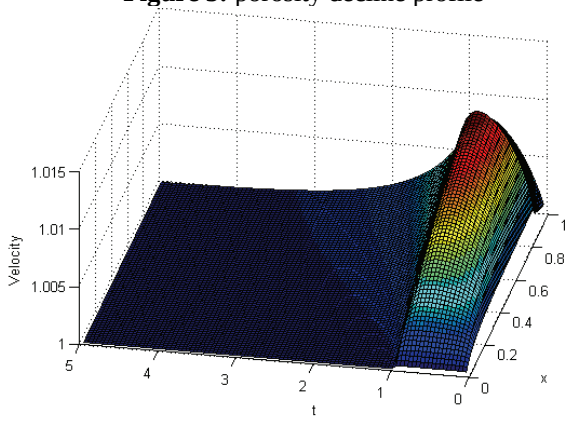

Figure 6: fluid velocity profile

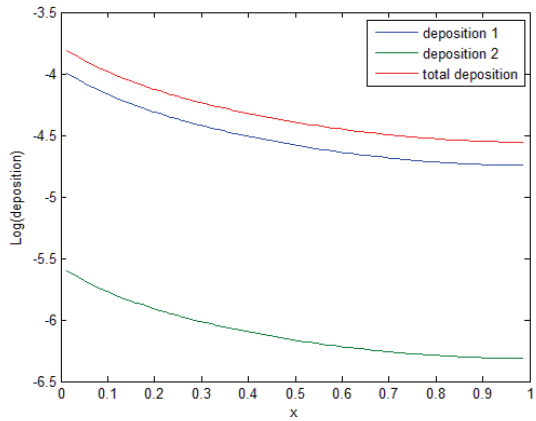

Figure 7: deposition accumulation profile

References

1. Shapiro, A.A., *Elliptic equation for random walks. Application to transport in microporous media.* Physica A: Statistical Mechanics and its Applications, 2007. **375**(1): p. 81-96.
2. Shapiro, A.A. and P.G. Bedrikovetsky, *Elliptic random-walk equation for suspension and tracer transport in porous media.* Physica A: Statistical Mechanics and its Applications, 2008. **387**(24): p. 5963-5978.
3. Shapiro, A., et al., *A stochastic model for filtration of particulate suspensions with incomplete pore plugging.* Transport in Porous Media, 2007. **67**(1): p. 135-164.
4. Santos, A. and P. Bedrikovetsky, *Size exclusion during particle suspension transport in porous media: stochastic and averaged equations.* Computational and Applied Mathematics, 2004. **23**(2-3): p. 259-284.
5. Tufenkji, N. and M. Elimelech, *Breakdown of Colloid Filtration Theory: Role of the Secondary Energy Minimum and Surface Charge Heterogeneities.* Langmuir, 2005. **21**(3): p. 841-852.
6. Tufenkji, N., J.A. Redman, and M. Elimelech, *Interpreting Deposition Patterns of Microbial Particles in Laboratory-Scale Column Experiments.* Environmental Science & Technology, 2003. **37**(3): p. 616-623.
7. Metzler, R. and J. Klafter, *The random walk's guide to anomalous diffusion: a fractional dynamics approach.* Physics Reports, 2000. **339**(1): p. 1-77.
8. Cortis, A. and B. Berkowitz, *Anomalous Transport in "Classical" Soil and Sand Columns.* Soil Sci Soc Am J, 2004. **68**(5): p. 1539-1548.
9. Barkai, E., R. Metzler, and J. Klafter, *From continuous time random walks to the fractional Fokker-Planck equation.* Physical Review E, 2000. **61**(1): p. 132.
10. Herzig, J.P., D.M. Leclerc, and P.L. Goff, *Flow of Suspensions through Porous Media-Application to Deep Filtration.* Industrial & Engineering Chemistry, 1970. **62**(5): p. 8-35.

Linfeng Yuan
Phone: +45 4525 2955
Fax: +45 4593 2906
E-mail: lfy@kt.dtu.dk
WWW: http://www.kt.dtu.dk/
Supervisors: Gunnar Jonsson
John M Woodley
Lars Korsholm, Novozymes A/S
Sune Jakobsen, Novozymes A/S

PhD Study
Started: March 2008
To be completed: March 2011

Membrane Assisted Enzyme Fractionation - Using Amino Acids as a Model

Abstract
An enzyme concentrate produced by fermentation will often contain two or more enzyme activities. For application it is often necessary therefore to separate the enzymes so as to remove any side activity. The aim of this project is to develop a suitable membrane fractionation process and to assess the economics of such a process for industrial scale production. Like enzymes, amino acids have an amphoteric character and therefore the separation of amino acids in solution is an interesting model for the separation of charged compounds with similar properties. In this work we report studies concerning the separation of L-leucine (Leu) from L-glutamic acid (Glu) by electro-membrane filtration (EMF) with an ultrafiltration (UF) membrane. The highest Leu fraction in the permeate and highest separation factor were 96.4% and 28.5 respectively.

Introduction
Large-scale economic purification of proteins is an increasingly important problem for the biotechnology industry. Separation of the desired protein from other proteins produced by the cell is usually attempted using a combination of different chromatography techniques. Adequate purity is often not achieved unless several purification steps are combined, thereby increasing cost and reducing product yield. Consequently there is a need for processes that purify protein mixtures using fewer steps and without the need for a costly affinity step.

Membrane processes are widely used in the biochemical industry for separation and concentration of protein. Traditionally fractionation of enzymes using membranes due to the variation in size of the proteins is rather limited, which is partly caused by concentration polarization and membrane fouling.

Motivation
Recent publications have shown that by careful control of the concentration polarization, and use of charged membranes, a dramatic effect can be seen on the separation efficiency of such membranes.

Enevoldsen et. al. has shown that by using an electrical field during crossflow ultrafiltration (EUF), a 3-7 times improvement in flux has been obtained. This indicates that using an overlaid electric field is an effective way to depolarize the membrane surface when operating with enzyme solutions [1,2]. It is possible that EUF can be used for the separation of two enzymes with opposite charge sign since enzymes can carry different charges by adjusting the pH of the solution. Another possibility is to separate the enzyme product from impurities in the solution by dragging the charged enzyme through the membrane. This could also improve the purity of the enzyme product.

In addition, Jonsson et. al. has shown that using high frequency backflushing of the membrane surface is very effective at reducing the concentration polarization and can further be used to tune the membrane selectivity and therefore in principle be used to make a fractionation of enzymes [3, 4].

Combining these techniques with the use of a charged membrane is expected to give the desired separation properties which can further be scaled-up to a feasible ultrafiltration membrane system.

Specific Obejctives
The project aims at developing and economically assessing a pilot scale membrane fractionation process as this might be more economical for bulk enzyme purification compared to current technologies.

The feasible membrane fractionation process to be considered or investigated will potentially include:

- EUF
- Charged membranes
- Membrane systems using high frequency pulsation and / or vibration

Feed solution properties such as pH, ionic strength, additives can be chosen as appropriate.

If an efficient process is developed then pilot up-scaling of the membrane fractionation process will be considered.

Experimental

Materials

The main physical-chemical properties of each amino acid under study are presented in Table 1. L-Leucine (≥ 99.5%(NT)), L-Lysine(≥ 97%) and L-Glutamic acid(≥99.5%(NT)) were obtained from Sigma-Aldrich. The feed solution of the amino acids for the experiments was prepared by dissolving the amino acids in RO water. Before all the EMF experiments the pH was adjusted to a certain value by adding 0.1M NaOH or 0.1M HCl.

Table1: Physical-chemical properties of amino acids used in the study [5]

Amino acid	MW	pI	pKa Values		
			α-COOH	α-$^{+}$NH3	Side chain
Leucine (Leu)	131.18	6.01	2.33	9.74	/
Lysine (Lys)	146.19	9.60	2.16	9.06	10.54
Glutamic acid (Glu)	147.13	3.15	2.10	9.47	4.07

-EMF module and set-up

To prevent direct contact between the solutes (enzymes or amino acids in this case) and the electrodes, the EMF cell is configured according to Figure 1.

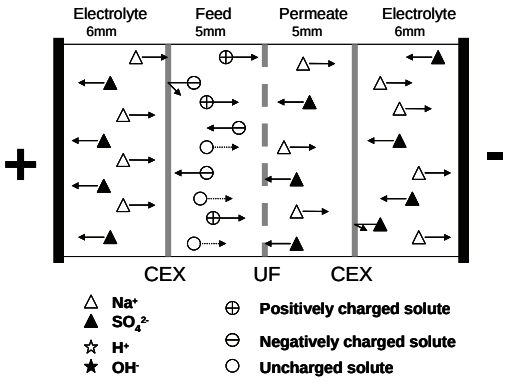

Figure 1: EMF module with an UF membrane (10KDa) placed between two cation exchange membranes [1].

A schematic representation of the EMF set-up used in this study is presented in Figure 2. The EMF cell consisted of four chambers. A UF membrane was placed between two cation exchange membranes (CEX), depending on the pore size of the UF membrane compared to the size of the solutes; it either retained solutes or let them pass through it. Flow spacers were used to enable adequate flow of the different streams. By using CEX membranes in front of both the anode and cathode it was possible to prevent an accumulation of salt ions in the feed stream.

The volume of the feed compartment (F), permeate compartment (P) and two electrolyte compartments (E) (including supply tank and piping volume) were 2.5L, 0.3L and 1L, respectively. The set-up was operated in a batch-wise manner. Both retentate and electrolyte were recirculated back to the feed and electrolyte tank, apart from that removed for sampling. The permeate stream was kept at a constant volume by an overflow pipe in the permeate tank, in which the excess amount of permeate was taken during a certain time for flux measurement and sampled for analysis. The recirculation flow rate of permeate and electrolyte solution were at a rate of 22L/h and 80L/h, respectively. In order to equalize the pH change in the anolyte and catholyte, the two streams were mixed. The two electrodes were made of platinized titanium. The electric field was generated by a power supply from xantrex (XHR 150-7). The TMP can be set by adjusting a valve placed on the retentate side. The electrolyte consisted of 0.1M Na_2SO_4. The initial permeate was 0.05M Na_2SO_4.The UF membrane was a 10kDa surface-modified PVDF ETNA 10PP membrane from Alfa Laval and the CEX membrane was a RELAX-CMH membrane from Mega. The membrane area was 10×10 cm^2. More details about the set-up have been described elsewhere [1,2].

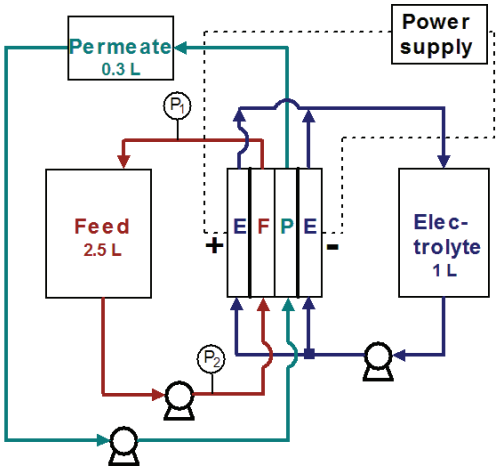

Figure 2: The experimental set-up, in which the EMF cell consists of 4 chambers separated by a 10KDa ultrafiltration(UF) membrane flanked by two cation exchange membrane(CEX)

Analytical methods

The concentration determination of Lys, Glu and Leu was done by HPLC (DIONEX, UltiMate 3000).
Column: Acclaim OA, 5 µm; Dimensions: 4 x 150 mm; Mobile Phase: 40 mM Na_2SO_4, pH 2.60 (adjusted with methanesulfonic acid); Temperature: 30 °C; Flow Rate: 0.6 mL/min; Injection Volume: 20 µL; Detection: UV, 210 nm

Results and Discussion

Calculation of the net charge percentage of amino acid at a given pH

We can calculate the relative fraction of the various forms of amino acid as a function of pH by using the Henderson-Hasselbalch equation described below:

$$pH = pKa + \log\frac{[A-]}{[HA]}$$

$$\text{and } pH = pKa + \log\frac{[base]}{[acid]}$$

pKa is –log(Ka), where Ka is the acid dissociation constant.

The relative fraction for various forms of Glu, Leu and Lys as a function of pH is shown in Figure 3a, Figure 3b and Figure 3c respectively.

These plots help to identify what forms of amino acid exist at a given pH value and eventually predict the migration direction through the membranes. In addition, one can obtain the specific form by adjusting the pH using these plots.

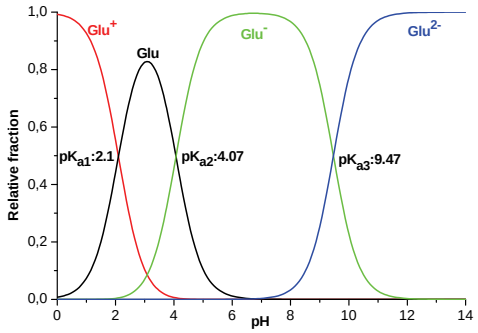

Figure 3a: Relative fraction for various forms of Glu as function of pH

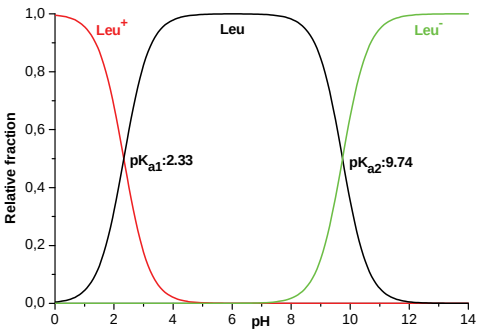

Figure 3b: Relative fraction for various forms of Leu as function of pH

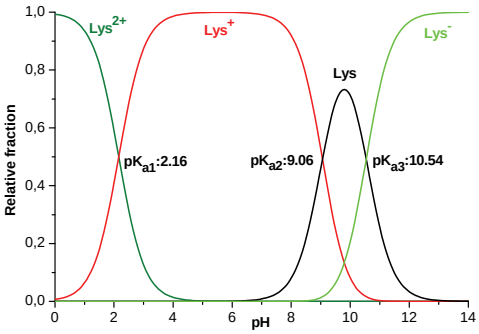

Figure 3c: Relative fraction for various forms of Lys as function of pH

Single amino acid

The transport of a single amino acid (Glu or Lys in this study) at different polarity was conducted in order to investigate the effect of electrophoresis due to the electric field.

Figure 4 shows the Glu concentration change in permeate both with and without applying electric field at 2 different polarities. The feed pH stayed at 6.5-8, hence Glu was negatively charged according to Figure 3a. The initial feed concentration of Glu was around 9mM. In the first 45min, there was no electric field applied, therefore the negatively charged Glu migrated into the permeate compartment because of convective transport due to trans membrane pressure (TMP). After 45min when applying the electric field in the direction of –UF+, it can be seen in Figure 4 the permeate concentration change of Glu was much enhanced due to the electrophoretic effect in addition to convective transport. While in the case of alternating the polarity into +UF-, the permeate concentration of Glu started slowing down after 45min, again due to the electrophoretic effect which dragged the Glu away from UF membrane in direct competition with convective transport.

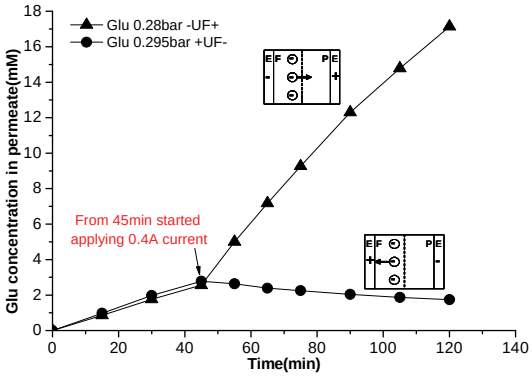

Figure 4: The change of Glu concentration in permeate with and without the application of electric field at different polarity when Glu was negatively charged in the feed.

Figure 5 shows the Lys concentration in permeate both with and without applying electric field at polarity +UF-. The feed pH stayed at 7-7.6, hence Lys was positively charged according to Figure 3c. The initial feed concentration of Lys was 8mM. As can be seen in Figure 5, the permeate concentration of Lys increased when the electric field was applied in comparison with the first 45min where there was only convective transport taking place. However, after 80min the permeate concentration of Lys started decreasing dramatically to 0mM at 160min. By checking the Lys concentration in the electrolyte compartment, we found that Lys started being transported into the electrolyte compartment from 80min. The phenomena that the permeate concentration of Lys decreased from 80min could be explained a follows: first, positively charged Lys can pass through the cation exchange membrane;

secondly, after 80min the conductivity of permeate was quite low hence the Lys was transported instead of Na+.

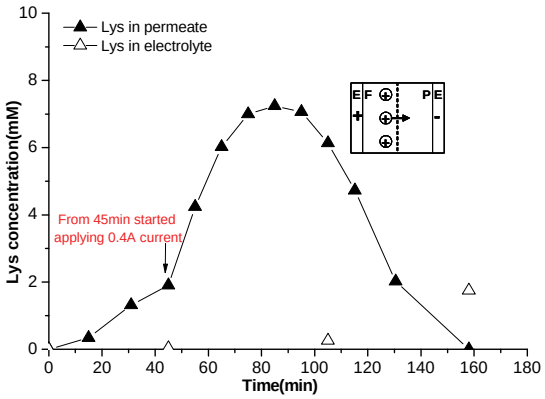

Figure 5: The change of Lys concentration in permeate without and with the application of electric field at polarity +UF- at constant TMP 0.28bar when Lys was positively charged in the feed

Binary mixture

Glu and Leu cannot be separated by a normal UF membrane based on the molecular size difference (data not show), therefore we have examined if separation could take place by applying an electric field.

The binary mixture of Glu and Leu with initial feed concentration around 10.5mM was used. The feed pH during the experiments stayed 6.3-6.7. According to Figure 3a and 3b, Leu is neutral and Glu is negatively charged.

As can be seen from Figure 6, separation of Leu and Glu proved possible by applying an electric field through the UF membrane. Leu was transported to the permeate only due to convective transport. However, the transport of charged Glu was controlled both by the electrophoretic effect and the convective effect, in which the electrophoretic effect dragged Glu away from UF membrane. Therefore the transport of Glu to permeate was a cause of the competition between convective transport and the electrophoretic transport due to TMP and current, respectively.

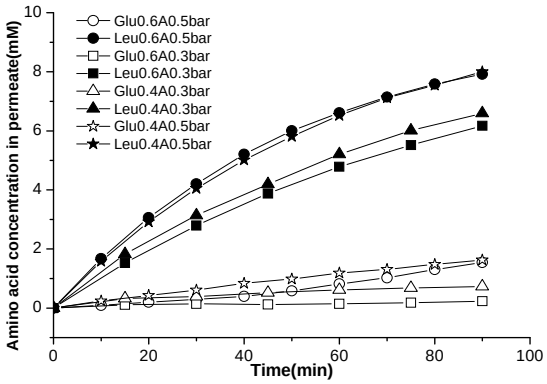

Figure 6: Leu and Glu concentration change in permeate at different current and TMP at polarity +UF-

In addition, as Table 2 shows, the selectivity and purity were very much dependent on the operational parameters (current and TMP). When having a combination of the highest current 0.6A and lowest TMP 0.3bar, the highest selectivity 28.5 and highest purity 96.4% can be obtained.

Table2: Selectivity and purity comparison of each experiment at 90min

Current, TMP	Selectivity($\alpha_{Leu/Glu}$)	Purity (Leu% in permeate)
0.6A,0.3bar	28,5	96,4
0.6A,0.5bar	6,5	83,7
0.4A,0.3bar	9,8	90
0.4A,0.5bar	5,4	83,1

Conclusions

In this study, we have used amino acids as model to investigate the possibility of using EMF to separate charged components. The experimental study was carried out with solutions of increasing complexity, i.e. single amino acid solution and subsequently, binary mixtures.

This work clearly indicates that the:

- electric field has a big effect on the transport of a charged amino acid
- EMF shows great potential to separate two amino acids with high separation factor and purity, which normal UF cannot achieve
- selectivity and purity can be tuned by using different combinations of current and TMP
- permeate conductivity is crucial to control the pH in the permeate (data not show)
- water splitting could take place when the permeate conductivity is low.

Acknwdegements

The Novozymes Bioprocess Academy is acknowledged for the financial support of this project.

References

1. A.D. Enevoldsen Electrically enhanced ultrafiltration of industrial enzyme solutions, Technical University of Denmark, Ph.D. thesis, 2007
2. A.D. Enevoldsen, E.B. Hansen and G. Jonsson, Journal of Membrane Science 299 (2007) 28-37
3. S. P. Beier and G. Jonsson, Separation and Purification Technology 53 (2007) 111–118.
4. G. Jonsson, Fractionation of macromolecules by dynamic ultrafiltration, 7th World Conference on Chemical Engineering in CD, Glasgow, 2005
5. http://www.unc.edu/~bzafer/aminoacids/

Adeel Zahid

Phone: +45 4525 2876
Fax: +45 4588 2258
E-mail: adz@kt.dtu.dk
WWW: http://www.ivc-sep.kt.dtu.dk/
Supervisors: Erling H Stenby
Alexander Shapiro

PhD Study
Started: January 2009
To be completed: December 2011

Advanced Waterflooding in Low Permeable Carbonate Reservoirs

Abstract
Careful design of Injecting brine composition in waterflooding is a part of strategy to improve the oil recovery both in carbonate and sandstone reservoirs. We are conducting experiments with ROP flooding rig and also investigating tracer wettability test to understand the mechanism of this waterflooding process. Experiments with AFM and SEM will also be conducted to study the interaction of seawater ions with rock and crude oil.

Introduction
It is still expected that more than half of the world's remaining oil exists in carbonate reservoirs [1]. They have rather low primary oil recovery; the improved oil recovery potential of these reservoirs is high. Many carbonate reservoirs are fractured and intermediate oil wet, so the improved oil recovery from such reservoirs is regarded as a great challenge.
Waterflooding is a secondary oil recovery process and is by far the most widely applied method for improving the oil recovery. Over the last decade, a number of studies have shown that waterflooding performance is dependent on the composition of injecting brine solution. Optimizing the injecting brine composition has been developed into an emerging IOR (Improved Oil Recovery) technology for both sandstone and carbonate reservoirs. Extensive laboratory research has been carried out by Austad and co-workers in order to understand improved oil recovery from chalk using surfactant solutions and later on using modified sea water [2],[3]. They explained wettability alteration towards more water wetting conditions as the reason for improvement in oil recovery. But still many things for understanding the mechanism of this process are not clear.
Research on this subject covered a broad range of disciplines, including colloid and surface chemistry, petroleum engineering and nano technology.

Fundamental Concept of Wettability
In a rock/brine/oil system, wettability is a measure of the preference that the rock has either for oil or water [4].

Wettability of formation is of utmost importance which controls the location, flow and spatial distribution of fluid in the rock. Wettability also has been shown to affect the waterflood behavior, relative permeability, capillary pressure, irreducible water saturation and electrical properties in the open literature. Fundamental understanding of wettability and the reliable data of the wettability of rock is extremely important for the development of a production scheme. Below is the illustration of different wetting states of reservoir rocks.

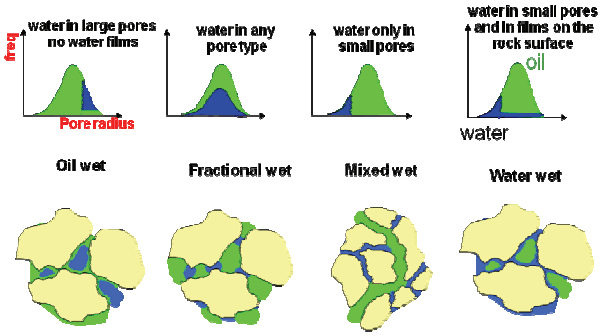

Figure 1: Illustration of different wetting conditions of rock

There are different methods for the measurement of wettability. Most Commonly used wettability measuring methods are contact angle, Amott Harvey index and USBM method. Recently Austad and coworkers developed a new tracer wettability method based on the adsorption of sulphate ions on water wetting surface area of chalk [5].

Specific Objectives

The Objectives of this PhD project are

- Understanding the effect of injecting brine composition, temperature and crude oil properties on waterflood oil recovery.
- What is the exact mechanism of increment in oil recovery with seawater ions (SO_4^{2-}, Ca^{2+} and Mg^{2+})?
- Exploring the possible benefit of these ions for limestone, dolomite and reservoir chalk cores.
- Wettability and microscopic and submicroscopic (nanoscale) analysis.

Experiments

As a first step of the experimental work, we measured the Acid number (AN) and Base number (BN) of three different crude oils using modified versions of ASTM D2896 for BN and D664 for AN [6].

As a second step we started to investigate the newly developed tracer wettability test by Austad and co-workers using both outcrop and reservoir chalk. Core plugs of different wettability are prepared with and without initial water saturation. We used different original crude oils for core preparation.

We are also investigating the reasons of observed improvement in oil recovery with sulphate ions. Is it really wettability alteration or something else? Most of the previous work has been done on the basis of spontaneous imbibition using core plugs aged in crude oil. Our study is based on flooding and using completely water wet core without being aged in crude oil, just saturated with crude oil under vacuum. Brine without sulphate is considered as the base fluid. After waterflooding with this brine, the cores are flooded with brine enriched with sulphate. The effect of temperature and flow rate of both brines on the recovery factor and the recovery rate are also under investigation.

Results and Discussion

Below is the potentiometric titration result for the crude oils.

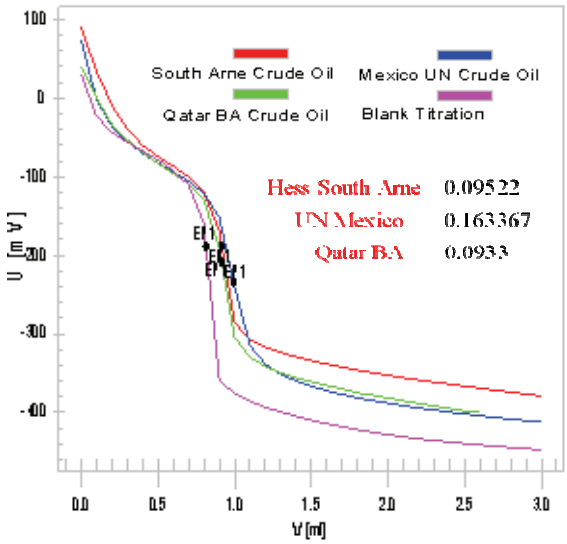

Figure 2: Titration result for AN measurement

In figure2 titrations of crude oils mixtures are compared with blank mixture. AN can be obtained from the difference between the end points with and without crude oil.

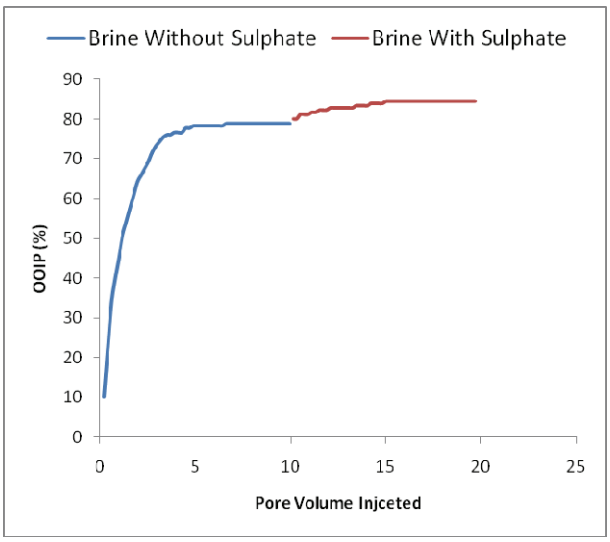

Figure 3: Core flooding with modified seawater with and without sulphate at 5 PV/day at 90 ºC.

In figure 3, for Stevin Klint outcrop core sample, we have observed 4-6 % increase of OOIP using brine with sulphate for water wet chalk at 90 ºC. This clearly indicates improvement in oil recovery without wettability alteration because chalk is already water wet. No improvement in oil recovery was observed at 40 ºC.

Future Work

Tracer wettability test will continue for other core plugs and we will also compare it with famous Amott Harvey wettability index.

We will focus on investigating the reasons of increment in oil recovery beside wettability alteration. Is it because of sulphate oil interaction or sulphate rock interaction and also why only at high temperature?

In future we also investigate the adsorption of seawater ions and wettability alteration phenomenon with Atomic force microscopy using calcite and APTES (3-aminopropyltriethoxy silane) coated mica substrates.

Acknowledgements

We are grateful to DONG Energy for funding this study as a part of the ADORE project.

References

1. Akbar, M. et al., Oilfield Review, 12(4), 20-21, 2000/2001.
2. T.Austad and D.C.Standnes, Journal of Petroleum Science and Engineering, 28(2002) 123-143.
3. T.Austad, P.Zhang, Colloid and Surfaces A: Physicochem Eng. Aspects 301(2007) 199-208.
4. W.G.Anderson, SPE 13932, JPT, 1986.
5. T.Austad et. al., Journal of Petroleum Science and Engineering, 52(2006) 187-197.
6. Fan, T and Buckley, J.S, SPE 99884, 2007.

Dayang Norulfairuz Abang Zaidel

Phone: +45 4525 2861
Fax: +45 4593 2906
E-mail: daz@kt.dtu.dk
Web page: http://www.kt.dtu.dk
Supervisors: Anne Meyer
John M. Woodley

PhD Study
Started: August 2008
To be completed: July 2011

Enzymatic Production of Cross-linked Plant Cell Wall Polymers

Abstract
This PhD project is based on the premise that improved emulsification and prebiotic effects in sugar beet pulp (SBP) and barley spent grain (BSG) can be achieved by cross-linking of feruloylated polysaccharide structures. The aims of the project are to establish the kinetic basis of the cross-linking reactions and characterize the macromolecular function of the resulting cross-linked polysaccharides in terms of their rheological properties and emulsion stabilizing effects.

Introduction
Recently, it has been recognized that polysaccharides, categorized as dietary fibres and prebiotic oligosaccharides, may exert potential physiological benefits beyond their classical effects. For instance, their ability to bind bile acids, cholesterol, and toxic compounds present in the digestive tract suggest that a number of oligosaccharides and polysaccharides may have an important preventative role against various chronic diseases such as coronary heart disease [1].

It is well established that many plant cell walls contain phenolic acids that are ester-linked to polysaccharides. They are mainly ester-linked to *O*-2 of the α-(1→5)-linked arabinan chains and to *O*-6 of β-(1→4)-linked type I of galactan chains [2]. It was reported that ferulic acid esters in plant cell walls could undergo oxidative coupling reactions to form dehydromers (diFAs) [2-4]. This oxidative reaction can be catalyzed by various systems such as peroxidases (with hydrogen peroxide), polyphenol oxidases, including laccases, as well as some purely chemical systems [4]. From these reactions various diFAs are formed: 5-5′, 8-O-4′, 8-5′ and 8-8′ (Figure 1). Formation of diFA enables covalent cross-linking of the polysaccharides they esterify. The previous studies indicated that the feruloylated polymers have an effect on the mechanical properties of plant cell wall *i.e.* a tightening effect on the plant cell wall (contributing to wall assembly, promotion of tissue cohesion and resistance against fungal penetration). This project is built on the premise that the cross-linked polysaccharides are able to enhance the emulsification stability of the polysaccharides [5].

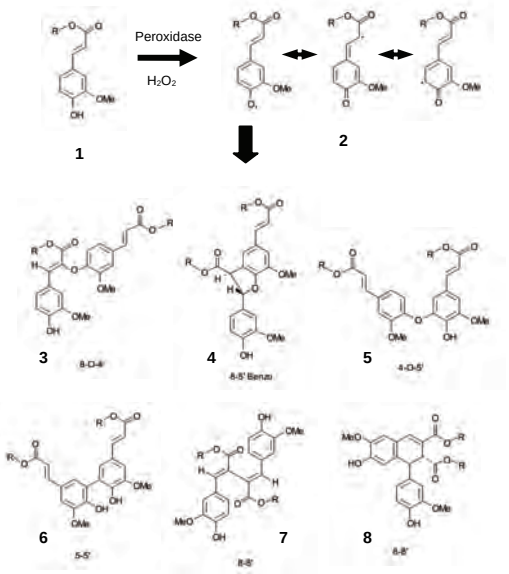

Figure 1: Dimerization of ferulate esters **1** via phenoxy radical **2** which react to form dehydrodiferulate esters **3-8** [4,6].

Objectives
The first objective of this project is to establish and describe the kinetic reactions of the enzymes involved in the *in vitro* cross-linking of the polysaccharides with

the various substrates. It is expected that the concentration of ferulic acid substrate and the size of the substrate affect the kinetics of the enzymatic reaction. The second objective is to characterize the macromolecular properties of the cross-linked polysaccharides in terms of rheological measurements and then establish the correlation between the macromolecular function of the cross-linked polysaccharides and the reaction kinetics. Finally, it is aimed to investigate the effect of emulsification stability of the cross-linked polysaccharide.

Current Work

In this work, cross linking of ferulic acid (FA) in arabinan sample was done by the addition of horseradish peroxidase (HRP) and hydrogen peroxide H_2O_2. The cross-linking was monitored by the disappearance of FA absorbance at 316 nm for 10 minutes. The absorbance decreased steeply at the beginning of the reaction and then decreased more gradually until it reached a stationary state (Figure 2).

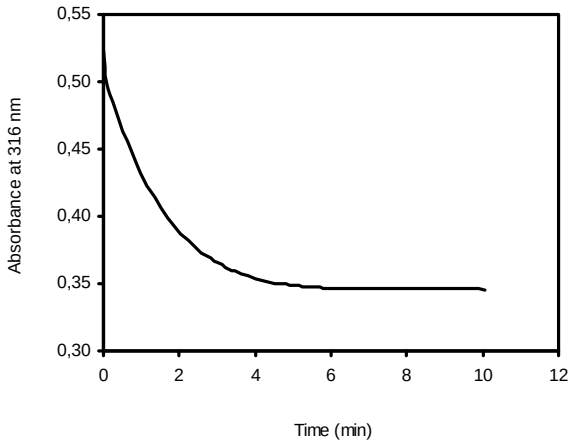

Figure 2: Influence of HRP/H_2O_2 addition on the absorbance of 0.50 g/L arabinan from SBP at 316 nm

From HPLC analysis, total FA content in the untreated arabinan residues extracted by saponification was about 1.5 mg/g dry matter. Naturally occurring diFAs was detected before the cross-linking. It was found that the amount of FA in the arabinan decreases about 90% and diFAs increases after the cross-linking. This indicates that the ferulic acid was cross-linked to produce ferulate dimers by addition of HRP and H_2O_2 as shown by the decreasing in absorbance.

Conclusion and Future Work

From this project, it is expected that a new enzymatic biocatalytis process will be developed, with a better understanding of the kinetics in order to improve the cross-linking of polysaccharides. This study will provide a distinctive contribution in the application of biological processes for the knowledge-based production of food ingredients, notably health promoting products. The knowledge gained will improve fundamental understanding of the molecular and kinetic basis of specific enzyme catalyzed processes.

Future work will be directed towards the establishment of enzyme kinetics of the cross-linked polysaccharides and their correlations with the macromolecular properties and emulsification stability.

Acknowledgement

The author would like to acknowledge Universiti Teknologi Malaysia, Skudai and the Ministry of Higher Education, Malaysia for their financial support.

References

1. T. Jalili, R.E.C. Wildman, Medeiros DM nutraceutical roles of dietary fiber. Journal of Nutraceuticals, Functional & Medical Foods. 2(4) (2000) 19-34.
2. M.-C. Ralet, G. Andre-Leroux, B. Quemener, J.-F. Thibault, Sugar beet *(Beta vulgaris)* pectins are covalently cross-linked through diferulic bridges in the cell wall. Phytochemistry. 66 (2005) 2800-2814.
3. K. Nishitani, D.J. Nevins, Enzymic analysis of feruloylated arabinoxylans (feraxan) derived from *Zea mays* cell walls. Plant Physiology. 93 (1990) 396-402.
4. L. Saulnier, J–F. Thibault, Ferulic acid and diferulic acids as components of sugar-beet pectins and maize bran heteroxylans. Journal of the Science of Food and Agriculture. 79 (1999) 396-402.
5. F. Littoz, D.J. McClements, Bio-mimetic approach to improving emulsion stability: cross-linking adsorbed beet pectin layers using laccase. Food Hydrocolloids. 22(7) (2008) 1203-1211.
6. J. Ralph, S. Quideau, J.H. Grabber, R.D. Hatfield, Identification and synthesis of new ferulic acid dehydrodimers present in grass cell walls. Journal of Chemical Society Perkin Transactions 1. The Royal Society of Chemistry. (1994). 3485-3498.

Muhd Nazrul Hisham Zainal Alam

Phone: +45 4525 2993
Fax: +45 4593 2906
e-mail: mza@kt.dtu.dk
www: www.kt.dtu.dk
Supervisors: Krist V. Gernaey
Anne Meyer
Gunnar Jonsson

Ph.D. Study
Started:
To be completed: June 2010

Continuous Membrane Microbioreactors for Development of Integrated Pectin Modification and Separation Processes

Abstract
The project aims at designing continuous membrane microbioreactors for the development of integrated pectin modification and separation processes. These microbioreactors should encompass the requirements to perform a continuous enzymatic reaction with simultaneous product separation and integration of optical sensors for on-line monitoring of relevant process variables. The project is linked to a new strategic research effort on enzymatic modification of pectins for producing pre-biotics initiated at the Department of Chemical and Biochemical Engineering at DTU.

Introduction
Pectin is a complex carbohydrate (heterosaccharide) mostly found in primary cell walls and intercellular regions of higher plants. Pectic substances are abundant in agro-industrial waste streams from sugar and potato starch production. Agro-industries are highly interested in converting these low-value waste streams into useful high-value products [1]. This conversion can be done by breaking down the pectin into oligosaccharides through the hydrolysis reaction catalyzed by combined action of pectinolytic enzymes, namely the pectinmethylesterase (PME) and polygalacturonase (PG). However; like any other enzymatic reaction, there is an abundance of factors dictating its reaction rate and kinetics [1 - 3].
Presently, the concept of microbioreactors to accommodate specific enzymatic reactions has been successfully demonstrated. However, most of the currently existing micro-scale systems for studying enzyme reactions are systems where the enzyme is immobilized [4]. Despite of its advantages in enzyme reutilization and elimination of enzyme recovery processes (recycle stream channel), this system is not suitable for the enzymatic depolymerization of pectin to oligosaccharides. This is due to the presence of multiple enzymes (PME and PG) and end-product inhibition. Under these circumstances, a free-cell system (stirred tank reactor) is most favorable. Microbioreactors (free-cell system) with a working volume ranging from milliliters down to nanoliters in different operating modes (batch, fed-batch and continuous operation) have been established. These microbioreactors are integrated with optical sensors for on-line monitoring of relevant process parameters (OD, DO, pH) [5]. Nevertheless, currently existing microbioreactors were mainly designed to facilitate the fermentation processes of bacterial and animal culture strains.
The development of micro-systems for high throughput screening of enzymatic reactions and for on site production of expensive bioproducts at the point of demand is an on-going research activity. At this stage, a feasible continuous membrane microbioreactor for pectin modification processes has yet to be established. Therefore, development of such a novel continuous membrane microbioreactor for pectin modification and separation processes will be the goal of this research project.

Motivation
When evaluating new enzymes for novel enzyme-catalysed production processes, the costs and availability of the enzymes are often a limit, as the production of limited quantities of new enzymes is costly.
In this respect, microbioreactors offer a number of cost-reducing advantages for assessing enzymatic processes (particularly screening of new enzymes). First, the microreactors operate with very small volumes, even when operated as a chemostat as envisaged in this project, thus offering significant cost reduction for assays with expensive substrates (e.g. labeled substrates) or expensive enzymes. Second, by adapting technologies from polymeric bio-microsystems,

microbioreactors can be made disposable to minimise reactor preparation efforts. Third, and maybe most important, due to the small size, the microbioreactors can mimic in a controlled fashion a wide range of environmental conditions, which can be related to conditions in full-scale bioprocesses. Moreover, the microbioreactors can be scaled out to platforms of multiple reactors, thus greatly increasing throughput for elucidating enzyme behaviour under various relevant bioprocessing conditions. [5,6].
All in all, the continuous operation of the microbioreactors is precisely the technology that will enable conducting experiments to unravel the kinetics governing enzymatic conversion processes under conditions relevant for actual industrial processes.

Continuous membrane microbioreactor prototype
The current continuous membrane microbioreactor prototype was realized as a loop reactor [6] with a working volume between 100 to 200 μL. The prototype (Figure 1) comprises both microbioreactor and micro membrane separation units pressed together in a housing made up of Polyethylene terephthalate (PETP). External microfluidic connections were established by standard Perfluoroalkoxy (PFA) tubing with commercially available chromatography fittings.

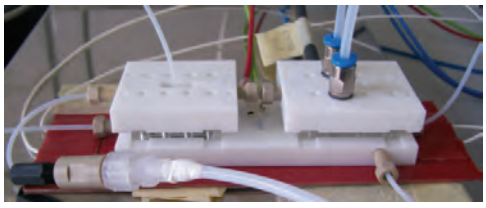

Figure 1.:The continuous membrane microbioreactor prototype

The microbioreactor (MBR) counterparts merely consist of a Polydimethylsiloxane (PDMS) layer sandwiched between two Poly methyl methacrylate (PMMA) layers. Both materials are cheap and biocompatible. This significantly reduces the cost for fabrication. The feature of the MBR includes mixing, temperature control and pH measurement. Mixing was established by a micro impeller placed inside the microreactor chamber. Temperature is measured with a Platinum resistance thermometer (Pt 100) and controlled with a heater mat placed underneath the prototype. pH is measured with fluorescent sensor spots which change both the amplitude and the phase of the emitted light with a change in the sensitive variable. A lock-in amplifier measures the phase difference and thus quantifies the measured variable.

The micro membrane separation (UF) unit on the other hand, is simply consists of a Regenerated Cellulose membrane pressed between two PMMA layers for tight sealing. Both layers have the same geometry design. An optical pressure sensor is integrated for measurement of pressure on the retentate side of the micro UF unit. A micro-gear pump is used to regulate the flow rate in the micro UF unit in such a way that a sufficiently large trans-membrane pressure for the separation process can be created. It is also used to establish the recycle stream for the entire system. Both units are illustrated in Figure 2.

(a) (b)

Figure 2.: (a) Microbioreactor counterparts (b) Micro membrane separation unit in the continuous membrane microbioreactor prototype

Work Done
We have successfully designed and fabricated the first continuous membrane microbioreactor prototype. This prototype was designed considering several aspects (geometry design, mixing. sensors, separation processes, and establishment of control loops). The cheap fabrication method allows us to re-design (if necessary) and fabricate the microbioreactor in a very short period of time. The prototype is used as a basis in understanding the basic principles of the operation of membrane microbioreactors. Its workability in real biological work in which pectin degradation with pectin lyase has also been demonstrated. Further testing is however required, before the prototype could be used for real biological work.

Next Steps
The next step of this research work will be on running more pectin modification and separation processes to further demonstrate its usefulness.

Acknowledgements
I would like to express my gratitude to Universiti Teknologi Malaysia (UTM), Skudai, Johor, Malaysia and the Malaysia Ministry of Education for their financial support of this project.

References
1. Todisco S. *et al.* (1994). *Mol. Cat.* . 92: 333 – 346.
2. Gallifuoco A. *et al.* (2003). *Ind. Eng. Chem. Res*. 42: 3937 – 3942.
3. Belafi-Bako K. *et al.* (2007). *Food. Eng*. 78: 438 – 442.
4. Miyazaki M. *et al.* (2006), *Trends. Biotechnol.*, 24 (10). 463-470.
5. Szita N. *et al.* (2005), *Lab on Chip*, 5, 819-826.
6. Muller D. H. *et al.* (2005), *Chem. Eng. Technol.*, 28 (12). 1569-1571.

Xuan Zhang

Phone: +45 4525 2892
Fax: +45 4588 2258
E-mail: xz@kt.dtu.dk
WWW: http://cere.dtu.dk
Supervisors: Alexander Shapiro
Erling H. Stenby

PhD Study
Started: September 2008
To be completed: August 2011

Multiphase Flow in Porous Media

Abstract

A novel approach to multiphase flow in porous media is to be developed. It will be based on the recent achievements in the area of thermodynamics of disperse systems, and on a deeper understanding of the flow mechanisms on the micro level: multiplicity of microstates, snap-off, and film flow. The anticipated results will change the approach to description of almost all the enhanced oil recovery processes. The second part of the work will be aiming at averaging/upscaling, in order to find out how the phenomena at micro level affect the flow at the laboratory and reservoir scales.

Current work is focused on upscaling of two phase flow, water and oil, in stratified fully communicating reservoir.

Introduction

Waterflooding is the most widely used method in improved oil recovery. Since the reservoir rocks are heterogeneous, and it is not practical for people to get very detailed information of reservoir, upscaling techniques are needed to get the pseudo properties of the reservoirs: pseudo relative permeabilities and pseudo fractional flow functions. These functions are used in the framework of the classical Buckley-Leverett theory of waterflooding.

Upscaling is to transfer from specific parameters of small scale to average (pseudo-) functions for the whole reservoir. Upscaling techniques are often used to coarsen the geological models to manageable levels for flow calculation. It is important that these coarsened flow models replicate the fine scale characteristics in terms of key behaviors, such as overall flow rate and the appearance of injected fluid. Upscaling techniques can be characterized as local, extended local, global or quasi-global, with regard to the size of the region used for calculating the coarse scale quantities. [1] Some of them focus on gridding methods, for example merging grids of same permeability or same porosity or same vorticity [2]. The others focus on algorithm.

A model of flow upscaling in a layered reservoir with perfect vertical connection has been developed in this article. The model describes displacement of oil by water in a viscous dominant regime. By using this method, we can calculate pseudo relative permeabilities, pseudo fractional flow function and pseudo water saturation profile without rearranging the layers, as Hearn did [5]. And we can apply this method to cases of any layers, as well as continuously distributed layers. Numerical and analytical algorithms to obtain the pseudo-functions have been worked out. The results were compared with the model of connected layer-cake reservoir.

Model Description

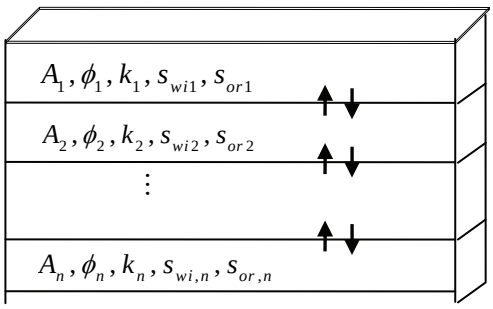

Figure 1: Sketch of stratified fully communicating reservoir. Each layer has individual area of cross section A_i, porosity ϕ_i, permeability k_i, irreducible water saturation $s_{wi,i}$, residual oil saturation $s_{or,i}$.

Case Study—Two-layer case

Mass conservation, modified Buckley-Leverrete equation

$$\Phi_1 \frac{\partial s_1}{\partial T} + \frac{\partial U_1 F_1(s_1)}{\partial X} = 0$$
$$\Phi_2 \frac{\partial s_2}{\partial T} + \frac{\partial U_2 F_2(s_2)}{\partial X} = 0 \qquad (1)$$

where Φ_i is porosity, s_i water saturation, U_i total flow velocity, F_i fractional flow function, of layer i. Φ_i, U_i, X and T are all dimensionless variables.

We assume water and oil are both incompressible and perfect pressure communication between layers, so we have

$$U_1 = \frac{\Lambda_1}{\Lambda_1\alpha_1 + \Lambda_2\alpha_2} Q$$
$$U_2 = \frac{\Lambda_2}{\Lambda_1\alpha_1 + \Lambda_2\alpha_2} Q \qquad (2)$$

Where Q is dimensionless injection rate, Λ_i is dimensionless total mobility from Darcy's law.

$$\Lambda_i = k_i \left(\frac{k_{rw,i}}{\mu_w} + \frac{k_{ro,i}}{\mu_o} \right) \qquad (3)$$

where $k_{rw,i}$ and $k_{ro,i}$ are relative permeabilities of water and oil respectively.

This model tells that total flow velocity is redistributed with regard to the total mobility of each layer.

Results and Discussion

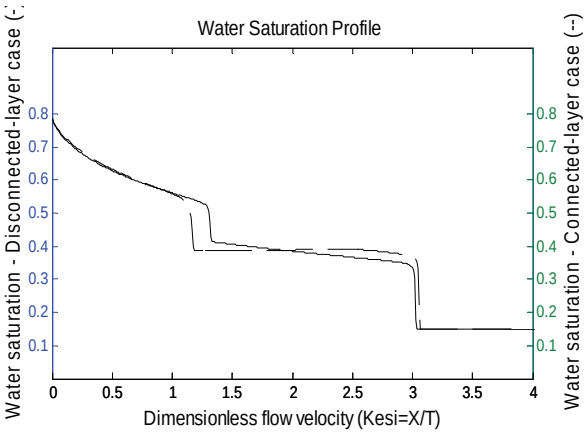

Figure 2: Water saturation profile $s^*(\xi)$. s^* is averaged water saturation, defined as

$$s^* = \frac{s_1 A_1 \Phi_1 + s_2 A_2 \Phi_2}{A_1\Phi_1 + A_2\Phi_2} \qquad (4)$$

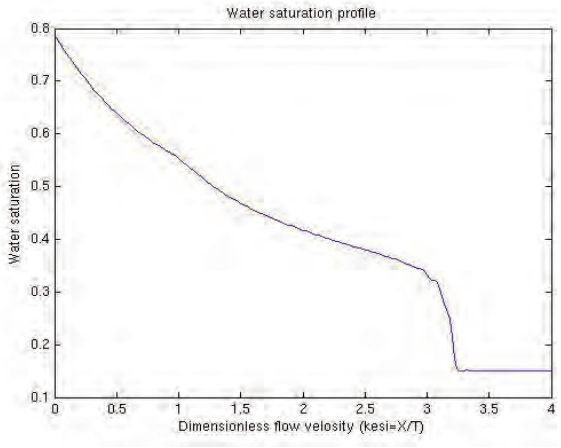

Figure 3: Water saturation profile $s^*(\xi)$, 2-dimentional simulation of communicating layers by Comsol.

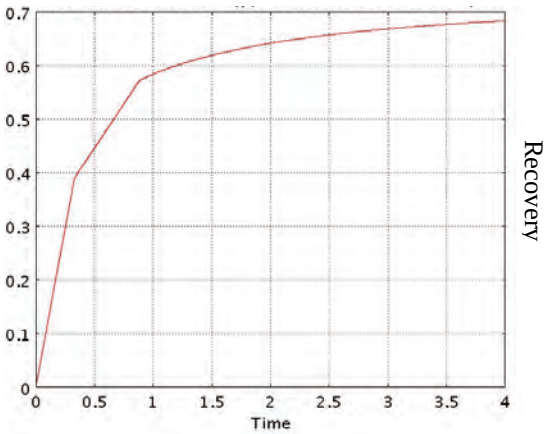

Figure 4: Recovery vs Time (PVI), by our model

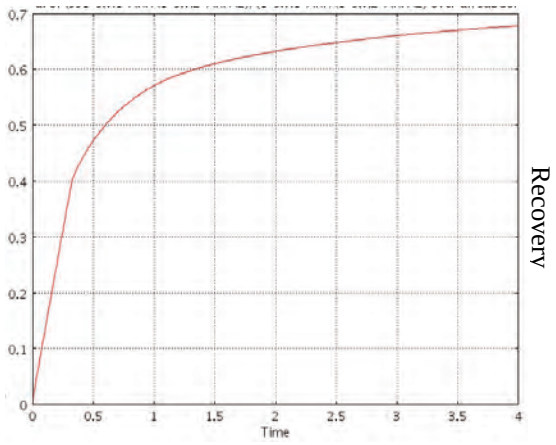

Figure 5: Recovery vs Time (PVI), 2-dimentional simulation of communicating layers by Comsol.

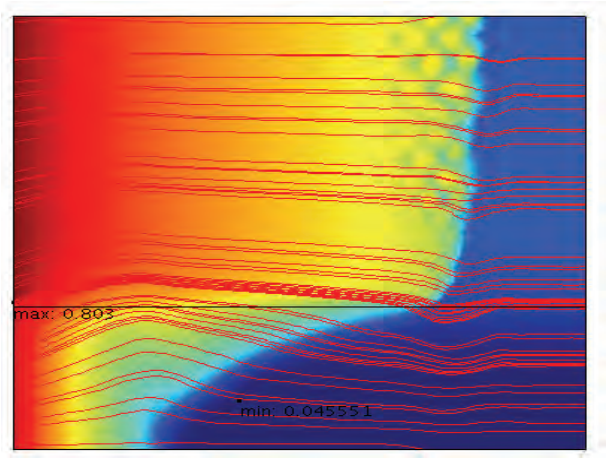

Figure 6: 2-dimentional water saturation profile, and stream line of total velocity U_i, simulation of communicating layers by Comsol.

Conclusions

Compare Figure 2 and 3, we find that the saturation profile of our model is different from the one done by Comsol. But they give similar front in the fast layer. Compare Figure 4 and 5, we see that our model and Comsol give very close recovery profile, for example the close break through time, at around 0.8 PVI, and close break through recovery. Our method is relatively simple, so it is better for practical application of upscaling.

Future Work

Future work involves generalization into multilayer and stochastically heterogeneous reservoirs.

Acknowledgements

The Danish Council of Technology and Production (FTP) is kindly acknowledged for financial support in the framework of the ADORE project. The authors are grateful to Kent Johansen, who has drawn their attention to apparent problems with the Hearn method.

References

1. Y. Chen, L. J. Durlofsky, M. Gerritsen, Department of petroleum engineering, Stanford University, X. H. Wen, Chevron texaco exploration & production technology company, San Ramon, A coupled local-global upscaling approach for simulating flow in highly heterogeneous formation, Advances in water resources 26 (2003) 1041-1060
2. H. Mahani, SPE, M. A. Ashjari, B. Firoozabadi, Sharif University of Technology, Iran, Reservoir flow simulation using combined vorticity-based gridding and multi-scale upscaling, SPE 110306, presented at 2007 SPE Asia Pacific Oil & Gas Conference and Exhibition
3. Jon Kleppe, Norwegian University of Science and Technology, Handout note 6-Dykstra-Parsons method, TPG 4150 Reservoir recovery techniques 2008
4. Rustam Rauf Gasimov, Petroleum engineering, Texas A&M University , Modification of the Dykstra-Parsons method to incorporate Buckley-Leverett displacement theory for water floods, August 2005, P3
5. C. L. Hearn , SPE-AIME Service Oil Co. Simulation of Stratified Water Flooding by Pseudo Relative Permeability Curves, SPE 2929, July 1971
6. Noaman El-Khatib, SPE, King Saud U, Waterflooding performance of communicating stratified reservoir with log-normal permeability distribution
7. Pavel Bedrikovetsky , Mathematical theory of oil and gas recovery-with applications to ex-ussr oil and gas fields, P3-7, P12, P22, ISBN 0-7923-2381-5, Kluwer academic publishers
8. Tore I. Bjørnaråa and Eyvind Aker, NGI, Norway Comparing Equations for Two-Phase Fluid Flow in Porous Media, COMSOL Conference 2008 Hannover
9. M.A. Diaz-Viera*,1, D.A. Lopez-Falcon1, A. Moctezuma-Berthier1, A. Ortiz-Tapia1 Instituto Mexicano del Petroleo, COMSOL Implementation of a Multiphase Fluid Flow Model in Porous Media

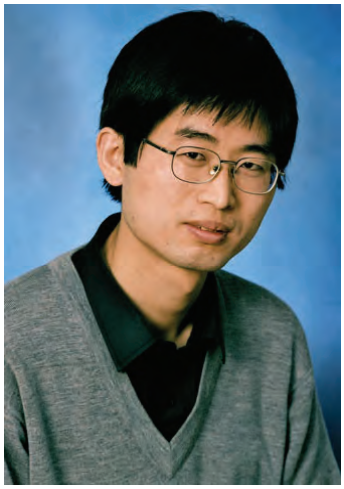

Yuanjing Zheng

Phone: +45 4525 2830
Fax: +45 4588 2258
E-mail: yjz@kt.dtu.dk
WWW: http://www.chec.dtu.dk
Supervisors: Anker Degn Jensen
Christian Windelin, FLSmidth Airtech

Industrial PhD Study
Started: April 2008
To be completed: March 2011

Mercury Removal from Cement Plants by Sorbent Injection upstream of a Pulse Jet Fabric Filter

Abstract
A fixed-bed reactor system has been built for mercury sorbent screening tests. In nitrogen atmosphere no mercury adsorption on sorbents is observed at 150°C except the bromine impregnated activated carbon. Simply adding a separate bed of $CaBr_2$ powder can improve the mercury adsorption significantly. Both fixed-bed and two-stage fabric filter adsorption models are developed. Investigations show that the low temperature, red brass converter system does not work according to the patent statement when using a gas composition of HCl with SO_2 or NOx.

Introduction
There has been an increased focus on mercury emission from industry during the latest years as a consequence of the environmental impact and potential risk for human health of mercury compounds. Some cement raw materials have high mercury contents and very high mercury emissions from cement plants have been observed. Mercury removal from cement plant flue gases has been required in both EU and US.

Due to rising energy costs and stricter energy and environmental regulations, alternative fuel technology is becoming an important factor in controlling costs for cement production. To gain a competitive edge, many cement producers worldwide have started to increase usage of alternative fuels. High mercury containing alternative fuels such as chemical waste, domestic waste and sewage sludge are also incinerated in cement plants and high mercury emissions have been encountered. FLSmidth's ambition is to address all the technological needs of the global cement industries related to utilization of alternative fuels. To ensure that the mercury emission limit is met, FLSmidth has initiated research on mercury removal from cement plants.

Mercury can be removed from the flue gas by fuel cleaning and switching, raw material cleaning, sorbent injection, sorbent fixed bed, oxidation and removal by catalyst and wet scrubber. Activated carbon injection upstream of a particulate control device such as fabric filter has been shown to have the best potential to remove both elemental and oxidized mercury from the flue gas for plants not equipped with a wet flue gas desulphurization plant. However, mercury adsorption by activated carbon is not clearly understood yet, research and development efforts are still needed before carbon injection is considered as a commercial technology for wide use. Low-cost, cement-friendly sorbents need to be developed to reduce the sorbent and disposal cost, the amount of sorbent injected needs to be kept to a certain level to reduce the operational cost. Furthermore, stability of mercury adsorbed by sorbents needs to be proved.

Extensive research has been carried out to reduce mercury emissions from coal combustion and waste incineration, but very little efforts have been concentrated on mercury removal in cement plant. The application of sorbent injection to cement kilns appears to be more challenging and knowledge obtained from mercury removal in power plant and incinerator might not be applied to cement plant directly.

Specific Objectives
The overall goal of this project is to develop and advance improved mercury control technologies using sorbent injection upstream of a pulse jet fabric filter for cement plants. Specific objectives are as follows:

1. To develop an experimental fixed-bed unit and screen sorbents for capturing mercury from cement kiln flue gas. To develop low-cost, cement-friendly sorbents and reveal mercury capture mechanisms and obtain kinetic rates.
2. To demonstrate the ability of developed sorbents and technology to control emissions of mercury from a full-scale cement plant or FLSmidth Airtech pilot

plant at Dania over a typical range of operating conditions.

3. To develop a mathematical model that can describe mercury removal and predict mercury removal efficiency in cement plant by injecting sorbent upstream of a fabric filter.

Experimental Setup

A lab-scale fixed bed reactor for screening the sorbents has been built. Figure 1 illustrates the sketch of the reactor system. The system consists of a mercury vapor generator, gas addition system, a gas-solid glass reactor, an electrical heated oven, oxidized mercury to elemental mercury converter, a mercury analyzer, flue gas treatment units, and data sampling. The mercury analyzer can analyze gas of up to 30% water, and therefore no drying of the gas is needed. To avoid mercury condensation and accumulation in the system, all the gas lines before and in the analyzer are heated at 130°C. The mercury source, reactor and heated gas lines are located in a dedicated ventilation hood.

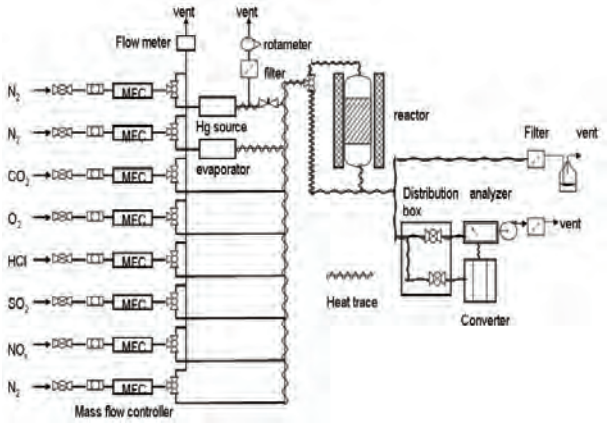

Figure 1: Sketch of the fixed bed reactor system.

More than 20 sorbent candidates are collected for screening tests. Particle size distributions are measured by Malvern laser diffraction equipment. Selected samples are analyzed by SEM-EDX.

Results

Leakage tests of the system have been conducted and mercury accumulation in the hot system was not observed. The analyzer has a good linearity and works well when measuring only elemental mercury under simulated flue gas condition. The converter holds red brass at 180°C and has been used in a waste incinerator according to the supplier (Lumex). However, tests in this project show that the converter works only when gases such as 15 ppmv HCl, 1000 ppmv SO_2, 1000 ppmv NO/34 ppmv NO_2 is added alone. Combination of HCl with SO_2 or NOx will result in oxidation or adsorption of elemental mercury and destroying the measurements.

Preliminary tests of some commercial sorbents have been conducted by mixing 5-10 mg sorbents with 2 g sand powder. These sorbents include Norit Darco Hg and Darco Hg-LH activated carbon, Sorbalit, Faxe Kalk Minsorb 1 and Minsorb 3. In nitrogen atmosphere no mercury adsorption on sorbents is observed at 150°C except Darco Hg-LH which is bromine impregnated (see Figure 2).

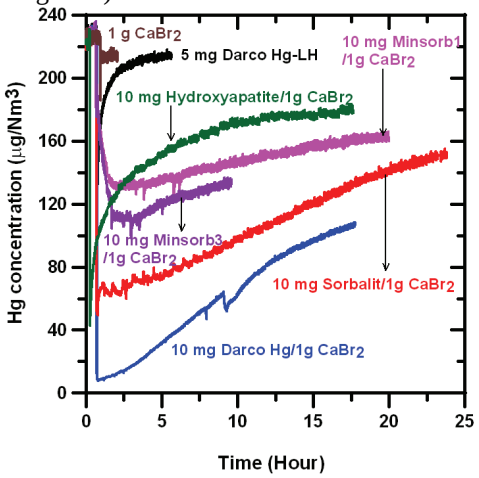

Figure 2. Adsorption curves of some commercial sorbents at 150°C in nitrogen atmosphere.

The sorbents were also tested by adding 1 g $CaBr_2$ powder on top of the sorbent/sand mixture and separated by quartz wool plug. The inlet elemental mercury level is about 230 µg/Nm^3 and decreases to about 215 µg/Nm^3 when the gas passes through 1 g $CaBr_2$ bed at 150°C. Instead of immediate breakthrough significant mercury adsorption is observed for sorbents having a 1 g $CaBr_2$ bed on top. This implies that $CaBr_2$ can be used to improve mercury adsorption by sorbents through ways such as injection of $CaBr_2$ solution at hot zone, mixing with or impregnating sorbents, adding of $CaBr_2$ in the fabric filter by impregnating the bags or adding $CaBr_2$ in the filter house.

Modeling Work

Mathematical models are developed assuming linear adsorption and local equilibrium within the sorbent particles. Orthogonal collocation method is used to solve mercury diffusion and adsorption inside a sorbent particle. For mercury adsorption in the duct another mass balance equation for bulk gaseous mercury is coupled and solved simultaneously using Matlab routine ode15s. The fixed-bed model is solved by tank-in-series method.

The fixed-bed model is then extended to moving boundary problem assuming a new sorbent layer is accumulated on the bag and acts as a well-mixed tank. Finally the duct model and fabric filter model are coupled to a two-stage model. The model can simulate the mercury removal profile with features of sorbent cake accumulation on the filter bag, and periodical cleaning fractions of the bags.

Acknowledgements

This project is a part of the Research Platform on New Cement Production Technology financed by Danish Advanced Technology Foundation, FLSmidth A/S, and DTU. Financial support of the industrial PhD study by the Ministry of Science Technology and Innovation is gratefully acknowledged.